Compressive Strength and Modulus of Elasticity Relationships for Alabama Prestressed Concrete Bridge Girders

by

Andric Hofrichter

A thesis submitted to the Graduate Faculty of
Auburn University
in partial fulfillment of the
requirements for the Degree of
Master of Science

Auburn, Alabama
August 2, 2014

Keywords: camber, concrete maturity, fresh properties, serviceability, stiffness

Approved by

Robert W. Barnes, Chair, James J. Mallett Associate Professor of Civil Engineering
Anton K. Schindler, Professor of Civil Engineering
J. Michael Stallings, Professor of Civil Engineering

Abstract

The state of Alabama constructs many of its bridges using precast, prestressed concrete bridge girders. There is a desire to more accurately predict girder cambers through the time of deck placement. Proper understanding of the short-term and long-term material properties of Alabama concretes is important information that must be obtained before consistently accurate camber predictions can be made.

Common practices of girder producers were observed and compared for predictable trends. Historical records including more than 1900 girder pours from four girder producers over a six-year period were analyzed for patterns in project requirements, fresh concrete properties, measured concrete compressive strengths, and producer practices. Using strength measurements and curing temperature measurements from 435 girder pours, the authors established trends in concrete maturity at prestress transfer and in compressive strength development over time.

Methods for predicting average concrete compressive strength at prestress transfer and at 28 days were developed based on historical records, and were compared to in-plant measured strengths. The compressive strength prediction methods were used to improve modulus of elasticity prediction accuracy for the 2012 *AASHTO LRFD Bridge Design Specifications*. Modulus of elasticity predictions were compared using five or more different prediction methods for both release and 28 days. Lastly, modulus of elasticity development over time was compared to concrete strength development over time.

Acknowledgments

In many ways, I am grateful to all of my Auburn professors, who are very knowledgeable and passionate about the training they provide. In particular, I am grateful to Dr. Schindler and Dr. Barnes. Dr. Schindler provided a wealth of knowledge and experience to help direct the focus of my work. Dr. Barnes has been a wonderful advisor—both challenging and encouraging, both friendly and professional. I am grateful for all the help and guidance he has given me along the way.

I am grateful for the hard work of Dave Mante, the leader of our project group, and Levent Isbiliroglu, the third member of our team. Dave's advice and experience was invaluable throughout this project. Both of these men worked very hard both in the field and in the office, and made this project possible. Also, I am grateful for all the willing help and useful information that was provided by Mr. Nathan Emmerich and Mr. Andrew Levens

I am very grateful for my parents, for their constant love, prayer, and encouragement. Also for my siblings, and most particularly for my brother, whose constant distractions and conversation helped to keep me energized and uplifted.

Lastly, but most importantly, I am grateful to the Lord my God, Who has provided so many amazing opportunities for me and brought so many wonderful people into my life. He is always faithful and gracious, and He has blessed me beyond what I could have hoped. I know that He is pleased when I work with energy and integrity, and that is the greatest encouragement of all.

Table of Contents

List of Figures

List of Tables

Chapter 1: Introduction

1.1. Background and Motivation

Camber is a fairly simple concept, capable of explanation using fundamental laws of mechanics or of definition in a single sentence. After all, camber in prestressed concrete bridge girders is simply the net upward deflection along the length of a member due to eccentric prestressing force. Camber involves the concepts of resolving an eccentric force into a force and a coupling moment, and the deflection response of a beam subjected to moment along its length.

But the quantification of camber, and the prediction thereof, involves a world of complications and interconnected variables that are left out of such a simple explanation. Time, temperature, humidity, concrete strength, concrete stiffness, prestressing force, prestressing eccentricity, aggregate type, and more, all play their part in the camber values of a given concrete girder.

Nevertheless, there is a strong desire to be able to reliably predict girder cambers during the design phase, before many of these variables are known. This prediction needs to be reasonably accurate—neither too high, nor too low—because errors on either side cause complications in the construction process. Prediction inaccuracy causes construction difficulties for projects both with and without cast-in-place concrete decks supported by the girders. Girders without a cast-in-place deck are typically members such as hollow-core slabs or box girders, which occasionally have a small topping applied. Hollow-core slabs are often seen used as floor systems in buildings, and box girders are often used for reasonably short-span bridges. Girders

with a cast-in-place deck are typically AASHTO girders or PCI bulb-tee girders, used in bridges.

When camber predictions are too high for girders that will receive a cast-in-place deck, and the camber actually achieved by the girder is less than predicted, a larger concrete deck buildup may be required to match the design grade levels. This then forces the contractor to use additional concrete in order to reach grade, which incurs additional costs and applies unplanned dead loads to the girder that were not included in the design. In extreme cases of overestimation, it is even possible for a finished bridge to sag under the superimposed dead loads such as the concrete deck and barrier rails.

When camber predictions are too small for girders that will receive a cast-in-place deck, and the girder cambers more than expected, it may be very difficult to achieve the desired deck elevations. Smaller seats may have to be used for reinforcing bars in the deck. In extreme cases, the girder may encroach into the planned deck location, and the deck thickness may need to be adjusted or deck elevations adjusted to accommodate the high cambers.

Lastly, variable cambers within a project are also undesirable. When adjacent girders in a bridge exhibit differing camber levels at the stage of erection, it causes difficulties in the construction process. If one girder has a 2 in. camber, and the adjacent girder has a 4 in. camber, alignment between the two becomes difficult.

Inaccurate camber predictions for girders that will not receive a cast-in-place deck often more directly affect the quality of the finished product, since there is no thick element to account for some of the camber variance. Placement of a thin topping and smooth transition between members becomes more difficult with varying cambers. Low cambers may result in sagging under sustained loads, and high cambers may result in undesirably high curvatures in a floor system or an overly bumpy ride in a bridge system.

Thus, being able to accurately predict cambers of prestressed concrete bridge girders during the design phase of the project is useful for those involved in the construction process. This research project was designed specifically for the purpose of helping to improve the accuracy of camber predictions by the Alabama Department of Transportation (ALDOT) engineers during the design phase and reduce the frequency of unexpected cambers experienced during construction.

1.2. Research Objectives

The primary objective of this research study was to provide the Alabama Department of Transportation (ALDOT) with a procedure that could be used during the girder design phase to more accurately predict girder camber prior to deck placement. Four secondary objectives were identified as necessary in order to achieve this primary objective.

1. Establish relationships between concrete modulus of elasticity and compressive strength at the time of prestress transfer for typical ALDOT girder concrete mixtures.
2. Identify relationships between specified concrete compressive strength at prestress transfer and actual compressive strengths achieved for typical ALDOT girder concrete mixtures and plant procedures.
3. Assess time-dependent deformation characteristics of typical ALDOT concretes.
4. Establish the best material property relationships for use in predicting initial camber and camber growth of ALDOT girders.

The primary focus of the research discussed in this thesis is related to Objectives 1 and 2, as they relate to the primary objective.

It was recognized in the early stages of this research project that the properties of a

prestressed concrete bridge girder at the time of prestress release are the most important aspects of the research project on which it would need to focus. This is because of the significant errors induced by inaccurate prediction of the cambers at release. Initial camber, which for the purposes of this project is defined as the camber immediately after prestress release, provides the baseline by which all future cambers are predicted in most methods.

- Perhaps the most commonly used method in the prestressed bridge girder industry is the PCI Multiplier Method (PCI 2003), originally developed by Leslie D. Martin (1977). He created a system of multipliers for different stages and components of the overall deflection, as may be seen in Table 1.1. The majority of these multipliers are used with values that are computed for the girder at the time of prestress release. Martin clearly stated all of the assumptions he used in developing these multipliers, allowing anyone who wished to do so to modify the multipliers to fit local conditions.

Table 1.1: PCI Multiplier Method Coefficients (PCI 2003)

	Without Composite Topping	With Composite Topping
At Erection:		
[1] Deflection (downward) component – apply to the elastic deflection due to the member weight at release of prestress	1.85	1.85
[2] Camber (upward) component – apply to the elastic camber due to prestress at the time of prestress release	1.80	1.80
Final:		
[3] Deflection (downward) component – apply to deflection calculated in [1] above	2.70	2.40
[4] Camber (upward) component – apply to camber calculated in [2] above	2.45	2.20
[5] Deflection (downward) – apply to elastic deformation due to superimposed dead load only	3.00	3.00
[6] Deflection (downward) – apply to elastic deflection caused by the composite topping	--	2.30

- A slightly newer, but lesser known method of predicting long-time cambers is the PCI Improved Multiplier Method (PCI 2003), developed by Tadros, Fawzy, and Hanna (1985). This method attempts to incorporate more girder-specific values of creep and prestress loss, but therefore requires more detailed knowledge of the concrete properties used in the project. The multipliers for this method may be seen in Table 1.2.

Table 1.2: PCI Improved Multiplier Method Coefficients (Tadros, Fawzy, and Hanna 1985)

	Erection Time		Final Time	
Load Condition	Formula	Average	Formula	Average
Initial Prestress	$1 + C_a$	1.96	$1 + C_u$	2.88
Prestress Loss	$\alpha(1 + \chi C_a)$	1.00	$(1 + \chi C_u)$	2.32
Self-weight	$1 + C_a$	1.96	$1 + C_u$	2.88
Dead Load on Plain Beam	1.00	1.00	$1 + C_u'$	2.50
Dead Load on Composite Beam	1.00	1.00	$1 + C_u'$	2.50

C_a = creep coefficient for loading applied immediately after transfer and strains measured at time of erection. Average value is 0.96.

C_u = ultimate creep coefficient for loads applied immediately after transfer. Average value is 1.88.

C_u' = ultimate creep coefficient for loads applied at time of erection. Average value is 1.50.

α = time-dependent prestress loss at erection divided by total time-dependent prestress loss. Average value is 0.60.

χ = Bazant's aging coefficient. Average value is 0.70.

- Kelly, Bradberry, and Breen (1987) also suggested a method of predicting time-dependent cambers, which used creep estimates, prestress loss estimates, and geometrical

changes to the girder to calculate multipliers for use with each of the different load components. These multipliers were based on time-dependent concrete properties, and were multiplied by the initial elastic deflections to produce time-dependent estimates.

Each of these methods uses the instantaneous, elastic deflection at the time of prestress release as the basis by which to predict all subsequent cambers. As such, the ability to accurately predict initial camber directly affects the ability to accurately predict cambers at all subsequent time periods.

Two groups of information are necessary in order to accurately predict initial cambers. They may be summed up as follows:

1. A good understanding of the interactions between self-weight, girder geometry, internal prestressing force, and the cambers that are induced by that combination. Barring several difficult-to-quantify components such as support friction and transfer length effects, many engineers are confident in the current camber calculation methods that are in place, provided that #2 is also available.
2. Much more difficult to obtain is accurate knowledge of the in-place stiffness of the concrete and actual prestressing force being applied to the concrete. This stiffness is invaluable, because it allows for accurate calculation of the longitudinal shortening of the girder, the relationship between curvature on a cross section and the moment resisted at the cross section, and the internal prestress force. The highly eccentric internal prestressing force produces large internal moments, which must be resisted at each location along the girder by curvature of the cross section at that location. The amount by which the cross section must rotate in order to resist the internal moment is largely determined by the stiffness of the cross section—namely, by the stiffness of the concrete.

Both of these information groups are necessary just for the prediction of initial cambers. Time-dependent camber predictions are then further complicated by concrete creep effects (which is usually considered to be a function of the initial elastic deformation) and relaxation of the prestressing strands. All of these components play a part in the prediction of girder cambers.

This research project as a whole was focused on the prediction of cambers until the time of bridge erection. However, the topics discussed in this thesis relate primarily to the relationships between concrete strength and stiffness up until 28 days and the prediction of concrete properties at the time of prestress release. In short, this thesis provides the necessary information for more accurate predictions of initial camber.

The importance of initial camber predictions has been clearly shown. As such, the largest portion of analysis discussed in this thesis is related to expected compressive strength at release and the relationship between release strength and release stiffness. Camber is, in most cases, not a life safety issue, but a serviceability issue. Thus, it is important to note that accurate knowledge of concrete strength is not, in and of itself, the ultimate goal of this analysis. A thorough understanding of concrete strength is merely used as a means of reaching accurate predictions of concrete stiffness, which is the crucial property for initial camber prediction. Ultimately, in addition to providing useful information about common plant practices and mixture proportions, this thesis aims to provide the following two pieces of information as top priority:

1. When a design engineer specifies any particular strength, f'_{ci} or f'_c, the goal is to provide the engineer with accurate and detailed knowledge as to the level of strength, f_{ci} or f_c, that should be expected to result from the production of that girder. Stiffness of the concrete at 28 days is not really significant for camber prediction, so all analyses will focus primarily on concrete properties at release.

2. When a design engineer either knows the actual strength of the concrete or has a firm understanding of the expected strength of the concrete from number 1 above, the next goal is to provide a much more accurate method of predicting the concrete stiffness than would have been provided by the use of f'_{ci} or f'_c.

1.3. Scope and Tasks

In order to accomplish the objectives outlined above, seven tasks were proposed:

1. *Review of literature and current ALDOT practice.*

Researchers would collect information on up-to-date material models for modulus of elasticity, creep, and shrinkage behavior of concrete used in prestressed concrete bridge girders. Recent findings by other researchers would also be examined. Common specifications, such as the AASHTO LRFD Bridge Design Specifications and the fib Model Code 2010, would also be included in the analysis.

Researchers would also study current ALDOT practice and plant procedures to determine what information is available to design engineers during design, and to identify possible variables that may contribute to inaccurate camber predictions. Construction practices would be studied to gain a thorough understanding of the role of camber predictions in the construction process.

2. *Design of Experimental Program.*

A detailed experimental program would be designed, using the information obtained in Task 1, to best accomplish the project objectives. All needed supplies and sensors would be identified and purchased. The experimental design is described in Chapter 4 of this Thesis.

3. *Collection, Review, and Analysis of Producer-Submitted Concrete Strength Data.*

In order to better understand the relationship between specified concrete design strength and the actual achieved strengths in plant-produced girders, producer- submitted strength test results would be collected and analyzed. By examining trends in girder production time, plant practices, fresh concrete properties, curing procedures, and any other plant-submitted data as they relate to the strength of the concrete, researchers would work to extend the applicability of the controlled test results.

4. *In-Plant Concrete Materials Testing and Camber Measurement.*

Researchers would perform camber measurements, girder instrumentation, and in-plant material testing on a variety of bulb-tee girders produced for actual ALDOT bridges. Embedded sensors would provide data for temperature and strain corrections, and camber growth would be measured until the girders were shipped to the construction site.

Material testing would be used to establish relationships between concrete modulus of elasticity and compressive strength of representative concrete mixes under typical casting and curing conditions, as well as relationships between specified concrete strengths (f'_{ci} and f'_{c}) and the actual concrete strengths at those times. Compressive strength and modulus of elasticity of representative concrete samples from these girders would be measured using standard test methods. Cylinders for testing would be match cured to girder temperatures in order to improve that applicability of test results.

In-plant testing would be organized and performed in such a way as to minimize disturbance of normal girder production procedures. If possible, this testing would be performed at three production facilities that cover a range of geographic conditions, aggregate sources, and production techniques characteristic of prestressed girders in ALDOT bridges.

5. *Creep and Shrinkage Testing.*

Creep and shrinkage properties of several representative girder concrete mixtures would be assessed using the Auburn University Highway Research Center (AUHRC) testing facility. These mixtures would be representative of common mix designs that are used in the production of ALDOT prestressed bridge girders.

6. *Analysis of Results.*

A detailed analysis of the results from Tasks 4 and 5 would be performed shortly after the results were obtained. This analysis would focus on the achievement of the stated primary objective, and particularly on developing a useful camber prediction procedure that accurately reflects current material properties and girder production techniques.

7. *Preparation of Final Report and Camber Prediction Procedure.*

A comprehensive report encompassing all components of the research project would be written. All data, analysis results, and a recommended camber prediction procedure for design purposes would be included. A software tool would be developed to easily implement this camber prediction procedure.

The information presented in this thesis only covers some of these tasks. Namely, this thesis discusses Tasks 1 and 3, and parts of Tasks 4, 6, and 7.

1.4. Thesis Organization

Chapter 2 examines modulus of elasticity equations and recent concrete strength and stiffness findings in related research.

Chapter 3 discusses the current state of the industry for prestressed girder production in Alabama. It examines common plant practices, common procedures for the production and storage of girders, and common concrete mixture designs properties.

Chapter 4 lays out the experimental design that was established for in-plant material testing and camber measurement. The experimental design for long-term concrete behavior, such as creep and shrinkage, is not included in this Thesis.

Chapter 5 outlines the collection and storage of all historical plant-submitted data, and provides descriptions of the results of all basic analyses. Concrete stiffness information was not available in plant-submitted data.

Chapter 6 explains and gives the results for the in-depth analysis of all strengths that were obtained from historical plant-submitted data. These findings are related to release strength, 28-day strength, and strength growth over time.

Chapter 7 discusses all in-plant experimental findings related to strength and modulus of elasticity in the concrete used. Findings related to release strength, 28-day strength, and strength growth over time are compared to the results from the historical analysis. Additional findings are related to release modulus, 28-day modulus, and modulus growth over time.

Chapter 8 summarizes the thesis and the conclusions reached.

Chapter 2: Previous Prestressed Concrete Materials Research

2.1. Introduction

This chapter examines strength relationships, modulus of elasticity equations, and recent concrete strength and stiffness findings in related research. First, in Section 2.2, different equations and methods for predicting concrete modulus of elasticity, along with some of their history, are presented and discussed. Different development methods for maturity, compressive strength, and modulus of elasticity are discussed in Section 2.3. Recent concrete strength and stiffness findings in related research are discussed in Sections 2.4 and 2.5, respectively.

2.2. Concrete Stiffness Prediction Methods

The origin of the current standard equation for the static modulus of normal weight concrete came from the work of Adrian Pauw (1960). He found that the static modulus of concrete depended on both the strength of the concrete and the unit weight of the concrete. After an extensive analysis of data encompassing different strengths of concrete and types of aggregates, he developed the following equation:

$$E_c = 33\omega^{\frac{3}{2}}\sqrt{f_c'} \qquad \textbf{Equation 2.1}$$

where:

E_c = static modulus of elasticity of the concrete, psi

ω = air-dry weight of concrete at the time of test, pcf

f_c' = specified compressive strength of the concrete, psi

This equation demonstrates that, as Pauw reported, the static modulus is more highly influenced by the weight of concrete than by the strength of the concrete, though it is affected by both. He also recognized that the method of testing the static modulus had a significant impact on its value. The equation was meant to provide a general means of estimating concrete modulus of elasticity for a wide range of strengths and concrete unit weights. It was developed using measured average strengths from a number of other sources, and it included both lightweight and normal weight concretes. Pauw recognized that the equation could be refined with the collection of more data and the adoption of a standard testing method.

Pauw's equation was later adopted and instituted in what is now known as the *Building Code Requirements for Structural Concrete* (ACI 318 2011), commonly referred to as simply the ACI 318 code. This equation has remained the standard method of predicting concrete modulus of elasticity for most structural concrete up to the present day, with concrete unit weights limited between 90 pcf and 160 pcf. Although Equation 2.1 includes no explicit provisions to account for different aggregate stiffness, the allowable range of unit weights includes even those concretes that would normally be considered lightweight concrete. Therefore, in determining concrete stiffness, the equation only indirectly accounts for aggregate stiffness by using concrete unit weight alone.

The American Society for Testing and Materials (ASTM) C469/C496M Standard (2010) provides the standard test method for the measurement of concrete modulus of elasticity that Pauw desired for uniform, comparable modulus values. This standard is called the "Standard Test Method for Static Modulus of Elasticity and Poisson's Ratio of Concrete in Compression." It was first approved in 1961, shortly after the publication of Pauw's paper. The adoption of this standard made possible the direct comparison of modulus of elasticity values taken by different

people in different areas, because it established a common method of measurement. This method measures the chord modulus of elasticity at 40% of the ultimate stress. This range, from a small stress to the $0.40f_c'$ limit, provides repeatable, relatively linear-elastic results.

Unlike the ACI 318 standard, the *AASHTO LRFD Bridge Design Specifications* (2012), hereafter referred to as simply the AASHTO code, did alter Pauw's equation to include subsequent findings about the effects of different aggregates on concrete modulus of elasticity. In the 2005 revisions of the AASHTO code, the following modified form of Equation 2.1 was adopted for the calculation of concrete modulus of elasticity:

$$E_c = 33{,}000K_1\omega^{\frac{3}{2}}\sqrt{f_c'} \qquad \textbf{Equation 2.2}$$

where:

E_c = static modulus of elasticity of the concrete, ksi

K_1 = correction factor for source of aggregate to be taken as 1.0 unless determined by physical test, and as approved by authority of jurisdiction

ω = unit weight of concrete at the time of test, kcf

f_c' = specified compressive strength of the concrete, ksi

This equation recognized the effect that aggregate source has on concrete stiffness, and created this K_1 factor to allow for engineers to modify the modulus of elasticity equation to accommodate local aggregate effects.

In addition to the effects of aggregate source, recent studies have shown that the common method of relating concrete strength to concrete stiffness may lose its accuracy when applied to modern, higher-strength concretes. In a report from ACI Committee 363 (1992), the authors discussed new data comparing the strength of concrete as related to its modulus of elasticity. They came to the conclusion that the Pauw equation used in ACI 318 overestimated the modulus

of elasticity for concretes with compressive strengths above 6,000 psi. Arguing that the Pauw equation was developed using primarily lower-strength concrete data, the authors included a new equation to accommodate a wider range of concrete strengths. A later report from ACI Committee 363 (2010) reported that this equation (Equation 2.3) provided a relatively reliable lower-bound prediction for normal-density high-strength concretes, but that some studies had shown the equation to significantly underestimate the modulus of elasticity.

$$E_c = 40{,}000\sqrt{f'_c} + (1.0 \cdot 10^6) \qquad \textbf{Equation 2.3}$$

for 3000 psi < f_c' < 12,000 psi

where:

E_c = static modulus of elasticity of the concrete, psi

f_c' = specified compressive strength of the concrete, psi

Common practice is still to use Equation 2.1 for most modulus of elasticity calculations, or the modified AASHTO version (Equation 2.2). However, since many prestressed concrete girders have concrete strengths above 6,000 psi, it is advisable to check Equation 2.3 for comparison as well.

Another method of modulus prediction which is often found to provide more accurate results is the method found in the *fib* Model Code (2010), often called the MC2010. The International Federation for Structural Concrete (literally, the *fédération internationale du béton*, or *fib*), a combined effort of the Euro-International Committee for Concrete (literally, the *Comité Euro-International du Béton*, or CEB) and the International Federation for Prestressing (literally, the *Fédération Internationale de la Précontrainte*, or FIP), first published the Model Code for Concrete Structures in 1978. Through this document, and its subsequent updates, the *fib* created a code that would serve as a basis for harmonization of European structural codes.

Since the *fib* Model Code was developed for European use, several differences must be addressed in order to apply the *fib* MC2010, the most recent Model Code, to the data found in this project. First, it should be noted that the MC2010 does not use "specified" and "average" strengths, as the US system does. The MC2010 uses something called a "characteristic strength" to represent the lower bound of expected concrete strengths based on strength testing. This characteristic strength is defined as the strength level at which 5% of strength tests would fall below this point (*fib* 2010). In this way, it is comparable to the US "design" or "specified" strength, which is usually expected to exceed approximately 1% of strength tests (ACI Committee 318 2011).

However, built into the MC2010 code is a provision that changes the characteristic strength, f_{ck}, into an estimated mean value of compressive strength, f_{cm}, for use in correlations to other concrete properties. This provision may be seen in Equation 2.4.

$$f_{cm} = f_{ck} + \Delta f \qquad \textbf{Equation 2.4}$$

where:

f_{cm} = mean value of compressive strength f_c at an age of 28 days, MPa

f_{ck} = characteristic value of f_c, MPa

Δf = 8 MPa (or approximately 1150 psi)

Thus, rather than using the lower bound estimate of strength, as is always the case when designing for strength (life safety), the *fib* Model Code uses an estimated mean of strength for calculations of related concrete properties. These related properties, such as modulus of elasticity, are serviceability-type computations where accuracy is more desirable than conservatism.

This concept of shifting to the mean strength is evident upon examination of the MC2010

equations for modulus of elasticity. Equation 2.5 is used with the characteristic strength. However, when the actual strength of the concrete is known (for example, when cylinders have been tested and an estimate of that concrete's stiffness is desired), Equation 2.6 is used instead.

$$E_{ci} = E_{c0} \cdot \alpha_E \cdot \left(\frac{f_{ck} + \Delta f}{10}\right)^{\frac{1}{3}} \quad \textbf{Equation 2.5}$$

$$E_{ci} = E_{c0} \cdot \alpha_E \cdot \left(\frac{f_{cm}}{10}\right)^{\frac{1}{3}} \quad \textbf{Equation 2.6}$$

where:

E_{ci} = modulus of elasticity at concrete age of 28 days, MPa

f_{ck} = characteristic value of f_c, MPa

f_{cm} = mean value of compressive strength f_c at an age of 28 days, MPa

Δf = 8 MPa (or approximately 1150 psi)

E_{c0} = $21.5 \cdot 10^3$ MPa, or approximately 3118 ksi

α_E = 1.2 for basalt or dolomitic limestone aggregates

= 1.0 for quartzite aggregates

= 0.9 for limestone aggregates

= 0.7 for sandstone aggregates

Additionally, it is also clear from the above two equations that the significant effects of aggregate source were directly included through the use of the α_E factor.

Some confusion may arise in tracking the use of variables due to the difference in notation utilized by the MC2010 as compared to American specifications. For the American specifications and reports, such as ACI 318 (2011) or the AASHTO code (2012), a subscript of *i* applied to a variable usually indicates that the variable applies at the time of prestress release. For example, f'_{ci} denotes the specified concrete compressive strength at the time of prestress

transfer, but f_c' denotes the specified concrete compressive strength at 28 days. The MC2010, on the other hand, has no such clear subscript designation. The *i* subscript is defined as denoting an "initial" variable, but the variable E_{ci} is actually defined as the modulus of elasticity at 28 days, not release. Therefore, care must be taken to check the variables used throughout this thesis. For all variables associated with American specifications or reports, a subscript *i* denotes the time of release, but this is not the case with MC2010 variables.

Many other modulus of elasticity prediction methods have been developed. However, the three methods described in detail here—namely Pauw's Equation, the AASHTO code method, and the *fib* Model Code method—are by far the most prevalent methods for structural concrete.

2.3. Development Methods for Concrete Compressive Strength and Stiffness with Time

The nature of concrete is such that its mechanical properties change quite substantially over time. Various methods have been developed to describe the development of concrete compressive strength and modulus of elasticity as the concrete ages. Moreover, some of the modulus of elasticity prediction equations described in Section 2.2 are only intended for use at certain concrete ages. Furthermore, a few methods have also developed to more specifically address the development of concrete properties as the concrete matures due to time and temperature effects.

2.3.1. Maturity Quantification

Most of the time, chronological age is used as the basis for quantifying concrete age. However, it is very well known that concrete strength gain at early ages is highly dependent on temperatures, and that higher temperatures induce more rapid strength gain. Therefore, ASTM

C1074 (2011) provides two methods by which concrete can be measured not in terms of chronological age, but in terms of "maturity" of the concrete. These methods incorporate a combination of time and temperature to accumulate the effective maturity of the concrete given its temperature history. It is then assumed that the same concrete with the same maturity has the same strength regardless of the curing temperature. Thus, concrete produced and maintained at 60°F and concrete produced and maintained at 95°F would have significantly different maturities at any given chronological age.

The two maturity methods are herein called the Temperature-Time Factor Method (TTFM) and the Equivalent Age Method (EAM). They have multiple differences, and each one has its advantages and disadvantages. The TTFM, described by Equation 2.7, yields maturity values with units of time × temperature (for example, ℃ × hrs).

$$M(t) = \sum[(T_a - T_o) \cdot \Delta t] \qquad \textbf{Equation 2.7}$$

where:

$M(t)$ = temperature-time factor at age t, ℃ × hrs

Δt = time interval, hrs

T_a = average concrete temperature during time interval Δt, ℃

T_o = datum temperature, ℃

The EAM, which is described by Equation 2.8, yields maturity values with units of just time. In general, then, the EAM provides results that are more conceptually straightforward.

$$t' = \sum\{\Delta t \cdot e^{\left[\left(\frac{1}{T_a} - \frac{1}{T_s}\right) \cdot \left(\frac{-E}{Q}\right)\right]}\} \qquad \textbf{Equation 2.8}$$

where:

t' = equivalent age of the concrete, hrs

Δt = change in chronological age, or the time increment being considered, hrs

T_a = average temperature during the time increment Δt being considered, K

T_s = specified (reference) concrete temperature to which the equivalent age shall be compared, K

E = activation energy, $\frac{\text{J}}{\text{mol}}$

Q = gas constant equal to 8.31 $\frac{\text{J}}{\text{K·mol}}$

Both of these equations were taken from ASTM C1074 (2011), but Equation 2.8 was slightly modified to allow for the specific selection of the activation energy. Examination of Equation 2.8 shows that the EAM models maturity growth as a nonlinear relationship with temperature, with maturity growing exponentially more rapidly at higher temperatures than at lower temperatures. Equation 2.7, on the other hand, shows that the TTFM models maturity growth as a linear relationship with temperature. A specific increase in temperature will result in a specific increase in the rate of maturity growth, no matter the temperature at which the concrete started.

Either of these two methods is used in the concrete industry. However, only the EAM was used for the analyses presented in this thesis. The EAM calculates an "equivalent age," t', relative to some specified temperature, T_s. Effectively, this can be seen by breaking down Equation 2.8 into two components—the time increment and the age factor (AF), a term used in ASTM C1074 (2011). The time increment is simply the short incremental time step over which each measurement is taken (Δt). The AF is the rest of the equation.

$$AF = e^{\left[\left(\frac{1}{T_a} - \frac{1}{T_s}\right) \cdot \left(\frac{-E}{Q}\right)\right]} \qquad \textbf{Equation 2.9}$$

where:

AF = age factor, calculated and multiplied by each time increment Δt

Within the exponent of the AF are two terms. The first term, $\left(\frac{1}{T_a} - \frac{1}{T_s}\right)$, includes all temperature effects, and is discussed in a moment. The second term, $\left(\frac{-E}{Q}\right)$, contains a universal constant and a material constant, defining the sensitivity of the hydration process to curing temperatures with the selected materials. Neither of these constants change after E has been selected.

The first term in the AF equation is the term that accounts for temperature differences between the actual measured temperature and the datum temperature. The factor $\left(\frac{1}{T_a} - \frac{1}{T_s}\right)$ indicates three possible ranges for the AF term, as outlined here:

1. If $T_a > T_s$, then $\left(\frac{1}{T_a} - \frac{1}{T_s}\right) < 0.0$. This yields an $AF > 1.0$, indicating that the concrete is expected to "mature" or "age" more quickly during the time increment in question than it would have matured at the datum temperature. Practically speaking, the concrete is expected to gain more strength than the same concrete would have over the same time interval if the concrete were at T_s.
2. If $T_a = T_s$, then $\left(\frac{1}{T_a} - \frac{1}{T_s}\right) = 0.0$. This yields an $AF = 1.0$, indicating that the concrete is expected to mature and gain strength at exactly the same rate as if the concrete had been at T_{dat}. Any other result would be nonsensical, since the concrete *is* at T_s.
3. If $T_a < T_s$, then $\left(\frac{1}{T_a} - \frac{1}{T_s}\right) > 0.0$. This yields an $AF < 1.0$, indicating that the concrete is expected to mature and gain strength at a slower rate than it would have if it were at T_s.

The TTFM and the EAM both provide a means of quantifying the apparent age of the

concrete, using known temperatures during curing to adjust the rate of maturity growth. Thus, they provide a more accurate way for predicting the development of concrete properties over time. Concrete compressive strength and modulus of elasticity are the primary topics of this thesis, so the development of these two properties is discussed in Sections 2.3.2 and 2.3.3, respectively.

2.3.2. Concrete Strength Development

The two primary strength growth equations are the *fib* Model Code equation (2010) and the ACI 209 equation (1992). The original MC2010 equation may be seen here:

$$f_{cm}(t) = \beta_{cc}(t) \cdot f_{cm} \qquad \textbf{Equation 2.10}$$

with

$$\beta_{cc}(t) = exp\left\{s \cdot \left(1 - \sqrt{\frac{28}{t}}\right)\right\}$$

where:

$f_{cm}(t)$ = the mean compressive strength at time t, MPa

f_{cm} = the mean compressive strength at an age of 28 days, MPa

$\beta_{cc}(t)$ = a function to describe strength development with time

s = coefficient which depends on the strength class of cement, as given in Table 2.1

t = the concrete age adjusted according to Equation 2.11 (taking into account temperature during curing), days

Table 2.1: Coefficient s from MC2010 Time Effects Equation for Strength Growth

Strength Class of Cement	32.5 N	32.5 R 42.5 N	42.5 R 52.5 N 52.5 R
s	0.38	0.25	0.20

The coefficients provided in Table 2.1 are associated with "strength classes" of cement, which are really labels for the type of cement (*fib* 2010). In this table, *N* denotes a normal rate of strength development, and *R* denotes a rapid rate of strength development. A similar table, provided in the context of predicting the development of modulus of elasticity, may be seen in Table 2.2 (*fib* 2010). This table uses the same s coefficients as Table 2.1, but more clearly defines the application of the coefficients. More detailed information as to the clear definition of the cement strength classes may be found in the report by the British Standard Institution (BS EN 197-1 2011).

Table 2.2: Coefficient s from MC2010 Time Effects Equation for Modulus Growth

f_{cm} **(MPa)**	**Strength Class of Cement**	s
≤ 60 (8.7 ksi)	32.5 N	0.38
	32.5 R, 42.5 N	0.25
	42.5R, 52.5 N, 52.5 R	0.20
> 60 (8.7 ksi)	All Classes	0.20

The MC2010 strength growth equation uses a time, t, adjusted for temperature during curing by the following equation:

$$t_T = \sum_{i=1}^{n} \Delta t_i \; exp\left[13.65 - \frac{4000}{273+T(\Delta t_i)}\right] \qquad \textbf{Equation 2.11}$$

where:

t_T = the temperature-adjusted concrete age which replaces t in the

corresponding equations, days

Δt_i = the time period over which a temperature T prevails, days

$T(\Delta t_i)$ = the temperature during the time period Δt_i, ℃

As is clear from the definition, t_T is much like an equivalent age or a maturity in that it creates a temperature-adjusted age which considers temperature during curing. At first glance, this equation seems very different from Equation 2.8 used in Section 2.3 for calculating equivalent age. However, it can be demonstrated that Equation 2.11 is the same as Equation 2.8.

First, the summation labels and the subscripts have been removed for simplicity in Equation 2.8. The Δt_i explicitly shows the step-wise nature of the summation, where the Δt of Equation 2.8 recognizes the implied step-wise nature caused by the summation. Next, the exponential portion of the equation may be modified with some rearrangement and some substitutions to match the exponential portion in Equation 2.11. First is to rearrange the exponent.

$$t' = \sum\{\Delta t \cdot e^{\left[\left(\frac{1}{T_s} - \frac{1}{T_a}\right) \cdot \left(\frac{E}{Q}\right)\right]}\} \qquad \textbf{Equation 2.12}$$

$$t' = \sum\left\{\Delta t \cdot e^{\left[\left(\frac{E/Q}{T_s} - \frac{E/Q}{T_a}\right)\right]}\right\} \qquad \textbf{Equation 2.13}$$

Next, some substitutions are made. The gas constant, Q, is defined as 8.31 $\frac{\text{J}}{\text{K·mol}}$ (ASTM C1074 2011). Also, it is known that the MC2010 uses 20℃ as its specified temperature. However, all temperatures in these strength growth equations must be expressed as Kelvin. Thus, the datum temperature must be increased by 273 before it may be used in the equation. If these known

values are substituted into Equation 2.13, together with a chosen value of $E = 33{,}200\ \frac{\text{J}}{\text{mol}}$, then the following results:

$$t' = \sum \left\{ \Delta t \cdot e^{\left[\left(\frac{33{,}200\ \text{J·K·mol}/8.31\ \text{J·mol}}{(20+273)\text{K}} - \frac{33{,}200\ \text{J·K·mol}/8.31\ \text{J·mol}}{T_a} \right) \right]} \right\}$$

Equation 2.14

Equation 2.14, when simplified, becomes Equation 2.15.

$$t' = \sum \left\{ \Delta t \cdot e^{\left[\left(13.64 - \frac{4000\ \text{K}}{T_a} \right) \right]} \right\}$$ **Equation 2.15**

Equation 2.15 is practically identical to Equation 2.11, which was provided in the MC2010 code.

$$t_T = \sum_{i=1}^{n} \Delta t_i \ exp\left[13.65 - \frac{4000}{273+T(\Delta t_i)} \right]$$ **Equation 2.11**

It is clear, then, that the equation for temperature-adjusted time given in the MC2010 code is nothing more than the standard equivalent age equation with assumed values of datum temperature and activation energy. This is important to note, though, because it means that the strength growth equation was designed to incorporate temperature effects into the age of the concrete. Therefore, extra care was taken to compare the MC2010 results using chronological age compared to those using equivalent age in the analyses presented in this thesis.

From examination of Equation 2.10, the MC2010 relationship between strength and equivalent age may be seen. The strength at any time, t, is taken as an age-dependent factor, $\beta_{cc}(t)$, multiplied by the strength at 28 days. This factor is less than one if the equivalent age of

the concrete is less than 28 days, and is greater than one if the equivalent age is greater than 28 days.

The rate of strength growth is then controlled by the coefficient, s, which has a positive value that depends on the properties of the cement or concrete mixture. Smaller values of s indicate a more rapid rate of early strength development and a less rapid rate of later strength development. A comparative plot of the MC2010 age factor with different values of s may be seen in Figure 2.1. A long-term version of this plot may be seen in Figure 2.2.

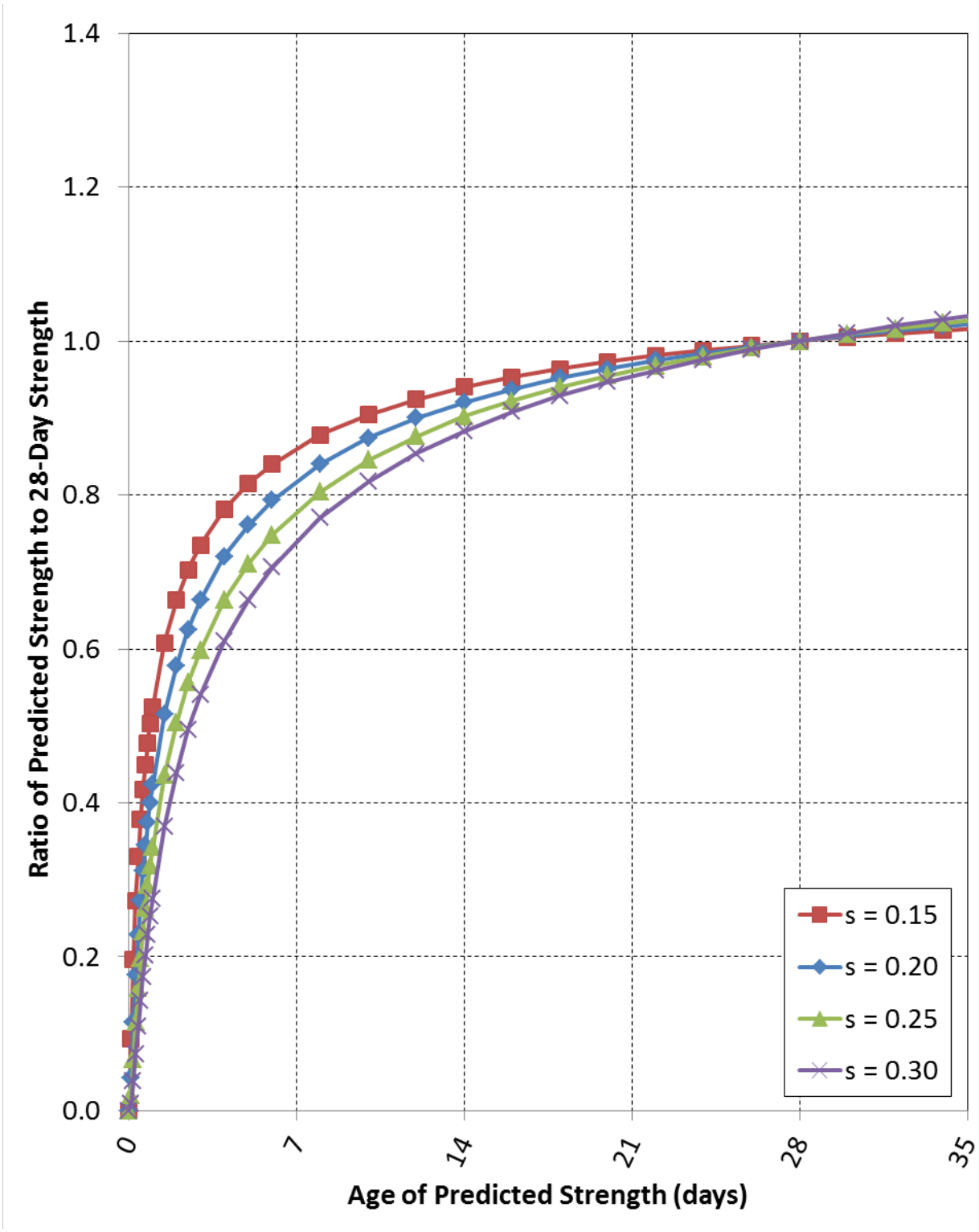

Figure 2.1: MC2010 Age Factor Comparison for Different *s* Parameters

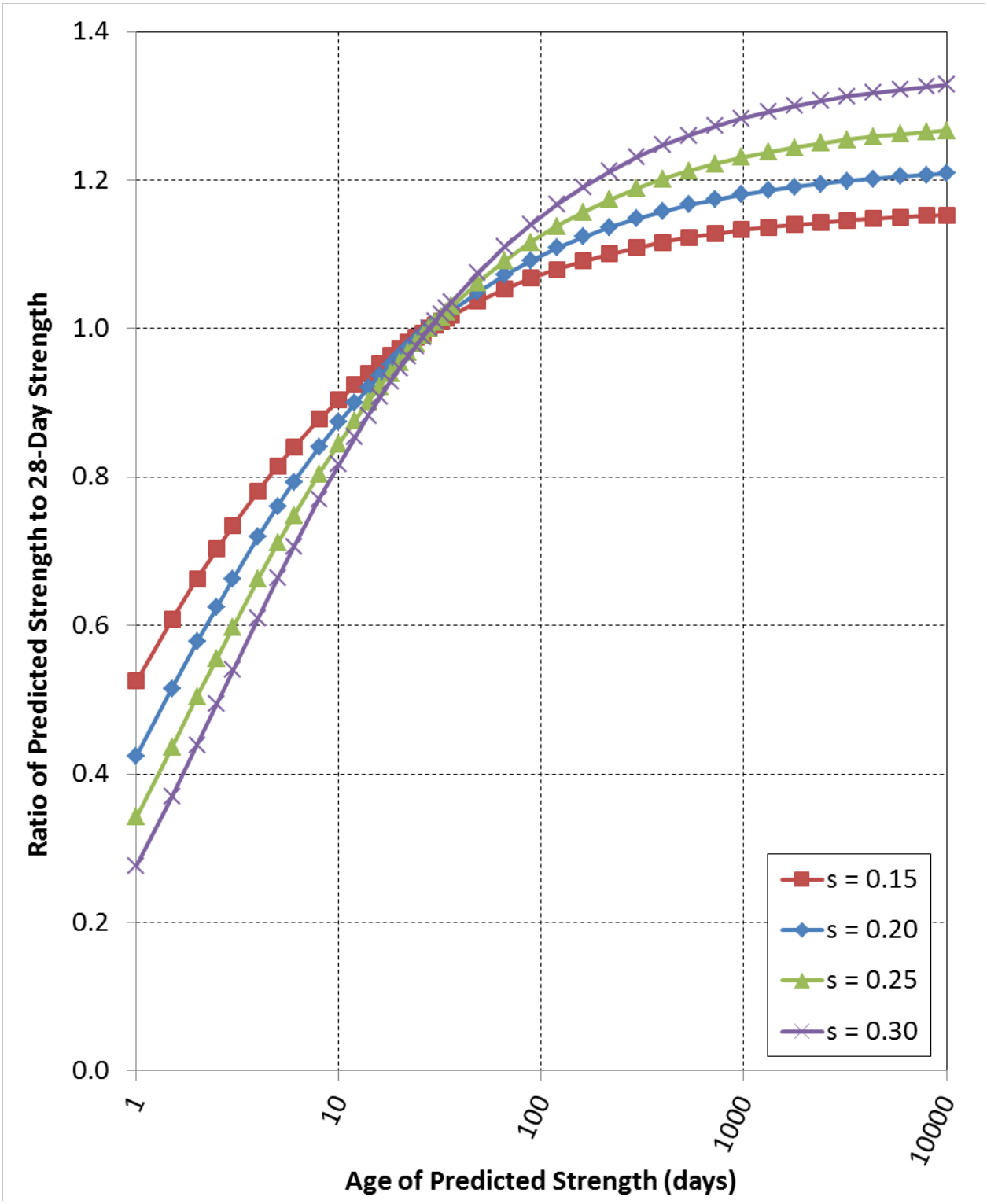

Figure 2.2: Extended MC2010 Age Factor Comparison for Different *s* Parameters

The ACI 209 (1992) strength growth equation may be seen in Equation 2.16 below.

$$f_c(t) = f_{c28}\left(\frac{t}{\alpha + \beta \cdot t}\right) \quad \textbf{Equation 2.16}$$

where:

$f_c(t)$ = concrete strength at any concrete age t, psi

f_{c28} = concrete strength at a concrete age of 28 days, psi

t = concrete age, days

α = constant used for shaping the strength growth function, days

β = constant used for shaping the strength growth function

In addition to shaping the overall function, the β constant also functions as a limiting factor for the long-term strength of the concrete. As the age of the concrete grows substantially larger and larger, the α term, which has large effects on the relationship at early ages, becomes insignificant. At that point, the β term controls the predicted strength. If $\beta > 1.0$, the time-dependent factor would always be less than one, meaning that the strength never actually reaches its 28-day strength. This is somewhat nonsensical, so most β factors used in practice are smaller than 1.0. A comparative plot of the ACI 209 time-dependent factors with the time-dependent factor constrained to equal 1.00 at 28 days may be seen in Figure 2.3, with a long-term version shown in Figure 2.4.

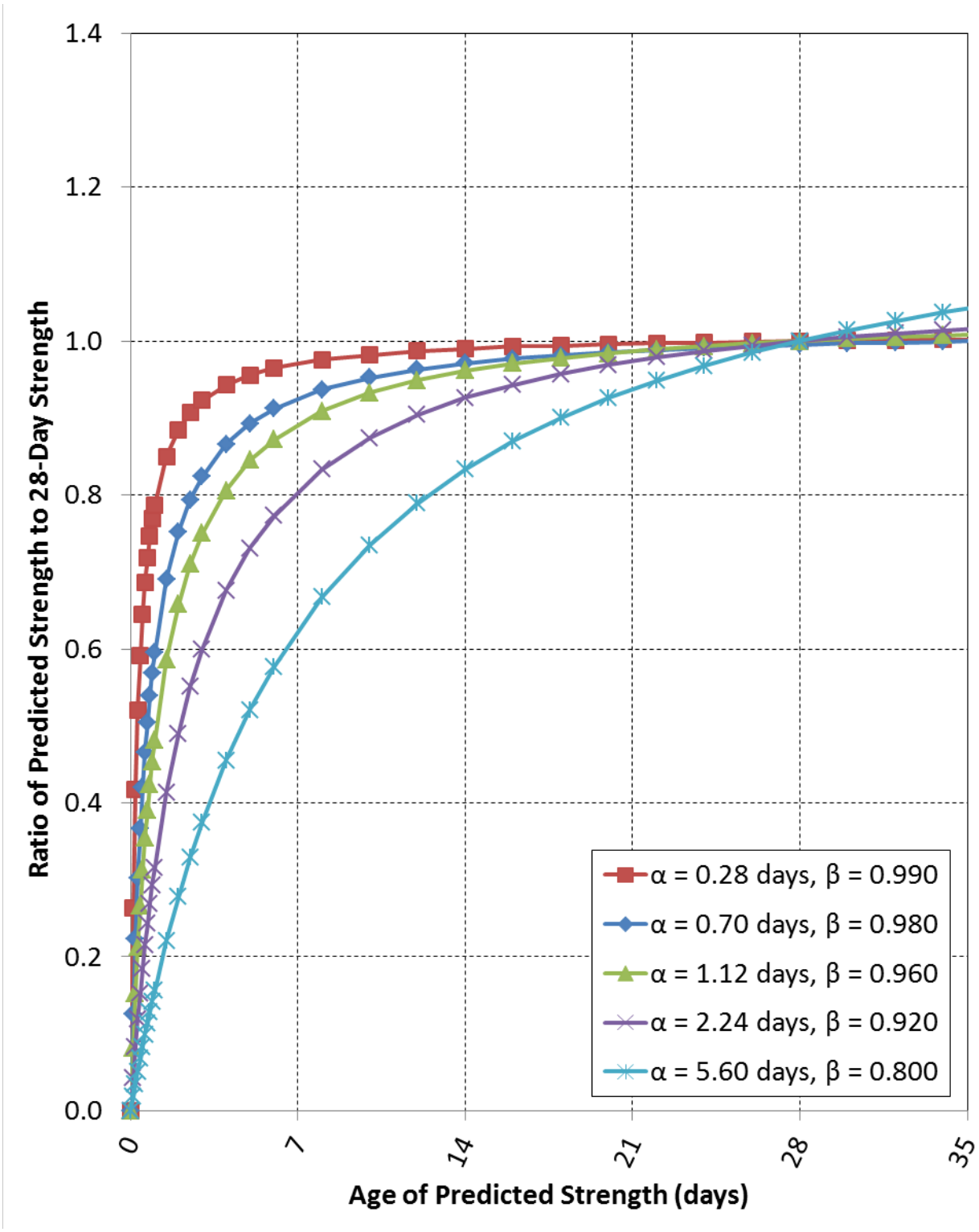

Figure 2.3: ACI 209 Time-Dependent Factor Comparison for Different Parameters

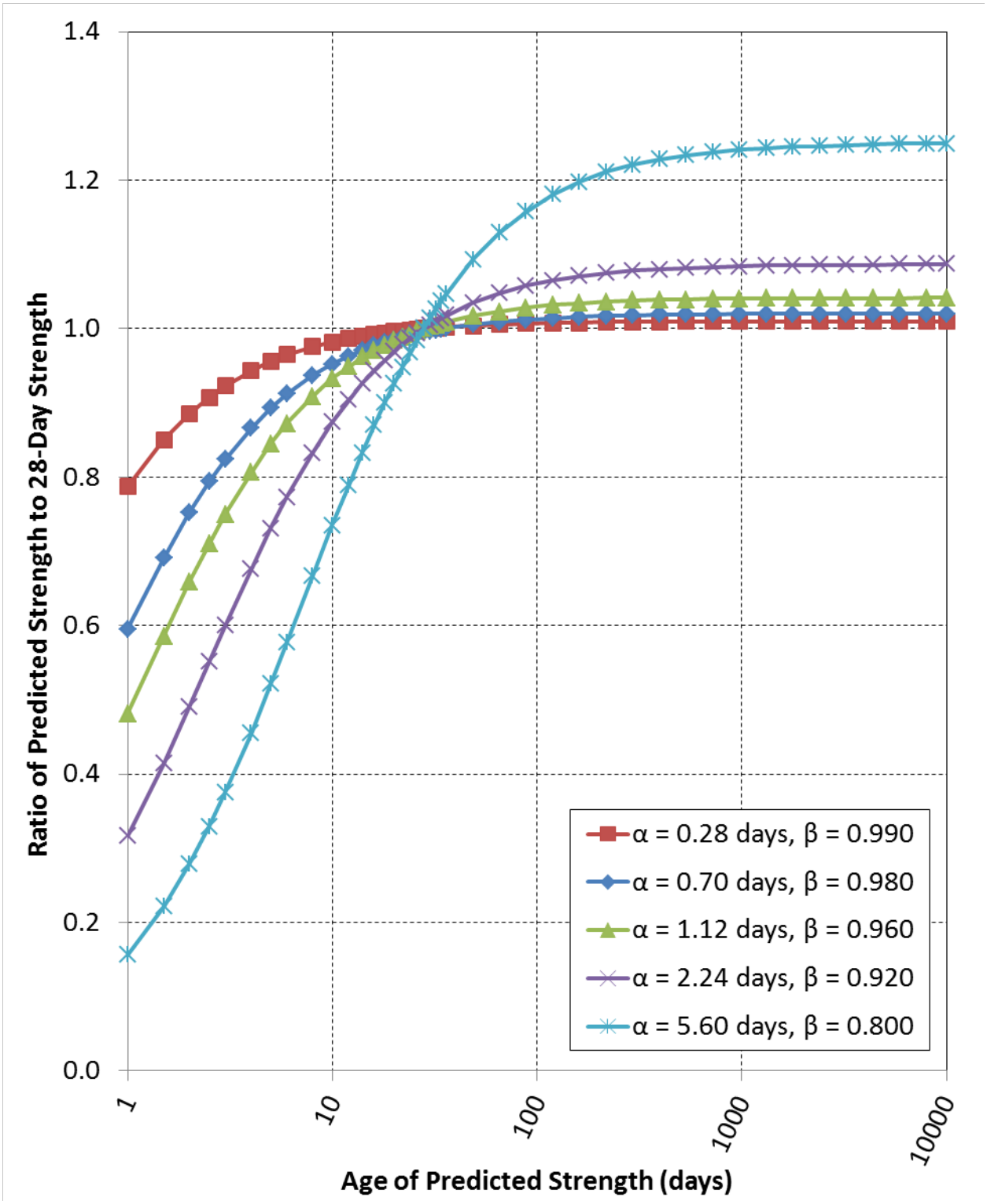

Figure 2.4: Extended ACI 209 Time-Dependent Factor Comparison for Different Parameters

For both α and β, smaller values indicate more rapid strength development. However, the influence of these parameters changes depending on the time being considered. Since α is not multiplied by the time t, its influence is greater at early ages when t is smaller. As t grows, the relative influence of α diminishes and the influence of β increases. At very high ages, the influence of α is practically negligible and β controls strength levels. The ultimate long-term strength that is predicted from concrete when $\beta < 1.0$ is equal to $\frac{1}{\beta} \cdot f_{c28}$.

Equation 2.16, like the MC2010 strength growth equation, uses a simple time-dependent factor multiplied by the 28-day strength to calculate concrete strength at any time. However, unlike the MC2010 equation, the time value used in the ACI 209 equation is not clearly defined as either chronological age or temperature-adjusted age. The inclusion of different suggested α and β parameters for steam-cured concrete as opposed to moist-cured concrete suggests that the method was designed for use with chronological ages, not equivalent ages. Both maturity quantifications are used in this thesis for comparison.

2.3.3. Modulus of Elasticity Development

The methods of predicting strength development described in Section 2.3.2 (*fib* 2010, ACI Committee 209 1992) are both specifically formulated for use in predicting concrete compressive strength, not modulus of elasticity. However, aside from those prediction methods, little information is usually given regarding the development of modulus of elasticity over time. The MC2010 code provides specifications that explicitly deal with modulus development over time, but none of the other methods do so.

Prediction of release modulus of elasticity is first component desired for establishing the development of modulus of elasticity over time. However, for most of the modulus of elasticity

prediction methods presented in Section 2.2, it is unclear whether the equation may be used for the prediction of release modulus or not (the MC2010 equation, which is discussed later, is an exception). Furthermore, if the equations may be used for the prediction of release modulus of elasticity, it is not clear whether this should be done using the specified release strength or the specified 28-day strength. The terms used in the equations do not explicitly prevent the use of release strengths. However, if it is allowable to use the equations for both release and 28-day predictions, it would have been beneficial for the equations to explicitly clarify that fact.

For example, consider the strength and modulus of elasticity terms used in the ACI 318 prediction method (2011), AASHTO method (2012), and ACI 363 method (2010). All of these equations (shown in Section 2.2) use the terms E_c and f_c', which are respectively defined in each equation as the "modulus of elasticity of concrete" and the "specified compressive strength of concrete." This wording does not explicitly define the equation for use at 28 days as opposed to release. However, each code or report also defines a variable f_{ci}', which is defined as the "specified compressive strength of concrete at time of initial prestressing." Furthermore, the AASHTO code defines a variable E_{ci}, which is defined as the "modulus of elasticity of concrete at transfer." The possible implication of these additional variables is that the equations shown in Section 2.2 might not be intended for use at that time of prestress transfer.

This leaves only three possible choices for predicting release modulus of elasticity based on ACI 318, ACI 363, or the AASHTO code.

1. The equation can be applied to predictions of release modulus, but using specified 28-day strengths. (The inevitable effect of this choice is that the predicted modulus of elasticity at release is equal to the predicted modulus of elasticity at 28 days.)
2. The equation can be applied to predictions of release modulus, but using specified release

strengths.

3. The equation can be used only for 28-day predictions, and some other method of predicting release modulus must be found.

If choice #2 is used, an assumption is included about the rate of strength development versus the rate of modulus development. Namely, it is assumed that relationship between the modulus of elasticity and compressive strength remains the same throughout the life of the concrete.

For example, consider Equation 2.1, taken from ACI 318 (2011).

$$E_c = 33\omega^{\frac{3}{2}}\sqrt{f_c'} \qquad \textbf{Equation 2.1}$$

where:

E_c = static modulus of elasticity of the concrete, psi

ω = unit weight of concrete at the time of test, pcf

f_c' = specified compressive strength of the concrete, psi

If this equation is used for predicting modulus of elasticity at both prestress transfer and at 28 days, then it is assumed that the modulus of elasticity develops at a rate that is proportional to the square root of the rate of strength development. In other words, if the strength quadruples between prestress transfer and 28 days ($f_{c,28}' = 4f_{ci}'$), then the modulus of elasticity is expected to double over the same period. This example is demonstrated in Equations 2.17 through 2.19.

$$E_{ci} = 33\omega^{\frac{3}{2}}\sqrt{f_{ci}'} \qquad \textbf{Equation 2.17}$$

$$E_{c,28} = 33\omega^{\frac{3}{2}}\sqrt{f_{c,28}'} = 33\omega^{\frac{3}{2}}\sqrt{4f_{ci}'} = 2 \cdot 33\omega^{\frac{3}{2}}\sqrt{f_{ci}'} \qquad \textbf{Equation 2.18}$$

$$E_{c,28} = 2 \cdot E_{ci} \qquad \textbf{Equation 2.19}$$

After making the choice to use the modulus of elasticity prediction equations for both release modulus and 28-day modulus, the rate of modulus of elasticity development is assumed to be equal to the square root of the rate of compressive strength development for the methods

other than the MC2010 method. The rate of strength development predicted by ACI Committee 209 (1992) has already been discussed in Section 2.3.2. This rate is purely controlled by the time-dependent factor multiplied by the 28-day strength, as shown in Equation 2.16.

$$f_c(t) = f_{c28}\left(\frac{t}{\alpha + \beta \cdot t}\right) \qquad \textbf{Equation 2.16}$$

where:

$f_c(t)$ = concrete strength at any concrete age t, psi

f_{c28} = concrete strength at a concrete age of 28 days, psi

t = concrete age, days

α = constant used for shaping the strength growth function, days

β = constant used for shaping the strength growth function

This time-dependent factor is designed to be $\frac{t}{\alpha + \beta \cdot t} = 1.00$ when $t = 28$ days. Therefore, the rate of strength development is $\frac{t}{\alpha + \beta \cdot t} < 1.00$ for all $t < 28$ days. Taking the square root of a value less than 1.00 results in a value greater than the original value. Thus, the implication is that the modulus of elasticity is expected to develop more rapidly than the compressive strength for all $t < 28$ days.

A very similar implied expectation may be seen in the MC2010 specifications. Based on equations presented in the *fib* Model Code (2010), it is expected that the modulus of elasticity will develop more rapidly through the time of prestress transfer, and probably beyond that. Unlike the ACI 318 equation, AASHTO equation, and ACI 363 equation, the MC2010 equations for modulus of elasticity use variables that are explicitly defined as 28-day values. These MC2010 equations have been restated below.

$$E_{ci} = E_{c0} \cdot \alpha_E \cdot \left(\frac{f_{ck} + \Delta f}{10}\right)^{\frac{1}{3}}$$ **Equation 2.5**

$$E_{ci} = E_{c0} \cdot \alpha_E \cdot \left(\frac{f_{cm}}{10}\right)^{\frac{1}{3}}$$ **Equation 2.6**

where:

E_{ci} = modulus of elasticity at concrete age of 28 days, MPa

f_{ck} = characteristic value of f_c, MPa

f_{cm} = mean value of compressive strength f_c at an age of 28 days, MPa

Δf = 8 MPa (or approximately 1150 psi)

E_{c0} = $21.5 \cdot 10^3$ MPa, or approximately 3118 ksi

α_E = 1.2 for basalt or dolomitic limestone aggregates

= 1.0 for quartzite aggregates

= 0.9 for limestone aggregates

= 0.7 for sandstone aggregates

Both of these equations use the E_{ci} variable, which is defined as the modulus of elasticity "at concrete age of 28 days." Furthermore, they are both intended to use f_{cm} or an approximation of f_{cm}, which is defined as the mean compressive strength "at an age of 28 days." Therefore, there is no uncertainty here—these equations are not intended for predictions of release modulus of elasticity.

However, MC2010 provides explicit accommodation for modulus-growth predictions. When modulus of elasticity is desired at concrete ages other than 28 days, predictions are to be made according to Equation 2.20, taken from the MC2010 (*fib* 2010).

$$E_{ci}(t) = \beta_E(t) \cdot E_{ci}$$ **Equation 2.20**

with

$$\beta_E(t) = [\beta_{cc}(t)]^{0.5}$$

and

$$\beta_{cc}(t) = exp\left\{s \cdot \left(1 - \sqrt{\frac{28}{t}}\right)\right\}$$

where:

$E_{ci}(t)$ = modulus of elasticity at an age t, MPa

E_{ci} = modulus of elasticity at an age of 28 days, MPa

$\beta_E(t)$ = a function to describe modulus of elasticity development with time

$\beta_{cc}(t)$ = a function to describe strength development with time

s = coefficient which depends on the strength class of cement, as given in Table 2.1

t = the concrete age adjusted according to Equation 2.11 (taking into account temperature during curing), days

Equation 2.20 simplifies to Equation 2.21.

$$E_{ci}(t) = E_{ci} \cdot exp\left\{\frac{s}{2} \cdot \left(1 - \sqrt{\frac{28}{t}}\right)\right\}$$ **Equation 2.21**

There are two ways to interpret Equation 2.21 when comparing the rate of modulus development to the rate of strength development. These are summarized as follows:

1. The impact of the s coefficient on development rate was discussed in Section 2.3.2, and it was shown that smaller values of s predict more rapid early development than larger values of s. Therefore, since the modulus development equation (Equation 2.21) uses $\frac{s}{2}$ where the strength development equation (Equation 2.10) uses simply s, it implies that the modulus of elasticity is expected to develop more rapidly than the strength at early

ages.

2. Alternatively, Equation 2.10 shows that the rate of compressive strength development is controlled by an age-dependent factor, $\beta_{cc}(t)$, multiplied by the 28-day strength. This age-dependent factor is $\beta_{cc}(t) < 1.00$ for most concrete ages less than 28 days, and the modulus of elasticity development equation takes $\beta_E(t) = \sqrt{\beta_{cc}(t)}$ to determine its rate of modulus development. Therefore, the implication is that $\beta_E(t) > \beta_{cc}(t)$ for concrete ages less than 28 days, and therefore the modulus of elasticity is expected to develop more rapidly for than the strength for ages less than 28 days.

The MC2010 differs from the other methods in that it both expects and explicitly states that its modulus of elasticity prediction equation is not meant to be used to calculate release modulus based on release strength. The code specifies that the release modulus of elasticity must be found by calculating the 28-day modulus of elasticity based on the 28-day strength and then using maturity quantification to calculate the release modulus based on the 28-day modulus.

Regardless of which modulus of elasticity development method is used, each method predicts that the modulus will develop more rapidly than the compressive strength through the time of prestress transfer.

2.4. Recent Compressive Strength Findings

Several recent research projects have provided recommendations to local designers which modify the specified strength for more accurate property predictions. Some suggested these strength adjustments purely for the purpose of more accurately predicting what strength would be achieved by a given project. In other cases this strength modification was used in prediction equations, in order to obtain more accurate predictions of related concrete properties.

Recognizing that the average girder in their region was developing a camber much smaller than that which was predicted, French and O'Neill (2012) conducted a historical analysis for the Minnesota Department of Transportation (MnDOT), studying concrete and girders from two different prestressed plants over a four year period. This analysis revealed several strength and material property trends that improved the accuracy of camber prediction methods. They discovered that concrete cylinders were breaking with an average strength 15.5% higher than the design release strength for that pour. To account for this "overstrength," it was advised that all calculations including release strength use a multiplier of 1.15, as may be seen here:

$$f_{ci}^{*} = 1.15 f_{ci}' \qquad \textbf{Equation 2.22}$$

where:

f_{ci}^{*} = expected release strength to be used in camber calculations, psi

f_{ci}' = design compressive strength at release, psi

Similarly, Storm (2011) performed an analysis of 381 girders for the North Carolina Department of Transportation (NCDOT), of which 49 were bulb-tee girders. Although much of his work related to cored slabs and box beams, and was therefore not directly applicable to research on bulb-tee girders, the material property trends found therein are still revealing. He found two similar strength trends, which are outlined here:

1. The average ratio of measured compressive strength at release to the specified design strength at release was 1.24, with a range of approximately 1.0 to 2.1. Therefore, for calculations it was suggested to use an expected release strength equal to

$$f_{ci}^{*} = 1.25 f_{ci}' \qquad \textbf{Equation 2.23}$$

where:

f_{ci}^{*} = expected release strength to be used in camber calculations, psi

f'_{ci} = design compressive strength at release, psi

2. The average ratio of measured compressive strength at 28 days to the specified design strength at 28 days was 1.45, with a range of approximately 1.0 to 2.2. Therefore, for calculations it was suggested to use an expected 28-day strength equal to

$$f_c^* = 1.45 f'_c \quad \textbf{Equation 2.24}$$

where:

f_c^* = expected 28-day strength to be used in camber calculations, psi

f'_c = design compressive strength at 28 days, psi

Like several many of the other projects reviewed, Rosa, Stanton, and Eberhard (2007) concluded that concrete strengths were often much higher than the required design strengths, and that this had significant impact on the resulting camber in prestressed girders. The authors in this study suggested two very similar conclusions for the Washington State Department of Transportation (WSDOT):

1. On average, it was found that the measured compressive strength at release was 11% higher than the specified release strength. The authors suggested the following modification for deflection calculations:

$$f_{ci}^* = 1.10 f'_{ci} \quad \textbf{Equation 2.25}$$

where:

f_{ci}^* = expected release strength to be used in camber calculations, psi

f'_{ci} = design compressive strength at release, psi

2. On average, it was found that the measured compressive strength at 28 days was 24% higher than the specified 28-day strength. The authors suggested the following modification for deflection calculations:

$$f_c^* = 1.25 f_c' \quad \textbf{Equation 2.26}$$

where:

f_c^* = expected 28-day strength to be used in camber calculations, psi

f_c' = design compressive strength at 28 days, psi

2.5. Recent Modulus of Elasticity Findings

Recent studies have also provided different recommendations for adjusting modulus of elasticity equations to better predict concrete stiffness based on known parameters. Some studies adjusted the strength, and then used this adjusted strength in modulus calculations. Other studies adjusted the modulus equations themselves, either independently or in tandem with adjusting the strength. In the context of all these adjustments, different researchers found that different equations better predicted the concrete modulus of elasticity in their region.

As was mentioned in Section 2.2, the ACI Committee 363 (2010) found that Pauw's equation (Equation 2.1) overestimated the modulus of elasticity for concrete strengths higher than 6000 psi.

In the four year historical analysis conducted by French and O`Neill (2012) for MnDOT, they discovered that Equation 2.1 provided the most accurate predictions for modulus of elasticity. However, these predictions were most accurate when using the modified value of f_{ci}^* instead of f_{ci}', as discussed in Section 2.4. Additionally, they quantified that the modulus of elasticity of a given batch of concrete increased an average of 15% from strand release to 28 days. This gave them a means of estimating 28-day stiffness based on a measured stiffness at strand release, which could be represented as follows:

$$E_c = 1.15 E_{ci} \quad \textbf{Equation 2.27}$$

where:

E_c = design modulus of elasticity at 28 days, psi

E_{ci} = design modulus of elasticity at release, psi

Storm (2011) used the Pauw equation, modified for use in the AASHTO code by the inclusion of an Aggregate Factor, K_1 (see Equation 2.2), for his prediction of modulus of elasticity. This equation was found to over-predict the average modulus of elasticity, and it was suggested that NCDOT use an aggregate factor $K_1 = 0.85$ to reduce the predicted modulus of elasticity for accommodation of NCDOT aggregate stiffness. No information about the aggregate source(s) used in this study was provided in the report.

Similarly, Rosa, Stanton, and Eberhard (2007) found that the Pauw equation would more accurately predict modulus of elasticity for WSDOT concrete with the inclusion of a 1.15 factor. Alternatively, it could be concluded that they found an aggregate factor, K_1, equal to 1.15. This aggregate factor, unlike the factor found by Storm (2011), was greater than 1.0. Thus, it was shown that the Pauw equation underestimated the modulus of elasticity for this area's concrete.

A study performed by Barr, Kukay, and Halling (2008), which focused on the loss of prestressing force in steel strands, found that the AASHTO method overestimated the concrete modulus of elasticity by an average of 28% for the studied WSDOT bridge. To account for this overestimation, the authors proposed a new equation for concrete modulus of elasticity, with two factors to account for aggregate effects:

$$E_c = 33{,}000K_1K_2(0.140 + \frac{f_c'}{1{,}000})^{1.5}\sqrt{f_c'} \qquad \textbf{Equation 2.28}$$

where:

E_c = static modulus of elasticity of the concrete, psi

K_1 = correction factor for aggregate type in predicting average modulus value

K_2 = correction factor for aggregate type in predicting lower bounds for prestress loss calculation and upper bound for crack control

f_c' = design compressive strength at 28 days, psi

Equation 2.28 was first proposed by Tadros et al. (2003), providing an equation that both included aggregate effects and did not require measurement of the unit weight. The unit weight is approximated as

$$\omega_c = 0.140 \text{ kcf} + \frac{f_c'}{1{,}000} \leq 0.155 \text{ kcf} \qquad \textbf{Equation 2.29}$$

where:

ω_c = unit weight of the concrete, kcf

f_c' = design compressive strength at 28 days, ksi

The data included in their study came from Nebraska, New Hampshire, Texas, and Washington. From their experimental results, Tadros et al. (2003) found that the average K_1 aggregate factor was less than 1.00 for Nebraska and New Hampshire, but substantially more than 1.00 for Texas and Washington.

Since Equation 2.28 is used much less often than the methods found in ACI 318, ACI 363, and the AASHTO Code, it will not be used for comparison with measured stiffness values in the remainder of this thesis.

2.6. Conclusion

A number of methods have been developed for the prediction of concrete modulus of elasticity. Some researchers have found some methods more accurate than others for their concretes, but the results are usually varied. Some found that the Pauw equation underestimated modulus of elasticity, while others found that it overestimated modulus. Furthermore, the

relationships between concrete modulus and strength are not always the same. Therefore the equations need to be compared, and sometimes optimized, for use in each location. This accommodates local materials and aggregates, making the equations more accurate.

Chapter 3: State of the Prestressed Bridge Girder Industry in Alabama

3.1. Introduction

In order to better understand the process and procedures involved in producing bulb-tee girders for the state of Alabama, researchers from the AUHRC traveled to four major prestressed girder producers. This was also done in order to begin the process of completing Task 3, discussed in Section 1.3. The producers that were visited were Hanson Pipe & Precast in Pelham, Alabama; Standard Concrete Products in Theodore, Alabama; and Gulf Coast Prestress in both Jonesboro, Georgia and Pass Christian, Mississippi. However, for simplicity, these producers are labeled for reference as Plant A, Plant B, Plant C, and Plant D. Hanson Pipe & Precast is called Plant A. Gulf Coast Prestress in Jonesboro, GA is called Plant B. Gulf Coast Prestress in Pass Christian, MS is called Plant C. Lastly, Standard Concrete Products in Theodore, Alabama is called Plant D.

For each prestressed plant, a narrative sheet was created which laid out many details for that plant, including the following:

- The plant's name and location,
- Approximate age of concrete at release,
- Curing practices for the girders and the cylinders,
- Weekend construction practices,
- Any differences between ALDOT girders and other states' girders,
- Storage conditions,

- Batch plant information,
- Material testing procedures, and
- ALDOT-approved mixture number and use.

In addition, many photographs were taken, and information was obtained as to the storage conditions of plant records. These records were either digitally recorded during the preliminary trip, or recorded at a later time, for use in Task 4 (see Section 1.3). The acquisition and analysis of this plant data is described in much more detail in Chapter 5. What follows in this chapter is a description of the information that was obtained regarding plant practices and mixture designs.

3.2. Common Practices

The following subsections are a description of common practices of prestressed plants in their production of ALDOT bulb-tee girders, unrelated to the materials used to make the concrete (see Section 3.3). Where applicable, entries from ALDOT specifications are included for comparison.

3.2.1. Bed Layouts and Girder Setup Procedure

Most girders are produced on production beds, or lines, that are long enough to hold more than one girder. For example, Figure 3.1 gives a general idea of some common Plant A girder layouts. Figure 3.1 shows that, for Plant A, it is common for multiple girders to be produced in a single day on the same bed, without removal of previously cast girders.

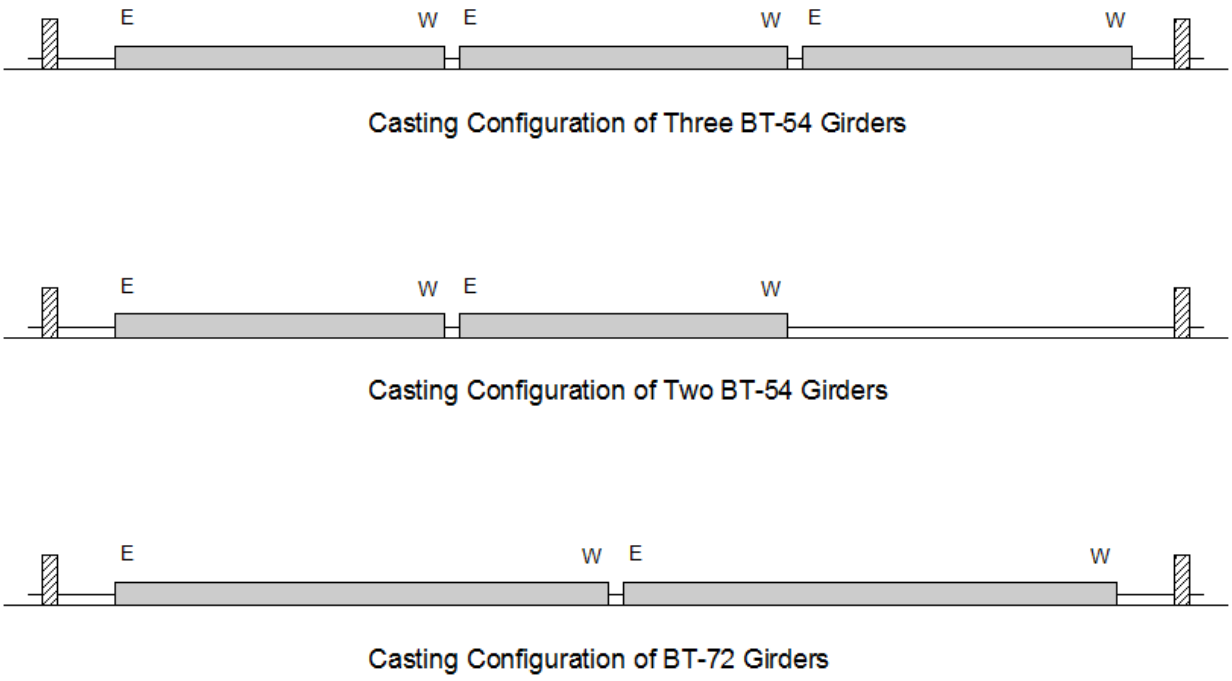

Figure 3.1: Sample Girder Layouts in a Casting Bed in Plant A

The number of girders that may be produced in a single day is dependent upon the number required for the project and the lengths of the girders being produced. Thus, a limiting factor is the length of each prestressing bed. Similarly, Figure 3.2 shows a partial map of the bulb-tee production beds for Plant B. From this image, it is apparent that some casting beds would have the capabilities of producing more girders at a time than others due to their increased length. On larger jobs with many similarly-designed girders, it is common practice to cast as many girders on a given bed in a single day as possible, thus maximizing efficiency. Casting beds always lay parallel to each other, with the metal forms stored nearly adjacent to the bed.

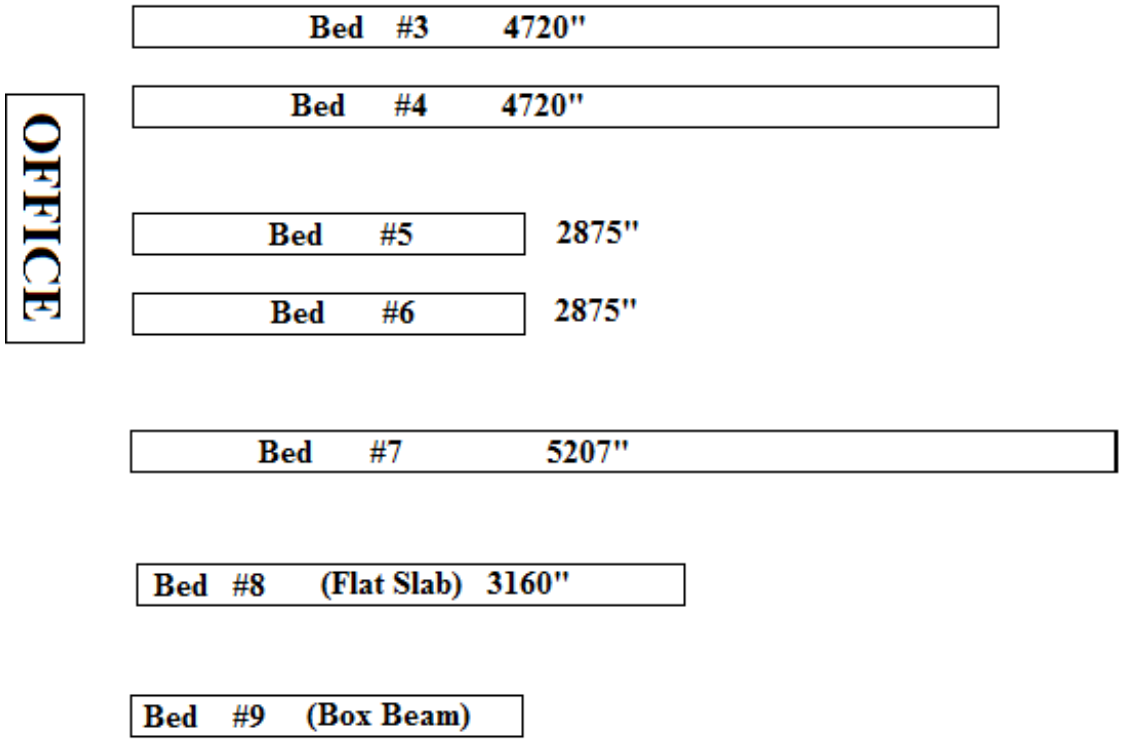

Figure 3.2: Sample Bed Layout Provided from Plant B

3.2.2. Casting Procedure

The ends of each girder are established by wooden bulkheads, usually fabricated in a carpentry area of each plant. These are usually made out of plywood or other wood, with holes predrilled and angled to allow for prestressing strand and skewed girder ends. Two bulkheads may be seen in Figure 3.3. These bulkheads, along with large metal strand deflection plates such as may be seen in Figure 3.4, go between each girder and are put in place first. However, plant operations differ at this point.

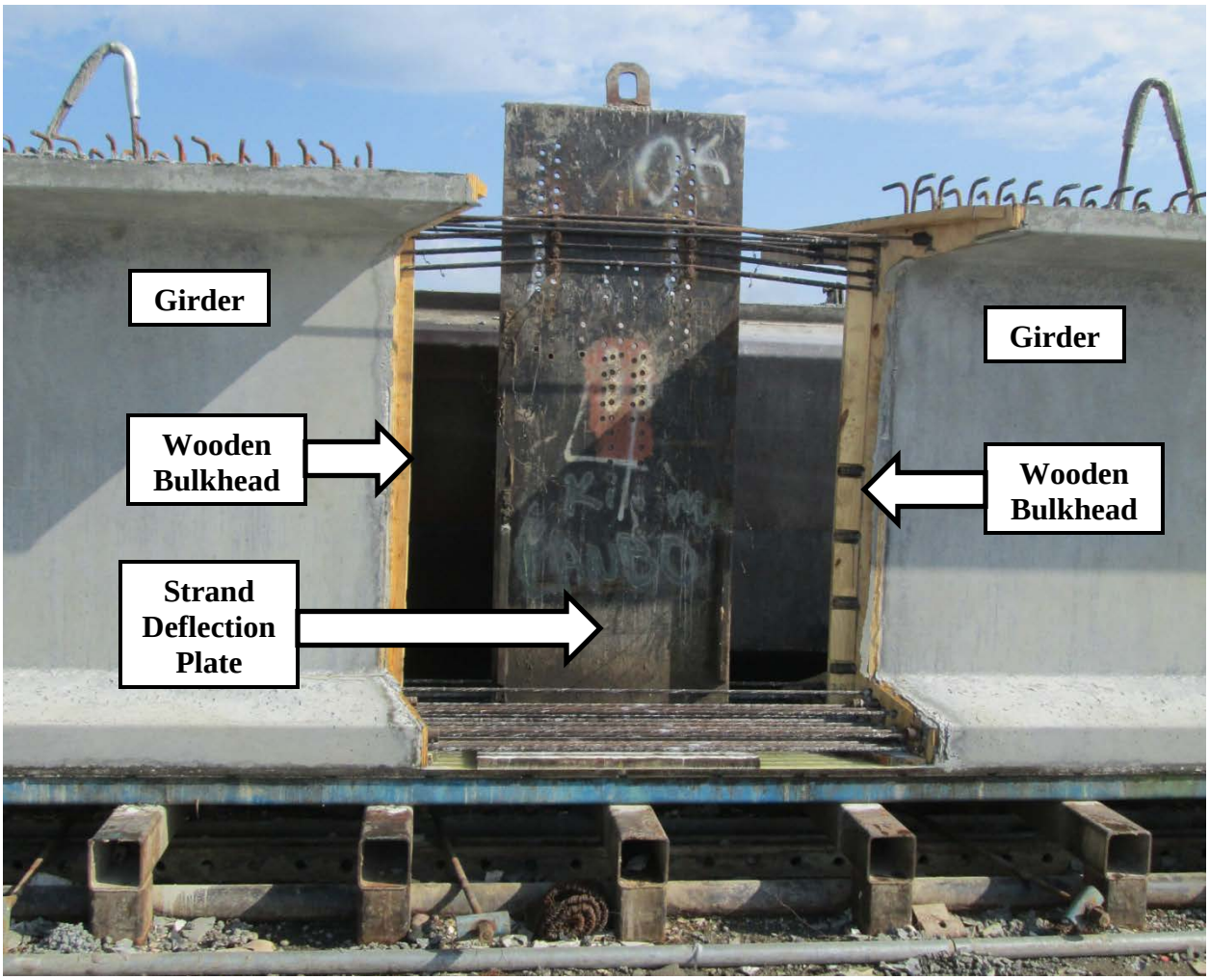

Figure 3.3: Sample Strand Deflection Plate from Plant C

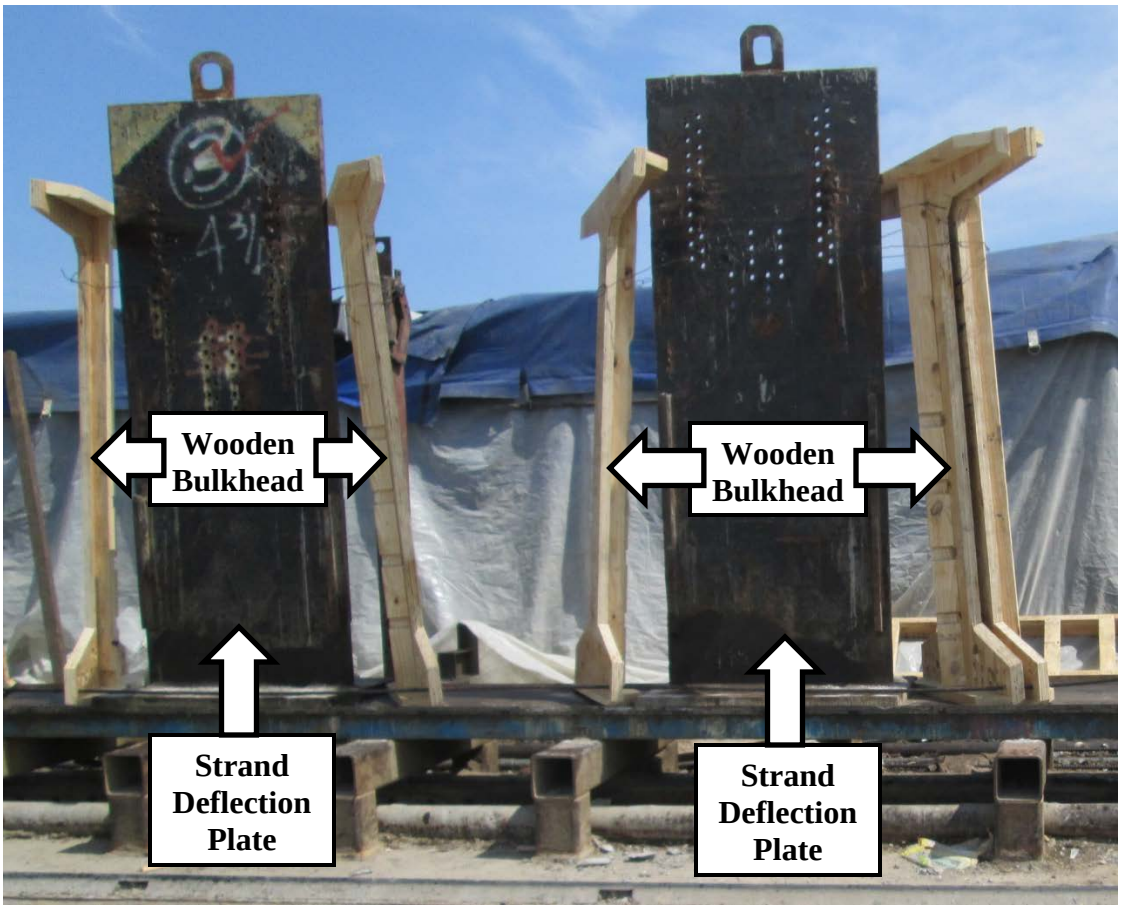

Figure 3.4: End Plates and Deflection Plates from Plant C

Commonly, the strand deflection plates are always set in place first and the end plates for each section of the bed are placed in their respective locations. Then prestressing strands are threaded through the holes in the plates and the assigned slots in the deflection plate. Using this method, the tie-down points would usually be the last component to be installed. These tie-down points, such as the small one that may be seen in Figure 3.5, are the components that change a sloping (draped) steel strand to a straight steel strand within the length of the girder. Therefore, they must stay in the girder after it has been cast.

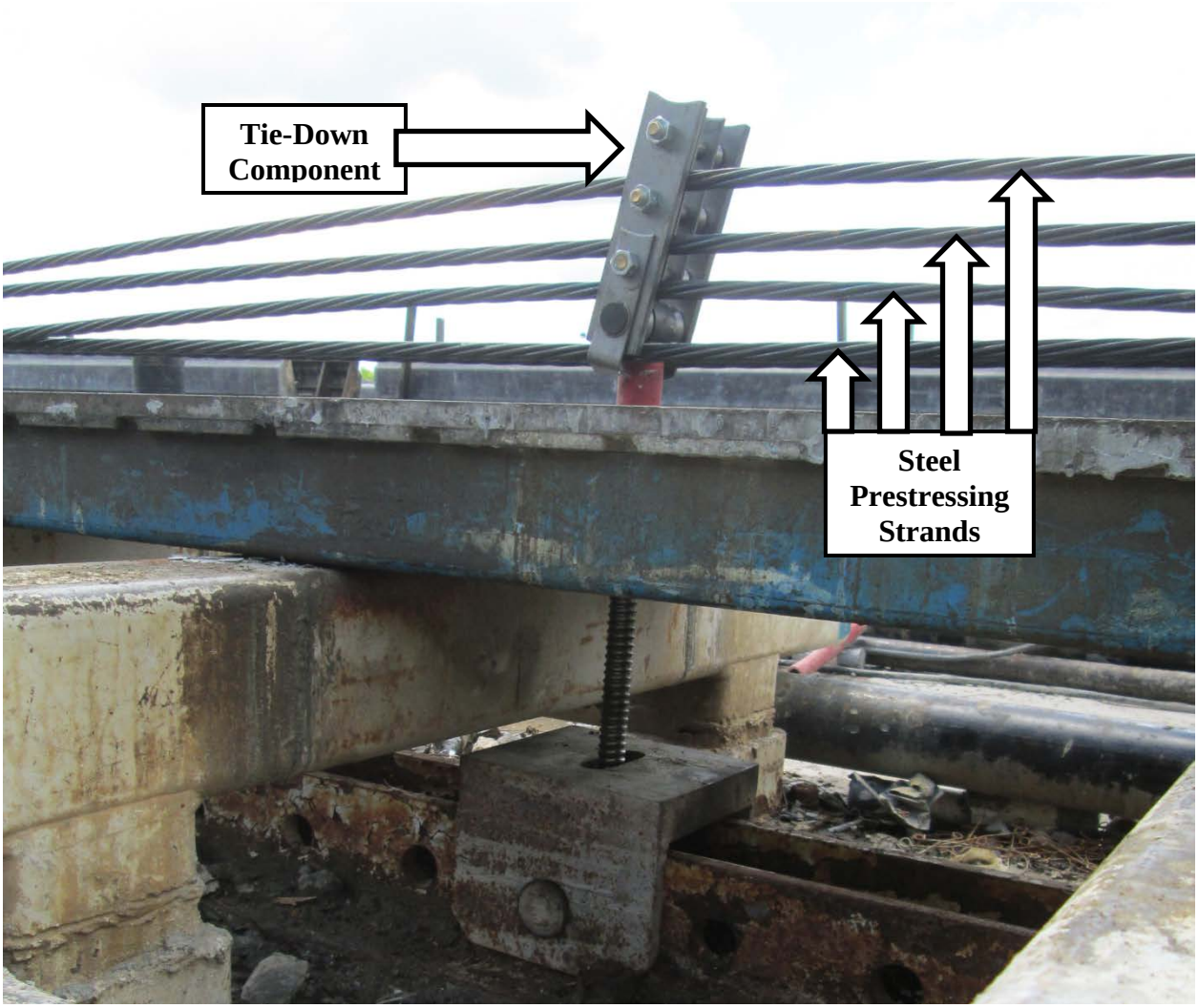

Figure 3.5: Tie-Down Component for a Small Girder

Alternatively, all of the end plates and strand deflection plates might be put at one end of the casting bed. Then some of the strands would be threaded through the holes. The plates would then be moved to their respective sections, and the rest of the strands would be threaded. This method is what was being performed in Figure 3.4. Using this method, tie-down points would be installed sometime after the strand deflection plates and the end plates had been moved to their respective sections.

No matter which method is used, the end plates, strand deflection plates, and tie-down

components are installed first. Then prestressing strands are put into place, and tensioned. There are different procedures for tensioning and locating the steel strands. Common practice now is to tension the strands in their final position, which requires that the tie-down points and the deflection plates be installed prior to strand tensioning. However, Plant A follows a different procedure. Plant A tightens its strands in the straight position, then deflects them to the appropriate location.

The arrangement of steel strands depends on ALDOT's design. However, two lightly tensioned prestressing strands are usually included in the top flange of the girder, to aid with hanging of the vertical stirrups, which consist of mild steel reinforcing bars (rebar). Strands are usually tensioned with a machine similar to the one shown in Figure 3.6, from Plant B, or by smaller hand-held hydraulic jacks.

Figure 3.6: An Example Strand Tensioning Machine from Plant B

The strands are pulled to the appropriate stress, while checking elongation and expected stresses to ensure the proper material properties of the strand, and then set to bear against a large steel bulkhead. A larger picture of one of these bulkheads may be seen in Figure 3.7, while a closer picture of the strands bearing against a bulkhead may be seen in Figure 3.8.

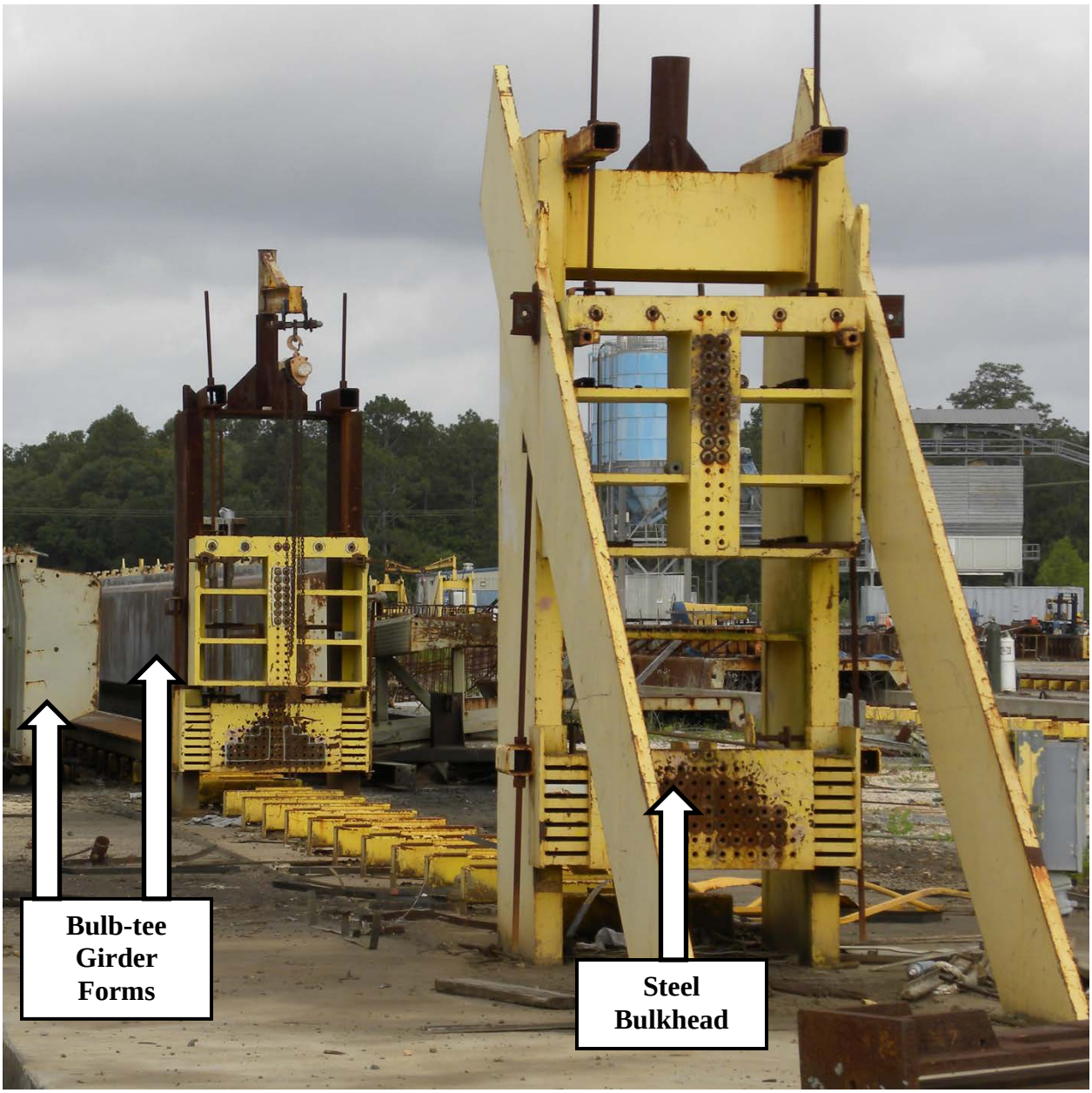

Figure 3.7: Steel Bulkhead from Plant D

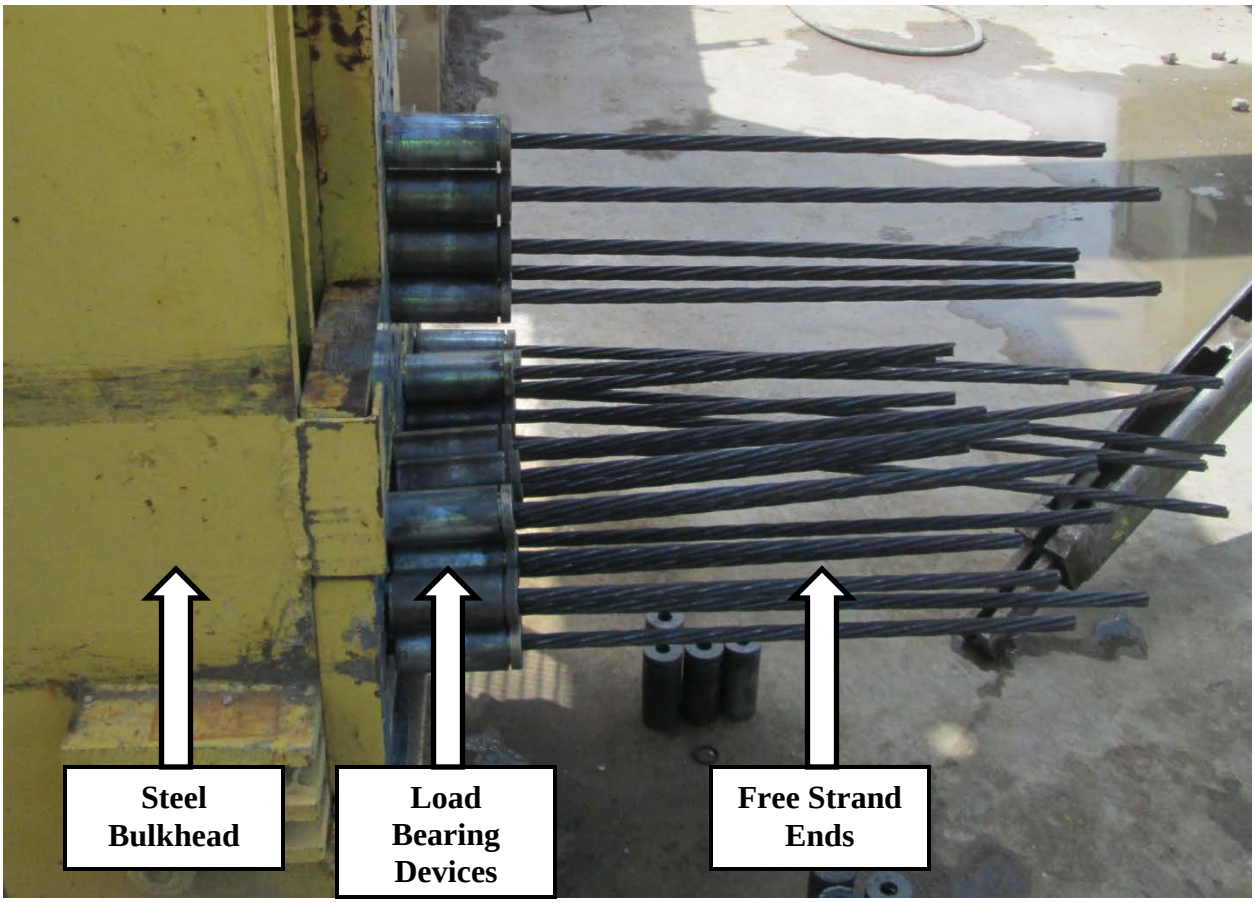

Figure 3.8: Close Picture of Strands Bearing on a Bulkhead

After all strands have been satisfactorily tensioned and supported, crews begin to hang stirrups from the strands. This is a relatively quick process. One person, usually the line foreman, goes down the line with plans and a tape measure and marks the location of each rebar. Other workers follow after him, tying in rebar to the marked locations. This is done by tightly twisting small wire ties around the rebar and the tendon. When desired, a stirrup is tied twice with crossing wire ties, to add to the strength of the connection and prevent the stirrups from translating during concrete placement. An example of double-tied rebar stirrups may be seen in Figure 3.9.

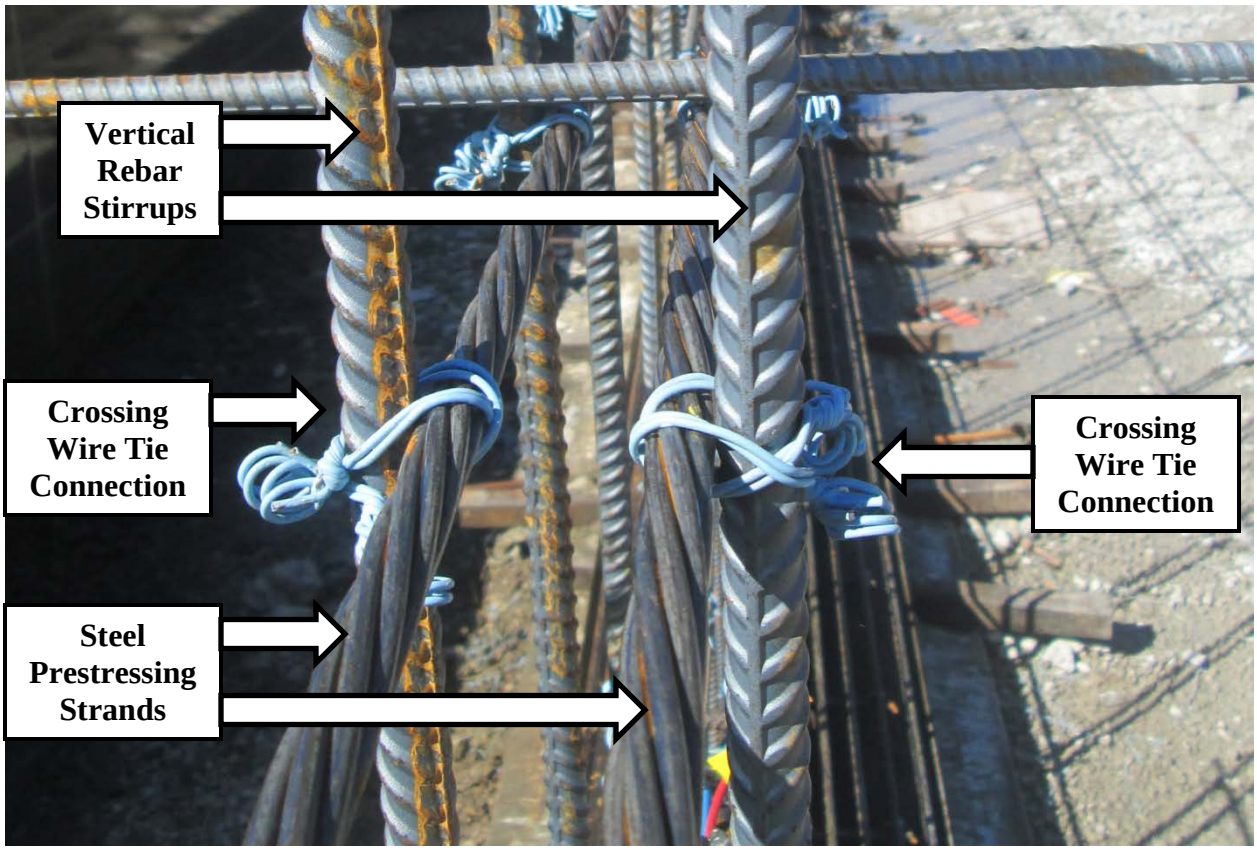

Figure 3.9: Double-tied Stirrup-to-Tendon Connections

After the rebar have been hung, inserts for diaphragms are tied in to the appropriate places of the girder. The finished product before placement of the forms and concrete may be seen in Figure 3.10. A close-up of the diaphragm insert may be seen in Figure 3.11.

Figure 3.10: Tensioned Strands, Hung Rebar, and Diaphragm Inserts in Plant C

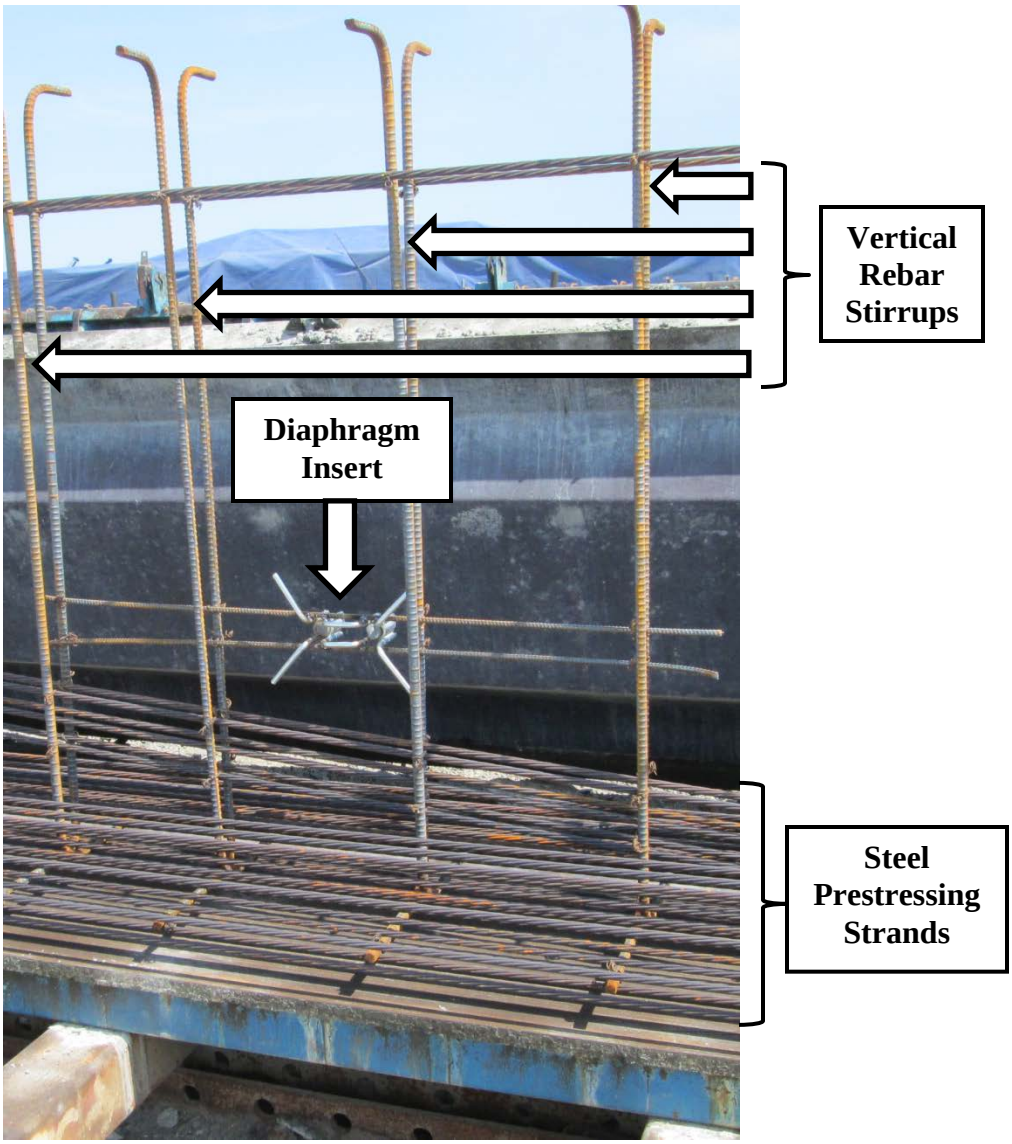

Figure 3.11: Close Picture of a Diaphragm Insert

Lastly, bent lifting points such as the one that may be seen in Figure 3.12 are inserted for easy handling of the girder after it has been cast. With all the strands tensioned, the rebar secured, and the diaphragm inserts and lifting points added, the line is finally ready for one last final pre-placement inspection by ALDOT personnel at this point. Upon approval, the line is ready to be cast.

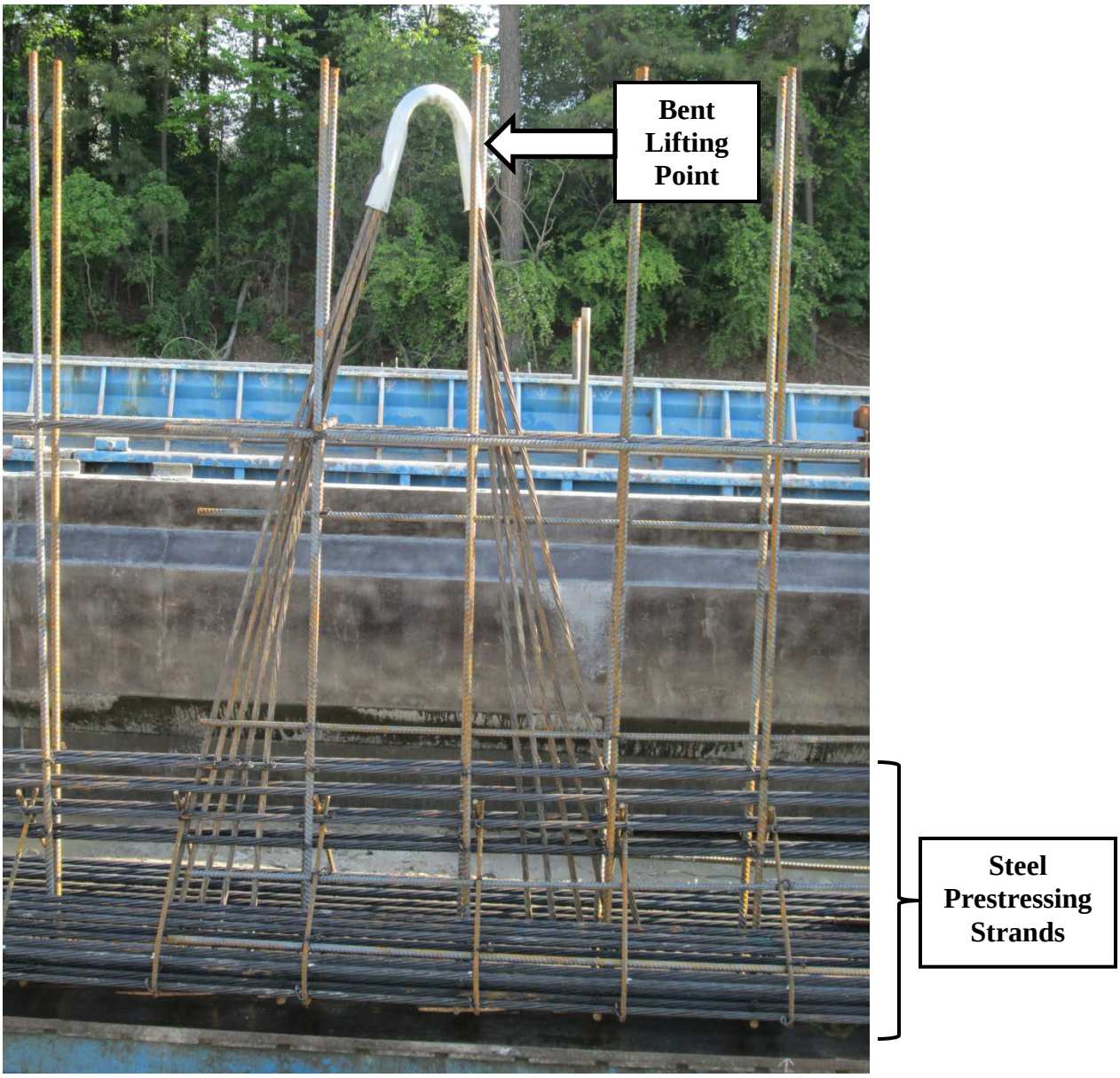

Figure 3.12: Example of a Lifting Point in a Georgia DOT Girder

Crews first clear any dirt, dust, or debris that may be sitting on the bottom of the bed. Then a bond breaker, or release agent, is lightly coated over the bottom of the bed and the insides of the steel forms, usually by spraying it. Different plants use different release agents, but an example of the one used in Plant D may be seen in Figure 3.13.

Figure 3.13: Example Release Agent from Plant D

When the bed and the forms are prepared, the forms are set into place by traveling cranes. Every plant that was visited batches its concrete on site, and the concrete is carted to the casting line in concrete delivery trucks like the ones shown in Figure 3.14. The first concrete batch is used for preliminary fresh concrete properties tests, such as slump, air content, unit weight, and temperature. If the concrete satisfies the specifications found in the ALDOT *Standard Specifications for Highway Construction* (2012), then the plant will begin casting of the girders.

Figure 3.14: Two Concrete Delivery Trucks Placing Concrete at Plant A

Sample cylinders are made and fresh concrete properties are tested in accordance with the portion of the ALDOT *Testing Manual* entitled "ALDOT 367: Production and Inspection of Precast Non-Prestressed and Prestressed Concrete" (2010), hereafter referred to as simply ALDOT 367. Namely, sample cylinders are made and fresh properties are tested "every 50 cubic yards, or fraction thereof, of concrete placed." This requirement usually means that for any given line of girders, concrete is sampled at one or two locations. ALDOT inspectors usually participate in the pour, both in the sampling procedures and in inspection of the concrete as it is placed into the forms.

After the primary crew has placed the concrete, a smaller crew follows them to rake the top surface for intended roughness and to insert any extra connection fittings that may have been included in the design. After everything is finished, the girders are covered in tarps and curing begins. Plants A, B, and C all use steam (accelerated) curing, with only a rare instance of wet (nonaccelerated) curing. Plant D, however, never applied steam, and only used nonaccelerated, wet curing. All plants claimed to provide consistent curing practices, without subjective curing

decisions made by the producers during the production process.

When sampling is required, test cylinders are molded and fresh concrete properties tests are performed. At this point in time, two 6 in. x 12 in. cylinders (150 mm x 300 mm) are usually used for strength testing. However, due to recent changes in ALDOT 367 (2010) allowing for the use of three 4 in. x 8 in. cylinders (100 mm x 200 mm), some plants have started to transition. Other plants that still use 6 in. x 12 in. cylinders have expressed interest in switching to the smaller cylinders due to the ease of handling and decrease of stress on testing machines.

In any case, these cylinders are made at each sampling location. Each plant handles the curing and storage of these cylinders a little bit differently, though all in compliance with ALDOT specifications. In almost all cases, the cylinders are stored under the tarp with the girder until the specified release strength has been achieved. The main exception to this is that Plant C prefers to use match-curing systems when possible, so 4 in. x 8 in. cylinders are used thar are not stored under the tarp.

When girders are expected to have achieved or nearly achieved their design release strength, the appropriate number of cylinders are removed from under the tarp and are tested for compressive strength. Each plant uses a very similar compression machine for their testing, with the primary differences being the age and capacity of the machine. Two examples may be seen in Figure 3.15 and Figure 3.16, which show the compression machines used in Plants B and D, respectively.

Figure 3.15: Compression Testing Machine from Plant B

Figure 3.16: Compression Testing Machine from Plant D

Due to the very rapid strength growth and early release ages, sulfur capping for release strength testing is not a viable option. All tests are performed using 70-durometer neoprene pads. When cylinder test results exceed the specified release strength, the girders are ready to be released and the producer proceeds to the practices laid forth in Section 3.2.3.

3.2.3. Post-Casting Practices

When the desired release strength has been achieved, accelerated curing is ended and the tarps are removed. Cylinders are transported to their respective curing locations, and the forms are removed by cranes and workmen on the ground. All of the forms are removed from the line before any prestressing strands are cut.

Curing practice for cylinders after tarps have been removed is rather different for each plant. Plant A demolds the cylinders and stacks them immediately adjacent to the Quality Assurance (QA) & Quality Control (QC) building, as may be seen in Figure 3.17. This provides partial shade for some cylinders, extensive shade for others, and possibly complete shade for a few.

Figure 3.17: Curing Conditions Used for Cylinders at Plant A

Plant B demolds the cylinders and lays them horizontally in shaded storage racks. Thus, all Plant B cylinders are shaded but also exposed to ambient temperatures. These curing racks may be seen in Figure 3.18.

Figure 3.18: Curing Racks Used for Cylinders at Plant B

Plant C demolds the cylinders and transports them to a storage area next to the QA/QC building, shown in Figure 3.19. Similarly to Plant A, the shading conditions for different cylinders is quite different due to the cylinder stacks. Cylinders on the top of the stack receive extensive sun exposure, while cylinders at the bottom and inside of the stack receive limited sun.

Figure 3.19: Curing/Storage Conditions for Cylinders at Plant C

And Plant D demolds its 4 in. x 8 in. cylinders and sets them in curing racks immediately adjacent to the QA/QC building. The curing racks for the 4 in. x 8 in. cylinders may be seen in Figure 3.20. These cylinders are shaded much of the time, but not all of the time. The 6 in. x 12 in. cylinders are allowed to cure on the gravel adjacent to the QA/QC building. Based on the observed arrangement, most of the cylinders receive reasonably similar sun exposure.

Figure 3.20: Curing Racks Used for Cylinders at Plant D

It is important to recognize that even though each of these plants handles long-term curing of the compressive strength cylinders differently, all of their curing methods fall within the specifications of ALDOT 367 (2010). All this document requires is that "the cylinders shall be cured in the exact same manner as the curing of the prestressed component that will be represented by the test cylinders." Some plants have taken this to mean that the cylinders shall be allowed to experience the same solar and weather exposure to which the girders are exposed.

However, due to the storage conditions of the girders, cylinders left in full exposure have the potential to receive much higher solar radiation than the girders. Furthermore, the thick

member sizes of the girders shelter internal concrete from drastic solar temperature variation and prevent excessive moisture loss, whereas cylinders have the potential for excessive heat fluctuation and drying during curing. Hence, some plants attempt to provide full or partial shade for the cylinders in order to prevent “baking” and to more accurately represent the concrete in the girder. Specifications are unclear on this matter, and thus both methods are acceptable.

Although plant practices for testing cylinders differ significantly after form release, plant practices for prestress release and girder removal are fairly uniform. Once the forms have been removed, a number of workers prepare to cut the strands. Usually this requires a number of workers with acetylene torches equal to one more than the number of girders. This is due to the fact that strands are cut at many different points simultaneously—one worker at each end of the line, and one worker in between each girder. One strand is cut at a time, following a predetermined pattern, and directed by the worker at the head of the line to ensure that all strands are cut at nearly the same time in each location. Usually, any draped strands are cut first. Then the tie-down connections for the draped strands are cut, as may be seen in Figure 3.21. Lastly, the bottom strands and the lightly tensioned top strands are cut, which may be seen in Figure 3.22.

Figure 3.21: Cutting of a Tie-Down Connection

Figure 3.22: A Worker Cutting the Bottom Strands

This is the point at which initial camber is measured. This is simply done with a tape measure, as may be seen in Figure 3.23. ALDOT 367 (2010) requires that camber be measured in a minimum of 50% of all members cast from the same setup and for the same ALDOT project. These measurements are used to verify consistency, not for acceptance or rejection of the girders. After camber has been measured, girders are lifted by traveling gantry cranes and transported to another area in the plant. First, the girders are transported to a finishing yard, where any unacceptable “bug holes” (surface irregularities) are filled. In some cases, this finishing occurs in the same location in which the girders will be stored. However, often the girders are later moved to a final storage area, where they await shipment to the job site.

Figure 3.23: Measuring the Initial Camber of a Girder after Release

Some examples of these final storage conditions for Plants A, B, C, and D may be seen in Figure 3.24, Figure 3.25, Figure 3.26, and Figure 3.27, respectively. As can be seen from those figures, the plants have fairly similar storage conditions. Girders are usually stored with supports as near to the ends as possible, or at a small nominal distance from the ends. Most plants store girders on concrete piles or other solid supports, with a layer of plywood or some similar material to act as a bearing surface as shown in Figure 3.28.

Figure 3.24: Example Girder Storage Conditions for Plant A

Figure 3.25: Example Girder Storage Conditions for Plant B

Figure 3.26: Example Girder Storage Conditions for Plant C

Figure 3.27: Example Girder Storage Conditions for Plant D

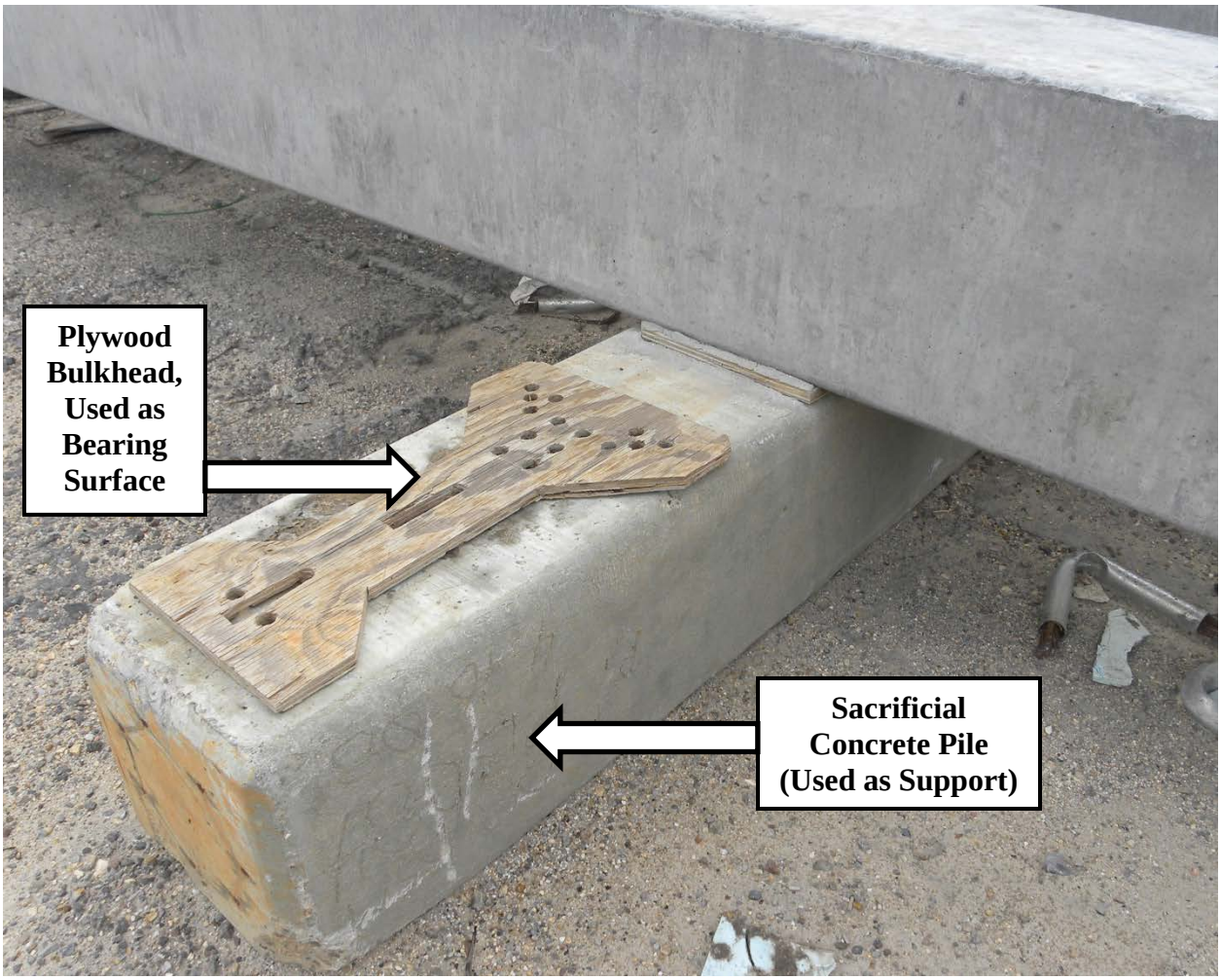

Figure 3.28: Plywood Bearing Surface on Concrete Pile

Plant D often used other means of support, such as stacks of timber, old conveyor belts, or used bearing pads. An example of a stack of timber used as a support may be seen in Figure 3.29.

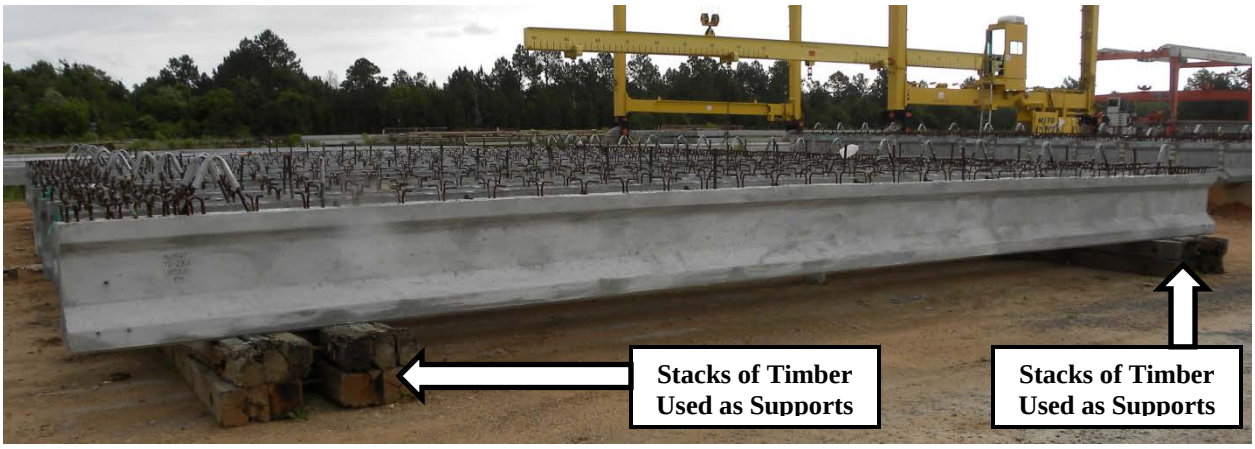

Figure 3.29: A Pile of Timber Used as Girder Supports

The location of supports during storage and the materials used for supports during storage are both important, as they can have a significant effect on long-term camber growth (Tadros, Fawzy, and Hanna 2011).

Lastly, when the girders are ready to be shipped to their respective job sites, they are most often transported by either a standard long-bed semi-trailer or by a split-bed semi-trailer, as may be seen in Figure 3.30. Producers try to use their own private transporters when possible, and only hire another company for transportation when necessary.

Figure 3.30: A Girder Being Transported by a Split-Bed Trailer

3.3. Common Mixture Design Properties

Becoming familiar with plant practices also included becoming familiar with common concrete mixture properties. As such, concrete mixture designs from each of the plants were collected and analyzed for mixture properties. Different mixtures were also compared to each other for similarities and differences, both within the same plant and between plants.

3.3.1. Specifications

There are various requirements found in ALDOT 367 (2010) and in Section 513 of the ALDOT *Standard Specifications for Highway Construction* (2012), hereafter referred to as the *Standard Specifications*, relating to the design of prestressed concrete mixtures. One

commonality, however, is that they allow a substantial amount of freedom in the details. The primary requirements of the *Standard Specifications* relating to concrete mixtures used for prestressed concrete bridge members are as follows:

1. The concrete mixture shall be designed for a minimum 28-day strength of 5000 psi or the 28-day compressive strength shown on the plans.
2. The concrete mixture shall have a target air content of 4.5% by volume, with an acceptable range of 2.5% to 6.0% by volume.
3. Chemical admixtures may be used to increase the concrete slump to a maximum of 9 inches, provided that this practice was included in the mixture approval process.
4. The water-to-cementitious material ratio (w/cm) of the approved mixture design shall not be exceeded to increase the slump.
5. Table 3.1 shows the other primary requirements applicable to prestressed concrete bridge members.

Table 3.1: Specifications for Prestressed Concrete Bridge Members

MIX DESIGN CRITERIA	ALL MEMBERS EXCEPT PILES	CONCRETE PILES
Minimum Cementitious Factor (Lbs/Yd^3) [kg/m^3]	550 [330]	600 [356]
Maximum Water/Cementitious Ratio	0.45	0.45
Maximum Slump (prior to admixture) (in.) [mm]	4.0 [100]	4.0 [100]

ALDOT 367 (2010) does not add any concrete proportioning requirements in addition to the requirements of the *Standard Specifications* (2012). Instead, ALDOT 367 merely points out the necessity of following those requirements.

3.3.2. Proportions

Concrete mixtures belonging to each girder producer are different. However, they share many common aspects. Table 3.2, Table 3.3, and Table 3.4 show a comparison of mixture proportions for different concrete mixtures from different producers. Each mixture was recently or is currently approved for use in prestressed bridge members in its respective plant. Table 3.2 compares the primary non-liquid ingredients of each mixture (cement, supplementary cementitious materials, fine aggregate, and coarse aggregate). Table 3.3 compares the liquid proportions of each mixture, and Table 3.4 compares the parameters that are calculated from these proportions for each mixture.

Table 3.2: Comparison of Basic Material Proportions between Plants, per Cubic Yard

	Plant A		Plant B		Plant C		Plant D	
Label	Mixture 1	Mixture 2	Mixture 1	Mixture 2	Mixture 1	Mixture 2	Mixture 1	Mixture 2
Cement Type	III	III	III	III	III	I / II	III	III
Cement (lbs/yd^3)	639	751	788	765	788	600	697	765
SCM #1 Type	Slag Cement	Slag Cement	Class F Fly Ash	Class F Fly Ash	Class F Fly Ash	Class F Fly Ash	Class F Fly Ash	Class F Fly Ash
SCM #1 (lbs/yd^3)	113	133	173	100	150	170	123	135
SCM #2 Type	None	None	None	Microsilica	None	Microsilica	None	None
SCM #2 (lbs/yd^3)	0	0	0	75	0	85	0	0
Fine Aggregate Type	#100 Sand	#100 Sand	#100 Sand	#100 Sand	#100 Sand	#100 Sand	#100 Sand	#100 Sand
Fine Aggregate (lbs/yd^3)	1172	1048	1301	1278	1091	1048	1249	1189
Specific Gravity of Fine Aggregate	2.66	2.66	2.62	2.62	2.62	2.62	2.63	2.63
Source of Fine Aggregate	Prattville, AL	Prattville, AL	Butler, GA	Butler, GA	Pearl River, LA	Pearl River, LA	Atmore, AL	Atmore, AL
Coarse Aggregate Type	#57/#67 Limestone (Dolomitic)	#57/#67 Limestone (Dolomitic)	#67 Granite	#67 Granite	#78 Limestone (Regular)	#67 Gravel	#67 Granite	#67 Granite
Coarse Aggregate (lbs/yd^3)	1860	1861	1345	1426	1720	1675	1655	1576
Specific Gravity of Coarse Aggregate	2.83	2.83	2.68	2.68	2.71	2.52	2.76	2.76
Source of Coarse Aggregate	Helena, AL	Helena, AL	Forest Park, GA	Forest Park, GA	Calera, AL	Pearl River, LA	Mulgrave, Canada	Mulgrave, Canada

Table 3.3: Comparison of Liquid/Admixture Proportions between Plants, per Cubic Yard

	Plant A		Plant B		Plant C		Plant D	
Label	Mixture 1	Mixture 2	Mixture 1	Mixture 2	Mixture 1	Mixture 2	Mixture 1	Mixture 2
Maximum Water (gal/yd^3)	33.3	33.8	35.0	33.0	30.4	29.8	31.0	34.0
Maximum Water (lbs/yd^3)	277	282	292	275	253	248	258	283
Air Entrainer (AE) Type	Daravair 1000	Daravair 1000	MB AE 90	MB AE 90	MB AE 90	MB AE 90	MB AE 90	MB AE 90
Max AE (oz/yd^3)	1.0	1.0	2.0	2.0	4.0	4.0	3.3	3.6
Type of Water Reducer	Recover	Recover	Delvo	Delvo	Pozzolith 100-XR	Pozzolith 100-XR	Delvo	Delvo
Max Water Reducer (oz/yd^3)	7.5	8.8	34.0	42.0	12.0	9.0	16.4	18.0
High-Range Water Reducing Admixture #1 Type (HRWRA)	ADVA CAST 575	ADVA CAST 575	Glenium 7700	Glenium 7700	Glenium 7700	Glenium 7700	Glenium 7700	Glenium 7700
Max HRWRA #1 (oz/yd^3)	45.1	53.0	57.0	66.0	48.0	43.0	53.3	49.5
High-Range Water Reducing Admixture #2 Type	ADVA CAST 555	ADVA CAST 555	NONE	NONE	NONE	NONE	NONE	NONE
Max HRWRA #2 (oz/yd^3)	30.1	35.4	0	0	0	0	0	0

Table 3.4: Comparison of Calculated Parameters between Plants

	Plant A		Plant B		Plant C		Plant D	
Label	Mixture 1	Mixture 2	Mixture 1	Mixture 2	Mixture 1	Mixture 2	Mixture 1	Mixture 2
Fine agg/total agg (*s/agg*)	0.387	0.360	0.492	0.473	0.388	0.385	0.430	0.430
Max *w/c*	0.435	0.376	0.371	0.360	0.322	0.414	0.371	0.371
Max *w/cm*	0.370	0.319	0.304	0.293	0.270	0.291	0.315	0.315

As can be seen from Table 3.2, most current concrete mixtures include Type III cement instead of the more common Type I or Type II cements. This is not surprising since the girders must reach design release strength in order for the prestressing strands to be cut. For precast

producers, it is optimal to remove the girders from a line as quickly as possible so that the process of setting up for the next set of girders may begin. Therefore, more rapid strength development in early ages is beneficial to the plant. Type III cement provides part of the equation for rapid early-strength development. High curing temperatures from the steam curing process provide the other part.

It is also apparent from Table 3.2 that the use of "mineral admixtures" (herein referred to as supplementary cementitious materials, or SCMs) is very common. In fact, of all approved mixtures that researchers from the AUHRC examined, only one mixture did not include an SCM of some kind. Most mixtures use fly ash, which is beneficial for later strength gain and lower costs. One plant preferred the use of slag cement. A few mixtures included small amounts of microsilica, a very fine byproduct useful for the production of high-strength concretes.

These SCMs are used in addition to high quantities of portland cement. From Table 3.4, it is clear that each mixture would have a low enough w/cm to satisfy the proportion requirements of Table 3.1 even without the addition of SCMs. It is also clear that each mixture contains more than enough cement by weight to satisfy the cement content requirements of Table 3.1. With both portland cement and SCMs, the mixtures reach w/cm well below the maximum ratios allowed by Table 3.1.

3.3.3. Aggregates

All of the aggregate proportions provided in Table 3.2 are measured in the saturated-surface-dry state. Many of the concrete mixtures are designed using the same or very similarly sized aggregates, though the amount, source, and type may differ. Note, for example, that every mixture outlined in Table 3.2 includes a #100 sand as its fine aggregate, but that the amount of

sand used and the source of the sand differ greatly from mixture to mixture. The fine aggregates for the eight mixtures outlined here are obtained from two different plants in Alabama, one in Pearl River, Louisiana, and one in Georgia. The amount of sand used varies by up to 24% between mixtures.

The coarse aggregate use is much more varied than the fine aggregate. Gradations range from #57/#67 aggregates to #78 aggregates. Also, the type of coarse aggregate changes significantly. Some mixtures use a dense dolomitic limestone aggregate, some use regular limestone, some use granite, and some use gravel. Each has a different source, different properties, and a different specific gravity (SG). One coarse aggregate is even shipped in from Mulgrave, Nova Scotia, Canada. The use of coarse aggregates by weight varies by up to 38%, and the SGs for each aggregate vary by up to 12%.

3.3.4. Chemical Admixtures

Some very important components of the concrete mixtures used in modern prestressed girder applications are the chemical admixtures. The consistency and similarity between plants in their use of chemical admixtures is surprising in some respects. As can be seen in Table 3.3, Plants B, C, and D all use an air entrainer called MB AE 90, while Plant A uses Daravair 1000. Again, Plants B, C, and D all use Glenium 7700 as their high-range water reducing admixture (HRWRA). However, Plant A uses ADVA CAST 555 and 575, two HRWRAs from a different company. The choice of water reducing (WR) admixtures is slightly more varied. Only Plants B and D use Delvo in common, while Plant A and Plant D use Recover and Pozzolith 100-XR, respectively.

Aside from this variance in type and number of admixtures, not much more can be said

regarding plant use of admixtures without extensive comparison of the products themselves. An important aspect to notice, though, is the high dosage of HRWRA used by each plant. The smallest amount used per cubic yard is a substantial dose of 43.0 $\frac{\text{oz}}{\text{yd}^3}$ in Plant C Mixture 2. The highest amount allowed for any mixture was 88.4 oz per cubic yard, in Plant A Mixture 2. This is approximately a 106% difference in dosage. It is clear, however, that all of these mixtures are designed to achieve a high degree of workability.

3.4. Summary

The visits made to each girder producer did a great deal in expanding the researchers' understanding of the details and processes involved in the production of prestressed concrete bridge girders for Alabama. Girder producers have set procedures in place to maximize the turnover rate of their lines—to maximize the efficiency of workers on the line, to increase the rate of strength gain, and to increase the overall speed of production.

This desire for rapid production has its counterpart in the material costs required to achieve it. Concrete mixtures use large quantities of portland cement with not insignificant portions of SCMs. Often producers aim for very rapid strength growth, so they use Type III cements and SCMs that aid in early strength development. However, they also aim for high total strength as an alternative way of increasing early strength. Therefore, they use very low w/cm ratios with high doses of water-reducing admixtures to maintain workability. Entrained air is usually acceptable, and WR admixtures are adjusted to ensure adequate fresh properties for placement and testing. All in all, it is a battle between the costs of unproductive time on the line against the costs of more or better materials. Most often, the additional material costs are outweighed by the speed of production and the consistency that the use of these different

materials allows.

Chapter 4: Experimental Design for In-Plant Testing

4.1. Introduction

With the knowledge that was gained during the site visits described in Chapter 3, researchers began the design of an extensive in-plant testing program to accomplish Task 4 listed in Section 1.3. This program combines actual girder instrumentation and monitoring with representative material testing and analysis to provide more useful data to designers. As such, the program was split into four major categories. These categories are delineated as Girder Strain and Temperature Measurement, Material Testing, Camber Measurement, and Cylinder Temperature/Maturity Measurement. This thesis gives a detailed description of the Material Testing and Cylinder Temperature/Maturity Measurement segments, but it only briefly describes the Girder Strain and Temperature Measurement and Camber Measurement segments.

Ultimately, the desire for the In-Plant Experimental Plan was to cover a range of geographic conditions, aggregate sources, and production techniques characteristic of prestressed girders in ALDOT bridges. To do so while obtaining adequate data to achieve statistically meaningful results, the original plan included in-plant testing at three different bridge girder producers and participation in eighteen different girder production cycles. As is commonly done in the industry, the combined concrete mixing and placement operations associated with the production of a single set of girders is referred to as a “pour” in this thesis. Thus far, researchers have only participated in six production cycles at two different plants.

4.2. Girder Strain and Temperature Measurement

Measurement of internal strains and temperatures was an important part of the in-plant testing program. Although the goal of the material testing methods was to most accurately represent the conditions of the in-place concrete, as is explained in Section 4.3, it was important to be able to directly compare and apply the results of these material tests to the girders they were intended to represent. As such, one girder in each pour from which material samples were taken was internally instrumented with a set of gauges. The extent of instrumentation depended on the level of detail expected for that set of girders. The “simple” girder instrumentation set was composed of only four vibrating-wire strain gauges (VWSGs), placed at midspan of the girder at the heights shown in Figure 4.1 and Table 4.1. The “detailed” girder instrumentation set included additional gauges.

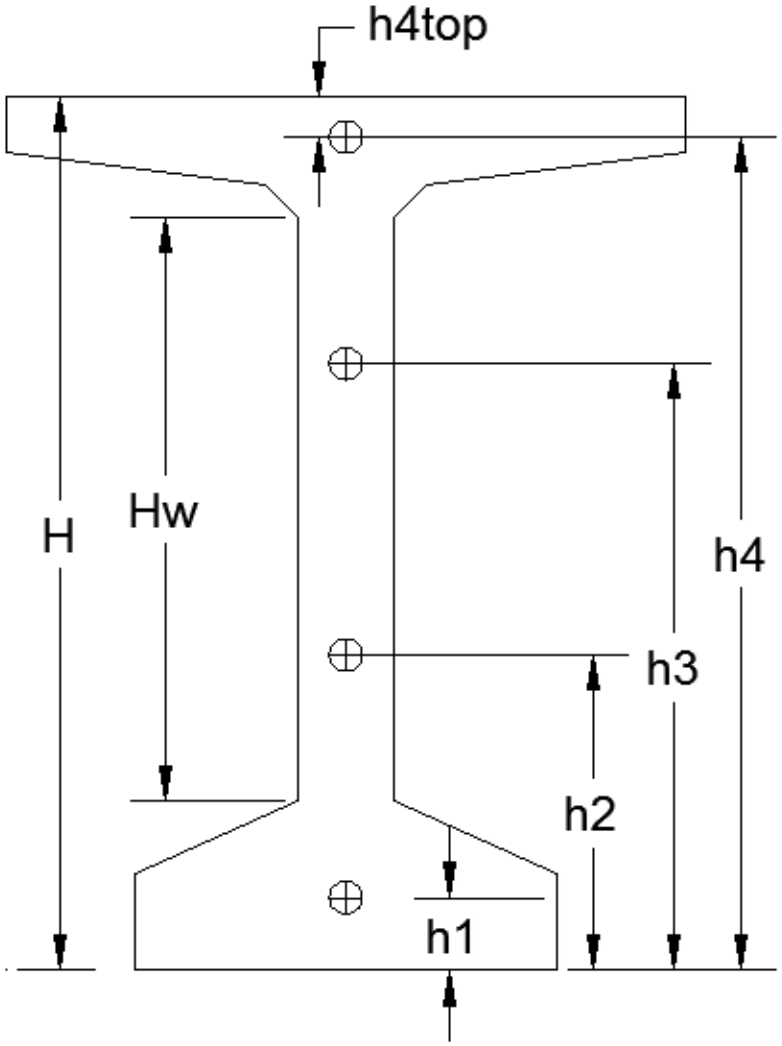

Figure 4.1: Sketch of Dimensions for VWSGs (see Table 4.1)

Table 4.1: Table of Dimensions for VWSGs (see Figure 4.1)

Girder Type	H (in.)	H_w (in.)	h_1 (in.)	h_2 (in.)	h_3 (in.)	h_4 (in.)	h_{4top} (in.)
BT-54	54	36	4.5	19.5	37.5	51.5	2.5
BT-63	63	45	4.5	21.8	44.3	60.5	2.5
BT-72	72	54	4.5	24	51	69.5	2.5

The locations that these heights represent are delineated as follows:

1. The centroid of concrete of the bottom flange. Since the focus of this research project was strictly PCI bulb-tee girders, and since all PCI bulb-tee girders have identical flange designs, this measurement came to 4.5 in. from the bottom of the girder.
2. The quarter height of the web as measured from the top of the bottom flange. The exact distances from the bottom of the girder were 19.5 in. for BT-54 girders, 21.75 in. for BT-63 girders, and 24 in. for BT-72 girders.
3. The three-quarter height of the web as measured from the top of the bottom flange. The exact distances from the bottom of the girder were 37.5 in. for BT-54 girders, 44.25 in. for BT-63 girders, and 51 in. for BT-72 girders.
4. The centroid of concrete of the top flange. Because all top flanges are the same between PCI bulb-tee girders, this distance was measured as being 2.5 in. down from the top of the girder for all bulb-tee sizes.

Each VWSG was installed in tandem with a thermistor, since it is necessary to correct the readings from a VWSG for gauge and concrete temperature.

In addition to the four VWSGs at midspan, a “detailed” girder contained an extra set of four VWSGs and one array of thermocouples. The second set of VWSGs was placed at the sixth-span point, because it approximated the average mid-drape point for most draped prestressing strands. Most ALDOT bult-tee girders contain a set of draped prestressing strands, such as those shown in the sketch in Figure 4.2.

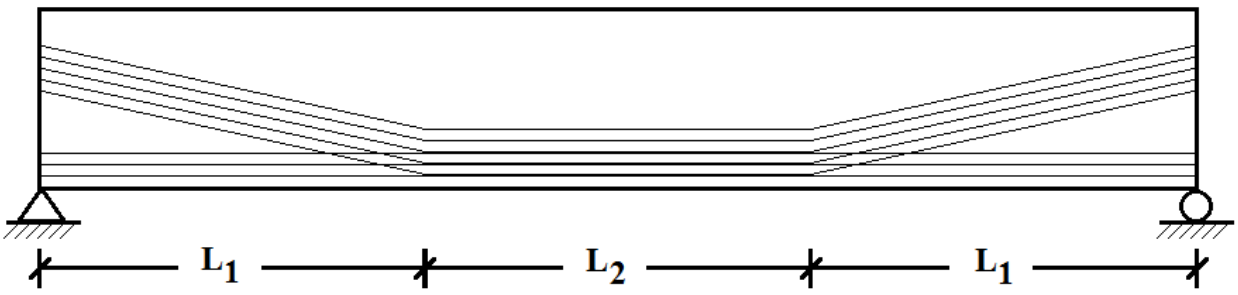

Figure 4.2: Sketch of Approximate Draped Strand Layout in ALDOT Girders

These draped strands often follow an approximate third-point profile. In other words, the prestressing strands are sloped toward the bottom of the girder for one third of the length, are parallel to the bottom of the girder for the middle one third of the length, and then slope back up away from the bottom of the girder for the last one third of the length. This is by no means exact, but is merely an approximation of average tendencies. The sixth-span location was also one of the locations at which camber survey points would be located, which is discussed in Section 4.4.

Gauges were installed after prestressing strands had been tensioned and sufficient rebar stirrups had been hung to provide supports. It was necessary for stirrups to be installed first because most of the gauges were installed by connecting them to pairs of stirrups. Care was taken during the installation to ensure that each gauge met the following goals:

- The gauge was level and oriented parallel to the longitudinal axis of the girder.
- The gauge was approximately in the middle of the girder in the lateral direction.
- The zip ties holding the gauge were loose enough to prevent distortion of that gauge, but tight enough to hold the gauge in place during concrete placement.
- The wires to which the zip ties attached were tight enough to provide support for the gauge, but loose enough to prevent the tension from displacing the supporting stirrups.

- The electrical cables running from the gauges were positioned to prevent excessive pull from the pressure of concrete.

Extra care was taken to ensure that the VWSGs, and the stirrups to which they were attached, would not be damaged or moved during placement of the concrete.

The thermocouple array consisted of a series of thermocouples attached to a fiberglass shaft positioned at midspan in the girder. A close view of one of these thermocouples may be seen in Figure 4.3, and the full array secured inside the girder reinforcement may be seen in Figure 4.4.

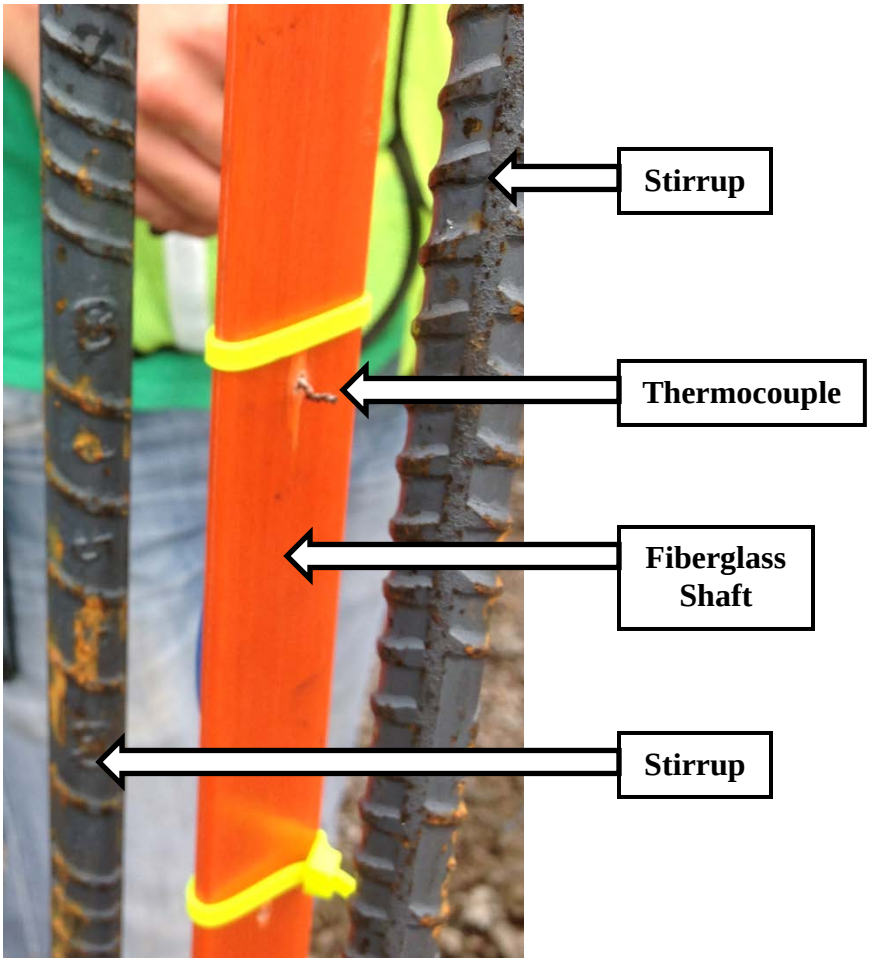

Figure 4.3: Thermocouple Attached to Fiberglass Shaft

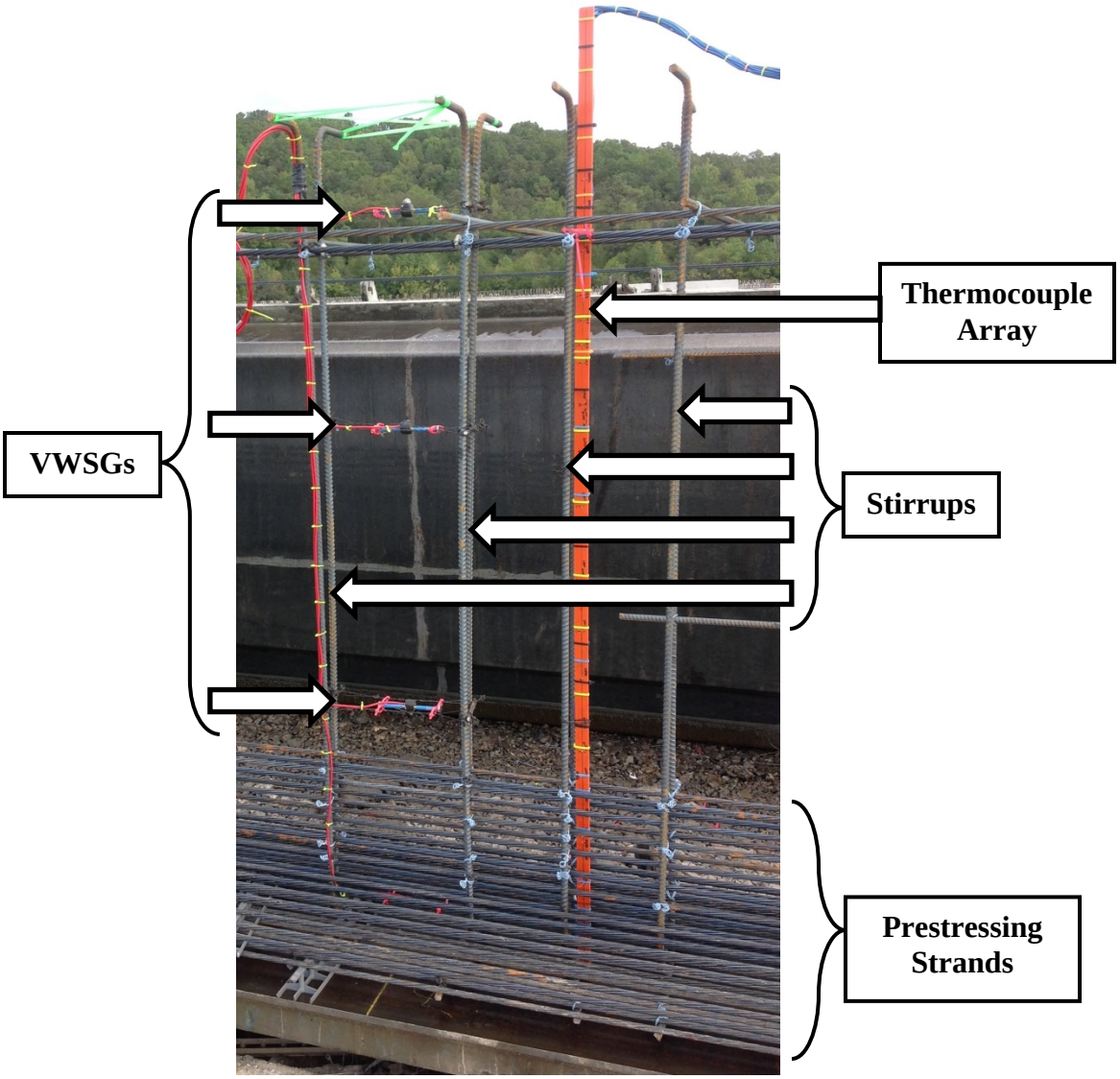

Figure 4.4: Thermocouple Array and VWSGs Secured in Girder Reinforcement

The thermocouple array provided a much more detailed internal temperature distribution than the VWSGs could provide. This temperature distribution was used to correct camber and strain measurements resulting solely from thermal effects. It is commonly known that thermal changes have the capacity to increase or decrease camber and strain measurements due to

nonuniform temperature distributions on a girder cross section. By knowing the coefficient of thermal expansion (α_T) of the concrete in question, a temperature distribution can be used to predict the proportion of field-measured camber or strain that is attributable to thermal effects.

Similarly to the VWSGs, the thermocouple array locations varied depending on the size of the girder. An array consisted of thirteen thermocouples placed at the locations described in Table 4.2.

Table 4.2: Thermocouple Array Positions

	Girder Size		
Thermocouple (TC) Label	BT-54	BT-63	BT-72
TC #1, Measured from Bottom, in.	1.0	1.0	1.0
TC #2, Measured from Bottom, in.	3.0	3.0	3.0
TC #3, Measured from Bottom, in.	6.0	6.0	6.0
TC #4, Measured from Bottom, in.	9.0	9.0	9.0
TC #12, Measured from Bottom, in.	12.5	13.0	14.0
TC #13, Measured from Bottom, in.	16.0	17.5	19.5
TC #5, Quarter Height of Web, Measured from Bottom, in.	19.5	21.8	24.0
TC #6, Mid-Height of Web, Measured from Bottom, in.	28.5	33.0	37.5
TC #7, Three-Quarter Height of Web, Measured from Bottom, in.	37.5	44.3	51.0
TC #8, Measured from Top, in.	6.5	6.5	6.5
TC #9, Measured from Top, in.	5.0	5.0	5.0
TC #10, Measured from Top, in.	3.0	3.0	3.0
TC #11, Measured from Top, in.	1.0	1.0	1.0

The thermocouple array was installed at the location of a stirrup. ALDOT girders use double-leg stirrups at each stirrup location, which creates a small space in the lateral direction. This small space is where the thermocouple array was installed, as may be seen in Figure 4.4 above. Care was taken during installation to ensure that the following requirements were met:

- The zip ties were a sufficient distance away from the end of the thermocouple to make sure it would not prevent concrete from reaching the thermocouple.
- The zip tie locations were spaced close enough together to prevent local deformations of the fiberglass shaft under nonuniform concrete pressures during placement. A buildup of fresh concrete on one side of the fiberglass shaft would cause nonuniform pressures, possibly causing the shaft to bend.
- The supporting stirrup set was adequately tied in place to prevent movement due to nonuniform concrete pressures during placement.
- The fiberglass shaft maintained vertical alignment during installation and concrete placement.

Detailed girders were subjected to one 24-hour test, during which an additional five gauges were temporarily installed. Three deflectometers were installed underneath the girder, and one tiltmeter was installed at each end.

The deflectometers, which are small devices that record linear deflection through the pull of a small wire from the main body, were installed at quarter length points of the girder. They provided frequent measurements of the girder's vertical deflection at each point throughout the 24-hour test.

The tiltmeters, which measure rotation of the object to which they are attached, were installed to the ends of the girder using a wooden U-shaped clamp. The clamp was attached directly to the end of the girder using a quick-set epoxy, and the tiltmeter was then attached to the end of the wooden clamp. These tiltmeters provided frequent measurements of the rotation of the ends of the girder, which could be correlated to the measured deflections taken from the deflectometers.

A full description of installation practices, measurement schedules, electronics used, plug-in mechanisms, and more is not contained in this thesis. The focus of this thesis is the material properties aspect of the concrete used in prestressed bridge girders, but these details relate more to the girder work that was performed.

4.3. Material Testing

The material testing portion of the experimental design was primarily focused on the production, curing, and testing of concrete cylinders. Researchers wished to perform material testing for the expected range of concrete behavior. Thus, it was decided to attempt to sample different girder designs—different girder sizes, different lengths, and different concrete strength levels. For each plant, three different girder designs were selected. Then, for each selected design, researchers participated in two different pours. Therefore, there were eighteen pours in all.

$$(3\ plants)\left(3\ \frac{girder\ designs}{plant}\right)\left(2\ \frac{pours}{girder\ design}\right) = 18\ pours$$

Each pour consisted of two random sampling locations. A total of 25 cylinders were cast, to be used as described below:

1. Three cylinders were created from each sampling location for strength and modulus of elasticity testing at the time of prestress transfer. Researchers used 40% of the release strength measured by the plant as the estimated upper stress limit for the first cylinder tested for modulus of elasticity. The upper limit for subsequent cylinders was determined based on the strength of the previously tested cylinders(s).
2. Three cylinders were created from each sampling location for strength and modulus of elasticity testing at a concrete chronological age of 24 hours. Unlike the cylinder testing

performed at prestress release, no plant cylinder strength tests were available for comparison at an age of 24 hours. Therefore, the measured release strengths were used for an estimate of the 24 hr strength, in order to allow for the collection of an additional modulus of elasticity measurement at 24 hours.

3. Three cylinders were created from each sampling location for strength and modulus of elasticity testing at a concrete chronological age of 28 days. One cylinder was tested to obtain an estimated 28-day field-cure strength, and then two modulus of elasticity measurements were obtained using the remaining cylinders before strength testing.
4. Three more cylinders were created from each sampling location for strength and modulus of elasticity testing at a concrete chronological age of 28 days. However, these cylinders were cured following the standard curing procedures set forth in ASTM C31/C31M (2009). After the first few pours, it was decided to use results from the 28-day field-cure cylinders to estimate the upper stress limit for modulus of elasticity testing for the standard-cured specimens.
5. One cylinder was created at one of the sampling locations for temperature history records. This cylinder was stored and cured in exactly the same manner as the other field-cure cylinders, but was not usable for strength or modulus of elasticity testing. A thermocouple was installed into the center of the cylinder while still in the fresh state, and this thermocouple was used for recording the temperature history.

Thus, for each pour, 25 cylinders were created. All cylinders that were tested for modulus of elasticity were also tested for strength, so the 25 cylinders yielded the following data:

1. At prestress release, the six cylinders yielded six concrete strength measurements and six modulus of elasticity measurements.

2. At a chronological age of 24 hours, the six cylinders yielded six concrete strength measurements and six modulus of elasticity measurements.
3. At a chronological age of 28 days, the six field-cure cylinders yielded six concrete strength measurements and four modulus of elasticity measurements.
4. At a chronological age of 28 days, the six standard-cure cylinders yielded six concrete strength measurements and six modulus of elasticity measurements.

For analysis, these measurements were averaged, as is discussed in Chapters 6 and 7. More detailed information about curing, storage, and testing of the cylinders follows.

Cylinders were set to be produced at two random sampling locations for each pour. Since it was already required that prestressed plants randomly sample their concrete every 50 yd^3, or fraction thereof (ALDOT 2010), it was agreed that the cylinders for in-plant material testing would be produced using the same batches of concrete that were used for the production of plant cylinders. Cylinders were created in single-use plastic molds, and capped with reusable plastic lids, following all the requirements of AASHTO T 23 (2009). Figure 4.5 shows an AUHRC researcher setting up the tools, wheelbarrow, and cylinder molds for cylinder production during a pour.

Figure 4.5: AUHRC Researcher Setting Up Testing Materials

As described in Section 3.2, concrete is delivered to the girder forms in concrete delivery trucks. Whenever a truck full of concrete was selected for testing, it first provided concrete for fresh concrete properties testing at the QA/QC building. This concrete was dumped into a wheelbarrow, from which samples would be tested for slump, concrete temperature, and air content. This same concrete was used for the production of 28-day standard-cure cylinders, as is described later. This was chosen so that the standard-cure cylinders could begin curing instantaneously, without high early temperatures or the need for transporting the cylinders long

distances to the QA/QC building.

The same truck of concrete proceeded to the casting line, where the inspectors produced their cylinders and where AUHRC researchers produced all cylinders except for the 28-day standard-cure cylinders. The truck then did one of two things. It either discharged concrete into a wheelbarrow for testing first, then emptied the rest of its contents into the girder formwork; or it first emptied a substantial portion of its contents into the formwork, and then discharged concrete for sampling. The first option was more commonly seen. In either case, whenever the truck was called to discharge concrete into a wheelbarrow for inspectors to use for the production of their cylinders, it also filled an additional wheelbarrow for AUHRC researchers to use. This method was chosen both for the ease of coordination and for the assurance that material property tests would very closely correlate to the tests performed by ALDOT inspectors. AUHRC cylinder production may be seen in Figure 4.6.

Figure 4.6: AUHRC Researcher Producing Test Cylinders

A clear labeling system, which may be seen in Figure 4.7, was used to track cylinders and to help ensure the reliability of measured data.

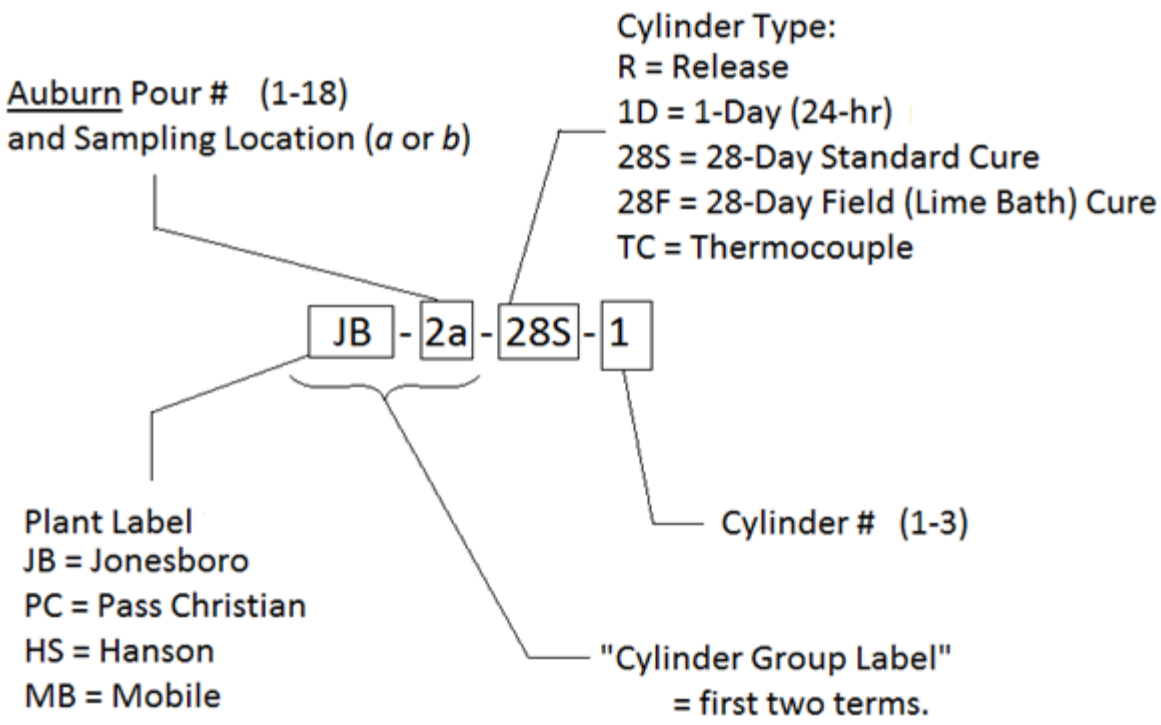

Figure 4.7: Labeling Convention for Test Cylinders

Each cylinder label consisted of the following four parts:

1. A shortened label for each girder producer.
2. The numerical order of the pour with regard to the AUHRC camber project (called the "Auburn pour number") and the sampling sequence within each pour. The sampling sequence was indicated by "a" or "b," as determined by the order in which the cylinders were produced.
3. The testing purpose of cylinder in question.
4. The number of the cylinder within the group intended for the purpose given in Part 3. In the case of the thermocouple cylinder, parts 3 and 4 were simply replaced by the letters "TC".

All of the cylinders produced at a given sampling location were immediately cleaned and

capped, before researchers continued to the next sampling location. This process may be seen in Figure 4.8. The purpose was to provide a level cylinder surface and ensure an adequate moisture-retaining seal with the cylinder cap.

Figure 4.8: Cleaning and Capping Test Cylinder Specimens

All cylinders except for the 28-day standard-cure cylinders were stored on the formwork underneath the tarps that were used to cover the girders during curing. However, they were not be moved to this location until after the primary casting crew had moved a sufficiently large enough distance down the line that the vibrations would have minimal effect on the cylinders. The forms used in the production of large bulb-tee girders are steel forms with large hollow spaces, so a sheet of plywood was laid across one of these hollow spaces to provide a level resting surface and the cylinders were placed on this sheet. This practice was identical to the procedure followed in the plant's cylinder testing program, as is shown in Figure 4.9.

Figure 4.9: Plant Placement of Cylinders during Girder Curing

Lastly, a 100-gal stock tank containing lime-saturated water (or a “lime bath”) was also placed beneath the tarp, for cylinder curing after removal of the forms. This tank is shown being filled with water in Figure 4.10. The lime bath sat adjacent to the casting line and adjacent to a heavy tote which contained the data acquisition system box, which is described later. The bath was purposefully placed under the curing tarp during curing so that it would reach approximately the same temperatures as the cylinders and girder, as is discussed in greater detail later. The final set up, showing the relative locations of the data collection tote, lime bath, and curing tarp, may be seen in Figure 4.11.

Figure 4.10: Filling the Field-Cure Lime Bath

Figure 4.11: Curing Tarp Coverage Conditions

There were two primary curing procedures that were used for this experimental design. For each pour, nineteen cylinders were cured under “field-cure” conditions and six cylinders were cured under “standard-cure” conditions, both of which are discussed in greater detail below.

Standard-cure cylinders utilized the previously existing temperature-controlled lime baths in the QA/QC building of each plant. These lime baths, such as the one shown in Figure 4.12, are often used for cylinder curing in projects for other Departments of Transportation (DOTs). Therefore, they already met the requirements set forth in ASTM C511 (2009) for curing temperature ranges.

Figure 4.12: Temperature-Controlled Lime Bath Used for Standard-Cure Cylinders

Cylinders produced for 28-day standard-cure testing were produced as described above, then cleaned and immediately capped with reusable plastic lids. These cylinders were either immediately submerged into the temperature-controlled lime bath, or submerged immediately after completion of the production of the field-cure specimens. Standard-cure cylinders remained in this lime bath until approximately the same time that all the other cylinders were demolded, as is described later in this section. At this time the standard-cure cylinders were also demolded, and then immediately re-submerged into the lime bath until they were ready to be transported back to the AUHRC facilities.

Field curing of cylinders followed a substantially different procedure. These cylinders were produced on the ground adjacent to the line, placed in the girder formwork after vibrations could no longer affect them, and kept under the tarp until the tarp was removed from the girder. This process was their initial curing procedure.

When release strength values were desired, two of the plant cylinders were removed and tested in compression. If adequate strength had not yet been reached, girder curing continued and the test was repeated at a later time. Upon reaching the design release strength, the tarps were removed, the cylinders were taken to their respective storage locations for long-term curing, and the removal of formwork began.

When the plant received confirmation that the compressive strength was sufficient for prestress transfer, AUHRC researchers began their own procedures for long-term cylinder curing. All cylinders intended for release tests were transported to the QA/QC building, where they were demolded and tested for compressive strength and modulus of elasticity.

The lime bath that was housed under the tarp was moved to the end of the line, where it was out of the way of traffic but still exposed to the same solar conditions as the girders. All 24-

hour cylinders, 28-day field-cure cylinders, and thermocouple cylinders were demolded and submerged into this lime bath, which was at approximately the same temperature as the cylinders due to its participation in the curing procedure. The tank was brought to approximately the same temperature as the cylinders to avoid possible thermal shock or microdamage that might occur to the cylinders if they were cooled too rapidly. The stock tank was covered by a thin plywood sheet to prevent uncharacteristic heating of the water due to solar effects.

At 24 hours, the cylinders intended for 24-hour chronological age tests were transported to the QA/QC building for testing. The 28-day field-cure cylinders remained in the lime bath until they were ready to be transported to the AUHRC facility.

In order for this process to work, it was required to have two lime baths on site. When the time came for the second pour, the first lime bath would already be in use and could therefore not be placed under the tarp for heating. To place the first lime bath under the tarp again would induce a second round of curing for the cylinders it contained, and would therefore skew earlier pours on a given trip towards higher maturities at the time of testing. Thus, a second lime bath was required.

The first lime bath, still containing the extra field-cure cylinders from the first pour, remained at the end of the prestressing bed. A second lime bath was placed under the tarp for the second pour. When the 24-hour, 28-day, and thermocouple cylinders from the second pour were demolded, they were placed into the second lime bath to avoid thermal shock. They were left in this second lime bath until the temperatures of the first and second lime baths were approximately equal (or in the case of the 24-hour cylinders, until the time came for testing). When the temperatures were equivalent, the cylinders from the second pour were transferred over to the first lime bath, thus emptying the second lime bath of all cylinders and freeing it for

use in yet another pour.

For transportation, all cylinders (including the standard-cure cylinders) were placed in the curing tanks or in plastic totes, both containing lime bath, and driven back to Auburn University. To prevent the cylinders in the tanks from damaging one another or receiving damage from the sides of the tank, the empty spaces between cylinders were filled with used cylinder molds. Upon arrival at the AUHRC facility, the cylinders were placed in their final stage of curing.

After transportation to the AUHRC facility, standard-cure cylinders were placed in the moist curing room, a room devoted to the curing of ASTM C31/C31M (2012) standard-cure cylinders. This room is maintained at the conditions described in ASTM C511 (2009).

Field-cure specimens were transferred into a large stock tank filled with a lime bath, which may be seen in Figure 4.13. This stock tank was set on a platform built specifically for that purpose, to provide a level resting surface. The stock tank itself was a galvanized steel, open-topped tank. Since this tank was to be much more permanent than the tanks used in each plant, it was important that it be durable enough to maintain its function over a long period of time. Thus, a permanent lid was constructed that would be sturdy enough to withstand the solar and moisture conditions for long periods of time. This lid was clearly labeled with warnings and contact information for anyone who might need to know more information about the tank or its contents.

Figure 4.13: Curing Tank Used for Field-Cure Cylinders

The location of the curing tank was carefully selected to ensure large percentages of solar exposure throughout the day, and complete exposure to ambient temperatures at all times. Solar exposure on the tank location was important because of the solar exposure to which girders are subjected. However, a lid was included on the curing tank to avoid uncharacteristic solar heating that might not occur in the girder, thus aiming to more accurately mimic conditions of the concrete within the girders. Lastly, the cylinders were cured in a high moisture environment that more characterized the inner portion of the concrete girder, not the surface.

Testing of the cylinders followed the procedures established in the ASTM C39/C39M (2012) and ASTM C469/C469M (2010) standards. The only significant variance from standard practices was with regard to the bearing surfaces. ASTM C1231/C1231M (2010) specifies that unbonded caps may be used in testing the strength of concretes with a strength up to 12,000 psi,

provided that qualification tests are performed to verify performance. An analysis of historical plant strength data, however, shows that concrete strength tests in prestressed plants occasionally reach strengths higher than 12,000 psi (see Chapters 5 and 6). Nevertheless, it is common practice for all of the included ALDOT girder producers to use unbonded 70 durometer elastomeric bearing pads in the testing of all their ALDOT cylinders for both release tests and 28-day tests. Furthermore, in the case of release strength tests there is no other option due to the setting time required by sulfur-capping compounds.

Strength and modulus of elasticity testing of the release cylinders and the 24-hour cylinders utilized compression machines in the prestressed plant QA/QC building. Figure 4.14 shows an AUHRC researcher performing modulus of elasticity tests on a cylinder, using the compression machine available at a plant. Testing at the AUHRC facility took place in either a Forney FX600 compression machine or, when the FX600 was down for maintenance, in an older Forney QC400 compression machine. These machines may be seen in Figure 4.15 and Figure 4.16 respectively.

Figure 4.14: Modulus of Elasticity Test Being Performed at a Plant

Figure 4.15: Forney FX600 Compression Machine Used for Testing

Figure 4.16: Forney QC400 Compression Machine Used for Testing

Cylinder strength tests were performed in accordance with ASTM C39/C39M (2012). Because the plants use 70 durometer elastomeric bearing pads for their strength tests, these strength tests also used those pads. A light coating of baby powder was used to reduce friction between the pads and the cylinder. When necessary, the top of the cylinder was hand-ground to produce a smoother, more uniform finish.

Modulus of elasticity tests were performed in accordance with ASTM C469/C469M (2010), and the cylinders were prepared in the same way as for strength tests. The only difference in preparation is that the compressometer was installed on the cylinder before the top retainer was added. A cylinder with the compressometer installed is shown sitting in the loading chamber of the Forney FX600 in Figure 4.17.

Figure 4.17: Cylinder Ready for Modulus Testing

Usually three loading cycles were performed for each cylinder used in modulus of elasticity testing, as is specified in ASTM C469/C469M (2010). The results of the first cycle were discarded, and the average result from the other two cycles was used for reporting modulus

of elasticity. However, when results between the two latter cycles were unreasonably different, additional cycles were performed for more consistent results.

After modulus test results were satisfactorily consistent, the compressometer was removed and the cylinder was tested for strength in accordance with ASTM C39/C39M (2012). The results from the strength and modulus of elasticity tests performed on all cylinders as part of the Task 4 in-plant material testing program, as well as the analysis of these results, are described in Chapters 6 and 7 of this thesis.

4.4. Camber Measurement

Measurement of actual girder cambers was a critical part of this research project on cambers. Thus, it had its own portion of the in-plant testing program. However, this part of the project is primarily included in the work of other individuals, and only a brief overview is given in this thesis.

To facilitate camber measurements, 2.5 in. lag screws were embedded in the top surface of each girder during the casting process. These screws provided a sufficiently wide, flat, and recognizable surface at each survey point for consistent measurements throughout the project. A total of five screws were embedded in each girder, at the five locations described below.

1. Near each end of the girder. To avoid conflict with metal plates that were often installed at the ends of the girder, these screws were placed near the end but not at the end itself.
2. At the approximate midspan of the girder.
3. At the approximate sixth point and five-sixths point of the girder. These were used to provide supplementary points in addition to the end and midspan points, to provide a better profile of the camber that occurred in each girder.

Except for during the 24-hr tests, as described in Section 4.2, cambers were always measured with a total station and prism rod. The total station was usually set up on the ground in a fairly central location for camber measurements.

Whenever camber was measured, one researcher operated the total station and another researcher walked along the top of the girder, obtaining readings at each lag screw location. These measurements, along with many different notes about the process and conditions, were written down by the researcher running the total station. This was done at four or five different times throughout the life of each girder.

1. Cambers were first surveyed immediately after removal of the girder formwork, but before the prestressing strands were cut. This reading provided the baseline against which all future readings would be compared. It established the relative elevations of the lag screws within a girder, when no quantifiable camber was present.
2. Cambers were surveyed immediately after the prestressing strands had been cut, but before the girders were lifted or moved from the bed.
3. Cambers were surveyed immediately after each girder had been transported to its temporary storage position. This survey provided what is called the “lift and set” survey. By comparing this survey to survey #2 above, the effects of end friction on camber may be quantified.
4. For those girders which took part in the 24-hr tests described in Section 4.2, cambers were surveyed an additional time while all gauges were recording. This provided a means of comparison between measured camber values and internal strain and temperature measurements.
5. Lastly, cambers were measured at least one more time shortly before shipment to the job

site. Since girders often sit in a storage yard for significant periods of time, this measurement provided a means of quantifying the growth of camber over time. A comparison of this nature could provide useful correlations to long term behaviors, such as creep and shrinkage of the concrete.

A detailed description of the survey results is not included in this thesis, as it was primarily the focus of other researchers.

4.5. Cylinder Temperature/Maturity Measurement

Temperature corrections proved to be an important part of this project. VWSG readings needed to be corrected for temperatures, camber measurements needed to be corrected for temperatures, and temperature corrections were useful for adjusting concrete tests and ages for more consistent relationships.

In order for the TTFM and EAM to be used (see Section 2.3.1), it is necessary to have consistent, continual temperature records of the concrete in question. The in-plant cylinder temperature/maturity monitoring plan was designed to provide these records. Monitoring and curing the cylinders and girders allowed correlation of strength and modulus of elasticity test results between the cylinders and the girders, taking into account possible differences in concrete maturities.

The primary means of measuring temperature histories for testing cylinders was through the thermocouple cylinders produced, cured, and stored as described in Section 4.3. One such thermocouple cylinder, capped and ready to be plugged in, is shown in Figure 4.18.

Figure 4.18: A Thermocouple Cylinder, Ready for Connection

These thermocouple cylinders were usually wired into a series of maturity meters—devices designed to measure temperatures at regular intervals and calculate different maturity factors based on those measurements. Occasionally, however, all available maturity meters were in use, and the thermocouple was wired into the same data collection system as all of the VWSGs and thermocouple array wires. In either case, this first connection was only used up until the point of prestress release.

The VWSGs and thermocouple array wires were connected into a data acquisition system box that contained a variety of measurement devices, which may be seen in Figure 4.19. This

box contained a CR1000 datalogger, three multiplexers, and a battery system.

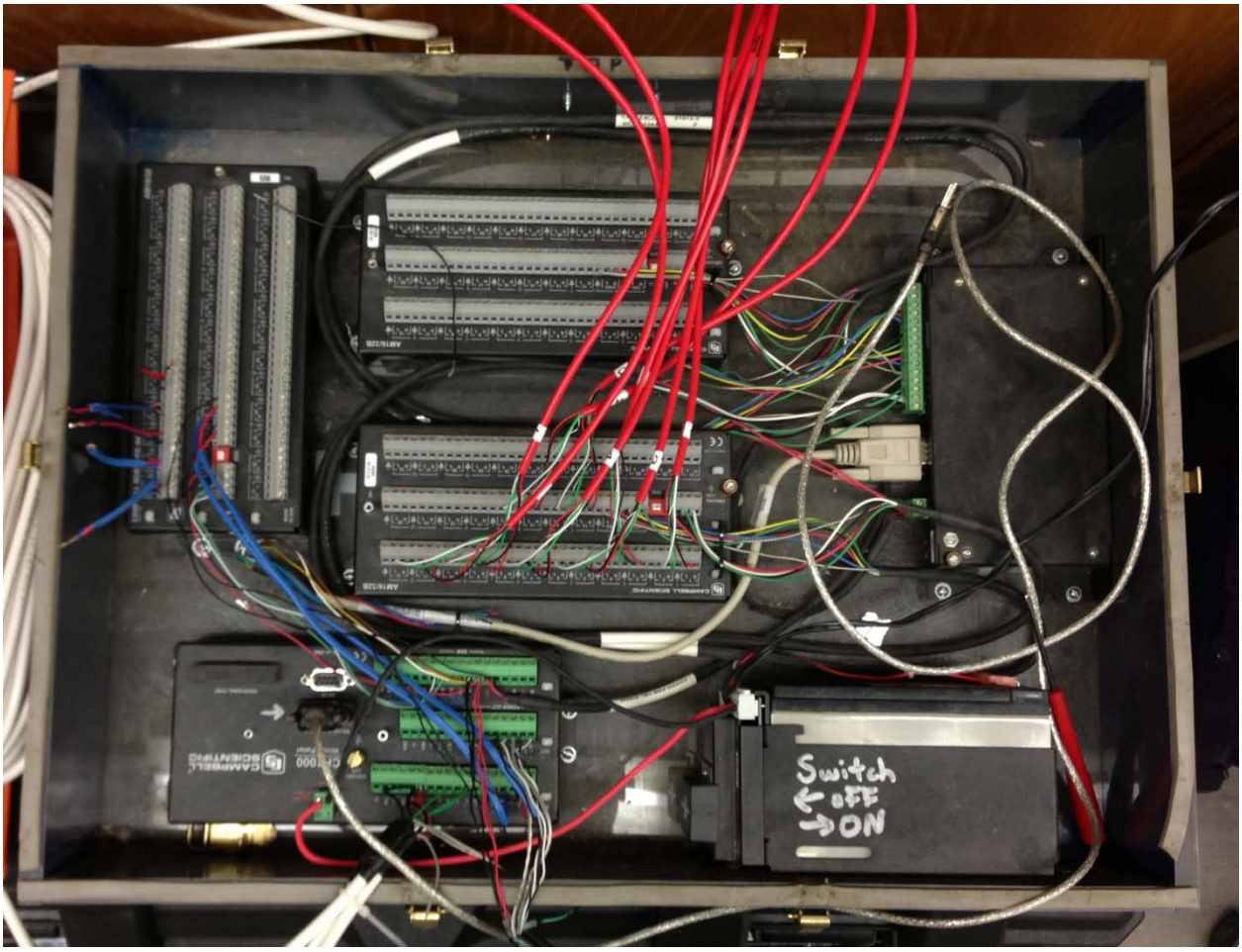

Figure 4.19: Measurement Devices of the Data Acquisition System

During initial curing, the thermocouple cylinder was stored under the tarp with the other cylinders. However, the thermocouple wire running from this cylinder connected to a measurement device that sat outside of the tarp to prevent damage from elevated temperatures and high humidity. Whichever device the thermocouple cylinder was connected to, its temperature was recorded at regular time intervals of 30 minutes or less. The ambient temperature of the air and the temperature of the air under the tarp were also measured during

this time.

When cylinders were demolded and moved to the lime bath as described in Section 4.3, the thermocouple cylinder was also demolded and submerged in the lime bath. At this point, it was disconnected from the previous means of measuring temperature and was connected to a second maturity meter which regularly measured the cylinder temperature, shaded ambient air temperature, and temperature of the water in the lime bath. This system was maintained until the cylinders were transported to AUHRC facilities. Upon arrival at least one thermocouple cylinder was submerged into the outdoor lime bath and was wired to a third maturity meter that regularly measured cylinder temperature, shaded ambient air temperature, and lime bath temperature.

Once the cylinders had been tested, segments from each of the three recording devices were combined to create a consistent, continuous temperature history for any given cylinder set from the time it was produced to the time it was tested. Thus, the tests of each cylinder set could be compared not just to its chronological age, but also to its equivalent age, for the possibility of establishing relationships. More detailed discussions of the EAM and the effects of analyzing concrete in terms of equivalent age may be found in Section 2.3.1 and in Chapters 5, 6, and 7.

4.6. Summary

The experimental design was meant to control every aspect of in-plant testing to ensure that the results were representative of plant practice, yet provided very detailed information about all aspects of the process. Girder instrumentation allowed examination of the internal strains and temperatures of a girder. Temporary girder instrumentation for the 24-hour test provided the ability to watch camber growth and girder end rotation with a full diurnal cycle.

Material testing allowed measurements of strength and modulus of elasticity at release

and 28-days, with an intermediate point for comparison and use in growth curve evaluation. Cylinders were cured to match the exposure conditions of girder concrete, for better correlation to actual girder behavior. Temperature of the cylinders was closely monitored all the way through testing for accurate calculation of temperature-adjusted concrete ages.

Lastly, camber measurements with total station and prism rod were performed at various times in the life of the girder. The first three measurements took place in close proximity to the release of prestressing force, allowing better understanding of instantaneous deflection. Subsequent measurements allowed examination of camber growth over time, for correlation with later research into the shrinkage and creep of girder concretes.

Chapter 5: Collection and Summary of Raw Historical Plant-Submitted Data

5.1. Introduction

This chapter details the collection and analysis results of the historical plant-submitted data as described in Section 1.3, Task 3. This task was the primary component involved in the accomplishment of Objective 2 from Section 1.2. By analyzing plant-submitted data from different plants, for a period of up to six years, researchers intended to obtain results that would be applicable to ALDOT girder designers and producers for the full spectrum of strength ranges, weather conditions, and girder designs. Plant data primarily consisted of fresh concrete properties, cylinder compressive strength values at prestress release and at 28 days, and curing information or mixture designs when available.

5.2. Collection and Organization of Historical Plant-Submitted Data

Collection of the historical plant-submitted data (hereafter, the historical data) took place at the same time as the preliminary plant visits described in Section 3.1. Most plant records were kept in paper form, organized by project number into folders housed in filing cabinets or boxes on site. Researchers from the AUHRC traveled with a flatbed scanner, a feeding scanner, and two private laptop computers for recording data. The feeding scanner was used as the primary scanner when possible.

Each plant provided an area in which the equipment could be set up and data could be scanned. Whenever a set of records was in a format that could easily be fed into the primary

scanner, it was chosen to use this method. This was much more efficient than using the flat scanner, since the pages could be nearly continuously fed into the scanner. As such, even records that were stapled or paper clipped together were run through this feeding scanner, with considerable care taken to ensure that records were put back together in the same order and groupings in which they were found. Only when data were not readily scannable through the feeding scanner was the flat scanner used. When it was available without interfering with plant operations, a large scanner/printer belonging to each plant was also used, and the digitized records were then transmitted via e-mail. This primarily took place after working hours, when office personnel had gone home, due to efforts at minimizing interruption to plant operations.

In this way, historical data were obtained from each of the four plants. This data usually consisted of the following elements:

- Project Information, including
    - Project numbers and counties;
    - Girder lengths and types;
    - Specified release and 28-day strengths, f'_{ci} and f'_c; and
    - Girder production dates.
- Conditions and fresh concrete properties for each concrete placement and sampling location, including
    - Slumps,
    - Air contents,
    - Ambient air temperatures,
    - Fresh concrete temperatures, and
    - Concrete unit weights, occasionally.

- Concrete mixture used for the pour, with the mixture defined by a plant-specific name (not the ALDOT designation).
- Measured cylinder compressive strengths at the time of prestress release and at 28 days. Occasionally, intermediate strength results were also included. These usually consisted of 7-day tests, but other times were also included.
- Prestressing strand force and elongation predictions and measurements.
- Curing temperature records for the girder or cylinders produced.

Not only was this information obtained from the plant records, but it was also obtained from ALDOT records kept on site. This added a level of redundancy and comparability, and allowed misplaced data to be filled in from corresponding records.

ALDOT records were entirely consistent from plant to plant—always organized the same way, with information readily available and easy to find. Detailed information was stored for up to five years in folders/binders on site, which contained information on material specifications, mixture approvals, concrete placement and strength test records, shipping records, and any repair or special circumstances that occurred. Less detailed information on these pours was kept in bound logbooks. These logbooks contained a summary of pertinent information, including fresh concrete properties, cylinder test records, ambient conditions, records of responsible parties, and the girder numbers produced in each pour. When ALDOT records were used to supplement plant-submitted records for the historical data analysis, these books were the primary source of information.

Plant records were not quite as consistent between plants. However, they contained the same basic information. Fresh concrete properties, pour numbers and dates, ambient conditions, prestressing strand stressing measurements, cylinder test results, temperature records, and

mixture designs were among the commonly contained information.

Temperature history data for each pour were particularly varied in consistency and in the methods used to measure them. First of all, the history was not always available for each pour. Furthermore, different plants kept records of different things. Some temperature history recordings showed the history of temperatures at the location of the test cylinders, with the thermocouple simply exposed to the air under the tarp. Other recordings showed the temperatures under the tarp at the location of the exposed deck-connection reinforcing steel above the girder, with the thermocouple tied between two adjacent bars. Still other recordings showed temperatures of a thermocouple embedded a specific distance into the girder concrete itself. Thus, these temperature histories were not necessarily directly comparable between plants. Furthermore, only a limited number of the temperature histories (namely, those which measured temperatures at the location of the test cylinders) were applicable to cylinder equivalent age calculations.

Temperature records were also stored differently. Some plants stored them on circular graphs, such as the one shown in Figure 5.1. Other plants created a normal, rectangular graph. Yet another plant stored its temperature histories in tabular form, with times and temperatures written side by side.

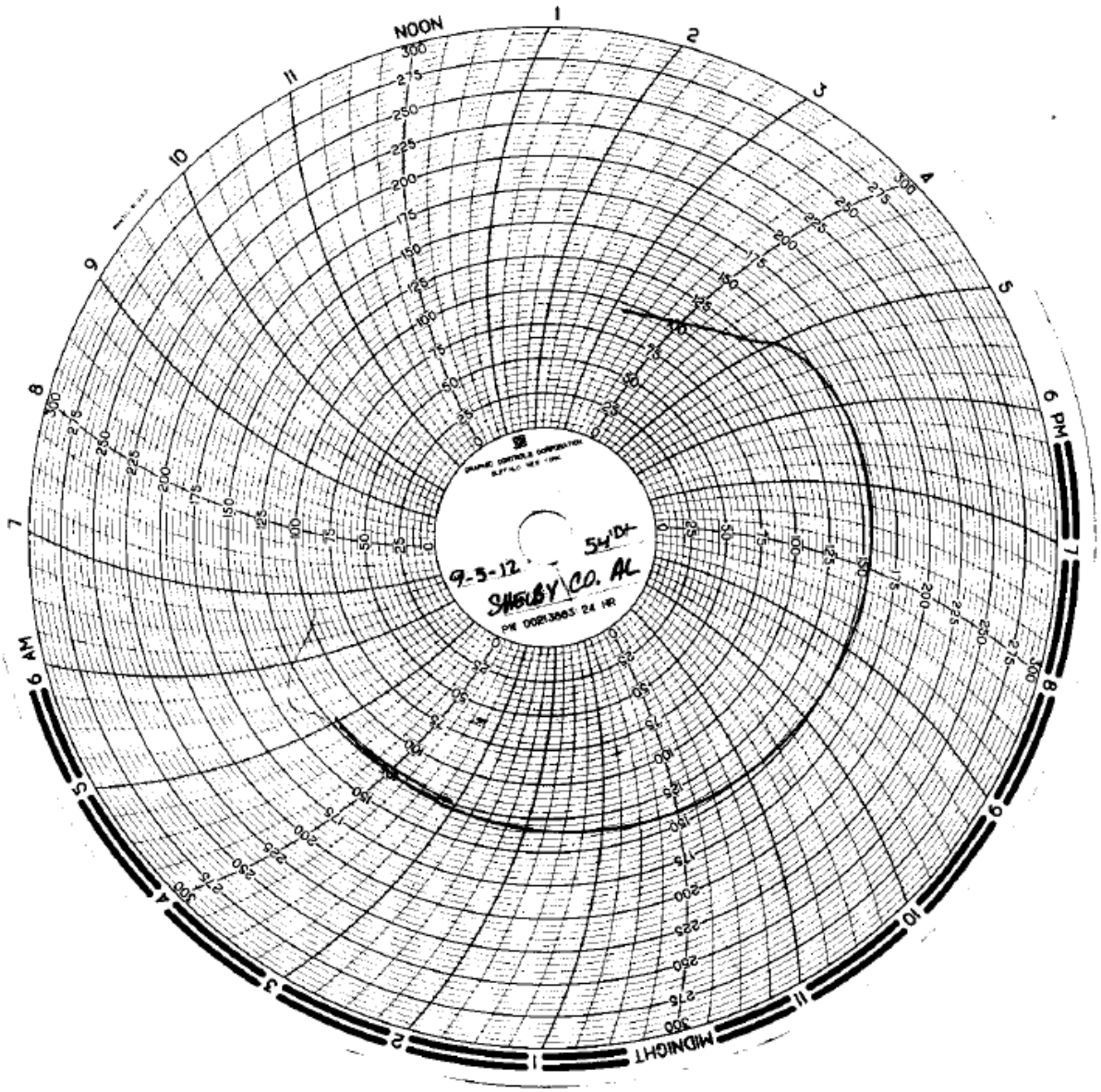

Figure 5.1: Example Circular Temperature Graph from Plant A

In any case, the diversity of plant records, the differences between plants, and the scanning methods used to obtain these records necessitated that the records be compiled by hand into a useful form for analysis. Thus, after scanning had been completed and data had been organized for easy access, all applicable records were input into a large computer database by hand. By the time record input had been completed and before data were eliminated based on

missing data components or suspected inaccuracy of the data, this database contained some estimated 10,000 cylinder test results, representing approximately 1900 girder pours. These pours occurred during the period from the end of the year 2007 until the data collection took place in 2013. The first version of the database consisted primarily of the following information:

- Producer and producer project number
- ALDOT project number
- Pour number and batch time
- Girder type and length for each pour
- Specified release and 28-day strengths, f'_{ci} and f'_c
- Measured slump for each cylinder set (or measured slump flow spread, where applicable)
- Measured air content for each cylinder set
- Measured unit weight, when provided
- Ambient air temperatures and fresh concrete temperatures
- Date and time of release cylinder tests, intermediate cylinder tests, and 28-day cylinder tests
- Calculated chronological ages for each cylinder at the time of testing, based on the above dates and times
- Weather conditions, when provided
- Mixture used for the pour, when provided

Later versions added several components, including the following:

- ALDOT mixture delineation
- Specific mixture proportions for the mixture used in each pour
- Calculated strength ratios, strength arithmetic differences, and percent increases for each

pour—based on comparisons to the specified strengths

- Predicted modulus of elasticity values based on the equations discussed in Section 2.2
- Temperature histories and calculated equivalent ages for each pour, when available
- Graphs and tables organizing and visualizing the data

The following sections in this chapter describe the specific analyses that were performed, and the findings discovered, using the data in this historical database.

Later, certain data entries were discarded. The two primary reasons for discarding data were because of the incomplete nature of the data or because of the unreliable nature of the data. Some pours contained only part of the information required for adequate analysis and comparison with other data. Examples include a missing air content measurement, or no recorded 28-day strength measurements, etc.

Data were deemed unreliable for a variety of reasons. First, due to the nature of the records themselves, the data were sometimes unreadable. Whether the handwriting was illegible, or the records sheet had been dirtied, or a poor scan was made, such data were discarded if it could not be ascertained with certainty what the data were. Furthermore, if there was no means of correlating the data with known facts about the pour, it was discarded. For example, sometimes temperature records for a given pour were provided, but with times and dates that did not in any way match with the time and date at which the pour took place. Because this temperature record could not be reliably matched with actual pour information, it was not used.

Analysis of the data began after all unusable data had been eliminated. For most analyses, the entire data set was used. However, for certain analyses, it was required to reduce or limit the data set to only that data which contained applicable information. The primary instance of this is explained in Section 6.5.

5.3. Range of Historical Data

The first and most preliminary analysis researchers performed was simply a survey of the range of all collected data. This survey included

- Release ages,
- Air contents,
- Slumps,
- Girder lengths,
- Air temperatures
- Concrete temperatures
- Specified strengths, f'_{ci} and f'_c, and
- Measured strengths, f_{ci} and f_c.

The summary of this data survey may be seen in Table 5.1, which includes all data from every plant included in this study. A similar summary table may be seen for each individual plant in Appendix A.

Table 5.1: Range of Plant-Submitted Data

Plants A, B, C, and D	10^{th} Percentile	Sample Mean, $\bar{x}$	90^{th} Percentile	Mode	Sample Standard Deviation, s	C.O.V. (%)
Specified Release Strength (psi)	5000	5835	6530	6000	754	12.9
Measured Release Strength (psi)	6480	7660	9020	7620	980	12.8
Specified 28-Day Strength (psi)	6000	6742	8000	7000	738	10.9
Measured 28-Day Strength (psi)	9250	10,590	11,850	10,650	1000	9.44
Air Content (%)	2.5	3.3	4.2	3.0	0.66	20.
Slump (in.)	7.5	8.5	9.0	9.0	0.69	8.1
Release Age (days)	0.63	1.04	2.70	0.82	0.8	72.4
Air Temp (°F)	50	73	92	90	16	22
Concrete Temp (°F)	66	80	91	90	10	12
Girder Length (ft)	48.6	95.9	134.4	99.2	31.6	32.9

5.4. Release Ages

Release ages were calculated by taking the recorded date and time at which the testing of release cylinders took place, and subtracting the recorded date and time at which the cylinders were produced. Trends in these release times were then analyzed for the entire reduced data set, and then also for data from each plant individually.

A histogram of chronological ages at the time of prestress release for the full data set may be seen in Figure 5.2. Two significant peaks occur in this histogram, which demonstrate the two usual situations in which girder production and release take place.

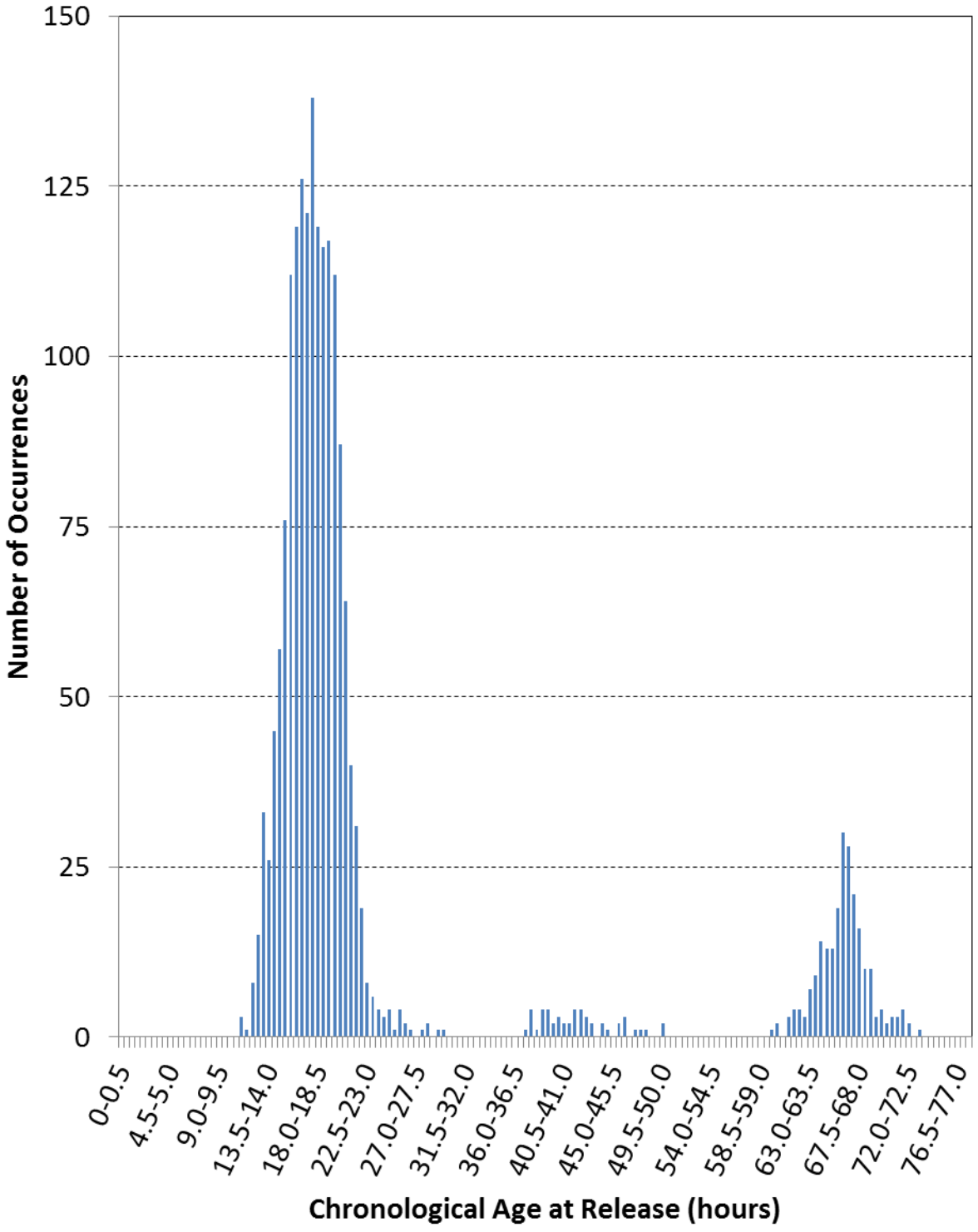

Figure 5.2: Full Histogram of Release Ages for All Plants

The first and primary peak occurs around the age of approximately 18 hours, which is representative of standard plant practices. Concrete is often placed during the late morning or early afternoon, with the intent to transfer prestress in the girders very early the next morning. Statistically, this time averages out to approximately 18 hours after the pour.

However, the secondary peak in the histogram represents a different set of pours—namely, non-standard pours which take place on Fridays. Plants often treat a Friday pour the same way as any other pour, and bring in a limited team on Saturday to release and move the girders at approximately the same time as any other day. However, this is not always the case. An often-seen alternative is that the plant produces the girders on Friday, leaves the girders in their formwork through the weekend, and then releases the prestressing strands early on the following Monday morning. Not coincidentally, the secondary peak centers on this release time of 66 hours.

Similar trends are seen in the histograms of chronological age at release which occur by splitting the data up according to the plant from which it was collected. The histograms of chronological age at release for Plant A, B, C, and D, may be see in Figures B.1, B.2, B.3, and B.4, respectively. The trends appear to be weaker for Plants C and D, which were also the plants for which the least number of data were available. Plant A, from which the most data was collected, shows trends nearly identical to the trends for the overall data set shown in Figure 5.2.

However, for more direct comparison between plants, it is useful to express these graphs in terms of the percentage of occurrences over each interval. Therefore, the histograms of release ages for the full data set and Plants A, B, C, and D are expressed as percentages of their respective data sets in Figure 5.3, B.5, B.6, B.7, and B.8, respectively. A version of Figure 5.3 showing the cumulative percentage of release age occurrences may be seen in Figure 5.4.

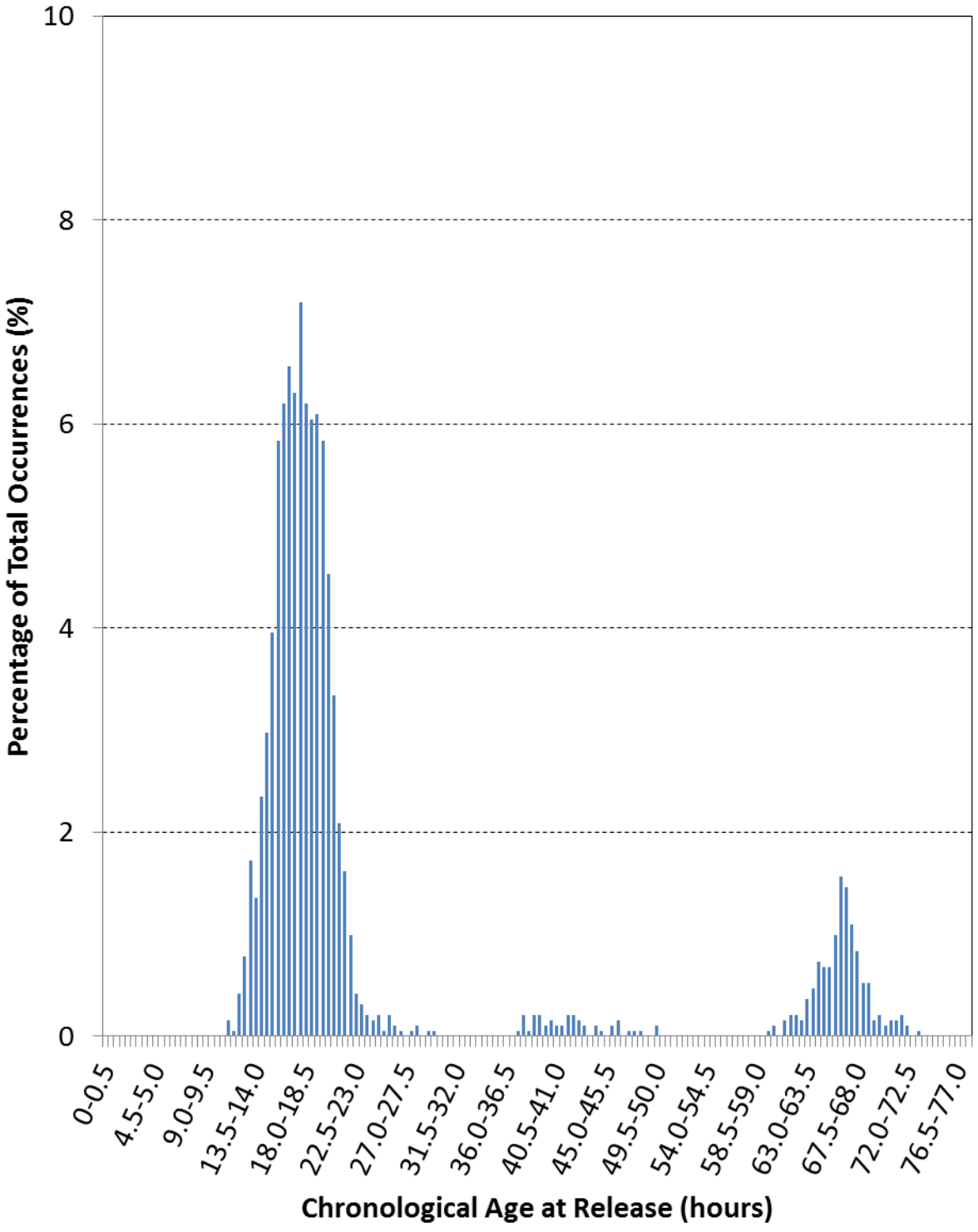

Figure 5.3: Normalized Histogram of Release Ages for All Plants

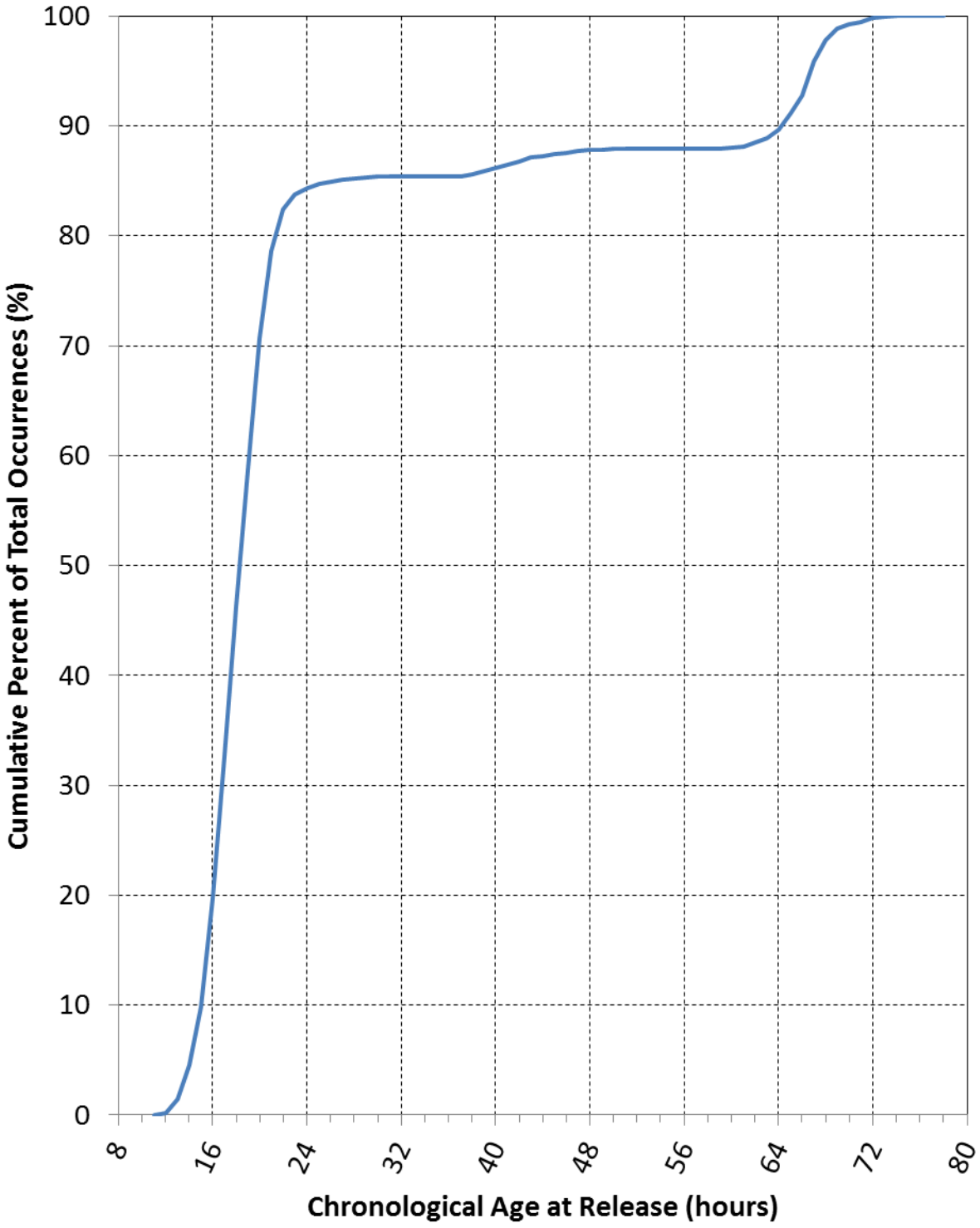

Figure 5.4: Cumulative Frequency Distribution of Release Ages for All Plants

Lastly, some plants show a noticeable, but not highly common, spread of data points outside of the two peaks described above. While a number of factors may contribute to this larger spread, the most probable and common cause is the delay of prestress transfer due to inadequate cylinder strength tests. Section 3.2.3 describes the process by which girder producers test their cylinders in order to ensure adequate strength for prestress transfer. As described there, when the strength tests are not sufficient, the plant allows the girders to remain in the formwork for continued curing. Only when sufficient strength has been reached are the forms removed and the prestressing strands cut. Thus, some release times spread out between the two peaks or beyond the secondary peak of the histogram, simply because the time of release was delayed in order to obtain adequate release strength. This is the most probable cause and explanation of the alternate release times.

The practices of weekend pours and delaying release for adequate strength shift the mean time of release away from the mode time of release. Under conditions of a perfectly normal distribution, one would expect the mean time and the mode time to be exactly equal. However, because of the secondary peak in release time occurrences, the mean value shifts to a higher number, while the mode stays at the primary peak. This difference may be seen in Table 5.2, which summarizes the statistical analysis of release times for each of the plants.

Table 5.2: Statistical Summary for Full Release Times Data Set

	Full Data Set	Plant A Only	Plant B Only	Plant C Only	Plant D Only
Number of Values	1919	1155	430	124	210
Sample Mean, $\bar{x}$ (hrs)	25.1	24.1	21.9	29.7	33.8
Sample Mode, Mo. (hrs)	17	18	16	14	17
Sample Standard Deviation, *s* (hrs)	18.1	16.3	15.1	26.4	23.9
Skewness Check, $\sqrt{\beta_1}$	2.47	2.43	2.52	2.81	1.20
Kurtosis Check, β_2	9.69	7.58	14.5	12.7	3.55

The skewness and kurtosis checks, which are both described by Cook (1989), aid in understanding the differences between the distribution of actual release ages as compared with a normal distribution. The skewness check, labeled as $\sqrt{\beta_1}$, is a measure of the symmetry of a set distribution. It may be calculated using Equation 5.1, shown below (Cook 1989):

$$\sqrt{\beta_1} = \frac{\frac{\Sigma(x-\bar{x})^3}{n}}{s^3} \qquad \textbf{Equation 5.1}$$

where:

$\sqrt{\beta_1}$ = value used for skewness check

x = any individual data point

$\bar{x}$ = sample mean

n = number of data points contained in the set being analyzed

s = sample standard deviation

If the value of $\sqrt{\beta_1}$ is equal to 0, then the data set may be said to be symmetrically oriented about the mean, as a perfectly normal distribution would be. On the other hand, if $\sqrt{\beta_1} < 0.0$, it means that the mean value of the data set is smaller than the mode value of the data set. In other words, if $\sqrt{\beta_1} < 0.0$, the data would appear to be more spread toward the lower end of the distribution

than the higher end. Likewise, a value of $\sqrt{\beta_1} > 0.0$ indicates that the mean value is higher than the mode value, or the data would appear to spread out toward the higher region.

The kurtosis check, defined as β_2, is a measure of the "peakedness" or "flatness" of the distribution. It may be calculated using the equation shown here (Cook 1989):

$$\beta_2 = \frac{\frac{\Sigma(x-\bar{x})^4}{n}}{s^4} \qquad \textbf{Equation 5.2}$$

where:

β_2 = value used for kurtosis check

x = any individual data point

$\bar{x}$ = sample mean

n = number of data points contained in the set being analyzed

s = sample standard deviation

This measure is unrelated to the Skewness check above, though they are both calculated in a very similar manner. If $\beta_2 = 3.0$, then the data set may be identified as having a "flatness" exactly identical to that of a perfectly normal distribution. If $\beta_2 > 3.0$, the data set exhibits a higher "peakedness" than a perfectly normal distribution, meaning that a histogram curve produced using the data set would tend to me more narrow and tall. A histogram curve produced using a data set that exhibited $\beta_2 < 3.0$, or more flatness than a perfectly normal distribution, would tend to be a shorter and broader curve.

Several statistical trends should be noticed from Table 5.2. First, it may be seen that the mean age of each data set is substantially higher than the mode age for that set. In the case of Plants C and D, the mean age approaches up to approximately double the mode age. Row 6 in Table 5.2 which shows that $\sqrt{\beta_1} > 0.0$ for each set of data analyzed, indicating that the data set

is skewed toward the higher values. Thus it is clear that the release age data set is not normally distributed when all data are considered.

In case the skewness results were not enough, the kurtosis results also indicated the abnormality of the data set. The fact that $\beta_2 > 3.0$ for each data set considered shows that, given the wide spread of release age values found at each plant, the primary peak for each plant is much higher than would be expected from a perfectly normal distribution.

The mean release age, $\bar{x}$, for each data set shown in Table 5.2 also raises difficulties when compared to standard plant practices. It was clearly stated and demonstrated during plant visits that the most common range for release ages was between 15 hrs and 21 hrs. Each $\bar{x}$ value shown in Table 5.2 clearly falls outside of this range, indicating that the mean age was not within range of common plant practices. Basing findings or predictions on such a mean value that is unrepresentative of practices in the industry would be irrational. The mode for most data sets, however, very nicely fell within the expected range of standard release ages, confirming the information found in each plant visit.

Lastly, the large sample standard deviation, s, for each data set compared to the sample mean for that set indicates a highly abnormal distribution. This, combined with the high mean-to-mode ratio, high $\sqrt{\beta_1}$ values, high β_2 values, and high $\bar{x}$ values, all suggest that an alternate system of analysis would be reasonable and justified. Thus, it was decided to split the release age data set into 2 primary groups. The first group, called the primary group or the primary peak, consisted of "standard pours"—those data points that lay within the most standard plant practice schedules. As described in Section 3.2, girder producers usually place concrete anywhere from the early morning to the midafternoon, with the express goal of releasing the prestressing strand early in the morning of the next day. Concrete is never placed as early in the morning as the

strands are released, so a reasonable cut-off point for the first release age data set was set at 24 hrs. Therefore, the primary group consisted of all release ages falling between 0 hrs and 24 hrs, inclusive.

The second group, also called the secondary peak, consisted of the fairly common though not standard instances in which the girders were produced on a Friday and were not released until the following Monday morning. Again, the maximum time that needed to be considered for these pours was an age of 72 hours, because concrete is never placed earlier in the morning than the strands would be cut on a Monday morning. The lower bound of the secondary peak was set at 58 hours by considering common plant practice of avoiding concrete pours on late Friday afternoons. If strands of a weekend pour were to be cut at 5:00 AM on the following Monday morning, a lower limit of 58 hrs for the data set would allow the concrete pour to occur as late as 7:00 PM Friday evening. Since plant practice was never to place concrete this late, this provided a conservative lower bound time estimate for capturing weekend pours into the second data set. Thus, the second group contained all release ages falling between 58 hrs and 72 hrs, inclusive.

It should be clarified that, although the second data set is referred to as “weekend pours,” not all Friday pours were included in this data set. Only those girders which were left in the forms until the following Monday were included in the second group, representing the secondary peak. Girder producers would frequently produce girders on a Friday, but still bring in a team of workers to release the prestressing on Saturday morning. These situations would still be included in the primary group, representing the most standard plant practices.

The results obtained from statistical analysis of the two data groups described above may be seen below. Table 5.3 and Table 5.4 provide a summary of the statistical parameters for the primary data group and the secondary data group, respectively.

Table 5.3: Statistical Summary for Primary Group of Release Times

	All Plants	Plant A Only	Plant B Only	Plant C Only	Plant D Only
Number of Values	1602	1013	373	85	131
Sample Mean, $\bar{x}$ (hrs)	17.7	18.2	16.5	17.3	17.6
Sample Mode, $Mo.$ (hrs)	17	18	16	14	17
Sample Standard Deviation, s (hrs)	2.2	1.9	2.4	3.2	2.2
Skewness Check, $\sqrt{\beta_1}$	0.197	0.138	0.365	0.130	0.375
Kurtosis Check, β_2	2.162	2.501	2.609	1.738	3.313
Percentage of Total Data Set (%)	83.5	52.8	19.4	4.4	6.8
Percentage of Respective Data Set (%)	83.5	87.7	86.7	68.6	62.4

Table 5.4: Statistical Summary for Secondary Group of Release Times

	All Plants	Plant A Only	Plant B Only	Plant C Only	Plant D Only
Number of Values	226	132	38	12	44
Sample Mean, $\bar{x}$ (hrs)	66.2	66.7	64.8	65.3	66.4
Sample Mode, $Mo.$ (hrs)	66	66	63	68	67
Sample Standard Deviation, s (hrs)	2.2	1.9	2.8	2.8	2.0
Skewness Check, $\sqrt{\beta_1}$	0.008	0.673	0.358	-0.076	0.538
Kurtosis Check, β_2	3.223	3.056	2.159	1.419	3.852
Percentage of Total Data Set (%)	11.8	6.9	2.0	0.63	2.3
Percentage of Respective Data Set (%)	11.8	11.4	8.8	9.7	21.0

Dividing the data set into these two groups greatly improved the statistical parameters of each data group. The first noticeable effect from both Table 5.3 and Table 5.4 is the shifting of each $\bar{x}$ value toward the $Mo.$ of the same data set. For example, $\bar{x}$ was approximately 34% larger than $Mo.$ for the data from Plant A before the data were divided. After the division, however, $\bar{x}$ was only 1.1% larger than Mo. for the primary group from Plant A, and only 1.1% larger for the secondary group. In both cases, there is a clear shift of the sample mean toward the sample mode. This trend holds for each of the different data sets.

Secondly, the sample standard deviation, s, for each data set was greatly reduced to a much more reasonable value. Before the division of data, s was a disproportionately large value, representing up to 88% of the value of the mean. This yields statistical results that are too sporadic to be truly useful. For example, even if the data from Plant B were normally distributed (which previous discussion has already shown is not the case), a mean of $\bar{x} = 21.9$ hrs with a standard deviation of $s = 15$ hrs would imply that only 68% of the data points would be found between the ages of 6.8 hrs and 37.0 hrs. This spread of values for such a limited percentage of data is not practically useful.

However, when the data has been analyzed as the primary group and the secondary group, the means and standard deviations become much more reasonable. The primary peak from Plant B, with $\bar{x} = 16.5$ hrs and $s = 2.4$ hrs, would contain 68% of the data between the ages of 14.1 hrs and 18.9 hrs under normal distribution conditions. Likewise, the secondary peak would contain 68% of the data between 62.0 hrs and 67.6 hrs. These distributions are much more useful for analysis than the wide distributions found before the division of data.

Thirdly, division of the data resulted in a dramatic shift toward a more symmetrical distribution for each data set. The full data set exhibited a skewness value, $\sqrt{\beta_1}$, equal to 2.468, indicating a data set strongly shifted toward the right. However, the division of data resulted in a primary peak skewness of $\sqrt{\beta_1} = 0.197$ and a secondary peak skewness of $\sqrt{\beta_1} = 0.008$, indicating a data set that is very slightly skewed to the right and a set that is almost perfectly symmetric, respectively.

Fourthly, the division resulted in values of β_2 for kurtosis that were much closer to a normal distribution than the full data set. This was true for all data sets except for the set from Plant D, which actually changed from $\beta_2 = 3.551$ for the complete set to $\beta_2 = 3.313$ for the

primary peak and $\beta_2 = 3.852$ for the secondary peak. This indicates that the distribution actually became less like a normal distribution when the secondary peak was analyzed by itself for Plant D.

A summary of the changes that occurred to the statistical parameters by division of the data into two groups may be seen in Table 5.5 for the primary peak and Table 5.6 for the secondary peak. Several of the values given in these tables may not be easily deciphered without further explanation, which is provided below.

Table 5.5: Summary of Statistical Changes from Complete Data Set to Primary Peak Set

	All Plants	Plant A Only	Plant B Only	Plant C Only	Plant D Only
Percent Change in Sample Standard Deviation, $\Delta s_{\%}$ (%)	-87.6	-88.4	-83.9	-87.9	-90.8
Percent Change in Sample Mean, $\Delta \bar{x}_{\%}$ (%)	-29.3	-24.5	-24.6	-42.0	-47.9
Percent Shift of Sample Mean, $\bar{x}$, toward Sample Mode, $\Delta \gamma_{\%}$ (%)	-43.2	-32.9	-33.7	-89.2	-95.4
Change in Skewness, $\Delta\left(\sqrt{\beta_1}\right)$	-2.27	-2.29	-2.16	-2.68	-0.83
Percent Change in Skewness, $\Delta\left(\sqrt{\beta_1}\right)_{\%}$ (%)	-92.0	-94.3	-85.5	-95.4	-68.8
Improvement of $\sqrt{\beta_1}$ toward Normality, $\delta(\sqrt{\beta_1})$	0.08	0.06	0.14	0.05	0.31
Change in Kurtosis, $\Delta\beta_2$	-7.53	-5.08	-11.88	-10.93	-0.24
Percent Change in Kurtosis, $\Delta(\beta_2)_{\%}$ (%)	-77.7	-67.0	-82.0	-86.3	-6.71
Improvement of Kurtosis toward Normality, $\delta(\beta_2)$	-2.51	-1.69	-3.96	-3.64	-0.08

Table 5.6: Summary of Statistical Changes from Complete Data Set to Secondary Peak Set

	All Plants	Plant A Only	Plant B Only	Plant C Only	Plant D Only
Percent Change in Sample Standard Deviation, $\Delta s_{\%}$ (%)	-87.7	-88.6	-81.2	-89.6	-91.8
Percent Change in Sample Mean, $\Delta \bar{x}_{\%}$ (%)	164.4	176.4	196.0	119.5	96.2
Percent Shift of Sample Mean, $\bar{x}$, toward Sample Mode, $\Delta \gamma_{\%}$ (%)	-47.0	-33.0	-34.0	-116.5	-99.9
Change in Skewness, $\Delta\left(\sqrt{\beta_1}\right)$	-2.46	-1.75	-2.16	-2.89	-0.66
Percent Change in Skewness, $\Delta\left(\sqrt{\beta_1}\right)_{\%}$ (%)	-99.7	-72.3	-85.8	-102.7	-55.2
Improvement of $\sqrt{\beta_1}$ toward Normality, $\delta(\sqrt{\beta_1})$	0.00	0.28	0.28	0.14	0.45
Change in Kurtosis, $\Delta\beta_2$	-6.47	-4.52	-12.33	-11.25	0.30
Percent Change in Kurtosis, $\Delta(\beta_2)_{\%}$ (%)	-66.8	-59.7	-85.1	-88.8	8.49
Improvement of Kurtosis toward Normality, $\delta(\beta_2)$	-2.16	-1.51	-4.11	-3.75	0.10

Each row of Table 5.5 and Table 5.6 gives some measure of a change in statistical parameters that took place by dividing the complete data set into the primary and secondary peak sets. However, it is first useful to clarify the subscripts that are used in the explanation of Table 5.5 and Table 5.6.

The $\sqrt{\beta_1}$ and β_2 variables maintain their subscripts of 1 and 2 at all times. However, when not contained within those defined variables, a subscript of 1 indicates that the variable belongs to the complete data set, before it was divided. A subscript of 2 indicates that the variable belongs to the divided data set, either the primary peak or the secondary peak,

whichever is under consideration at the time. When equations include the skewness or kurtosis checks, these subscripts are simply added to the existing ones. An example of this is $(\beta_2)_1$, which indicates a kurtosis value for the complete data set, in the same way that $(\sqrt{\beta_1})_2$ indicates a skewness value for one of the divided data sets.

The second row in Table 5.5 and Table 5.6 gives the percent change in the sample standard deviation, $\Delta s_{\%}$. This was calculated using the following equation:

$$\Delta s_{\%} = \frac{s_2 - s_1}{s_1} \cdot 100\% \qquad \textbf{Equation 5.3}$$

where:

$\Delta s_{\%}$ = percent change in the sample standard deviation, %

s_2 = sample standard deviation of the primary or secondary data set

s_1 = sample standard deviation of the complete data set

The highly negative values of this parameter in both tables indicate that dividing the data resulted in two data sets that were much more concentrated about the sample mean. A value of $\Delta s_{\%} = -100\%$, which is the largest (negative) theoretically possible value for $\Delta s_{\%}$, would indicate that the divided data set exhibited no spread whatsoever (i.e., s was reduced by 100%). This result is not truly possible for all practical purposes.

Moving on to the next parameter in Table 5.5 and Table 5.6, the third row gives the percent change in the sample mean, $\Delta \bar{x}_{\%}$, calculated using the following equation:

$$\Delta \bar{x}_{\%} = \frac{\bar{x}_2 - \bar{x}_1}{\bar{x}_1} \cdot 100\% \qquad \textbf{Equation 5.4}$$

where:

$\Delta \bar{x}_{\%}$ = percent change in the sample mean, %

$\bar{x}_2$ = sample mean of the primary or secondary data set

$\bar{x}_1$ = sample mean of the complete data set

The percent change in sample mean, or $\Delta\bar{x}_{\%}$, is not a strictly useful parameter on its own. It is most useful when combined with the next row of data, the percent shift of the sample mean toward the sample mode.

From the rationalization for dividing the data set into two groups, it was expected that the mean strength would drop to a lower value for the primary peak, since the sample mean was pulled higher by the secondary peak values. This expectation was fulfilled, as the large negative percentages in Table 5.5 demonstrate. For example, the sample mean of the data from Plant C was decreased by approximately 42%, from 29.7 hrs in the complete data set to 17.3 hrs in the primary peak group.

Conversely, it was expected that the mean value for the secondary group would be much higher than the mean for the complete data set. This expectation was also fulfilled, as was shown by the large positive $\Delta\bar{x}_{\%}$ values in Table 5.6. For example, the sample mean of the data from Plant C increased by approximately 120%, from 29.7 hrs in the complete data set to 65.3 hrs in the secondary peak group.

However, this data is best combined with the fourth row of the Table 5.5 and Table 5.6. This row shows the percent shift of the sample mean toward the sample mode, or $\Delta\gamma_{\%}$. This parameter gives some comparison of difference between $\bar{x}_2$ and $Mo._2$ compared with the difference between $\bar{x}_1$ and $Mo._1$. It is calculated using the following equation:

$$\Delta\gamma_{\%} = \left(\frac{\bar{x}_2 - Mo._2}{Mo._2} - \frac{\bar{x}_1 - Mo._1}{Mo._1} \right) \cdot 100\% \qquad \textbf{Equation 5.5}$$

where:

$\Delta\gamma_{\%}$ = percent shift of sample mean toward sample mode, %

$\bar{x}_2$ = sample mean of the primary or secondary data set

$Mo._2$= sample mode of the primary or secondary data set

$\bar{x}_1$ = sample mean of the complete data set

$Mo._1$= sample mode of the complete data set

Positive values of $\Delta\gamma_{\%}$ indicate that the discrepancy between the sample mean and sample mode became worse after the data division. Negative values of $\Delta\gamma_{\%}$ indicate that the discrepancy between mean and mode decreased by the data division.

All of the values for $\Delta\gamma_{\%}$ found in Table 5.5 and Table 5.6 are largely negative, indicating that the discrepancies between the means and modes for both of the divided data sets are much smaller than the discrepancy in the complete data set. For example, consider the discrepancy difference from the complete data set of Plant D to the primary peak set of Plant D. For this data set, $\Delta\gamma_{\%} = -95.4\%$, as seen in Table 5.5. This means that $\bar{x}_2$ is approximately 95% closer to $Mo._2$ for the primary peak set than $\bar{x}_1$ is to $Mo._1$. As suspected by this number, $\bar{x}_2 = 17.6$ hrs is very close to $Mo._2 = 17$ hrs, whereas $\bar{x}_1 = 33.8$ hrs is not very close to $Mo._1 = 17$ hrs.

The fifth row of data describes the difference between $(\sqrt{\beta_1})_1$ and $(\sqrt{\beta_1})_2$, or simply $\Delta(\sqrt{\beta_1})$. It is calculated by Equation 5.6.

$$\Delta(\sqrt{\beta_1}) = (\sqrt{\beta_1})_2 - (\sqrt{\beta_1})_1 \qquad \textbf{Equation 5.6}$$

where:

$\Delta(\sqrt{\beta_1})$ = change in $\sqrt{\beta_1}$ from complete set to divided set

$(\sqrt{\beta_1})_2$ = measure of the skewness for the primary or secondary data set

$(\sqrt{\beta_1})_1$ = measure of the skewness for the complete data set

The explanation of $\Delta(\sqrt{\beta_1})$ is fairly straightforward. If $\Delta(\sqrt{\beta_1}) > 0.0$, then division of the data

shifted the distribution to the right. Likewise, $\Delta\left(\sqrt{\beta_1}\right) < 0.0$ means that division of the data shifted the distribution to the left, and $\Delta\left(\sqrt{\beta_1}\right) = 0.0$ indicates that the data maintained the same level of skewness.

The complete data set exhibited $\sqrt{\beta_1}$ values significantly higher than the base value of 0.0, and one goal of dividing the data into two groups was to reduce this skewness (in this case, reduce $\sqrt{\beta_1}$). This goal was accomplished, as evidenced by the large negative $\Delta(\sqrt{\beta_1})$ values shown in Table 5.5 and Table 5.6. The quantification of how large this change was when compared to the original value is given in the sixth row, and the quantification of just how much this improved the skewness of the distribution is given in the seventh row.

The sixth row of data quantifies how large the change in $\sqrt{\beta_1}$ was when compared to the original value. It is called the percent change in skewness, and is defined by the following equation:

$$\Delta\left(\sqrt{\beta_1}\right)_{\%} = \frac{\Delta\left(\sqrt{\beta_1}\right)}{\left(\sqrt{\beta_1}\right)_1} \cdot 100\% \qquad \textbf{Equation 5.7}$$

where:

$\Delta\left(\sqrt{\beta_1}\right)_{\%}$ = percent change in $\sqrt{\beta_1}$ from complete set to divided set, %

$\Delta\left(\sqrt{\beta_1}\right)$ = change in $\sqrt{\beta_1}$ from complete set to divided set

$\left(\sqrt{\beta_1}\right)_1$ = measure of the skewness for the complete data set

The information that could be gleaned from $\Delta\left(\sqrt{\beta_1}\right)_{\%}$ is purely controlled by the values of $\Delta\left(\sqrt{\beta_1}\right)$, which is described above. However, as an example, consider the $\Delta\left(\sqrt{\beta_1}\right)_{\%} = -99.7\%$ value for the secondary peak of all plant data. This comes from $\left(\sqrt{\beta_1}\right)_2 = 0.008$ and $\left(\sqrt{\beta_1}\right)_1 =$

2.468, resulting in a difference of $\Delta(\sqrt{\beta_1}) = -2.46$. This difference is very nearly as large as the original value itself, meaning that this value was reduced nearly 100%. Since the value is reduced, $\Delta(\sqrt{\beta_1})_{\%}$ is negative.

The seventh row of data quantifies just how much skewness of the distribution was improved by dividing the data. The row is defined as the improvement of $\sqrt{\beta_1}$ toward normality. It is calculated using Equation 5.8, shown below.

$$\delta(\sqrt{\beta_1}) = \frac{(\sqrt{\beta_1})_2}{(\sqrt{\beta_1})_1} \qquad \textbf{Equation 5.8}$$

where:

$\delta(\sqrt{\beta_1})$ = improvement of $\sqrt{\beta_1}$ toward normality

$(\sqrt{\beta_1})_2$ = measure of the skewness for the primary or secondary data set

$(\sqrt{\beta_1})_1$ = measure of the skewness for the complete data set

The results from this equation may be split into several zones, as described here:

- If $1.0 < \delta(\sqrt{\beta_1}) < \infty$, then the data distribution was made worse by division of the data. In other words, the data set was more skewed after the division than it was before the division.
- If $\delta(\sqrt{\beta_1}) = 1.0$, then the distribution was skewed just as much after the division as it was before the division. This skewness was not necessarily in the same direction, however.
- If $0.0 < \delta(\sqrt{\beta_1}) < 1.0$, then the distribution was shifted closer to a symmetric distribution by the division of data. In other words, the data set was less skewed after the division than it was before the division.
- Lastly, if $\delta(\sqrt{\beta_1}) = 0.0$, the skewness became exactly identical to the skewness in a

normal distribution by the division of data. In other terms, $(\sqrt{\beta_1})_2 = 0.0$.

Every $\delta(\sqrt{\beta_1})$ value in Table 5.5 and Table 5.6 was a small, positive value less than 1.0, indicating that the skewness was greatly reduced for all data sets by division of the data. For example, the skewness of Plant B was $(\sqrt{\beta_1})_2 = 0.365$ when considering the primary peak and $(\sqrt{\beta_1})_1 = 2.522$ when considering the complete data set, resulting in $\delta(\sqrt{\beta_1}) = 0.14$. One might say that the data division improved the skewness of Plant B data by approximately $\left(1 - \delta(\sqrt{\beta_1})\right) \cdot 100\% = (1 - 0.14) \cdot 100\% = 86\%$ when considering the primary peak. This relationship works as long as the values of $\delta(\sqrt{\beta_1})$ remain positive and between 0.00 and 1.00.

The eighth row of data in each table is very similar to the fifth row, except that it measures the difference in kurtosis instead of skewness. It is defined by the following equation:

$$\Delta\beta_2 = (\beta_2)_2 - (\beta_2)_1 \qquad \textbf{Equation 5.9}$$

where:

$\Delta\beta_2$ = change in β_2 from complete set to divided set

$(\beta_2)_2$ = measure of the kurtosis for the primary or secondary data set

$(\beta_2)_1$ = measure of the kurtosis for the complete data set

Like $\Delta(\sqrt{\beta_1})$, the explanation for $\Delta\beta_2$ is fairly straightforward. If $\Delta\beta_2 > 0.0$, then division of the data caused the distribution to have a more peaked nature. Likewise, $\Delta\beta_2 < 0.0$ means that division of the data flattened out the data, and $\Delta\beta_2 = 0.0$ indicates that the data maintained the same level of peakedness. A flatter distribution indicates that the data is less concentrated about the mean. It was expected that division of the data into two groups would cause each group to appear more peaked than the complete data set. For the most part, this expectation was correct, as is indicated by the negative values of $\Delta\beta_2$ shown for most of the data sets. However, the

secondary peak data from Plant D actually became flatter by the division of data.

The fact that a data set became flatter does not necessarily imply that the data set became less like a normal distribution—it simply indicates that the data set became flatter. If the original set were more peaked than a normal distribution, becoming flatter would actually bring it closer to a normal distribution. Therefore, the $\Delta\beta_2$ value is further quantified by the ninth and tenth rows of each table.

The ninth row parallels the sixth row by quantifying how large the change in $\Delta\beta_2$ was when compared to the original value. It is called the percent change in kurtosis, and is defined by the following equation:

$$\Delta(\beta_2)_{\%} = \frac{\Delta\beta_2}{(\beta_2)_1} \cdot 100\% \qquad \textbf{Equation 5.10}$$

where:

$\Delta(\beta_2)_{\%}$ = percent change in β_2 from complete set to divided set, %

$\Delta\beta_2$ = change in β_2 from complete set to divided set

$(\beta_2)_1$ = measure of the kurtosis for the complete data set

The information that could be gleaned from $\Delta(\beta_2)_{\%}$ is purely controlled by the values of $\Delta\beta_2$, which is described above.

Lastly, the tenth row parallels the seventh row by quantifying just how much kurtosis of the distribution was improved by dividing the data. The row is defined as the improvement of kurtosis toward normality. It is calculated using Equation 5.11, shown below.

$$\delta(\beta_2) = \left|\frac{(\beta_2)_2}{3.0}\right| - \left|\frac{(\beta_2)_1}{3.0}\right| \qquad \textbf{Equation 5.11}$$

where:

$\delta(\beta_2)$ = improvement of kurtosis toward normality

$(\beta_2)_2$ = measure of the kurtosis for the primary or secondary data set

$(\beta_2)_1$ = measure of the kurtosis for the complete data set

The results from this equation may be split into several zones, as described here:

- If $0.0 < \delta(\beta_2) < \infty$, then the data distribution was made worse by division of the data. In other words, a flat data set was made flatter, or a highly peaked set increased in peakedness.
- If $\delta(\beta_2) = 0.0$, then the distribution was peaked just as much after the division as it was before the division.
- Lastly, if $-\infty < \delta(\beta_2) < 0.0$, then the distribution was shifted closer to a normal distribution by the division of data.

It is the $\delta(\beta_2)$ value which demonstrates that the data division made each data set much more normal except the secondary peak set for Plant D. The $\Delta\beta_2$ values from the eighth row showed that the secondary peak from Plant D decreased in peakedness while all the other data sets increased in peakedness. However, only by the $\delta(\beta_2)$ values in the tenth row is it clear that the secondary peak from Plant D became less like a normal distribution, while all other data sets became more like a normal distribution.

It was important that the division of the complete data set into the primary peak group and secondary peak group would not ignore an unreasonable percentage of release ages, so the percentage of data points contained in each peak group was calculated and shown in Table 5.3 and Table 5.4. The primary peak contained a vast majority of collected data, comprising 83.5% of collected data points. The secondary peak contained another sizeable section, with 11. 8% of the data. This confirmed the idea that standard plant practices are adequately captured in the primary peak, but that the rest of the common plant practices are contained in the secondary

peak. Together, these two peaks contain 95.3% of all collected release ages, which is more than enough to justify reasonable statistical summarizations from these groups.

Of course, it could reasonably be expected that delaying girder release an additional 48 hrs, even without continued steam curing during that time, might significantly increase the observed release strengths for that pour. Therefore, a quick statistical check was performed, and it indeed discovered that a higher percentage of the 28-day strength was developed prior to release in secondary peak girders than in primary peak girders. This may be seen in Table 5.7, which provides a simple summary of the mean strengths for the two groups.

Table 5.7: Summary of Comparisons for Release Age Peak Group Strengths

Mean Values	Specified Release Strength (psi)	Measured Release Strength (psi)	Specified Release Strength Ratio	Release / 28-Day Strength Ratio	Specified 28-Day Strength (psi)	Measured 28-Day Strength (psi)	Specified 28-Day Strength Ratio
Primary Peak	5810	7480	1.30	0.71	6720	10,500	1.58
Secondary Peak	5850	8820	1.54	0.83	6730	10,440	1.58

The “specified release strength ratio” is the ratio of the measured release strength to the specified release strength. Likewise, the “specified 28-day strength ratio” is the ratio of the measured 28-day strength to the specified 28-day strength. The “release / 28-day strength ratio” is the ratio of the measured release strength to the measured 28-day strength.

Even though the mean specified release strengths, mean specified 28-day strengths, mean measured 28-day strengths, and mean 28-day ratios are all nearly identical for both peaks, the mean release strength for the secondary peak is 18% larger than the mean release strength for the primary peak. Likewise, the mean specified release strength ratio for the secondary peak is 18%

larger than the mean ratio for the primary peak, and the mean release / 28-day strength ratio for the secondary peak is 17% larger than the mean ratio for the primary peak. From this, it can be concluded that the delay of girder releases over the weekend does indeed increase the measured release strengths of those pours and the percentage of 28-day strength developed prior to release.

5.5. Equivalent Ages at Release

The data set available for equivalent age analysis was much more limited than the set for chronological age at release. This was due primarily to the limited temperature history data available, as well as the questionable reliability of some temperature history data that was available. In the end, a limited set of temperature histories were selected from Plant A, with selection based on the following criteria:

1. The first and primary requirement was that reliable temperature data needed to be available for any pour selected. This factor eliminated a large portion of the data. For many pours, temperature records were simply not available. Furthermore, for several of those pours for which temperature data was available, the temperature data could not be confidently correlated to the pour.
2. Secondly, only pours that followed standard plant procedures were selected. This excluded any pour that was labeled as a “weekend pour” according to the data division described in Section 5.3. Standard pours accounted for a large majority of the data anyway, and focusing on that set of data would provide the most applicable findings.
3. It was also required that the strength records, fresh concrete records, and girder records for each pour be complete. This was instituted so that any findings for equivalent ages could be correlated with other properties if desired.

After the data set had been selected based on these criteria, it consisted of 435 girder pours from Plant A and none from the other three plants.

Calculation of the equivalent age (EA) at release for each pour was conducted based on Equation 2.8, taken from ASTM C1074 (2011). This equation is restated in Equation 5.12.

$$t' = \sum\{\Delta t \cdot e^{\left[\left(\frac{1}{T_a} - \frac{1}{T_s}\right) \cdot \left(\frac{-E}{Q}\right)\right]}\} \qquad \textbf{Equation 5.12}$$

where:

t' = equivalent age of the concrete, hrs

Δt = change in chronological age, or the time increment being considered, hrs

T_a = average temperature during the time increment Δt being considered, K

T_s = specified concrete temperature to which the equivalent age shall be compared, K

E = activation energy, $\frac{\text{J}}{\text{mol}}$

Q = gas constant equal to 8.31 $\frac{\text{J}}{\text{K·mol}}$

The activation energy, E, is known to be highly variable between different concretes. It is primarily dependent on the type of cement used, the presence of SCMs, and the proportions between the two. Based on the work performed by Carino and Tank (1992), E for most concretes ranges somewhere between $30{,}000$ $\frac{\text{J}}{\text{mol}}$ and $65{,}000$ $\frac{\text{J}}{\text{mol}}$. It was decided to use $E = 45{,}000$ $\frac{\text{J}}{\text{mol}}$, which is fairly close to the constant found by Carino and Tank for concretes with Type III cements, for all equivalent age calculations. This value was also used by Kavanaugh (2008) to improve the accuracy of creep and shrinkage predictions using the *CEB-FIP Model Code* (CEB 1990) instead of the assumed value of $E = 33{,}240$ $\frac{\text{J}}{\text{mol}}$. The specified temperature

for the equivalent age method (EAM) was set at 73°F (296 K), because this is considered "room temperature" and is approximately equal to the target curing temperature for standard-cure cylinders (ASTM C31/C31M 2012).

The equivalent age (also referred to as EA) of a concrete pour at the time of testing was calculated by the following procedure:

1. A graph of temperature versus time was acquired for the pour in question.
2. This graph was divided into a number of time increments for the analysis. Most intervals were set at 30 minutes, which provided sufficient accuracy for the purposes of this project. The length of each time increment became Δt for that increment.
3. Using the graph, an estimated temperature was established for the beginning and end of each time increment (T_1 and T_2, respectively). All readings were approximate in nature by necessity, since all records used in the analysis were scanned graphs in paper form.
4. An average temperature, T_{av}, was calculated for each time interval by the following equation:

$$T_{av} = \frac{T_1 + T_2}{2} \qquad \textbf{Equation 5.13}$$

where:

T_{av} = average temperature during the time increment Δt being considered, °F

T_1 = temperature at the beginning of the time increment Δt being considered, °F

T_2 = temperature at the end of the time increment Δt being considered, °F

5. An EA increment for each time increment was calculated using the following equation, which is simply the incremental version of Equation 5.12:

$$\Delta t' = \Delta t \cdot e^{\left[\left(\frac{1}{T_a} - \frac{1}{T_s}\right) \cdot \left(\frac{-E}{Q}\right)\right]} \qquad \textbf{Equation 5.14}$$

where:

t' = equivalent age of the concrete, hrs

Δt = change in chronological age, or the time increment being considered, hrs

T_a = average temperature during the time increment Δt being considered, K

T_s = specified concrete temperature to which the equivalent age shall be compared, K

E = activation energy, $\frac{\text{J}}{\text{mol}}$

Q = gas constant equal to 8.31 $\frac{\text{J}}{\text{K·mol}}$

6. All EA increments were summed together using Equation 5.12, giving the total EA at the time of testing.

It was desired that the reduced data set would cover the full range of seasons and ambient temperatures. This was confirmed by the creation of Figure 5.5, which shows a histogram of the number of pours that occurred during each week of the year. In this graph, weeks are delineated by number. Thus, 1 = January 1st through January 7th, 2 = January 8th through January 14th, etc. The wide range of values indicates that, except for a small segment between 29 and 31 (roughly mid-July through early August), the equivalent age data set incorporates pours from all times of the year.

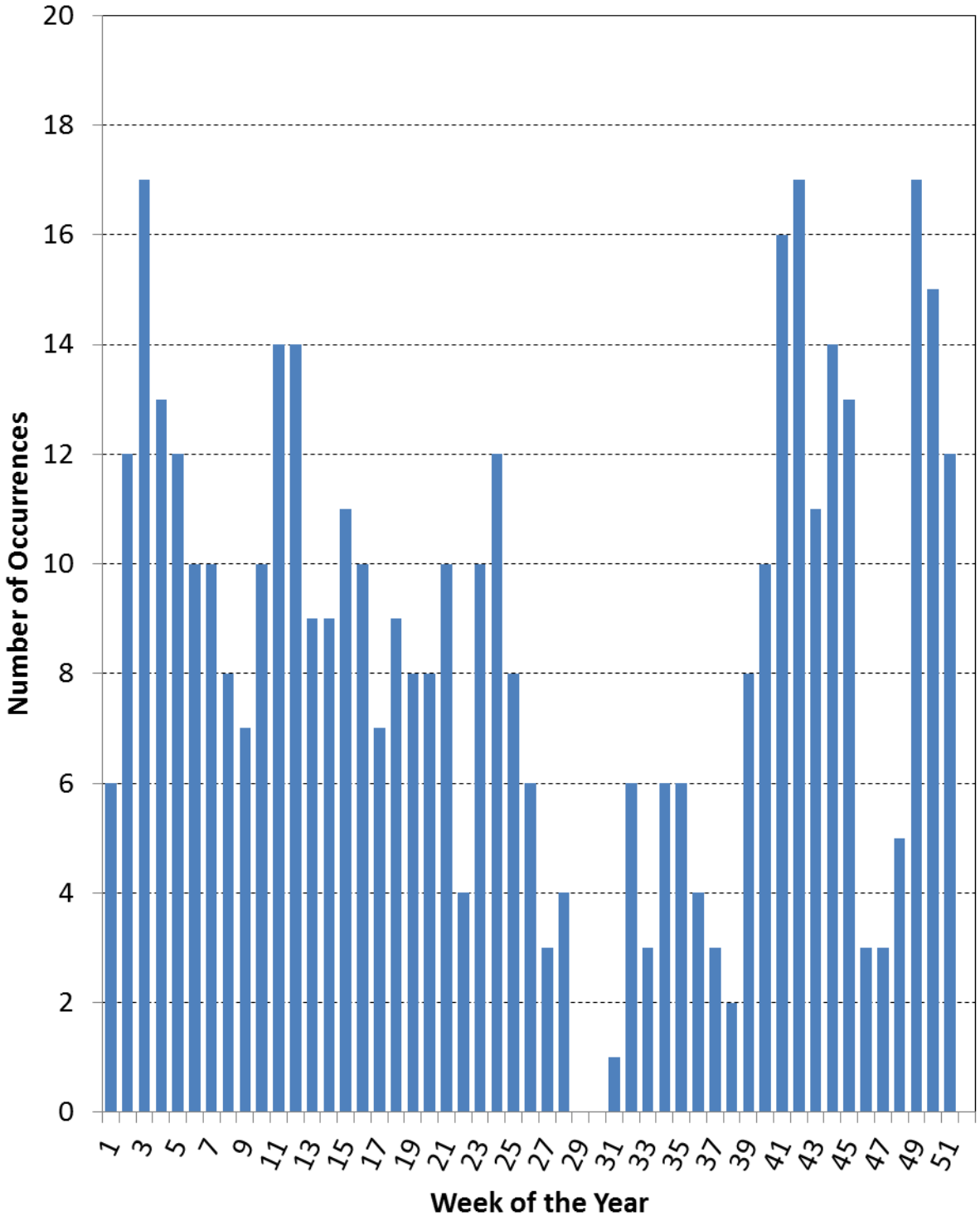

Figure 5.5: Histogram of Girder Pours by the Week of the Year

A histogram of EA values calculated from this data set may be seen in Figure 5.6.

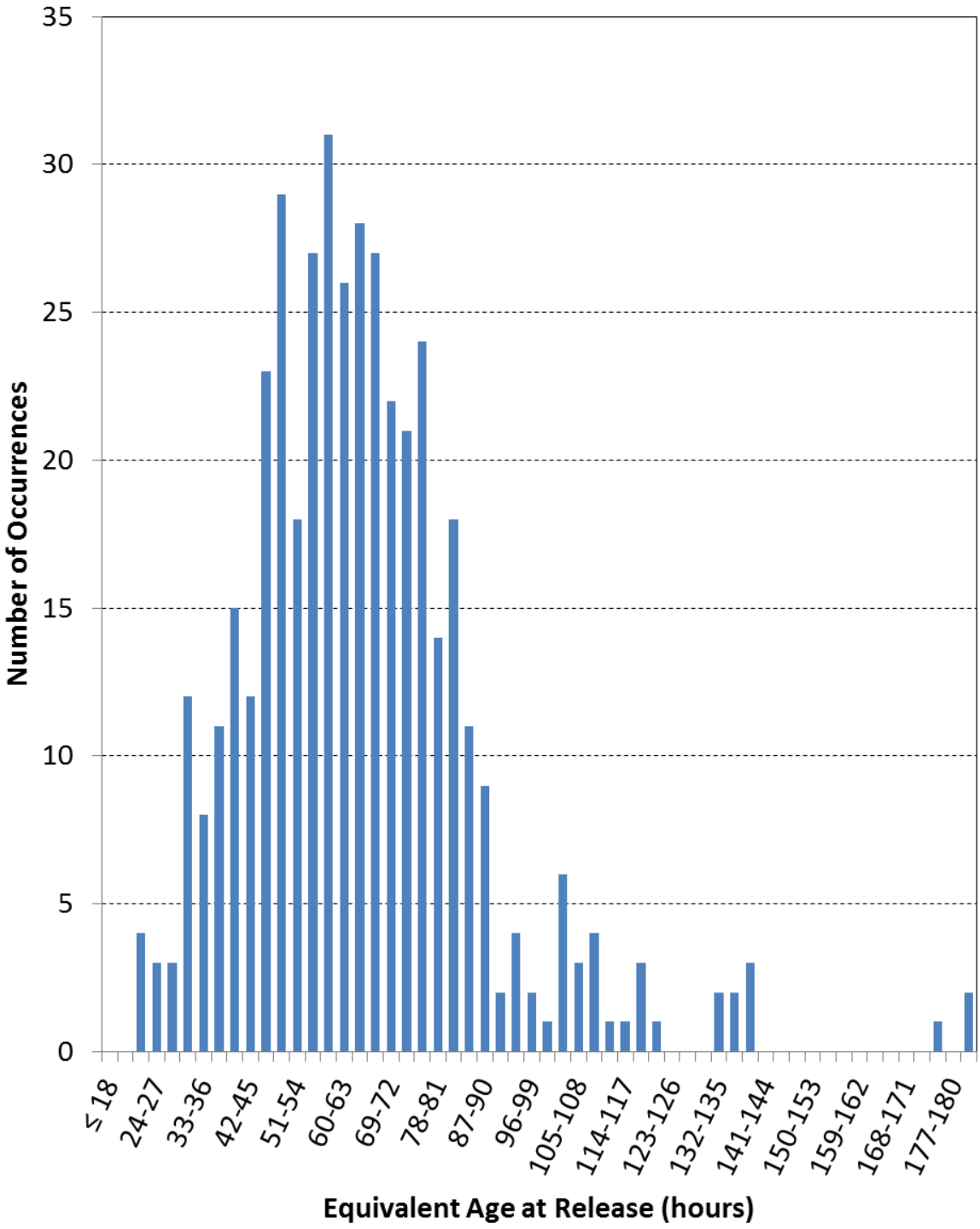

Figure 5.6: Histogram of Calculated Equivalent Ages

Figure 5.6 is expressed as a cumulative frequency distribution graph in Figure 5.7.

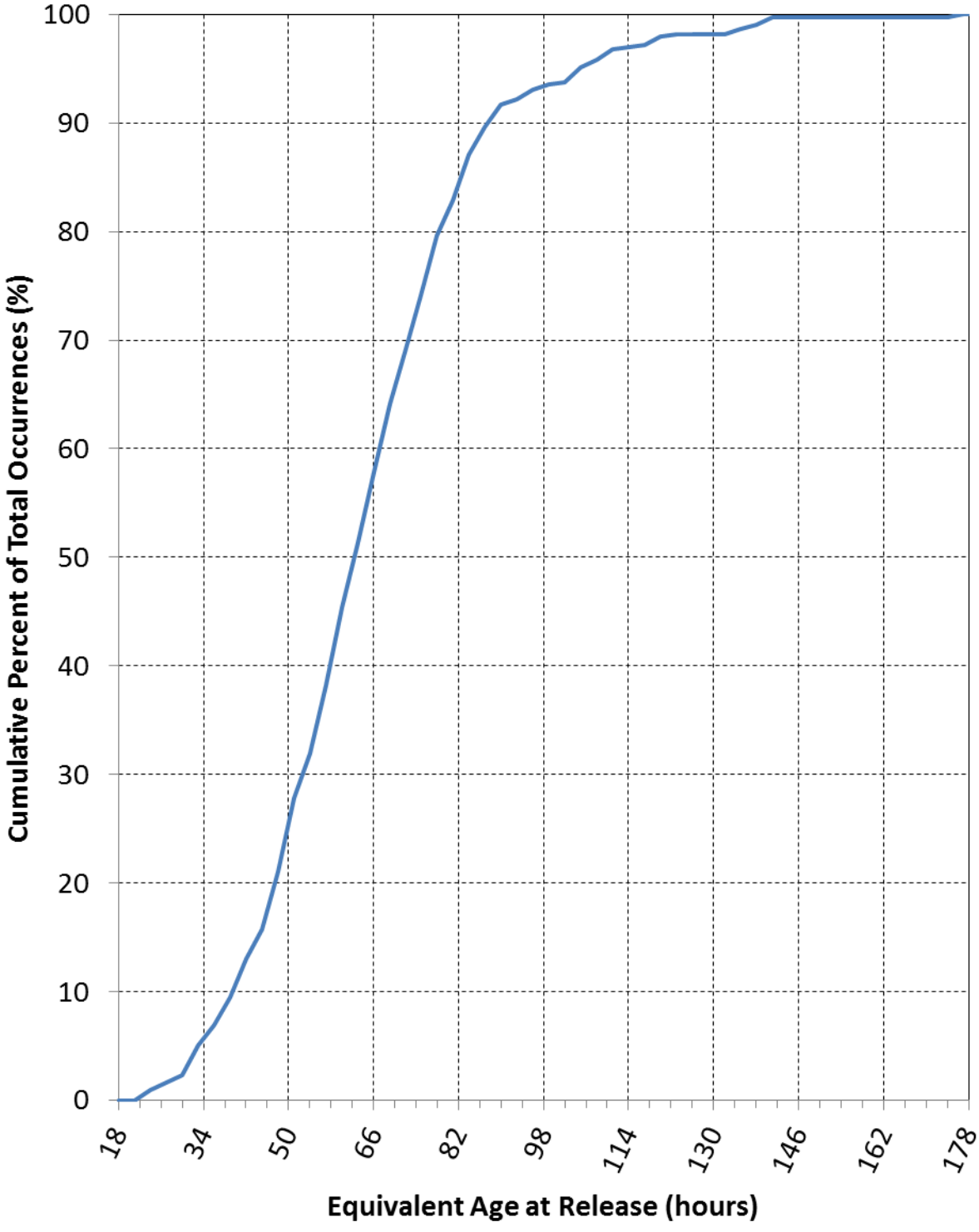

Figure 5.7: Cumulative Frequency Distribution of Calculated Equivalent Ages

From first glance, it would appear that this data set is less coherent than the primary peak data set discussed in Section 5.3. However, statistical analysis is required to confirm this suspicion. Table 5.8 was created to show the statistical parameters of the EA data set. By comparing this table to Table 5.3, it is clear that the distribution of equivalent ages is not nearly as normal as the distribution of the primary peak group.

Table 5.8: Statistical Summary for Equivalent Age Distribution

	All EA Data
Number of Values, n	435
Sample Mean, $\bar{x}$ (hrs)	65.0
Sample Mode, $Mo.$ (hrs)	50
Sample Standard Deviation, s (hrs)	24.4
Coefficient of Variation, COV (%)	37.5
Skewness Check, $\sqrt{\beta_1}$	2.352
Kurtosis Check, β_2	16.652

There is a large discrepancy between $\bar{x}$ and $Mo.$ for the EAs, while the $\bar{x}$ and $Mo.$ for the primary peak of Plant A are almost identical. The coefficient of variation (COV) of the EAs is very large, indicating a wide spread of the data. In fact, it is more than 3.5 times as large as the COV for the primary. Furthermore, $\sqrt{\beta_1} = 2.352$ and $\beta_2 = 16.652$ indicate that the distribution of EAs is highly skewed to the right, and much more peaked than a normal distribution would be.

In fact, based on the statistical parameters alone (with no prior knowledge of the shape of the distribution), the distribution of equivalent age values is much closer to the distribution of the complete data set before it was divided into the primary and secondary peaks than to the primary

peak of Plant A.

The effects on calculated strength growth, or the shift in measured release strengths caused by using equivalent age, are discussed in Section 6.5.

5.6. Air Contents

As discussed in Section 3.3.1, the ALDOT *Standard Specifications for Highway Construction* (2012) call for any concrete mixture to have a target air content of 4.5%, with an acceptable range of 2.5% to 6.0% by volume. Air contents are measured using the ASTM C231/C231M (2010) procedure. Higher air contents are invaluable for increasing freeze-thaw resistance in concrete, among other things. However, a concrete mixture that achieves a low air content will have a higher strength than the same concrete mixture that achieves a higher air content. This relationship between air content and strength for the same concrete mixture is what was used to "adjust" measured concrete strengths for air content, as is discussed in Section 6.3.2. That relationship corresponds to the fact that lower air contents usually imply a lower porosity, which in many instances provides much longer durability for the concrete due to decreased permeability. Thus, there may be incentive for different producers to aim for different air contents.

As such, one of the analyses that were performed was a comparison of the requirements of the *Standard Specifications* to the trends seen in plant practices. This section describes the results of analyzing the data set air contents by themselves, without correlation to other properties. A summary of air content statistical analyses for the full data set and by plant may be seen in Table 5.9, and a histogram of the air contents for the full data set may be seen in Figure 5.8. Plant-specific histograms of air content may be seen in Appendix C.

Table 5.9: Statistical Summary of Air Contents

	Full Data Set	Plant A Only	Plant B Only	Plant C Only	Plant D Only
Number of Values	1916	1156	430	124	206
Sample Mean, $\overline{x}$ (%)	3.3	3.4	3.2	3.6	3.1
Sample Mode, Mo. (%)	3.0	2.5	3.0	2.5	2.5
Sample Standard Deviation, s (%)	0.66	0.68	0.50	0.89	0.58
Coefficient of Variance (%)	19.9	20.1	15.6	24.8	19.1
Skewness Check, $\sqrt{\beta_1}$	0.503	0.421	1.139	0.553	-1.096
Kurtosis Check, β_2	5.604	4.714	4.642	2.342	16.06

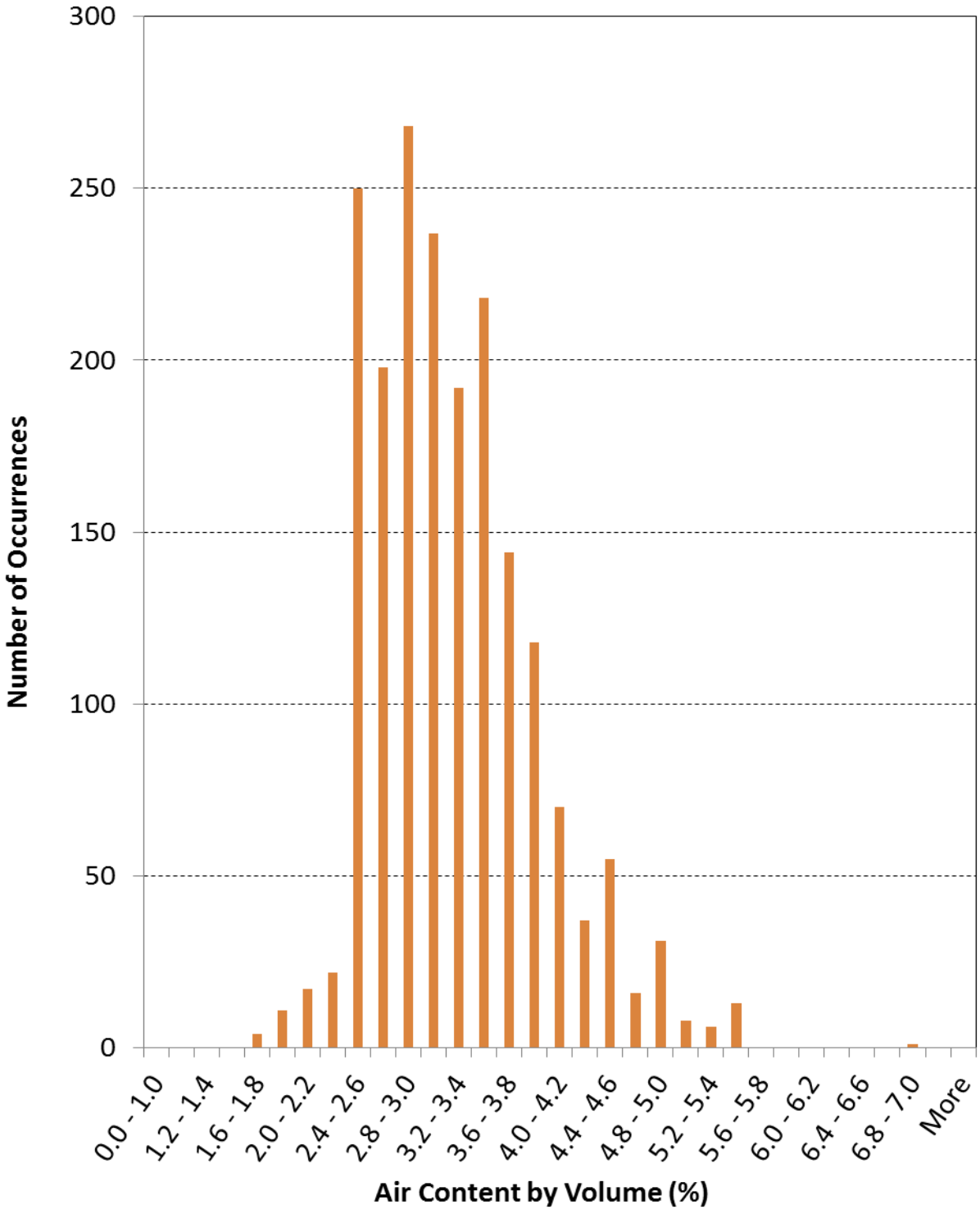

Figure 5.8: Histogram of Air Contents for Full Data Set

Table 5.9 and Figure 5.8 clearly show that air contents for each girder manufacturer do not center on the stated target air content of 4.5% by volume. In fact, the mean air contents are roughly 1% less than the target, and the modes for each data set are between 1.5% and 2.0% below the target. In all cases, the mean air content was higher than the mode air content, which would normally indicate that the data set was skewed to the right. The distribution for Plant D, however, exhibits a distribution that is actually skewed to the left, even though the mean is higher than the mode.

Since the distributions for each data set have a mean and mode well below the target value of 4.5%, it makes sense that the distribution would have a wider distribution toward the higher air contents. It would not make sense for the data distribution to be skewed to the right if it were centered on 4.5%, because there is a smaller tolerance between 4.5% and 6.0% as compared with the tolerance between 4.5% and 2.5%.

Even ignoring all other factors, such as high curing temperatures and mixture target strengths well above the specified strengths, these reduced air contents would be expected to cause concrete strengths somewhat higher than the expected strengths for the concrete mixture at 4.5% air content. More detailed information with regards to the effects of air content related to strength findings is discussed in Section 6.6.

5.7. Slump Measurements

In girder production plants, concrete slumps are measured in accordance with ASTM C143/C143M (2010). The ALDOT *Standard Specifications* (2012) allow a maximum slump of 4 inches without chemical admixtures. With the use of chemical admixtures, this slump is allowed to reach up to 9 inches. As was discussed in Section 3.3.2, virtually every concrete mixture used

in the production of Alabama prestressed concrete bridge girders utilizes one or more water-reducing admixtures, which is the primary method of increasing the slump. This is not surprising, due to the fact that the use of these admixtures allows for low w/cm ratios while still maintaining workability. Achieving these lower w/cm ratios allows for higher strength concretes, thus allowing producers to cut prestressing strands and remove girders from the bed as quickly as possible.

The vast majority of data collected for this research project consisted of vibrated concrete (as opposed to self-consolidating concrete), so a slump measurement was usually reported. For those pours that employed self-consolidating concrete, which only occurred during research projects, a slump flow spread value was reported instead. Slump flow spread values were not included in the slump analysis.

Figure 5.9 shows a histogram of all the slump measurements for the full data set. Plant-specific histograms are provided in Appendix D. There is a clear, definite trend of reaching slump values at the highest allowable level by the *Standard Specifications*, and this is not surprising. High slumps usually imply high workability, allowing girder producers to more easily and consistently produce high quality, well consolidated concrete girders. Low slump concretes are much harder to fill throughout the girder, especially in areas that are somewhat congested with reinforcement or have narrow flow channels, which is fairly common in prestressed girders.

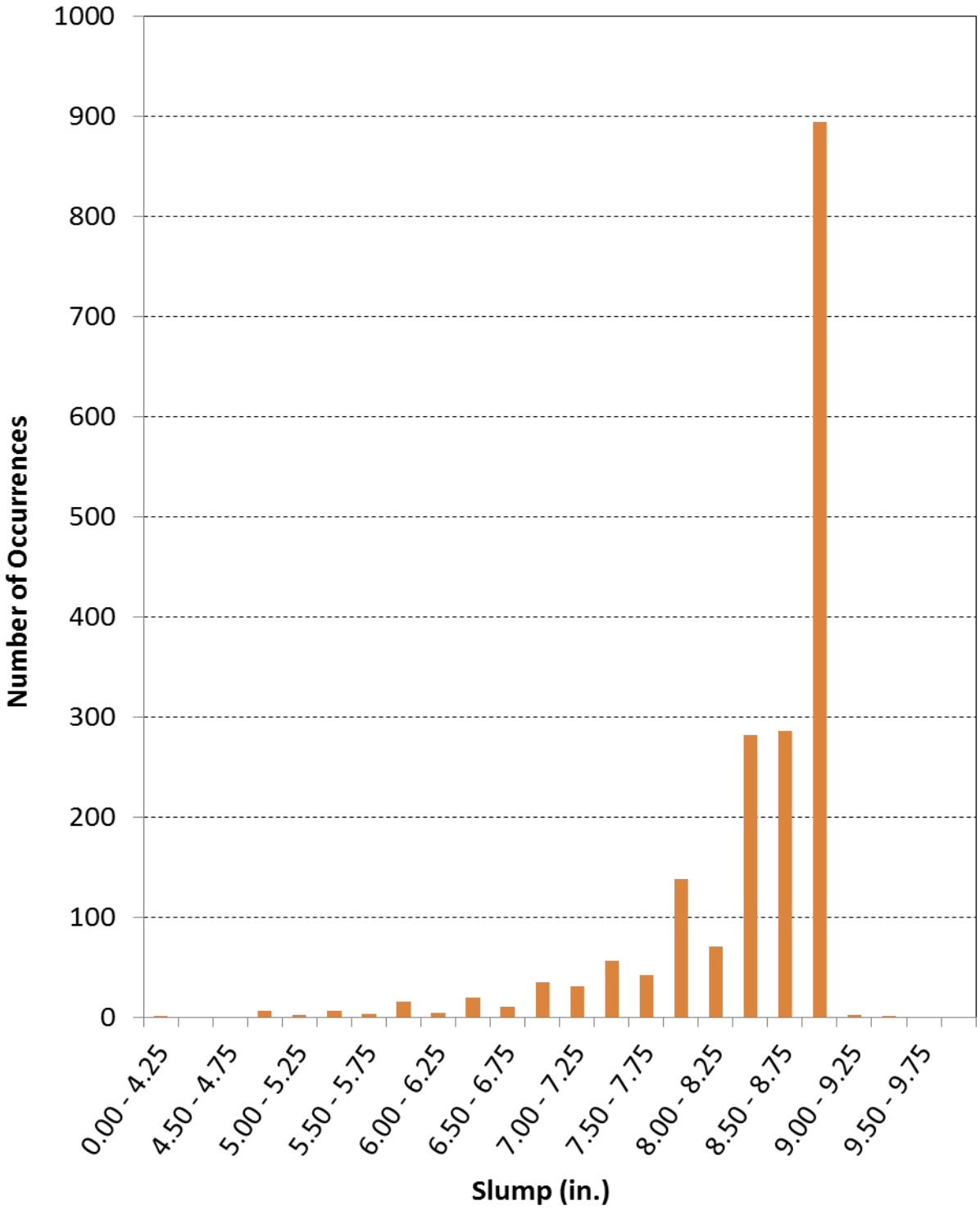

Figure 5.9: Histogram of Slump Measurements for Full Data Set

The cost of discarding a girder due to unusable concrete is monumental compared to the cost of adding admixtures to the concrete mixture for increased workability. Therefore, it would be expected that girder producers would wish to use high-slump concretes. This is further supported by Table 5.10, which provides a summary of the means and modes for the slumps from the full data set and from each plant.

Table 5.10: Slump Means and Modes for Each Data Set

	Full Data Set	Plant A Only	Plant B Only	Plant C Only	Plant D Only
Sample Mean, $\bar{x}$ (in.)	8.5	8.7	8.5	7.5	8.6
Sample Mode (in.)	9.0	9.0	9.0	8.0	9.0

The data distribution visualized in Figure 5.9 and Table 5.10 appears more logarithmic or exponential than normal. In fact, 80% of all slump measurements were between 8.0 in. and 9.0 in., inclusive. Approximately 20% had smaller slumps, and only a rare few measurements were higher than 9.0 in. Since the data does not exhibit any trends similar to a normal distribution (nor was it expected to), treating this data set as normally distributed would be highly inaccurate. Hence, no information about standard deviation, coefficient of variation, skewness, or kurtosis is provided.

5.8. Girder Types, Sizes, and Strengths

The data set gathered from girder producers was quite large, and covered a wide range of projects. As such, researchers wanted to have some measure of the types and sizes of girders that were included in the data set. Furthermore, a simple analysis was performed to see if there was any correlation between the type of girder and the average strengths that are specified. Table

5.11 details the number of girder pours that were included in the data set. It also clearly shows how many of these pours came from each girder producer. This table shows that no AASHTO Type IV girders were included in this study. Furthermore, only a limited number of Type V girders were included, and these girders were all a part of the same project.

Table 5.11: Number of Girder Pours by Type and Plant

	Full Data Set	Plant A Only	Plant B Only	Plant C Only	Plant D Only
Number of Type I Girder Pours	225	97	7	7	95
Number of Type II Girder Pours	191	123	51	17	0
Number of Type III Girder Pours	252	123	69	53	7
Number of Type IV Girder Pours	0	0	0	0	0
Number of Type V Girder Pours	36	36	0	0	0
Number of BT-54 Girder Pours	505	176	239	0	90
Number of BT-63 Girder Pours	187	134	20	16	17
Number of BT-72 Girder Pours	520	464	44	12	0
Total Number of Girder Pours	1916	1153	430	124	209

Table 5.12, Table 5.13, and Table 5.14 then provide the reader with an idea of the range of lengths, specified release strengths, and specified 28-day strengths, respectively, that were associated with each girder type and each plant. It is important to note that, for all of the tables in this section, the girder types were combined into general categories for ease of analysis and presentation. Any modified girder types, or any SI-unit girder types, were included in the group of girder to which they would have belonged under normal circumstances. For example, the BT-54 girder group actually consists of all BT-54 girders, Modified BT-54 girders, and BT-1370 girders (which are SI girders practically equivalent to BT-54 girders). Any abnormalities in girder type were lumped into the girder groups analyzed here.

Table 5.12: Girder Lengths by Girder Type

		Full Data Set (ft)	Plant A Only (ft)	Plant B Only (ft)	Plant C Only (ft)	Plant D Only (ft)
Type I	90%	75.5	75.5	33.3	39.7	89.1
	Mean	48.7	47.2	32.4	38.1	54.2
	10%	38.4	38.3	30.6	34.0	39.2
Type II	90%	59.5	59.3	59.3	79.3	NA
	Mean	57.4	55.9	56.0	71.9	NA
	10%	48.6	48.5	53.7	55.3	NA
Type III	90%	99.2	84.3	106.9	99.2	86.4
	Mean	80.3	74.4	87.8	85.8	69.5
	10%	62.9	62.9	58.2	75.1	47.3
Type V	90%	138.1	138.1	NA	NA	NA
	Mean	138.1	138.1	NA	NA	NA
	10%	138.1	138.1	NA	NA	NA
BT-54	90%	104.7	105.0	104.6	NA	99.2
	Mean	94.1	97.3	89.9	NA	99.1
	10%	75.8	88.5	70.7	NA	98.1
BT-63	90%	133.2	143.2	115.2	120.4	123.5
	Mean	114.9	117.4	115.1	119.5	90.4
	10%	94.8	100.8	115.0	118.5	53.1
BT-72	90%	140.6	140.5	134.5	157.8	NA
	Mean	130.1	129.8	125.5	157.8	NA
	10%	120.8	123.1	115.4	157.8	NA

Table 5.13: Specified Release Strengths by Girder Type

		Full Data Set (psi)	Plant A Only (psi)	Plant B Only (psi)	Plant C Only (psi)	Plant D Only (psi)
Type I	90%	6700	6490	5600	5500	9000
	Mean	5790	5500	4600	4980	6380
	10%	5000	5000	4000	4000	5500
Type II	90%	6600	6600	6500	8000	NA
	Mean	5830	5780	5910	6050	NA
	10%	5000	5000	5700	5000	NA
Type III	90%	6500	6200	7500	6400	6200
	Mean	5660	5320	6190	5820	5230
	10%	4600	4600	4500	5000	4000
Type V	90%	7500	7500	NA	NA	NA
	Mean	7500	7500	NA	NA	NA
	10%	7500	7500	NA	NA	NA
BT-54	90%	6200	6300	6200	NA	6000
	Mean	5710	5630	5660	NA	6000
	10%	5000	5200	5000	NA	6000
BT-63	90%	7000	7000	6000	6200	6200
	Mean	6000	6080	6000	6200	5170
	10%	5220	5220	6000	6200	4000
BT-72	90%	6530	6530	6500	7500	NA
	Mean	5890	5850	5980	7500	NA
	10%	5390	5390	5600	7500	NA

Table 5.14: Specified 28-Day Strengths by Girder Type

		Full Data Set (psi)	Plant A Only (psi)	Plant B Only (psi)	Plant C Only (psi)	Plant D Only (psi)
Type I	90%	8000	8000	7000	7000	9000
	Mean	6700	6290	5860	6100	7350
	10%	5000	5000	5000	5000	6500
Type II	90%	7000	7000	7000	8000	NA
	Mean	6450	6500	6300	6590	NA
	10%	6000	6000	6000	6000	NA
Type III	90%	7400	7000	8000	7000	7500
	Mean	6560	6320	6860	6740	6360
	10%	6000	6000	6000	6000	5000
Type V	90%	8000	8000	NA	NA	NA
	Mean	8000	8000	NA	NA	NA
	10%	8000	8000	NA	NA	NA
BT-54	90%	7000	7250	7000	NA	7000
	Mean	6590	6470	6530	NA	7000
	10%	6000	6000	5500	NA	7000
BT-63	90%	8000	8000	7000	7000	8000
	Mean	7090	7180	7000	7000	6590
	10%	6500	6500	7000	7000	5000
BT-72	90%	7500	7250	8000	8500	NA
	Mean	6890	6800	7430	8500	NA
	10%	6000	6000	6600	8500	NA

By close examination of Table 5.12, Table 5.13, and Table 5.14, it becomes apparent that there is little correlation between the girder type and the specified girder strengths. In fact the highest specified strengths actually occurred with some Modified Type I girders from Plant D, and Type I girders are the smallest girder sizes that were considered in this research project. There does appear to be a general trend of increasing girder lengths with larger girder heights, based on Table 5.12, but this trend is not strictly followed. Figure 5.10 provides a graphical representation of this trend, showing increased girder lengths with increased girder heights.

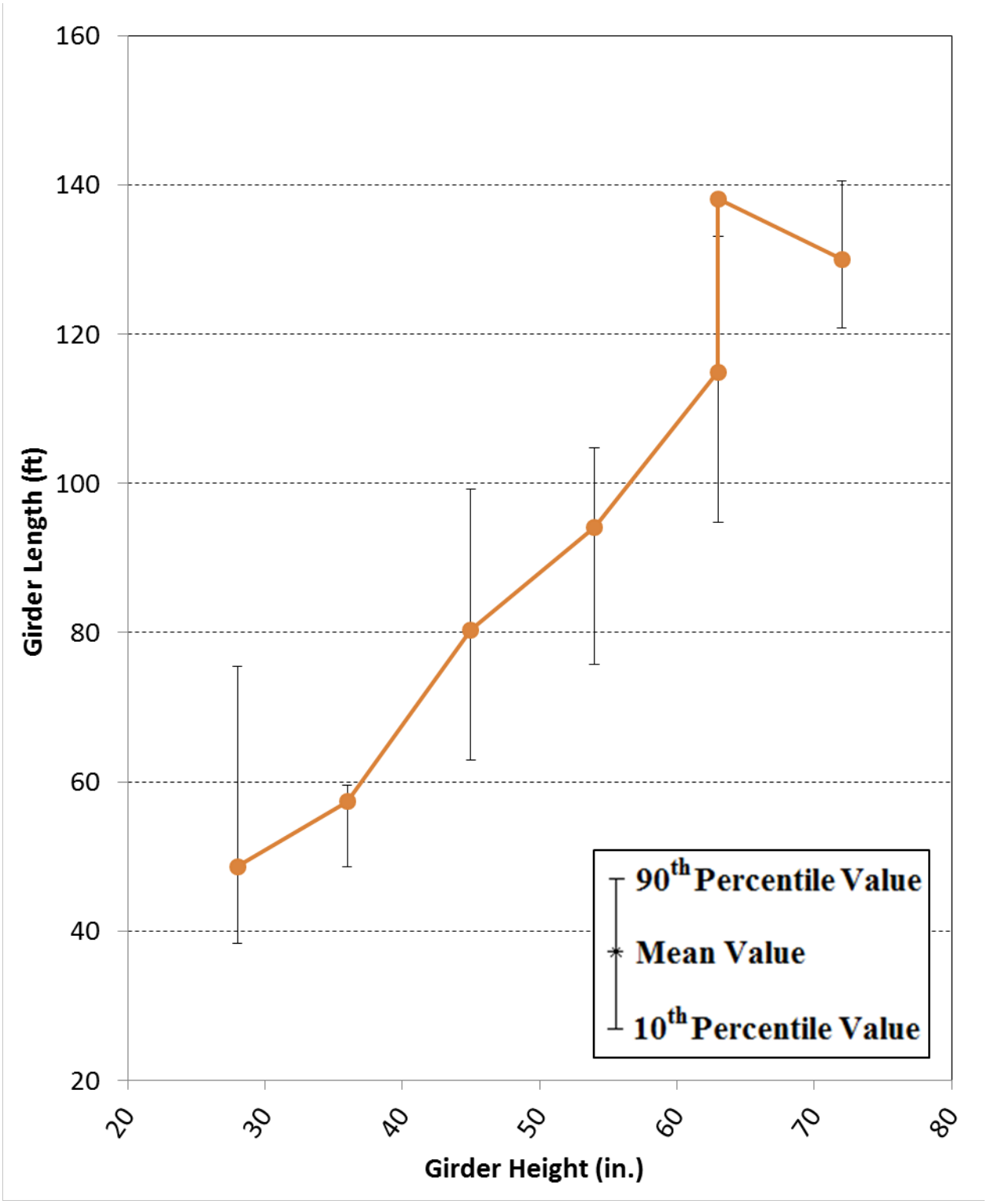

Figure 5.10: Average Girder Heights for each Girder Height, with Percentile Range

5.9. Release Strengths

The full data set for measured concrete compressive strengths at the time of prestress release that was gathered by AUHRC researchers contained 1917 data points, each representing an average of 2 or 3 concrete cylinders produced during the girder pour. This data set was, unsurprisingly, highly variable and scattered. This was to be expected, considering the large number of factors that contribute to measured concrete strength at release, including the following factors:

- Concrete mixture design
- Cylinder production quality
- Temperature conditions during curing
- Moisture conditions during curing
- Concrete age at release

The release strength data set, without any modification or analysis, is briefly shown in this section. However, such presentation of raw data provides only a little useful information. Chapter 6 provides information on the data in terms of grouping, analysis, and modification for best results.

A basic analysis of the ranges and general properties of the release strength data set was also performed, and the summary of release strength measurements may be seen in Table 5.15.

Table 5.15: Statistical Summary of Measured Release Strengths

	Full Data Set	Plant A Only	Plant B Only	Plant C Only	Plant D Only
Number of Points	1917	1155	430	123	209
Sample Mean, $\bar{x}$ (psi)	7660	7873	7271	6960	7699
Sample Standard Deviation, s (psi)	983	907	837	1154	1120
Coefficient of Variance (%)	12.83	11.52	11.51	16.58	14.55
Skewness Check, $\sqrt{\beta_1}$	0.329	0.300	0.739	0.442	0.421
Kurtosis Check, β_2	3.015	2.913	3.623	2.884	1.685
Maximum Measured Value (psi)	10,990	10,800	9,940	10,530	10,990
90^{th} Percentile Value (psi)	9,020	9,080	8,310	8,580	9,340
10^{th} Percentile Value (psi)	6,480	6,740	6,290	5,560	6,440
Minimum Measured Value (psi)	4,750	5,230	5,060	4,750	5,550

Scatter of the complete data set may be seen in Figure 5.11, which shows a plot of measured release strength versus specified release strength. Figures E.1, E.2, E.3, and E.4 in Appendix E show the same data comparison, but with the data set limited to only those data which came from Plants A, B, C, and D, respectively. These figures, combined with the plot for the full data set, reveal the difficulty in establishing useful trends from the complete data set without modification.

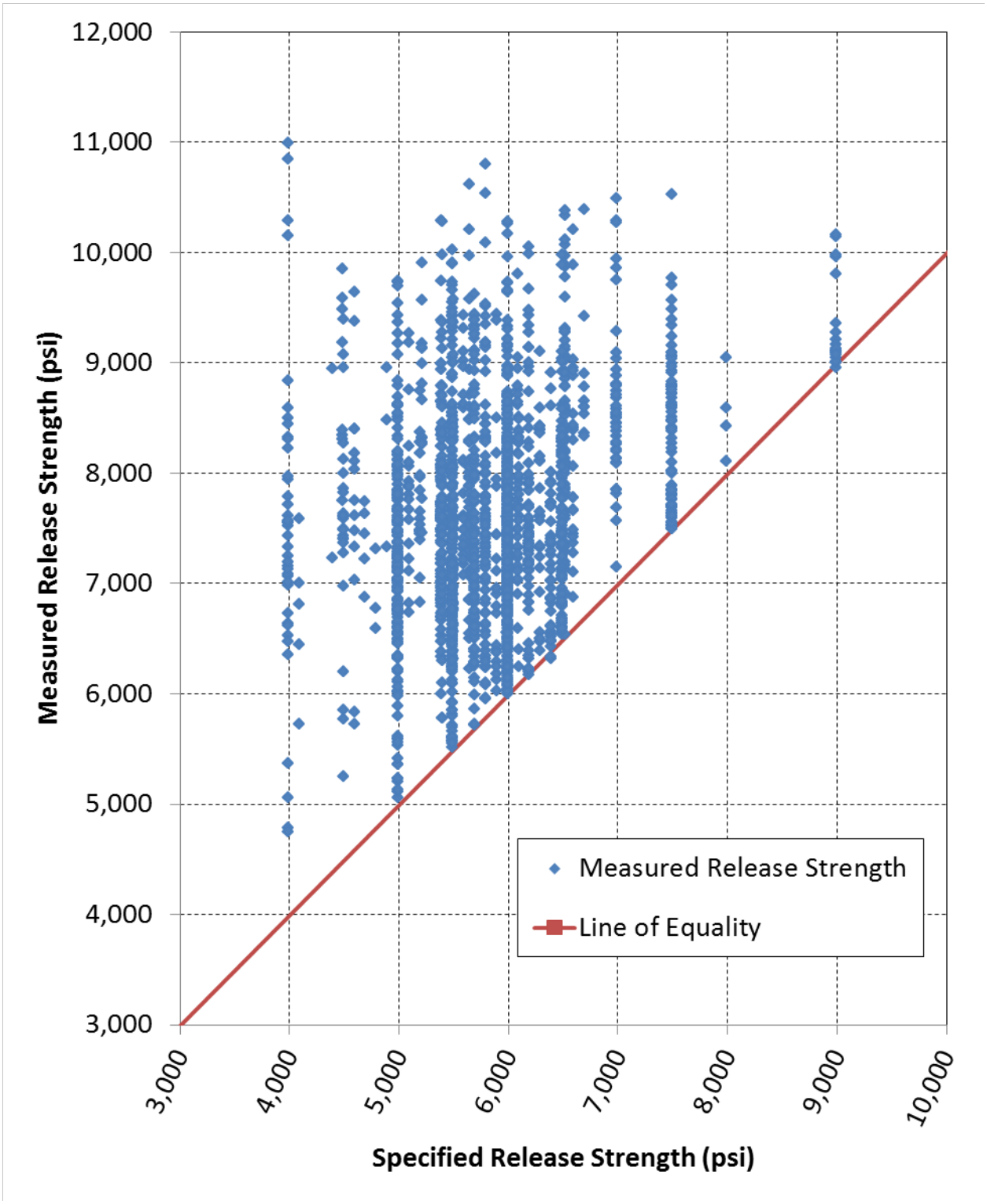

Figure 5.11: Full Data Set, Measured Release Strength versus Specified Release Strength

The only trend that may be readily seen by visual examination of this plots is that the lower bound for each plot is strictly set as the one-to-one ratio of measured strength versus specified strength, with very few entries falling below this line. This is not because tests never yielded strengths below the specified release strength. If they did, prestress transfer was usually delayed until adequate strength was achieved in later cylinder tests. Therefore, these low-strength test results were excluded from the data set due to not being representative of the girder concrete at the actual time of prestress transfer.

A histogram of the occurrences of release strengths may be seen in Figure 5.12. Plant-specific histograms are also provided in Appendix E.

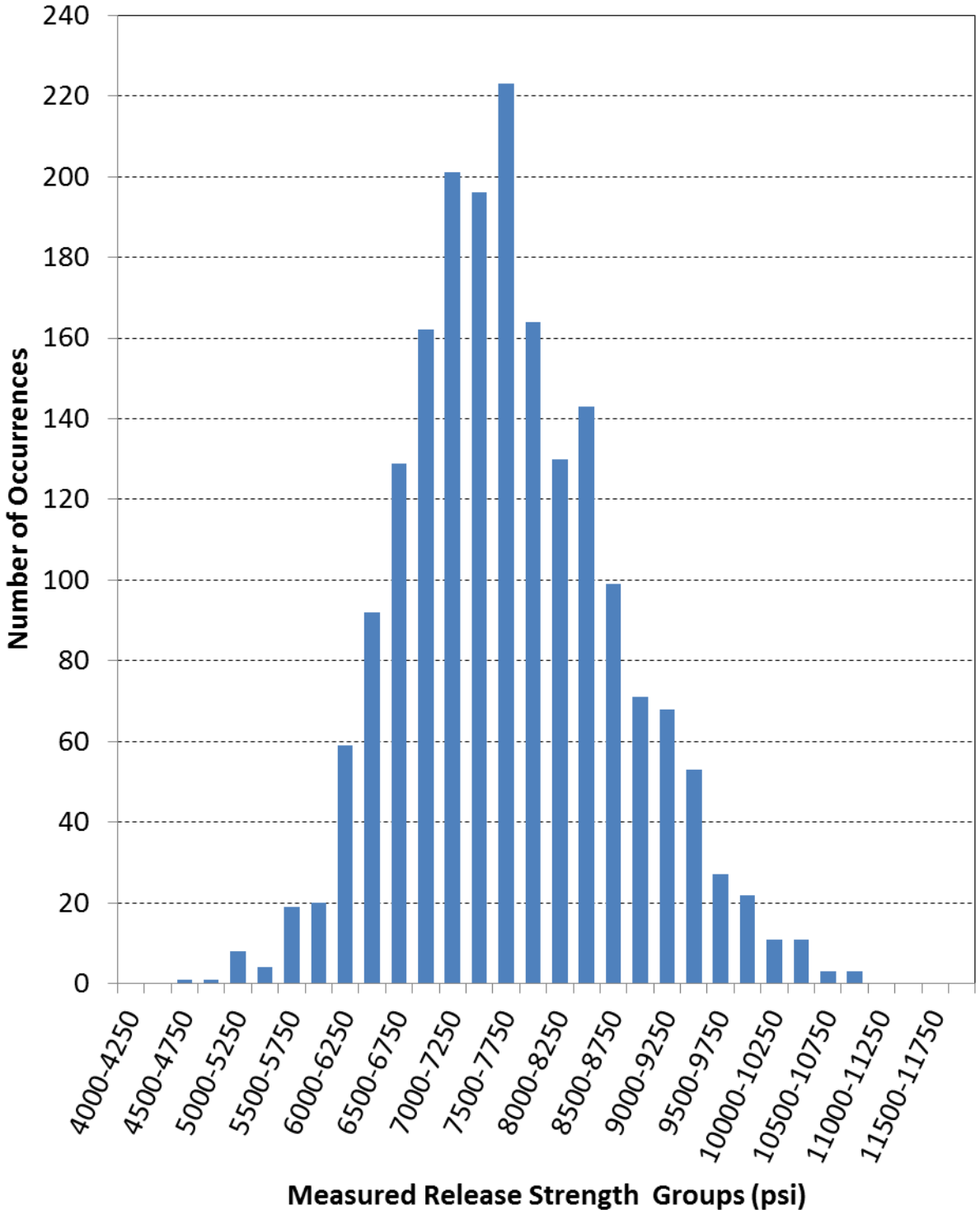

Figure 5.12: Histogram of Measured Release Strengths for Full Data Set

5.10. 28-Day Strengths

The raw data for 28-day concrete compressive strengths are presented in this section, similar to the release strengths in Section 5.9. A full description of the analysis results from the data set is given in Section 6.4, and the relationships between release strengths and 28-day strengths are analyzed in Sections 6.5 and 6.6. A plot of measured 28-day strengths compared to their respective specified 28-day strengths may be seen in Figure 5.13. As was the case with the release strengths plotted in Figure 5.11, there is clearly a large amount of scatter in the measurements, and highly accurate predictions of strength will be practically impossible.

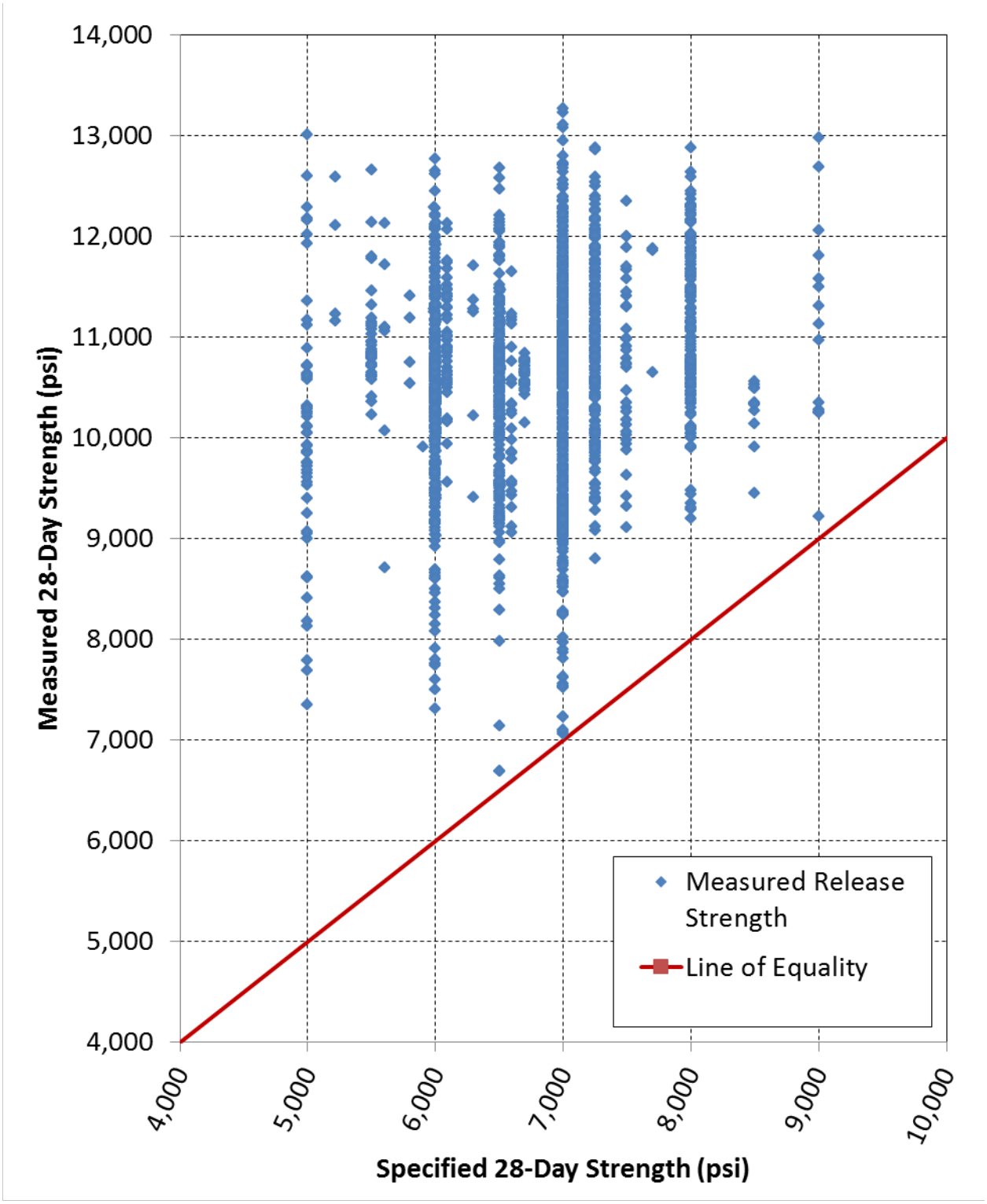

Figure 5.13: Full Data Set, Measured 28-Day Strengths versus Specified 28-Day Strength

A summary table of collected 28-day strength values may be seen in Table 5.16, which directly parallels Table 5.15 for release strengths. Likewise, Figure 5.14 shows a histogram of measured 28-day strength occurrences which parallels Figure 5.12 for release strengths. Plant-specific versions of both Figure 5.13 and Figure 5.14 have been provided in Appendix F.

Table 5.16: Statistical Summary of Measured 28-Day Strengths

	Full Data Set	Plant A Only	Plant B Only	Plant C Only	Plant D Only
Number of Points	1897	1150	421	121	205
Sample Mean, $\bar{x}$ (psi)	10590	10728	10826	8886	10333
Sample Standard Deviation, s (psi)	995	894	698	979	1062
Coefficient of Variance (%)	9.40	8.33	6.45	11.01	10.28
Skewness Check, $\sqrt{\beta_1}$	-0.439	-0.212	0.095	0.028	0.684
Kurtosis Check, β_2	3.678	3.070	5.893	2.286	2.826
Maximum Measured Value (psi)	14,140	13,230	13,270	11,090	14,140
90^{th} Percentile Value (psi)	11,850	11,910	11,740	10,290	11,890
10^{th} Percentile Value (psi)	9,250	9,550	10,140	7,540	9,150
Minimum Measured Value (psi)	6,690	6,690	7,560	6,690	9,020

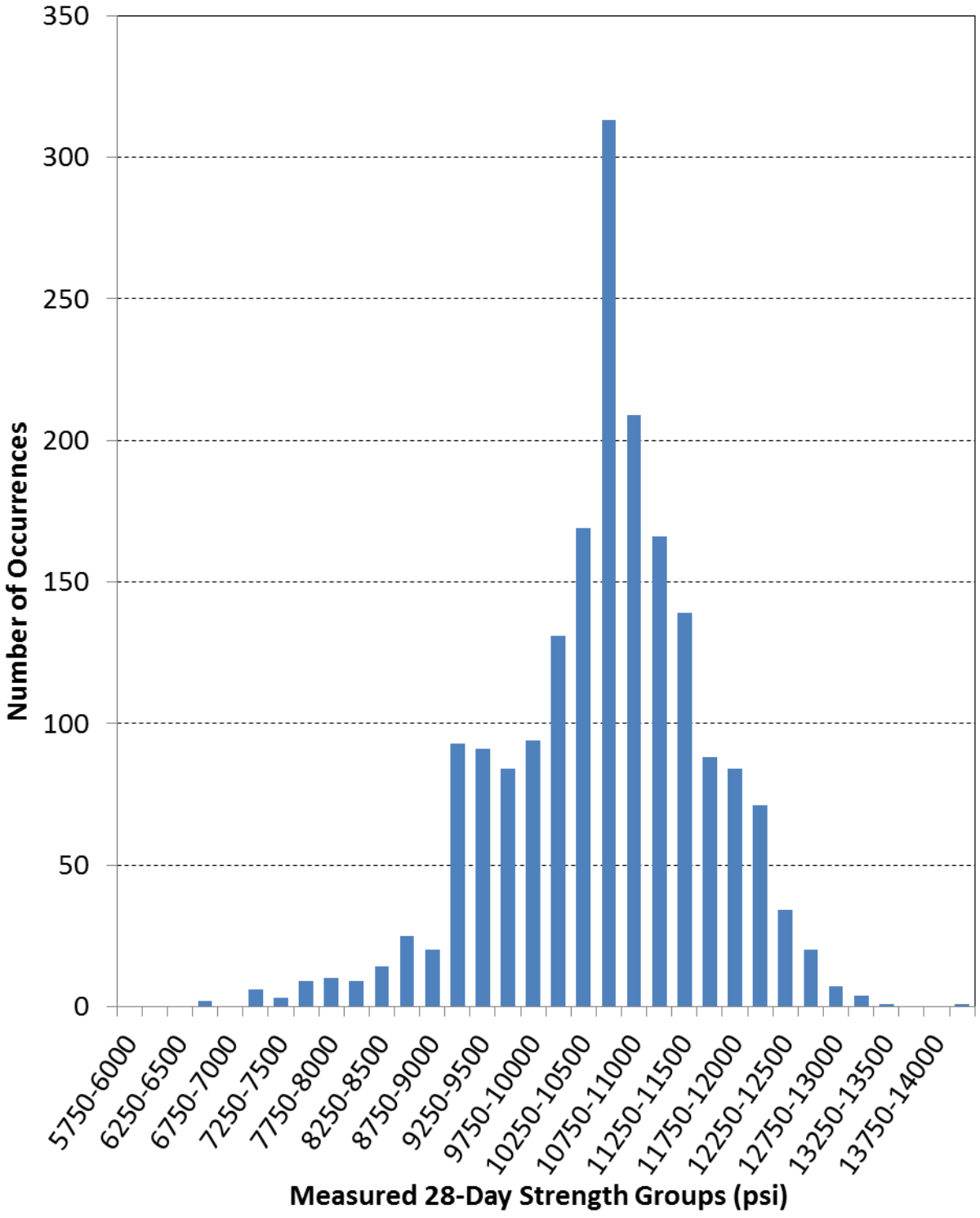

Figure 5.14: Histogram of Measured 28-Day Strengths for Full Data Set

5.11. Summary

The historical plant-submitted data collected for this research project provided a large number of measurements. Over 1900 pours were included, and these pours occurred during all times of the year, for girder sizes ranging from AASHTO Type I girders to PCI BT-72 girders, with a wide range of strengths and plant locations. Analyzed historical data included release ages, equivalent ages at release, air contents, slump measurements, girder types, girder lengths, and strengths at both release and 28 days. A summary of pertinent findings and conclusions from this chapter is as follows:

- The ages at which girders were released fell into two general categories—standard pours and extended weekend pours.
- Standard pours, in which there was a normal rate of strength development and nothing prevented release of the girders, had a mean curing time of approximately 18 hrs. Standard pours included 83.5% of the pours.
- Extended weekend pours, in which the girders were cast on a Friday and left in the forms until Monday morning, had a mean curing time of approximately 66 hrs. Extended weekend pours included 11.8% of the pours.
- Extended weekend pours exhibited higher mean release strengths than standard pours, though the mean specified release strengths were the same and the mean 28-day strengths were the same. A higher percentage of the 28-day strength was developed by the time of prestress transfer in extended weekend pours.
- Extended weekend pours exhibited higher release strength ratios than standard pours.
- The sample mean of calculated equivalent ages at the time of prestress transfer was more than three times as large as the mean of chronological ages at the time of prestress

transfer. The mean equivalent age at transfer was in the vicinity of 2.5 days, while the mean chronological age of the primary peak at release was in the vicinity of 0.75 days.

- Concrete air contents fell well below the target value specified by the ALDOT *Standard Specifications* (2012).
- Most girder pours used the maximum allowable slump with chemical admixtures.
- On average, girder lengths tended to increase with increasing girder height. This was true for both AASHTO girders and PCI Bulb-tee girders.
- There was little correlation between girder type and specified strengths.
- The two most produced girder types seen in this study were PCI BT-54 and BT-72 girders.

Chapter 6: Historical Strength Analysis

6.1. Introduction

Probably the most numerous and detailed of all the findings discussed in this thesis are the findings related to strength. As discussed in Section 1.2, for the purposes of camber prediction, concrete strength is not the most important parameter. The most important parameter is the modulus of elasticity (MOE) of the concrete at the time of release. However, all methods of predicting MOE incorporate concrete compressive strength in some way or another, and this strength has been the single most thoroughly demonstrable means of predicting MOE. Perhaps most importantly, compressive strength is the universally measured property associated with the quality of the concrete. A thorough investigation of concrete strengths at the time of prestress release can be used to better predict MOE at the time of release, thus aiding in the prediction of girder cambers.

The major compressive strength relationships are discussed in detail in this chapter. First is the relationship between the specified strength of a girder at any age and the actual achieved strength of the girder at that age. This relationship is very valuable to design engineers, as it provides them with a means of estimating the average strength they expect whenever they specify a certain strength. The *fib* Model Code (2010) has built-in relationships for establishing a mean strength, f_{cm}, based on the specified characteristic strength, f_{ck}. This mean strength is used for serviceability calculations, as is discussed in Section 2.2. Estimation of average strengths is useful for predicting service-level behaviors. Therefore this relationship is discussed for release

strengths in Section 6.3 and 28-day strengths in Section 6.4.

The second major strength relationship is that between concrete strength and concrete age. There are a number of methods and options that have been used to quantify this relationship, and these are discussed in detail in Sections 6.5 and 6.6.

6.2. Concrete Compressive Strength Variables

Before an in-depth discussion of strength results begins, however, it is first practical to explain the different variables that are used to describe the different "types" of compressive strength at any given age. This prevents the necessity of writing the full phrase "specified release strength" or "measured 28-day strength" every time the phrase is desired.

There are four "types" of strength at any given age that are discussed or used in the rest of this thesis. The system used for differentiating between these four types is as follows:

1. The strength level that is measured by cylinder testing at any given age is simply called the "measured strength" at that age. The variable form used to describe this is the simplest of the four types, and is shown here:

   f_{ci} = measured compressive strength of concrete at prestress release, psi

   f_c = measured compressive strength of concrete at 28 days, psi

   Note the lack of any exponent on the f variable. This is the defining characteristic that marks this variable as a measured value.

2. The strength level specified on the contract drawings, or specified by the design engineer, at a given time is called the "specified" strength at that age. The variable form used to describe this type is shown here:

   f'_{ci} = specified compressive strength of concrete at prestress release, psi

f_c' = specified compressive strength of concrete at 28 days, psi

The apostrophe in the f' variable marks it as a specified value. The factors that combine to determine the values of f_{ci}' and f_c' are discussed later.

3. The strength level which concrete producers target during mixture approval testing, to provide sufficient probability that the measured f_{ci} or f_c will be higher than the specified f_{ci}' or f_c', is known as the "required" strength. Strength measurements performed on concrete cylinders usually follow a normal or nearly normal distribution. Any given strength test has the potential to be much higher than the actual average strength of the concrete, or much lower than the actual average strength, or somewhere in between. The use of a minimum of two cylinders for any strength test reduces this issue, but it does not eliminate it. Therefore, for any f_c', a related required strength is established. The required strength is established such that there is a large probability that the average of two or more cylinder tests will be equal to or stronger than the specified strength. For example, the average cylinder tests are supposed to be larger than the specified strength 99% of the time according to the ACI 318 code (2011) In this thesis, the required strength is denoted using the following variable format:

   f_{cir}' = required measured compressive strength at prestress release, psi

   f_{cr}' = required measured compressive strength at 28 days, psi

4. The strength level that is expected or predicted based on statistical analysis of the common relationships between specified strengths and measured strengths is called the "expected" strength at a given age. The variable form used to describe this type is shown here:

   f_{ci}^* = expected compressive strength of concrete at prestress release, psi

f_c^* = expected compressive strength of concrete at 28 days, psi

The asterisk in the f^* variable marks it as an expected value.

The clarification of these terms allows much more fluid discussion of the strength results in the rest of this thesis.

Many factors contribute to the selection of f'_{ci} and f'_c. The value of f'_{ci} is primarily controlled by the requirements of satisfying certain allowable concrete stresses at the time of prestress transfer. Stresses due to the combined self-weight of the girder and internal prestressing forces just after release must not exceed code-specified limits, such as those presented in the AASHTO (2012).

The value of f'_c has multiple determining factors. Ultimate stress or strength limits and long term performance requirements are both contributing factors to the selected f'_c value. However, the combined requirements that control f'_c often do not require strengths significantly higher than f'_{ci}. It is also much more difficult to achieve f'_{ci} in a limited time frame (see Section 5.4) than to achieve f'_c in 28 days. Thus, the value of f'_{ci} is often found to control strength throughout the girder life, with the 28-day f'_c requirements easily fulfilled if the f'_{ci} requirements are satisfied.

6.3. Analysis and Predictions of Release Strength

This section focuses on the release strength data found in the historical plant-submitted data set. No findings related to 28-day strength are discussed, and the relationships between release strength and 28-day strength, time or maturity, or air content, are not discussed. These issues are found in later sections.

A major difficulty with analyzing the release strength data set as a group had to do with

the indiscriminate nature of the data grouping. With all data points lumped together, without discrimination based on age at release, specified strengths, mixture proportions, or any other parameter, uncovering meaningful trends in the data becomes much more difficult. Therefore, it was necessary to split the data into different groups and subdivisions for analysis.

Two major divisions were made for better data analysis. The first major division was the choice to analyze the data from two different perspectives. The first perspective, which is more directly correlated with the express goals of the project as stated in Section 1.2, was to analyze the data from the perspective of bridge design engineers (ALDOT or consultants) during the design phase. This is called the "specified strength focus" perspective. The second perspective was that of plant managers or girder producers, and is called the "measured strength focus" perspective. Different information would be available to these different groups during the time at which they would use the findings described in this thesis. After all, design engineers aim to estimate girder cambers during the design phase without prior knowledge of the girder producer or mixture design. However, once any project has been let to a given producer, that producer has the potential for much more detailed information about plant practice and materials than the design engineers would have available. Thus, strength findings can be tailored to meet the needs of each group based on the information available to them.

The second major division that took place was the decision to analyze the strength data in "strength bins." In other words, rather than analyzing the full data set as a single unit, or even analyzing all data from any plant as a single unit, the data was divided into groups for more detailed analysis. For design engineers, the primary pieces of information available for camber prediction are the specified strengths at release and 28 days. However, girder producers are primarily focused on the release strength, and 28-day strengths are usually easily achieved if

release strength requirements are met on the time scale described in Section 5.4. Therefore, when analyzing data from the perspective of design engineers, the data was split into groups based on specified release strengths.

Girder producers, on the other hand, know the strength for which they are aiming during any pour. This strength, as is shown by the analysis of strength results later in this chapter, is often very different from the specified strength. Therefore, when analyzing data from the perspective of girder producers, the data was divided into groups based on measured release strengths.

In theory, the goal was to obtain a sort of 2-dimensional strength distribution—a relationship between the distribution of specified strengths and the relationship between measured strength over limited sections of that specified strength range. In other words, one could select a specified strength, and have a statistical measurement of the distribution of historical measured strengths for that specified strength. Bins based on specified release strength would provide design engineers with a much better understanding of the strength results that are actually obtained for any specified strength. Bins based on measured release strength would provide producers with a detailed breakdown of the distribution of strength results for any strength level they attempt to produce. In either case, the division of data would provide much more accurate understanding of the actual behavior. Sections 6.3.1 and 6.4.1 focus on the perspective of the design engineer, while Sections 6.3.2 and 6.4.2 focus on the perspective of girder producers.

6.3.1. Specified Strength Focus

A surprisingly small amount of production-specific information is available to bridge

design engineers during the design phase of a project. They have control over girder type, girder length, f'_{ci}, f'_c, and reinforcement. The values of f'_{cir} and f'_{cr} are established by ALDOT specifications, based on the addition of an arithmetical strength increase above the specified strength (ALDOT 2009). Typically, however, engineers are not aware of which plant will be producing the girders, the date on which the girders shall be produced, and many other production-related aspects. Furthermore, historical records indicate that girder type and length do not correlate to standard strength levels, as is shown in Section 5.8. The most consistent pieces of information controlled and known by the design engineers are f'_{ci} and f'_c.

Table 6.1 provides a summary of the statistical analysis of all release strength tests, both in strength bins based on f'_{ci} and as a complete set. For better understanding of the results, and in case the design engineers actually knew beforehand which plant would be producing their girders, the same analysis is summarized in plant-specific form in Appendix G.

Table 6.1: Full Set Release Strength Distributions –Bins Divided by f'_{ci}

Strength Bins	*n*	Sample Standard Deviation, s (psi)	Sample Mean, $\bar{x}$ (psi)	Sample Coefficient of Variance, COV (%)	Skewness Check, $\sqrt{\beta_1}$	Kurtosis Check, β_2
4000 psi $\leq f'_{ci} <$ 4500 psi	53	1400	7680	18.2	0.243	3.037
4500 psi $\leq f'_{ci} <$ 5000 psi	49	960	7580	12.7	-0.175	3.082
5000 psi $\leq f'_{ci} <$ 5500 psi	402	950	7500	12.7	0.181	3.204
5500 psi $\leq f'_{ci} <$ 6000 psi	518	1010	7520	13.4	0.527	2.904
6000 psi $\leq f'_{ci} <$ 6500 psi	558	850	7550	11.2	0.524	3.095
6500 psi $\leq f'_{ci} <$ 7000 psi	191	930	8010	11.6	0.496	2.671
7000 psi $\leq f'_{ci} <$ 7500 psi	43	730	8640	8.47	0.771	3.370
7500 psi $\leq f'_{ci} <$ 8000 psi	79	670	8370	8.02	0.588	2.834
8000 psi $\leq f'_{ci} <$ 8500 psi	4	390	8550	4.58	0.188	1.077
8500 psi $\leq f'_{ci} <$ 9000 psi	0	NA	NA	NA	NA	NA
9000 psi $\leq f'_{ci} <$ 9500 psi	20	420	9340	4.46	0.949	2.140
Full f'_{ci} Range	1917	980	7660	12.8	0.329	3.015

These analyses revealed some interesting trends in release strength data. These trends may best be understood by graphs produced using the data. Therefore, Figure 6.1 shows a graph of the mean release strength for each data set, plotted for each strength bin. This plot is called a "traveling mean" plot, and allows comparison between plants and between strength bins.

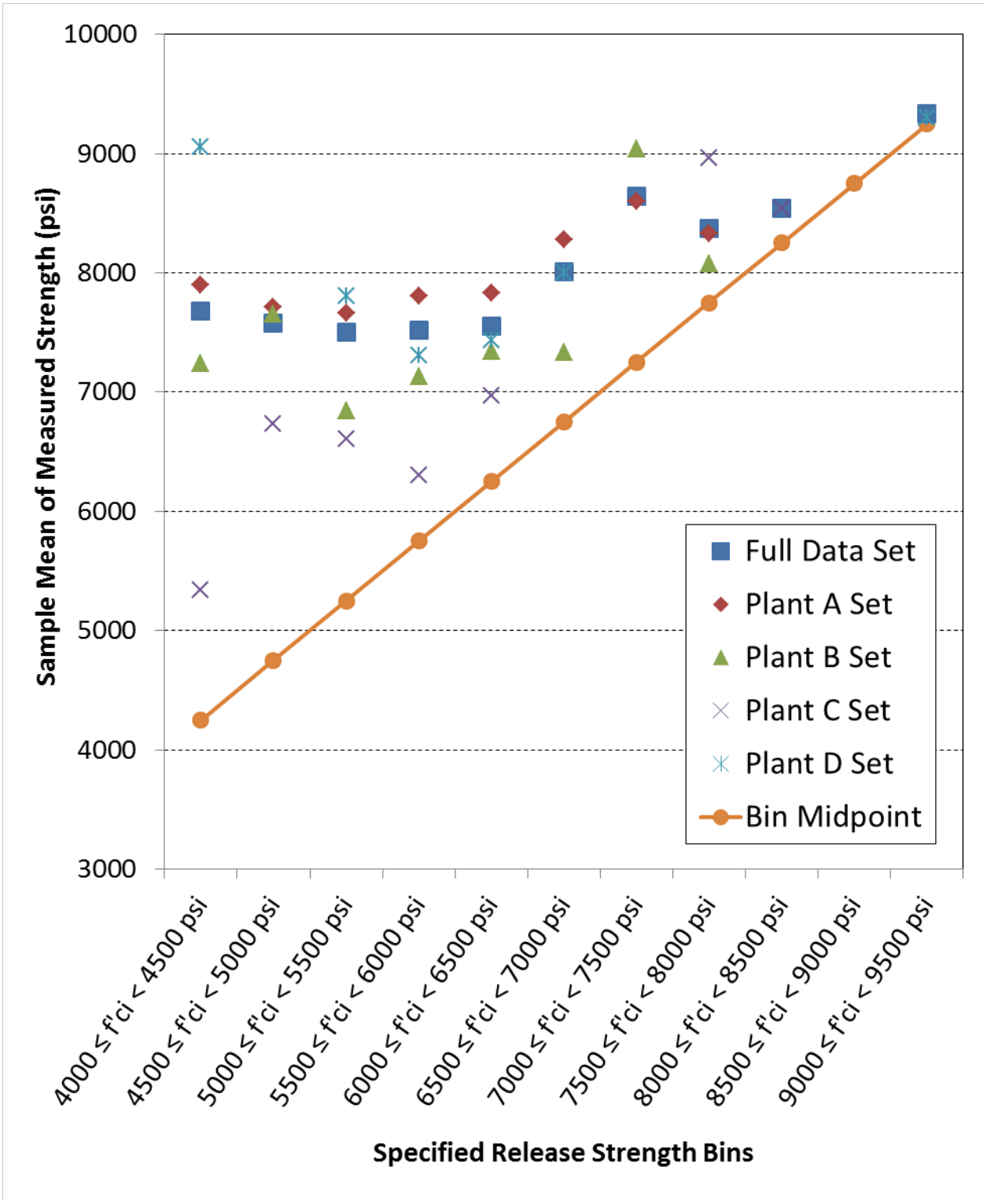

Figure 6.1: Traveling Mean for Full Data Set and Each Plant

Figure 6.2 shows a graph of the traveling mean for the full data set compared to the midpoint of each strength bin, along with the 10^{th} Percentile and 90^{th} Percentile limits of those values. Lastly, Figure 6.3 shows a graph of the traveling mean difference between the measured strengths and the specified strengths, with the 10^{th} Percentile and 90^{th} Percentile limits of those values.

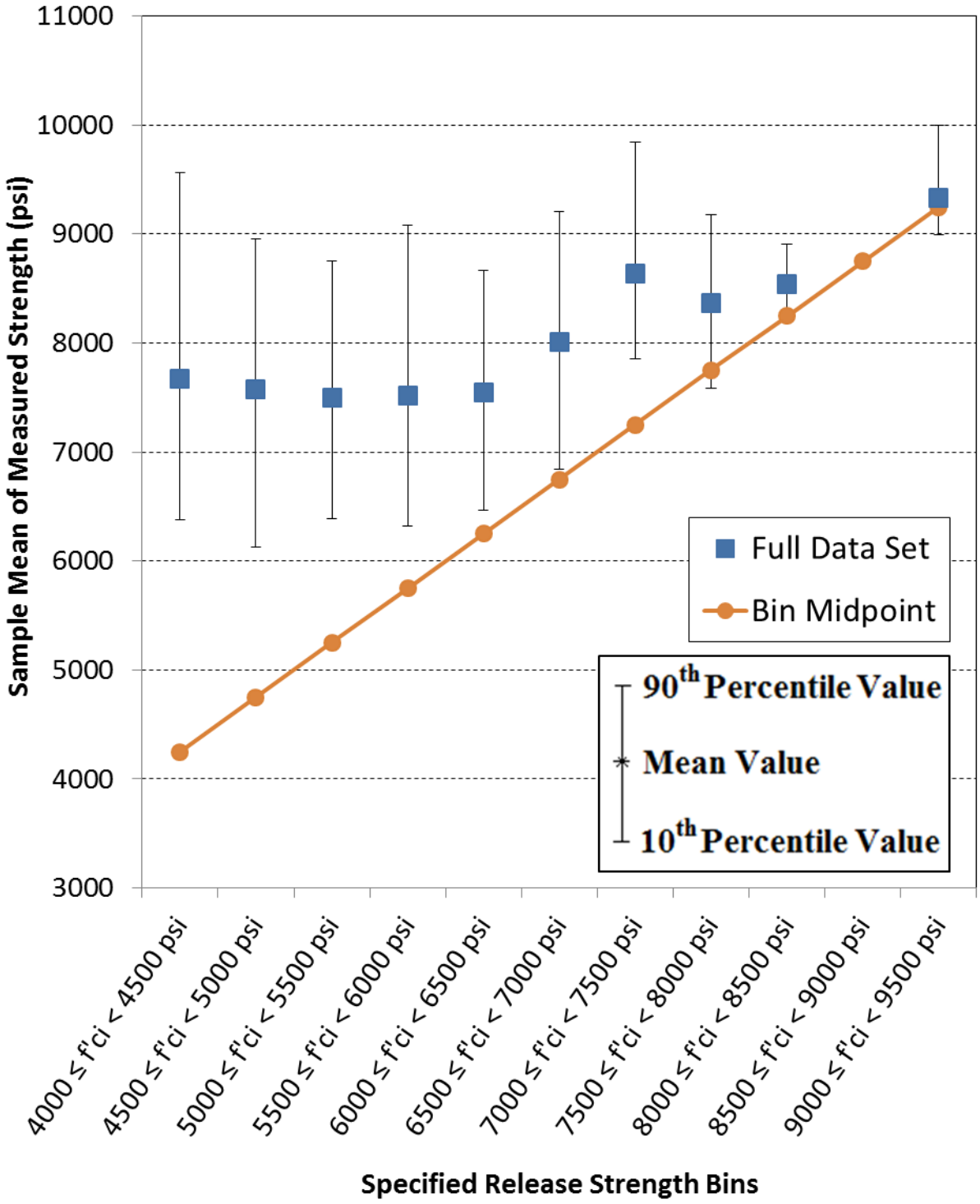

Figure 6.2: Traveling Mean of Full Data Set with Percentile Bounds

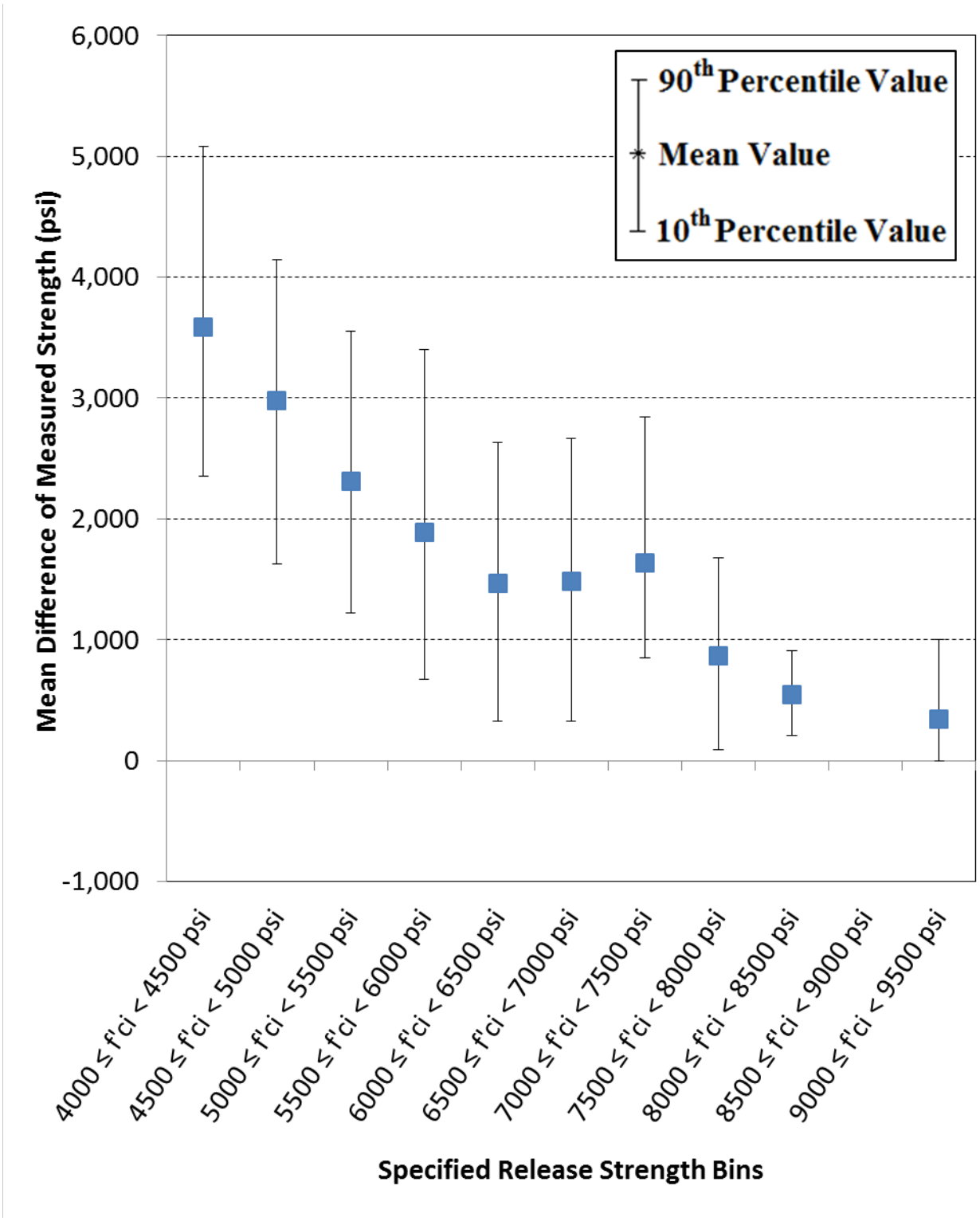

Figure 6.3: Traveling Mean Difference for Full Data Set with Percentile Bounds

Not surprisingly, the traveling mean of the full data set closely resembles the traveling mean of the Plant A data set. Considering the large percentage of the overall data set which Plant A provided, it is reasonable for the results from Plant A to have the largest impact on the overall results. This is acceptable, because the proportion of data received from Plant A is related to the fact that Plant A has also produced the largest number of girders for ALDOT over the course of time covered by this research project.

Figure 6.2 shows a distinct trend of maintaining a relatively constant strength in the lower range of f'_{ci}. For all $f'_{ci} < 6500$ psi, the mean measured strength for each strength bin does not change by more than 200 psi. This is confirmed by the summary found in Table 6.1. The mean strength then starts to climb at $f'_{ci} = 6500$ psi.

Figure 6.3 shows this same trend, but from a different perspective. For $f'_{ci} < 6500$ psi, there is a clear, near-linear decrease in the mean difference between measured strengths and specified strengths ($f_{ci} - f'_{ci}$). This linear trend breaks at $f'_{ci} = 6500$ psi, and then levels off at higher f'_{ci} values.

Figure 6.4 was constructed after the data set had been divided into bins based on f'_{ci}. It had been noticed earlier, based on mixture approval requirements, plant practices, and strength measurements, that most girder producers only had one or two approved mixture at any given time. Because producers were not allowed to deviate from the approved mixture in order to adjust for required strengths, it seemed as though a plant would use what is called a “minimum-strength preferred mixture” for any f'_{ci} below a certain level. They would then switch to the second mixture for any specified f'_{ci} higher than that “break” point. To confirm this idea, and to find the break point if it existed, Figure 6.4 was created.

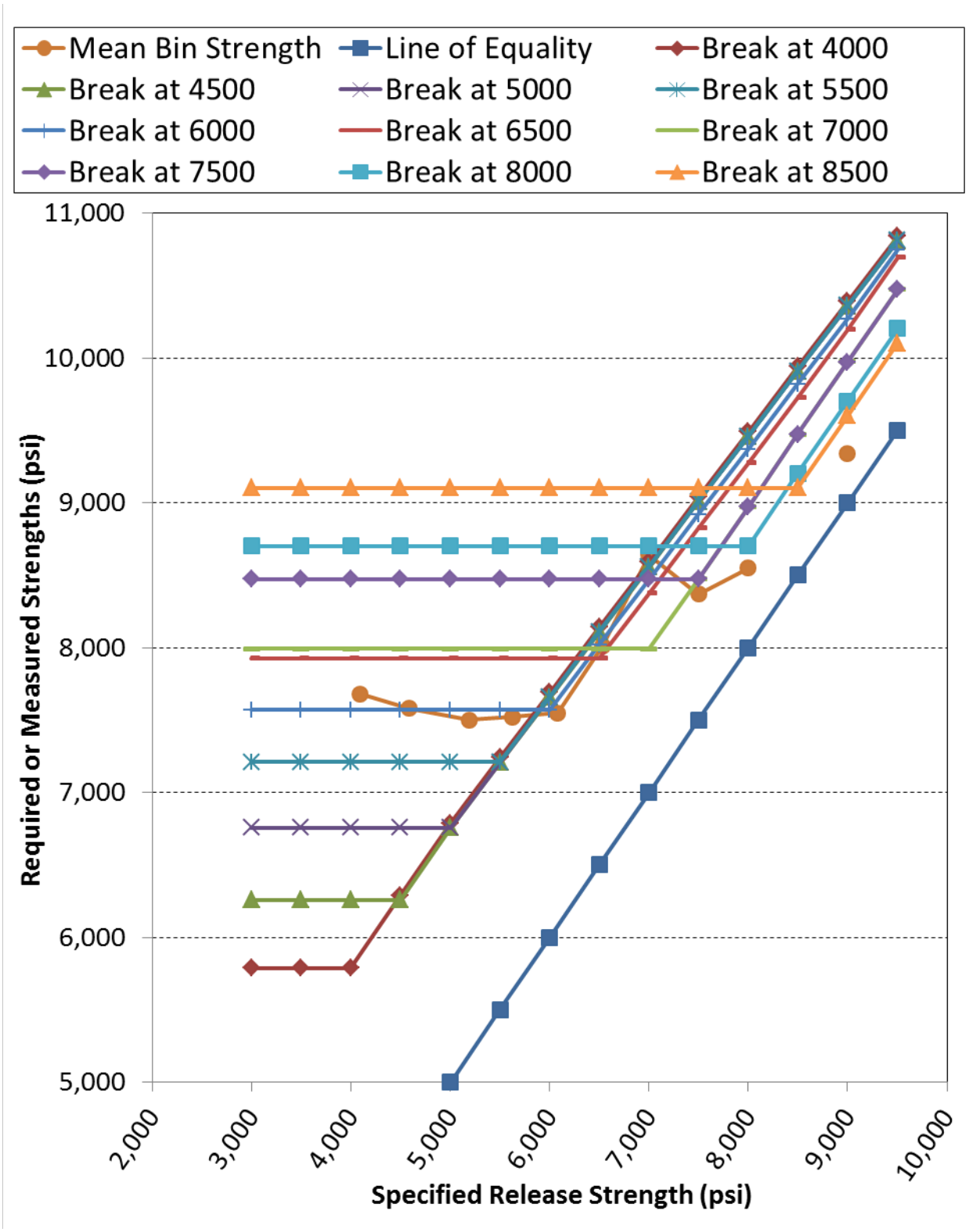

Figure 6.4: Break Points in Release Strength Measurements, All Data

An iterative approach was used to produce Figure 6.4, using the following steps for each iteration:

1. All measured strengths with a f'_{ci} greater than or equal to the break point were combined into a single group of data. For example, for the line marked as "Break at 6000" all measured strengths with $f'_{ci} \geq 6000$ psi were included in a single group for the subsequent steps, and all measured strengths with $f'_{ci} < 6000$ psi were not included.
2. A sample standard deviation, s, was calculated for this single group of data.
3. For each f'_{ci} greater than or equal to the break point, a required strength was calculated as the greater of Equations 6.1, 6.2, and 6.3 (modified from ACI Committee 214 2011), which may be seen below.

   Equation 6.1 established the required strength f'_{cr} of a running average of n consecutive tests that corresponded to a certain probability, determined by z, that the actual strength will equal or exceed f'_{ci}.

$$f'_{cir} = f'_{ci} + \left(\frac{zs}{\sqrt{n}}\right) \qquad \textbf{Equation 6.1}$$

where:

f'_{cir} = required strength for concrete mixture at 28 days, psi

f'_{ci} = specified concrete strength at release, psi

z = reliability factor for sufficiently high probability that the actual strength will equal or exceed f'_{ci}

= 2.33 for 98% probability that the actual strength will equal or exceed f'_{ci}

s = sample standard deviation for all data above the break point, psi

n = number of tests included for consecutive average

= 3 for all f'_{cir} calculations in this thesis

A value of $z = 2.33$, corresponding to a probability of 98%, is one of the most commonly used probabilities for these types of calculations in structural engineering applications (ACI Committee 214 2011). This is also confirmed by back-calculating the same value from the required strength equations found in the ACI 318 Building Code Requirements (2011). Both of these documents are focused on life-safety (strength) design, not service-life performance design.

Equation 6.2, applicable only to specified strengths less than or equal to 5000 psi (ACI Committee 214 2011), established the required strength of a concrete mixture for a certain maximum probability that any individual test would fall below $(f'_{ci} - k)$.

$$f'_{cir} = (f'_{ci} - k) + zs \qquad \textbf{Equation 6.2}$$

for $f'_{ci} \leq 5000$ psi

where:

f'_{cir} = required strength for concrete mixture at release, psi

f'_{ci} = specified concrete strength at release, psi

k = maximum amount by which f_{ci} is allowed to fall below f'_{ci} for a sufficiently high probability that the actual strength will meet or exceed f'_{ci}, psi

= 500 psi for calculations in this thesis

z = reliability factor for sufficiently high probability that the actual strength will equal or exceed f'_{ci}

= 2.33 for 98% probability that the actual strength will equal or exceed f'_{ci}

s = sample standard deviation for all data above the break point, psi

Equation 6.3, applicable only to specified strengths greater than 5000 psi (ACI Committee 214 2011), established the required strength of a concrete mixture for a

certain maximum probability that any individual test would fall below k% of f'_{ci}.

$$f'_{cir} = kf'_{ci} + zs \qquad \textbf{Equation 6.3}$$

for $f'_{ci} > 5000$ psi

where:

f'_{cir} = required strength for concrete mixture at release, psi

k = minimum percentage of f'_{ci} that f_{ci} must reach for a sufficiently high probability that the actual strength will equal or exceed f'_{ci}, %

= 90% for calculations in this thesis

f'_{ci} = specified concrete strength at release, psi

z = reliability factor for sufficiently high probability that the actual strength will equal or exceed f'_{ci}

= 2.33 for 98% probability that the actual strength will equal or exceed f'_{ci}

s = sample standard deviation for all data above the break point, psi

For all data groups the standard deviation had to be modified by the multiples found in Table 6.2, taken and modified from the ACI Committee 214 report (2011), with linear interpolation where required.

Table 6.2: Modification Factors for Standard Deviation (ACI 214 2011)

Number of Tests	Modification Factors
< 15	Refer to Table 6.3
15	1.16
20	1.08
25	1.03
30	1.00

For those few data groups with fewer than 15 tests, the equations from Table 6.3 were

used instead of the Equations 6.1, 6.2, and 6.3. This table was also taken and modified from ACI Committee 214 (2011).

Table 6.3: Minimum Required Average Strength without Sufficient Historical Data (ACI 214 2011)

Required Average Compressive Strength	Specified Compressive Strength
$f'_{creq} = f'_c + 1000psi$	when $f'_c < 3000psi$
$f'_{creq} = f'_c + 1200psi$	when $3000psi \leq f'_c \leq 5000psi$
$f'_{creq} = 1.10f'_c + 700psi$	when $f'_c > 5000psi$

Both tables were originally found in the ACI 318 code (2011). In any case, the use of these equations and tables established a "required" strength level, calculated for any specified strength greater than or equal to the assumed break point strength.

4. The calculated strength level at the break point was then used for all specified strengths less than the break point.

As an example, consider the "Break at 6000" line. For this line, all measured strengths with $f'_{ci} \geq 6000$ psi were used to calculate a sample standard deviation, $s = 931$ psi. This standard deviation was used in Equations 6.1 and 6.3 to calculate a required strength for $f'_{ci} = 6000$ psi, $f'_{ci} = 6500$ psi, etc. For $f'_{ci} = 6000$ psi,

$$f'_{cir,6000} = MAX\left[f'_{ci} + \left(\frac{zs}{\sqrt{n}}\right), kf'_{ci} + zs\right]$$

$$f'_{cir,6000} = MAX\left[6000 \text{ psi} + \left(\frac{2.33 \cdot 931 \text{ psi}}{\sqrt{3}}\right),\ 0.90 \cdot (6000 \text{ psi}) + (2.33 \cdot 931 \text{ psi})\right]$$

$$f'_{cir,6000} = MAX[7252 \text{ psi},\ 7569 \text{ psi}] = 7569 \text{ psi}$$

Similarly, for $f'_{ci} = 6500$ psi in the "Break at 6000" line, using the same $s = 931$ psi,

$$f'_{cir,6500} = MAX[7752 \text{ psi},\ 8019 \text{ psi}] = 8019 \text{ psi}$$

And the calculated value of f'_{cir} found at $f'_{ci} = 6000$ psi was also used for $f'_{ci} = 5500$ psi, $f'_{ci} = 5000$ psi, etc. Thus, the following would both be true for the "Break at 6000" line:

$$f'_{cir,5500} = f'_{cir,6000} = 7569 \text{ psi}$$

$$f'_{cir,5000} = f'_{cir,6000} = 7569 \text{ psi}$$

This process was repeated for each assumed break. Most of the time, the addition of the next strength bin increased the sample standard deviation, because the addition of more data points spread out the distribution. Occasionally, however, the additional data points actually decreased the standard deviation by filling in "gaps" in the previously existing distribution. In either case, there were usually a number of curves for each plant, and for the full data set, that converged on the chart. In effect, the addition of extra strength bins did not significantly change the expected strength at higher specified strengths. This may be seen by examining Figure 6.4 once more, and noticing that the lines for "Break at 4000" through "Break at 5500" are nearly identical above their respective break points. Furthermore, the lines for "Break at 4000" through "Break at 6500" do not differ greatly above their respective break points.

Figure 6.4 was used as the basis for developing some method of predicting the average strength that would actually be expected for any level of specified strength, without prior knowledge of which plant would produce the girders. Using the mean strengths ($\bar{x}$), the sample standard deviations (s), and the general line shapes generated by the production of this graph, a number of trial fit lines were developed. These trial fit prediction methods are shown in Table 6.4, and are graphed next to the break lines that most closely matched the mean values release strengths in Figure 6.5.

Table 6.4: Possible Release Strength Prediction Methods

Current Practice	$f_{ci}^{*} = f_{ci}'$
Trial Fit #1	$f_{ci}^{*} = 7500$ psi for $f_{ci}' \leq 6000$ psi and $f_{ci}^{*} = f_{ci}' + 1000$ psi for $f_{ci}' > 6000$ psi
Trial Fit #2	$f_{ci}^{*} = 7600$ psi for $f_{ci}' \leq 6000$ psi and $f_{ci}^{*} = \frac{4}{5} f_{ci}' + 2800$ psi for $f_{ci}' > 6000$ psi
Trial Fit #3	$f_{ci}^{*} = 7500$ psi for $f_{ci}' \leq 6500$ psi and $f_{ci}^{*} = f_{ci}' + 1000$ psi for $f_{ci}' > 6500$ psi
Trial Fit #4	$f_{ci}^{*} = 7500$ psi for $f_{ci}' \leq 7000$ psi and $f_{ci}^{*} = f_{ci}' + 500$ psi for $f_{ci}' > 7000$ psi

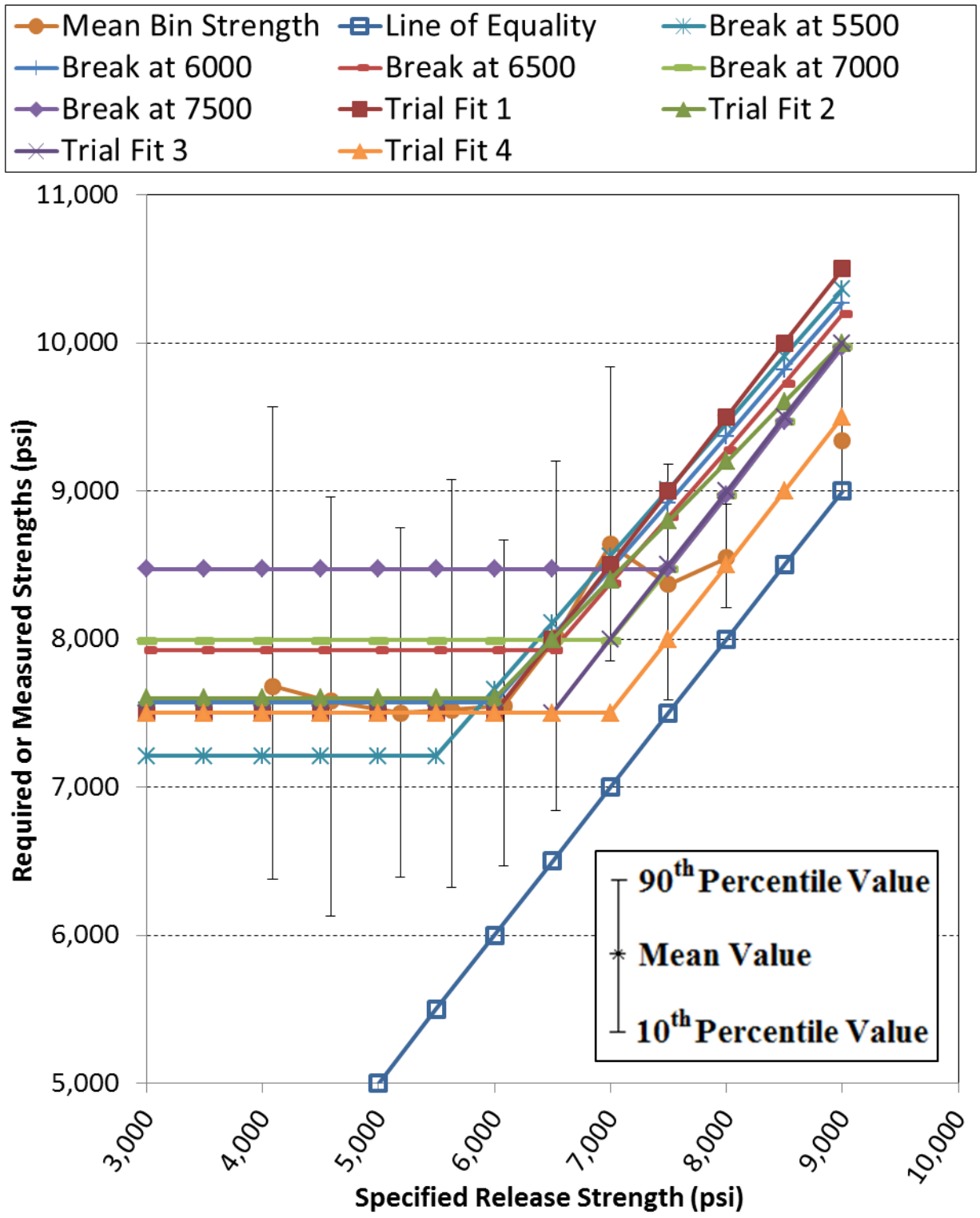

Figure 6.5: Release Strength Break Points and Trial Fits, All Data

It may be apparent from examining Figure 6.5 that the first two trial fit lines (Trial Fit 1 and Trial Fit 2) were predominately fitted to match the mean strengths in the lower f'_{ci} range. There are several good reasons for this.

- The lower range of data is much more consistent. Therefore, it is much more realistic to have a constant function that matches those strengths.
- The lower range of data contains a much larger number of data points than the high range. The number of girders with $f'_{ci} > 7500$ psi drops drastically compared to those with $f'_{ci} \leq 7500$ psi.
- Not only do the number of girders drop off, but the number of plants that have produced girders with high f'_{ci} also drops off. Only Plant D produced girders with $f'_{ci} > 8000$ psi, and that was fewer than 20 pours. Only Plant C produced girders with $f'_{ci} = 8000$ psi, and that was also fewer than 20 pours. Every other pour, from every plant, had $f'_{ci} \leq 7500$ psi.

Because of these reasons, fitting the strength prediction model to the lower values of f'_{ci} was more statistically accurate than trying to force the model to match the higher values of f'_{ci}. However, there was some uncertainty as to how designers might respond to the appearance of predicting strengths higher than the mean bin strengths at higher f'_{ci} values, so Trial Fit 4 was created to err slightly on the side of safety.

It should be mentioned again, however, that the purpose of these strength prediction methods is to provide accurate predictions of average behavior for the prediction of service-life behavior, not conservative predictions of lower-bound behavior for life safety or strength design. The whole point of the specified f'_{ci} value is that it is supposed to be a form of reasonable lower-bound strength, as mentioned in Section 2.4. However, when it comes to predicting service-level

behavior, under-predicting average behavior is no better or worse than over-predicting average behavior. The goal is to most accurately predict actual behavior, not provide for life safety.

Statistical accuracy was only one of the factors by which the choice of strength prediction methods was made. It was desired that the prediction model would have a number of traits, as may be seen here.

- First, it was desired that the prediction model employ a two-part linear piecewise function, as this was expected to reasonably accurately model the exhibited strength patterns while still maintaining a fairly simple equation set.
- Second, it was desired that the statistical accuracy of the model significantly improve the predictions when compared to current practice. Current practice is simply to use the specified strengths, f'_{ci} and f'_c, as the expected strengths. Checking the statistical accuracy was primarily done using the standard error of estimate (SEE), which is explained below.
- It was also desired that the prediction model be simple without sacrificing substantial accuracy. Thus it would be linear, without unduly precise numbers. This aspect primarily came into effect when selecting between various prediction models. When the model could be made much simpler without significant cost to the statistical accuracy, this aspect provided motivation to use the simpler of the two.

These three desired traits were considered when determining which model was best for use.

The standard error of estimate, otherwise referred to as the SEE, was the primary means of determining the statistical accuracy of any prediction model. It was calculated using Equation 6.5, a modified form of Equation 6.4, found in *Statistical Methods for Engineers* (McCuen 1985). Equation 6.5 was changed simply to match the variable forms used in this thesis.

$$S_e = \left[\frac{1}{\nu}\sum_{i=1}^{n}\left(\hat{Y}_i - Y_i\right)^2\right]^{0.5}$$ **Equation 6.4**

where:

S_e = standard error of estimate

ν = degrees of freedom in the equation

$= n - (number\ of\ unknowns)$

n = number of data values

$\hat{Y}_i$ = the *i*th predicted value of the criterion variable

Y_i = the *i*th measured value of Y

$$S_e = \left\{\frac{1}{\nu}\sum_{j=1}^{n}\left[(f_{ci}^{*})_j - (f_{ci})_j\right]^2\right\}^{0.5}$$ **Equation 6.5**

where:

S_e = standard error of estimate, psi

ν = degrees of freedom in the equation

$= n - (number\ of\ unknowns)$

n = number of data values

$(f_{ci}^{*})_j$ = the *j*th predicted value of the concrete strength at release, psi

$(f_{ci})_j$ = the *j*th measured concrete strength at release, psi

This equation provided a measure of how accurately each prediction method predicted strengths compared to the actual measured values.

Table 6.5 was created to summarize the statistical accuracy of some of the final release strength prediction methods compared to the current practice of using $f_{ci}^{*} = f_{ci}'$. It can readily be seen from this table that the prediction methods greatly improved strength predictions. In every

case except for the results from Plant C, the SEE was reduced approximately 50% or more by using one of the trial fit prediction models. When one considers the wide variability of data measurements, and the massive range of data included (described in Section 5.3), an improvement of 50% in the errors for a prediction model is quite substantial.

Table 6.5: Standard Errors of Estimate for Release Strength Predictions

		Standard Error of Estimate for Release Strength Predictions				
Strength Prediction Method		Full Data Set (psi)	Plant A Only (psi)	Plant B Only (psi)	Plant C Only (psi)	Plant D Only (psi)
Current Practice	$f_{ci}^* = f'_{ci}$	2120	2310	1750	1400	2050
Trial Fit #1	$f_{ci}^* =$ 7500 psi for $f'_{ci} \leq$ 6000 psi and $f_{ci}^* = f'_{ci} +$ 1000 psi for $f'_{ci} >$ 6000 psi	950	920	890	1230	1040
Trial Fit #2	$f_{ci}^* =$ 7600 psi for $f'_{ci} \leq$ 6000 psi and $f_{ci}^* = \frac{4}{5} f'_{ci} +$ 2800 psi for $f'_{ci} >$ 6000 psi	940	900	920	1280	1000
Trial Fit #3	$f_{ci}^* =$ 7500 psi for $f'_{ci} \leq$ 6500 psi and $f_{ci}^* = f'_{ci} +$ 1000 psi for $f'_{ci} >$ 6500 psi	950	940	860	1180	1000
Trial Fit #4	$f_{ci}^* =$ 7500 psi for $f'_{ci} \leq$ 7000 psi and $f_{ci}^* = f'_{ci} +$ 500 psi for $f'_{ci} >$ 7000 psi	970	940	860	1210	980

The standard error of estimate is, in this case, also called the standard deviation of errors.

Therefore, a complementary way of viewing these results would be to view them as a distribution of errors, where the error is defined as follows (McCuen 1985):

$$e_i = \hat{Y}_i - Y_i \qquad \textbf{Equation 6.6}$$

where:

e_i = error of the *i*th prediction

$\hat{Y}_i$ = the *i*th predicted value of the criterion variable

Y_i = the *i*th measured value of Y

Or, in the case of release strengths

$$e_j = \left(f^*_{ci}\right)_j - \left(f_{ci}\right)_j \qquad \textbf{Equation 6.7}$$

where:

e_j = error of the *j*th strength prediction, psi

$(f^*_{ci})_j$ = the *j*th predicted value of the concrete strength at release, psi

$(f_{ci})_j$ = the *j*th measured concrete strength at release, psi

Using this definition of errors, Table 6.6 was created to summarize the comparison of error distributions between predicted release strengths, specified release strengths, and measured release strengths.

Table 6.6: Error Distributions for Release Strength Predictions

90th Percentile Prediction Error	Full Data Set (psi)	Plant A Only (psi)	Plant B Only (psi)	Plant C Only (psi)	Plant D Only (psi)
Current Practice	-3300	-3490	-3001	-2458	-3416
Trial Fit #1	1220	913	1300	1938	1370
Trial Fit #2	1230	960	1350	2038	1182
Trial Fit #3	1021	790	1211	1938	1056
Trial Fit #4	1020	753	1211	1938	1056
Mean Prediction Error					
Current Practice	-1825	-2075	-1468	-1076	-1618
Trial Fit #1	35	-190	369	820	133
Trial Fit #2	96	-127	441	864	166
Trial Fit #3	-76	-308	273	686	40
Trial Fit #4	-117	-352	249	621	-8
10th Percentile Prediction Error					
Current Practice	-470	-857	-289	-72	-186
Trial Fit #1	-1240	-1440	-653	-374	-1350
Trial Fit #2	-1160	-1353	-580	-368	-1250
Trial Fit #3	-1381	-1526	-772	-576	-1350
Trial Fit #4	-1430	-1550	-772	-590	-1350

Table 6.5 and Table 6.6, when combined, demonstrate just how much the trial fit prediction methods improved release strength predictions over the current practice. Simply using the SEE is not enough. The SEE acts like a standard deviation, quantifying how dispersed the errors are in their distribution. However, because of its practice of squaring all the errors (see Equation 6.4 or 6.5), the SEE cannot indicate whether the predictions are too high, or too low, or in the middle. It only quantifies how tightly distributed the errors are.

Thus, Table 6.6 is provided to demonstrate how the predictions compare with the distribution. In this table, examination of the “Current Practice” rows shows that, because of the requirements of adequate strength for release and plant practice of obtaining strengths much

higher than the specified strength, current practice consistently under-predicts the strength. The 90th Percentile value is the most negative, the Mean value less negative, and the 10th Percentile value the least negative. The point is—they're all negative. They're all less than the actual strength, whether by a little bit or a large amount.

Examination of Table 6.6 demonstrates that the trial fit prediction methods are tailored to pass through the approximate average behavior of the strength distributions. The 90th Percentile values are largely positive, the Mean values are in the vicinity of zero, and the 10th Percentile values are largely negative. This means that the predicted value falls close to the mean of the measured values. Such behavior is exactly what is desired for service-level behavior prediction.

Combined examination of Table 6.5 and Table 6.6 shows that the trial fit prediction methods developed in this project serve to both improve the distribution of errors between predicted values and measured values, and to improve the location of the predicted strength relative to the mean strength of the group.

For design engineers, with no prior knowledge of which plant will be producing the girders they design, Trial Fit 4 is suggested for predicting actual release strengths for any given specified strength.

$$f_{ci}^{*} = 7500 \text{ psi} \qquad \text{for } 4000 \text{ psi} \leq f_{ci}' \leq 7000 \text{ psi} \qquad \textbf{Equation 6.8}$$

$$f_{ci}^{*} = f_{ci}' + 500 \text{ psi} \qquad \text{for } 7000 \text{ psi} < f_{ci}' \leq 9000 \text{ psi}$$

where:

f_{ci}^{*} = expected concrete strength at release, psi

f_{ci}' = specified concrete strength at release, psi

This piecewise function is very simple to apply, and provides a means of approximating the average expected strength at release based on the specified strength at release. A graph of this

suggested function compared to the mean strengths of each strength bin and the ranges contained in each strength bin may be seen in Figure 6.6. A graph of the suggested function compared to the raw set of data points may be seen in Figure 6.7.

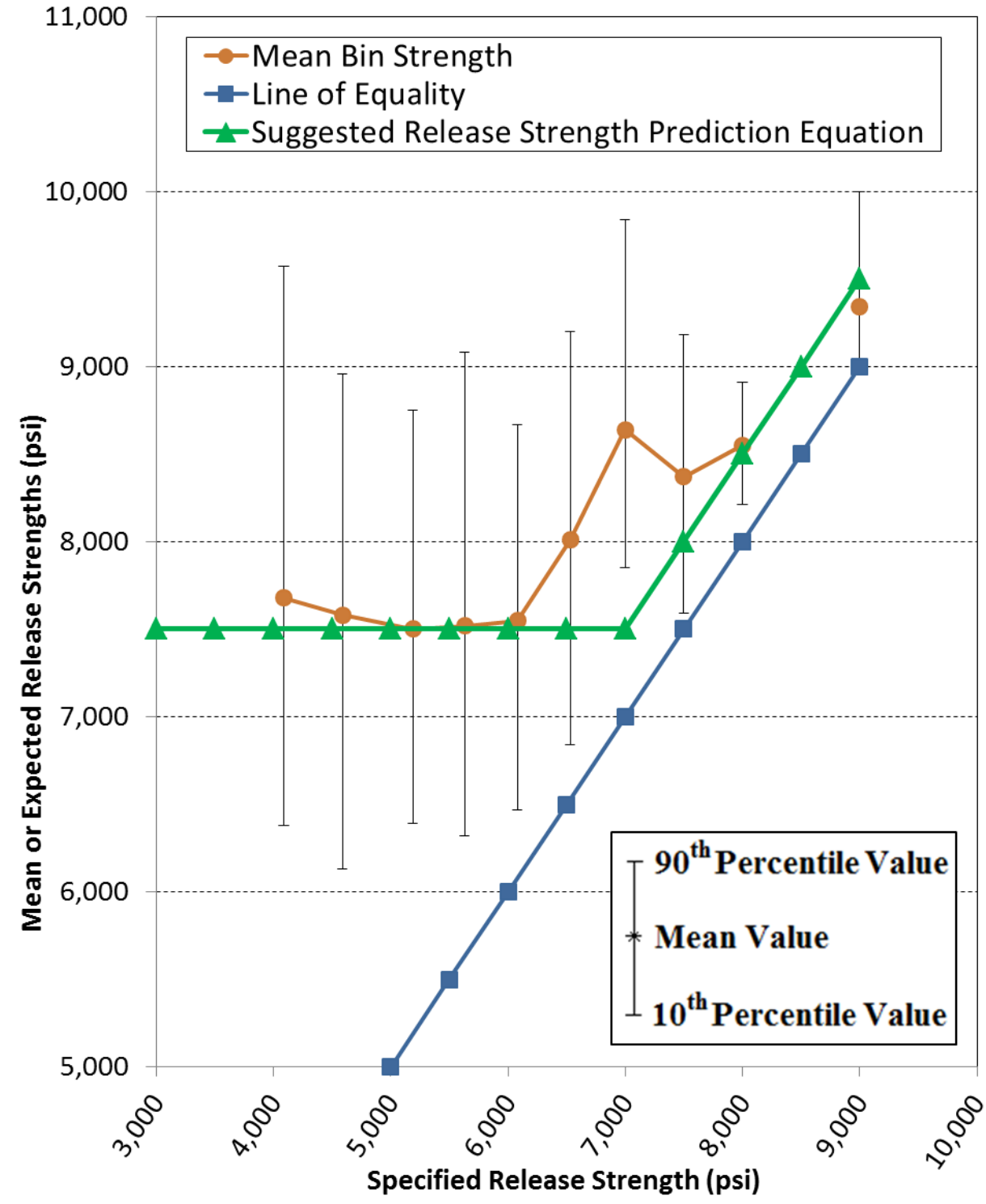

Figure 6.6: Predicted Release Strengths Compared to Mean Bin Release Strengths

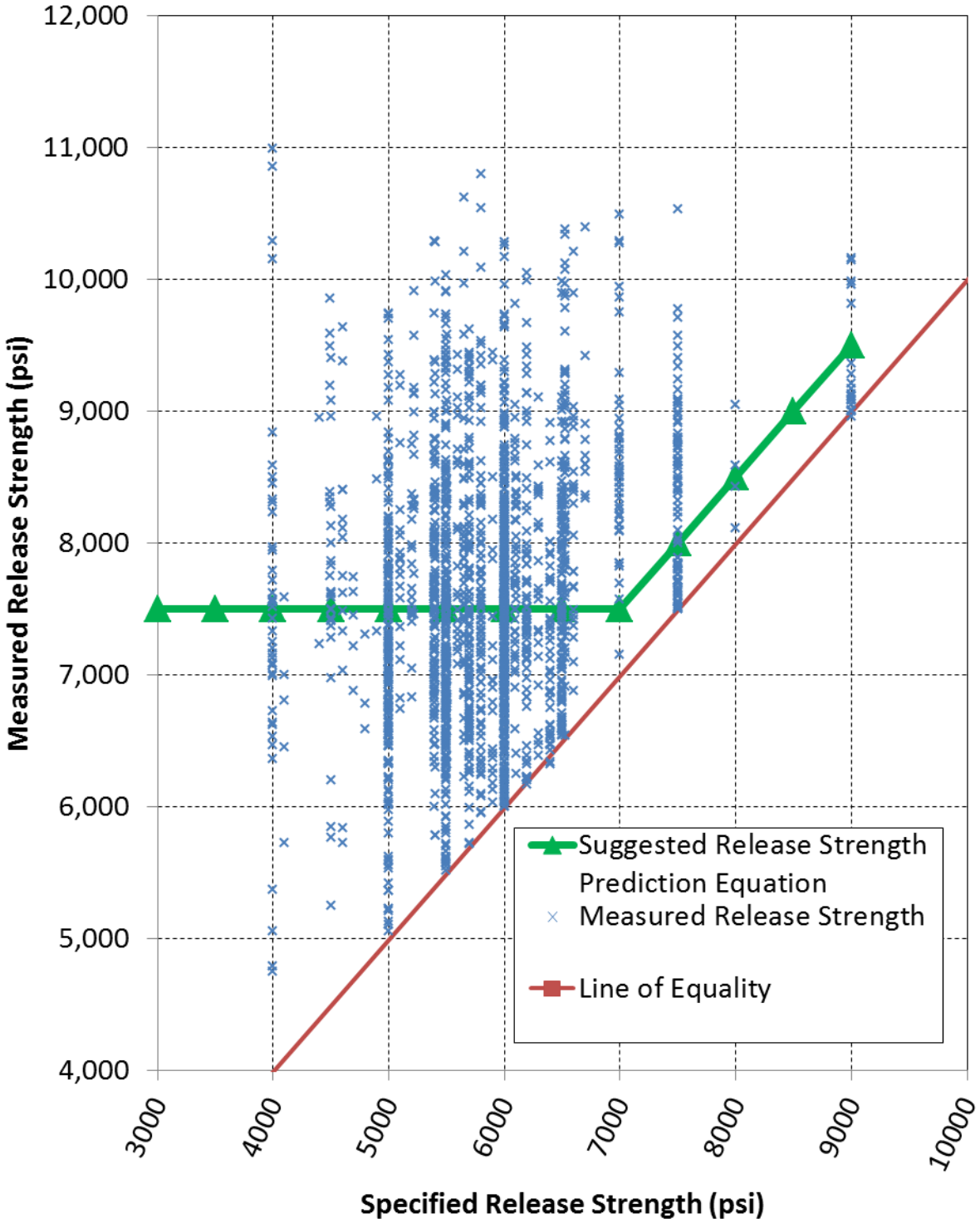

Figure 6.7: Predicted Release Strengths Compared to Raw Release Strength Data

The upper branch of the Trial Fit 4 prediction line was largely dictated by the upper strength bins, especially when $f'_{ci} \geq 7500$ psi. These upper bins had limited data, though—few data values, only one or two producers per strength bin, and only one or two projects per bin. Therefore, this prediction method could be refined as more projects are produced with high specified release strengths. The lack of adequate numbers of "well behaved" data for the higher specified strengths also contributed to the suggestion of the slightly-more conservative Trial Fit 4 instead of Trial Fit 3, which was slightly more accurate for the same level of complexity.

Both of these prediction methods, aside from their piecewise nature, are similar in concept to the provisions found in the *fib* Model Code (2010) for converting the characteristic strength (f_{ck}) into the mean strength (f_{cm}). As is discussed in Section 2.2, when no better information is available by which to establish the mean strength, the MC2010 specifies that 8 MPa be added to the characteristic strength (or approximately 1200 psi). This arithmetic difference is used no matter the level of specified characteristic strength.

In that regard, then, the trial fit prediction methods differ from the MC2010. In the lower strength levels well below the break point, the difference between f^*_{ci} and f'_{ci} are substantially greater than 1000 psi. Nearer the break point, however, the difference becomes less than 1200 psi. Eventually, when the break point is reached and beyond, the difference between f^*_{ci} and f'_{ci} is only 500 psi—only half as large as the MC2010 specifies.

6.3.2. Measured Strength Focus

The measured strength focus is an alternative way of analyzing strength distributions. It would not be useful for design engineers, because they would not know the actual strength of the producer-selected concrete mixture. However, this analysis might provide producers with a sense

of the consistency of their strength distributions within a certain range. The only information that is provided in this thesis is a detailed bin analysis of the full data set, which may be seen in Table 6.7 below, and bin analyses of each plant. The plant-specific analyses are summarized in Appendix G.

Table 6.7: Full Set Release Strength Distributions – Bins Divided by f_{ci}

Strength Bins	n	Sample Standard Deviation, s (psi)	Sample Mean, $\bar{x}$ (psi)	Sample Coefficient of Variance, COV (%)	Skewness Check, $\sqrt{\beta_1}$	Kurtosis Check, β_2
f_{ci} < 5500 psi	40	250	5190	4.84	-1.160	3.598
5500 psi ≤ f_{ci} < 6000 psi	125	140	5790	2.33	-0.391	2.055
6000 psi ≤ f_{ci} < 6500 psi	263	150	6280	2.37	-0.309	1.841
6500 psi ≤ f_{ci} < 7000 psi	409	140	6760	2.10	-0.212	1.929
7000 psi ≤ f_{ci} < 7500 psi	405	150	7230	2.02	0.117	1.820
7500 psi ≤ f_{ci} < 8000 psi	328	140	7720	1.83	0.189	1.860
8000 psi ≤ f_{ci} < 8500 psi	184	140	8230	1.69	0.086	1.973
8500 psi ≤ f_{ci} < 9000 psi	99	150	8720	1.72	0.020	1.597
9000 psi ≤ f_{ci} < 9500 psi	45	120	9220	1.34	0.179	2.324
9500 psi ≤ f_{ci} < 10,000 psi	20	170	9690	1.73	0.549	1.821
10,000 psi ≤ f_{ci}	3	30	10,100	0.32	-0.343	0.667
Full f_{ci} Range	1921	910	7200	12.7	0.299	3.067

This table is very similar in concept to Table 6.1. The difference between the two is in the division of the strength bins. Table 6.1 was divided into bins according to the specified release

strength of each pour, f'_{ci}. Table 6.7 is divided into bins according to the measured strength at the time of release, f_{ci}.

Aside from the first and last bins, which both cover a much wider set of possible values, the mean bin strength for each bin was fairly close to the center of that bin. The number of data values in each bin also closely resembles the pattern that was seen in Figure 5.12 for the distribution of release strengths.

The standard deviations and COVs for each bin, with the possible exception of the COV for the "f_{ci} < 5500 psi" bin, were very small, indicating tight control over the distribution of strengths within that bin. The COV and s for the "f_{ci} < 5500 psi" bin were still less than the suggested values for "excellent" control of general construction testing in the ACI 214 report (2011), but they were substantially larger than the COVs and standard deviations for the other bins.

The skewness values of most bins were reasonably close to zero, indicating symmetric distributions of strength measurements about the mean bin strength. The kurtosis values for almost all bins, however, were substantially less than 3.0, indicating that the distribution of measurements within each bin were flatter (less peaked) than a normal distribution would be. The largest exception to both of these trends occurred in the "f_{ci} < 5500 psi" bin.

6.4. Analysis and Prediction of 28-Day Strengths

Concrete strengths at 28 days are the most commonly specified concrete parameter in construction. Furthermore, standard-cure cylinders broken at 28 days are the most common method of measuring the quality of concrete as delivered to the site of construction. However, as discussed in Section 1.2, concrete strengths at the time of prestress release are much more

important with regards to the objectives of this research project. Therefore, less analysis was performed on the 28-day strength tests than the release strength tests.

6.4.1. Specified Strength Focus

The analysis of unadjusted 28-day strength measurements provides a method of predicting concrete strength for bridge design engineers, just like the analysis of unadjusted release strength measurements. Although the ability to predict 28-day strengths does not substantially benefit engineers in the prediction of girder cambers, it is still useful information for design engineers to know.

Figure 5.13 shows a plot of all measured 28-day strengths compared to the specified 28-day strength of each respective pour. Based on knowledge of plant practices, it was assumed that 28-day strength measurement distributions would not be as consistent or as meaningful as release strength values. Table 6.8 was created to summarize the statistical distributions of 28-day strengths for the full data set. Plant-specific versions of the summary found in Table 6.8 may be found in Appendix H.

Table 6.8: All 28-Day Strength Distributions –Bins Divided by f'_c

Strength Bins	n	Sample Standard Deviation, s (psi)	Sample Mean, $\bar{x}$ (psi)	Sample Coefficient of Variance, COV (%)	Skewness Check, $\sqrt{\beta_1}$	Kurtosis Check, β_2
5000 psi ≤ f'_c < 5500 psi	61	1270	10,180	12.46	0.067	2.707
5500 psi ≤ f'_c< 6000 psi	56	600	10,950	5.52	-0.115	5.994
6000 psi ≤ f'_c < 6500 psi	455	890	10,480	8.52	-0.533	3.828
6500 psi ≤ f'_c < 7000 psi	307	860	10,470	8.19	-0.818	5.475
7000 psi ≤ f'_c < 7500 psi	782	1100	10,580	10.38	-0.405	3.046
7500 psi ≤ f'_c < 8000 psi	38	840	10,790	7.75	-0.067	2.011
8000 psi ≤ f'_c < 8500 psi	170	770	11,100	6.90	-0.047	2.493
8500 psi ≤ f'_c < 9000 psi	12	320	10,270	3.07	-1.409	4.074
9000 psi ≤ f'_c< 9500 psi	16	1250	11,300	11.07	0.531	2.591
Full f'_cRange	1897	1000	10,590	9.40	-0.439	3.678

Table 6.8 shows the distributions of measured 28-day compressive strengths without any modification. Surprisingly, the 28-day strength distributions were reasonably similar in normality compared to the release strength distributions. In fact, they were in many cases arguably closer to a normal distribution than the release strength distributions. However, they did appear to be somewhat more sporadic. The release strength distributions showed clear trends toward more controlled strength distributions with higher specified strengths, whereas the 28-day strength distributions showed no trends in the COV, even though individual bins were often closer to a normal distribution than the release strength distributions were (comparing the coefficients of variance from Table 6.1 and Table 6.8).

Another thing that was somewhat surprising from the 28-day strength tests was the

sometimes massive level of overstrength that was measured. This may best be demonstrated by examination of Figure 6.8, which was created using a process identical to the one described in Section 6.3.1. This figure represents a comparison between possible required strengths by the methods of ACI Committee 214 (2011) with a minimum plant-preferred mixture strength and the actual measured strengths for the full data set.

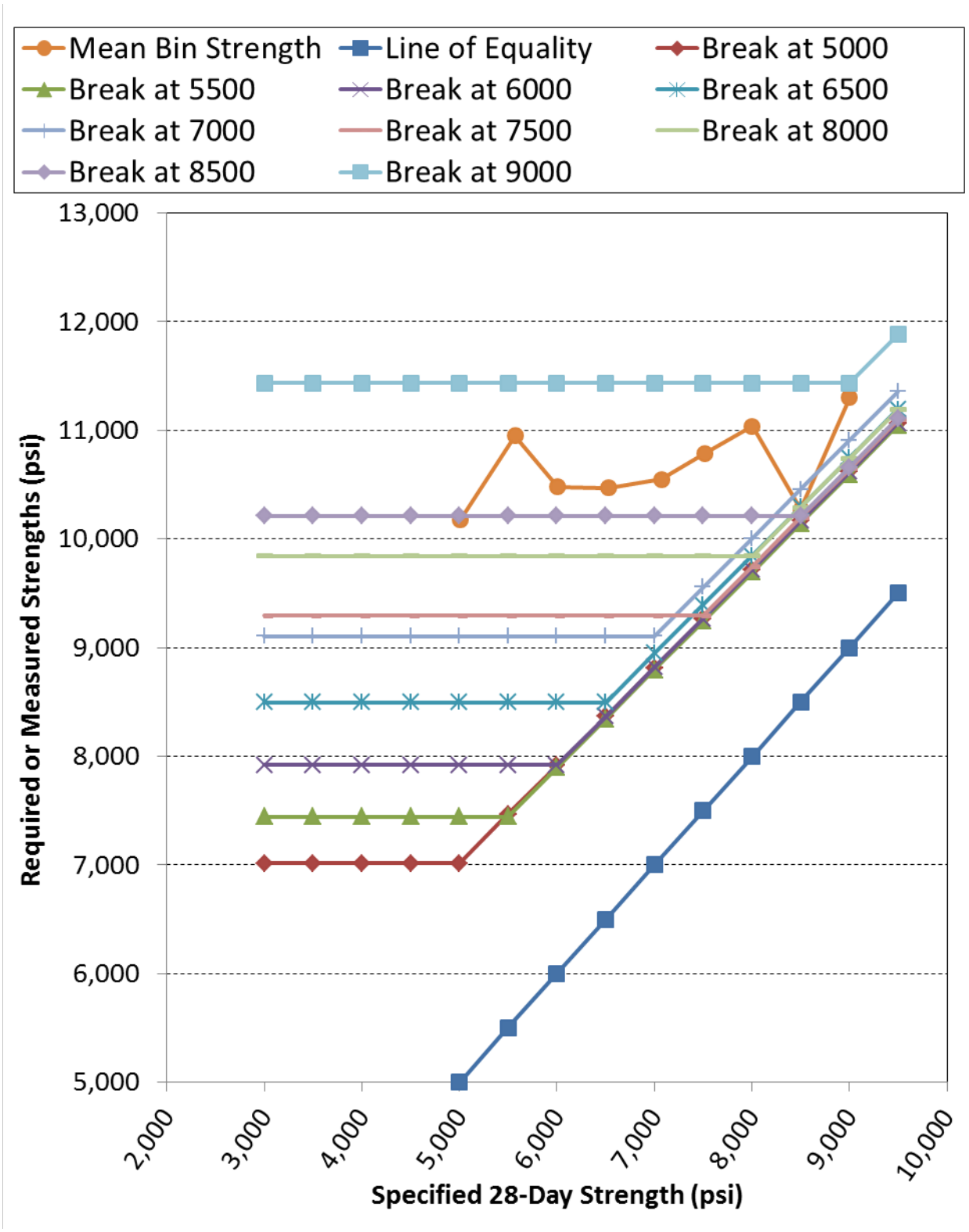

Figure 6.8: Break Points in 28-Day Strength Measurements, All Data

The results for this analysis were very similar to those found for release strengths, as may be seen by comparing Figure 6.8 to Figure 6.4. The strengths exhibited in Figure 6.8 are higher than the strengths in Figure 6.4, which is to be expected. However, two other differences may be noted.

First, the apparent break point for Figure 6.4 was much lower than that for Figure 6.8 for reasonably accurate prediction of strengths below the break point. For Figure 6.8, the most accurate break point for lower f_c' values was at 8500 psi. However, for Figure 6.4 the most accurate break point for lower f_{ci}' values was at 6000 psi.

In tandem with that, the 28-day mean strengths shown in Figure 6.8 exhibit a higher degree of scatter than the mean release strengths shown in Figure 6.4. There appears to be less control, or less consistency, in the 28-day strengths than in the release strengths, thus providing further confirmation for the idea that girder producers focus on release strengths more than 28-day strengths.

This analysis provided some of the first confirmation for the expectation that 28-day strengths would take a place of secondary importance relative to release strengths. As Figure 6.8 and the mean strengths calculated in Table 6.8 demonstrate, the 28-day strengths found in plant-submitted data are much higher than the strengths specified by design engineers. Viewing the requirements of strength at 28 days without considering the other aspects of the production process, it would make very little sense for girder producers to use this high strength concrete unless it was required. The concrete mixtures that achieve high strengths have high cement contents, high SCM contents, and large doses of chemical admixtures, making them expensive mixtures to be used when not required. If 28-day strength were the sole measure of acceptance, there would be no reason for a girder producer to supply strengths so much higher than the

specified strength.

However, two primary factors explain why producers would want to use a concrete mixture that ultimately achieves a strength much higher than specified.

1. In order for any concrete mixture to be used for the production of prestressed concrete girders for ALDOT, that mixture must undergo a rigorous approval process as described in ALDOT Procedure 170 (ALDOT 2009). The costs associated with this approval process, as well as the requirements of maintaining documentation of multiple mixtures, encourage producers to simply maintain one or two concrete mixtures for use on all girder pours. The simplest approach is to ensure that all concrete mixtures have a high strength and can be used for all or most of the girder pours, regardless of the specified strength. For example, then, a plant may create a concrete mixture that is approved for use in any girder with $f_c' \leq 10{,}000$ psi. That plant may then use that mixture for any girder with $f_c' \leq 10{,}000$ psi, even if the actual f_c' for a specific project is only 5500 psi. The actual strength would correspond to the strength of the mixture, not to the specified strength of the girder.
2. Perhaps even more importantly, the use of high strength mixtures requires a smaller percentage of the total long-term strength to be developed by the time of prestress transfer. As is discussed many places in this thesis, prestress release governs everything in prestressed girder production. The earlier a girder may be released, the earlier it may be removed from the casting line. The longer girders must stay on the line, the fewer girders may be produced in a year.

   The use of a high strength mixture has the potential to reduce the amount of time a girder must cure before the prestressing strands may be cut. After all, consider a project with

$f'_{ci} = 4500$ psi. If the producer decides to use a concrete mixture with a target 28-day strength of $f_c^* = 6000$ psi, then approximately 75% of the target strength must be developed in that girder before it may be removed from the line on which it was produced. However, if the producer decides to use a concrete mixture with a target 28-day strength of $f_c^* = 10{,}000$ psi, then only 45% of the target strength must be developed before the girder may be removed. Thus the required 28-day strength becomes easily satisfied because of the steps taken to gain rapid early strength, as was discussed in Section 6.2. By using a higher strength mixture, the producer is potentially able to reduce the amount of time required before the production line may be prepared for the next pour. In consideration of these two factors, it is not surprising that measured 28-day strengths greatly exceed the specified strengths for which they were produced.

The ultimate goal of the strength analyses, as explained in Section 1.2, was to have a means of more accurately estimating modulus of elasticity for a given strength level. The intermediate goal, therefore, was to gain a reasonably accurate estimate of what the expected strength would be for any specified strength. As such, a two-part piecewise function was created to approximate the average strength level expected for any given specified strength. The process used to determine this prediction equation was identical to the process used to determine the trial fit release strength prediction model as described in Section 6.3.1. Therefore, the figures and tables that follow in this section directly parallel similar figures and tables in Section 6.3.1. The only difference is that everything in this section is related to 28-day strength instead of release strength.

The trial fit curves that were developed to predict 28-day strength may be seen in Figure 6.9, together with the most accurate break lines and the bin mean strengths for comparison. This

figure corresponds to Figure 6.5 for release strengths.

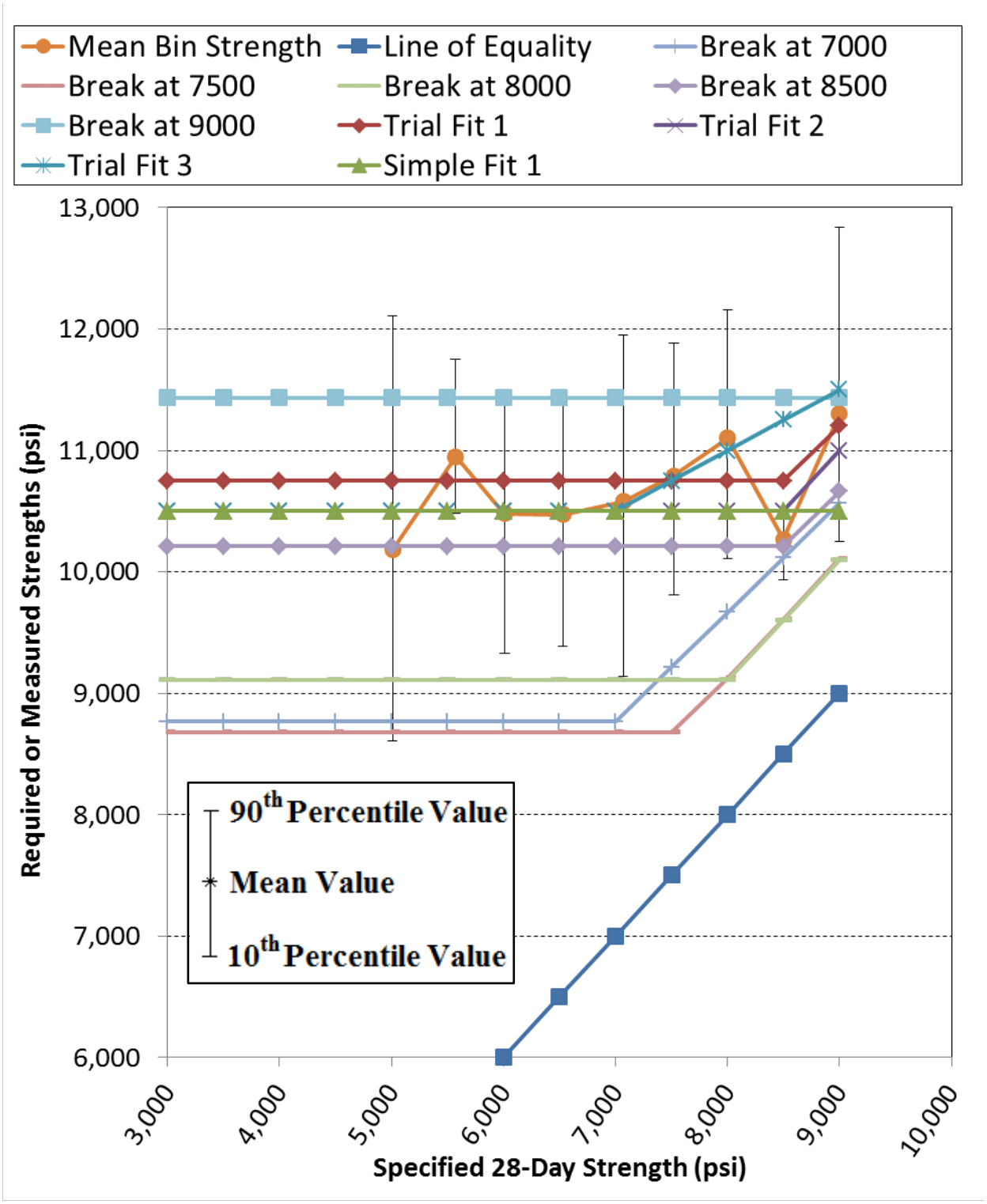

Figure 6.9: 28-Day Strength Break Points and Trial Fits, All Data

As may be seen from either Figure 6.8 or Figure 6.9, the mean bin strengths exhibited some definite non-linear behavior between the first three bins. Trial Fit 1 was shaped to match the overall average of all lower-strength bins. It was outside of the range for the 8500 psi bin, but it was well within the bounds of the other bins.

The Trial Fit 2 and Trial Fit 3 lines, on the other hand, attempted to minimize error by bisecting the means of the first two bins and matching the short linear portion in the next two bins. Trial Fit 2 continued until 8500 psi before breaking, thus attempting to better match the higher-strength bins. Trial Fit 3 broke the piecewise function into its second component in a location that allowed it to best match the next three bins after the short linear portion.

The scatter of the data, together with the mean values of the full data set and the calculated values of SEE that were found for each prediction method, led researchers to also include the Simple Fit line. This line simply expected the 28-day strength to be 10,500 psi, regardless of the specified 28-day strength, provided that it was within the bounds of the collected data.

In this case, as with the release strength analysis, there was no break point line that adequately matched the behavior of strength distributions without modification. Therefore the trial fit lines were created to statistically match the behavior, while still being simple and easy to remember. The requirements for the suggested method of strength prediction are outlined in Section 6.3.1.

Table 6.9 and Table 6.10 compare the trial fit curves to current design practice for predicting 28-day strengths. Table 6.9 serves to quantify the spread of the errors, while Table 6.10 shows how the predicted strengths compare to the average strengths of the bin.

Table 6.9: Standard Errors of Estimate for 28-Day Strength Predictions

Strength Prediction Method		Standard Error of Estimate for 28-Day Strength Predictions				
		Full Data Set (psi)	Plant A Only (psi)	Plant B Only (psi)	Plant C Only (psi)	Plant D Only (psi)
Current Practice	$f_c^* = f_c'$	4020	4150	4270	2350	3500
Trial Fit #1	$f_c^* = 10{,}750$ psi for $f_c' \leq 8500$ psi and $f_c^* = \frac{9}{10} f_c' + 3100$ psi for $f_c' > 8500$ psi	1010	890	700	2100	1130
Trial Fit #2	$f_c^* = 10{,}500$ psi for $f_c' \leq 8500$ psi and $f_c^* = f_c' + 2000$ psi for $f_c' > 8500$ psi	1000	920	770	1890	1050
Trial Fit #3	$f_c^* = 10{,}500$ psi for $f_c' \leq 7000$ psi and $f_c^* = \frac{1}{2} f_c' + 7000$ psi for $f_c' > 7000$ psi	980	890	740	1910	1030
Simple Fit #1	$f_c^* = 10{,}500$ psi	1000	920	770	1890	1070

Table 6.10: Error Distributions for 28-Day Strength Predictions

90th Percentile Prediction Error	Full Data Set (psi)	Plant A Only (psi)	Plant B Only (psi)	Plant C Only (psi)	Plant D Only (psi)
Current Practice	-5260	-5290	-5440	-3410	-4766
Trial Fit #1	1500	1200	610	3210	1606
Trial Fit #2	1250	950	360	2960	1356
Trial Fit #3	1270	990	450	2960	1366
Simple Fit #1	1250	950	360	2960	1346
Mean Prediction Error					
Current Practice	-3855	-4028	-4170	-2114	-3267
Trial Fit #1	164	22	-76	1864	452
Trial Fit #2	-86	-228	-326	1614	206
Trial Fit #3	-13	-149	-274	1705	271
Simple Fit #1	-90	-228	-326	1614	167
10th Percentile Prediction Error					
Current Practice	-2290	-2679	-3000	-900	-2104
Trial Fit #1	-1100	-1160	-990	460	-1082
Trial Fit #2	-1350	-1410	-1240	210	-1332
Trial Fit #3	-1230	-1290	-1140	540	-1232
Simple Fit #1	-1354	-1410	-1240	210	-1388

Errors were calculated using Equation 6.9, which is the 28-day counterpart to Equation 6.7.

$$e_j = \left(f_c^*\right)_j - \left(f_c\right)_j \qquad \textbf{Equation 6.9}$$

where:

e_j = error of the *j*th strength prediction, psi

$(f_c^*)_j$ = the *j*th predicted value of the concrete strength at 28 days, psi

$(f_c)_j$ = the *j*th measured concrete strength at 28 days, psi

From these two tables, it is clear that any of provided prediction models greatly improves 28-day

strength predictions when compared to current practice. This improvement is quite substantial (up to a 75% decrease in the SEE for several cases), but Plant C does not experience the same improvement. This is largely due to the fact that Plant C had strengths that were smaller than the other plants, in general. However, the small number of pours from Plant C made the other plants more important for statistical accuracy. As was seen with release strengths in Section 6.3.1, the prediction results from Plant C show little improvement, and the distributions from Plant C show only limited improvement. However, when considering the data group as a whole, the improvement is quite substantial.

When all trial fits had been considered, Trial Fit 3 was found to be the most accurate. However, as may be seen in Figure 6.9 and Table 6.9 and Table 6.10, the simple fit method was only slightly less accurate than the piecewise functions. It also had a tendency to very slightly underestimate the actual strength on average. For engineers who much more commonly design for life safety, in which an overestimation of strength is dangerous, this may provide an additional level of comfort without substantial loss of accuracy over the range of concrete strengths covered.

Therefore, for the full data set, there are two functions this research project suggests for use in predicting 28-day concrete strengths—the Trial Fit #3 function and the Simple Fit #1 function. Both of these functions may be seen in Figure 6.10 and Figure 6.11, along with the range of values for which they were intended to approximate the strength. Figure 6.10 shows these suggested prediction equations in comparison with the bin mean strengths and bin strength ranges. Figure 6.11 show these suggested prediction equations in comparison with the raw 28-day strength data

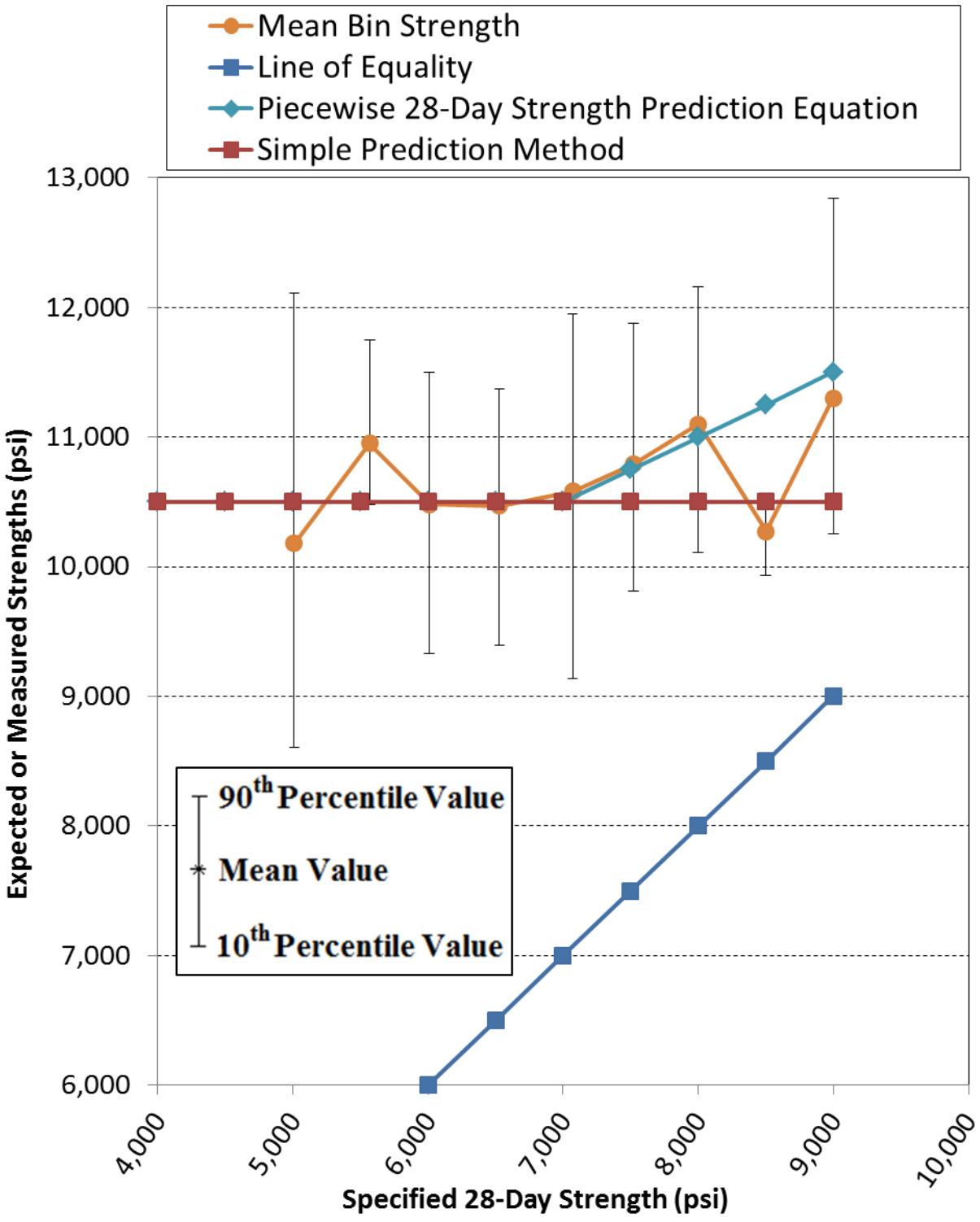

Figure 6.10: Predicted 28-Day Strengths Compared to Mean Bin 28-Day Strengths

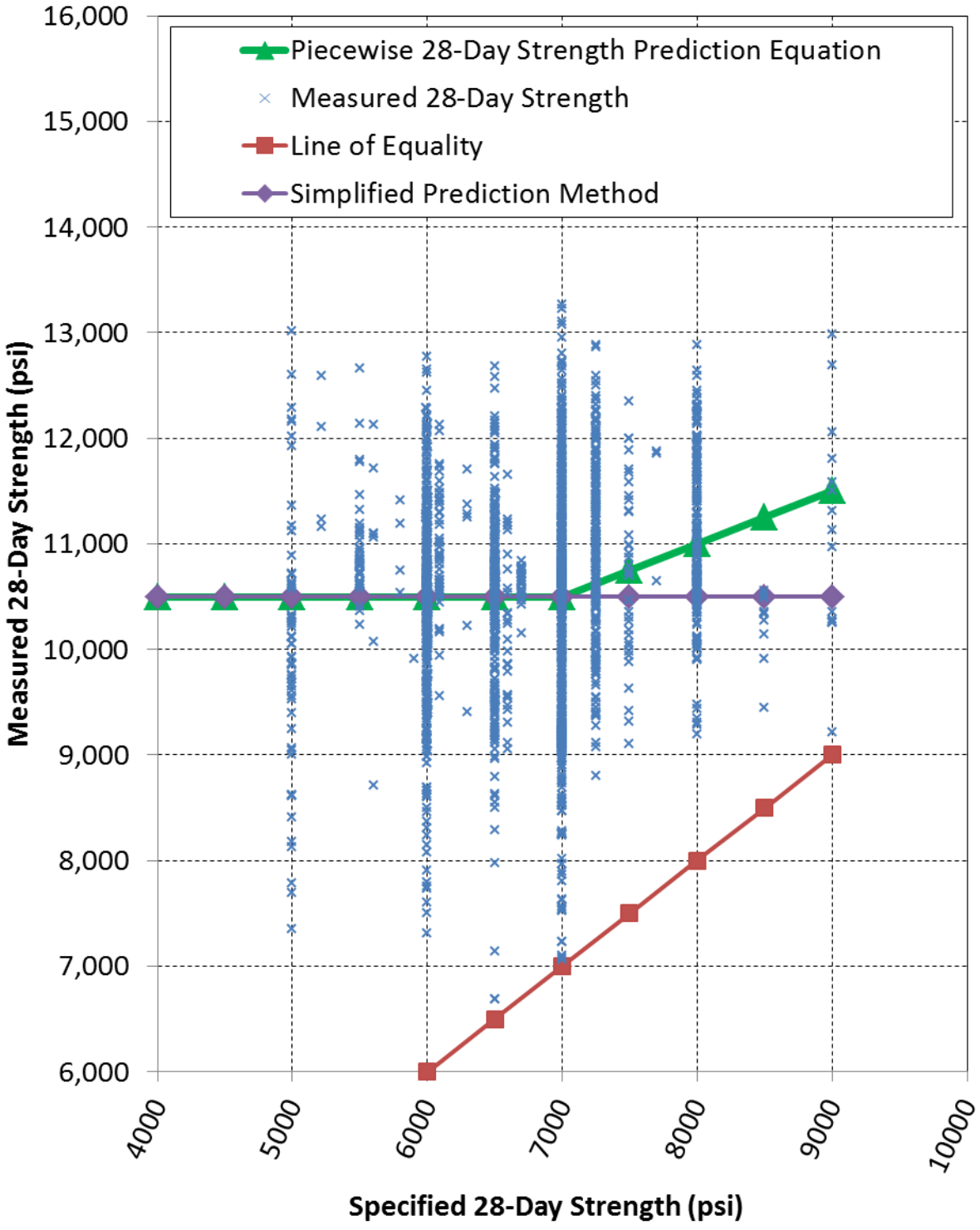

Figure 6.11: Predicted 28-Day Strengths Compared to Raw 28-Day Strength Data

The piecewise trial fit function, Trial Fit #3, is defined as Equation 6.10.

$$f_c^* = 10{,}500 \text{ psi} \qquad \text{for } 5000 \text{ psi} \leq f_c' \leq 7000 \text{ psi} \qquad \textbf{Equation 6.10}$$

$$f_c^* = \frac{1}{2} f_c' + 7000 \text{ psi} \qquad \text{for } 7000 \text{ psi} < f_c' \leq 9000 \text{ psi}$$

where:

f_c^* = expected concrete strength at 28 days, psi

f_c' = specified concrete strength at 28 days, psi

This piecewise function should be fairly simple to remember, and provides a means of approximating the average expected strength at 28 days based on the specified 28-day strength.

However, Equation 6.10 is somewhat unusual compared to previously seen expected strength prediction equations. Some expected strength prediction methods, such as the MC2010 method for estimating f_{cm} based on f_{ck} (see Section 2.2), use the addition of a small strength increase to estimate the expected strength. Other methods, such as some of those presented in Section 2.4, use a constant multiplier greater than 1.0 to estimate the expected strength. Equation 6.10 is unusual because it uses a multiplier (less than 1.0) *and* adds a substantial strength increase (7000 psi). This method was chosen because it fit the behavior of the strength bins well. However, the Trial Fit #2 line presented in Table 6.9 could also be used without substantial decreases in the error of estimation.

If the Simple Fit #1 prediction method would rather be used, it is defined in Equation 6.11.

$$f_c^* = 10{,}500 \text{ psi} \qquad \textbf{Equation 6.11}$$

$$\text{for } 5{,}000 \text{ psi} \leq f_c' \leq 9{,}000 \text{ psi}$$

where:

f_c^* = expected concrete strength at 28 days, psi

f_c' = specified concrete strength at 28 days, psi

The piecewise function uses an arithmetic addition to the strength in establishing the expected mean strength, as the MC2010 specifies. However, unlike the MC2010, Equation 6.10 does not increase the expected strength at the same rate as the specified strength increases above the break point. The Simple Fit #1 method follows neither of these trends, and merely predicts a constant strength no matter what the specified strength may be. This is clearly not what the MC2010 specifies.

6.4.2. Measured Strength Focus

A bin analysis was performed on 28-day strengths with bins divided according to the measured 28-day strength, f_c. The results of this analysis for 28-day strengths may be seen in Table 6.11, which parallels Table 6.7 for release strengths. Plant-specific versions of Table 6.11 may be seen in Appendix H.

Table 6.11: Full Set 28-Day Strength Distributions – Bins Divided by f_c

Strength Bins	n	Sample Standard Deviation, s (psi)	Sample Mean, $\bar{x}$ (psi)	Sample Coefficient of Variance, COV (%)	Skewness Check, $\sqrt{\beta_1}$	Kurtosis Check, β_2
f_c < 8000 psi	30	360	7520	4.80	-0.688	2.563
8000 psi ≤ f_c < 8500 psi	21	130	8280	1.55	-0.035	2.165
8500 psi ≤ f_c < 9000 psi	46	160	8730	1.87	0.292	1.584
9000 psi ≤ f_c < 9500 psi	178	130	9260	1.44	0.084	1.873
9500 psi ≤ f_c < 10,000 psi	180	150	9750	1.54	-0.053	1.694
10,000 psi ≤ f_c < 10,500 psi	296	140	10,260	1.38	-0.138	1.875
10,500 psi ≤ f_c < 11,000 psi	525	130	10,720	1.18	0.212	2.092
11,000 psi ≤ f_c < 11,500 psi	305	150	11,230	1.30	0.141	1.786
11,500 psi ≤ f_c < 12,000 psi	175	140	11,740	1.21	0.020	1.857
12,000 psi ≤ f_c < 12,500 psi	108	120	12,190	1.01	0.387	2.276
12,500 psi ≤ f_c < 13,000 psi	28	130	12,680	1.04	0.675	2.440
13,000 psi ≤ f_c	6	420	13,310	3.15	1.203	2.661
Full f_c Range	1898	1000	10,590	9.40	-0.438	3.676

This table shows nearly identical trends to those shown by Table 6.7 for release strengths. Except for the smallest and largest strength bins, the mean bin strength for each bin was close to the center of that bin. The standard deviations and COVs were all very small. The largest standard deviations and COVs occurred in the smallest and largest strength bins, but were still within the bounds of what would be labeled “excellent” concrete control by ACI Committee 214 (2011).

Many of strength bins had a skewness relatively close to zero, although there were more exceptions to this in Table 6.11 than there were in Table 6.7. The smallest strength bin had a sizeable skewness value, and the three largest strength bins also had relatively large skewness values. Furthermore, similar to what was seen in Table 6.7, all of the bins had kurtosis values less than 3.0, indicating distributions that were less peaked than a normal distribution would be.

6.5. Time and Maturity Effects

It is well known in the concrete industry that concrete strength and stiffness develop over time. It is also well known that this development is, especially at younger concrete ages, highly dependent on the temperature at which the concrete is cured. This is the reason for the development of methods for describing a concrete "age" in terms of both time and temperature, creating a "maturity" or an "equivalent age" (EA). The Temperature-Time Factor Method (TTFM) and the Equivalent Age Method (EAM), the most common methods used for calculating these adjusted ages, are discussed in Sections 2.3.1 and 5.5.

However, the TTFM and the EAM are only designed to deal with the maturity of the concrete. They do not inherently describe the strength of that concrete at said maturity. Various strength growth equations have been developed for that purpose, and some of these are used in this section to describe the strength growth of the concretes studied in this project with respect to time. This data set was limited to only those points which met the requirements laid out in Section 5.5, and covered 435 girder pours from Plant A.

6.5.1. Strength Growth Analyses

The strength growth analysis, described in Section 2.3.1, was performed on the limited data set as two groups. Optimization was performed using a least-squares approach. The data was either treated as a single data group, or the data was divided according to concrete mixture. Although Plant A used only a small number of concrete mixtures during the time over which these data were collected, the labeling system used was not always consistent. As such, nine different concrete mixture labels were found in the data set. Since it was not always clear which label was the same as a different label, each label was treated as its own mixture. Of the nine possible mixtures, two mixtures clearly did not have enough data points to provide meaningful results. Therefore, when the data was analyzed by concrete mixture, only seven mixtures were included. The number of data values available for each mixture is summarized in Table 6.12.

Table 6.12: Number of Data Values for Each Mixture

	Number of Data Values
Mixture #1	125
Mixture #2	117
Mixture #3	53
Mixture #4	87
Mixture #5	9
Mixture #6	18
Mixture #7	23

Analysis of the strength growth equations took place in two main stages.

1. The data was first filled into a digital spreadsheet. Each girder pour contained release ages, equivalent ages calculated according to Section 5.5, release strengths, and 28-day strengths. Using these four pieces, it was possible to try various combinations of

prediction and comparing using the ACI 209 (1992) equations and the *fib* Model Code (2010) equations. In any case, the strength growth equations were used to create predictions for each pour. An error was then calculated between that prediction and the measured value. These errors were squared, and summed.

A SOLVER function was implemented to minimize the sum of these squared errors. This SOLVER function used the GRG Nonlinear Solving Method, designed for smooth non-linear functions. For the MC2010 predictions, the SOLVER function varied the value of s until the sum of the squares of the errors had been minimized. For the ACI 209 predictions, the SOLVER function varied the values of α and β values until the sum of the errors had been minimized. This was done for both the full 435-pour set, and for each mixture individually.

For all SOLVER iterations, bounds or other constraints were required on the varied parameters. The following constraints were used to control the optimized parameter values:

- $0.00 \leq s \leq 1.00$
- $0.00 \leq \alpha \leq 28.00$
- $0.000 \leq \beta \leq 1.000$
- $\alpha = (1 - \beta)28$

The last two constraints were required to enforce logical values for the ACI 209 predicted strength at 28 days and at the final (long-term) age.

2. The second stage of the optimization process measured how well the prediction method, with its optimized values from stage #1, predicted the strength growth of that group. One

component of checking the predicted fit was by using the following equation (Brown 2000):

$$R^2 = 1 - \frac{\Sigma\left(y - y_{fit}\right)^2}{\Sigma\left(y - y_{mean}\right)^2} \qquad \textbf{Equation 6.12}$$

where:

R^2 = correlation index, or coefficient of determination – measure of how well the predicted curve fits the measured data

y = measured data point

y_{fit} = predicted data point

y_{mean} = mean of the measured data points

This equation provided the R^2 value for each prediction method. The closer R^2 approached 1.0, the better the prediction method predicted the measured values. The closer R^2 come to 0.0, the worse the fit. For linear equations, the range of R^2 was from 0.0 to 1.0. However, when fitting non-linear equations to measured data, it is possible to have an $R^2 < 0.0$. Mathematically, $R^2 < 0.0$ simply means that the errors between the predicted values and the measured values are greater than the errors between the measured values and the mean of the measured values.

The other two components of checking the predicted fit was by use of the standard error of estimate, which is explained in Section 6.3.1, and the standard percent error of estimate, which is explained in Section 6.5.2.

In short, stage #1 resulted in the values of s, α, and β that would make the functions most accurately predict strength growth. Then stage #2 checked to see just how accurate each function was once it had been optimized.

In addition to analyzing the data set as two groups (one with all 435 pours, one divided by concrete mixture), the data was also analyzed in what is called two different "directions." As may be seen from Equations 2.10 and 2.16, prediction of time-dependent strength usually uses the 28-day strength as the basis for all other strengths. In other words, if it was desired to predict concrete strength at release using a strength-growth equation, it would first be necessary to have knowledge or accurate predictions of the 28-day strengths. For practical real-time purposes, this seems illogical—requiring knowledge of a later strength to predict an earlier strength.

Bearing this issue in mind, Equations 2.10 and 2.16 were rearranged in an attempt to try predicting 28-day strengths using measured release strengths, rather than the other way around. Equation 2.10 was turned into Equation 6.13, and Equation 2.16 was turned into Equation 6.14. No true restructuring of the prediction method took place—simply a rearrangement of the time-dependent factor relative to the strengths. These equations are written in terms of the 28-day strength, rather than a generalized later-age strength, because all later-age strength tests included in this analysis were performed at 28 days.

$$f_{cm} = \frac{f_{cm}(t)}{\beta_{cc}(t)} \qquad \textbf{Equation 6.13}$$

with

$$\beta_{cc}(t) = exp\left\{s \cdot \left(1 - \sqrt{\frac{28}{t}}\right)\right\}$$

where:

f_{cm} = the mean compressive strength at an age of 28 days, MPa

$f_{cm}(t)$ = the mean compressive strength at time t, MPa

$\beta_{cc}(t)$ = a function to describe strength development with time

s = coefficient which depends on the strength class of cement, as given in Table

2.1

t = the concrete age adjusted according to Equation 6.13 (taking into account temperature during curing), days

$$f_{c28} = \left(\frac{\alpha + \beta \cdot t}{t}\right) \cdot f_c(t) \qquad \textbf{Equation 6.14}$$

where:

f_{c28} = concrete strength at a concrete age of 28 days, psi

t = concrete age, days

α = constant used for shaping the strength growth function, days

β = constant used for shaping the strength growth function

$f_c(t)$ = concrete strength at any concrete age t, psi

These two equations were used to predict 28-day strengths based on known release strengths and concrete ages at the time of release. These ages could be either chronological age or equivalent age.

In short, there were a total of four possible divisions, resulting in a large number of analyses. The four divisions may be summed up as follows:

1. The source of the strength growth prediction model. This could be either the MC2010 method or the ACI 209 method.
2. The direction of prediction. Each method could use 28-day strengths to predict release strengths, or it could use release strengths to predict 28-day strengths.
3. The chosen maturity (or age) quantification. The maturity could be quantified in terms of chronological age, or in terms of equivalent age based on temperatures during curing.

4. The size of the data set. Each analysis could be on the complete 435-pour set, or on each individual mixture.

A summary of where to find each strength-growth analysis that is discussed in this thesis may be seen in Table 6.13. Calculation of optimized s, α, and β parameters was only performed when predicting release strengths. However, the measures of fit were compared for both prediction directions, to see if the prediction methods could reasonably be used for the prediction of later strengths based on release strengths.

Table 6.13: Strength-Growth Analyses Included in this Thesis

				MC2010	ACI 209
Full Data Set	Predicting Release Strengths	Chronological Age	Not Adjusted	Sect. 6.5.2	Sect. 6.5.2
			Air-Adjusted	Sect. 6.6.2	Sect. 6.6.2
		Equivalent Age	Not Adjusted	Sect. 6.5.2	Sect. 6.5.2
			Air-Adjusted	Sect. 6.6.2	Sect. 6.6.2
	Predicting 28-Day Strengths	Chronological Age	Not Adjusted	Sect. 6.5.2	Sect. 6.5.2
			Air-Adjusted	Sect. 6.6.2	Sect. 6.6.2
		Equivalent Age	Not Adjusted	Sect. 6.5.2	Sect. 6.5.2
			Air-Adjusted	Sect. 6.6.2	Sect. 6.6.2
By Mixture	Predicting Release Strengths	Chronological Age	Not Adjusted	Sect. 6.5.2	Sect. 6.5.2
			Air-Adjusted	Sect. 6.6.2	Sect. 6.6.2
		Equivalent Age	Not Adjusted	Sect. 6.5.2	Sect. 6.5.2
			Air-Adjusted	Sect. 6.6.2	Sect. 6.6.2
	Predicting 28-Day Strengths	Chronological Age	Not Adjusted	Sect. 6.5.2	Sect. 6.5.2
			Air-Adjusted	Sect. 6.6.2	Sect. 6.6.2
		Equivalent Age	Not Adjusted	Sect. 6.5.2	Sect. 6.5.2
			Air-Adjusted	Sect. 6.6.2	Sect. 6.6.2

6.5.2. Strength-Growth Prediction Results

This section summarizes the results of all unadjusted data analyses contained in Table 6.13. There were far too many parts to this analysis to easily display all the results in a single instance. Therefore, the results must be presented in a number of tables and summaries.

When considering all 435 pours as a single data set, the analyses results may be condensed enough to nicely fit into a single table. Table 6.14 provides a summary of the strength growth parameters (s, α, and β) for each prediction method, prediction direction, and maturity quantification.

Table 6.14: Summary of Strength-Growth Prediction Results for Full Data Set

			Predicting Release Strengths		Predicting 28-Day Strength	
			Chronological Age	**Equivalent Age**	**Chronological Age**	**Equivalent Age**
MC2010	Optimized	s	0.069	0.147	0.069	0.147
		SEE (psi)	620	610	880	900
		SPEE (%)	8.6	8.5	8.2	8.4
		R^2	0.38	0.39	-0.05	-0.10
	Suggested by MC2010	s	0.20	0.20	0.20	0.20
		SEE (psi)	3670	1080	10,170	1920
		SPEE (%)	48.4	14.2	96.2	18.0
		R^2	-20.9	-0.88	-139	-4.00
ACI 209	Optimized	α (days)	0.34	1.13	0.34	1.13
		β	0.988	0.960	0.988	0.960
		SEE (psi)	620	710	900	1100
		SPEE (%)	8.6	9.8	8.4	10.2
		R^2	0.37	0.18	-0.09	-0.63
	Suggested by ACI 209	α (days)	0.70	0.70	0.70	0.70
		β	0.98	0.98	0.98	0.98
		SEE (psi)	1990	1100	3800	1370
		SPEE (%)	25.8	15.4	36.1	12.7
		R^2	-5.40	-0.96	-18.6	-1.53

Two different sets of these strength growth parameters are provided for each method. The "optimized" parameters are those that were calculated using the process discussed in Section 6.5.1. These values are the values determined to minimize errors in the prediction method. The

"suggested" parameters, on the other hand, are those parameters that were suggested by the authors of the Model Code (*fib* 2010) and the ACI Committee 209 Report (1992) for the concrete mixtures and curing conditions used in these pours.

Table 6.14 uses a curve-fit measurement called the standard percent error of estimate (SPEE) in addition to the SEE. This variable is defined in Equation 6.15, and expresses the distribution of normalized errors, or errors as a percentage of the measured value.

$$SPEE = 100\% \cdot \left\{ \frac{1}{\nu} \sum_{j=1}^{n} \left[\frac{\left(f_c^*\right)_j - \left(f_c\right)_j}{\left(f_c\right)_j} \right]^2 \right\}^{0.5} \qquad \textbf{Equation 6.15}$$

where:

$SPEE$ = standard percent error of estimate, %

ν = degrees of freedom in the equation

$= n - (number\ of\ unknowns)$

n = number of data values

$(f_{ci}^*)_j$ = the *j*th predicted value of the concrete strength, psi

$(f_{ci})_j$ = the *j*th measured concrete strength, psi

This SPEE variable provides a more realistic means of comparing the accuracy of strength predictions between prediction directions, or before and after air adjustments. This is discussed in greater detail later.

For the MC2010 (*fib* 2010), the suggested parameter was $s = 0.20$, which corresponded to a high-strength, rapid early strength concrete mixture (42.5R or 52.5R designation in MC2010) (ACI Committee 209 2008). The ACI 209 report (1992) suggested an $\alpha = 0.70$ days and a $\beta = 0.98$ for steam-cured concretes with Type III cement. These conditions most closely matched the true mixture designs and curing conditions, so they were used for comparison.

Comparison of the accuracy of prediction methods with optimized parameters against the suggested parameters shows how much the predictions could be improved using the calculated values.

Lastly, Table 6.14 also provides a summary of how well each prediction method fits the measured data by providing the SEE, SPEE, and R^2 values for each for each set.

Both the differences and the similarities shown in Table 6.14 are interesting. Consider, for example, the results shown for the MC2010 analysis. Even though the s parameter was not changed between prediction directions, the SEE and R^2 values changed substantially. For both chronological age and EA results, the SEE increased by over 40% and R^2 decreased to a value less than zero (over 110% decrease) when predicting 28-day strengths. In both cases R^2 became negative, which means that the measured 28-day strengths were more consistent about their own mean than about the predicted strengths.

However, even though the SEE increased by 40% for both forms of maturity quantification, the SPEE stayed very close to the values obtained from predicting release strengths (and even became slightly smaller). This indicates that the increase in SEE was primarily due to the increase in the magnitude of predicted and measured values, not to an increase in the relative error of prediction. Expressed as a percentage of the measured value, the errors remained equivalent.

For the most part, the ACI 209 method showed very similar trends. When prediction direction was switched, the SEE increased by close to 50% for both chronological age and EA. R^2 showed a major decrease when predicting 28-day strengths instead of release strengths. The SPEE of 28-day predictions decreased by approximately 3% for chronological age predictions and increased by approximately 4% for EA predictions.

The suggested MC2010 equation showed substantial improvement for the full data set when using EA instead of chronological age. This should not be surprising, because the MC2010 method was designed to use EA, but was not suggested for use with chronological age. This is why the errors are so large for chronological age predictions with the MC2010 using chronological age (3670 psi for release strength predictions, and 10,170 psi for 28-day strength predictions). Even though the MC2010 was not intended for use with chronological age, the results have been shown for comparison. The suggested ACI 209 equation also showed substantial improvement when using EA instead of chronological age.

For the optimized ACI 209 equation, however, there was an increase in SEE and SPEE when using EA of approximately 15% to 22%. This increase in error occurred both when predicting release strengths and when predicting 28-day strengths. The SEE value for the optimized ACI 209 parameters with chronological age was approximately equal to the SEE for optimized MC2010 EA predictions. The corresponding SPEEs behaved the same way.

One of the last comparisons to be made from Table 6.14 alone is a comparison of the optimized strength growth parameters compared to the parameters suggested by each code. For the MC2010 method, the optimized s parameter was always less than the suggested s. As was discussed in Section 2.3.2, a smaller value of s indicates a more rapid rate of early strength development, and slower later-age strength development. Thus smaller values of s than suggested indicate more rapid strength development than was expected.

When using equivalent age, optimized s values were a little more than 25% less than the suggested s. When using chronological age, however, optimized s values were approximately 66% less than the suggested s. This difference makes sense, due to the time-stretching nature of equivalent age calculations. Equivalent age calculations use the high temperatures during early

girder curing to effectively "stretch out" the early curing time. In other words, the concrete "ages" much more rapidly before release compared to after release. Chronological age predictions do not have this stretching effect included.

Therefore, the ratio of aging before release to after release is much larger for equivalent age predictions, allowing the use of a slower strength development. Because the ratio of aging before release to after release was much smaller for chronological age predictions, a smaller s was required to increase the rate of strength gain. In both cases, the strength development was more rapid than the MC2010 predicted.

The ACI 209 optimized parameters are slightly harder to compare to the suggested values, because there are two parameters which both affect the shape and growth of the curve. The effect of both α and β are discussed in detail in Section 2.3.2. The time-dependent factor was constrained to equal 1.00 at time $t = 28$ days by using the fourth constraint listed in Section 6.5.1.

For the results shown in Table 6.14, it is clear that the optimized α value was substantially less than the suggested value when using chronological age, but substantially more than the suggested value when using equivalent age. The β value was slightly higher than the suggested value when using chronological age, but slightly less than the suggested value when using EA. α was approximately 44% less for chronological age calculations and 61% more for EA calculations. For chronological age, this indicates a similar trend as was discussed for the MC2010 s parameter, showing that early strength development was more rapid than the model predicted. For EA, however, the early strength development needed to be slower than the suggested model predicted.

If α were to remain fixed, an increased β value would indicate an overall decreased rate of strength development. Therefore, in some respects the increased β values for chronological age counteract the decreased α values. When the optimized values of α and β are compared to the suggested values, the net combined effect for chronological age was that early strength development was increased while later strength development was decreased. The combined effect for EA was the opposite—reducing the rate of early strength development but increasing the rate of later strength development.

In general, when comparing the two methods directly, the MC2010 equation was usually more accurate than the ACI 209 equation. The only exceptions were that the ACI 209 method was more accurate when using suggested parameters for chronological age calculations (as was expected) and for 28-day strength predictions with EA. All in all, it appears that the most accurate strength-growth equation for the full data set is to use the MC2010 strength-growth equation with calculated equivalent ages. This is approximately 20% more accurate than using the ACI 209 equation with chronological ages or EAs.

To visually support and clarify the comparisons made from Table 6.14, several figures have been provided. Figure 6.12 shows a comparison of all of the prediction methods used to predict release strengths based on chronological age. The data in this group is very closely grouped near 0.75 days, due to standard plant practices of releasing their girders at 18 hours. It is clear from this image that the optimized curve passes right through the approximate center of the data grouping for both methods, while the suggested curves pass below the group in both methods.

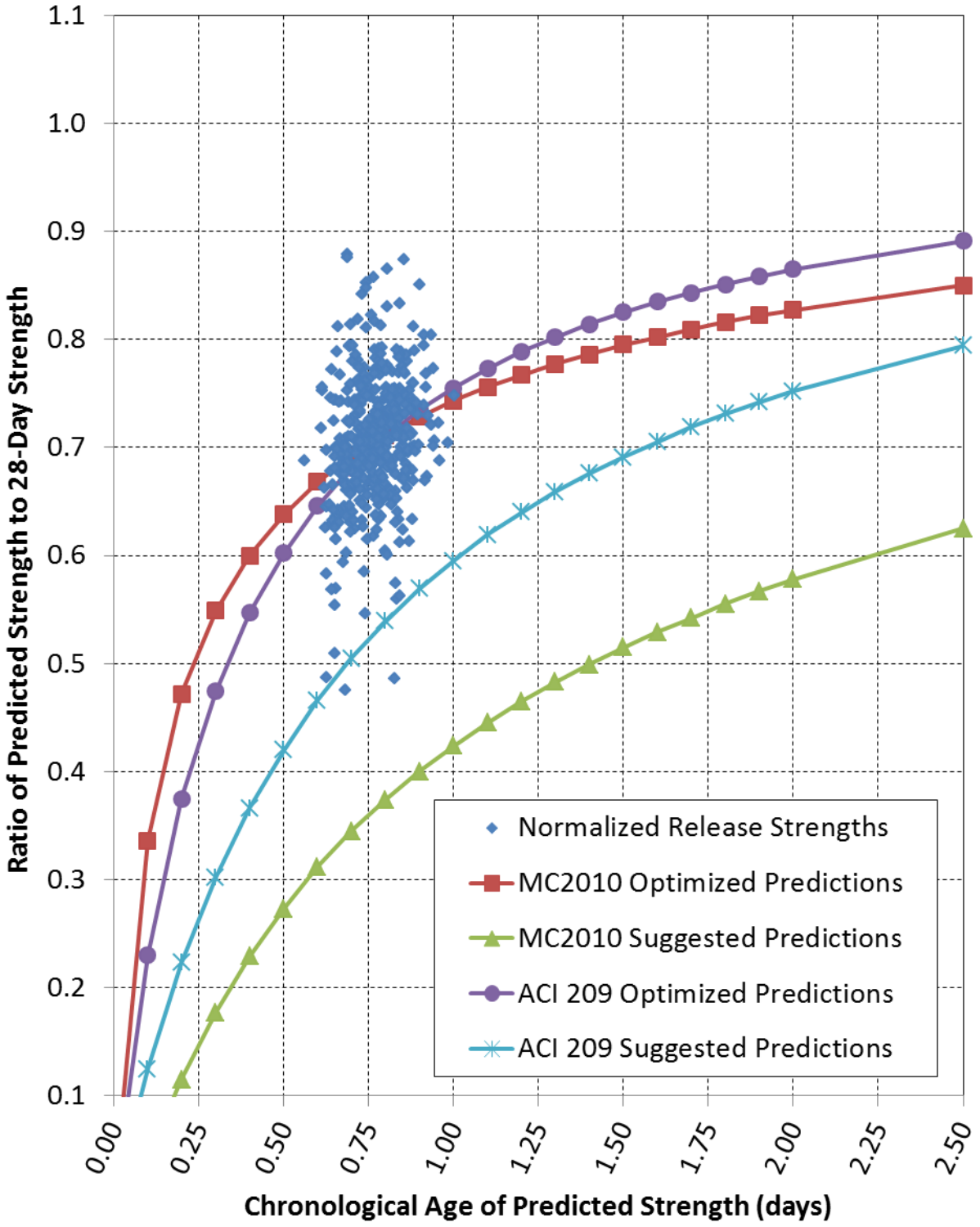

Figure 6.12: Prediction Curves for Release Strengths with Chronological Age

Figure 6.13 shows the same comparison as Figure 6.12, but all using equivalent age instead of chronological age. It may first be noticed from this figure that the data has been greatly spread out on the time scale by the use of equivalent age. Whereas in Figure 6.12 all of the data was grouped between 0.50 days to 1.00 days, in Figure 6.13 the data ranges all of the way from approximately 1.0 days to 8.0 days. Extended versions of Figure 6.12 and Figure 6.13 that show the behavior of each curve through much larger maturities may be seen in Figure 6.14 and Figure 6.15, respectively.

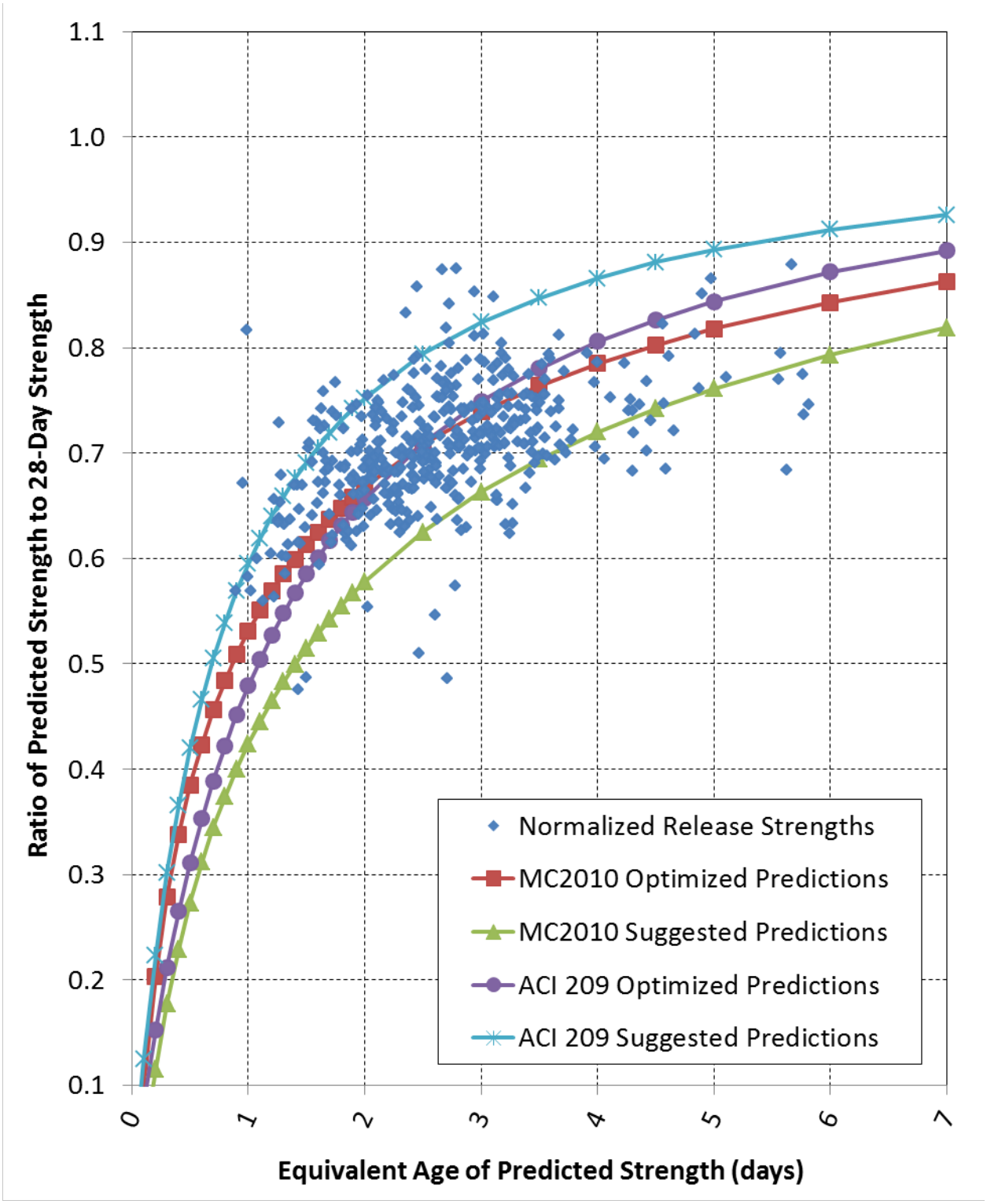

Figure 6.13: Prediction Curves for Release Strengths with Equivalent Age

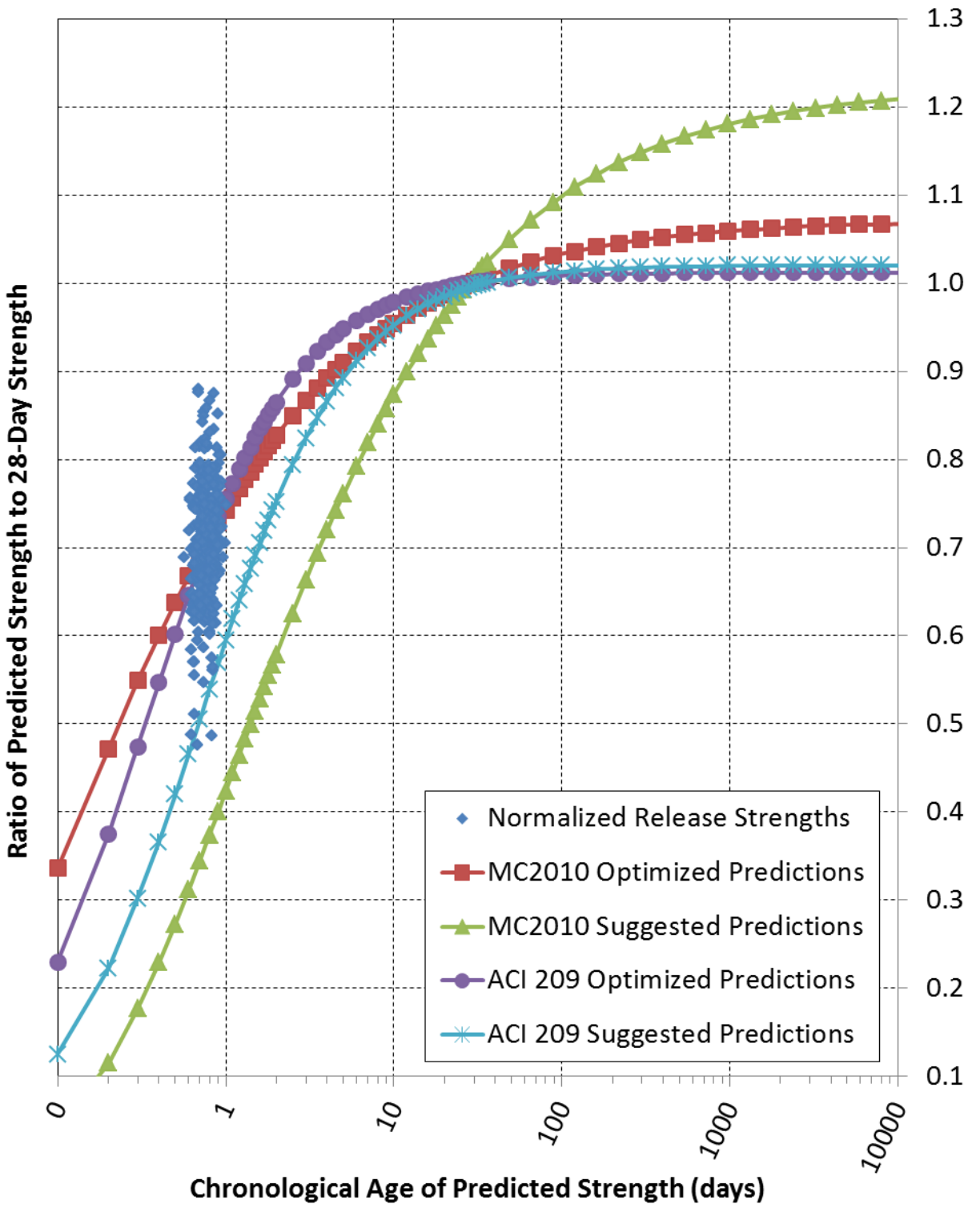

Figure 6.14: Extended Curves for Release Strengths with Chronological Age

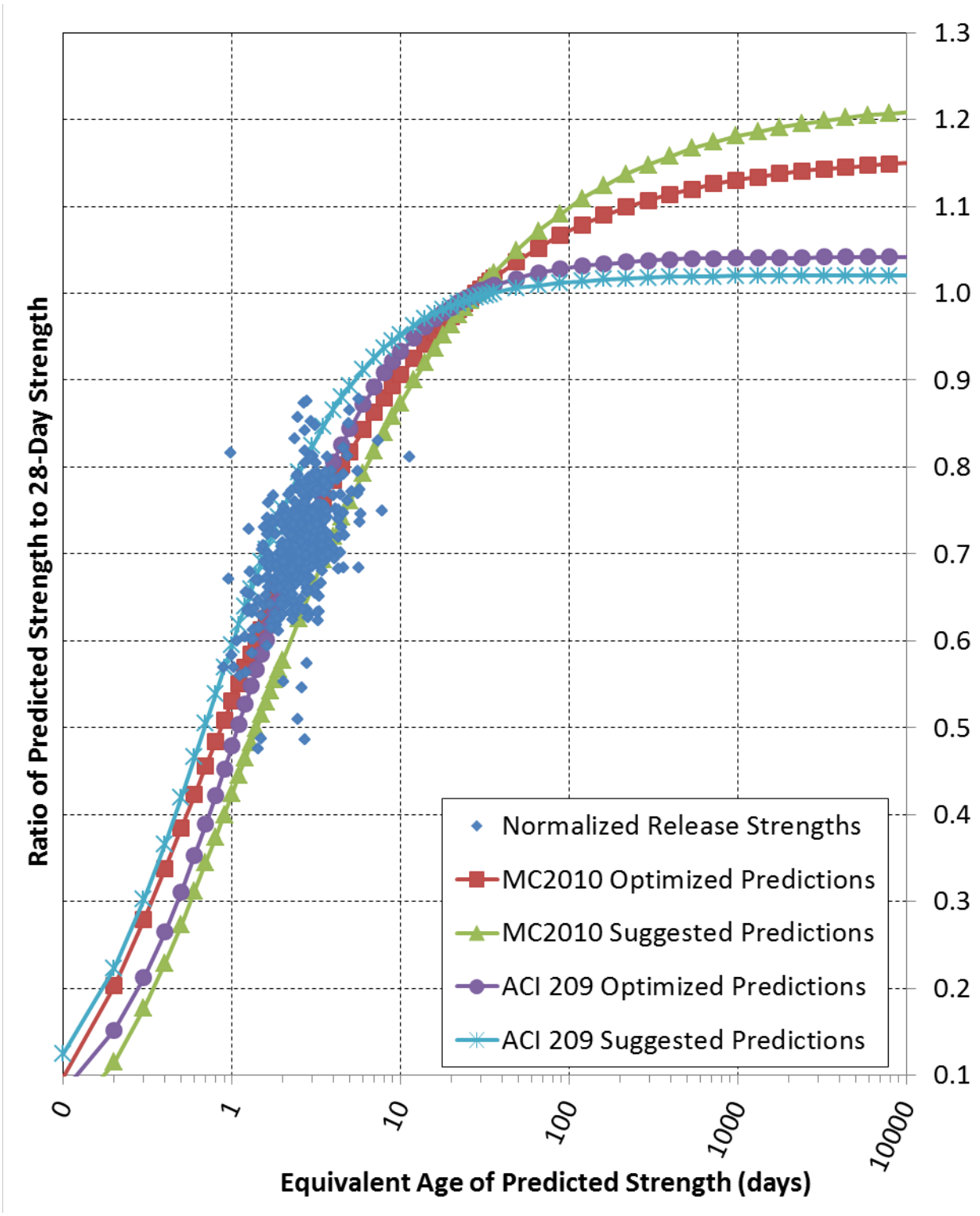

Figure 6.15: Extended Curves for Release Strengths with Equivalent Age

From Table 6.14, it appears three of the four prediction methods maintained or improved their accuracy when using EA instead of chronological age. When using suggested parameters, the use of EA instead of chronological age greatly increased the accuracy of predictions. However, the suggested MC2010 curve still appeared to be underestimating release strengths, while the suggested ACI 209 curve switched to overestimating release strengths. The optimized curves both still passed through the center of the data group.

Notice that, as was predicted based on the α and β values found in Table 6.14, the optimized ACI 209 curves do appear to cross over the suggested ACI 209 curves at later ages. For the majority of the plot, the optimized chronological age curve predicts a higher release strength ratio than the suggested curve. However, at a certain point (which is difficult to tell from the graphs, but appears to be slightly higher than 35 days) the curves cross over, and the optimized curve predicts a lower strength ratio than the suggested curve. The EA curves show the opposite trend, with the crossover occurring at approximately 20 days. This confirms what was said earlier in regards to Table 6.14.

Figure 6.16 and Figure 6.17 (with extended versions shown in Figure 6.18 and Figure 6.19, respectively) show similar trends in the prediction of 28-day strengths, although each of these trends is graphically flipped. In other words, although the suggested prediction curves still predict a slower rate of growth than reality when predicting 28-day strengths with chronological age, the curves in Figure 6.16 are actually above the data rather than below it. Likewise, in Figure 6.13 the suggested MC2010 curve underestimated the strengths and the suggested ACI 209 overestimated the strengths. This relationship is still true in Figure 6.17, but the location of each curve has switched to the opposite side of the data.

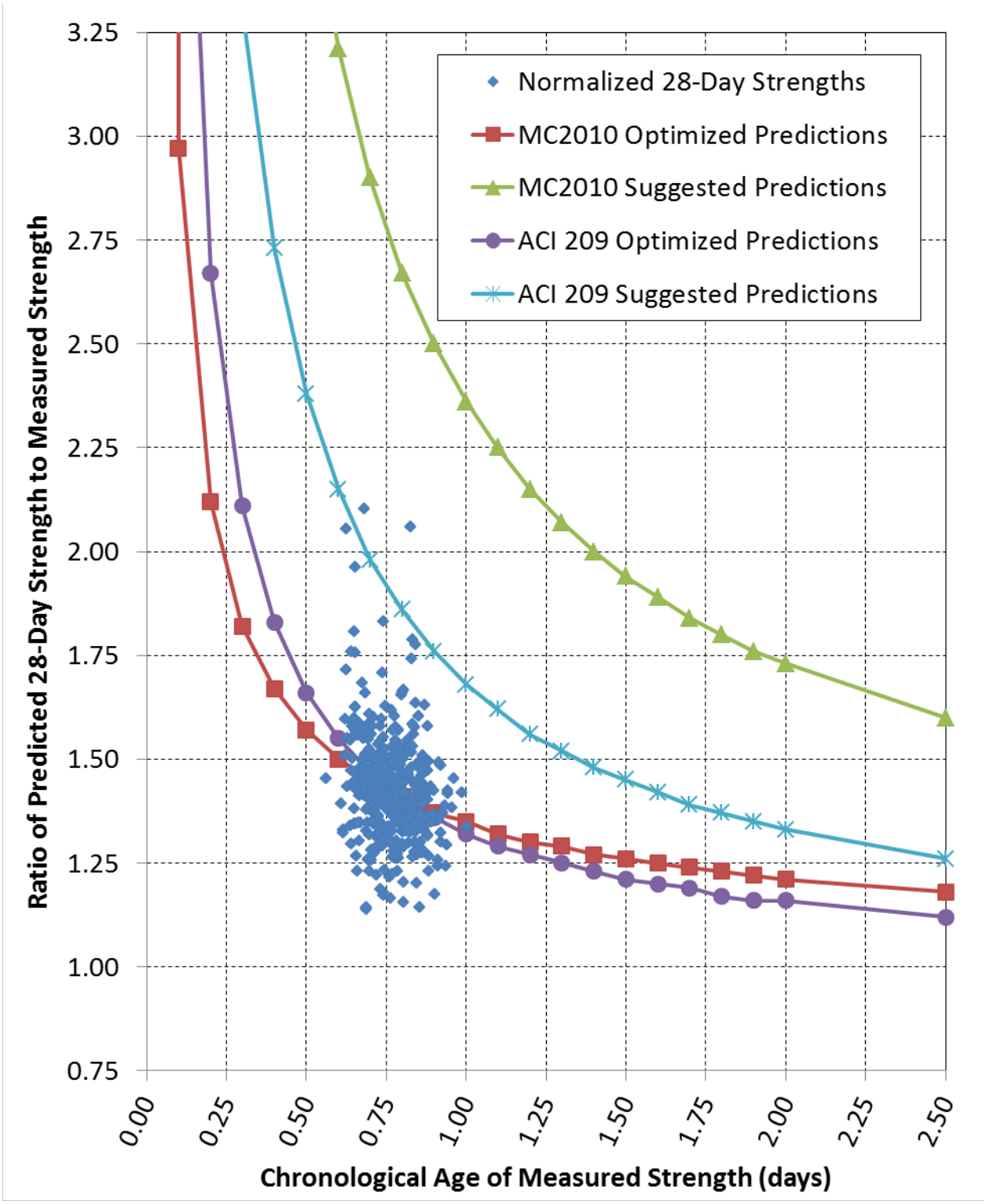

Figure 6.16: Prediction Curves for 28-Day Strengths with Chronological Age

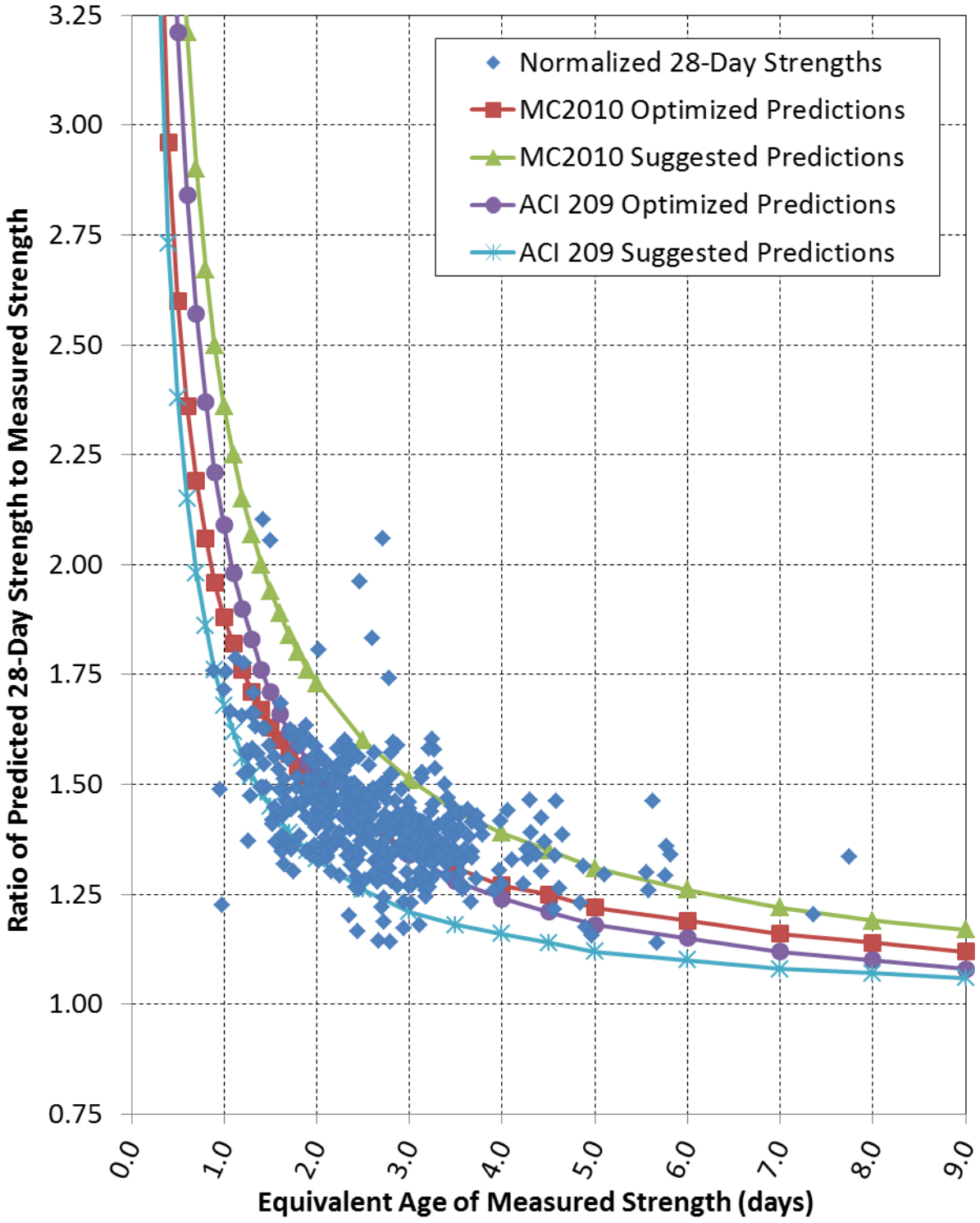

Figure 6.17: Prediction Curves for 28-Day Strengths with Equivalent Age

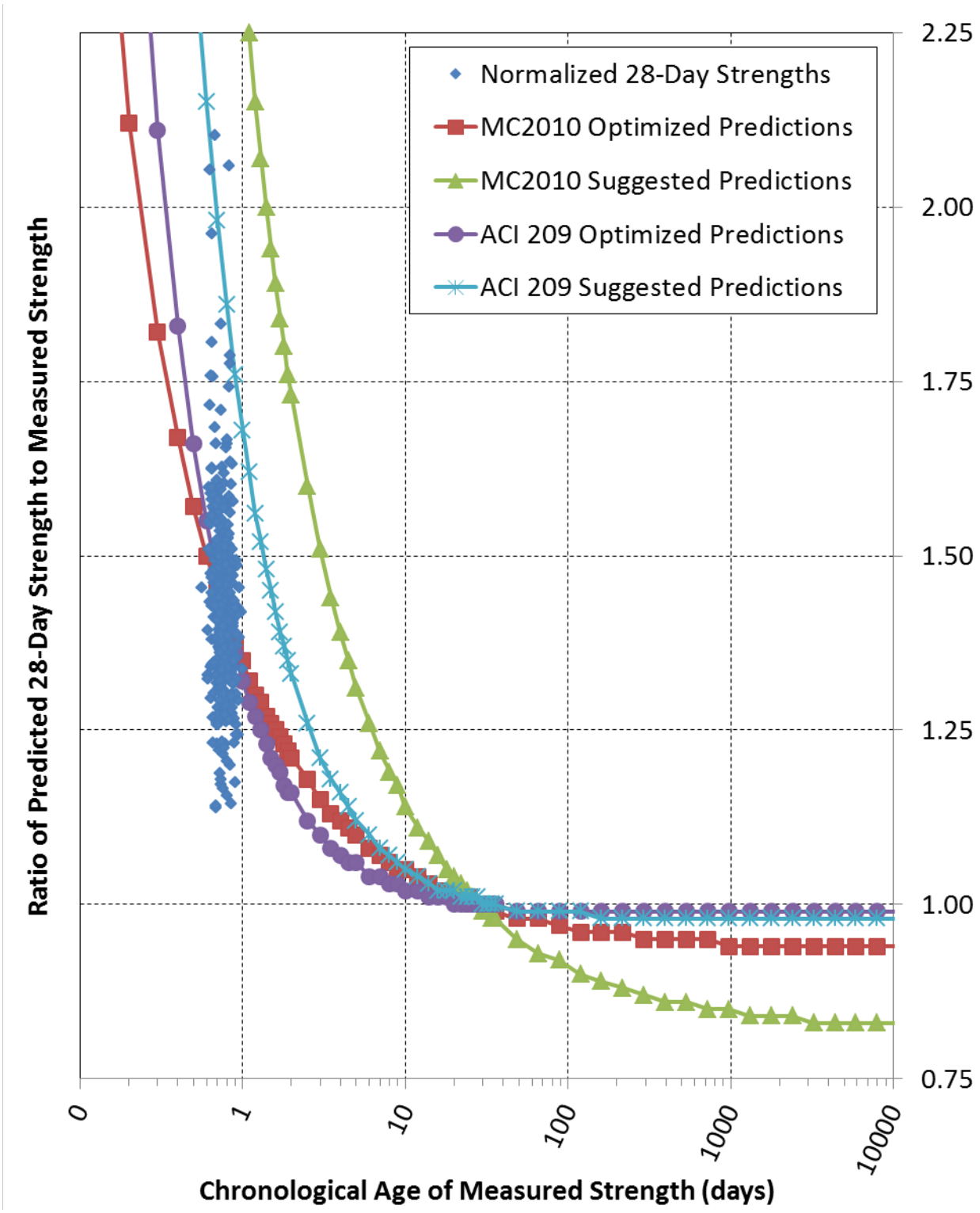

Figure 6.18: Extended Curves for 28-Day Strengths with Chronological Age

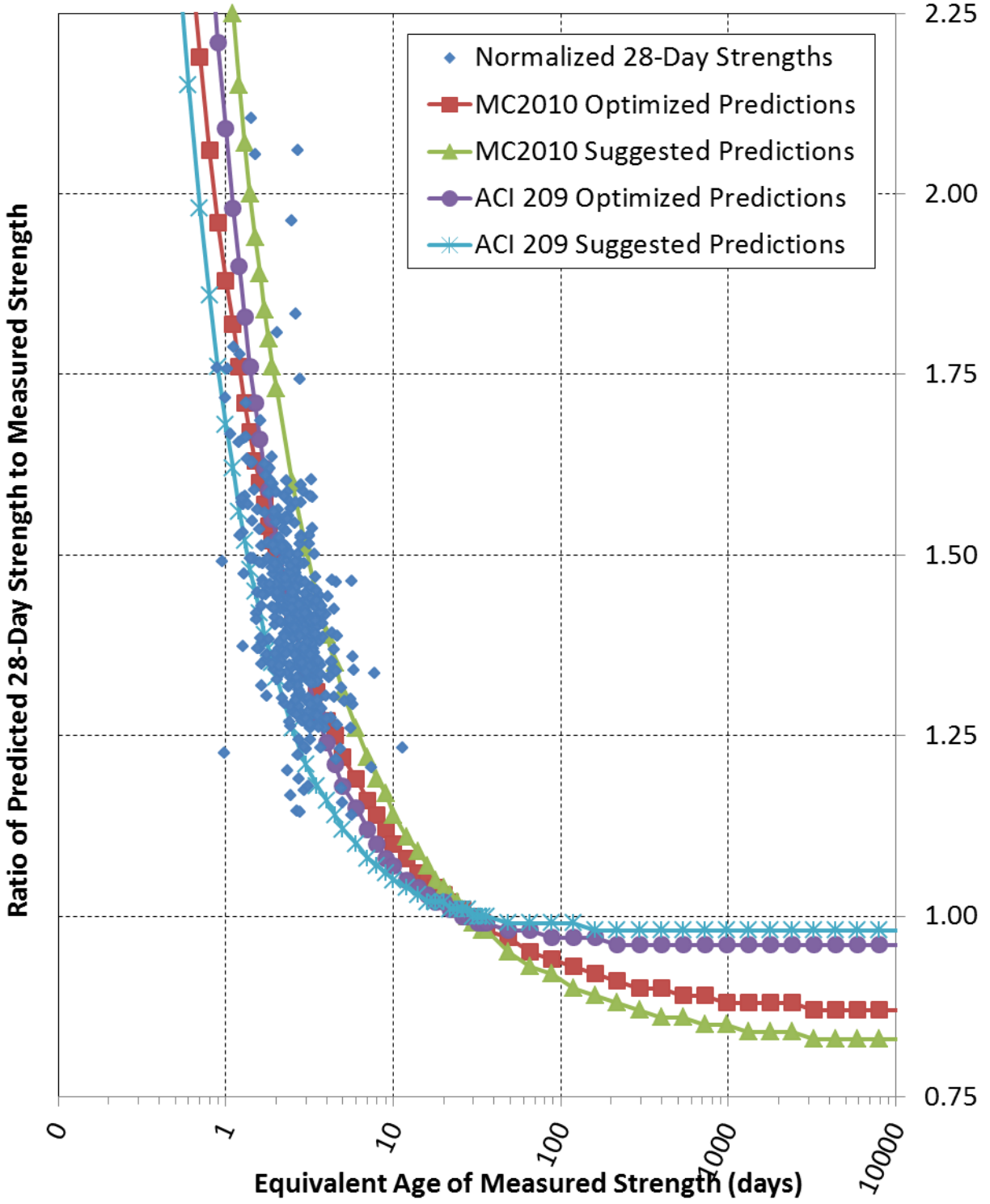

Figure 6.19: Extended Curves for 28-Day Strengths with Equivalent Age

For additional information to compare the fit of each prediction method, Table 6.15 was created to compare the distribution of errors. As may be seen from this table, each optimized prediction method for the full data set was fairly consistent in obtaining a mean error close to zero. This means that each method was not consistently over- or under-predicting values, but that the predictions were accurate on average. The 90th Percentile and 10th Percentile values were also approximately equidistant from the mean, which means that the distribution was fairly symmetric about the mean.

Table 6.15: Strength-Growth Prediction Error Distributions for Full Data Set

		Predicting Release Strengths		**Predicting 28-Day Strength**	
		Chronological Age (psi)	**Equivalent Age (psi)**	**Chronological Age (psi)**	**Equivalent Age (psi)**
MC2010	90th Percentile	660	700	1020	1100
	Mean	-10	20	20	10
	10th Percentile	-720	-730	-920	-940
ACI 209	90th Percentile	660	860	1110	1400
	Mean	-60	30	90	40
	10th Percentile	-760	-910	-930	-1100

The optimized ACI 209 methods have very similar error distributions compared to the MC2010 methods. The range of errors found in Table 6.15 did appear to be a little larger for both equivalent age prediction methods.

The next step is to break the data set into groups and to analyze each mixture individually. Table 6.16 provides a summary of the optimized equation parameters (s, α, and β) for each mixture, for each prediction method, and for each prediction direction. These results are discussed and compared to the parameters from the full data set before a summary of the fit of

each curve is presented. The optimized values calculated from release strength predictions were also used for 28-day strength predictions.

Table 6.16: Strength-Growth Prediction Parameters by Mixture

		Predicting Release Strengths	
		Chronological Age	**Equivalent Age**
Mixture #1	s	0.063	0.137
	α (days)	0.30	1.04
	β	0.989	0.963
Mixture #2	s	0.069	0.147
	α (days)	0.34	1.15
	β	0.988	0.959
Mixture #3	s	0.076	0.153
	α (days)	0.38	1.15
	β	0.987	0.959
Mixture #4	s	0.072	0.150
	α (days)	0.36	1.15
	β	0.987	0.959
Mixture #5	s	0.068	0.167
	α (days)	0.31	1.40
	β	0.989	0.950
Mixture #6	s	0.080	0.140
	α (days)	0.42	0.98
	β	0.985	0.965
Mixture #7	s	0.069	0.174
	α (days)	0.34	1.43
	β	0.988	0.949

It has been recognized that any strength/time relationship is only valid for the specific concrete mixture for which it was developed. Therefore, it was desired that each concrete mixture should be analyzed individually. This would allow comparison between different

mixtures, and also between the mixtures individually and the data set as a whole. Thus, it would be possible to see how well the results from the full data set match the results from each mixture.

The range of values was fairly consistent. Table 6.17 shows the range of s, α, and β values obtained from the mixture-specific analysis compared to the s, α, and β values obtained from the full data set analysis or suggested with the equations. For many of the parameters and methods, the range of values found was not substantially large. More significantly, the parameter values obtained from the full data set analysis were well within the range of mixture-specific values for both the MC2010 equation and the ACI 209 equation.

Table 6.17: Range and Comparison of Prediction Parameters

	Predicting Release Strengths	
	Chronological Age	**Equivalent Age**
Max Mixture s	0.080	0.174
Min Mixture s	0.063	0.137
Full Set s	0.069	0.147
Suggested s by Code	NA	0.20
Max Mixture α (days)	0.42	1.43
Min Mixture α (days)	0.30	0.98
Full Set α (days)	0.34	1.13
Suggested α by Report (days)	0.70	NA
Max Mixture β	0.989	0.965
Min Mixture β	0.985	0.949
Full Set β	0.988	0.960
Suggested β by Report	0.98	NA

From Table 6.16 and Table 6.17, it may be determined that the values of s, α, and β remain fairly consistent from mixture to mixture. Mixture-specific s values were within 16% of the full set s value for chronological age calculations, and within 18% for equivalent age

calculations. Mixture-specific β values were nearly identical to the full set value. Mixture-specific α values were within 24% of the full set α value for chronological age calculations, and within 27% for equivalent age calculations.

Of course, it was desirable not only to know the parameter values obtained from each mixture analysis, but also to know how well the optimized equation predicted strength growth for each mixture in each situation. Therefore, Table 6.18 was created to summarize the measurement of fit for each curve by providing SEE and R^2 values in each case. Table 6.19 was also created to summarize the SPEE values for each case.

Table 6.18: Strength-Growth Prediction Curve Fits by Mixture

			Predicting Release Strengths		Predicting 28-Day Strengths	
			Chronological Age	**Equivalent Age**	**Chronological Age**	**Equivalent Age**
Mixture #1	MC2010	SEE (psi)	540	520	740	690
		R^2	0.40	0.45	-0.35	-0.17
	ACI 209	SEE (psi)	560	620	780	850
		R^2	0.35	0.20	-0.50	-0.75
Mixture #2	MC2010	SEE (psi)	740	790	1050	1190
		R^2	0.16	0.02	-0.79	-1.27
	ACI 209	SEE (psi)	740	890	1070	1420
		R^2	0.15	-0.24	-0.85	-2.24
Mixture #3	MC2010	SEE (psi)	490	570	720	930
		R^2	0.62	0.48	0.19	-0.35
	ACI 209	SEE (psi)	490	710	720	1220
		R^2	0.63	0.20	0.19	-1.33
Mixture #4	MC2010	SEE (psi)	560	490	810	730
		R^2	0.31	0.47	-0.03	0.16
	ACI 209	SEE (psi)	560	590	810	920
		R^2	0.32	0.24	-0.03	-0.32
Mixture #5	MC2010	SEE (psi)	380	330	520	430
		R^2	0.56	0.66	0.46	0.63
	ACI 209	SEE (psi)	420	420	560	540
		R^2	0.47	0.46	0.37	0.42
Mixture #6	MC2010	SEE (psi)	540	300	800	450
		R^2	-0.09	0.66	-0.95	0.39
	ACI 209	SEE (psi)	560	410	850	600
		R^2	-0.17	0.36	-1.19	-0.12
Mixture #7	MC2010	SEE (psi)	460	430	640	620
		R^2	-0.50	-0.37	-0.52	-0.42
	ACI 209	SEE (psi)	480	470	690	680
		R^2	-0.67	-0.63	-0.72	-0.69

Table 6.19: Optimized Standard Percent Errors of Estimate by Mixture

		SPEE when Predicting Release Strengths		SPEE when Predicting 28-Day Strengths	
		Chronological Age (%)	Equivalent Age (%)	Chronological Age (%)	Equivalent Age (%)
Mixture #1	MC2010	7.3	7.0	7.3	6.8
	ACI 209	7.4	8.5	7.7	8.3
Mixture #2	MC2010	10.2	10.8	9.5	10.6
	ACI 209	10.1	12.0	9.7	12.8
Mixture #3	MC2010	6.9	8.2	6.9	8.9
	ACI 209	6.6	10.1	6.8	11.6
Mixture #4	MC2010	8.1	6.9	7.3	6.8
	ACI 209	8.0	8.2	7.3	8.5
Mixture #5	MC2010	5.8	4.7	5.8	4.5
	ACI 209	6.4	5.9	6.1	5.6
Mixture #6	MC2010	8.1	4.2	7.5	4.3
	ACI 209	8.2	5.9	8.1	5.9
Mixture #7	MC2010	7.1	6.6	6.4	6.2
	ACI 209	7.3	7.2	6.9	6.8

The trends seen in the full data set analyses were closely mimicked in the mixture-specific analyses. All MC2010 SEE values increased approximately 30% – 60% when predicting 28-day strengths rather than predicting release strengths. This should not be surprising for a couple of reasons. First, the strength-growth equations were developed and designed to predict strengths based on 28-day strengths. With such nonlinear functions, going the other direction can induce larger errors. Secondly, the 28-day strengths had a much larger magnitude than release strengths, so the magnitude of errors is increased.

This second reason is proven to be the primary cause of the increased MC2010 SEE values for 28-day predictions by Table 6.19. This table shows that the MC2010 SPEE for each mixture and each maturity quantification stayed relatively constant for both prediction directions, indicating that the values of SEE were larger because of the larger strength magnitudes.

The ACI 209 SEE values showed a very similar trend in Table 6.18 compared to the MC2010 SEE values. All mixtures had greater SEE values when predicting 28-day strengths by approximately 30% – 60%. The SPEE values for the ACI 209 method also exhibited a similar level of consistency between prediction directions, as was seen for the MC2010 method. This again confirms that the increase in SEE was primarily due to the increase in strength magnitudes. For both prediction methods, several of the mixtures actually exhibited very slight improvements in the SPEE value when predicting 28-day strengths.

To match these SEE findings, it was also found that the R^2 value decreased in every instance when predicting 28-day strengths instead of release strengths. These changes in R^2 were highly varied.

Most of the methods and mixtures showed some improvement to SEE when using EA instead of chronological age. However, when using the MC2010 equation with mixtures 2 and 3, the SEE actually increased when using EA. There was also a corresponding decrease in R^2 to accompany the increase in SEE. For the other mixtures there was a decrease in SEE of 3% to 44%, depending on the mixture and method.

The ACI 209 method exhibited the opposite trend in response to maturity quantification. All mixtures except 5, 6, and 7 had larger SEEs when using equivalent age.

For both methods and all mixtures, the trends in SPEE mimicked the trends in SEE. All mixtures except 2 and 3 had smaller SPEEs for EA than for chronological age with the MC2010 equation, and all mixtures except 5, 6, and 7 had larger SPEEs with the ACI 209 equation.

The use of EA made the MC2010 equation more accurate in prediction of both release strengths and 28-day strengths than the ACI 209 equation. This was almost always true, whether the ACI 209 equation used chronological age or equivalent age. The two exceptions to this were

in Mixture #2 and Mixture #3, in which the ACI 209 method with chronological ages was more accurate than the MC2010 method with EAs.

When predicting release strengths with the same maturity quantification, the SEE was anywhere from 0% to 10% smaller for the MC2010 equation. Furthermore, for predicting 28-day strengths with the same maturity quantification, the SEE was anywhere from 9% to 25% smaller for the MC2010 equation. Excluding Mixture #2 and Mixture #3, the MC2010 equation using EAs had SEEs that were 7% – 47% smaller than the ACI 209 equation using chronological ages.

All in all, it appears that the most accurate strength-growth equation for the full data set is the MC2010 strength-growth equation with calculated equivalent ages.

6.6. Air Content Effects

Up until this point, all analyses have dealt with the measured values of strength without any adjustments. This yields the most directly applicable and easily understood results. A more theoretical approach to analyzing strength data, however, is to first adjust the measured strength for the actual air content. J.E. Cook (1989) quantified the amount by which concrete strength is dependent on air content, and determined that a 1% change in air content resulted in approximately a 5% change in strength for a given concrete mixture. As long as the proportions of the mixture remained the same, this held true.

Basically, the pore structure of concrete with a low air content is denser than the pore structure of concrete with a higher air content, even though the chemical composition and the proportions of that concrete may in all other ways be identical. This means that concrete with a low air content would have a higher strength than the same concrete with a high air content.

Therefore, this more theoretical approach to analyzing concrete strengths asks the

question: “What would the strengths be like if they were all at the same air content?” Any air content could be selected. However, since the ALDOT *Standard Specifications* (2012) specify that the target air content for concrete used in the production of prestressed concrete bridge girders is 4.5% by volume, this was set as the reference value for comparison. All strength values were adjusted according to the following equation:

$$f_{c,adj} = \left\{\left[\left(\frac{AC-4.5\%}{100\%}\right)\cdot 5\right] + 1\right\}\cdot f_c \qquad \textbf{Equation 6.16}$$

where:

$f_{c,adj}$ = adjusted concrete strength at 28 days, psi

AC = measured air content of the concrete test specimens by volume, %

f_c = measured concrete strength at 28 days, psi

The net effect of Equation 6.16 is to adjust the measured strength by 5% for every 1% difference in air content from the target content of 4.5%. Examination of Equation 6.16 shows that

- When $AC < 4.5\%$, the measured strength is adjusted downward. A lower air content means that the pore structure is denser than it would have been at the target air content. This implies that the strength is higher than it would have been, and needs to be shifted downward.
- When $AC > 4.5\%$, the measured strength is adjusted upward. The air content is higher than the target air content, meaning that the pore structure is less dense than it would have been at the target air content. This implies that the strength is lower than it would have been, and needs to be shifted upward.

6.6.1. General Analysis Effects from Air-Adjustment

Because of the more theoretical nature of air-adjusted strength analysis, the direct

implementation of its results is somewhat less prevalent. Therefore, the results of air-adjusted analysis are not discussed in nearly the level of detail that the unadjusted data was discussed. However, the basic findings are presented in this section and compared to the corresponding findings from Sections 6.3.1 and 6.4.1 for the benefit of the reader. These comparisons demonstrate the general effects that air-adjustment had on the measured strength data.

In Section 6.3.1, Table 6.1 provided a detailed breakdown of the statistical distribution of strengths within bins divided according to the specified release strength, f'_{ci}. Table 6.20 takes the same bin divisions and provides the statistical distribution details of the air-adjusted release strengths instead of the measured release strengths. Figure 6.20 then shows a comparative plot of the mean bin release strengths and the suggested release strength prediction equation provided in Section 6.3.1.

Table 6.20: All Release Strength Distributions – Air-Adjusted Data, Bins Divided by f'_{ci}

Strength Bins	*n*	Sample Standard Deviation, s (psi)	Sample Mean, $\bar{x}$ (psi)	Sample Coefficient of Variance, COV (%)	Skewness Check, $\sqrt{\beta_1}$	Kurtosis Check, β_2
4000 psi ≤ f'_{ci} < 4500 psi	53	1250	7190	17.42	0.075	2.572
4500 psi ≤ f'_{ci} < 5000 psi	49	840	7160	11.77	-0.327	2.876
5000 psi ≤ f'_{ci} < 5500 psi	402	860	7140	12.06	0.028	3.284
5500 psi ≤ f'_{ci} < 6000 psi	518	960	7040	13.69	0.506	2.997
6000 psi ≤ f'_{ci} < 6500 psi	558	810	7080	11.38	0.510	3.171
6500 psi ≤ f'_{ci} < 7000 psi	191	870	7520	11.63	0.485	2.774
7000 psi ≤ f'_{ci} < 7500 psi	43	730	7950	9.21	0.940	3.463
7500 psi ≤ f'_{ci} < 8000 psi	79	650	7790	8.30	0.940	3.834
8000 psi ≤ f'_{ci} < 8500 psi	4	380	8030	4.73	-0.469	1.125
8500 psi ≤ f'_{ci} < 9000 psi	0	NA	NA	NA	NA	NA
9000 psi ≤ f'_{ci} < 9500 psi	20	420	8620	4.83	0.151	1.223
Full f'_{ci} Range	1917	910	7200	12.68	0.288	3.039

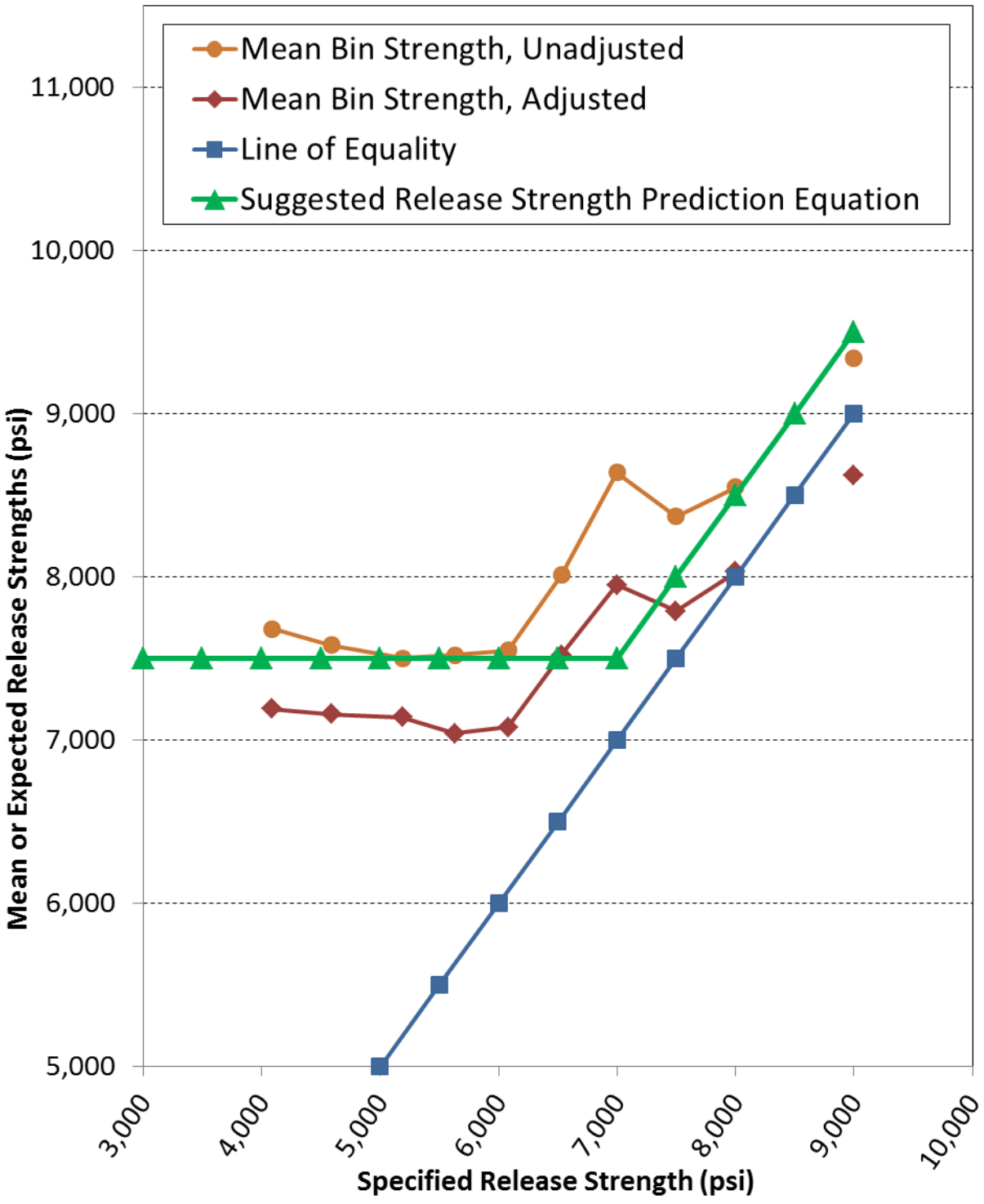

Figure 6.20: Comparative Plot of Air-Adjusted Mean Bin Release Strengths

A direct comparison may be made between Table 6.1 and Table 6.20 to determine the effects of air-adjustment on release strengths. Plant-specific versions of Table 6.20 may be seen in Appendix I.

The most obvious effect of air-adjustments may be seen by comparing the sample means from both tables. Air-adjustments had the obvious effect of shifting the majority of all strength measurements down. Comparison of the sample means between the two tables shows that the mean strengths of any air-adjusted bin are approximately 350 psi to 700 psi smaller (5% to 8% smaller) than the unadjusted bins. This is further supported by examination of Figure 6.20, which shows the net effect the air-adjustment had of shifting measured release strengths to a lower level.

Such results are not surprising considering the air content findings discussed in Section 5.6. In that section, it was shown that even though the target air content for the concretes in this study was 4.5% by volume, the mean air contents were roughly 1% less than the target and the modes for each data set were between 1.5% and 2.0% below the target. By adjusting the measured strengths to meet the target air content, then, it would be expected that the majority of strengths would be shifted downward by Equation 6.16.

A comparison of sample standard deviations from Table 6.1 and Table 6.20 shows that the standard deviation decreased for nearly every data division by adjusting for air. Two strength bins did not change. This decrease in standard deviation was not extraordinarily large in most cases, but varied from approximately 2.5% to 12.5%. Normally, this would indicate that the distribution became “better.” In other words, it would be assumed that because the standard deviation decreased, the distribution has become more tightly controlled.

However, an examination of sample coefficients of variance (COVs) shows an opposite

trend, in which all but four of the data groups reached a larger COV because of air-adjustment. This is because the decrease in mean strength caused by air-adjustment was proportionately larger than the decrease in standard deviation, resulting in a net decrease in distribution control. The three lowest strength bins, together with the complete data set as a whole, did achieve better distribution control in spite of the decrease in mean strength.

The changes caused in skewness and kurtosis were somewhat inconsistent. Although there were multiple exceptions in both cases, the general trend was that skewness was slightly shifted toward normality by air-adjustment and kurtosis was slightly shifted away from normality.

The results of analyzing all 28-day strength measurements after adjustment may be seen in Table 6.21 and Figure 6.21. Table 6.21 compares directly to Table 6.8. Plant-specific versions of Table 6.21 may be seen in Appendix I. As was seen in comparing release strengths, the most obvious difference noticed in comparing Table 6.8 and Table 6.21 was the noticeable decrease in mean strengths that occurs for every strength bin. The mean strength of every data division decreased by 500 psi to 800 psi (a 5% to 8.5% decrease) regardless of the strength level. This result was expected, considering the distribution of air contents that was found in Section 5.6.

Table 6.21: All 28-Day Strength Distributions – Air-Adjusted Data, Bins Divided by f_c'

Strength Bins	*n*	Sample Standard Deviation, s (*psi*)	Sample Mean, $\bar{x}$ (*psi*)	Sample Coefficient of Variance, COV (%)	Skewness Check, $\sqrt{\beta_1}$	Kurtosis Check, β_2
5000 psi ≤ f_c' < 5500 psi	61	1000	9620	10.44	-0.320	2.864
5500 psi ≤ f_c'< 6000 psi	56	570	10250	5.52	-0.418	4.777
6000 psi ≤ f_c' < 6500 psi	455	760	9950	7.59	-0.646	4.262
6500 psi ≤ f_c' < 7000 psi	307	850	9820	8.68	-0.646	5.086
7000 psi ≤ f_c' < 7500 psi	782	1060	9920	10.68	-0.472	3.130
7500 psi ≤ f_c' < 8000 psi	38	650	10120	6.39	-0.141	2.537
8000 psi ≤ f_c' < 8500 psi	170	650	10290	6.28	-0.185	2.612
8500 psi ≤ f_c' < 9000 psi	12	520	9770	5.29	-3.610	9.056
9000 psi ≤ f_c'< 9500 psi	16	1090	10350	10.52	0.595	2.236
Full f_c'Range	1897	910	9950	9.18	-0.567	3.920

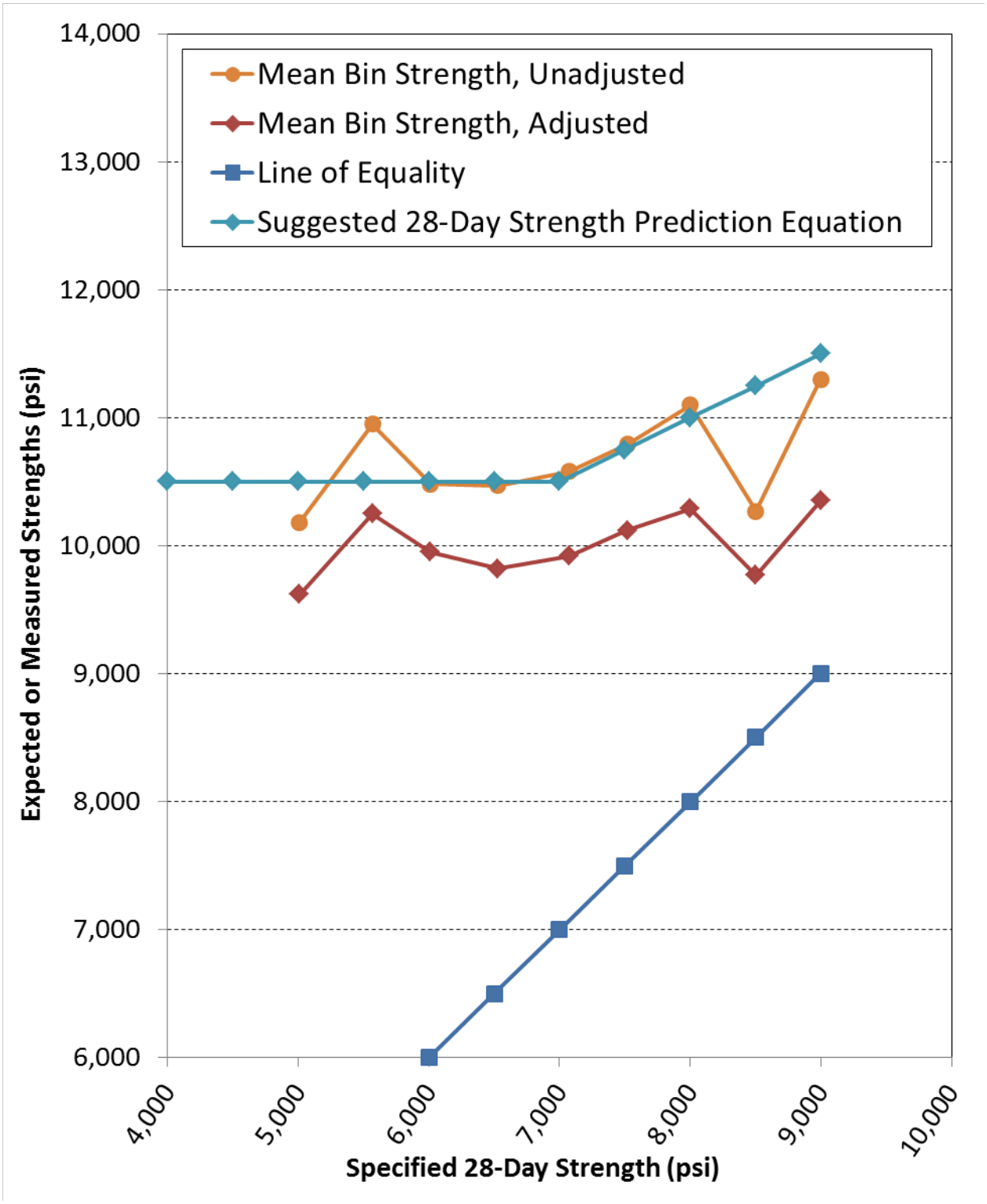

Figure 6.21: Comparative Plot of Air-Adjusted Mean Bin 28-Day Strengths

In most of the data divisions, air-adjustments to 28-day strengths decreased the sample standard deviation. This change was highly variable, decreasing by anywhere from 1% to 23%. Only in the 7500 psi $\leq f_c' <$ 8000 psi bin was the standard deviation increased, but this increase was a quite substantial 62.5%. The COV decreased or remained constant in most of the bins. Only in three strength bins did the COV increase.

Examination of the $\sqrt{\beta_1}$ values for skewness showed that all data divisions except the 6500 psi $\leq f_c' <$ 7000 psi strength bin were shifted away from normality by the air-adjustments. Treating the entire data set as a single group, the skewness was shifted approximately 29% away from normality by the adjustments.

Likewise, the kurtosis of the entire data group was shifted approximately 6.5% away from normality. However, the strength bins were fairly equally distributed in the number that were shifted toward normality compared to the number that were shifted away from it. Four strength bins were shifted away from normality and five strength bins were shifted toward normality by air adjustments.

Comparison of Figure 6.4 to Figure 6.22 and Figure 6.8 to Figure 6.23 reveals another interesting trend caused by air content adjustments. The creation of these break point graphs was mostly independent of the mean strength of each strength bin, but highly dependent on the standard deviation of all data points above the break point. Although all the lines were shifted by differing amounts, it is clear that the required strength lines in Figure 6.22 are all equivalent or lower than the corresponding lines from Figure 6.4, and the required strength lines in Figure 6.23 are all lower than the corresponding lines from Figure 6.8.

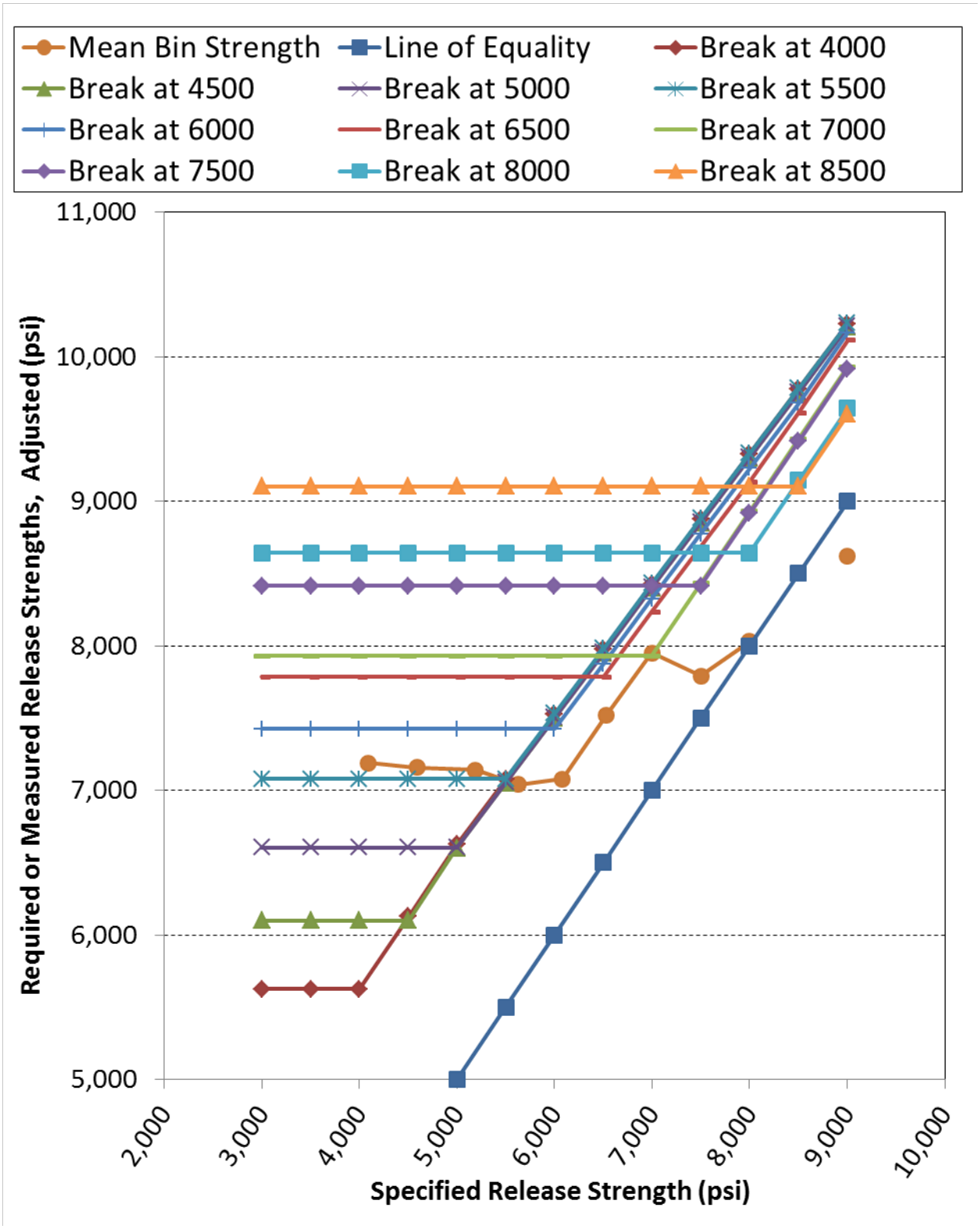

Figure 6.22: Break Points in Release Strength Measurements, All Data, Air-Adjusted

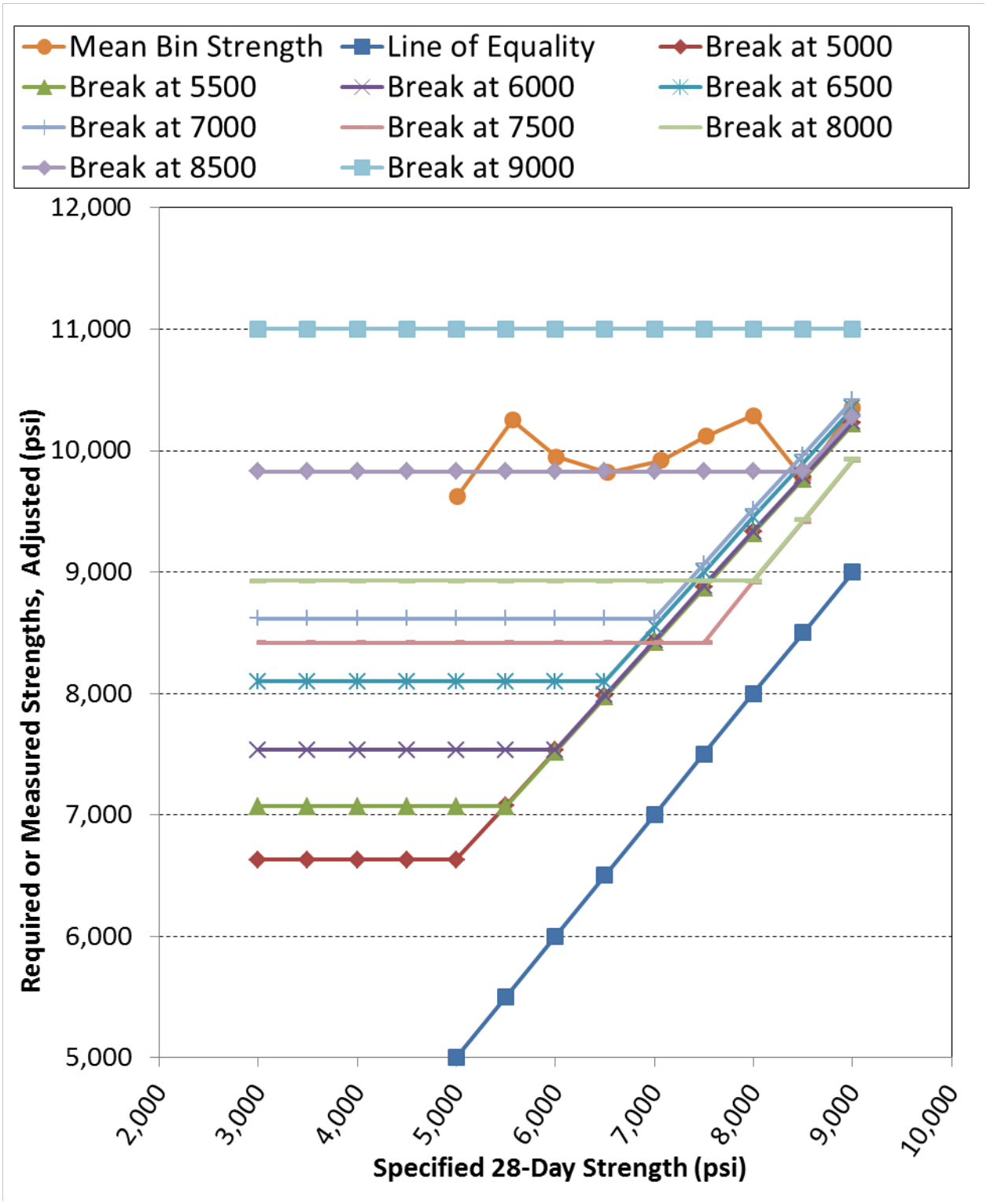

Figure 6.23: Break Points in 28-Day Strength Measurements, All Data, Air-Adjusted

Since these lines are purely dependent on the standard deviation of all data above the break point, this means that the standard deviation of every break group improved by adjusting for air content. In other words, even though the standard deviation of each individual bin did not improve, the standard deviation of any given bin combined with all the bins higher than it did improve. Thus, although the standard deviation of the $7500 \text{ psi} \leq f_c' < 8000 \text{ psi}$ 28-day strength bin was actually made larger by the air content adjustment, the standard deviation of the $7500 \text{ psi} \leq f_c' < 9500 \text{ psi}$ group was made smaller. This same trend continues for lower strength bins. The standard deviation of the break groups compiled in this way decreased by anywhere from 0% to 17%.

Overall, then, the effects of adjusting measured strengths for air content had two significant trends. First, it very consistently and clearly decreased the average strengths contained in each data division. Secondly, it reduced the standard deviation in almost all cases. However, the effects of air-adjustment on COV, $\sqrt{\beta_1}$, or β_2 values were more sporadic and unpredictable.

6.6.2. Strength-Growth Prediction Effects from Air-Adjustment

One of the main purposes of the air-adjustments was to create what had the potential to be a more consistent and accurate relationship between strength and concrete age. Analyzing measured strength results without any modification was the first level of analysis, and it provided useful means of predicting expected strengths with very little prior knowledge. The next level was to include the effects of time and temperature, in an attempt to gain a better understanding of the growth of concrete strength as it develops. Now, including adjustments for time, temperature, and actual air content provides the third and most detailed analysis of the behavior of these

concretes. It is the most detailed analysis, but therefore it also requires the most prior knowledge about the concrete.

In order to see the effects of adjusting for air content in the context of strength growth predictions, the analyses described in Sections 2.3.1 and 6.5.1 were repeated with air-adjusted strengths. The information presented in the rest of this section is both compared within itself, just like the results in Section 6.5.1 were presented, and also compared to the results in Section 6.5.1. This comparison will clearly show the effects of adjusting the strengths.

Table 6.22 shows the air-adjusted results that parallel Table 6.14.

Table 6.22: Strength-Growth Prediction Results for Full Air-Adjusted Data Set

			Predicting Release Strengths		Predicting 28-Day Strength	
			Chronological Age	**Equivalent Age**	**Chronological Age**	**Equivalent Age**
MC2010	Optimized	s	0.069	0.146	0.069	0.146
		SEE (psi)	580	570	830	840
		SPEE (%)	8.6	8.5	8.2	8.3
		R^2	0.31	0.32	-0.16	-0.19
	Suggested by MC2010	s	0.20	0.20	0.20	0.20
		SEE (psi)	3470	1010	9600	1800
		SPEE (%)	48.4	14.2	96.2	18.0
		R^2	-23.7	-1.11	-155	-4.51
ACI 209	Optimized	α (days)	0.34	1.12	0.34	1.12
		β	0.988	0.960	0.988	0.960
		SEE (psi)	590	670	840	1020
		SPEE (%)	8.6	9.8	8.4	10.2
		R^2	0.30	0.08	-0.20	-0.77
	Suggested by ACI 209	α (days)	0.70	0.70	0.70	0.70
		β	0.98	0.98	0.98	0.98
		SEE (psi)	1870	1040	3590	1290
		SPEE (%)	25.8	15.4	36.1	12.7
		R^2	-6.21	-1.22	-20.8	-1.83

The MC2010 results found in Table 6.22 are practically identical to the results found in Table 6.14, with the primary noticeable difference being that the SEE values are approximately 7% smaller and the R^2 values are slightly larger in Table 6.22. However, the SPEE values indicate that the air-adjusted strength predictions had approximately the same percent error as the unadjusted predictions. The primary cause of the decreased SEE values was the decrease in the average magnitude of the measured strengths, as was discussed in Section 6.6.1.

The suggested ACI 209 functions showed identical trends. The SEE and R^2 values are slightly smaller in Table 6.22 than in Table 6.14. However, the SPEE values remained the same,

indicating that the decrease in SEE was caused by the decrease in average strength.

The optimized ACI 209 functions were the only portion of the table in which there were changes to the SPEE values. The SPEEs for equivalent age calculations remained the same, but the SPEEs for chronological age calculations decreased by 11% – 22% due to air-adjustments.

When treating the full data set as a single group, the optimized MC2010 method did not show any significant signs of improvement by the use of EA instead of chronological age. The optimized ACI 209 method, on the other hand, showed an approximate 14% increase in SEE when predicting release strengths and a 21% increase in SEE when predicting 28-day strengths. Both suggested methods showed significant improvement in SEE when using EA instead of chronological age.

In general, when comparing the two methods directly, the MC2010 equation was usually equivalent to or more accurate than the ACI 209 equation. All in all, it appears that the most accurate strength-growth equation for the full data set with air-adjustments is the MC2010 strength-growth equation with calculated equivalent ages.

For additional information to compare the fit of each prediction method, Table 6.23 was created to compare the distribution of errors. As may be seen from this table, each prediction method for the full data set was fairly consistent in obtaining a mean error close to zero. The error distributions found in Table 6.23 were similar to those found in Table 6.15. The 90^{th} and 10^{th} percentile values differed by a larger amount, but usually no more than approximately 10%.

Table 6.23: Strength-Growth Prediction Error Distributions, Full Air-Adjusted Data Set

		Predicting Release Strengths		Predicting 28-Day Strength	
		Chronological Age (psi)	**Equivalent Age (psi)**	**Chronological Age (psi)**	**Equivalent Age (psi)**
MC2010	90^{th} Percentile	610	670	960	1020
	Mean	-10	40	20	-20
	10^{th} Percentile	-690	-670	-860	-910
ACI 209	90^{th} Percentile	610	800	1030	1260
	Mean	-60	40	80	20
	10^{th} Percentile	-720	-840	-850	-1030

One important similarity between the adjusted values and the unadjusted values is in the values of s, α, and β. These optimized values are basically identical for the analyses involving adjusted strength values compared to the unadjusted strength values. This indicates that the air-adjustments did not alter the shape of the optimized curve, but shifted all values in such proportions that the variable parameters remained constant. This was the expected result, since adjustment for air content shifts each set of cylinder strength tests in proportion, as a percentage of the measured strengths. Thus, the relationship between the release tests and 28-day tests should remain approximately the same.

An important comparison to make is the accuracy of fit between adjusted values and unadjusted values. Table 6.24 was created to better quantify the effects of adjustment on curve fits.

Table 6.24: Summary of Prediction Fit Changes from Air Adjustment for Full Data Set

			Predicting Release Strengths		Predicting 28-Day Strength	
			Chronological Age (%)	**Equivalent Age (%)**	**Chronological Age (%)**	**Equivalent Age (%)**
MC2010	Optimized	$\Delta SEE_{\%}$	-6.45	-6.56	-5.68	-6.67
		$\Delta SPEE_{\%}$	0.00	0.00	0.00	-0.83
		$\Delta R^2{}_{\%}$	-19.0	-17.5	-227	-90.0
	Suggested	$\Delta SEE_{\%}$	-5.45	-6.48	-5.60	-6.25
		$\Delta SPEE_{\%}$	0.00	0.00	0.00	0.00
		$\Delta R^2{}_{\%}$	-13.5	-25.3	-11.6	-12.8
ACI 209	Optimized	$\Delta SEE_{\%}$	-4.84	-5.63	-6.67	-7.27
		$\Delta SPEE_{\%}$	-0.12	-0.10	-0.12	-0.49
		$\Delta R^2{}_{\%}$	-20.1	-54.7	-120	-22.3
	Suggested	$\Delta SEE_{\%}$	-6.03	-5.45	-5.53	-5.84
		$\Delta SPEE_{\%}$	0.00	0.00	0.00	0.00
		$\Delta R^2{}_{\%}$	-15.0	-27.0	-11.8	-19.2

This table uses three variables, $\Delta SEE_{\%}$, $\Delta SPEE_{\%}$ and $\Delta R^2{}_{\%}$, to show the overall effects of adjustment in each instance. These variables were calculated by Equations 6.17, 6.18, and 6.19, shown below. The percent change in standard error of estimate, labeled as $\Delta SEE_{\%}$, quantifies the amount by which air-adjustment changed the SEE relative to the unadjusted value.

$$\Delta SEE_{\%} = \left(\frac{SEE_2 - SEE_1}{SEE_1}\right) \cdot 100\% \qquad \textbf{Equation 6.17}$$

where:

$\Delta SEE_{\%}$ = percent change in SEE due to air-adjustments, %

SEE_2 = standard error of estimate after air-adjustments, psi

SEE_1 = standard error estimate before air-adjustments, psi

$$\Delta {R^2}_{\%} = \left(\frac{\left(R^2\right)_2 - \left(R^2\right)_1}{\left|\left(R^2\right)_1\right|} \right) \cdot 100\% \qquad \textbf{Equation 6.18}$$

where:

${\Delta R^2}_{\%}$ = percent change in R^2 due to air-adjustments, %

$(R^2)_2$ = correlation index after air-adjustments

$(R^2)_1$ = correlation index before air-adjustments

$$\Delta SPEE_{\%} = \left(\frac{SPEE_2 - SPEE_1}{SPEE_1} \right) \cdot 100\% \qquad \textbf{Equation 6.19}$$

where:

$\Delta SPEE_{\%}$ = percent change in SPEE due to air-adjustments, %

$SPEE_2$ = standard percent error of estimate after air-adjustments, psi

$SPEE_1$ = standard percent error estimate before air-adjustments, psi

If $\Delta SEE_{\%} < 0.00$, the air-adjustments decreased the SEE, meaning that the errors between the prediction method and the measured values were decreased. If $\Delta SEE_{\%} > 0.00$, it indicates that the adjustments increased the errors of the prediction method.

If ${\Delta R^2}_{\%} < 0.00$, it indicates that the correlation index decreased due to air-adjustments, meaning that the prediction method fit the data worse than it had originally. If ${\Delta R^2}_{\%} > 0.00$, it indicates that the air-adjustments improved the fit of the prediction method.

If $\Delta SPEE_{\%} < 0.00$, the air-adjustments decreased the SPEE, meaning that the normalized errors between the prediction method and the measured values were decreased. If $\Delta SPEE_{\%} > 0.00$, it indicates that the adjustments increased the normalized errors of the prediction method.

The values for $\Delta SEE_{\%}$ shown in Table 6.24 are all negative, showing that air-adjustments improved the errors of each strength-growth prediction method, regardless of prediction direction or maturity quantification. All of these decreases in SEE were in the vicinity of 5.5% to 7.5%. However, this range of $\Delta SEE_{\%}$ was actually caused by the decrease in average strength values due to air-adjustments. The average air content, as discussed in Section 5.6, was 1% – 2% below the target value, so the average strength values were reduced by 5% – 10%. The values of $\Delta SPEE_{\%}$ in Table 6.24 are all very close to zero, supporting the idea that the change in SEE was primarily caused by the change in average strength.

The $\Delta SEE_{\%}$ and $\Delta SPEE_{\%}$ percentages are more directly applicable than the percentages shown for $\Delta R^2{}_{\%}$, for reasons which are explained below.

The values for the percent change in correlation index, labeled as $\Delta R^2{}_{\%}$, show a counterpoint to the improved SEE values caused by air-adjustments. This variable quantifies the amount by which air-adjustment changed the correlation index, R^2, relative to its unadjusted value. $\Delta R^2{}_{\%} < 0.00$ for every prediction method, direction, maturity quantification, and set of parameters. At first glance, this appears to contradict the values found for $\Delta SEE_{\%}$, which showed that air-adjustments decreased the prediction errors in every instance. In this regard, however, the results of this analysis are much like the results of air-adjustments on standard deviation (s) and coefficient of variation (COV) discussed in Section 6.6.1. In that instance, the decrease in data distribution was offset by the decrease in the mean, resulting in a net effect of worsened statistical coherence.

Similarly, in this case, the decrease in prediction errors shown by the $\Delta SEE_{\%}$ values is actually offset by the decrease in errors between the measured values and the mean of the measured values. In other words, negative $\Delta R^2{}_{\%}$ values show that the decrease in prediction

errors caused by air-adjustments to the full data set was less than the increase of the data's coherence about itself.

It is important to note that the magnitude of the $\Delta R^2{}_{\%}$ value is not a reliable indicator of the magnitude of the change. This is due to the possibility of having $(R^2)_1$ values very close to zero. Consider, for example, a comparison of the R^2 values for the optimized MC2010 method, both before and after adjustment. The values of $\Delta R^2{}_{\%}$ in Table 6.24 imply that the change in R^2 when using chronological age must be substantially greater than the change when using equivalent age, because the $\Delta R^2{}_{\%}$ is -274% instead of -201%. In reality, however, the change in R^2 was actually exactly the same when using chronological age—a change of -0.11 to R^2 in both cases. The $\Delta R^2{}_{\%}$ value simply makes the change appear much larger for chronological age because $(R^2)_1$ had a smaller value for chronological age. Both changes appear rather large in spite of a fairly small magnitude, because both have a magnitude of $(R^2)_1$ close to zero.

This is not a problem when dealing with $\Delta SEE_{\%}$ because all of the SEE values are positive and substantially greater than zero. Therefore, while $\Delta SEE_{\%} = 6.5\%$ gives the reader a reliable sense of how substantial the change was, $\Delta R^2{}_{\%} = 6.5\%$ could indicate a wide range of changes because of the influence of the $(R^2)_1$ magnitude.

Figure 6.24, Figure 6.25, Figure 6.26, and Figure 6.27 show the same graphical comparisons for air-adjusted data that were provided for the unadjusted data earlier in this section. Extended versions are not provided, since the relationships remain nearly the same.

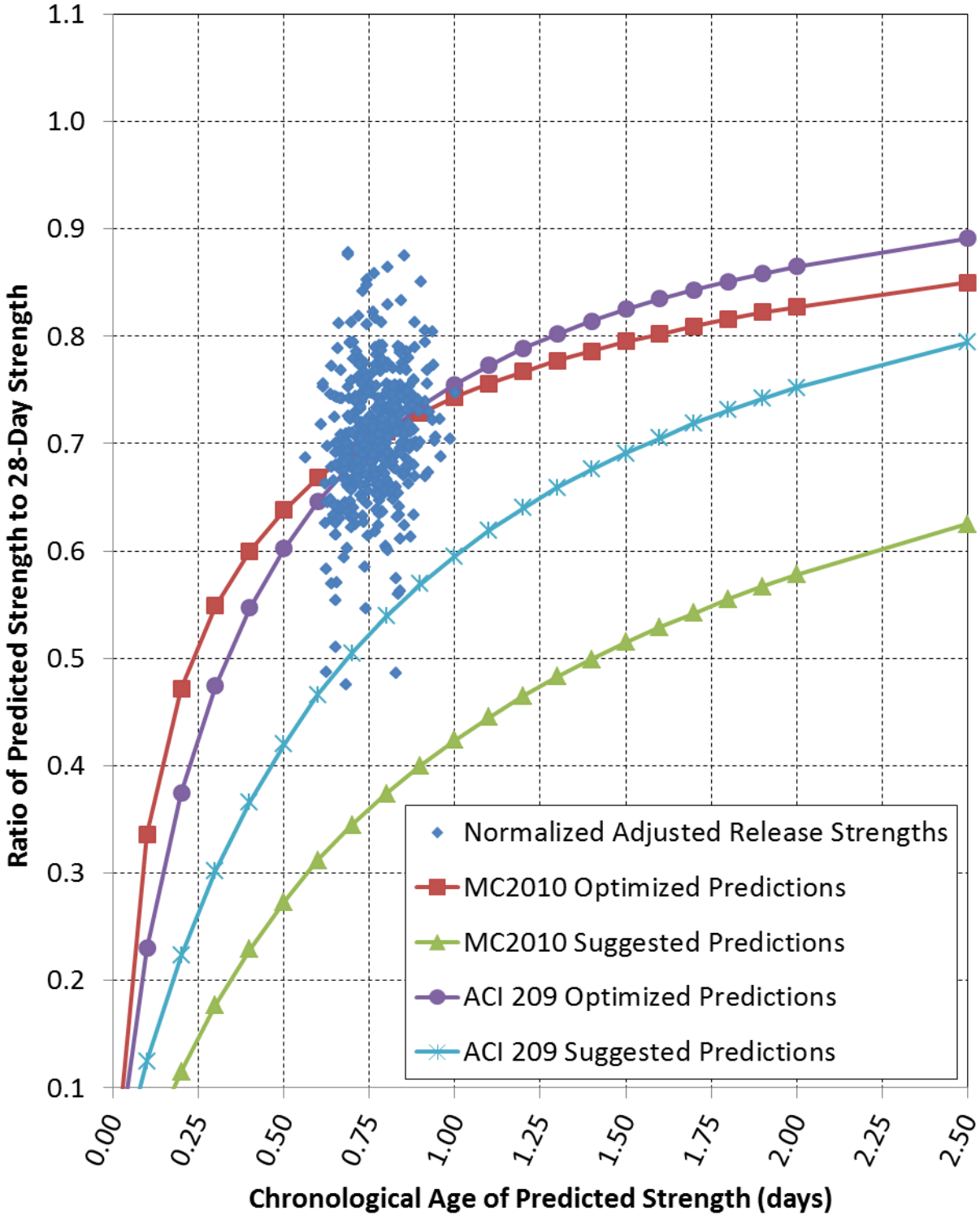

Figure 6.24: Prediction Curves for Air-Adjusted Release Strengths with Chronological Age

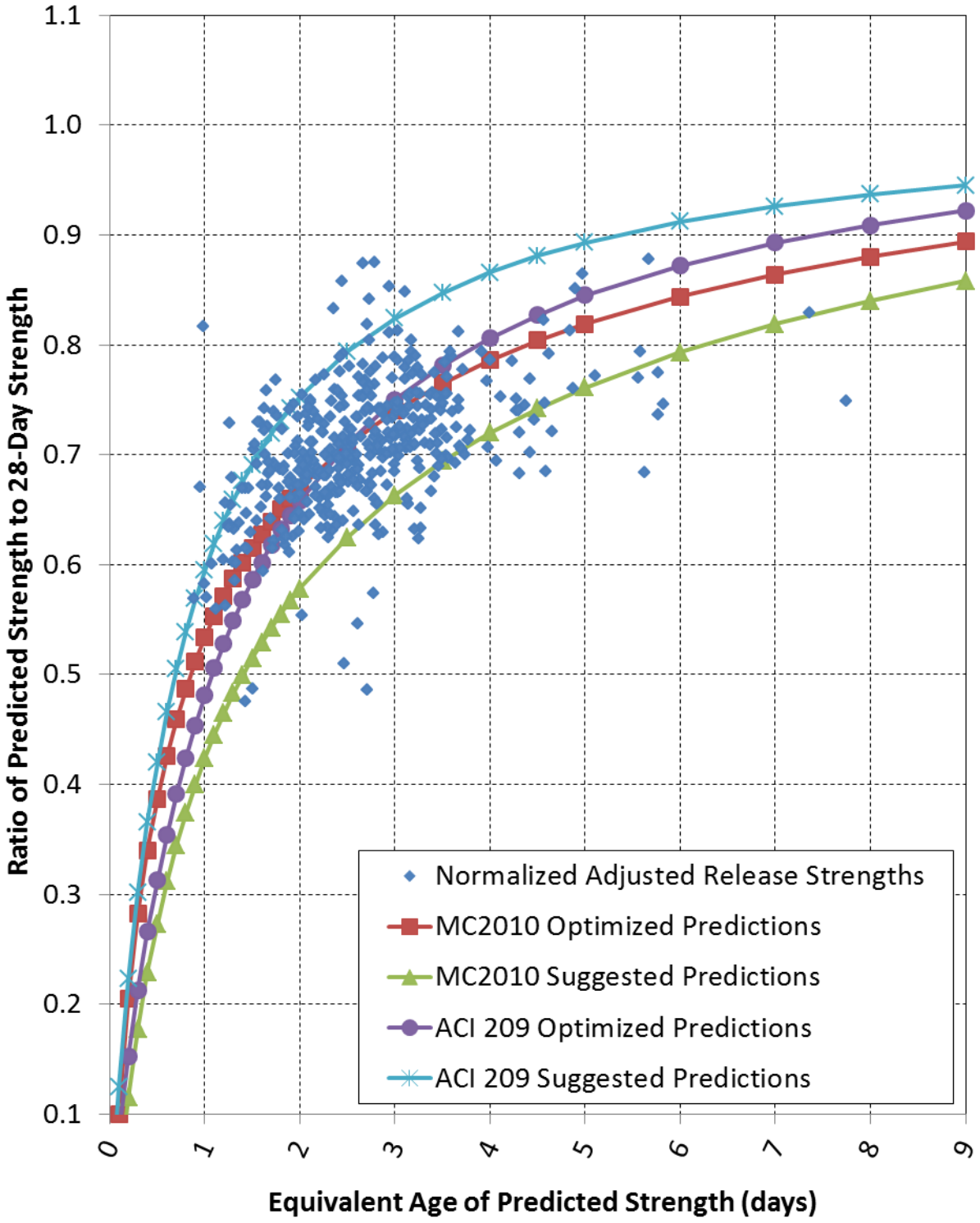

Figure 6.25: Prediction Curves for Air-Adjusted Release Strengths with Equivalent Age

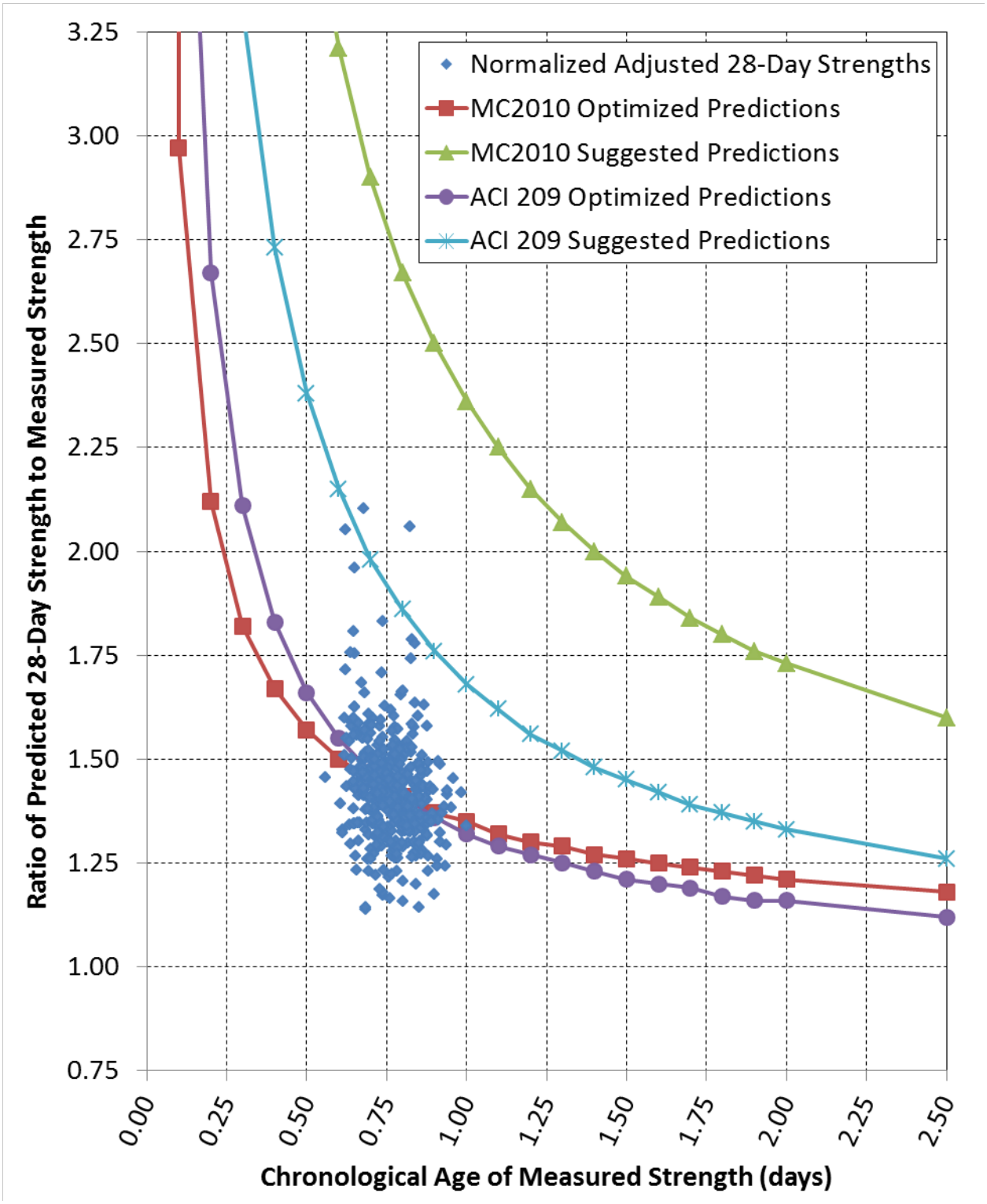

Figure 6.26: Prediction Curves for Air-Adjusted 28-Day Strengths with Chronological Age

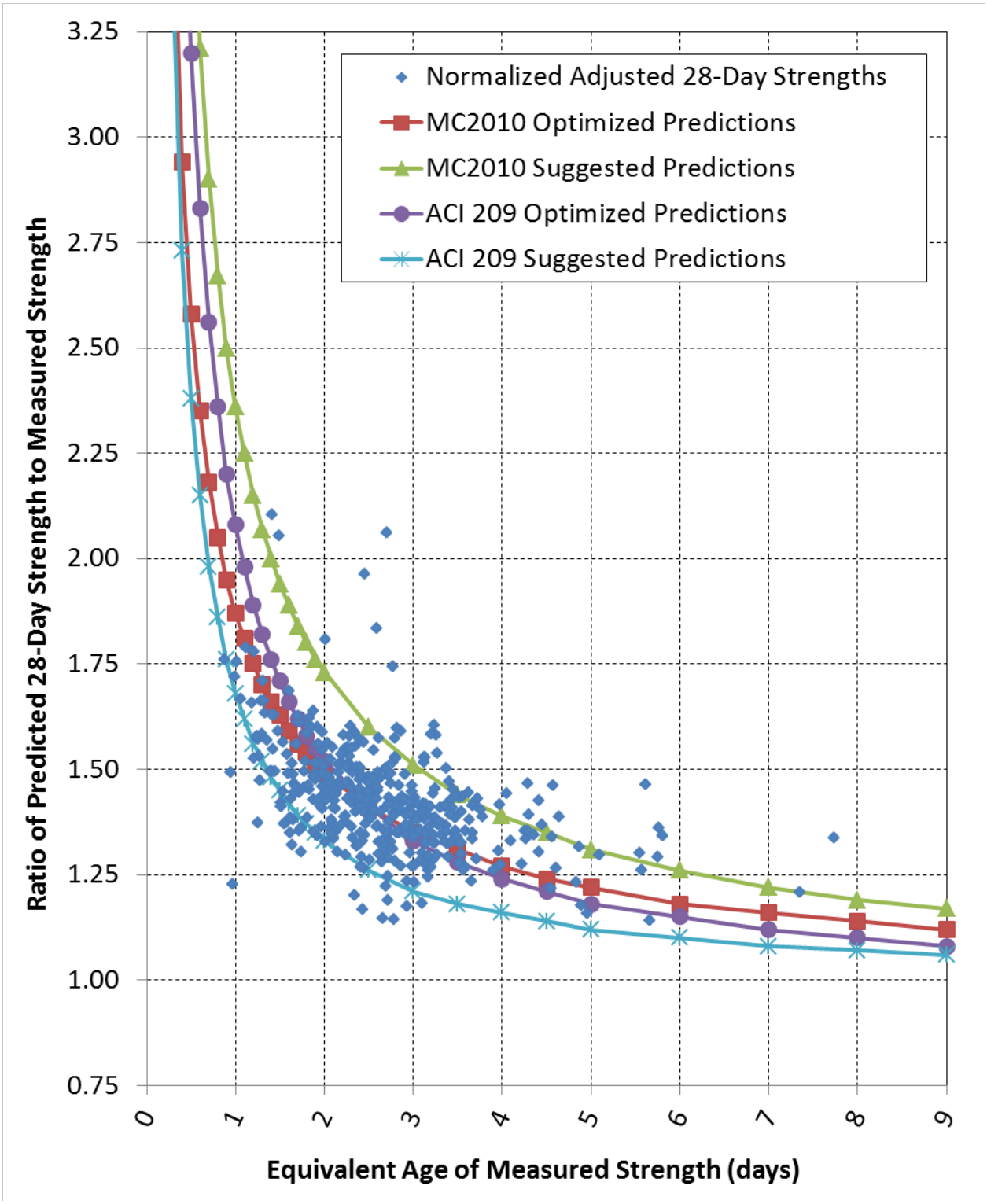

Figure 6.27: Prediction Curves for Air-Adjusted 28-Day Strengths with Equivalent Age

It can easily be seen from these graphs that all of the same trends hold for the adjusted data that held for the unadjusted data curves. One interesting change between the two sets of graphs, though (Figure 6.12, Figure 6.13, Figure 6.16, and Figure 6.17 compared to Figure 6.24, Figure 6.25, Figure 6.26, and Figure 6.27, respectively), should be mentioned.

It was discussed before that the use of equivalent age instead of chronological age had the capacity to shift data in the x-axis direction, but not in the y-axis direction. Air adjustments, on the other hand, only have the potential to shift data values in the y-axis direction. These adjustments cannot shift the data in the x-axis direction. Only by combining the use of EA instead of chronological age and adjustment for air content may the data be shifted in both directions. By adjusting the data in both the x and y directions, it is possible to group the data more coherently about a prediction relationship. This is why the prediction of air-adjusted strengths with the use of EA should provide the most accurate means of prediction.

When analyzing the full data set, and when speaking in terms of SEE, this was often found to be the case. All methods showed reduced SEE values (with nearly constant SPEE values) due to air-adjustments. However, not all methods showed increased accuracy by the use of EA. This assumed relationship between shifted data and improved accuracy was not found to hold true in all cases. However, the single method of strength prediction with the smallest error was the prediction of air-adjusted strengths with the use of equivalent ages in the MC2010 method. Therefore, there is some support to the idea.

The next step would normally be to break the data up and present the mixture-specific results for comparison. However, an examination of Table 6.25 and Table 6.16 reveals that none of the mixture-specific strength growth parameters changed significantly due to air-adjustments.

Table 6.25: Strength-Growth Prediction Parameters by Mixture, Air-Adjusted Data

		Predicting Release Strengths	
		Chronological Age	**Equivalent Age**
Mixture #1	s	0.063	0.137
	α (days)	0.31	1.04
	β	0.989	0.963
Mixture #2	s	0.069	0.148
	α (days)	0.34	1.15
	β	0.988	0.959
Mixture #3	s	0.076	0.152
	α (days)	0.38	1.15
	β	0.987	0.959
Mixture #4	s	0.072	0.150
	α (days)	0.36	1.15
	β	0.987	0.959
Mixture #5	s	0.069	0.167
	α (days)	0.34	1.37
	β	0.988	0.951
Mixture #6	s	0.081	0.140
	α (days)	0.42	0.98
	β	0.985	0.965
Mixture #7	s	0.068	0.172
	α (days)	0.34	1.46
	β	0.988	0.948

In fact, every adjusted parameter was nearly identical to the corresponding unadjusted parameter. This was expected, due to the proportional nature of air-adjustments on both release values and 28-day values.

Therefore, at this point a number of additional comparisons are unnecessary. Because the equation parameters remained virtually unchanged by the air-adjustments, both in the full set analysis and in the mixture-specific analyses, the relationships among all of these parameters

have already been discussed above. The only results that really changed were the curve fit measurements—SEE, SPEE, and R^2.

Table 6.26 provides a summary of the range of strength-growth parameters found in the air-adjusted analyses.

Table 6.26: Range and Comparison of Prediction Parameters, Air-Adjusted Data

	Predicting Release Strengths	
	Chronological Age	**Equivalent Age**
Max Mixture s	0.081	0.172
Min Mixture s	0.063	0.137
Full Set s	0.069	0.146
Suggested s by Code	NA	0.20
Max Mixture α (days)	0.42	1.46
Min Mixture α (days)	0.31	0.98
Full Set α (days)	0.34	1.12
Suggested α by Report (days)	0.70	NA
Max Mixture β	0.989	0.965
Min Mixture β	0.985	0.948
Full Set β	0.988	0.960
Suggested β by Report	0.98	NA

Table 6.27 and Table 6.28 were created to summarize the measurement of fit for each curve. Table 6.27 provides the SEE and R^2 values for each mixture, and Table 6.28 provides the SPEE values for each mixture.

Table 6.27: Strength-Growth Prediction Curve Fits by Mixture, Air-Adjusted Data

			Predicting Release Strengths		Predicting 28-Day Strengths	
			Chronological Age	**Equivalent Age**	**Chronological Age**	**Equivalent Age**
Mixture #1	MC2010	SEE (psi)	520	500	710	660
		R^2	0.31	0.36	-0.61	-0.41
	ACI 209	SEE (psi)	540	590	750	810
		R^2	0.25	0.08	-0.79	-1.11
Mixture #2	MC2010	SEE (psi)	680	730	970	1100
		R^2	0.05	-0.11	-0.59	-1.04
	ACI 209	SEE (psi)	680	830	990	1310
		R^2	0.04	-0.41	-0.64	-1.90
Mixture #3	MC2010	SEE (psi)	460	540	680	860
		R^2	0.61	0.47	0.16	-0.37
	ACI 209	SEE (psi)	460	670	680	1130
		R^2	0.62	0.18	0.16	-1.35
Mixture #4	MC2010	SEE (psi)	530	470	770	700
		R^2	0.22	0.40	-0.28	-0.05
	ACI 209	SEE (psi)	530	560	770	870
		R^2	0.23	0.14	-0.29	-0.63
Mixture #5	MC2010	SEE (psi)	360	300	500	400
		R^2	0.10	0.34	0.27	0.54
	ACI 209	SEE (psi)	370	380	520	490
		R^2	0.03	-0.04	0.21	0.30
Mixture #6	MC2010	SEE (psi)	510	280	770	420
		R^2	-0.37	0.59	-0.16	0.65
	ACI 209	SEE (psi)	530	380	800	570
		R^2	-0.46	0.23	-0.27	0.37
Mixture #7	MC2010	SEE (psi)	420	410	590	580
		R^2	0.23	0.28	-0.97	-0.87
	ACI 209	SEE (psi)	450	450	640	650
		R^2	0.13	0.13	-1.29	-1.33

Table 6.28: Optimized Standard Percent Errors of Estimate by Mixture, Air-Adjusted Data

		SPEE when Predicting Release Strengths		SPEE when Predicting 28-Day Strengths	
		Chronological Age (%)	Equivalent Age (%)	Chronological Age (%)	Equivalent Age (%)
Mixture #1	MC2010	7.3	7.0	7.3	6.8
	ACI 209	7.4	8.4	7.7	8.3
Mixture #2	MC2010	10.2	10.8	9.5	10.7
	ACI 209	10.1	11.9	9.7	12.8
Mixture #3	MC2010	6.9	8.2	6.9	8.8
	ACI 209	6.6	10.1	6.8	11.6
Mixture #4	MC2010	8.2	6.9	7.2	6.8
	ACI 209	8.0	8.2	7.3	8.5
Mixture #5	MC2010	5.7	4.7	5.8	4.5
	ACI 209	6.0	5.9	6.1	5.5
Mixture #6	MC2010	8.0	4.2	7.6	4.3
	ACI 209	8.2	8.9	8.1	5.9
Mixture #7	MC2010	7.1	6.7	6.4	6.2
	ACI 209	7.3	7.2	6.9	6.9

The trends seen in the full data set analyses were closely mimicked in the mixture-specific analyses. All SEE values increased approximately 30% to 50% when predicting 28-day strengths rather than predicting release strengths.

To match these SEE findings, it was also found that the R^2 value decreased in almost every instance when predicting 28-day strengths instead of release strengths. This decrease was highly varied, with no clear pattern. The only exceptions to the general trend of having worse accuracy when predicting 28-day strengths than when predicting release strengths were in mixtures 5 and 6. In both of those mixtures, the R^2 value actually increased, despite the fact that the SEE for those mixtures increased. However, in both of these mixtures the SPEEs were fairly similar for both prediction directions. Mixture #6 did show a sizeable decrease in SPEE for chronological age predictions.

The mixture-specific analyses did not all exhibit improvement or equivalence when using EA instead of chronological age. Most of the MC2010 predictions showed improvement in SEE when using EA, with several exceptions. In contrast, most of the ACI 209 predictions had smaller SEEs for chronological age predictions, with several exceptions.

When using chronological age as the maturity quantification, results between the ACI 209 equation and the MC2010 equation were very similar. When they were different, the MC2010 method was usually slightly more accurate. The differences between the two are negligible considering their scale. This similarity between methods when using chronological age matches the trend that was found when analyzing the full data set with optimized parameters.

The use of EA always made the MC2010 equation more accurate in prediction of both release strengths and 28-day strengths than the ACI 209 equation with EAs. The use of EA usually, though not always, made the MC2010 equation more accurate in prediction of both release strengths and 28-day strengths than the ACI 209 equation with chronological ages. Excluding the exceptions, the SEE for the MC2010 method with EAs was anywhere from 7% to 47% smaller than the ACI 209 equation for release strength predictions. For predicting 28-day strengths, the SEE was anywhere from 9% to 47% smaller for the MC2010 equation.

One last comparison is the comparison between the mixture-specific curve fits after adjustment and before adjustment. For this purpose, Table 6.29 was created to summarize some of the percent changes that occurred in each mixture-specific analysis during the air-adjustment process. The methods of calculating $\Delta SEE_{\%}$ and $\Delta R^2{}_{\%}$ are described above in Equations 6.17 and 6.18, along with a description of what the results would mean. Table 6.30 shows a summary of the percent changes that occurred in SPEE due to air-adjustments, calculated in accordance with Equation 6.19.

Table 6.29: Summary of Prediction Fit Changes from Air Adjustment by Mixture

			Predicting Release Strengths		Predicting 28-Day Strengths	
			Chronological Age (%)	**Equivalent Age (%)**	**Chronological Age (%)**	**Equivalent Age (%)**
Mixture #1	MC2010	$\Delta SEE_{\%}$	-3.70	-3.85	-4.05	-4.35
		$\Delta R^2{}_{\%}$	-23.3	-20.1	-74.9	-141
	ACI 209	$\Delta SEE_{\%}$	-3.57	-4.84	-3.85	-4.71
		$\Delta R^2{}_{\%}$	-28.4	-61.2	-58.6	-46.8
Mixture #2	MC2010	$\Delta SEE_{\%}$	-8.11	-7.59	-7.62	-7.56
		$\Delta R^2{}_{\%}$	-66.1	-602	24.8	17.8
	ACI 209	$\Delta SEE_{\%}$	-8.11	-6.74	-7.48	-7.75
		$\Delta R^2{}_{\%}$	-71.7	-70.2	24.2	15.1
Mixture #3	MC2010	$\Delta SEE_{\%}$	-6.12	-5.26	-5.56	-7.53
		$\Delta R^2{}_{\%}$	-1.64	-2.18	-15.9	-5.62
	ACI 209	$\Delta SEE_{\%}$	-6.12	-5.63	-5.56	-7.38
		$\Delta R^2{}_{\%}$	-1.57	-8.47	-15.0	-2.09
Mixture #4	MC2010	$\Delta SEE_{\%}$	-5.36	-4.08	-4.94	-4.11
		$\Delta R^2{}_{\%}$	-28.6	-14.6	-853	-132
	ACI 209	$\Delta SEE_{\%}$	-5.36	-5.08	-4.94	-5.43
		$\Delta R^2{}_{\%}$	-27.7	-40.0	-757	-97.3
Mixture #5	MC2010	$\Delta SEE_{\%}$	-5.26	-9.09	-3.85	-6.98
		$\Delta R^2{}_{\%}$	-81.6	-48.2	-40.2	-14.5
	ACI 209	$\Delta SEE_{\%}$	-11.90	-9.52	-7.14	-9.26
		$\Delta R^2{}_{\%}$	-94.1	-110	-43.5	-28.5
Mixture #6	MC2010	$\Delta SEE_{\%}$	-5.56	-6.67	-3.75	-6.67
		$\Delta R^2{}_{\%}$	-329	-10.7	83.3	66.8
	ACI 209	$\Delta SEE_{\%}$	-5.36	-7.32	-5.88	-5.00
		$\Delta R^2{}_{\%}$	-170	-36.1	77.1	407
Mixture #7	MC2010	$\Delta SEE_{\%}$	-8.70	-4.65	-7.81	-6.45
		$\Delta R^2{}_{\%}$	147	175	-85.6	-108
	ACI 209	$\Delta SEE_{\%}$	-6.25	-4.26	-7.25	-4.41
		$\Delta R^2{}_{\%}$	120	121	-78.5	-93.3

Table 6.30: Summary of $\Delta SPEE_{\%}$ Changes by Mixture

		$\Delta SPEE_{\%}$ when Predicting Release Strengths		$\Delta SPEE_{\%}$ when Predicting 28-Day Strengths	
		Chronological Age (%)	Equivalent Age (%)	Chronological Age (%)	Equivalent Age (%)
Mixture #1	MC2010	-0.14	0.00	-0.14	0.00
	ACI 209	0.13	-0.12	0.26	0.00
Mixture #2	MC2010	0.00	-0.19	-0.11	0.38
	ACI 209	-0.10	-0.08	-0.10	0.00
Mixture #3	MC2010	0.00	0.00	-0.29	-0.34
	ACI 209	0.00	0.20	-0.15	-0.09
Mixture #4	MC2010	0.25	-0.14	-0.28	0.00
	ACI 209	0.00	0.00	0.00	0.00
Mixture #5	MC2010	-0.87	0.00	0.87	-0.22
	ACI 209	-7.0	0.00	0.16	-1.6
Mixture #6	MC2010	-0.50	0.47	0.40	0.47
	ACI 209	0.12	0.34	0.00	0.34
Mixture #7	MC2010	0.42	0.60	-0.63	-0.64
	ACI 209	-0.27	0.00	-0.15	1.6

It can be seen from Table 6.29 that air-content adjustments decreased the SEE value for every prediction method, prediction direction, maturity quantification, and mixture by anywhere from 3% to 9%. However, the values of $\Delta SPEE_{\%}$ shown in Table 6.30, which are almost all very close to zero, confirm that this decrease in SEE was primarily due to the decrease in average strengths.

For most of the mixtures, the R^2 value was also decreased. Mixtures 2 and 6 were the only exceptions to this, showing an increase in R^2 for both chronological age and equivalent age when predicting 28-day strengths.

After extensive analysis and comparison, then, the following general conclusions are made with regard to strength-growth predictions with these concretes:

- In terms of SEE, predicting release strengths is much more accurate than predicting 28-day strengths. In terms of SPEE, the error is reasonably equivalent for either prediction direction.
- The optimized s, α, and β parameters calculated for the full data set provide a much better curve fit for the full data set than the use of the suggested parameters from the MC2010 code or ACI 209 report.
- Using chronological age with the suggested s value in MC2010 strength-growth predictions yields excessively large errors, and is not advised.
- Using equivalent age as the basis for strength predictions yields substantially more accurate results for both the ACI 209 method and the MC2010 method when the methods are used with suggested parameters.
- Adjusting the measured values for actual air content decreases the prediction errors (SEE), but does not substantially change the shape of the optimized prediction curve. The normalized prediction errors (SPEE) do not change significantly.
- The most accurate method of predicting strength-growth over any maturity quantification is to use the optimized MC2010 prediction method with equivalent ages to predict air-adjusted release strengths. This is only slightly more accurate than using the optimized ACI 209 prediction method with chronological ages.

6.7. Summary

The analysis results provided in this chapter quantify the relationship between specified strengths and expected strengths at both release and 28 days, and the relationship between concrete strength and concrete age. From these results, several suggestions are made.

First, when predicting average concrete strengths at the time of prestress release, the following relationship is suggested:

$$f_{ci}^{*} = 7500 \text{ psi} \qquad \text{for } 4000 \text{ psi} \leq f_{ci}' \leq 7000 \text{ psi} \qquad \textbf{Equation 6.8}$$

$$f_{ci}^{*} = f_{ci}' + 500 \text{ psi} \qquad \text{for } 7000 \text{ psi} < f_{ci}' \leq 9000 \text{ psi}$$

where:

f_{ci}^{*} = expected concrete strength at release, psi

f_{ci}' = specified concrete strength at release, psi

The standard error of estimate for this equation, when considering the full set of release strength measurements, is $SEE = 970$ psi. This means that approximately 68% of all measured release strengths are within 970 psi of the estimated strength, and approximately 95% of all measured release strengths are within 1940 psi of the estimated strength. This SEE is an improvement of approximately 54% over the current practice of treating the average strength as equal to the specified strength. These predictions also place the estimate near the mean of measured values, rather than as a lower bound of measured values. The effects of the SEE error range on modulus of elasticity predictions are discussed in greater detail in Chapter 7.

When predicting average concrete strengths at 28 days, the following two relationships are suggested as alternatives:

$$f_{c}^{*} = 10{,}500 \text{ psi} \qquad \text{for } 5000 \text{ psi} \leq f_{c}' \leq 7000 \text{ psi} \qquad \textbf{Equation 6.10}$$

$$f_{c}^{*} = \frac{1}{2} f_{c}' + 7000 \text{ psi} \qquad \text{for } 7000 \text{ psi} < f_{c}' \leq 9000 \text{ psi}$$

or:

$$f_{c}^{*} = 10{,}500 \text{ psi} \qquad \textbf{Equation 6.11}$$

$$\text{for } 5{,}000 \text{ psi} \leq f_{c}' \leq 9{,}000 \text{ psi}$$

where:

f_c^* = expected concrete strength at 28 days, psi

f_c' = specified concrete strength at 28 days, psi

The standard errors of estimate for these two prediction methods, when considering the full set of 28-day strength measurements, are 980 psi and 1000 psi, respectively. Both of these are an approximate 75% improvement over current practice, and place the estimated value near the mean of the measured values rather than at a lower bound.

In Section 6.5, a limited data set was analyzed for strength-growth predictions using various methods and options. Both the MC2010 method (2010) and the ACI Committee 209 method (1992) of predicting strength growth were tested, both with suggested values from the authors and with optimized values calculated based on the measured data. In all cases, it was found that the optimized values were substantially more accurate than the suggested values. The optimized s parameter for the MC2010 method was always less than the suggested value of $s = 0.20$ from the code, indicating that strength development in ALDOT concretes is more rapid than predicted by this method. The optimized α and β parameters for the ACI 209 method with chronological ages combined to cause more rapid early strength development than the suggested parameters, but somewhat slower later strength development. The optimized α and β parameters for the ACI 209 method with EAs combined to have the opposite effect.

When using chronological (unadjusted) age, the optimized MC2010 method and the optimized ACI 209 method were found to have very similar accuracy in predicting strengths. The use of equivalent (adjusted for temperature) age, however, made the MC2010 method usually slightly more accurate.

One additional analysis performed was to rearrange the MC2010 and ACI 209 prediction equations to predict 28-day strengths based on measured early-age strengths. It was found that

using the equations in this way resulted in normalized errors (SPEE) of approximately the same magnitude in either case.

In Section 6.6, these same strength-growth analyses were performed on strength measurements that had been adjusted to a theoretical strictly controlled air content. This analysis caused most of the strength-growth prediction methods to improve in SEE, but the SPEE remained nearly unchanged. The optimized strength-growth parameters also remained virtually unchanged. All in all, the most accurate method of strength-growth prediction was to use the optimized MC2010 method with equivalent ages to predict air-adjusted release strengths.

From these analyses, Table 6.31 was created to summarize the suggested values of s, α, and β based on the optimized values, compared to the values suggested by the MC2010 code and the ACI Committee 209 report. These "optimized" values were based on the analyses found in Sections 6.5 and 6.6, but are not exactly the same as the values found there. Since the values were so nearly identical in many situations, it was decided that it would be best to simplify the suggested optimized values by ignoring the slight differences caused by a different prediction direction.

Table 6.31: Summary of Suggested Strength-Growth Parameters for Full Data Set

			Chronological Age	Equivalent Age
MC2010	Suggested based on Plant Data	s	0.07	0.15
	Suggested by MC2010	s	NA	0.20
ACI 209	Suggested based on Plant Data	α (days)	0.34	1.13
		β	0.988	0.960
	Suggested by ACI 209	α (days)	0.70	NA
		β	0.98	NA

Chapter 7: In-Plant Strength and Stiffness Findings

7.1. Introduction

Up until this point in this thesis, all findings that have been discussed have been related to concrete strength and other concrete properties other than modulus of elasticity, based on historical plant-submitted data that was collected from four different prestressed girder producers. This chapter discusses all results that were found thus far through in-plant testing performed by AUHRC researchers, related to both concrete strength and concrete modulus of elasticity.

In Sections 7.2 and 7.3, the strength findings from in-plant testing are compared to the findings based on historical data and the prediction methods based on those findings. The in-plant results related to concrete modulus of elasticity, and the application of the previously discussed prediction methods to the prediction of stiffness values and growth, are discussed in Section 7.4.

Due to the limited production of ALDOT bulb-tee girders during the time period over which this research project took place, combined with the difficulty of scheduling in-plant testing during the times when girders were being produced, only six girder production cycles had been completed by the time this thesis was written. This was not regarded as being enough data for drawing any definitive conclusions about modulus of elasticity (MOE) findings. Therefore, the findings discussed in this section are somewhat preliminary in nature, and await the inclusion of

additional data as the project continues.

However, to improve the applicability of these preliminary findings, additional data was collected from previous AUHRC research projects to be included in this analysis. The collection of these additional data sources had the added bonus of diversifying the concrete type, since both of the added projects were used for comparing vibrated concrete (VC) to self-consolidating concrete (SCC). It is anticipated that at least some, if not all, girder producers will begin using SCC for some of their girder production in Alabama as soon as ALDOT updates the relevant specification later this year.

SCC and VC data groups were not separated for analysis. This was partly due to the reality that girder designers do not know which plant will produce the girders or which type of concrete will be used. It was also due to the fact that the strength/modulus relationship has been found to be fairly similar for SCC and VC when strength levels are equivalent and curing conditions are the same. Some researchers have found that SCC and VC have nearly identical modulus of elasticity under these circumstances (Long, Khayat, and Hwang 2012). Others have found that SCC has slightly lower modulus of elasticity than VC under these circumstances (Keske 2014). In either case, SCC and VC were analyzed together for the purposes of this project.

The additional data that was included in the in-plant analysis came from two primary sources. The first source was the study conducted by Keske (2014), comparing the short- and long-term properties of VC girders to SCC girders in a four-span ALDOT bridge. The second source was the study conducted by Boehm, Barnes, and Schindler (2010), comparing transfer lengths and flexural testing in AASHTO Type I girders for VC and SCC.

However, not all of the data from these projects were used for all aspects of the in-plant

analysis. This is due to the differences in testing processes that occurred between these projects and the in-plant testing performed for this thesis. Table 7.1 was created to show which source of data was used for which analyses, based on availability of the data and reliability of the data.

Table 7.1: Summary of Data Sources for In-Plant Testing Results

	VC	SCC	Delay of Plant Practice	Expected Strength Results	Strength Growth Results	Prediction of E_{ci} and E_c	Growth Comparison of E to f_c
Current Project	X			X	X	X	X
Keske	X	X	X	X	X	X	X
Boehm	X	X	X			X	X

One of the express goals of the methodology chosen for in-plant testing in this project was to minimize or eliminate interruptions or disturbances to standard plant practices. Researchers did not alter girder production, or delay prestress release or movement of the girders, in any way. On previous projects, however, this was not always the case. The work of Keske and Boehm et al. delayed release of the girders, thus potentially influencing some of the measured values.

Several of the strength tests performed in the project conducted by Boehm et al. (2010) were below the corresponding specified strength, which is unrepresentative of actual girder production practices. Therefore Boehm's data were used for all modulus of elasticity relationships to strength, but were not used for comparison of predicted strengths to measured strengths or for strength growth.

7.2. Expected Strengths and Measured Strengths

In Sections 6.3.1 and 6.4.1, the strength records of the historical plant-submitted data are used to establish some fairly simple methods of predicting the average concrete strength at release and at 28-days, respectively, given knowledge of the specified strengths. The in-plant testing data was not included in the establishment of these prediction methods. Therefore, one comparison that was desired from the in-plant testing was an analysis of how well these prediction methods worked when predicting the strengths seen during in-plant testing. For this analysis, the data from the current project and the Keske project were used. The Boehm data points were not included due to low strength test results that were not representative of actual plant practices and concrete strengths at the time of release and the experimental nature of the production.

Figure 7.1 shows a comparison of the measured release strengths used in this analysis compared to the specified release strengths and the release strength prediction method formulated in Section 6.3.1.

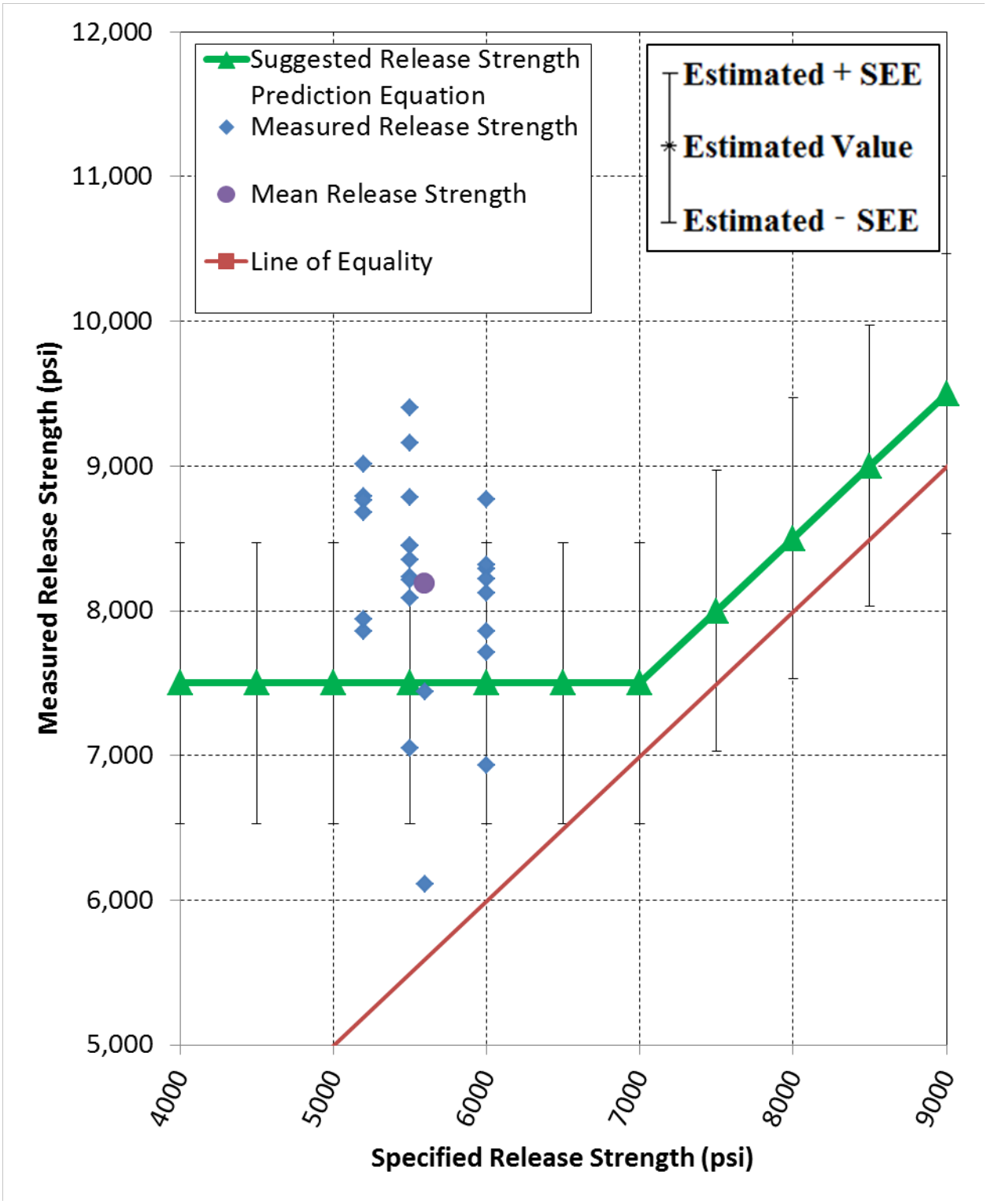

Figure 7.1: Release Strength Predictions for In-Plant Testing

The piecewise prediction method was defined as Equation 6.8, which may be seen below.

$$f_{ci}^{*} = 7500 \text{ psi} \qquad \text{for } 4000 \text{ psi} \leq f_{ci}' \leq 7000 \text{ psi} \qquad \textbf{Equation 6.8}$$

$$f_{ci}^{*} = f_{ci}' + 500 \text{ psi} \qquad \text{for } 7000 \text{ psi} < f_{ci}' \leq 9000 \text{ psi}$$

where:

f_{ci}^{*} = expected concrete strength at release, psi

f_{ci}' = specified concrete strength at release, psi

This equation was expected to have a standard error of estimate (SEE) equal to 970 psi based on the historical data from which it was formulated. The range of error established by this SEE may be seen in Figure 7.1. Since the SEE is basically a standard deviation of the errors, it would be expected that approximately 68% of the data points would lie within the bounds of $Predicted\ Strength \pm SEE$. This appears to be true based on Figure 7.1.

To confirm these findings, a statistical analysis was performed on the release strength values. The results of this analysis have been summarized in Table 7.2. From this table, it can be seen that the SEE between the prediction model and all historical release strengths is approximately the same as the SEE between the prediction model and the measured in-plant release strengths. Thus, it can be concluded that the prediction model was as accurate as was expected in predicting the in-plant release strengths. The SEE increased greatly for the current practice of treating the expected strength as equal to the specified strength.

Table 7.2: SEE Comparison for In-Plant Release Strength Predictions

	SEE Based on Historical Data (psi)	SEE Based on In-Plant Data (psi)
Prediction Model	970	990
Specified Strengths	2120	2730

In both of these cases, though, the error may have been slightly increased by the inclusion of data from the Keske project. As was mentioned earlier, release times were delayed for approximately two hours by research-related tasks in this project, so actual release strengths may have been slightly higher than they normally would have been under standard plant practices. This is supported by examination of Figure 7.1, which shows that the general trend of both the prediction model and the specified strength model was to underestimate the actual strength. Although consideration of the extra strength caused by release delay does not drastically improve either prediction method, it does slightly improve both. This improvement, however, cannot be quantified.

The same strength prediction comparison was made for 28-day strengths. Figure 7.2 shows a comparison of the measured 28-day strengths obtained from in-plant testing compared to the specified 28-day strengths and the 28-day strength prediction methods formulated in Section 6.4.1. These two prediction methods are restated below.

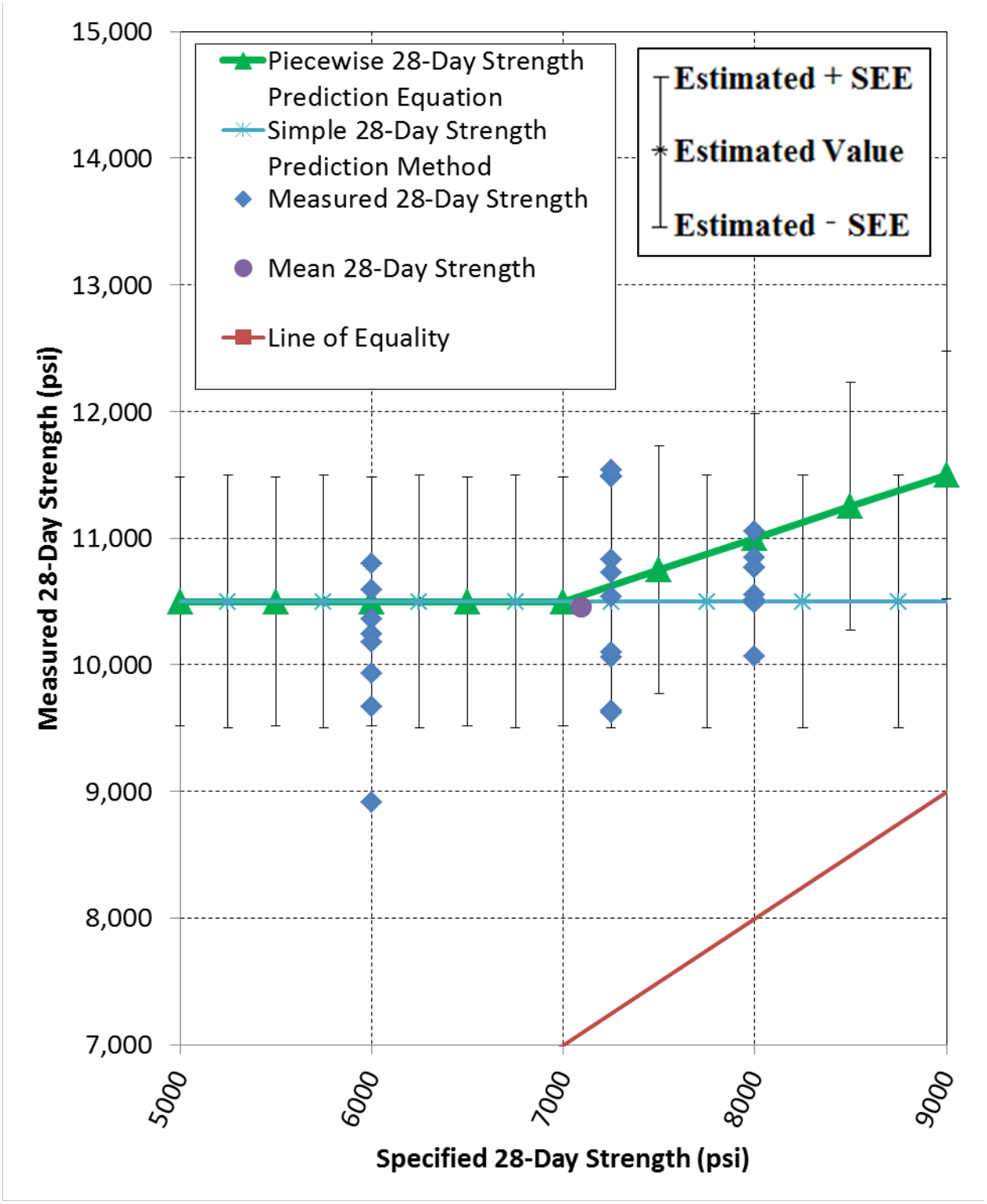

Figure 7.2: 28-Day Strength Predictions for In-Plant Testing

Equation 6.10 defines the piecewise 28-day strength prediction method.

$$f_c^* = 10{,}500 \text{ psi} \qquad \text{for } 5000 \text{ psi} \leq f_c' \leq 7000 \text{ psi} \qquad \textbf{Equation 6.10}$$

$$f_c^* = \frac{1}{2} f_c' + 7000 \text{ psi} \qquad \text{for } 7000 \text{ psi} < f_c' \leq 9000 \text{ psi}$$

where:

f_c^* = expected concrete strength at 28 days, psi

f_c' = specified concrete strength at 28 days, psi

Equation 6.11 defines the simple 28-day strength prediction method.

$$f_c^* = 10{,}500 \text{ psi} \qquad \textbf{Equation 6.11}$$

$$\text{for } 5{,}000 \text{ psi} \leq f_c' \leq 9{,}000 \text{ psi}$$

where:

f_c^* = expected concrete strength at 28 days, psi

f_c' = specified concrete strength at 28 days, psi

It can easily be seen from Figure 7.2 that both of these methods performed admirably in predicting the 28-day strengths. Table 7.3 provides a summary of the SEE values obtained from the historical data set and the in-plant data set for 28-day strength predictions.

Table 7.3: SEE Comparison for In-Plant 28-Day Strength Predictions

	SEE Based on Historical Data (psi)	SEE Based on In-Plant Data (psi)
Piecewise Prediction Model	980	630
Simple Prediction Model	1000	610
Specified Strengths	4020	3450

The SEE values obtained from the historical data analysis for these two methods were 980 psi for the piecewise function and 1000 psi for the simple function. The range of

$Predicted\ Strength \pm SEE$ has been shown in Figure 7.2 for both of these methods, and it is clear that much more than the expected 68% of the data is included within this range. In fact, as may be seen from Table 7.3, the expected SEEs that were calculated from the in-plant data for these two prediction methods are substantially less than the SEEs calculated from the historical data set. Therefore, both methods did an excellent job of predicting the 28-day strengths for these in-plant 28-day strength values.

The 28-day strength values were not significantly affected by the delayed release caused by AUHRC researchers in the Keske (2014) project, because the testing times of these cylinders were independent of the time of release. Thus, although the delays may have slightly raised the in-plant release strengths, it is not expected that they had any significant effect on the 28-day strengths.

From these two analyses, then, it can be concluded that the strength prediction methods created in Sections 6.3.1 and 6.4.1 performed well in predicting strengths for the in-plant testing values. Furthermore, as was expected, these methods were a great deal more accurate than the current practice of using specified strengths—specifically, 64% more accurate for release strength predictions and 82% more accurate for 28-day strength predictions.

7.3. Strength Growth

In Section 6.5, an extensive analysis is performed of 435 pours from the historical data set to examine the accuracy of various strength-growth prediction models. Again, the in-plant testing data was not included in the analysis of these prediction methods. Therefore, it was desired that a comparison be made between the accuracy of the strength-growth prediction models when applied to the historical data set compared to when applied to the in-plant testing

data set. For this analysis, the data from the current project and the Keske (2014) project were included. The Boehm, Barnes, and Schindler (2010) data points were not included, since the break strengths were uncharacteristically low in that project, making them unrepresentative of standard plant practices.

A summary of the parameters used, as well as the SEE and R^2 values for measuring the fit of the prediction curves, may be seen in Table 7.4. This table contains three divisions for each method of strength-growth prediction, and three sections within each method for both prediction directions. For most of the following discussion, predictions are made for "early strengths" and not strictly "release strengths." This is because not all of the strength measurements were taken at release or at 28 days. Many of the early strengths do not correspond to the time of prestress transfer. Some of the data points are from a chronological age of 24 hours, which was almost always after release had already occurred. However, this does not affect the relationship between concrete strength and concrete age, so they may be included without uncertainty.

Table 7.4: Summary of Strength-Growth Parameters and Curve Fits for In-Plant Testing

			Predicting Early Strengths			Predicting 28-Day Strengths		
			Ch. Age	Eq. Age	Adj. EA	Ch. Age	Eq. Age	Adj. EA
MC2010	Optimized from Historical	s	0.07	0.15	0.15	0.07	0.15	0.15
		SEE (psi)	930	820	700	1280	1110	940
		$SPEE$ (%)	11.5	10.5	8.4	12.8	11.3	9.4
		R^2	-0.01	0.21	0.43	-2.58	-1.70	-0.95
	Optimized from In-Plant Strengths	s	0.05	0.14	0.13	0.05	0.14	0.13
		SEE (psi)	720	810	650	920	1080	840
		$SPEE$ (%)	10.4	10.7	8.2	9.5	10.9	8.4
		R^2	0.39	0.23	0.52	-0.85	-1.53	-0.54
	Suggested in Code	s	NA	0.20	0.20	NA	0.20	0.20
		SEE (psi)	4030	1110	1140	10,080	1700	1740
		$SPEE$ (%)	48.7	13.1	13.6	97.6	17.0	17.1
		R^2	-17.90	-0.42	-0.52	-221.0	-5.35	-5.63
ACI 209	Optimized from Historical	α (days)	0.34	1.13	-----	0.34	1.13	-----
		β	0.988	0.960	-----	0.988	0.960	-----
		SEE (psi)	900	900	-----	1220	1180	-----
		$SPEE$ (%)	11.3	11.72	-----	12.3	11.93	-----
		R^2	0.06	0.06	-----	-2.26	-2.04	-----
	Optimized from In-Plant Strengths	α (days)	0.26	1.18	-----	0.26	1.18	-----
		β	0.991	0.958	-----	0.991	0.958	-----
		SEE (psi)	730	900	-----	930	1200	-----
		$SPEE$ (%)	10.52	11.51	-----	9.56	12.15	-----
		R^2	0.38	0.07	-----	-0.87	-2.14	-----
	Suggested in Report	α (days)	0.70	NA	-----	0.70	NA	-----
		β	0.98	NA	-----	0.98	NA	-----
		SEE (psi)	2330	1140	-----	920	1320	-----
		$SPEE$ (%)	27.70	15.72	-----	9.55	13.13	-----
		R^2	-5.30	-0.51	-----	-0.87	-2.82	-----

The three sections are defined as follows:

1. "Optimized from Historical" – These are the "suggested optimized" values provided in Table 6.31 in Section 6.7. They are nearly identical to the optimized values that were

found from analysis of the historical data set.

2. "Optimized from In-Plant Strengths" – These are the values that were calculated to optimize the fit of each strength-growth prediction method to the data points found in the in-plant testing data set. Thus, they will inevitably provide the most accurate predictions for this data set.
3. "Suggested in Code" or "Suggested in Report" – These are the values that were suggested by the MC2010 (*fib* 2010) code or the ACI Committee 209 report (1992), respectively, for use with the concrete mixtures and curing conditions seen in this data set.

Each section provides the values of the applicable strength-growth parameters that were used (s for the MC2010 method or α and β for the ACI 209 method) and the curve fit measurements, SEE and R^2. It is important to note that all of the SEE and R^2 values reported in Table 7.4 are a measure of how well the prediction fits the in-plant data set, with no influence by the historical data set. Even the values of SEE and R^2 provided for the "Optimized from Historical" section are a measure of how well the historically-optimized curve fit the in-plant data points.

The last possibly unclear portions of Table 7.4 are the maturity quantifications. Each prediction direction is broken up into three maturity quantifications, which are defined as follows:

1. "Ch. Age" – These values predicted strength growth on the basis of chronological age, unadjusted for temperatures during curing.
2. "Eq. Age" – These values predicted strength growth on the basis of calculated equivalent ages, adjusted for temperatures during early curing. Only the ages of early tests, such as tests at the time of prestress release or at a chronological age of 24 hours, were adjusted in this column.

3. "Adj. EA" – This stands for "adjusted equivalent age." In order for this column to make sense, the MC2010 equation for strength growth (Equation 6.12) must be reexamined. It has been provided again below for easy reference.

$$f_{cm}(t) = \beta_{cc}(t) \cdot f_{cm} \qquad \textbf{Equation 6.12}$$

with

$$\beta_{cc}(t) = exp\left\{s \cdot \left(1 - \sqrt{\frac{28}{t}}\right)\right\}$$

where:

$f_{cm}(t)$ = the mean compressive strength at time t, MPa

f_{cm} = the mean compressive strength at an age of 28 days, MPa

$\beta_{cc}(t)$ = a function to describe strength development with time

s = coefficient which depends on the strength class of cement, as given in Table 2.1

t = the concrete equivalent age adjusted for curing temperatures, days

Examination of the $\beta_{cc}(t)$ factor, which is basically the ratio of the strength at any time t to the strength at 28 days, reveals that the effects of the concrete age are controlled by the ratio contained in the exponent, $\sqrt{\frac{28}{t}}$. This ratio is supposed to be $\sqrt{\frac{28}{t}} = 1$ when the time t is equal to 28 days. With $t = 28$ days, $f_{cm}(28 \text{ days}) = f_{cm}$, which is the only logical solution based on the definition of $f_{cm}(t)$ and f_{cm}.

However, this assumes that the concrete age at the time of 28-day strength testing is actually 28 days; in other words, it is assumed that $t = 28$ days when the 28-day strength is measured. This is only significant because the equation is designed to use equivalent age, and yet the 28-day strength is measured at a chronological age of 28 days. Therefore when

the 28-day strength is measured, the value for t may be greater than 28 days or less than 28 days, depending on the curing conditions leading up to that point. Using such values of t could lead to nonsensical answers that would literally translate as "the concrete strength at 28 days is greater than the concrete strength at 28 days."

Therefore, the "Adj. EA" maturity quantification applies equivalent ages to both ends of the equation, and uses the following modified form of the MC2010 equation for its predictions:

$$f_{cm}(t) = \beta_{cc}(t) \cdot f_{cm} \qquad \textbf{Equation 7.1}$$

with

$$\beta_{cc}(t) = exp\left\{s \cdot \left(1 - \sqrt{\frac{t_{28}}{t}}\right)\right\}$$

where:

$f_{cm}(t)$ = the mean compressive strength at time t, MPa

f_{cm} = the mean compressive strength at a chronological age of 28 days, MPa

$\beta_{cc}(t)$ = a function to describe strength development with time

s = coefficient which depends on the strength class of cement,

t_{28} = the concrete equivalent age adjusted for curing temperatures that corresponds to a chronological age of 28 days, days

t = the concrete equivalent age adjusted for curing temperatures, days

Equation 7.1 could not be used in the historical data set analyses because no information was available about the equivalent ages of the cylinders at the time of 28-day strength testing. For the in-plant pours included in this research project, however, detailed temperature profiles were kept from cylinder production to cylinder testing. Therefore the 28-day strengths in this research project had known equivalent ages, and could be compared to Equation 7.1. The ACI 209 method could not be adjusted in a similar fashion because it does not use the 28-day age as a

direct reference point.

The first comparison made from Table 7.4 is the comparison between the historically optimized strength growth parameters and the optimized parameters obtained from the in-plant data. Figure 7.3 and Figure 7.4 provide graphical comparison of each of the different methods, with extended versions in Figure 7.5 and Figure 7.6, respectively.

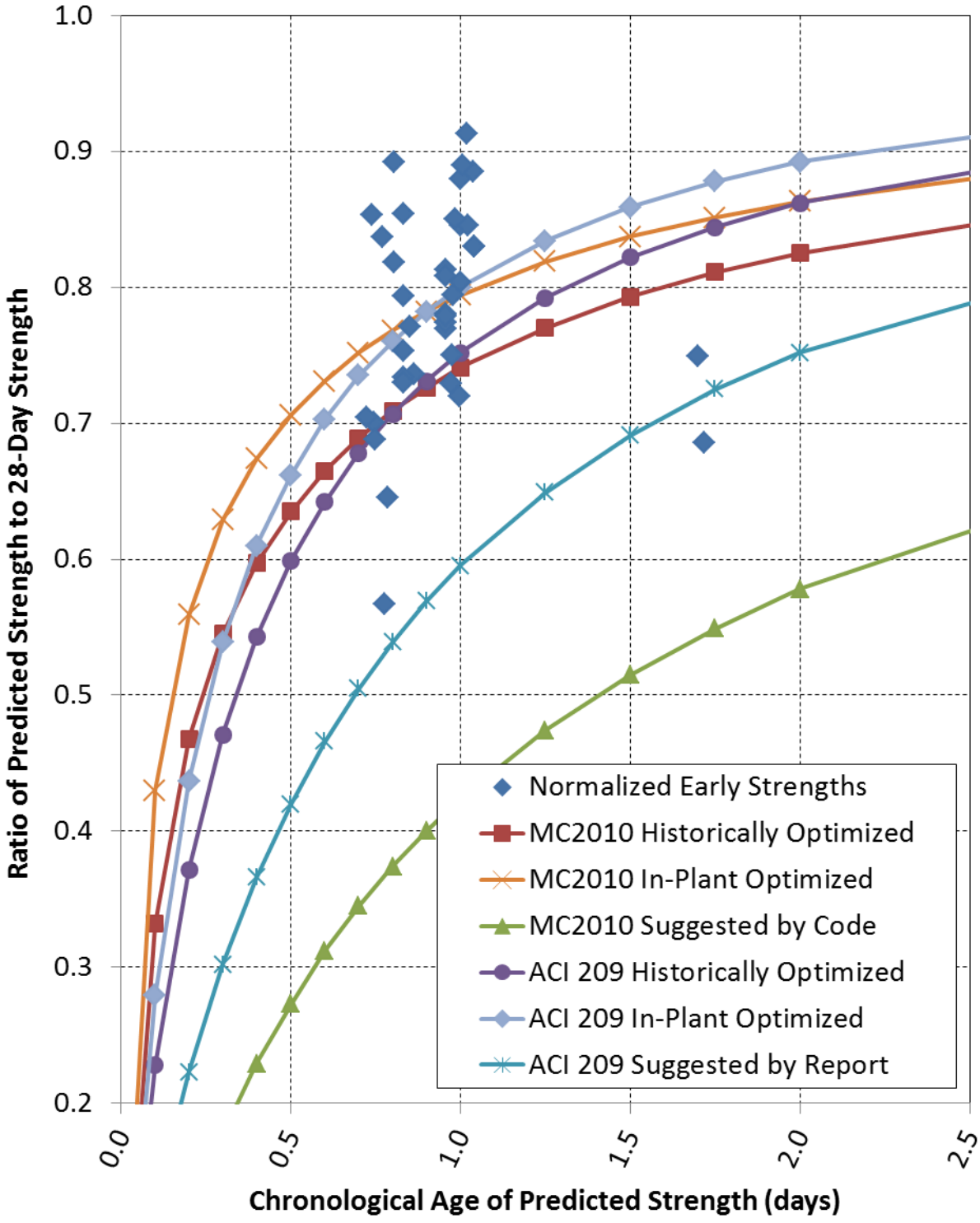

Figure 7.3: Prediction Curves for In-Plant Early Strengths with Chronological Age

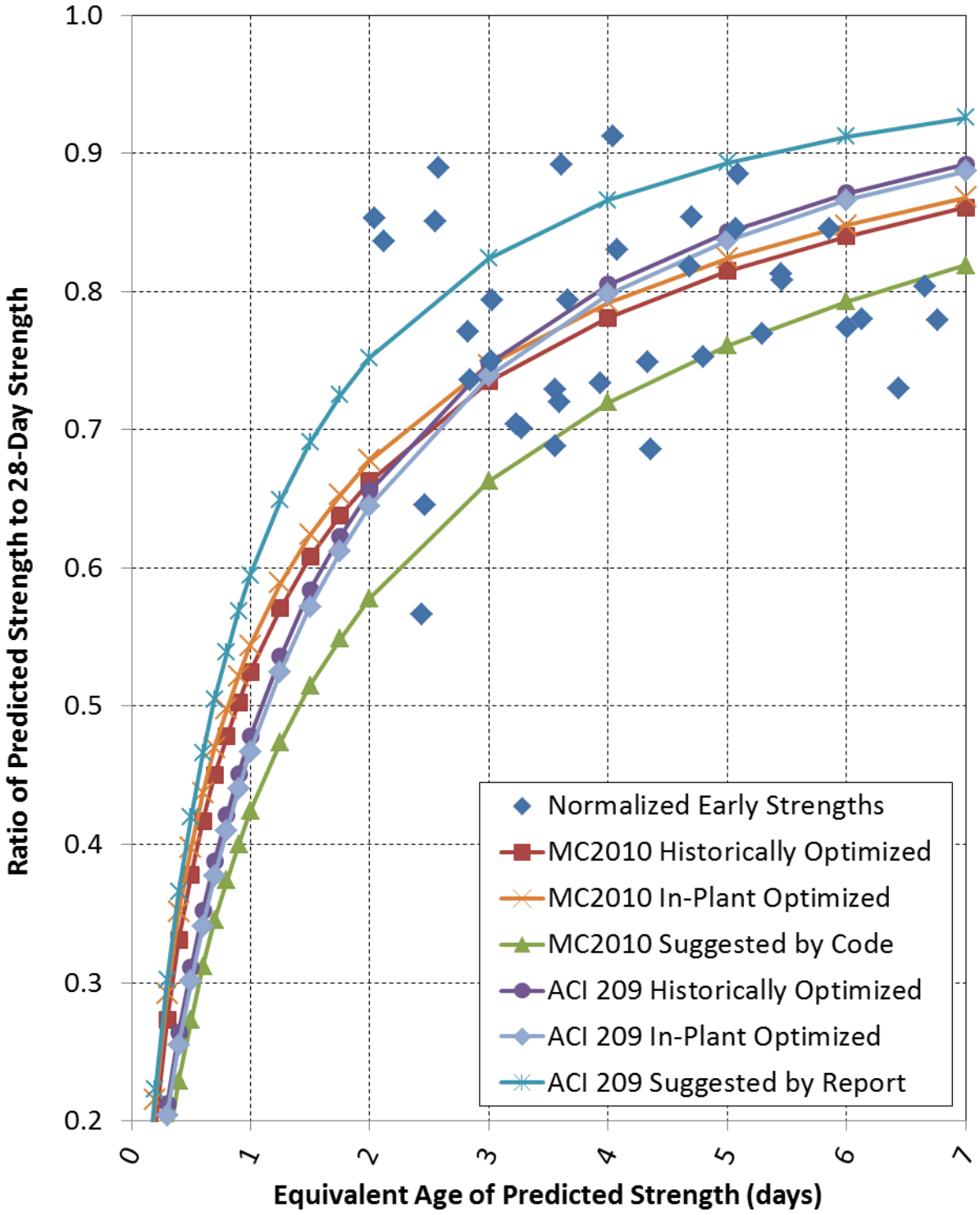

Figure 7.4: Prediction Curves for In-Plant Early Strengths with Equivalent Age

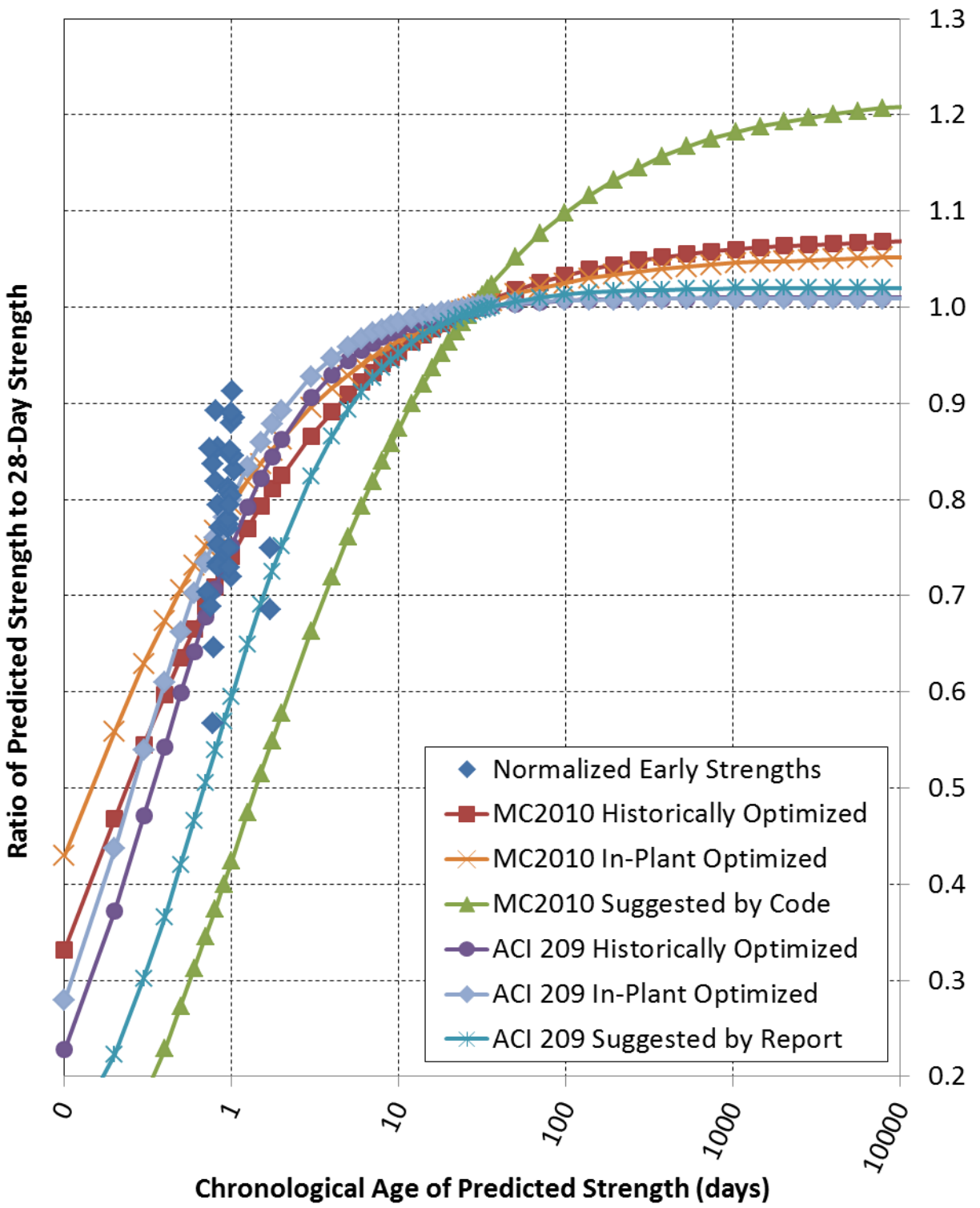

Figure 7.5: Extended Prediction Curves for In-Plant Early Strengths, Chronological Age

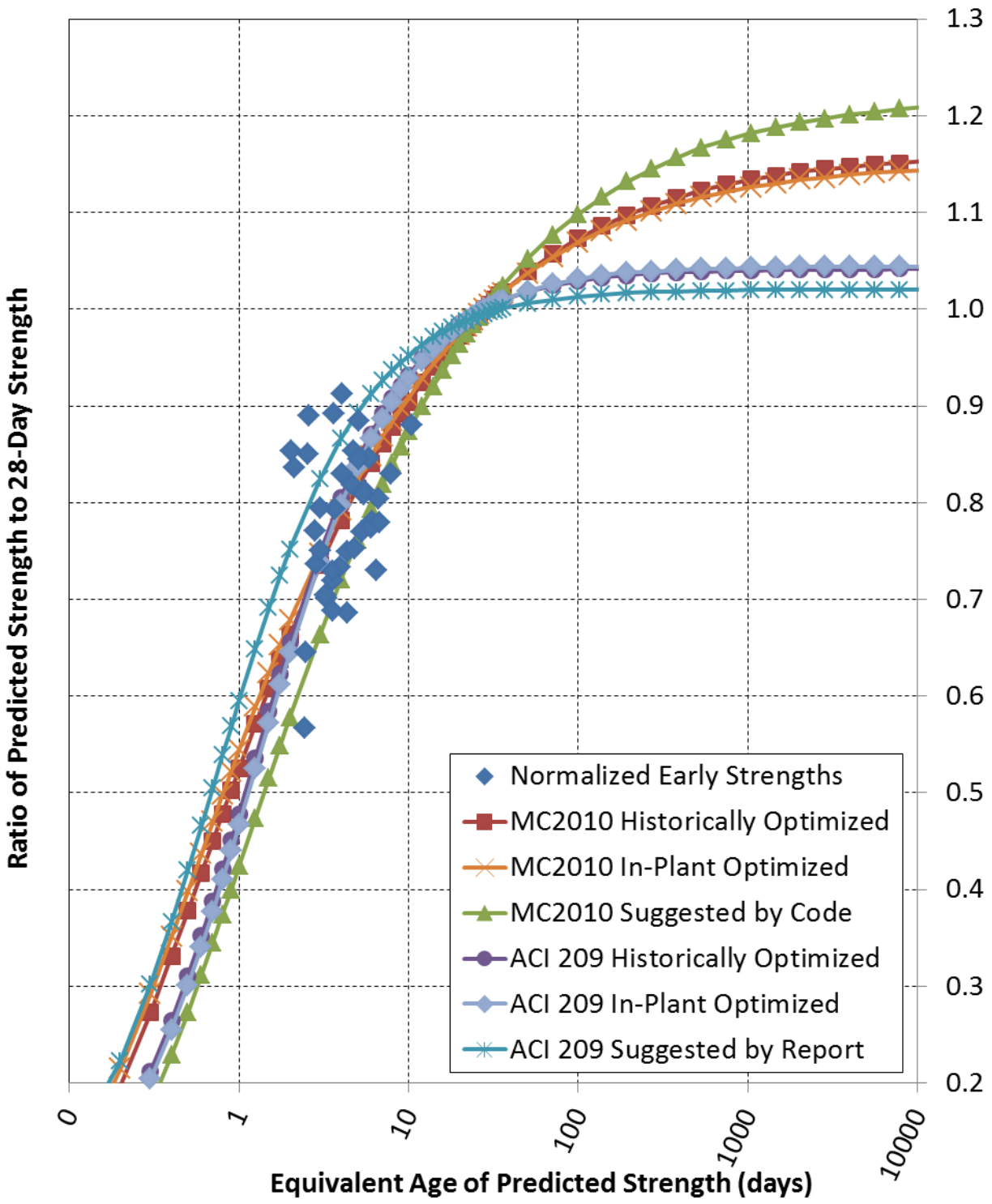

Figure 7.6: Extended Prediction Curves for In-Plant Early Strengths, Equivalent Age

Note first of all that all of the s values for the in-plant optimized curves are slightly less than the values from the corresponding historically optimized curves. This indicates that the in-plant data exhibited slightly more rapid early strength development than was predicted by the parameters from the historical data set. It is also known from the discussion in Section 6.5 that the historically optimized s values predicted much more rapid early strength development than the MC2010 code suggested, so it is clear that the in-plant data's strength development was much more rapid than the MC2010 code predicted.

The in-plant optimized ACI 209 parameters, α and β, took the trends found from the historically optimized parameters in the same direction, but to a greater extent. This is supported by the values of α and β shown in Table 7.4. For chronological age calculations, the in-plant optimized α value was smaller than the historically optimized value, which in turn was smaller than the suggested value. This indicates a progression in the prediction of more and more rapid early strength development based on more specific knowledge of the values. For EA calculations, the in-plant optimized α value was larger than the historically optimized value, which in turn was larger than the suggested value, indicating a progression in the prediction of slower and slower early strength development against EA.

In-plant β values were so close to the corresponding historically optimized values that rounding makes them appear the same, indicating equivalent long-term strength growth.

Not surprisingly, it was found that the in-plant optimized curves provided the most accurate predictions of strength growth for the in-plant data set in almost all cases. The only exception to this occurred when predicting 28-day strengths based on historically optimized values instead of in-plant optimized values, with the ACI 209 method. Because the in-plant optimized parameters were optimized on the basis of early strength predictions, it was possible

for 28-day predictions to still be more accurate using the historically optimized values.

The SEEs calculated from the historically optimized prediction curves were almost always substantially smaller than those suggested by the authors. The only exception was in the ACI 209 method with the use of chronological ages to calculate 28-day strengths, in which the SEE increased by 34%. All of the other historically optimized curves had SEEs from 36% to 87% smaller than the corresponding author-suggested curve. Similarly, aside from the exception mentioned above, the SEEs from the in-plant optimized curves were all 0%–28% smaller than the corresponding historically optimized curve.

It may be ascertained from Figure 7.3 through Figure 7.6 that direct graphical comparison of all the different possible prediction methods quickly becomes too muddled to see clearly. Therefore, since the in-plant data set is much smaller than the historical data set used for strength-growth prediction optimization, it is easier to use a different form of comparison. Since there are far too many graphs to show at once, only a few graphs are shown and discussed, and the rest are provided in Appendix J.

For the purposes of direct comparison, the three graphs that may be seen in Figure 7.7, Figure 7.8, and Figure 7.9 are all for unadjusted early strength predictions using the MC2010 method. Figure 7.7 uses chronological age, Figure 7.8 uses equivalent age, and Figure 7.9 uses Equation 7.1 with known 28-day equivalent ages. Again, these predictions are marked as “early strengths” and not “release strengths” because they do not all correspond to the time of prestress transfer. Some of the data points are from a chronological age of 24 hours.

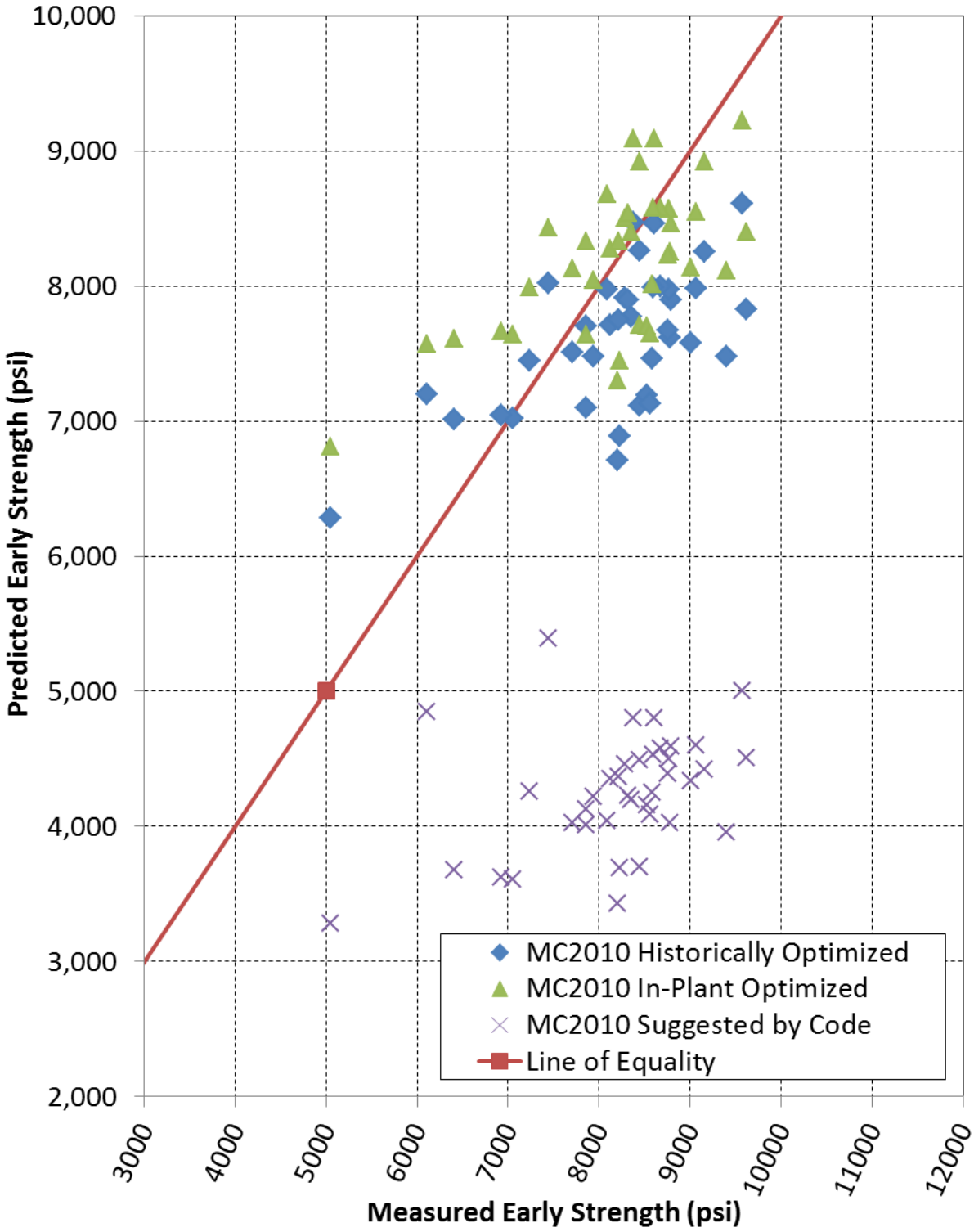

Figure 7.7: MC2010 Early Strength Predictions for In-Plant Data using Chronological Age

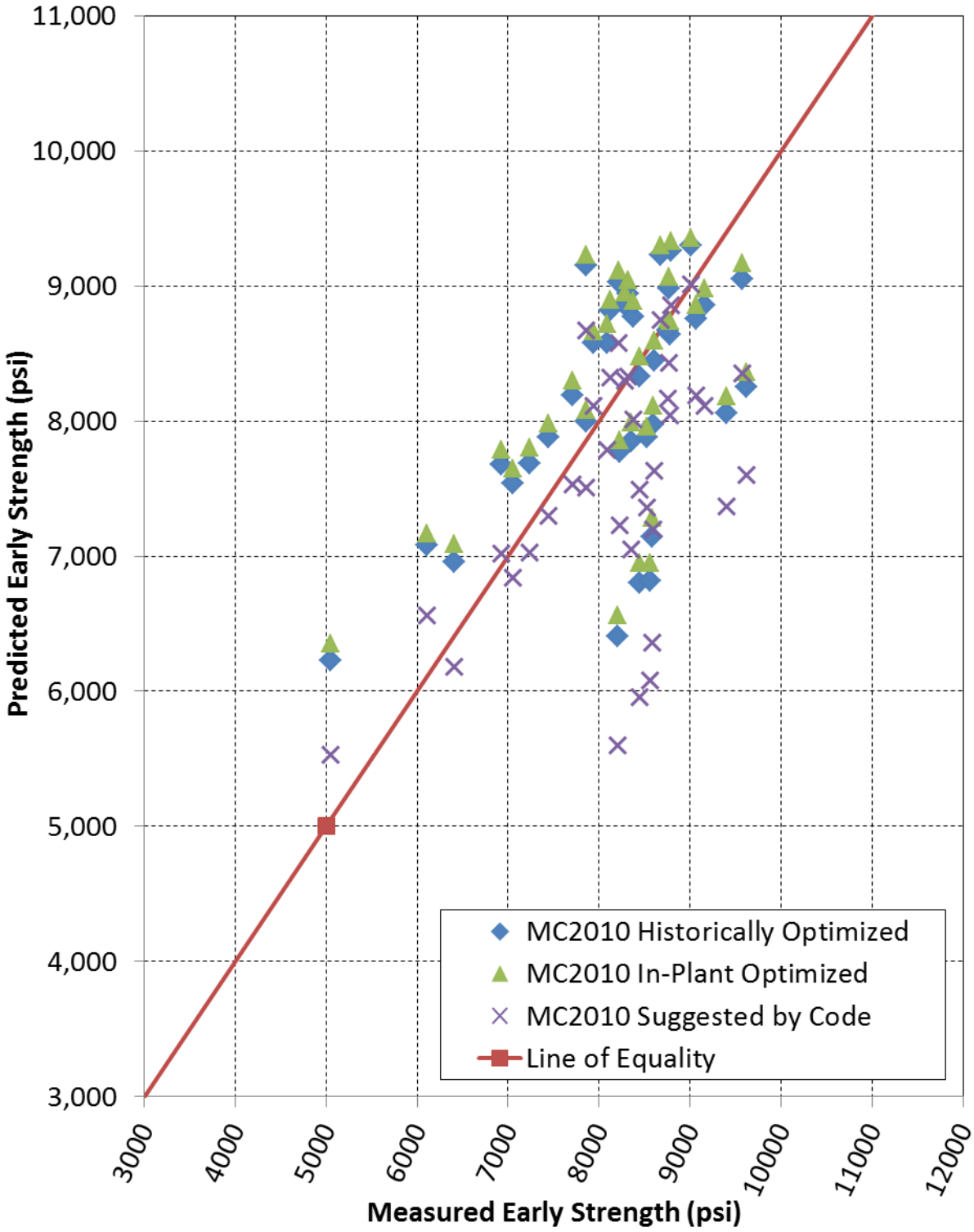

Figure 7.8: MC2010 Early Strength Predictions for In-Plant Data using Equivalent Age

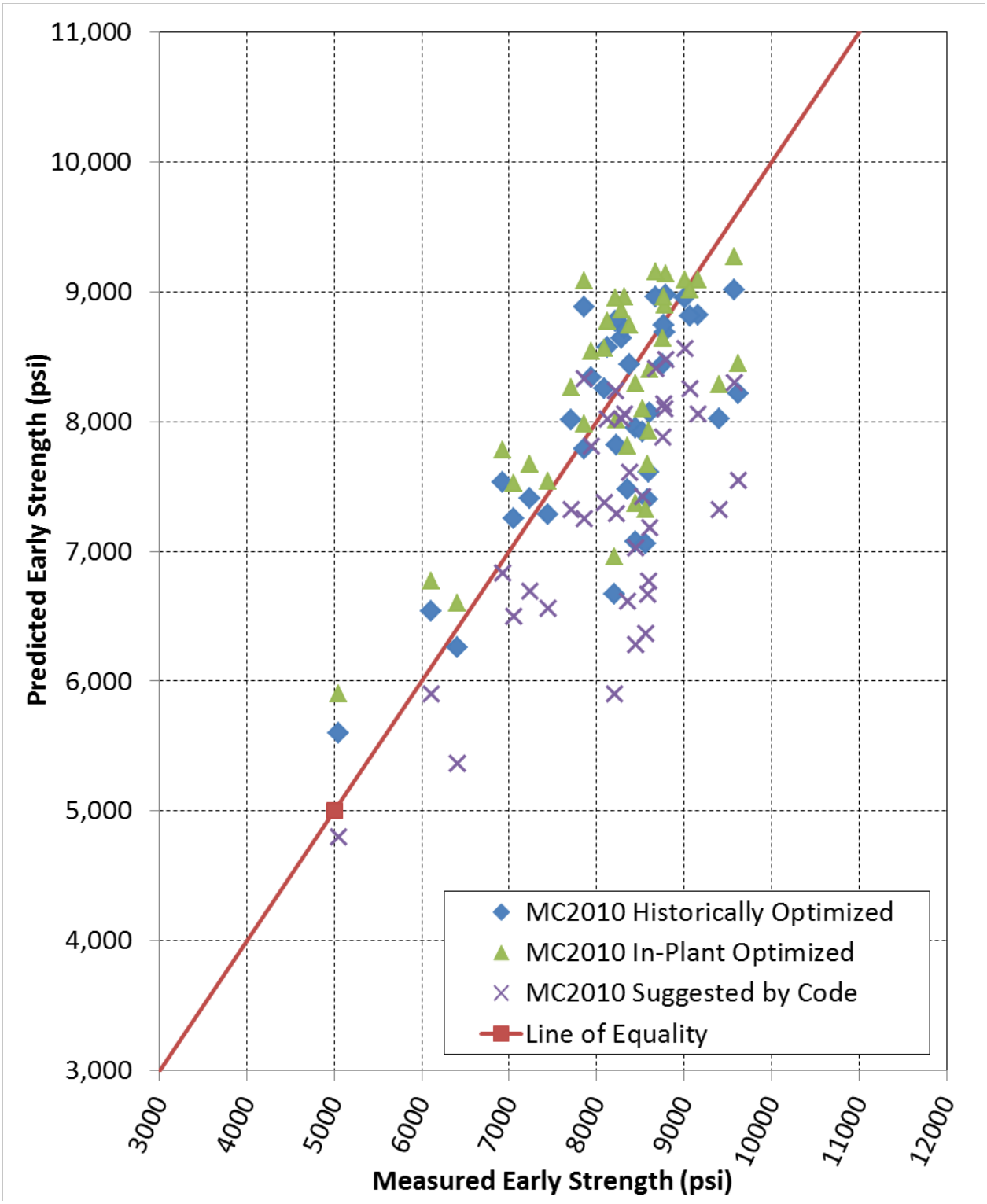

Figure 7.9: MC2010 Early Strength Predictions for In-Plant Data using Adjusted EA

The effects of each change are readily visible for comparison from this series of figures. Within each figure, it is clear that the MC2010 Suggested by Code values are by far the most inaccurate for predicting the in-plant early strengths. However, it may also be seen that the MC2010 Historically Optimized values are much more accurate than the suggested values, and that the MC2010 In-Plant Optimized values are slightly more accurate still. The progression from least specific knowledge about the measurements to most specific knowledge about the measurements shows a clear increase in the possible accuracy of those predictions.

A comparison from Figure 7.7 to Figure 7.8 to Figure 7.9 also shows increasing prediction accuracy with better knowledge of the maturity quantification for each set of values. The optimized curves pass through the core of the chronological age data. However, it is a data cloud—not a line or a clear relationship. With the use of equivalent ages in Figure 7.8, the data starts being drawn more tightly toward the Line of Equality, which is the line at which the predicted value equals the measured value. Thus, the use of equivalent age makes the relationship more clear and consistent. The use of equivalent age most significantly improves the prediction made with the suggested parameter of $s = 0.20$, as is expected.

The relationship then becomes clearest when predictions are made with knowledge of the equivalent ages at both the time of prediction and the time of 28-day strength testing. By the time the transition has been made from Figure 7.7 to Figure 7.9, the data group has changed in appearance from something like a cloud to something closely following the Line of Equality.

All in all, the strength-growth prediction methods in place do indeed accurately describe the relationship of concrete strength with concrete age, provided that sufficient information is known regarding the points at which data measurements are taken. The more knowledge about the maturity quantification that is available, the higher accuracy is possible in predicting strength

growth. Graphs showing predictions of 28-day strengths, as well as predictions using the ACI 209 method, may be seen in Appendix J.

For the data seen in this project, it is concluded that the historically optimized strength growth parameters that were suggested in Table 6.31 may be used for reasonably accurate predictions of strength using either the MC2010 method or the ACI 209 method. The error of these predictions increases if they are used for predicting later-age strengths on the basis of early strengths. The normalized error (SPEE) also increases, but not as substantially.

7.4. Modulus of Elasticity Prediction and Growth

At last, all of the discussion and analysis that has been presented in this thesis comes to what is probably the single most important component in terms of reaching the goals set forth for the project—namely, the prediction and growth of concrete stiffness. Knowledge of concrete stiffness at the time of prestress release is necessary for accurate estimation of the initial girder camber, and knowledge of the initial camber is vital for accurate predictions of later cambers. Even the strength analyses presented in the previous chapter were meant to provide a means of more accurately estimating the concrete modulus of elasticity.

This section has been divided into four subsections. Prediction of release modulus of elasticity is discussed in Section 7.4.1, prediction of 28-day modulus of elasticity is discussed in Section 7.4.2, and the comparison of modulus growth and strength growth over time is discussed in Section 7.4.3. All suggestions based on the discussions found in these three sections are found in Section 7.4.4.

7.4.1. Release Modulus Predictions

Prediction of release modulus of elasticity required some choices to be made regarding prediction methods. As discussed in Section 2.3.3, the modulus of elasticity prediction equations are either unclear as to their applicability to release modulus predictions or, in the case of the MC2010 equation, explicitly a step along the way to the prediction of release modulus. Nevertheless, for the other equations from ACI and AASHTO, the choice was made to use release strengths (f'_{ci}, f^*_{ci}, or f_{ci}) in the modulus prediction equations for predicting release modulus of elasticity. This is common practice in the United States. It is more logical to expect correlation between release strengths and release modulus of elasticity than between 28-day strengths and release modulus.

The MC2010 equation was treated differently, due to its specifications regarding the calculation of release modulus of elasticity. To provide some justification for using release strengths instead of 28-day strengths, which was still regarded as the more logical option, both methods were used for the preliminary analysis. Deciding to use release strengths instead of 28-day strengths for release modulus predictions also bypasses the need for knowledge of the concrete maturity at the time of prestress release, which would be required if calculation were to be performed strictly according to the MC2010.

The expected concrete modulus of elasticity at release was initially calculated using seven basic methods to provide a benchmark by which to judge future calculations and improvements. A summary of the accuracy of these predictions may be seen in Table 7.5. Figure 7.10, Figure 7.11, and Figure 7.12 provide graphical representation of Table 7.5, showing the accuracy and trends found therein. A more full description of the analysis that was performed is given after this table and these figures.

Table 7.5: Summary of Release Modulus Prediction Accuracy for Basic Equations

		Specified Strengths	Expected Strengths	Measured Strengths
ACI 318, "Normalweight" ($\omega \cong 145$ pcf)	SEE (ksi)	2000	1390	1250
	$SPEE$ (%)	31.4	21.4	20.0
	R^2	-9.51	-4.06	-3.10
ACI 318, Known Weights	SEE (ksi)	1650	990	830
	$SPEE$ (%)	25.8	15.2	13.5
	R^2	-6.11	-1.56	-0.82
AASHTO, $K_1 = 1.2$	SEE (ksi)	840	550	510
	$SPEE$ (%)	13.0	10.5	8.6
	R^2	-0.86	0.19	0.33
ACI 363	SEE (ksi)	2280	1850	1740
	$SPEE$ (%)	35.9	28.8	27.7
	R^2	-12.62	-7.95	-6.96
MC2010, Direct, Using 28-Day, $\alpha_E = 1.2$	SEE (ksi)	910	1260	1130
	$SPEE$ (%)	17.3	23.4	20.7
	R^2	-1.17	-3.19	-2.34
MC2010, Explicit, Using 28-Day, $\alpha_E = 1.2$	SEE (ksi)	780	630	600
	$SPEE$ (%)	12.2	11.1	10.1
	R^2	-0.61	-0.06	0.04
MC2010, Using Release, $\alpha_E = 1.2$	SEE (ksi)	610	650	510
	$SPEE$ (%)	11.1	12.4	9.4
	R^2	0.03	-0.11	0.31

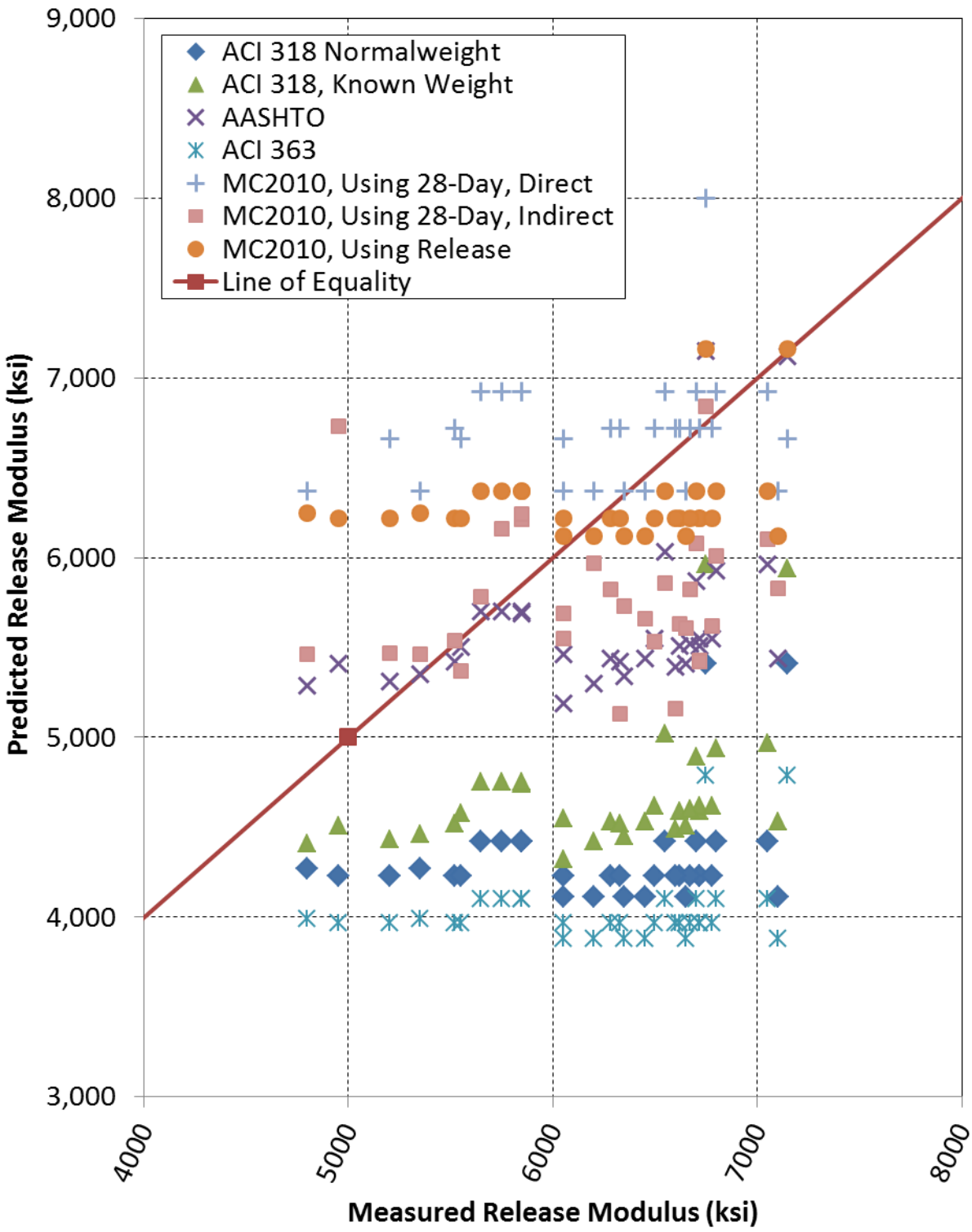

Figure 7.10: Release Modulus Predictions using Basic Equations, Specified Strength

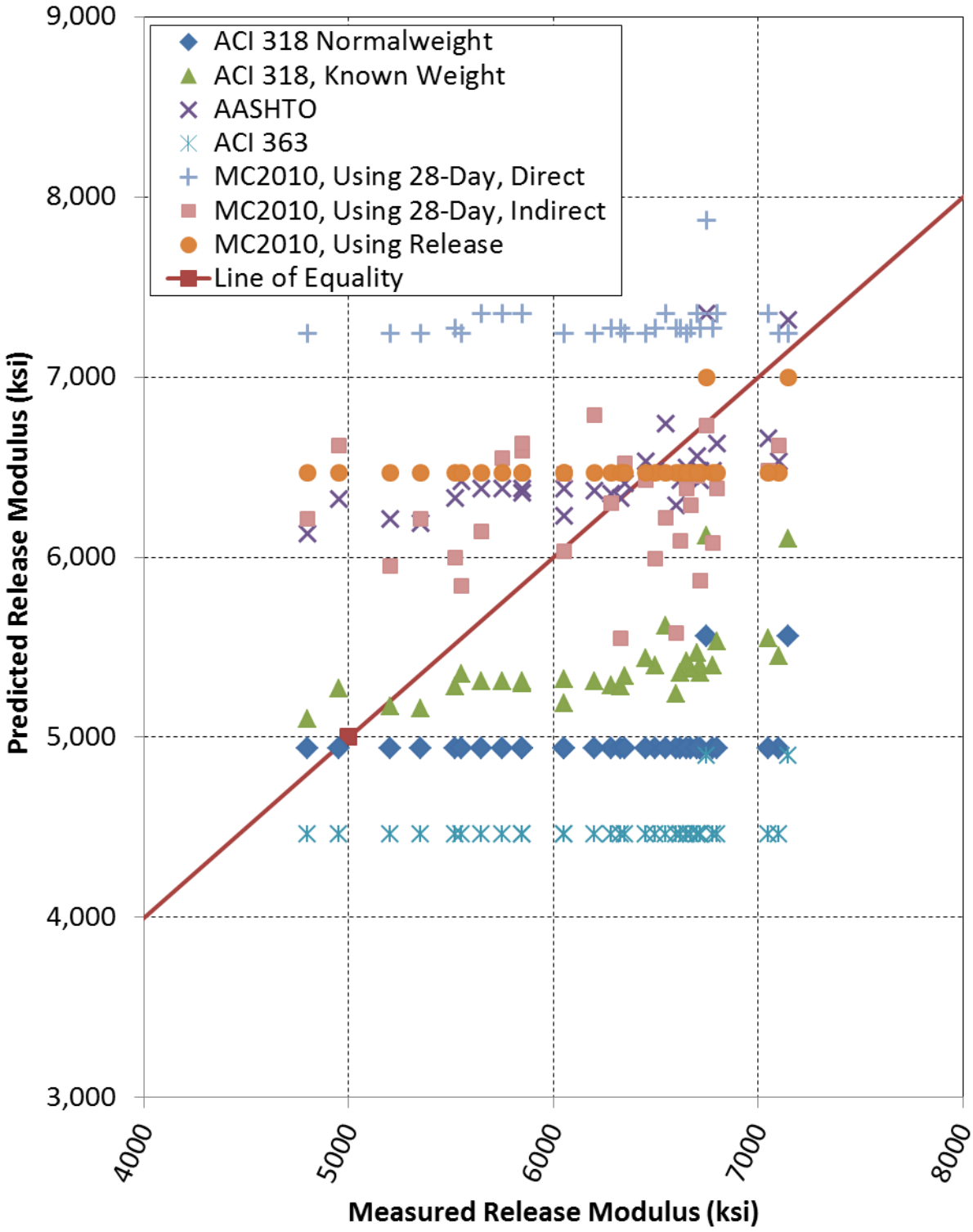

Figure 7.11: Release Modulus Predictions using Basic Equations, Expected Strength

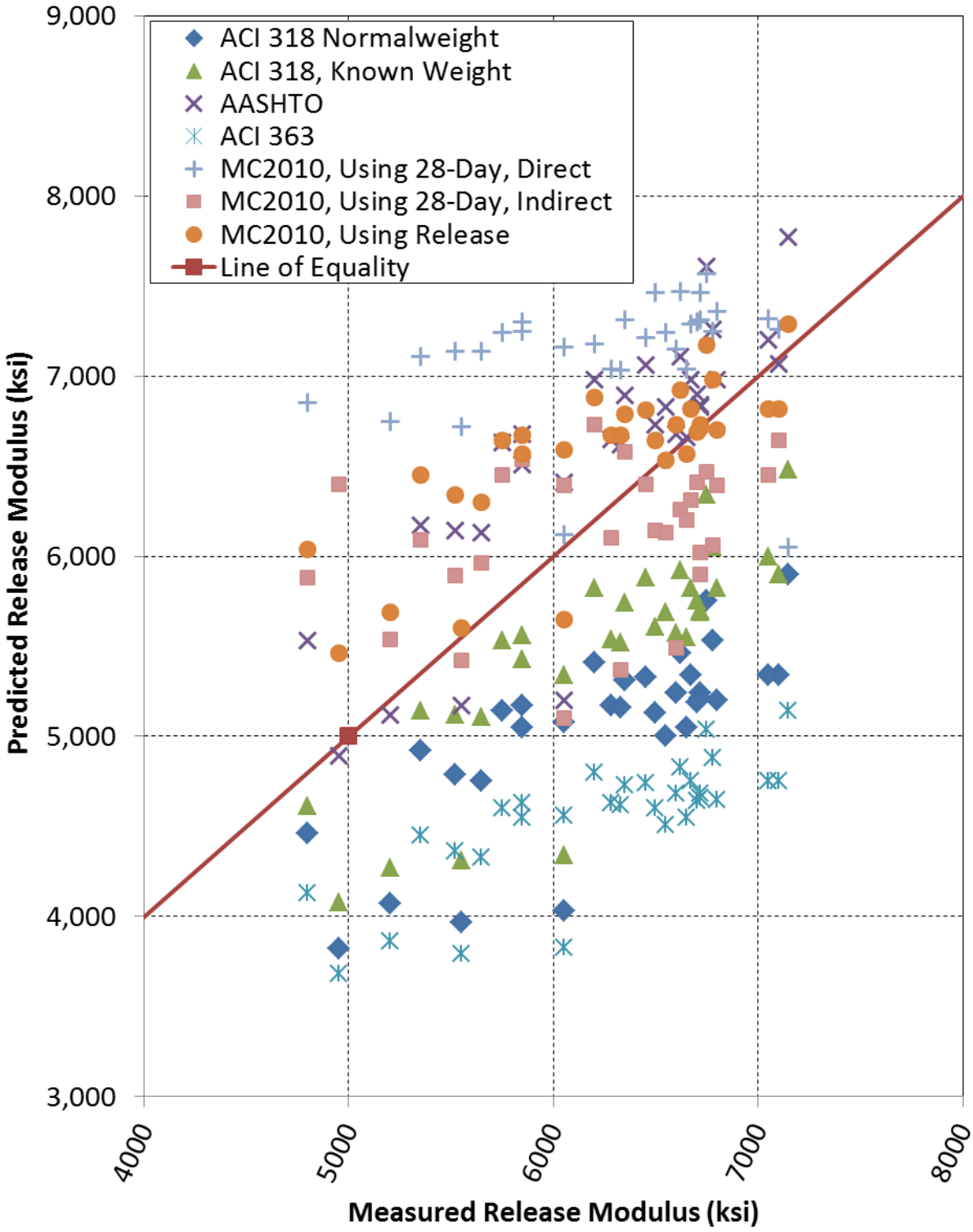

Figure 7.12: Release Modulus Predictions using Basic Equations, Measured Strength

Seven prediction methods are shown in Table 7.5, along with three levels of strength knowledge. These prediction methods and strength levels are explained below.

- ACI 318, "Normalweight" ($\omega \cong 145$ pcf) refers to the simplified form of Equation 2.1 which may be found in the building code from ACI Committee 318 (2011). This simplified form is allowed for use in all normalweight concretes, which includes the concrete types used in this research project, and may be seen in Equation 7.2 below.

$$E_c = 57{,}000\sqrt{f_c'} \qquad \textbf{Equation 7.2}$$

where

E_c = the concrete modulus of elasticity, psi

f_c' = compressive strength of the concrete, psi

Equation 7.2 uses an assumed unit weight of ($\omega \cong 145$ pcf) to simplify Equation 2.1.

- ACI 318, Known Weights refers to the calculation of modulus of elasticity using Equation 2.1 and known unit weights rather than an assumed unit weight. Equation 2.1 has been restated below. It is important to note that the unit weight, ω, was only measured in a few of the pours from which data were taken for this analysis. For most of the pours, the unit weight was calculated after-the-fact by using either concrete batch tickets (when available) or known mixture designs. These calculated unit weights were all adjusted for the air content, which was measured in each case.

$$E_c = 33\omega^{\frac{3}{2}}\sqrt{f_c'} \qquad \textbf{Equation 2.1}$$

where

E_c = static modulus of elasticity of the concrete, psi

ω = unit weight of concrete at the time of test, pcf

f_c' = compressive strength of the concrete, psi

- AASHTO, $K_1 = 1.2$ refers to the use of Equation 2.2, taken from the *AASHTO LRFD Bridge Design Specifications* (AASHTO 2012). It was known that the dolomitic limestone used in Plant A was very dense and stiff compared to other aggregates, and only one pour out of all of the collected in-plant data was from a producer other than Plant A. Therefore, an assumed value of $K_1 = 1.2$ was used as a starting point for reference with Equation 2.2. This value was not suggested by the AASHTO code, but was used as a starting estimate based on the suggested values of α_E for the *fib* Model Code (2010), discussed below. Using $K_1 = 1.2$ was substantially more accurate than using $K_1 = 1.0$, which is the same thing as the ACI 318 Known Weights method.

$$E_c = 33{,}000 K_1 \omega^{\frac{3}{2}} \sqrt{f_c'} \qquad \textbf{Equation 2.2}$$

where

E_c = static modulus of elasticity of the concrete, ksi

K_1 = correction factor for source of aggregate to be taken as 1.0 unless determined by physical test, and as approved by authority of jurisdiction

ω = unit unit weight of concrete at the time of test, kcf

f_c' = compressive strength of the concrete, ksi

- ACI 363 refers to the use of Equation 2.3, which may be found in the report from ACI Committee 363 (1992). This equation was developed specifically for high-strength concretes, which clearly applies to the concretes involved in this study. However, a more recent report from ACI Committee 363 (2010) mentioned that several more recent projects showed that this equation substantially underestimated modulus of elasticity, so it was not expected to provide the best results for this project.

$$E_c = 40{,}000 \sqrt{f'_c} + (1.0 \cdot 10^6) \qquad \textbf{Equation 2.3}$$

for 3000 psi < f_c' < 12,000 psi

where

E_c = static modulus of elasticity of the concrete, psi

f_c' = compressive strength of the concrete, psi

- MC2010, Direct, Using 28-Day, $\alpha_E = 1.2$ refers to the baseline established with either Equation 7.3 or Equation 7.4. These equations are slightly modified forms of Equation 2.5 and Equation 2.6, respectively, which were taken from the *fib* Model Code (2010). However, this method of predicting release modulus of elasticity is not specified in the MC2010. It was simply included for comparison, as a half-way point between the MC2010 Explicit method and the MC2010 Using Release method.

  Equation 2.5 has a built-in method of converting the characteristic strength, which is basically the Model Code version of the specified strength, into an average strength. This is done by adding Δf to the characteristic strength. Therefore, Equation 2.5 was changed into Equation 7.3 for use with specified strengths.

  However, two of the strength levels used for the modulus of elasticity predictions are already intended to function as an average strength. Therefore, Equation 2.6 was modified to form Equation 7.4. Equation 7.4 is used with expected strengths or measured strengths, so no arithmetical increase is included.

  In both equations, the aggregate coefficient was chosen as $\alpha_E = 1.2$ for dolomitic limestone, which matches the $K_1 = 1.2$ assumption used in the AASHTO code equation. This method was called the “Direct” method because it used 28-day values to directly calculate the release modulus of elasticity, as opposed to the method described next. This method is referred to as the MC2010 Direct method.

$$E_{ci} = E_{c0} \cdot \alpha_E \cdot \left(\frac{f_{ck} + \Delta f}{10}\right)^{\frac{1}{3}}$$ **Equation 2.5**

$$E_{ci} = E_{c0} \cdot \alpha_E \cdot \left(\frac{f_{cm}}{10}\right)^{\frac{1}{3}}$$ **Equation 2.6**

$$E_{ct,i} = E_{c0} \cdot \alpha_E \cdot \left(\frac{f'_{c28} + \Delta f}{10}\right)^{\frac{1}{3}}$$ **Equation 7.3**

$$E_{ct,i} = E_{c0} \cdot \alpha_E \cdot \left(\frac{f^{**}_{c28}}{10}\right)^{\frac{1}{3}}$$ **Equation 7.4**

where

$E_{ct,i}$ = predicted concrete modulus of elasticity at release, MPa

f_{ck} = characteristic value of f_c at 28 days, MPa

f_{cm} = mean value of f_c at 28 days, MPa

Δf = 8 MPa (or approximately 1150 psi)

E_{c0} = $21.5 \cdot 10^3$ MPa, or approximately 3118 ksi

α_E = 1.2 for basalt or dolomitic limestone aggregates

= 1.0 for quartzite aggregates

= 0.9 for limestone aggregates

= 0.7 for sandstone aggregates

f'_{c28} = specified concrete strength at 28 days, MPa

f^{**}_{c28} = expected or measured concrete strength at 28 days, MPa

- MC2010, Explicit, Using 28-Day, $\alpha_E = 1.2$ refers to calculation of the release modulus of elasticity in strict accordance with the MC2010 specifications. In other words, the expected release modulus of elasticity was calculated based on Equation 2.21, which is a simplified combination of three equations from the Model Code (*fib* 2010). This method

is referred to as the MC2010 Explicit method.

$$E_{ci}(t) = E_{ci} \cdot exp\left\{\frac{s}{2} \cdot \left(1 - \sqrt{\frac{28}{t}}\right)\right\} \quad \textbf{Equation 2.21}$$

where:

$E_{ci}(t)$ = modulus of elasticity at an age t, MPa

E_{ci} = modulus of elasticity at an age of 28 days, MPa

s = coefficient which depends on the strength class of cement, as given in Table 2.1

t = the concrete age adjusted according to Equation 2.11 (taking into account temperature during curing), days

E_{ci} was calculated based on either Equation 2.5 or Equation 6.5, shown above. Knowledge of the equivalent age of the test cylinder at the time of release testing was used in Equation 2.21 to predict the modulus of elasticity at release based on the 28-day modulus using 28-day strengths.

- MC2010, Using Release, $\alpha_E = 1.2$ refers to the baseline established with either Equation 7.5 or Equation 7.6. These equations are slightly modified forms of Equation 7.3 and Equation 7.4, respectively. These equations were used with release strength levels rather than 28-day strength levels, to provide justification for optimization using release strengths instead of 28-day strengths.

$$E_{ct,i} = E_{c0} \cdot \alpha_E \cdot \left(\frac{f'_{ci} + \Delta f}{10}\right)^{\frac{1}{3}} \quad \textbf{Equation 7.5}$$

$$E_{ct,i} = E_{c0} \cdot \alpha_E \cdot \left(\frac{f^{**}_{ci}}{10}\right)^{\frac{1}{3}} \quad \textbf{Equation 7.6}$$

where

$E_{ct,i}$ = predicted concrete modulus of elasticity at release, MPa

Δf = 8 MPa (or approximately 1150 psi)

E_{c0} = $21.5 \cdot 10^3$ MPa, or approximately 3118 ksi

α_E = 1.2 for basalt or dolomitic limestone aggregates

= 1.0 for quartzite aggregates

= 0.9 for limestone aggregates

= 0.7 for sandstone aggregates

f'_{ci} = specified concrete strength at release, MPa

f^{**}_{ci} = expected or measured concrete strength at release, MPa

The three strength levels shown in Table 7.5 are defined as follows:

1. Specified Strengths are the strengths that were specified by bridge design engineers for the girders (f'_{ci} and f'_c).
2. Expected Strengths are the strengths that were predicted using the suggested strength prediction equations presented in Chapter 6, based on the specified strengths of that project (f^*_{ci} and f^*_c).
3. Measured Strengths are the strengths that were actually measured at the time of each modulus test, produced from the same batch of concrete and cured in the same manner as one another (f_{ci} and f_c).

Combined, these seven prediction methods and three strength levels make for a large number of possible analysis models. The addition of various optimization options for these prediction equations rapidly expands the number of possible models to a number well beyond that which might be reasonably presented and understood. Therefore, the results reported in Table 7.5 were used to eliminate some possible prediction methods, and some consideration about the format of

desired results was used to eliminate some potential optimization options.

Before these optimization options are discussed, a thorough comparison of the results from Table 7.5 is first examined. First, for all of the modulus prediction methods except two of the MC2010 methods (the MC2010 Direct method and the MC2010 Using Release method), the accuracy of the method increased with more detailed knowledge of the strength. In other words, the use of f_{ci}^{*} provided more accurate modulus predictions than the use of f_{ci}', and the use of f_{ci} provided more accurate predictions than the use of f_{ci}^{*}. This increased accuracy was the goal of the extensive strength analyses seen in Chapter 6. They were meant to provide much more accurate means of predicting f_{ci}^{*} and f_{c}^{*}, which could then be used for more accurate predictions of the modulus of elasticity. For the most part, this was the case. However, the MC2010 Direct method and the MC2010 Using Release method were slightly more accurate with the use of specified strengths and the built-in strength increase that they were with the use of expected strengths and no strength increase. They were both still most accurate when using measured strengths with no strength increase.

Of course, it would not be possible to know the actual measured strength of the concrete during the design phase. However, the increased accuracy of the Measured Strengths column over the other two columns shows that the prediction methods can do a good job of predicting modulus of elasticity if the strength is known. This implies that if accurate predictions of strength can be obtained, accurate predictions of modulus are possible.

One very important comparison is the degree of accuracy between the ACI 318, Known Weights method and the AASHTO, $K_1 = 1.2$ method. The AASHTO method has an error 39% or more less than the errors of the ACI 318 method. This is significant because, at this point of the process, the only difference between the two prediction methods is that the AASHTO

equation has been multiplied by the K_1 factor equal to 1.2. Basically, by shifting the ACI 318 prediction equation up by a factor of 1.2, the accuracy was improved by 39% or more. This kind of improvement was used to much greater extent in the optimization process.

It is clear from Table 7.5 that the ACI 318 "Normalweight" method and the ACI 363 methods do not predict modulus of elasticity nearly as well as the other methods. Not only do these two methods have higher errors, though, but they also have fewer possibilities for optimization of the method. Therefore, both of these methods were excluded from the optimization process.

Furthermore, two of the MC2010 methods were excluded from the optimization process. Table 7.5 shows that the MC2010 Direct method was substantially more inaccurate than either the MC2010 Explicit method or the MC2010 Using Release method. Since this method was neither accurate, nor specified by the MC2010, nor inherently logical as a means of predicting release modulus of elasticity, it was readily excluded from the optimization process.

The MC2010 Explicit method was slightly more inaccurate than the MC2010 Using Release method, except when expected strengths were used. Even when expected strengths were used, the MC2010 Explicit was only very slightly more accurate. Therefore, since the MC2010 Using Release method was more accurate and did not require any knowledge about the maturity of the concrete, it was decided that the MC2010 Using Release method would be used for optimization. It is a reasonable approach to predicting the release modulus of elasticity, in spite of the fact that the MC2010 does not specify this method. The MC2010 Explicit method was excluded from the optimization process, leaving only the ACI 318, Known Weights method, the AASHTO, $K_1 = 1.2$ method, and the MC2010 Using Release method.

At this stage of the analysis, the MC2010 Using Release method was found to most

accurately predict release modulus of elasticity using specified strengths, likely because this was the only method that incorporates an estimate of the expected strength based on the specified strength. This equation also used an aggregate factor of $\alpha_E = 1.2$, but was more accurate than the AASHTO method. However, the AASHTO method most accurately predicted release modulus of elasticity when using expected strengths. The AASHTO method and the MC2010 Using Release method were nearly equally accurate when using measured strengths.

Another interesting trend may be seen in Figure 7.10, and even more so in Figure 7.11, that was not noticeable in Table 7.5. In both of these figures, the distribution of predicted modulus points appears as a nearly horizontal line. The MC2010 Explicit method was a major exception to this trend. In Figure 7.10, the relatively linear appearance of the data was primarily due to the fact that the specified release strengths were fairly consistent throughout this portion of the project. In Figure 7.11, however, the linear appearance shows the effect of using the expected strength equation. Since almost all of the specified release strengths were less than the break point of the piecewise release strength prediction equation, they almost all received the exact same expected strength—7500 psi. This makes the distribution of predictions a nearly horizontal line. It is only when knowledge of the actual measured strengths is applied that the distribution of predictions grows closer to the Line of Equality.

It may be concluded from Table 7.5 and these graphs that the prediction methods discussed so far should be improved for use in predicting the modulus of elasticity for the concretes in this project. Thus, each of the three most accurate methods were optimized to better fit the material properties found in this project. The number of possible optimization option combinations for these three equations was far too large to analyze and present in a meaningful fashion, so the optimization pattern was limited. For the ACI 318, Known Weights method

(hereafter called the ACI 318 method), three optimization combinations were included. These combinations are described below Equation 7.7, which is a restated form of Equation 2.1 ready for optimization. Each combination has been given a label for easy reference.

$$E_c = 33\omega^A (f_c^-)^B \qquad \textbf{Equation 7.7}$$

where

E_c = estimated modulus of elasticity of the concrete, psi

ω = unit weight of concrete at the time of test, pcf

f_c^- = specified, expected, or measured compressive strength of the concrete at the time of test, psi

1. ACI 318-1: Optimization of only A.
2. ACI 318-2: Optimization of only B.
3. ACI 318-3: Optimization of A and B together.

The constant in front of the equation (33) was not adjusted in any way. This was because the only difference between the AASHTO method and the ACI 318 method is the inclusion of that K_1 aggregate factor in the AASHTO method. The K_1 factor simply acts as a constant multiplier in front of the equation, so its effects were included in the AASHTO optimization (variable C). For the AASHTO optimization, the combinations below Equation 7.8 were included.

$$E_c = 33 \cdot C\omega^A (f_c^-)^B \qquad \textbf{Equation 7.8}$$

where

E_c = estimated modulus of elasticity of the concrete, ksi

C = optimization coefficient

ω = unit unit weight of concrete at the time of test, kcf

f_c^- = specified, expected, or measured compressive strength of the concrete at

the time of test, ksi

1. AASHTO-1: Optimization of only C.
2. AASHTO-2: Optimization of A and C together.
3. AASHTO-3: Optimization of A, B, and C together.
4. AASHTO-4: Optimization of B and C together.

The MC2010 method was a lot different from the other two methods, so more optimization combinations were included for it. These combinations may be seen below Equations 7.9 and 7.10, the restated optimization-ready versions of Equations 7.3 and 7.4, respectively.

$$E_{ct} = E_{c0} \cdot C \cdot \left(\frac{f_c' + A}{10}\right)^B \quad \textbf{Equation 7.9}$$

$$E_{ct} = E_{c0} \cdot C \cdot \left(\frac{f_c^{**}}{10}\right)^B \quad \textbf{Equation 7.10}$$

where

E_{ct} = predicted concrete modulus of elasticity at time of test, MPa

E_{c0} = $21.5 \cdot 10^3$ MPa, or approximately 3118 ksi

C = optimization coefficient

f_c' = specified concrete compressive strength at time of test, MPa

A = factor used to convert strength input to an estimated average strength

= optimization equivalent of Δf strength addition

f_c^{**} = expected or measured concrete strength at time of test, MPa

1. MC2010-1: Optimization of only C.
2. MC2010-2: Optimization of only A.
3. MC2010-3: Optimization of only B.

4. MC2010-4: Optimization of A and C together.
5. MC2010-5: Optimization of A, B, and C together.
6. MC2010-6: Optimization of B and C together

It is worthwhile to re-emphasize that the A term is only found in Equation 7.9, for use with specified strengths. The defined purpose of A, which is the optimization equivalent of Δf in the original equation, is to convert a lower-bound strength (f_c', or f_{ck} in the original equation) into an estimated average strength (f_c, or f_{cm} in the original equation). However, the expected strength or measured strength (combined into f_c^{**}) is supposed to act as an average strength, not a lower bound. Therefore no A term is necessary, and A is only applied to the specified strength equation.

The term "optimization" is here used to indicate that the variables being optimized are allowed to vary within a certain range of values, while the other variables are held constant at the original value suggested in the equation, until the predictions from that equation cause the least sum of squared errors. Not all of the optimizations would necessarily provide useful answers in and of themselves, but together they could reveal trends in the material behavior that might otherwise have gone unnoticed. The optimizations for each prediction method were summarized into their own tables and figures, which are presented and discussed below.

The ACI 318 method was analyzed first, since this is the current standard practice and also the simplest of all considered methods. A summary of the optimized parameters for this method, together with the curve-fit measurements SEE, SPEE, and R^2 may be seen in Table 7.6. This table refers back to Equation 7.7, which showed the optimization-ready form of the ACI 318 equation. A and B are the exponents on the concrete unit weight and the concrete strength, respectively. There are three combinations shown, which correspond to the optimization

combinations mentioned above.

Table 7.6: Summary of Optimized Release Modulus Predictions with the ACI 318 Method

		Specified Strengths	Expected Strengths	Measured Strengths
ACI 318-1	A	1.56	1.53	1.53
	B	**0.50**	**0.50**	**0.50**
	SEE (ksi)	600	500	360
	$SPEE$ (%)	10.2	9.1	6.2
	R^2	0.07	0.34	0.66
ACI 318-2	A	**1.50**	**1.50**	**1.50**
	B	0.53	0.52	0.51
	SEE (ksi)	610	500	370
	$SPEE$ (%)	10.4	9.0	6.4
	R^2	0.01	0.34	0.64
ACI 318-3	A	1.99	2.18	1.83
	B	0.25	0.14	0.33
	SEE (ksi)	500	480	310
	$SPEE$ (%)	8.9	8.7	5.4
	R^2	0.35	0.40	0.75

Graphical representation of Table 7.6 may be seen in Figure 7.13, Figure 7.14, and Figure 7.15 for predictions with specified strengths, expected strengths, and measured strengths, respectively. These figures show a high range of consistency between the optimized combinations of the ACI 318 method, and the general trends mentioned below. Clearly, the use of measured strengths provides what are by far the most accurate predictions of modulus of elasticity. Graphical comparison of the other methods is not provided in the text, but may be found in Appendix K.

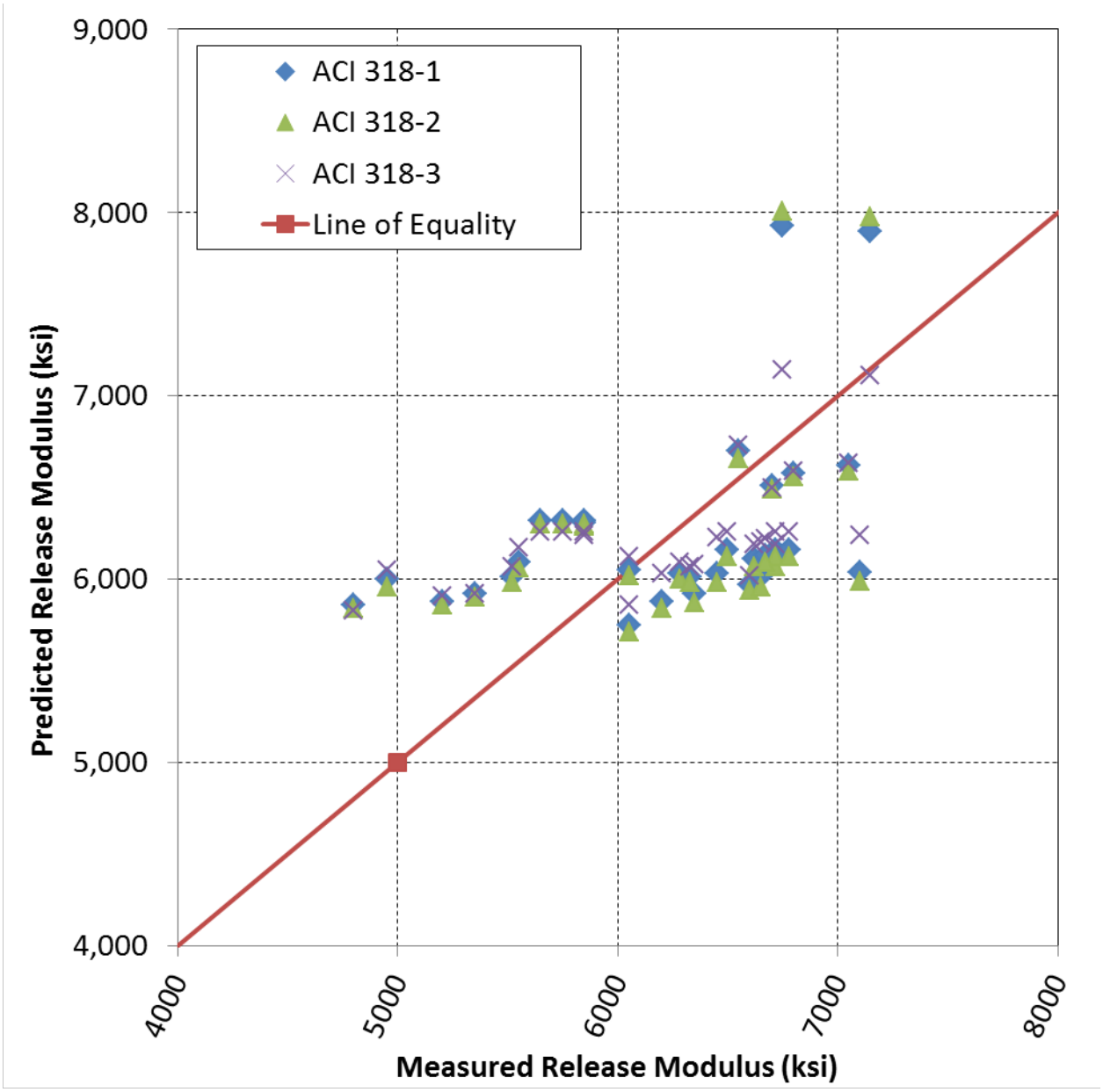

Figure 7.13: Optimized ACI 318 Release Modulus Predictions with Specified Strengths

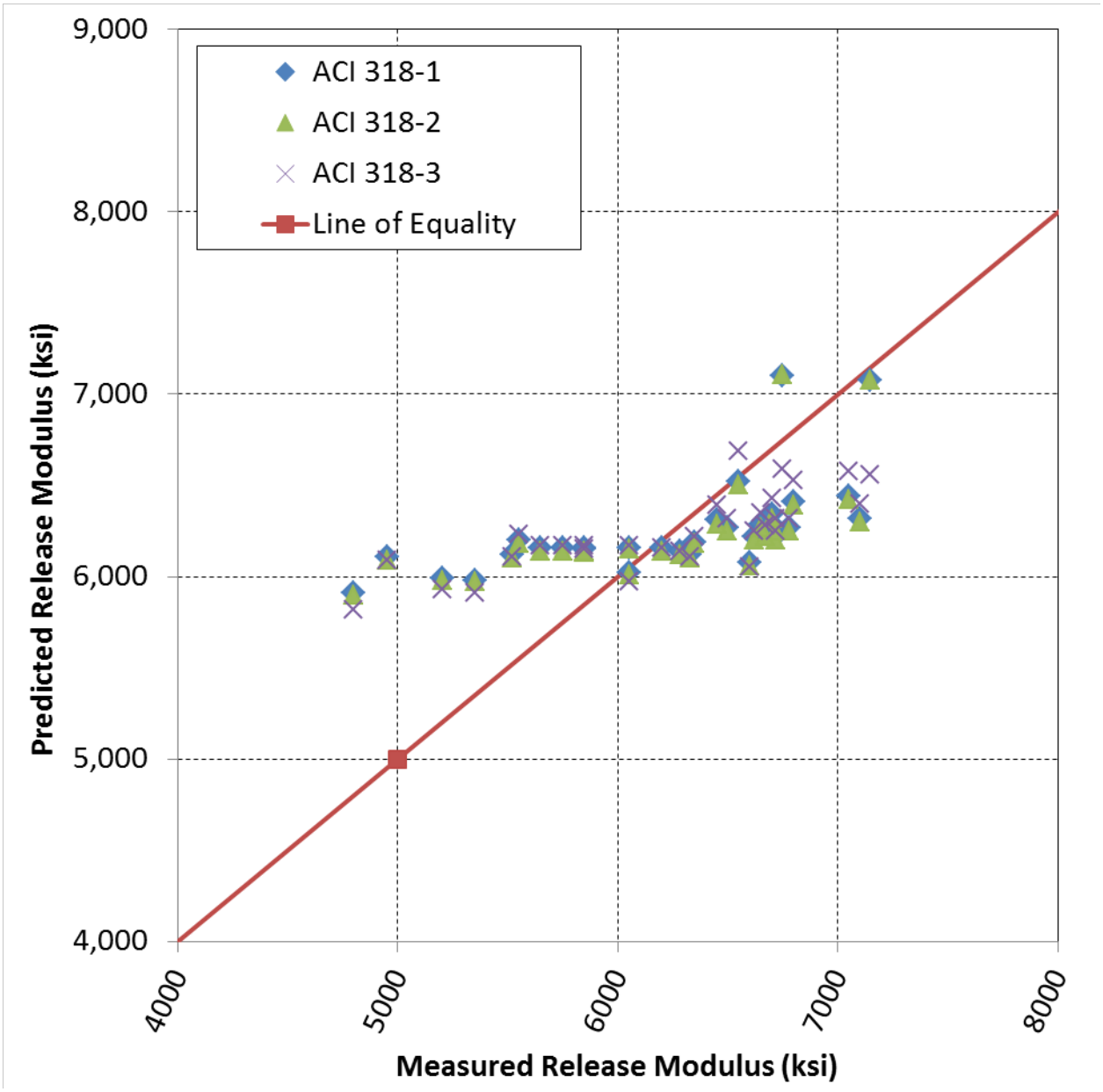

Figure 7.14: Optimized ACI 318 Release Modulus Predictions with Expected Strengths

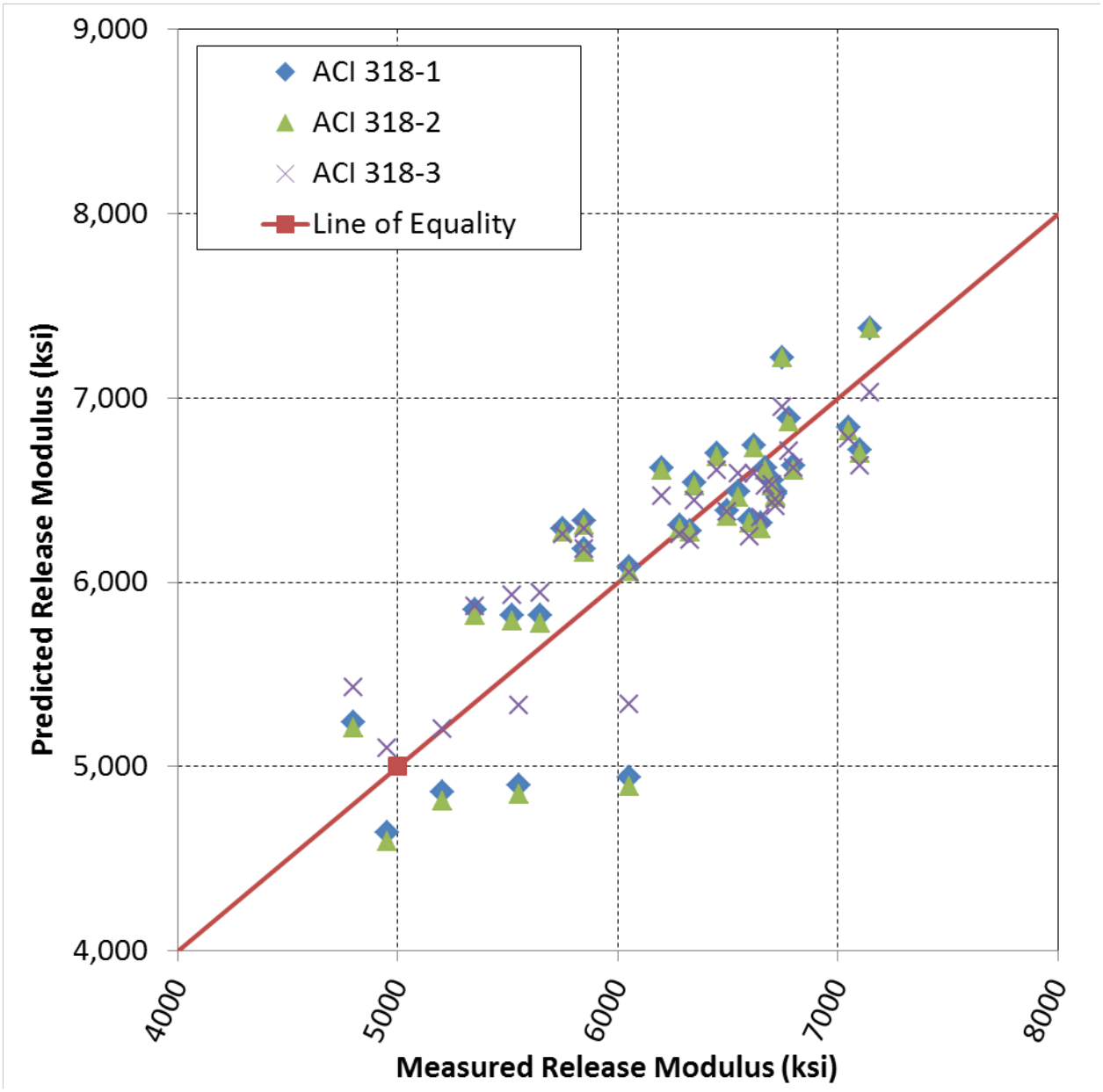

Figure 7.15: Optimized ACI 318 Release Modulus Predictions with Measured Strengths

All of the combinations in Table 7.6 showed the expected trend of increasing accuracy with improved knowledge of strength. Not surprisingly, the ACI 318-3 combination, in which both *A* and *B* were varied, was more accurate than either of the other two combinations. However, there were some other interesting trends to note.

First examine the ACI 318-1 combination, in which B was kept as 0.50 (square root of the strength) and only A was varied. The optimized A values in this method were surprisingly close to 1.50, which is the standard value used in the ACI equation. Likewise, when the A value was fixed at 1.50 and the B value was varied in ACI 318-2, the optimized B values came surprisingly close to 0.50. It could be concluded from this that the relative influence of unit weight and concrete strength on modulus of elasticity is well predicted with the ACI 318 equation.

When both A and B were allowed to vary, however, the optimized prediction method tended to increase the influence of unit weight and decrease the influence of concrete strength. This is indicated by the values of A that are all larger than the code-standard $A = 1.50$ and the values of B that are all smaller than the code-standard $B = 0.50$. The concrete unit weight had more influence than the code predicted, and the concrete strength had less influence, for optimized solutions.

The AASHTO prediction method was examined next, since it was nearly identical to the ACI 318 method except for the addition of the optimization coefficient C. A summary table for the four considered AASHTO method optimization combinations, similar to Table 7.6 for the ACI 318 combinations, may be seen in Table 7.7. This AASHTO table refers back to Equation 7.8, which showed the optimization-ready form of the AASHTO equation. A and B are the exponents on the concrete unit weight and the concrete strength, respectively. C is related to the K_1 factor, but was labeled as C to mark it as one of the variables that was optimized. There are four combinations shown, which correspond to the optimization combinations mentioned above.

Table 7.7: Summary of Optimized Release Modulus Predictions with the AASHTO Method

		Specified Strengths	Expected Strengths	Measured Strengths
AASHTO-1	A	**1.50**	**1.50**	**1.50**
	B	**0.50**	**0.50**	**0.50**
	C	1.32	1.16	1.14
	SEE (ksi)	600	500	360
	$SPEE$ (%)	10.1	9.1	6.2
	R^2	0.06	0.34	0.66
AASHTO-2	A	1.50	1.52	1.70
	B	**0.50**	**0.50**	**0.50**
	C	1.36	1.06	0.41
	SEE (ksi)	600	500	360
	$SPEE$ (%)	10.1	9.0	6.2
	R^2	0.06	0.34	0.66
AASHTO-3	A	2.10	2.05	1.82
	B	0.11	0.13	0.31
	C	1.99	1.99	1.27
	SEE (ksi)	480	480	310
	$SPEE$ (%)	8.7	8.8	5.4
	R^2	0.39	0.38	0.75
AASHTO-4	A	**1.50**	**1.50**	**1.50**
	B	0.45	0.45	0.46
	C	2.08	1.86	1.68
	SEE (ksi)	580	500	340
	$SPEE$ (%)	9.8	9.0	5.9
	R^2	0.13	0.34	0.69

Graphical representation of the relationships and trends seen in Table 7.7 may be seen in Appendix K. In many ways, despite the large differences in the optimized variables, the accuracy and the graphical representation of the ACI 318 combinations are nearly identical to those of the AASHTO combinations.

The first trend shown in Table 7.7 is the clear improvement of prediction accuracy with more detailed knowledge of the concrete strength. This has already been discussed multiple

times.

Next, examination of the AASHTO-1 combination, in which only C was varied, shows that this concrete did indeed have stiffer aggregates than standard. This provides some justification for the $K_1 > 1.00$ factor that was used above in establishing the baseline. Note, however, that C was greater than 1.20 when using specified strengths but was smaller than 1.20 when using expected or measured strengths. More detailed knowledge of strength allowed for more accurate predictions of strength, even with a reduced C factor.

The AASHTO-2 combination allowed A and C to vary, but forced the power of the strength to remain at 0.50. This combination showed that control over the influence of unit weight allowed for more accurate predictions than simply the use of a controlled aggregate factor. With improved knowledge of the concrete strength and increased influence of the unit weight, the C value was decreased substantially while still achieving better prediction accuracy. These two values are not independent, since aggregate stiffness is usually directly related to its density. However, the optimized solution showed that control over the unit weight power was more effective than control over the aggregate factor.

Similarly to ACI 318-3, the AASHTO-3 combination showed that the influence of unit weight was much more significant than the influence of strength. The B factor was reduced to substantially less than the standard 0.50 value, but both A and C were increased to values higher than the standard values.

Lastly, an interesting similarity seen in Table 7.7 was the identical curve fit measurements for AASHTO-1 and AASHTO-2. Both of these methods had nearly identical SEE, SPEE, and R^2 values, although one had an optimized power on the unit weight and the other was only optimized for the constant coefficient.

The summary table for the six considered MC2010 optimization combinations may be seen in Table 7.8, which refers back to Equations 7.9 and 7.10 from above. In Equation 7.9, A is a constant strength increase which is added to the strength before use in the equation. In both equations, B is the power to which the strength ratio is raised and C relates to the α_E aggregate stiffness factor, but was marked as C to signify that it was optimized in these combinations. The combination labels refer back to the list described above. All of the three optimization combinations for which it was applicable showed the expected trend of increasing prediction accuracy with more detailed knowledge of the concrete strength.

Table 7.8: Summary of Optimized Release Modulus Predictions with the MC2010 Method

		Specified Strengths	Expected Strengths	Measured Strengths
MC2010-1	A (psi)	**1160**	**NA**	**NA**
	B	**0.333**	**0.333**	**0.333**
	C	1.19	1.15	1.14
	SEE (ksi)	600	590	400
	$SPEE$ (%)	10.8	10.7	7.0
	R^2	0.05	0.08	0.58
MC2010-2	A (psi)	946		
	B	**0.333**		
	C	**1.20**		
	SEE (ksi)	600		
	$SPEE$ (%)	10.8		
	R^2	0.05		
MC2010-3	A (psi)	**1160**	**NA**	**NA**
	B	0.33	0.31	0.31
	C	**1.20**	**1.20**	**1.20**
	SEE (ksi)	600	590	410
	$SPEE$ (%)	10.8	10.8	7.21
	R^2	0.05	0.08	0.57
MC2010-4	A (psi)	4030		
	B	**0.33**		
	C	1.06		
	SEE (ksi)	600		
	$SPEE$ (%)	10.8		
	R^2	0.07		
MC2010-5	A (psi)	5700		
	B	0.35		
	C	0.97		
	SEE (ksi)	600		
	$SPEE$ (%)	10.8		
	R^2	0.07		
MC2010-6	A (psi)	**1160**	**NA**	**NA**
	B	0.26	0.40	0.38
	C	1.33	1.03	1.06
	SEE (ksi)	600	590	390
	$SPEE$ (%)	10.8	10.7	6.9
	R^2	0.06	0.09	0.60

The graphs corresponding to Table 7.8 may be seen in Appendix K. It is really quite remarkable how very similar all of the optimized methods are, even with such different parameters.

The MC2010-1 combination showed the same trend that the AASHTO-1 combination showed, requiring smaller and smaller aggregate stiffness factors with more detailed strength knowledge while still achieving improved accuracy. Nearly identical levels accuracy for each strength level were possible by varying both B and C while holding A constant (MC2010-6) or by varying only B while holding both A and C constant (MC2010-3). When using specified strengths, MC2010-2, MC2010-4, and MC2010-6 were all able to obtain nearly identical accuracies compared to the other three methods.

A suggested method for predicting release modulus of elasticity is presented in Section 7.4.4.

7.4.2. 28-Day Modulus Predictions

Even though 28-day modulus predictions are not quite as important for camber predictions as release modulus, it was desired that this research project might provide better means of estimating modulus at both times. Therefore, a similar analysis as was described in Section 7.4.1 was also performed on 28-day modulus predictions, comparing the various methods before and after optimization. However, 28-day modulus of elasticity predictions were a lot less complicated than release modulus predictions, since each of the modulus prediction equations used in this study were developed for 28-day predictions. Because of this, it would not be unreasonable to expect that the accuracy of these prediction methods would be greater at 28-days than at release.

Interestingly enough, this was not always found to be the case. Table 7.9 shows a summary of the curve fit measurements for the five standard equations. This table is basically the 28-day version of Table 7.5. Graphical representation of the relative accuracies of each method may be seen in Appendix L.

Table 7.9: Summary of 28-Day Modulus Prediction Accuracy for Basic Equations

		Specified Strengths	**Expected Strengths**	**Measured Strengths**
ACI 318, "Normalweight" ($\omega \cong 145$ pcf)	SEE (ksi)	2100	1130	1260
	$SPEE$ (%)	30.0	15.5	17.9
	R^2	-10.3	-2.28	-3.07
ACI 318, Known Weights	SEE (ksi)	1720	730	830
	$SPEE$ (%)	24.5	9.8	11.7
	R^2	-6.54	-0.35	-0.74
AASHTO, $K_1 = 1.2$	SEE (ksi)	900	1000	750
	$SPEE$ (%)	12.4	15.7	11.7
	R^2	-1.05	-1.54	-0.44
ACI 363	SEE (ksi)	2530	1830	1940
	$SPEE$ (%)	36.3	25.8	27.8
	R^2	-15.4	-7.59	-8.61
MC2010, $\alpha_E = 1.2$	SEE (ksi)	640	740	560
	$SPEE$ (%)	9.0	11.8	8.8
	R^2	-0.03	-0.38	0.21

Each of the prediction methods shown in Table 7.9 is exactly the same as the methods shown in Table 7.5, except for the fact that they are using 28-day strengths instead of release strengths for the predictions. The MC2010, $\alpha_E = 1.2$ method (hereafter called the MC2010 method) is most closely related to the MC2010, Direct, Using 28-Day, $\alpha_E = 1.2$ method from Table 7.5, except that it is now predicting 28-day modulus of elasticity instead of release modulus of elasticity. The values are the same, since MC2010, Direct, Using 28-Day, $\alpha_E = 1.2$

used 28-day strengths for its predictions.

For both SEE and SPEE measurements, 28-day modulus of elasticity predictions were sometimes more accurate and sometimes less accurate than release modulus predictions. There was no consistent pattern or increased or decreased accuracy by strength level or by prediction method. The MC2010 method was more accurate at predicting 28-day modulus of elasticity than the MC2010, Direct, Using 28-Day, $\alpha_E = 1.2$ method was at predicting release modulus. This is the logical result that was expected.

The relationship shown in Table 7.9 between the level of strength knowledge used and the accuracy of 28-day modulus predictions was somewhat inconsistent between methods. In the three ACI methods, the use of expected strengths caused the smallest SEE compared to specified strengths or measured strengths. However, in the AASHTO method and the MC2010 method, the use of expected strengths had the highest SEE.

As was the case when predicting release modulus, the ACI 318, “Normalweight” method and the ACI 363 method were by far the most inaccurate methods for predicting 28-day modulus. Therefore, both of these methods were excluded from the optimization process. The other three methods were optimized in the exact same way as described in Section 7.4.1, with the same combination labels. The optimized parameters and curve fits for each method have been summarized in Table 7.10, Table 7.11, and Table 7.12 below, paralleling Table 7.6, Table 7.7, and Table 7.8, respectively, for release modulus.

Table 7.10: Summary of Optimized 28-Day Modulus Predictions with the ACI 318 Method

		Specified Strengths	Expected Strengths	Measured Strengths
ACI 318-1	A	1.55	1.51	1.52
	B	**0.50**	**0.50**	**0.50**
	SEE (ksi)	760	560	480
	$SPEE$ (%)	10.8	8.1	7.2
	R^2	-0.48	0.20	0.41
ACI 318-2	A	**1.50**	**1.50**	**1.50**
	B	0.53	0.51	0.51
	SEE (ksi)	790	560	480
	$SPEE$ (%)	11.2	8.1	7.2
	R^2	-0.60	0.20	0.41
ACI 318-3	A	2.28	2.02	1.85
	B	0.092	0.23	0.32
	SEE (ksi)	530	540	450
	$SPEE$ (%)	7.8	7.9	6.6
	R^2	0.28	0.26	0.47

Table 7.11: Summary of Optimized 28-Day Modulus Predictions with AASHTO Method

		Specified Strengths	Expected Strengths	Measured Strengths
AASHTO-1	A	**1.50**	**1.50**	**1.50**
	B	**0.50**	**0.50**	**0.50**
	C	1.29	1.07	1.11
	SEE (ksi)	760	560	480
	$SPEE$ (%)	10.8	8.1	7.2
	R^2	-0.48	0.20	0.41
AASHTO-2	A	1.50	1.52	1.65
	B	**0.50**	**0.50**	**0.50**
	C	1.29	0.97	0.51
	SEE (ksi)	760	560	480
	$SPEE$ (%)	10.8	8.1	7.2
	R^2	-0.48	0.20	0.41
AASHTO-3	A	2.15	1.78	1.80
	B	0.09	0.29	0.32
	C	1.84	1.80	1.30
	SEE (ksi)	530	540	450
	$SPEE$ (%)	7.8	8.0	6.6
	R^2	0.28	0.24	0.47
AASHTO-4	A	**1.50**	**1.50**	**1.50**
	B	0.44	0.45	0.50
	C	2.13	1.77	1.15
	SEE (ksi)	710	550	480
	$SPEE$ (%)	10.0	8.1	7.2
	R^2	-0.28	0.21	0.41

Table 7.12: Summary of Optimized 28-Day Modulus Predictions with the MC2010 Method

		Specified Strengths	Expected Strengths	Measured Strengths
MC2010-1	A (psi)	**1160**	**NA**	**NA**
	B	**0.333**	**0.333**	**0.333**
	C	1.22	1.13	1.16
	SEE (ksi)	620	600	500
	$SPEE$ (%)	9.0	8.9	7.4
	R^2	0.02	0.07	0.37
MC2010-2	A (psi)	1792		
	B	**0.333**		
	C	**1.20**		
	SEE (ksi)	610		
	$SPEE$ (%)	9.0		
	R^2	0.04		
MC2010-3	A (psi)	**1160**	**NA**	**NA**
	B	0.34	0.30	0.32
	C	**1.20**	**1.20**	**1.20**
	SEE (ksi)	620	600	500
	$SPEE$ (%)	9.02	8.9	7.4
	R^2	0.01	0.07	0.36
MC2010-4	A (psi)	6026		
	B	**0.33**		
	C	1.05		
	SEE (ksi)	590		
	$SPEE$ (%)	8.8		
	R^2	0.10		
MC2010-5	A (psi)	1714		
	B	0.18		
	C	1.60		
	SEE (ksi)	590		
	$SPEE$ (%)	8.7		
	R^2	0.11		
MC2010-6	A (psi)	**1160**	**NA**	**NA**
	B	0.15	0.38	0.40
	C	1.70	1.02	1.01
	SEE (ksi)	590	600	490
	$SPEE$ (%)	8.7	8.9	7.4
	R^2	0.11	0.08	0.38

Graphical representation of Table 7.10 may be seen in Figures L.4, L.5, and L.6 in Appendix L. Graphical representation of Table 7.11 may be seen in Figures L.7, L.8, and L.9 in the Appendix. Lastly, graphical representation of Table 7.12 may be seen in Figures L.10, L.11, and L.12 in Appendix L.

Table 7.10 provides the optimized results for the ACI 318 method. The ACI 318-1 and ACI 318-2 combinations showed very similar trends compared to the values seen in Table 7.6 for release modulus. When only the power on the unit weight was allowed to vary, it stayed fairly close (within 3.3%) to the standard value of $A = 1.50$. When only the power on the strength was allowed to vary, it also stayed fairly close (within 6.0%) to the standard value of $B = 0.50$. Thus the relative influence of the unit weight and the strength provided a fairly accurate equation. However, when both A and B were allowed to vary, the influence of the unit weight was increased and the influence of the strength was decreased, just like in the release modulus predictions.

The SEE was greater for 28-day modulus predictions than for release modulus predictions for all three ACI 318 combinations and all three strength knowledge levels. However, the SPEE values indicate that this increased SEE was primarily due to an increase in prediction magnitudes. For specified strengths and measured strengths, the SPEE was slightly larger when predicting 28-day modulus of elasticity. However, for expected strength the SPEE was smaller when predicting 28-day strengths. This is most likely due to the accuracy of the 28-day strength prediction method, as was discussed earlier.

Table 7.11 shows the optimized parameters and fit measurements for the three AASHTO method optimization combinations. All combinations except AASHTO-3 followed the expected decrease in SEE with improved strength knowledge. The SEE for AASHTO-3 was slightly

higher with expected strengths than with specified strengths. AASHTO-3 was the most accurate of the optimized AASHTO combinations, which was expected based on the free variables during the optimization process.

When comparing Table 7.11 to Table 7.7, which is the release modulus equivalent, some important trends are visible. First, the SEEs for 28-day modulus predictions were always larger than the corresponding release modulus predictions. With the consistent exception of expected strength calculations, the SPEEs for 28-day modulus predictions were usually slightly larger than the corresponding release modulus predictions. The other exception to this was in the AASHTO-3 combination with specified strengths.

The percent decrease in SPEE relative to the release modulus predictions for expected strength predictions was approximately 10%. The percent increase in SPEE relative to the release modulus predictions for specified strength and measured strength predictions ranged from 2% to 6% and from 15% to 22%, respectively. Just as was seen in Table 7.7, the SEE values of AASHTO-1 and AASHTO-2 for 28-day modulus predictions were identical.

The optimized parameters and fit measurements for the five MC2010 method combinations may be seen in Table 7.12. All three of the combinations that applied to multiple strength levels followed the expected path of improved prediction accuracy with more detailed strength knowledge. When using specified strengths, the most accurate MC2010 combination for 28-day modulus predictions was to use a higher value of A and a lower value of B, with a substantially larger value of C. When using either expected strengths or measured strengths, the most accurate MC2010 combination for 28-day modulus predictions was to use a C factor very close to 1.00, with a higher power of B.

A number of useful trends may be seen by comparison of Table 7.12 to Table 7.8. The

optimized C values were very similar for MC2010-1 in both tables. The value of C did not change by more than 2.5% between tables, no matter which strength level is examined. Similarly, the maximum change in the MC2010-3 B values between tables was a mere 3.3%. Thus, the results were surprisingly similar when only one variable was changed to optimize the equation. Values of A changed more drastically between tables, but this is not surprising. Since the A value is an arithmetically added value and is raised to a power of $1/3$ in the standard MC2010 equation, it takes a greater change in A to have the same effect that a small change in B or C would have.

An important note to make between Table 7.12 to Table 7.8 is the plurality of possible methods of obtaining the most accurate prediction. In Table 7.8, all combinations had practically equal accuracy when using specified strengths. In Table 7.12, the SEE didn't change between combinations by more than 5% when using specified strengths. Both tables exhibited nearly identical accuracies across all applicable methods when using expected or measured strengths. Therefore, the equation could either be highly complicated by the adjustment of all three variables, or it could be slightly changed by the adjustment of only one variable, and the accuracy of the two would be approximately the same. When confronted with multiple options like this, it is better to choose the simpler of the two.

A suggested method for predicting 28-day modulus of elasticity is presented in Section 7.4.4.

7.4.3. Modulus Growth

Extensive analysis has already been discussed regarding the development of strength with concrete age for the concretes used in this research project. However, these analyses do not

examine the rate of growth of concrete stiffness over time. Neither do they compare the development rates of compressive strength and modulus of elasticity. Therefore, this section examines the rate of modulus development over concrete age, and compares the development rate of concrete strength and stiffness.

There were two main ways to go about this analysis, and both are presented here. One way is to use modulus-growth prediction equations with the growth parameters found in previous analyses, and compare the results to results obtained from newly calculated parameters. The second and less direct way is to calculate an "aggregate factor" (hereafter called an optimization coefficient) for the modulus of elasticity prediction equation at both release and 28-days, then compare the two optimization coefficients to see if they follow the expected relationship when used with measured concrete strengths. Since the cylinders were tested in sets that were each produced from the same batch of concrete, the optimization coefficient should be equal in both cases if the modulus of elasticity develops at the expected rate relative to the strength. This is discussed in Section 2.3.3, and is explained further later.

The reason the previous paragraph places the term "aggregate factor" in quotation marks is that it is not truly an aggregate factor if it changes based on the time of testing. An aggregate stiffness factor, such as K_1 in the AASHTO equation (2012), should be independent of the time of testing. Thus, since the coefficient may not truly be an aggregate factor, it is called the optimization coefficient. This is discussed in greater detail in Section 7.4.4.

Both of the above methods have been included in this section. The modulus-growth prediction equation method is discussed first, and then the aggregate factor method.

The MC2010 specifies the expected rate of development of modulus of elasticity. The simplified modulus growth equation is shown in Equation 2.21, which was explained in Section

2.3.3. This is directly comparable to Equation 7.11, which is a simplified form of Equation 2.10.

$$E_{ci}(t) = E_{ci} \cdot exp\left\{\frac{s}{2} \cdot \left(1 - \sqrt{\frac{28}{t}}\right)\right\} \quad \textbf{Equation 2.21}$$

$$f_{cm}(t) = f_{cm} \cdot exp\left\{s \cdot \left(1 - \sqrt{\frac{28}{t}}\right)\right\} \quad \textbf{Equation 7.11}$$

where:

$E_{ci}(t)$ = modulus of elasticity at an age t, MPa

E_{ci} = modulus of elasticity at an age of 28 days, MPa

s = coefficient which depends on the strength class of cement

t = the concrete age adjusted according to Equation 2.11 (taking into account temperature during curing), days

$f_{cm}(t)$ = the mean compressive strength at time t, MPa

f_{cm} = the mean compressive strength at an age of 28 days, MPa

These two equations demonstrate that the form of growth prediction is identical for compressive strength and modulus of elasticity, except that the modulus prediction equation uses a constant equal to half of the s constant used for strength prediction. Therefore, the optimized s values that were calculated from the historical data set and the in-plant strength measurements may be used in Equation 2.21 for predicting modulus of elasticity, even though they were developed for strength predictions.

The ACI Committee 209 report (1992) does not provide any such accommodation for the prediction of modulus of elasticity development. However, as was discussed in Section 2.3.3, if the decision is made to use release strength to predict release modulus of elasticity and 28-day strength to calculate 28-day modulus, then the rate of modulus growth is implied from the proportionality of strength and modulus. The ACI 318 equation (2011), AASHTO equation

(2012), and ACI 363 equation (2010) all use the square root of strength, $\sqrt{f_c'}$, to estimate modulus of elasticity. Therefore, the rate of modulus of elasticity development is expected to be proportional to the square root of the rate of strength development (see the discussion in Section 2.3.3).

Using ACI 209, the strength is expected to develop according to Equation 2.16.

$$f_c(t) = f_{c28}\left(\frac{t}{\alpha + \beta \cdot t}\right) \qquad \textbf{Equation 2.16}$$

where:

$f_c(t)$ = concrete strength at any concrete age t, psi

f_{c28} = concrete strength at a concrete age of 28 days, psi

t = concrete age, days

α = constant used for shaping the strength growth function, days

β = constant used for shaping the strength growth function

This equation shows that the rate of strength developed is determined solely by the $\left(\frac{t}{\alpha + \beta \cdot t}\right)$ factor. Therefore, it is reasonable to expect that the modulus of elasticity will develop at a rate equal to $\sqrt{\left(\frac{t}{\alpha + \beta \cdot t}\right)}$, as is shown in Equation 7.12.

$$E_c(t) = E_{c28}\sqrt{\left(\frac{t}{\alpha + \beta \cdot t}\right)} \qquad \textbf{Equation 7.12}$$

where:

$E_c(t)$ = concrete modulus of elasticity at any concrete age t, ksi

E_{c28} = concrete modulus of elasticity at a concrete age of 28 days, ksi

t = concrete age, days

α = constant used for shaping the strength growth function, days

β = constant used for shaping the strength growth function

Thus, similarly to the MC2010 method, the same α and β parameters that were optimized in the previous analyses may be used in Equation 7.12 to predict modulus of elasticity development.

To directly compare to the results that were presented in Section 7.3, a modulus of elasticity equivalent of the Adj. EA maturity quantification is needed. Therefore, using the same principles as were used to create Equation 2.21, Equation 7.1 was modified to create Equation 7.13.

$$E_{ci}(t) = E_{ci} \cdot exp\left\{\frac{s}{2} \cdot \left(1 - \sqrt{\frac{t_{28}}{t}}\right)\right\} \quad \textbf{Equation 7.13}$$

where:

$E_{ci}(t)$ = modulus of elasticity at an age t, MPa

E_{ci} = modulus of elasticity at an age of 28 days, MPa

s = coefficient which depends on the strength class of cement

t_{28} = the concrete equivalent age adjusted for curing temperatures that corresponds to a chronological age of 28 days, days

t = the concrete equivalent age adjusted for curing temperatures, days

A summary of the parameters used for each method, in each prediction direction, and with each maturity quantification may be seen in Table 7.13. This table also shows the curve fit measurements for each of these combinations. For reference, this table of values may be compared to Table 7.4.

Table 7.13: Summary of Modulus-Growth Parameters and Curve Fits for In-Plant Testing

			Predicting Release Modulus			Predicting 28-Day Modulus		
			Ch. Age	Eq. Age	Adj. EA	Ch. Age	Eq. Age	Adj. EA
MC2010	Optimized from Historical Strengths	s	0.07	0.15	0.15	0.07	0.15	0.15
		SEE (psi)	600	510	480	700	590	560
		$SPEE$ (%)	9.6	8.2	7.7	10.4	8.6	8.2
		R^2	0.19	0.42	0.47	-0.26	0.11	0.19
	Optimized, Strength, In-Plant	s	0.05	0.14	0.13	0.05	0.14	0.13
		SEE (psi)	520	500	460	580	570	520
		$SPEE$ (%)	8.7	8.1	7.4	8.5	8.4	7.6
		R^2	0.40	0.44	0.53	0.13	0.15	0.29
	Optimized, Modulus, In-Plant	s	0.05	0.13	0.12	0.05	0.13	0.12
		SEE (psi)	510	490	450	570	550	510
		$SPEE$ (%)	8.8	8.2	7.5	8.2	8.0	7.3
		R^2	0.42	0.46	0.54	0.18	0.21	0.34
ACI 209	Optimized from Historical Strengths	α (days)	0.34	1.13	-----	0.34	1.13	-----
		β	0.988	0.960	-----	0.988	0.960	-----
		SEE (psi)	590	500	-----	680	580	-----
		$SPEE$ (%)	9.5	8.2	-----	10.1	8.5	-----
		R^2	0.22	0.43	-----	-0.19	0.13	-----
	Optimized, Strength, In-Plant	α (days)	0.26	1.18	-----	0.26	1.18	-----
		β	0.991	0.958	-----	0.991	0.958	-----
		SEE (psi)	520	510	-----	580	590	-----
		$SPEE$ (%)	8.8	8.3	-----	8.5	8.6	-----
		R^2	0.40	0.42	-----	0.13	0.10	-----
	Optimized, Modulus, In-Plant	α (days)	0.23	1.02	-----	0.23	1.02	-----
		β	0.992	0.964	-----	0.992	0.964	-----
		SEE (psi)	510	500	-----	570	570	-----
		$SPEE$ (%)	8.8	8.3	-----	8.3	8.3	-----
		R^2	0.42	0.44	-----	0.18	0.17	-----

There were two primary differences in the way that modulus growth was predicted compared to strength growth. The first is the equations that were used—Table 7.13 used Equations 2.21, 7.12, and 7.13, whereas Table 7.4 used Equations 7.11, 2.16, and 7.1,

respectively. The second primary change was that the suggested values of $s = 0.20$, $\alpha = 0.70$ days, and $\beta = 0.98$ were not used for comparison. These values were already shown to perform very poorly when predicting concrete strength, so using them to predict modulus of elasticity would not be beneficial in comparing the growth of strength and modulus.

Instead of using these suggested values, newly optimized values were calculated from the modulus of elasticity measurements. These optimized values could then be compared to the parameters optimized from the historical data set and the parameters optimized from the in-plant strength measurements, providing a valuable comparison of growth rates.

A few trends are able to be identified from Table 7.13. It is evident that, as was the case with the previous analyses, predicting 28-day modulus always caused larger SEEs than predicting release modulus. This increase in SEE was largely caused by the increase in prediction magnitudes, however, because the trend was not closely followed by the SPEE values. In fact, with the parameters optimized from the in-plant modulus tests, SPEE values consistently decreased when predicting 28-day modulus instead of release modulus, even though the SEE values increased.

Comparing the growth parameters reveals some behavioral differences between strength growth and modulus of elasticity growth. For example, the modulus-optimized s values for the MC2010 method were always slightly less than the in-plant strength-optimized s values (or equivalent). Furthermore, it was already known from Section 7.3 that the in-plant strength-optimized s values were less than the historically optimized values. The lower modulus-optimized values of s indicate that the early-age development of modulus of elasticity is very slightly more rapid than would be expected based on the development of strength over the same period.

This same trend was followed in the ACI 209 prediction optimizations. The modulus-optimized α values were slightly smaller than the in-plant strength-optimized α values, indicating a slightly more rapid rate of early modulus development. The modulus-optimized β values were slightly larger than the in-plant strength-optimized β values, indicating a slightly smaller long-term modulus development relative to the 28-day value.

In both the MC2010 method and the ACI 209 method, then, the modulus of elasticity developed more rapidly at early ages than concrete strength—even more rapidly than expected. Therefore, it was expected that an optimization coefficient calculated for use in predicting release modulus would need to be slightly larger than the proportional amount for use in predicting 28-day modulus.

This expectation was indeed confirmed by a few of the results present in Sections 7.4.1 and 7.4.2. When the AASHTO-1 combination was optimized, the only portion of the equation that was allowed to vary was the optimization coefficient, C. When using measured strengths, which is the only reliable method of this comparison for growth predictions, the optimization coefficient was found to be $C = 1.14$ for release modulus and $C = 1.11$ for 28-day modulus. This difference is not substantial, but it does support the idea that the modulus of elasticity had developed slightly more than the corresponding square root of the strengths at the time of prestress transfer.

This idea is even further supported by a comparison of the ratios of 28-day values to release values. Each pour consists of a group of cylinder tests—one test set at release, and one test set at 28 days. When all in-plant 28-day strengths were divided by the corresponding release strength, the mean ratio was equal to 1.30. On the other hand, when all 28-day moduli were divided by the corresponding release moduli, the mean ratio equal to 1.11. This is shown in the

following two equations:

$$\left(\frac{f_{c28}}{f_{ci}}\right)_{avg} = 1.30 \qquad \textbf{Equation 7.14}$$

$$\left(\frac{E_{ct,28}}{E_{ct,i}}\right)_{avg} = 1.11 \qquad \textbf{Equation 7.15}$$

where:

f_{c28} = concrete compressive strength at an age of 28 days, psi

f_{ci} = concrete compressive strength at prestress transfer, psi

$E_{ct,28}$ = concrete modulus of elasticity at an age of 28 days, ksi

$E_{ct,i}$ = concrete modulus of elasticity at prestress transfer, ksi

Therefore, on average, 28-day strengths were 30% larger than release strengths, but 28-day moduli were only 11% larger than release moduli. The prediction models expect that the modulus of elasticity should develop at a rate that is the square root of the rate of strength development. Therefore, if the development of modulus of elasticity and strength had followed the expected behavior, the modulus ratio shown above would have been $\sqrt{1.30} = 1.14$. The actual ratio shown in Equation 7.15 is smaller than 1.14, indicating that the modulus of elasticity values at release were larger relative to the 28-day modulus values than was expected. A higher percentage of the 28-day modulus had developed by the time of release than the strength. Thus, the modulus developed at a more rapid rate than the square root of the strength development.

7.4.4. Suggested Modulus Prediction Methods

There are two aspects of the optimized prediction methods presented in Sections 7.4.1, 7.4.2, and 7.4.3 that make them impractical or unusable for everyday application.

1. It was found that the optimized prediction combinations were sometimes extremely

sensitive to changes in the optimized values. As a perfect example of this sensitivity, compare the ACI 318, Known Weights results from Table 7.5 to the ACI318-1 optimized results from Table 7.6 when using expected strengths. The only difference between these two prediction methods is that the ACI 318-1 equation raised the unit weight to a power of 1.53, while the ACI 318, Known Weights equation raised the unit weight to the original power of 1.50. In equation form, the ACI 318-1 equation is Equation 7.16, while the ACI 318, Known Weights equation is Equation 2.1.

$$E_c = 33\omega^{1.53}\sqrt{f_c'} \qquad \textbf{Equation 7.16}$$

where:

E_c = static modulus of elasticity of the concrete, psi

ω = unit weight of concrete at the time of test, pcf

f_c' = compressive strength of the concrete at the time of test, psi

The difference in the power of the unit weight, ω, between the two equations was equal to 0.03, or 2%. This tiny change increased the SEE in Equation 2.1 to nearly 100% larger than the SEE in Equation 7.16.

A similar sensitivity was seen in the power to which strength was raised. Compare the ACI 318, Known Weights results from Table 7.5 to the ACI318-2 optimized results from Table 7.6 when using measured strengths. The only true difference between these two prediction methods is that the ACI 318-2 equation raised the strength to a power of 0.51, while the ACI 318, Known Weights equation raised the unit weight to the original power of 0.50. In equation form, the ACI 318-2 equation is Equation 7.17, while the ACI 318, Known Weights equation is Equation 2.1.

$$E_c = 33\omega^{\frac{3}{2}}(f_c')^{0.51} \qquad \textbf{Equation 7.17}$$

where:

E_c = static modulus of elasticity of the concrete, psi

ω = unit weight of concrete at the time of test, pcf

f_c' = compressive strength of the concrete at the time of test, psi

The difference in the power of the strength, f_c', between the two equations was 3%. This tiny change increased the SEE in Equation 2.1 to nearly 225% larger than the SEE in Equation 7.17.

If such small differences in optimized parameters could create such a large difference in curve fit error, and if each optimized combination provided different parameter values, it would be nearly impossible to suggest parameter values that would be accurate in all situations.

2. The optimized parameter values were, as mentioned above, quite varied. In some instances they changed by only a little, but in other instances they changed by a large amount.

In addition to these two problematic aspects of the optimized prediction methods, there was also concern about the limited nature of the modulus data set. The complete data set, including all of the data from this project's in-plant work, the work by Keske (2014), and the work by Boehm, Barnes, and Schindler (2010), consisted of 32 girder pours. Not only that, but the included range of in-plant specified strengths and unit weights was small. Out of the 32 pours, 30 had specified release strengths from 5200 psi to 6000 psi, inclusive. The range of 28-day strengths was not much larger, with 30 of the 32 pours specifying 28-day strengths from 6000 psi to 8000 psi, inclusive. Unit weights were the most limited of all, ranging from 147.2 pcf to 156.9 pcf (a maximum difference of only 6.6%). Therefore, the range and number

of data available for these analyses were not significant.

With these considerations in mind, it was recognized that the findings and suggestions presented herein are somewhat preliminary in nature—a framework for future optimization with the inclusion of additional data as the project continues. It was also decided that it would be best to minimize alterations to the modulus of elasticity equations. These equations have been in use for quite some time, and their form should not be significantly changed without a substantial amount of justification. The limited data set used for this analysis is simply insufficient for such justification.

In both the AASHTO method and the MC2010 method, however, there is a built-in variable intended for adjusting the modulus of elasticity equation to local concretes. In both equations, this variable is intended to modify the equation for aggregate properties. This variable is K_1 for the AASHTO method and α_E for the MC2010 method. It is fully justifiable to calculate values of these variables for use in predicting modulus of elasticity for ALDOT projects.

Of the two equations with this built-in factor, the AASHTO method is the more well-known in ALDOT practice. Furthermore, with simple optimizations the AASHTO method was found to usually provide more accurate predictions than the MC2010 method when using either expected strengths or measured strengths. Therefore the AASHTO method was chosen as the method for which suggestions would be made.

Table 7.14 was created to aid in the process of deciding which parameter values to suggest. This table provides only a basic summary of the optimized C coefficients and the SEEs caused by predictions with that value. For the meaning of the C coefficient, refer to Equation 7.8.

Table 7.14: Simplified Summary of AASHTO-1 Optimized Parameters

		Specified Strengths	Expected Strengths	Measured Strengths
Release Modulus	K_1	**1.00**	**1.00**	**1.00**
	SEE (ksi)	1650	990	830
	K_1	**1.20**	**1.20**	**1.20**
	SEE (ksi)	840	550	510
	C, Optimized	1.32	1.16	1.14
	SEE (ksi)	600	500	360
28-Day Modulus	K_1	**1.00**	**1.00**	**1.00**
	SEE (ksi)	1720	730	830
	K_1	**1.20**	**1.20**	**1.20**
	SEE (ksi)	900	1000	750
	C, Optimized	1.29	1.07	1.11
	SEE (ksi)	760	560	480

Table 7.14 also provides the same summary for the unadjusted AASHTO baseline function, with $K_1 = 1.20$, and the ACI 318 function ($K_1 = 1.00$). The ACI 318 method of prediction is the current standard ALDOT practice. Clearly, all of the optimized methods substantially improved the accuracy of predictions over the use of the standard equations alone.

It is apparent from Table 7.14 that the optimized C coefficient is different for every combination of strength level and age of prediction. However, as was mentioned in Section 7.4.3, an aggregate factor should be independent of the age of the concrete. The stiffness of the aggregate does not change as the concrete matures, but rather the stiffness of the cement paste. Therefore, any chosen value of K_1 should remain constant, regardless of whether predictions are being made for release modulus of elasticity or 28-day modulus of elasticity.

Nevertheless, there is a distinct different in the optimized C coefficient depending on the age of prediction. Therefore, it was decided to divide the influence of the C coefficient between

two separate factors. A portion of the C coefficient was distributed to the suggested aggregate stiffness factor, K_1, which is independent of the age of loading. An additional time-dependent factor, K_t, was included to account for the age at which modulus of elasticity is predicted. The optimization coefficient, C, was divided in such a way that $C = K_1 K_t$. The suggested prediction equations, as well as the suggested values for K_1 and K_t, are presented below.

Two sets of equations for predicting modulus of elasticity were established for use under different circumstances. Predicting both the release modulus and the 28-day modulus was more accurate with expected strengths than with specified strengths, and both of these strength levels could be known during the design phase of the project. Therefore, it made sense to only provide an equation that utilized expected strengths for predicting modulus. However, there may also arise a situation in which bridge design engineers or girder producers desire to predict concrete modulus of elasticity at the time of strength testing. In this case, measured strengths would be known, and it would be beneficial to have an equation based on measured strengths rather than specified or expected strengths. Therefore, two time-dependent K_t factors are provided for the prediction of both release modulus and 28-day modulus based on strength—four equations in total.

Table 7.15 provides a summary of the suggested K_1 and K_t factors, together with the SEEs and SPEEs from each prediction method. Of course, the SEEs and SPEEs from the measured strength predictions are smaller than the expected strength predictions. However, this requires knowledge of the actual concrete strength, which will not be available during girder design.

Table 7.15: Summary of Suggested AASHTO Modulus K_1 Factors and Accuracies

		Expected Strengths	Measured Strengths
Predicting Release Modulus	K_1	**1.12**	**1.12**
	K_t	1.04	1.02
	SEE (ksi)	500	360
	$SPEE$ (%)	9.1	6.3
Predicting 28-Day Modulus	K_1	**1.12**	**1.12**
	K_t	0.96	0.99
	SEE (ksi)	560	480
	$SPEE$ (%)	8.1	7.2

Table 7.15 shows that the suggested aggregate stiffness factor is equal to $K_1 = 1.12$ for all ages and strength levels. This was selected as the suggested aggregate stiffness factor for two reasons.

1. $K_1 = 1.12$ is close to the average value of C for modulus predictions with both expected strengths and measured strengths. For expected strengths, C ranged from 1.07 to 1.16. For measured strengths, C ranged from 1.11 to 1.14.
2. More importantly, $K_1 = 1.12$ closely matches historical studies of aggregate stiffness performed using this aggregate source. Roberts (2005) found in laboratory testing that the AASHTO LRFD equation underestimated modulus of elasticity for SCC mixtures using this aggregate source by 0% – 10%. His research was performed prior to the inclusion of the K_1 aggregate stiffness factor in the AASHTO equation, but his findings would imply that the optimized K_1 factor would be somewhere between 1.00 to 1.10. Similarly, Jones (2004) performed laboratory testing with the same aggregate source and provided Equation 7.18 as a suggested method for predicting modulus of elasticity.

$$E_c(t) = 37 w_c^{1.5} \sqrt{f_c(t)} \qquad \textbf{Equation 7.18}$$

where:

$E_c(t)$ = concrete modulus of elasticity at time t, psi

w_c = unit weight of concrete at the time of test, pcf

$f_c(t)$ = concrete compressive strength at time t, psi

This equation is identical to the ACI 318 equation, except that the coefficient is 37 instead of 33. This is equivalent to suggesting an aggregate stiffness factor of $K_1 = 1.12$, since $1.12 \cdot 33 = 37$. Jones (2004) did not have the option of suggesting a K_1 factor for the AASHTO equation, because the K_1 factor was not included in the AASHTO equation until 2005. Therefore, the equation suggested by Jones exactly matches the $K_1 = 1.12$ factor suggested in this thesis.

The suggested aggregate factor $K_1 = 1.12$ was developed based on data that mostly came from Plant A, which uses a dolomitic limestone as its coarse aggregate. In the past, Plant A has produced the majority of ALDOT girders. However, it is important to recognize that these K_1 factors are intended for use with this dolomitic limestone aggregate, and will most likely slightly overestimate average modulus of elasticity for less dense aggregates. These factors were developed using a range of specified release strengths from 5200 psi to 6000 psi, with two pours specifying a release strength of 9000 psi. The range of specified 28-day strengths was from 6000 psi to 8000 psi, with two pours specifying a 28-day strength of 13,000 psi. The inclusion of additional data as the project continues may expand the number of aggregate sources and the specified strength range.

The suggested equations for predicting modulus of elasticity are shown below. These equations are simply modified forms of the AASHTO (2012) standard equation for modulus of elasticity, with varying K_t factors depending on the situation. During the design phase, when

only specified strength and expected strength are known, the following equation is suggested for modulus of elasticity predictions:

$$E_{c,t} = 33K_1K_t\omega^{\frac{3}{2}}\sqrt{f^*_{c,t}} \qquad \textbf{Equation 7.19}$$

where:

$E_{c,t}$ = static modulus of elasticity of the concrete at release or 28-days, psi

K_1 = aggregate stiffness factor

= 1.12

K_t = time-dependency factor to account for age of predictions

= 1.04 when predicting release modulus of elasticity

= 0.96 when predicting 28-day modulus of elasticity

ω = unit weight of concrete at the time of test, pcf

$f^*_{c,t}$ = expected compressive strength of the concrete at the time for which modulus is predicted, psi

The $f^*_{c,t}$ expected strength is calculated in accordance with the methods suggested in Sections 6.3.1 and 6.4.1 for release predictions and 28-day predictions, respectively.

When the modulus of elasticity is to be predicted using measured strengths, the following equation is suggested:

$$E_{c,t} = 33K_1K_t\omega^{\frac{3}{2}}\sqrt{f_{c,t}} \qquad \textbf{Equation 7.20}$$

where:

$E_{c,t}$ = static modulus of elasticity of the concrete at release or 28-days, psi

K_1 = aggregate stiffness factor

= 1.12

K_t = time-dependency factor to account for age of predictions

= 1.02 when predicting release modulus of elasticity

= 0.99 when predicting 28-day modulus of elasticity

ω = unit weight of concrete at the time of test, pcf

$f_{c,t}$ = measured compressive strength of the concrete at the time for which modulus is predicted, psi

For both of these equations, it is important that the time is kept consistent throughout the equation. For example, if the goal is to predict release modulus then it is important that the K_t factor be the release factor and the strength be the release strength.

The SEEs and SPEEs for expected strength predictions are somewhat large. However, these accuracies are in the same vicinity of the optimized errors from the other methods, so they are as accurate as was possible based on the data. Furthermore, the errors are substantially less than the errors calculated using the current practice.

For example, the suggested release modulus of elasticity equation using expected strengths (Equation 7.11) has a calculated SPEE $= 9.1\%$ for the in-plant data. This means that approximately 68% of measured release modulus of elasticity values occurred within the range of $E_{c,t} \pm 9.6\%$. This is substantially more accurate than the original ACI 318 equation, which predicted that 68% of measured release moduli would fall within the range of $E_{c,t} \pm 26\%$ with specified strengths or $E_{c,t} \pm 15\%$ with expected strengths.

Equation 7.19 and Equation 7.20 were both developed using measured or calculated unit weights. However, it is recognized that measurements of unit weight are not usually available. Therefore, if it is known which concrete mixture will be used for the production of the girders, it is suggested that the unit weight be calculated using the approved mixture proportions with an assumed air content of 3.2% by volume (this is the median value of the air contents from the

historical data set). If the mixture to be used is unknown, then an estimated concrete unit weight of $\omega = 152$ pcf is suggested for use in Equations 7.19 and 7.20. This is the mean concrete unit weight that was seen from the in-plant data.

If the modulus of elasticity is known at release, it can be used to estimate the 28-day modulus based on the rate of modulus development. In Section 7.4.3, it was mentioned that the mean ratio of 28-day modulus to release modulus was 1.11. This can be turned into an equation, which is shown below.

$$E_{c28} = 1.11E_{ci} \qquad \textbf{Equation 7.21}$$

where:

E_{c28} = static modulus of elasticity of the concrete at 28-days, ksi

E_{ci} = static modulus of elasticity of the concrete at release, ksi

This method allows the prediction of 28-day moduli using release moduli with a calculated error of $SEE = 520$ ksi (or $SPEE = 7.5\%$), which is approximately as accurate as the prediction of either modulus using expected strengths.

7.5. Summary

This chapter provided useful feedback on the prediction methods developed in Sections 6.3, 6.4, and 6.5 for concrete strength and strength development. It also provided important findings related to the actual concrete stiffness, which was an express goal for the purposes of this research project. The main goal of these analyses was to obtain more accurate predictions for the concrete modulus of elasticity at release, which is the most important concrete material property needed for estimating initial camber. However, some additional analyses were performed on the data, including prediction of 28-day modulus and the rate of modulus

development compared to strength development. Additional in-plant data were collected from projects conducted by Keske (2014) and Boehm, Barnes, and Schindler (2010) to supplement the limited data set available from this project.

In Section 7.2 the expected strength prediction methods developed in Sections 6.3.1 and 6.4.1 are compared to the measured strengths seen in the in-plant testing. The analysis results shown there led to the conclusion that the prediction method developed in these two sections performed well in predicting the strengths seen in the in-plant testing. Furthermore, as was expected, these methods were a great deal more accurate than the current practice of using specified strengths—specifically, 64% more accurate for release strength predictions and 82% more accurate for 28-day strength predictions.

In Section 7.3 the optimized strength-growth prediction methods developed in Section 6.5 are compared to the strength development seen in the in-plant testing. It was found that the in-plant strengths developed slightly more rapidly than was predicted by the historically optimized equation parameters. This difference in strength development was not significant enough to warrant a change to the historically optimized equations, and it was concluded that the historically optimized strength growth parameters suggested in Table 6.31 may be used for reasonably accurate predictions of strength using either the MC2010 method or the ACI 209 method. It was also recognized that, although it was possible to predict 28-day strengths based on release strengths, the error of these predictions was usually slightly larger than predicting release strengths based on 28-day strengths.

Lastly, in Section 7.4 all of the analyses related to concrete stiffness are compared. The accuracy of five different methods in predicting the release modulus for the in-plant data using different levels of knowledge as to the strength behavior were first compared, in Section 7.4.1.

All five methods showed the best accuracy when using measured strength values for the predictions, as was expected. All five methods also showed improved accuracy with the use of expected strengths rather than specified strengths. Section 7.4.1 then also showed the optimization possibilities of the ACI 318 method, AASHTO method, and MC2010 method for predicting concrete modulus of elasticity at release. The optimization process was able to greatly reduce prediction errors, but the optimized parameters were quite varied.

Section 7.4.2 showed all of the same analyses as 7.4.1 for 28-day modulus predictions. All of the unchanged ACI prediction methods were most accurate with the use of expected strengths, rather than measured strengths. The AASHTO method was least accurate with expected strengths, and the MC2010 method followed the expected trend. All of the errors in these analyses were also greatly reduced by optimization, but the optimized parameters were quite varied.

Section 7.4.3 compared the rate of modulus development to the rate of strength development for the same concrete, and showed that the modulus tends to develop slightly more rapidly during early ages than the strength for concretes used in ALDOT girders. When the MC2010 modulus-growth equation was used, the optimized values of s calculated for modulus-growth were very slightly less than the values of s optimized for strength-growth. This indicates a slightly more rapid rate of early modulus development than was expected based on strength growth. The optimized values of α and β in the ACI 209 method indicated the same trend, with modulus-optimized α values slightly smaller than the corresponding strength-optimized α values. It was also found that the average ratio of 28-day moduli to release moduli was only 1.11. This 1.11 ratio is smaller than the square root of the average ratio of 28-day strengths to release strengths, which was $\sqrt{1.30} = 1.14$. This showed that a higher percentage of the 28-day modulus

had developed at release than was expected based on strength development.

Lastly, Section 7.4.4 provided some practical suggestions based on Sections 7.4.1, 7.4.2, and 7.4.3, for use in modulus of elasticity predictions. Predictions during the design phase of the project, or without prior knowledge of the concrete strength, should be made using Equation 7.11, with the appropriate K_t factor and strength for the age at which the prediction is made.

$$E_{c,t} = 33K_1K_t\omega^{\frac{3}{2}}\sqrt{f^*_{c,t}} \qquad \textbf{Equation 7.19}$$

where:

$E_{c,t}$ = static modulus of elasticity of the concrete at release or 28-days, psi

K_1 = aggregate stiffness factor

= 1.12

K_t = time-dependency factor to account for age of predictions

= 1.04 when predicting release modulus of elasticity

= 0.96 when predicting 28-day modulus of elasticity

ω = unit weight of concrete at the time of test, pcf

$f^*_{c,t}$ = expected compressive strength of the concrete at the time for which modulus is predicted, psi

Predictions of modulus with prior knowledge of the concrete strength should be made using Equation 7.12, with the appropriate K_t factor and strength for the age at which the prediction is made.

$$E_{c,t} = 33K_1K_t\omega^{\frac{3}{2}}\sqrt{f_{c,t}} \qquad \textbf{Equation 7.20}$$

where:

$E_{c,t}$ = static modulus of elasticity of the concrete at release or 28-days, psi

K_1 = aggregate stiffness factor

= 1.12

K_t = time-dependency factor to account for age of predictions

= 1.02 when predicting release modulus of elasticity

= 0.99 when predicting 28-day modulus of elasticity

ω = unit weight of concrete at the time of test, pcf

$f_{c,t}$ = measured compressive strength of the concrete at the time for which modulus is predicted, psi

If it is known which concrete mixture will be used for the production of the girders, it is suggested that the unit weight be calculated using the approved mixture proportions with an assumed air content of 3.2% by volume.

If it is unknown which concrete mixture will be used, then an estimated concrete unit weight of $\omega = 152$ pcf is suggested for use in Equations 7.19 and 7.20. This is the mean concrete unit weight that was seen from the in-plant data.

If the concrete modulus of elasticity is desired at 28 days, and modulus of elasticity is known at release, then the 28-day modulus can be estimated using Equation 7.21.

$$E_{c28} = 1.11E_{ci} \qquad \textbf{Equation 7.21}$$

where:

E_{c28} = static modulus of elasticity of the concrete at 28-days, psi

E_{ci} = static modulus of elasticity of the concrete at release, psi

Chapter 8: Final Summary & Conclusions

8.1. Summary

The camber of prestressed concrete bridge girders is a highly variable phenomenon dependent on a wide range of factors. The accurate prediction of cambers is a serviceability and constructability issue, with the usual price of inaccuracy being increased costs, construction delays, and possibly strained relationships on the job site. It is the occasional large errors in predicting these cambers which has been the motive for a research project to examine the short-term and long-term material properties of ALDOT concretes, together with measurements of the girders produced with these concretes, to develop an updated computer software program for the prediction of girder cambers. This thesis discusses primarily the short-term material properties of ALDOT concretes and concrete strength and stiffness up until 28 days.

Plant practices and historical data were both examined for trends and predictable patterns that could be used to improve the prediction of modulus of elasticity. Extensive analysis of approximately 1900 girder pours over the last 6 years, containing approximately 10,000 cylinder tests, was used to map patterns in fresh concrete properties, curing patterns, casting conditions, and concrete strengths. A more limited data set of 435 girder pours was used for detailed examination of strength development over time.

Release and 28-day strengths were examined in great detail, because they had the potential to provide more accurate means of predicting modulus of elasticity. Relationships between the specified strength and the expected strengths were developed based on the historical

data, and were used to predict more accurate strengths for use in predicting modulus of elasticity. The development of strength with time was also examined, to judge the accuracy of existing prediction methods when applied to typical ALDOT concretes. Other parts of this research project, not discussed in this thesis, included extensive in-plant girder instrumentation and long-term material testing for the prediction of long-term camber growth.

Modulus of elasticity prediction methods from ACI 318 (2011), the *AASHTO LRFD Bridge Design Specifications* (2012), ACI 363 (1992), and MC2010 (*fib* 2010) were examined for accuracy when predicting release and 28-day moduli for ALDOT concretes. Optimized forms of three of these equations were produced to see the potential accuracy available with sufficient pour-specific knowledge. The growth of modulus was compared to the growth of strength in the same concrete.

8.2. Conclusions

Conclusions were made based on the observed plant practices followed by the four plants that produce prestressed concrete bridge girders for ALDOT and the analysis of both historical plant data and in-plant data. All four primary producers of ALDOT girders were included for the observation of plant practices and the collection of historical project data. The following conclusions were made regarding the plant practices observed in this study:

- Plant practices are very similar in most ways, and nearly identical in several. The primary differences between plants are the pre-release curing of girders and the post-release curing of cylinders.
- Most plants use accelerated (steam) curing methods for their girders, with thick tarps for covering.

- Concrete mixtures used in ALDOT girders tend to have high cement contents, often with the use of one or two mineral admixtures, and low water-to-cement ratios. These mixtures also employ large doses of high-range water-reducing admixtures to increase slump and workability.
- Most girder producers keep a limited number of approved mixtures available for girder production. These mixtures are used for projects with specified strengths much lower than the strength capacity of the mixture, either for workability or because of a lack of other options.
- The ages at which girders are released fall into two general categories—standard pours and extended weekend pours.
- Standard pours, in which there is a normal rate of strength development and nothing preventing release of the girders, have a mean curing time of approximately 18 hours. Standard pours included 83.5% of the pours examined in this study.
- Extended weekend pours, in which the girders are cast on a Friday and left in the forms until Monday morning, have a mean curing time of approximately 66 hours. Extended weekend pours included 11.8% of the pours examined in this study.

Historical data included the records of more than 1900 girder pours, collected from the four girder producers. These records included girder sizes covering the full range of AASHTO girders (Type I through Type V) and PCI bulb-tee girders (BT-54 through BT-72). Specified release strengths ranged from 4000 psi to 9000 psi, and specified 28-day strengths ranged from 5000psi to 9000 psi. Coarse aggregates included granite, limestone, and dolomitic limestone. All fine aggregates were a #100 sand.

The following conclusions were made regarding the fresh concrete properties and project

trends observed in the historical plant-submitted data:

- The sample mean of calculated equivalent ages at the time of prestress transfer is more than three times as large as the mean of chronological ages at the time of prestress transfer. The mean equivalent age at transfer is in the vicinity of 2.5 days, while the mean chronological age of standard pours at release is in the vicinity of 0.75 days.
- Concrete air contents fall well below the target value specified by the ALDOT *Standard Specifications* (2012). The differences between the mean air contents and the target air contents are approximately 1% for each data group, and the differences between the mode air contents and the target air contents are approximately 1.5% – 2.0% for each data group.
- Most girder pours use the maximum allowable slump with chemical admixtures.
- On average, girder lengths tend to increase with increasing girder height. This is true for both AASHTO girders and PCI bulb-tee girders.
- There is little correlation between girder type and specified strengths.
- The two most produced girder types seen in this study were PCI BT-54 and BT-72 girders.
- The time of year during which girders are produced was not found to significantly impact the strengths of the girder.
- Concrete unit weights were found to be slightly higher than the typically assumed value of $\omega = 145$ pcf.

The following conclusions were made regarding strength findings from the historical plant-submitted data:

- Both release strengths and 28-day strengths are often much higher than the specified

strengths. 28-day strengths exhibit this behavior to a greater degree.

- Release strength measurements are nearly normally distributed, with a slight skew toward higher strength values.
- 28-day strength measurements are not quite as normally distributed as release strength measurements, with a slight skew toward lower strength values and a higher peakedness.
- Extended weekend pours exhibit higher mean release strengths than standard pours, though the mean specified release strengths are the same and the mean 28-day strengths are the same. A higher percentage of the 28-day strength was developed by the time of prestress transfer in extended weekend pours.
- Specified strengths alone are found to be poor predictors of average concrete strength, partially because they are supposed to be lower-bound strength values.
- Mean release strengths remain fairly constant for specified release strengths not greater than 6500 psi.
- Mean 28-day strengths remain fairly consistent for specified 28-day strengths not greater than 7000 psi.
- Selecting a constant, average strength for predicting 28-day strengths is almost as accurate as selecting a simple piecewise strength prediction equation.
- The use of the suggested parameters in the MC2010 (*fib* 2010) and ACI 209 (1992) strength-growth equations has large errors, and consistently underestimates the strength of concrete when using chronological age.
- In general, concrete strength in ALDOT concretes develops more rapidly than the MC2010 (*fib* 2010) and ACI 209 (1992) equations predict.
- The ACI 209 (1992) strength-growth prediction method over-predicts strength

development when equivalent age is used.

- It was found that the ACI 209 and MC2010 strength-growth equations could be rearranged for prediction of 28-day strengths using measured release strengths. The errors associated with this rearrangement were not substantially greater than the errors of the original version when using the optimized parameters. However, the errors caused by the rearrangement were usually substantially larger than the errors of the original version when using the suggested parameters from ACI 209 (1992) and MC2010 (*fib* 2010).
- The optimized ACI 209 and MC2010 methods were found to be approximately equally accurate in their strength-growth predictions when chronological age is used.
- The optimized MC2010 method was found to more accurately predict the development of strength than the optimized ACI 209 method when equivalent age is used.
- Adjustment of the strength measurements for known air content decreased all mean strength values.
- Air content adjustments do not significantly affect the accuracy of all full-set strength-growth predictions.

Lastly, in-plant conclusions were drawn from the analysis of material testing performed by AUHRC researchers, as well as data collected from Keske (2014) and Boehm, Barnes, and Schindler (2010). All of the research from these sources was performed almost solely at Plant A, so the vast majority of the in-plant testing used dolomitic limestone as a coarse aggregate. Specified release strengths for the in-plant testing ranged from 5200 psi to 6000 psi, with two pours specifying a release strength of 9000 psi. The range of specified 28-day strengths was from 6000 psi to 8000 psi, with two pours specifying a 28-day strength of 13,000 psi. The following conclusions were made regarding the results of in-plant material testing:

- The use of the proposed release strength prediction method greatly reduces the errors in predicting release strengths compared to current practice.
- The use of either of the proposed 28-day strength prediction methods greatly reduces the errors in predicting 28-day strengths compared to current practice.
- All three proposed strength prediction methods are reasonably accurate in their strength predictions when compared to in-plant measurements.
- In-plant strengths were found to develop slightly more rapidly at early ages than historical strengths.
- The suggested strength-growth parameters from the historical data set can be used to predict strength growth with reasonable accuracy for the in-plant data.
- Predictions of release modulus of elasticity based on release strengths are more accurate than predictions of release modulus based on 28-day strengths.
- Without optimization or the inclusion of an assumed aggregate factor, all prediction methods tend to underestimate the modulus of elasticity at release.
- Optimization of the ACI 318, AASHTO, and MC2010 modulus prediction methods is able to achieve a reasonably similar level of accuracy in predicting release modulus of elasticity. The MC2010 method was found to have the highest minimum error.
- When powers were allowed to freely vary, optimization of the modulus prediction equations increases the power of the unit weight and decreases the power of concrete strength.
- Without optimization or the inclusion of an assumed aggregate factor, all prediction methods underestimate the modulus of elasticity at 28 days.
- The AASHTO method provides the simplest form of modulus prediction for the same

level of accuracy.

- The modulus of elasticity develops slightly more rapidly at early ages than expected based on strength growth.
- In all optimized modulus prediction combinations, the use of measured strengths provides the most accurate predictions.
- In most optimized modulus prediction combinations, the use of the suggested strength prediction equations provides more accurate modulus predictions than the use of specified strengths.
- A higher percentage of the 28-day modulus is developed at the time of prestress transfer than is expected based on the percentage of 28-day strength that has developed at the time of prestress transfer.

8.3. Recommendations for Future Work and Implementation

After completion of this study, the following recommendations can be made for future investigations:

- An examination of modulus of elasticity relationships over a much larger data set could be used to better test the accuracy of the suggested prediction equations.
- A mixture-specific analysis of a large data set with clearly designated mixture designs could reveal more accurate means of strength and modulus prediction, since many aspects of such predictions depend on mixture-specific properties.

The following recommendations can be made to ALDOT for possible implementation of the results presented in this thesis:

- The average expected concrete compressive strength at release may be estimated using

Equation 6.8. Using this expected release strength equation reduces the standard error of estimate by approximately 50% when compared to using the specified release strengths.

$f_{ci}^{*} = 7500$ psi for 4000 psi $\leq f_{ci}' \leq 7000$ psi **Equation 6.8**

$f_{ci}^{*} = f_{ci}' + 500$ psi for 7000 psi $< f_{ci}' \leq 9000$ psi

where:

f_{ci}^{*} = expected concrete strength at release, psi

f_{ci}' = specified concrete strength at release, psi

- The average expected concrete compressive strength at 28 days may be estimated using either Equation 6.10 or 6.11. Using either of these expected 28-day strength equations reduces the standard error of estimate by approximately 75% when compared t using the specified 28-day strengths.

$f_{c}^{*} = 10{,}500$ psi for 5000 psi $\leq f_{c}' \leq 7000$ psi **Equation 6.10**

$f_{c}^{*} = \frac{1}{2} f_{c}' + 7000$ psi for 7000 psi $< f_{c}' \leq 9000$ psi

where:

f_{c}^{*} = expected concrete strength at 28 days, psi

f_{c}' = specified concrete strength at 28 days, psi

Equation 6.11 is simpler than Equation 6.10, but slightly less accurate for higher specified strengths.

$f_{c}^{*} = 10{,}500$ psi **Equation 6.11**

for $5{,}000$ psi $\leq f_{c}' \leq 9{,}000$ psi

where:

f_{c}^{*} = expected concrete strength at 28 days, psi

f_{c}' = specified concrete strength at 28 days, psi

- If knowledge of curing temperatures is known and maturity may be calculated, the MC2010 (*fib* 2010) method of strength-growth prediction may be used. If maturity cannot be calculated, then the ACI 209 (1992) strength-growth prediction method should be used instead. The suggested strength-growth parameters for these two methods are shown in Table 8.1, along with the parameters suggested in MC2010 and the ACI 209 report.

Table 8.1: Summary of Suggested Strength-Growth Parameters for Full Data Set

			Chronological Age	**Equivalent Age**
MC2010	Suggested based on Plant Data	s	NA	0.15
	Suggested by MC2010	s	NA	0.20
ACI 209	Suggested based on Plant Data	α (days)	0.34	NA
		β	0.988	NA
	Suggested by ACI 209	α (days)	0.70	NA
		β	0.98	NA

- For modulus of elasticity predictions, a modified form of the standard equation found in the *AASHTO LRFD Bridge Design Speicifications* (2012) may be used with the factors, accuracies, and strength levels shown in Table 8.2. The equations that correspond to this suggestion are shown after the table.

Table 8.2: Summary of Suggested AASHTO Modulus K_1 Factors and Accuracies

		Expected Strengths	Measured Strengths
Predicting Release Modulus	K_1	**1.12**	**1.12**
	K_t	1.04	1.02
	SEE (ksi)	500	360
	$SPEE$ (%)	9.1	6.3
Predicting 28-Day Modulus	K_1	**1.12**	**1.12**
	K_t	0.96	0.99
	SEE (ksi)	560	480
	$SPEE$ (%)	8.1	7.2

During the design stage, when measured strengths of the concrete are not available, modulus of elasticity at release or 28 days may be calculated using Equation 7.19.

$$E_{c,t} = 33K_1K_t\omega^{\frac{3}{2}}\sqrt{f^*_{c,t}} \qquad \textbf{Equation 7.19}$$

where:

$E_{c,t}$ = static modulus of elasticity of the concrete at release or 28-days, psi

K_1 = aggregate stiffness factor

= 1.12

K_t = time-dependency factor to account for age of predictions

= 1.04 when predicting release modulus of elasticity

= 0.96 when predicting 28-day modulus of elasticity

ω = unit weight of concrete at the time of test, pcf

$f^*_{c,t}$ = expected compressive strength of the concrete at the time for which modulus is predicted, psi

If measured strengths of the concrete are available, modulus of elasticity at release or 28

days may be calculated using Equation 7.20.

$$E_{c,t} = 33K_1K_t\omega^{\frac{3}{2}}\sqrt{f_{c,t}} \qquad \textbf{Equation 7.20}$$

where:

$E_{c,t}$ = static modulus of elasticity of the concrete at release or 28-days, psi

K_1 = aggregate stiffness factor

= 1.12

K_t = time-dependency factor to account for age of predictions

= 1.02 when predicting release modulus of elasticity

= 0.99 when predicting 28-day modulus of elasticity

ω = unit weight of concrete at the time of test, pcf

$f_{c,t}$ = measured compressive strength of the concrete at the time for which modulus is predicted, psi

These suggested aggregate factors were determined using primarily dolomitic limestone as the coarse aggregate, which is the aggregate used by Plant A.

If it is known which concrete mixture will be used for the production of the girders, it is suggested that the unit weight be calculated using the approved mixture proportions with an assumed air content of 3.2% by volume.

If it is unknown which concrete mixture will be used, then an estimated concrete unit weight of $\omega = 152$ pcf is suggested for use in Equations 7.19 and 7.20.

- If the modulus of elasticity at release is known, then the modulus of elasticity at 28 days may be estimated using Equation 7.21. This is approximately as accurate as using Equation 7.20.

$$E_{c28} = 1.11E_{ci} \qquad \textbf{Equation 7.20}$$

where:

E_{c28} = static modulus of elasticity of the concrete at 28-days, ksi

E_{ci} = static modulus of elasticity of the concrete at release, ksi

Lastly, the following recommendations can be made to ALDOT for possible practice and specification changes:

- The addition of modulus of elasticity testing to the mixture approval process could provide bridge design engineers with more specific knowledge of the modulus properties in Alabama concretes. The prediction equations could be tailored to better match the values found with these tests.
- The requirement for concrete unit weights to be measured and reported at regular intervals, or whenever fresh properties are tested, would provide a much more thorough database for the prediction of concrete modulus of elasticity. Additionally, keeping continual records of such measurements would allow design engineers to track gradual changes in the unit weights as mixture designs change, giving them the opportunity to adjust modulus prediction equations to account for this change. These could be done according to the standard method described in ASTM C138/C138M (2012).
- Regular testing of the modulus of elasticity, strength, and unit weight in tandem would allow design engineers to see gradual changes in the relationship between those three components as mixture designs change or material components are altered.

References

AASHTO. 2005. *AASHTO LRFD Bridge Design Specifications: Interim Revisions*. 3rd ed. Washington D.C.: American Association of State Highway and Transportation Officials (AASHTO).

AASHTO. 2012. *AASHTO LRFD Bridge Design Specifications*. 6th ed. Washington D.C.: American Association of State Highway and Transportation Officials (AASHTO).

ACI Committee 209. 1992. *Prediction of Creep, Shrinkage, and Temperature Effects in Concrete Structures*. Farmington Hills, Michigan: American Concrete Institute, 209R-92 (Reapproved 2008).

ACI Committee 209. 2008. *Guide for Modeling and Calculating Shrinkage and Creep in Hardened Concrete*. Farmington Hills, Michigan: American Concrete Institute, 209.2R-08.

ACI Committee 214. 2011. *Guide to Evaluation of Strength Test Results of Concrete*. Farmington Hills, Michigan: American Concrete Institute, 214R-11.

ACI Committee 318. 2011. *Building Code Requirements for Structural Concrete (ACI 318-11) and Commentary*. Farmington Hills, Michigan: American Concrete Institute, 318-11.

ACI Committee 363. 1992. *State-of-the-Art Report on High-Strength Concrete*. Farmington Hills, Michigan: American Concrete Institute, 363R-92.

ACI Committee 363. 2010. *Report on High-Strength Concrete*. Farmington Hills, Michigan: American Concrete Institute, 363R-10.

ALDOT. 2008. ALDOT 425: Maturity Method to Determine Early-Age Strengths of Concrete. In *ALDOT Testing Manual*. Montgomery, AL: Alabama Department of Transportation Bureau of Materials and Tests, ALDOT-425-08.

ALDOT. 2009. ALDOT 170-82: Method of Controlling Concrete Operations for Structural Portland Cement Concrete. In *ALDOT Testing Manual*. Montgomery, AL: Alabama Department of Transportation Bureau of Materials and Tests, ALDOT-170-82.

ALDOT. 2010. ALDOT 367: Production and Inspection of Precast Non-Prestressed and Prestressed Concrete. In *ALDOT Testing Manual*. Montgomery, AL: Alabama Department of Transportation Bureau of Materials and Tests, ALDOT-367-89.

ALDOT. 2012. *Standard Specifications for Highway Construction*. Alabama Department of Transportation.

Anderson, F. D. 1985. Statistical Controls for High-Strength Concrete. *High-Strength Concrete* SP-87: 71-82.

ASTM C31/C31M. 2012. Standard Practice for Making and Curing Concrete Test Specimens in the Field. In *Annual Book of ASTM Standards*, Vol 4: Concrete and Aggregates. West Conshohocken, Pennsylvania: ASTM International. 23-29.

ASTM C39/C39M. 2012. Standard Test Method for Compressive Strength of Cylindrical Concrete Specimens. In *Annual Book of ASTM Standards*, Vol 4: Concrete and Aggregates. West Conshohocken, Pennsylvania: ASTM International. 23-29.

ASTM C138/C138M. 2012. Standard Test Method for Density (Unit Weight), Yield, and Air Content (Gravimetric) of Conrete. In *Annual Book of ASTM Standards*, Vol 4: Concrete and Aggregates. West Conshohocken, Pennsylvania: ASTM International. 103-106.

ASTM C143/C143M. 2010. Standard Test Method for Slump of Hydraulic-Cement Concrete. In *Annual Book of ASTM Standards*, Vol 4: Concrete and Aggregates. West Conshohocken, Pennsylvania: ASTM International. 109-112.

ASTM C231/C231M. 2010. Standard Test Method for Air Content of Freshly Mixed Concrete by the Pressure Method. In *Annual Book of ASTM Standards*, Vol 4: Concrete and Aggregates. West Conshohocken, Pennsylvania: ASTM International. 162-171.

ASTM C469/C469M. 2010. Standard Test Method for Static Modulus of Elasticity and Poisson's Ratio of Concrete in Compression. In *Annual Book of ASTM Standards*, Vol 4: Concrete and Aggregates. West Conshohocken, Pennsylvania: ASTM International. 274-278.

ASTM C511. 2009. Specification for Mixing Rooms, Moist Cabinets, Moist Rooms, and Water Storage Tanks Used in the Testing of Hydraulic Cements and Concretes. In *Annual Book of ASTM Standards*, Vol 4: Concrete and Aggregates. West Conshohocken, Pennsylvania: ASTM International. 306-308.

ASTM C1074. 2011. Standard Practice for Estimating Concrete Strength by the Maturity Method. In *Annual Book of ASTM Standards*, Vol 4: Concrete and Aggregates. West Conshohocken, Pennsylvania: ASTM International. 582-591.

ASTM C1231/C1231M. 2010. Standard Practice for Use of Unbonded Caps in Determination of Compressive Strength of Hardened Concrete Cylinders. In *Annual Book of ASTM Standards*, Vol 4: Concrete and Aggregates. West Conshohocken, Pennsylvania: ASTM International. 665-669.

Barr, P. J., B. M. Kukay, and M. W. Halling. 2008. Comparison of Prestress Losses for a Prestress Concrete Bridge made with High-Performance Concrete. *Journal of Bridge Engineering* (September/October): 468-475.

Boehm, K. M., R. W. Barnes, and A. K. Schindler. 2010. *Performance of Self-Consolidating Concrete in Prestressed Girders*. Alabama Department of Transportation. Report No. FHWA/ALDOT 930-602.

Brown, A. M. 2001. A Step-by-Step Guide to Non-Linear Regression Analysis of Experimental Data Using a Microsoft Excel Spreadsheet. *Computer Methods and Programs in Biomedicine* 65: 191-200.

BS EN 197-1. 2011. Cement, Composition, Specifications and Conformity Criteria for Common Cements. London, England: British Standard Institution (BSI).

Buettner, D. R., and J. R. Libby. 1979. "Camber" Requirements for Pretensioned Members. *Concrete International* (February): 66-72.

Carino, N. J., and R. C. Tank. 1992. Maturity Functions for Concretes Made with Various Cements and Admixtures. *ACI Materials Journal* (March-April): 188-196.

CEB. 1990. *CEB-FIP Model Code 1990*. Lausanne, Switzerland: *Comité Euro-International du Béton* (CEB).

Cook, J. E. 1989. 10,000 psi Concrete. *Concrete International* (October): 67-75.

fib. 2010. *Model Code 2010*. Lausanne, Switzerland: International Federation for Structural Concrete.

FHWA. 1996. *Implementation Program on High Performance Concrete: Guidelines for Instrumentation of Bridges*. U.S. Department of Transportation (August).

French, C. E., and C. O'Neill. 2012. *Validation of Prestressed Concrete I-Beam Deflection and*

Camber Estimates. Minnesota Department of Transportation. Report No. MN/RC 2012-16.

Johnson, B. R. 2012. Time-Dependent Deformations in Precast, Prestressed Bridge Girders. Master's thesis, Auburn University.

Jones, K. L. 2004. The Age-Dependent Stiffness Development of Concrete. Master's thesis, Auburn University.

Kavanaugh, B. P. 2008. Creep Behavior of Self-Consolidating Concrete. Master's thesis, Auburn University.

Kelly, D. J., T. E. Bradberry, and J. E. Breen. 1987. *Time Dependent Deflections of Pretensioned Beams*. Research Report 381-1, University of Texas at Austin.

Keske, S. E. 2014. Use of Self-Consolidating Concrete in Precast, Prestressed Girders. Ph.D. dissertation, Auburn University.

Long, W., K. H. Khayat, and S. Hwang. 2012. Mechanical Properties of Prestressed Self-Consolidating Concrete. *Materials and Structures*.

Martin, L. D. 1977. A Rational Method for Estimating Camber and Deflection of Precast Prestressed Members. *PCI Journal* (January/February): 100-108.

McCuen, R. H. 1985. *Statistical Methods for Engineers*. Englewood Cliffs, New Jersey: Prentice-Hall, Inc.

Pauw, A. 1960. Static Modulus of Elasticity of Concrete as Affected by Density. *ACI Journal, Proceedings* 57, no. 6 (December): 679-687.

PCI. 2003. Chapter 8.7. In *Bridge Design Manual*. Chicago, Illinois: Precast/Prestressed Concrete Institute (July).

PCI Committee on Bridges – Camber FAST Team. 2012. 2012 Committee Days.

Precast/Prestressed Concrete Institute.

Roberts, J. B. 2005. Evaluation of Self-Consolidating Concrete for Use in Prestressed Girder Applications. Master's thesis, Auburn University.

Rosa, M. A., J. F. Stanton, and M. O. Eberhard. 2007. *Improving Predictions for Camber in Precast, Prestressed Concrete Bridge Girders*. Washington State Transportation Center. Report No. WA-RD 669.1.

Stallings, J. M., R. W. Barnes, and S. Eskildsen. 2003. Camber and Prestress Losses in Alabama HPC Bridge Girders. *PCI Journal* (September-October): 1-16.

Storm, T. K. 2011. Predicting Prestress Losses, Camber, and Deflection in Prestressed Concrete Members. Master's thesis, North Carolina State University.

Storm, T. K., S. H. Rizkalla, and P. Z. Zia. 2013. Effects of Production Practices on Camber of Prestressed Concrete Bridge Girders. *PCI Journal* (Winter): 96-111.

Tadros, M. K., N. Al-Omaishi, S. J. Seguirant, and J. G. Gallt. 2003. *Prestress Losses in Pretensioned High-Strength Concrete Bridge Girders*. National Cooperative Highway Research Program, Transportation Research Board. NCHRP Report No. 496. Washington, D. C.

Tadros, M. K., F. Fawzy, and K. E. Hanna. 2011. Precast, Prestressed Girder Camber Variability. *PCI Journal* (Winter): 135-154.

Appendices

Appendix A: Plant-Specific Tables for the Range of Historical Data

Table A.1: Range of Plant-Submitted Data from Plant A

Plant A	10^{th} Percentile	Sample Mean, $\bar{x}$	90^{th} Percentile	Mode, Mo.	Sample Standard Deviation, s	C.O.V. (%)
Specified Release Strength (psi)	5000	5798	6600	6000	682	11.76
Measured Release Strength (psi)	6750	7870	9080	7620	910	11.56
Specified 28-Day Strength (psi)	6000	6703	8000	7000	710	10.59
Measured 28-Day Strength (psi)	9550	10730	11910	10590	890	8.29
Air Content (%)	2.5	3.4	4.2	2.5	0.7	20.08
Slump (in.)	8.0	8.7	9.0	9.0	0.5	5.71
Release Age (days)	0.66	1.00	2.71	0.70	0.68	67.44
Air Temp (°F)	48	72	92	75	17	23.09
Concrete Temp (°F)	65	79	91	89	10	13.06
Member Length (ft)	54.4	102.9	138.1	127.2	32.4	31.53

Table A.2: Range of Plant-Submitted Data from Plant B

Plant B	10^{th} Percentile	Sample Mean, $\bar{x}$	90^{th} Percentile	Mode, Mo.	Sample Standard Deviation, s	C.O.V. (%)
Specified Release Strength (psi)	5000	5803	6500	6000	680	11.72
Measured Release Strength (psi)	6290	7270	8310	7100	840	11.55
Specified 28-Day Strength (psi)	5600	6660	7500	7000	686	10.29
Measured 28-Day Strength (psi)	10140	10830	11740	13270	10640	700
Air Content (%)	2.7	3.2	3.9	3.0	0.5	15.63
Slump (in.)	7.5	8.5	9.0	9.0	0.7	8.61
Release Age (days)	0.56	0.91	1.65	0.68	0.6	69.04
Air Temp (°F)	50	72	93	68	16	21.70
Concrete Temp (°F)	66	78	89	82	8	10.72
Member Length (ft)	54.3	89.4	115.2	54.3	22.8	25.53

Table A.3: Range of Plant-Submitted Data from Plant C

Plant C	10^{th} Percentile	Sample Mean, $\bar{x}$	90^{th} Percentile	Mode, Mo.	Sample Standard Deviation, s	C.O.V. (%)
Specified Release Strength (psi)	5000	5884	7500	6000	905	15.38
Measured Release Strength (psi)	5560	6960	8580	7410	1150	16.52
Specified 28-Day Strength (psi)	6000	6786	8000	7000	877	12.92
Measured 28-Day Strength (psi)	7540	8890	10290	9180	980	11.02
Air Content (%)	2.5	3.6	5.0	2.5	0.9	24.75
Slump (in.)	6.0	7.5	8.8	8.0	1.1	14.57
Release Age (days)	0.58	1.25	2.69	0.91	1.1	87.83
Air Temp (°F)	53	72	86	80	13	17.89
Concrete Temp (°F)	69	83	93	91	9	10.91
Member Length (ft)	39.0	85.2	120.5	99.2	34.8	40.89

Table A.4: Range of Plant-Submitted Data from Plant D

Plant D	10^{th} Percentile	Sample Mean, $\bar{x}$	90^{th} Percentile	Mode, Mo.	Sample Standard Deviation, s	C.O.V. (%)
Specified Release Strength (psi)	5500	6081	6500	6000	1074	17.66
Measured Release Strength (psi)	6440	7700	9340	8590	1120	14.55
Specified 28-Day Strength (psi)	6500	7103	8000	7000	800	11.26
Measured 28-Day Strength (psi)	9150	10330	11890	14140	1060	10.26
Air Content (%)	2.5	3.1	3.7	2.5	0.6	19.06
Slump (in.)	7.8	8.6	9.0	8.0	0.6	7.54
Release Age (days)	0.65	1.41	2.80	0.91	1.0	70.54
Air Temp (°F)	62	79	91	80	11	13.74
Concrete Temp (°F)	70	83	92	91	8	10.23
Member Length (ft)	39.7	77.0	99.2	99.2	27.7	36.02

Appendix B: Plant-Specific Release Age Histograms

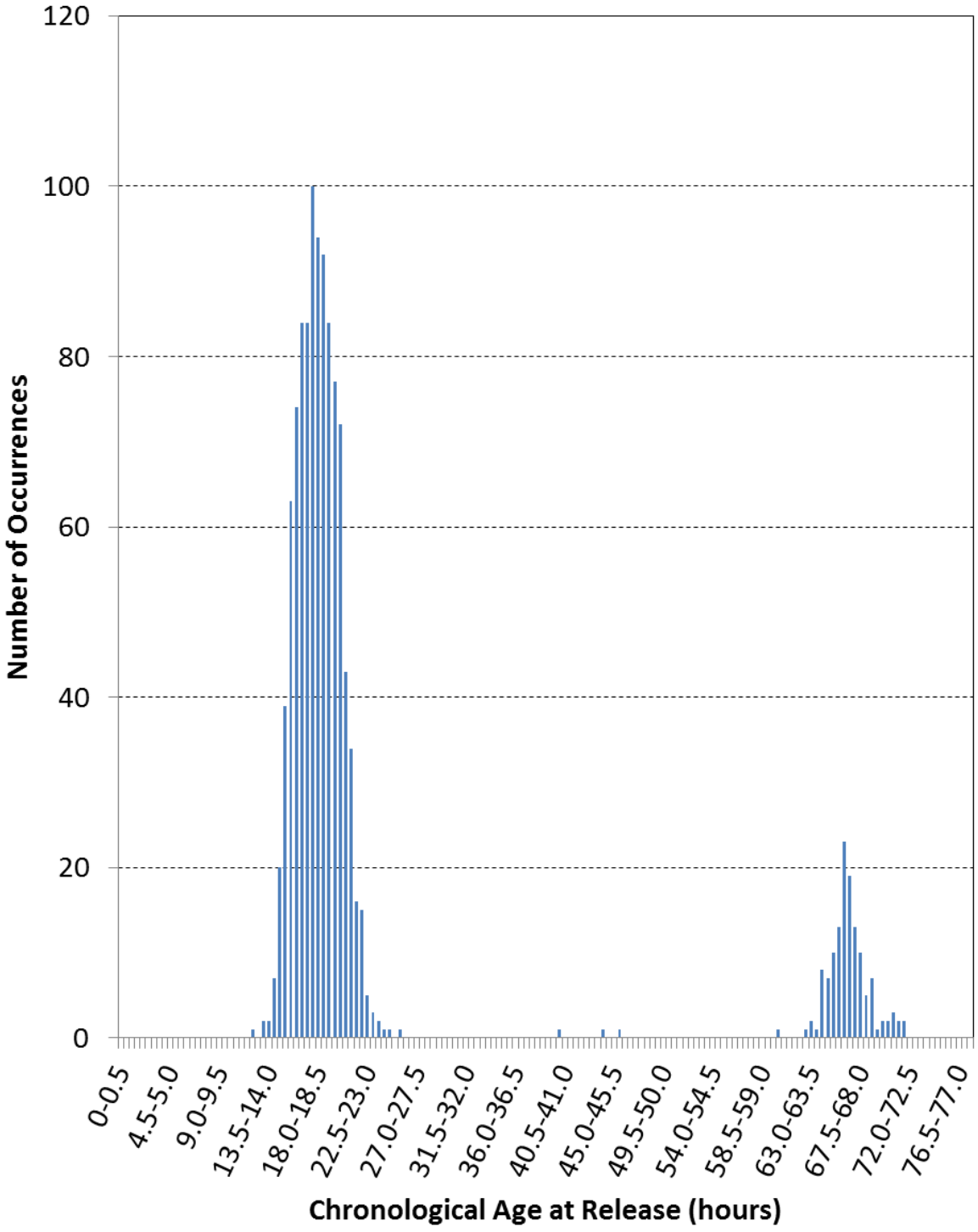

Figure B.1: Full Histogram of Release Ages for Plant A

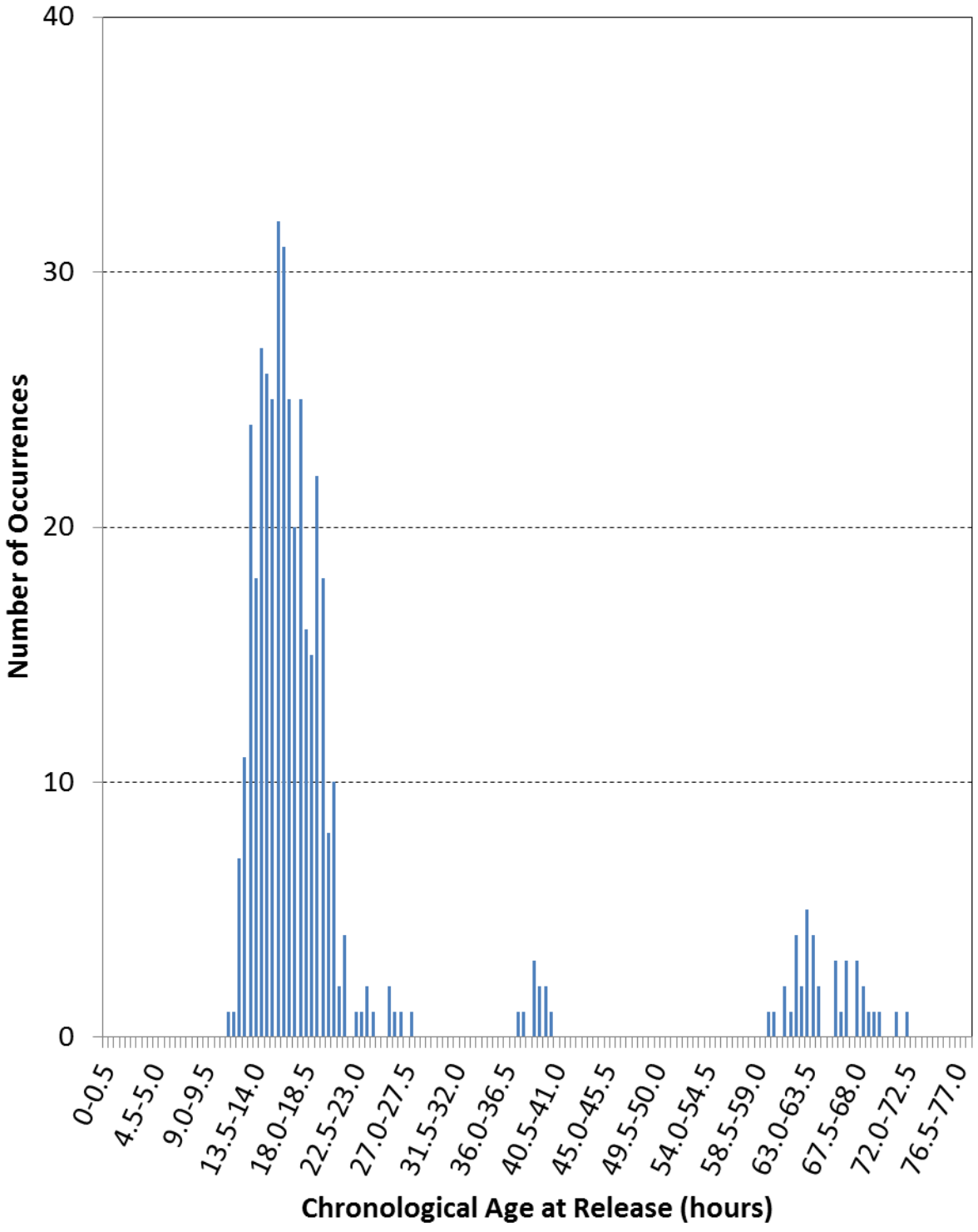

Figure B.2: Full Histogram of Release Ages for Plant B

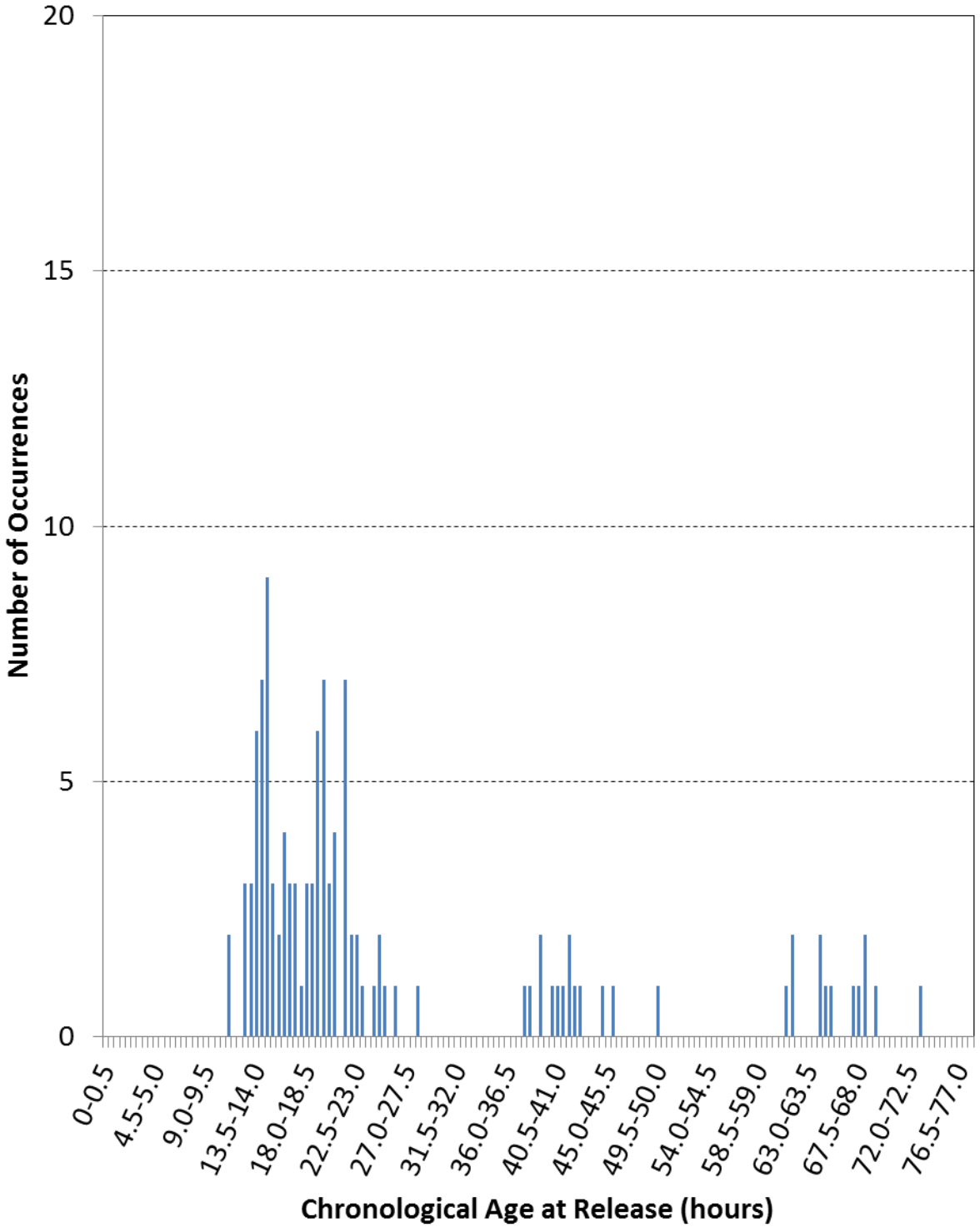

Figure B.3: Full Histogram of Release Ages for Plant C

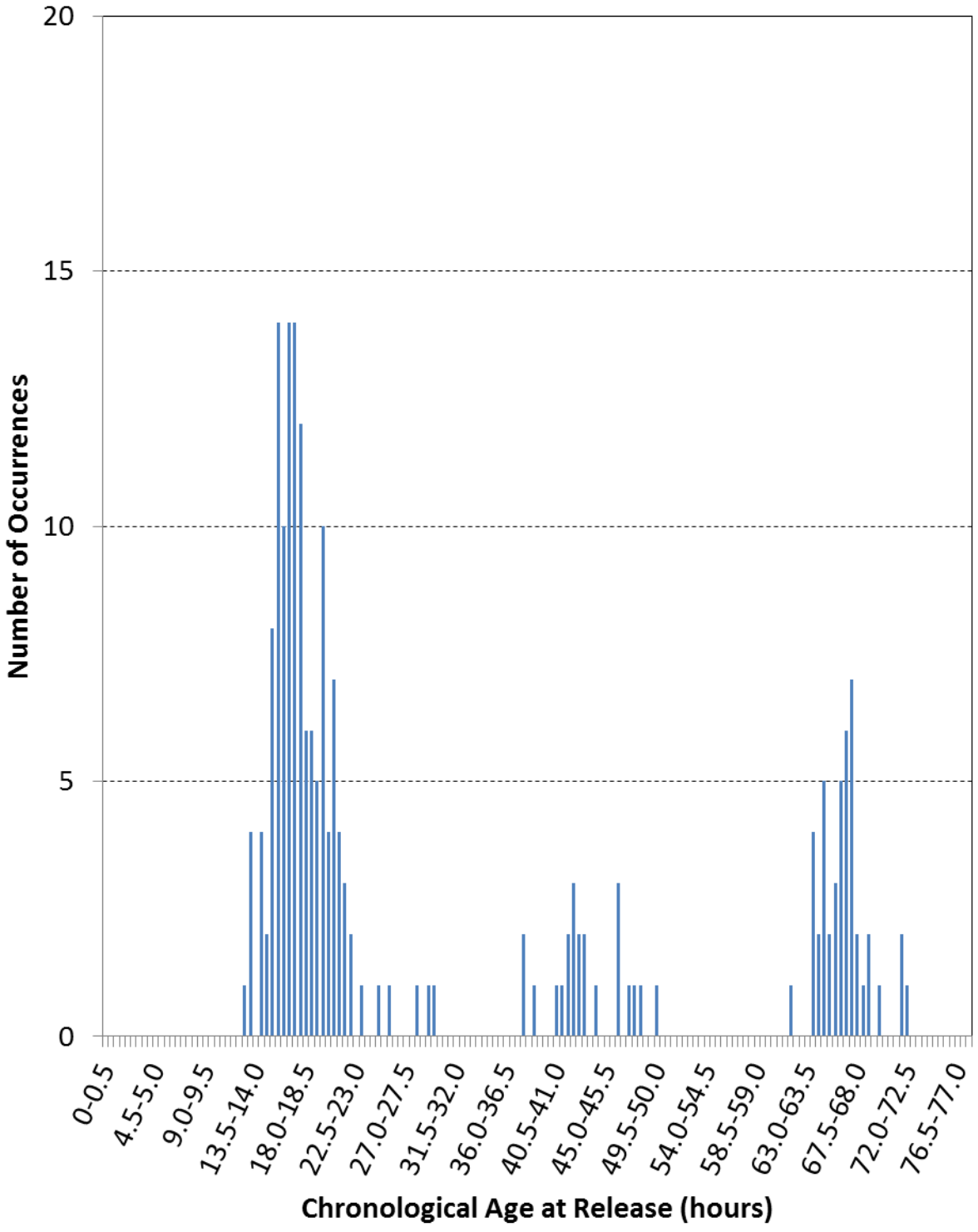

Figure B.4: Full Histogram of Release Ages for Plant D

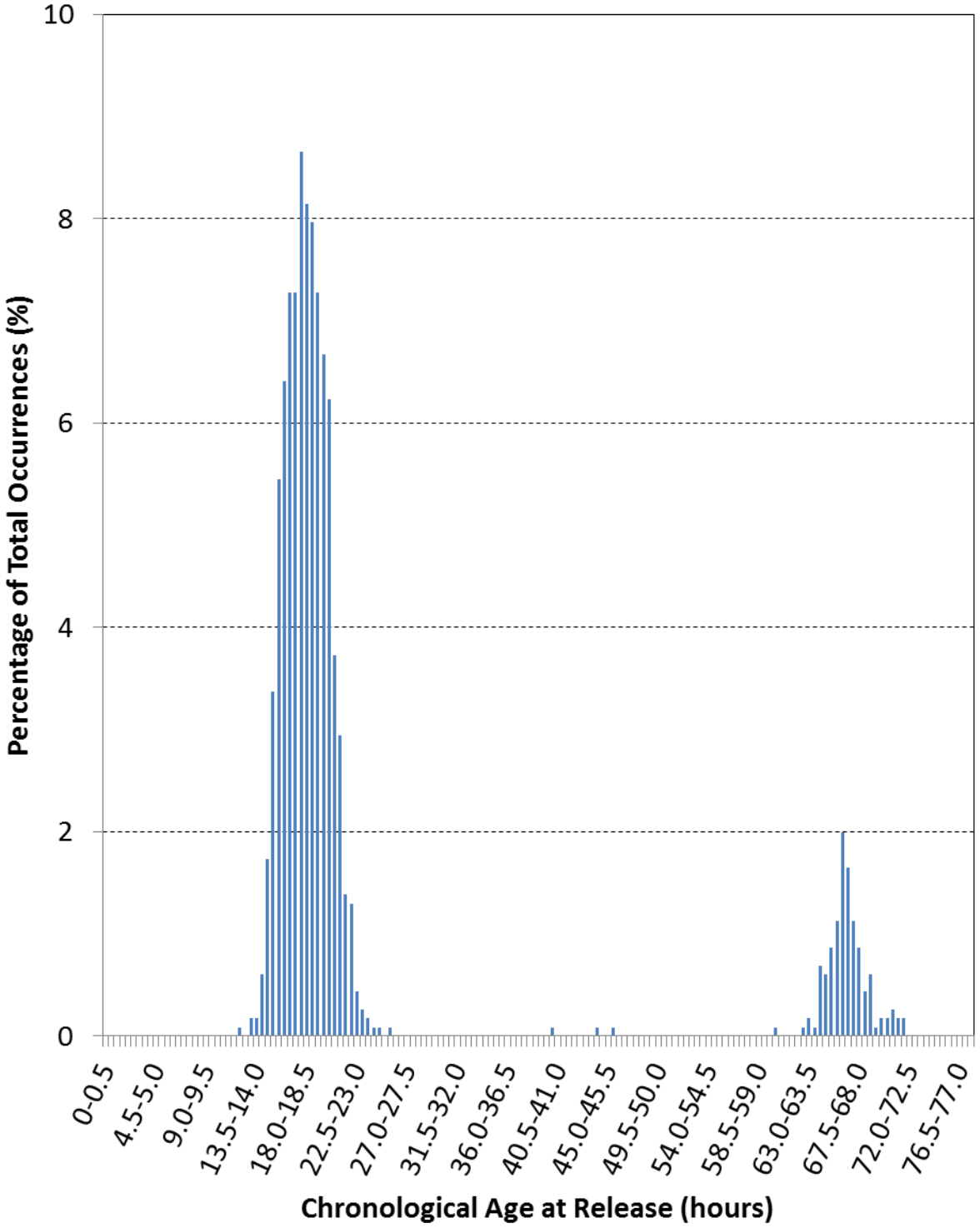

Figure B.5: Normalized Histogram of Release Ages for Plant A

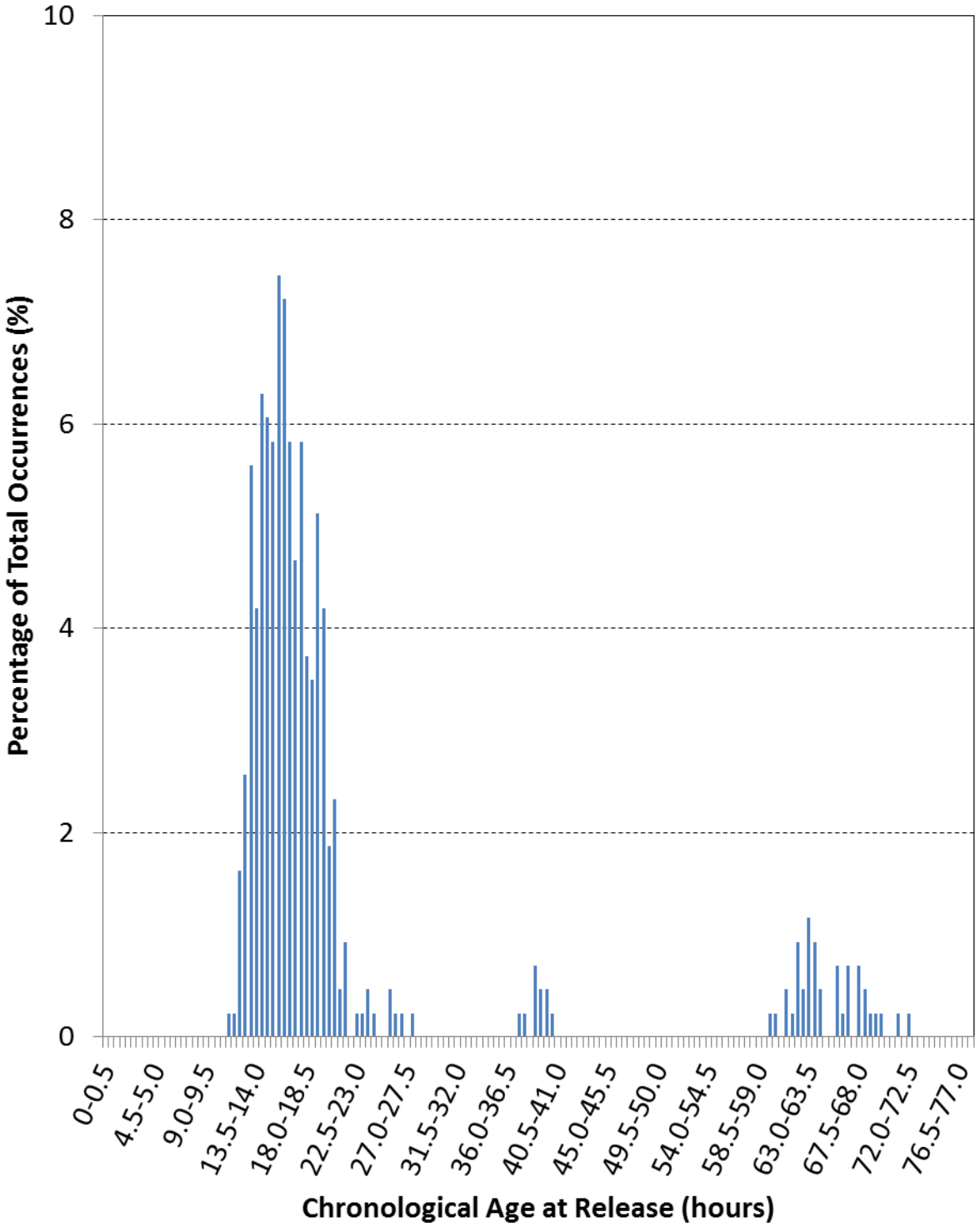

Figure B.6: Normalized Histogram of Release Ages for Plant B

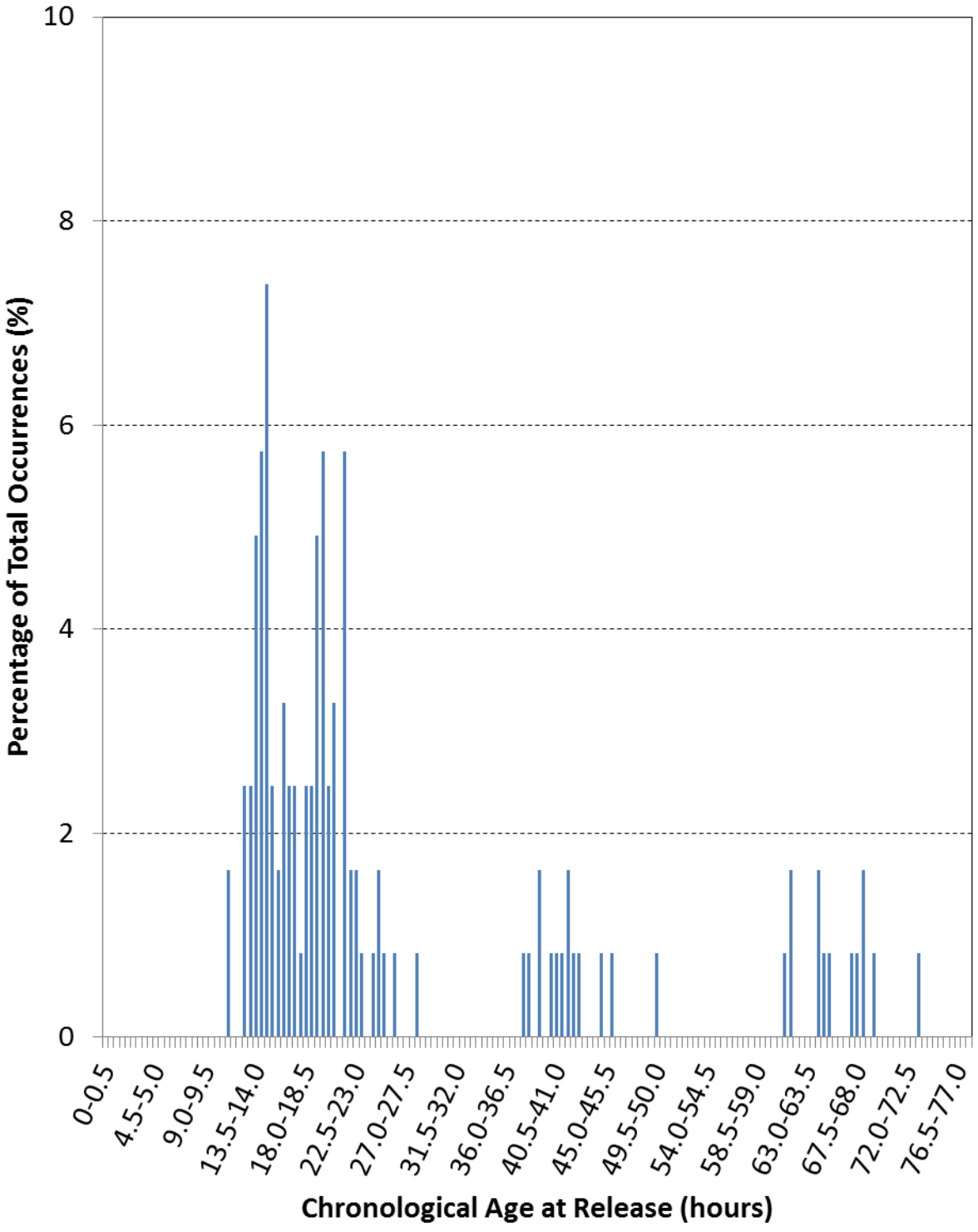

Figure B.7: Normalized Histogram of Release Ages for Plant C

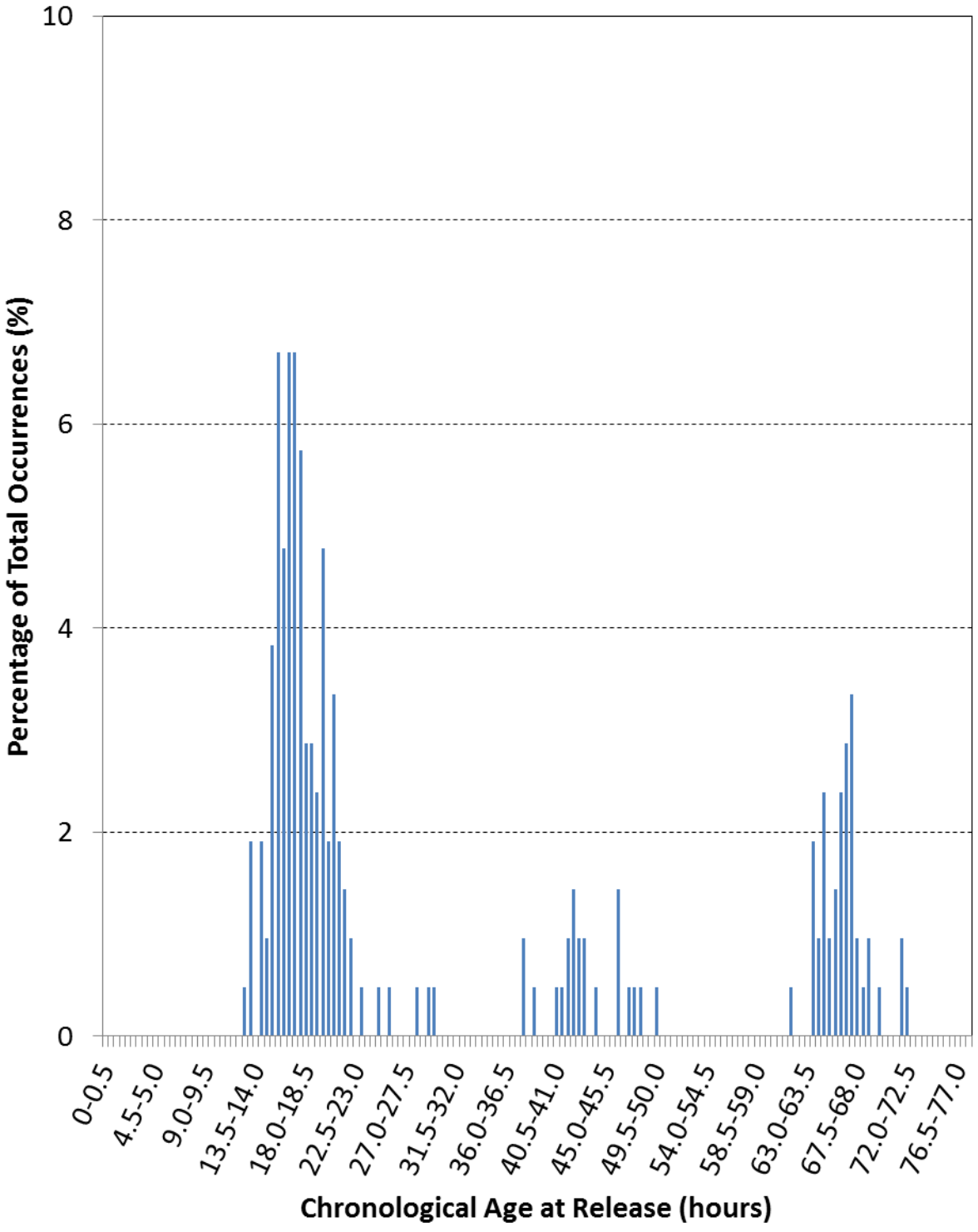

Figure B.8: Normalized Histogram of Release Ages for Plant D

Appendix C: Plant-Specific Air Content Histograms

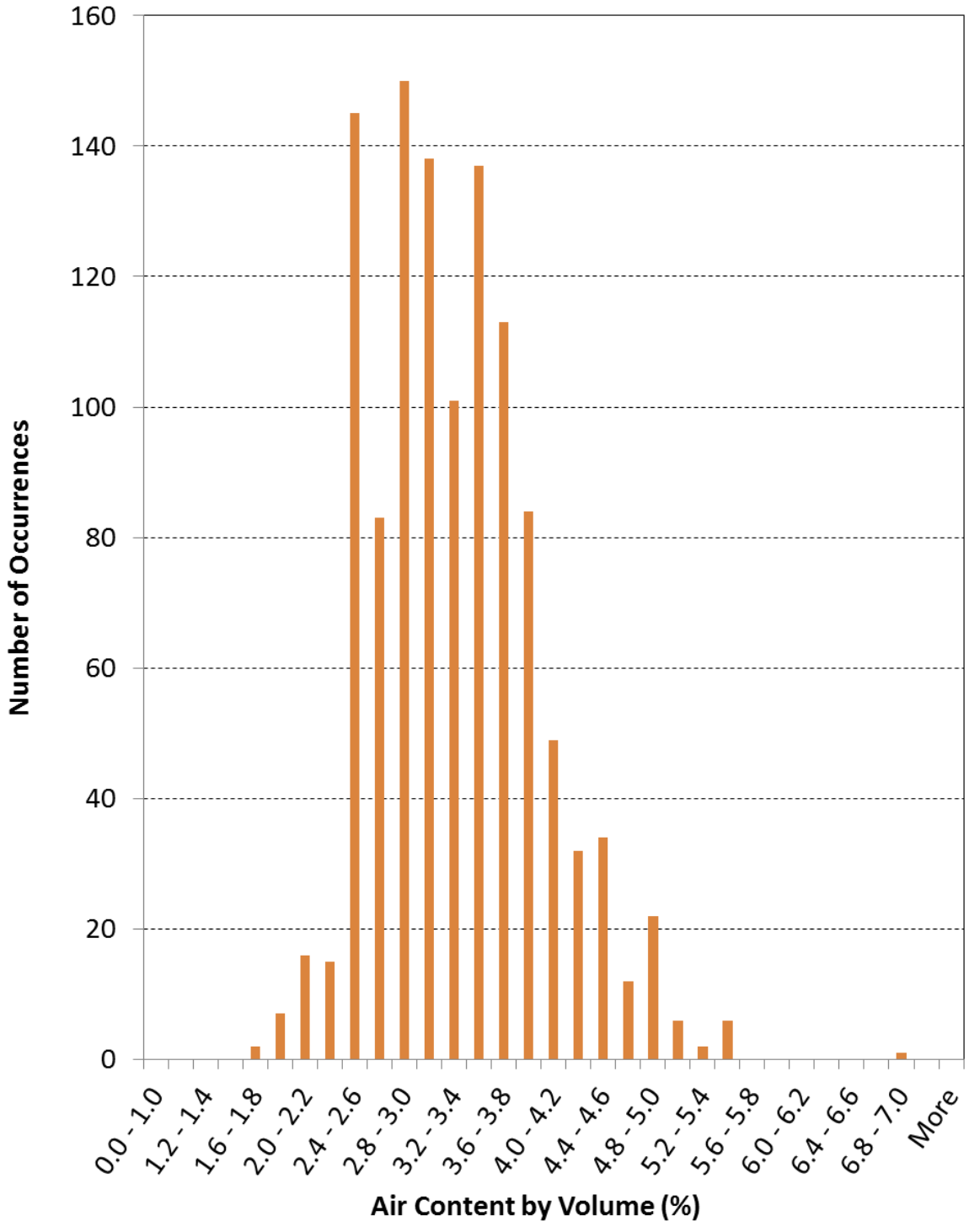

Figure C.1: Histogram of Air Contents for Plant A

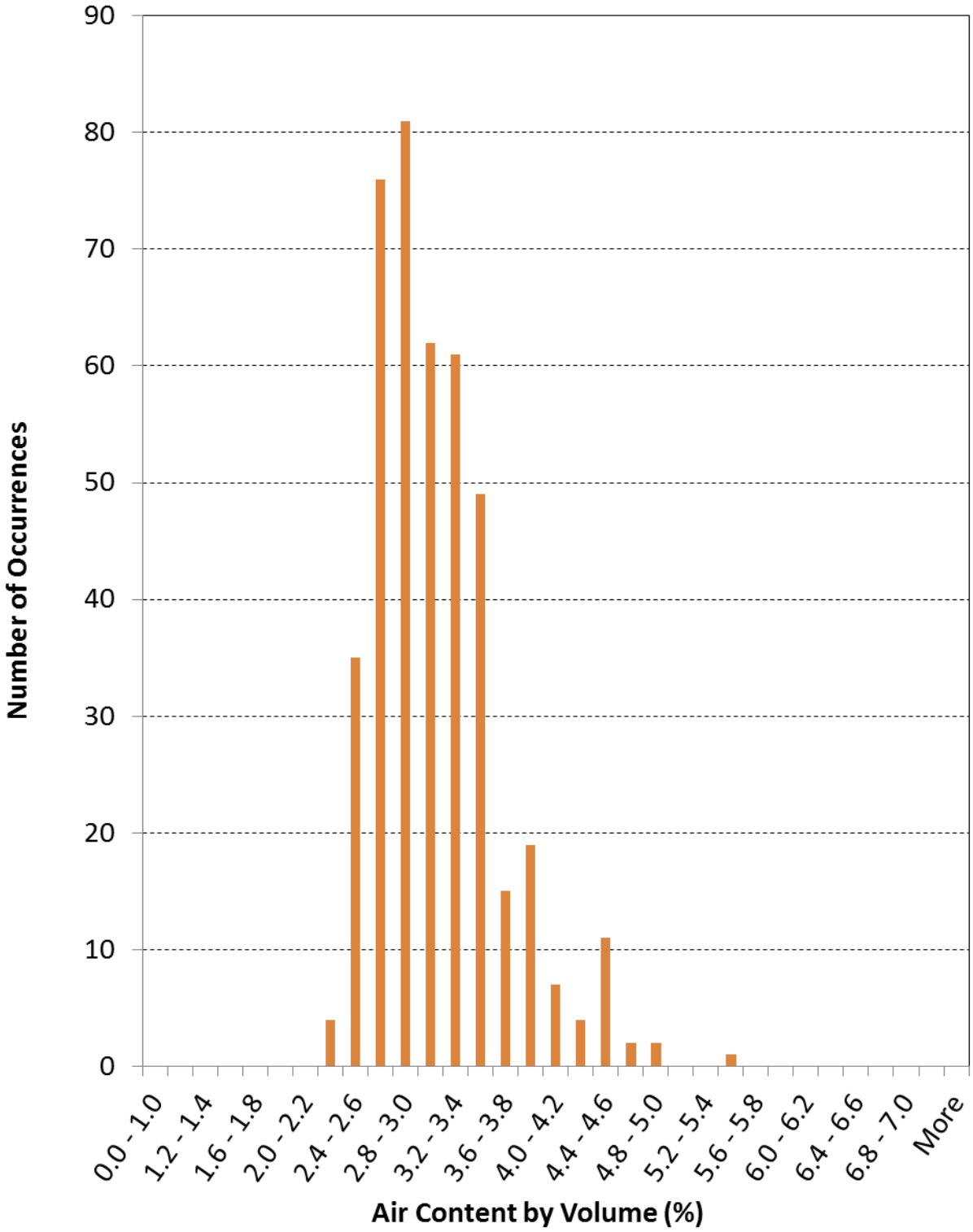

Figure C.2: Histogram of Air Contents for Plant B

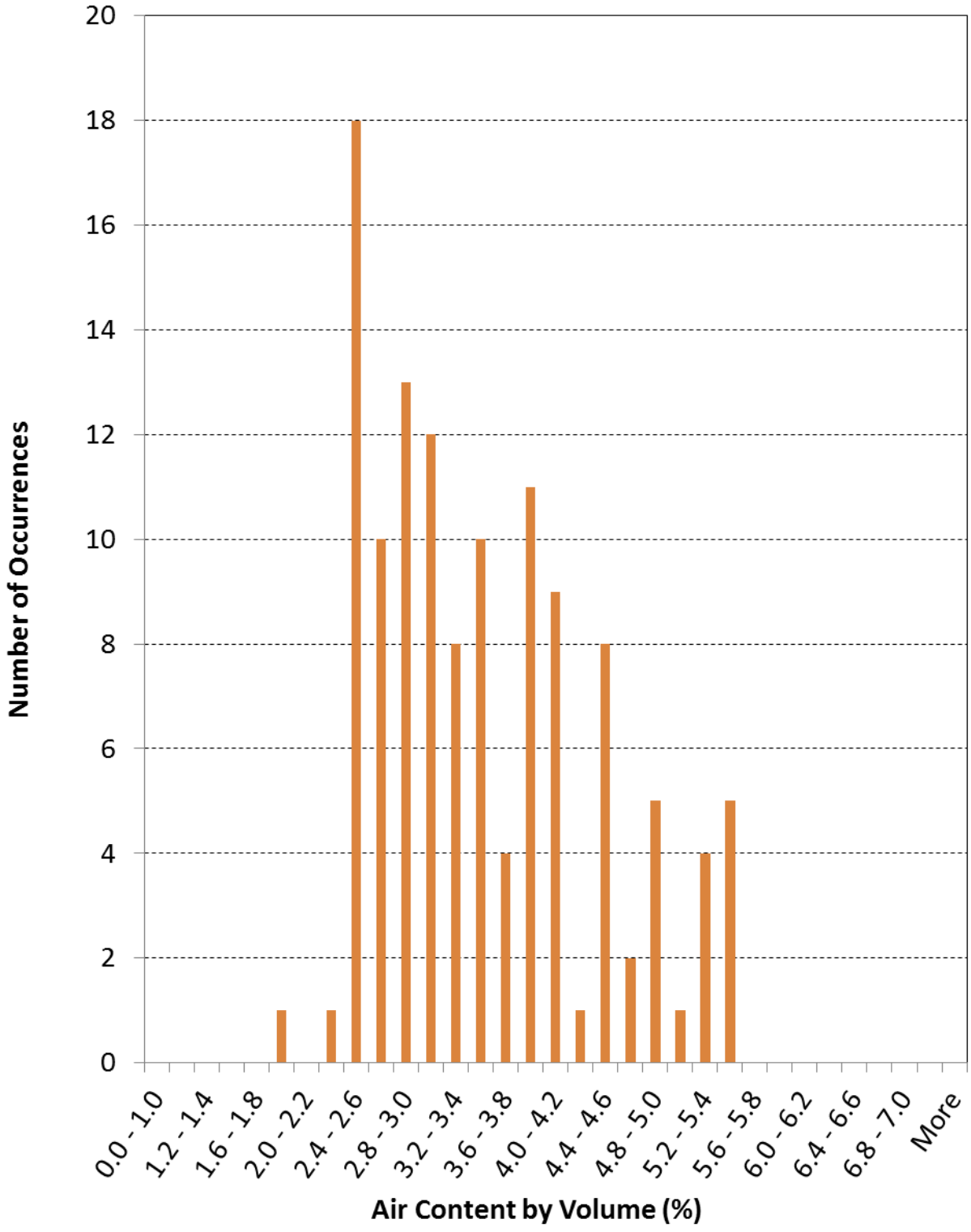

Figure C.3: Histogram of Air Contents for Plant C

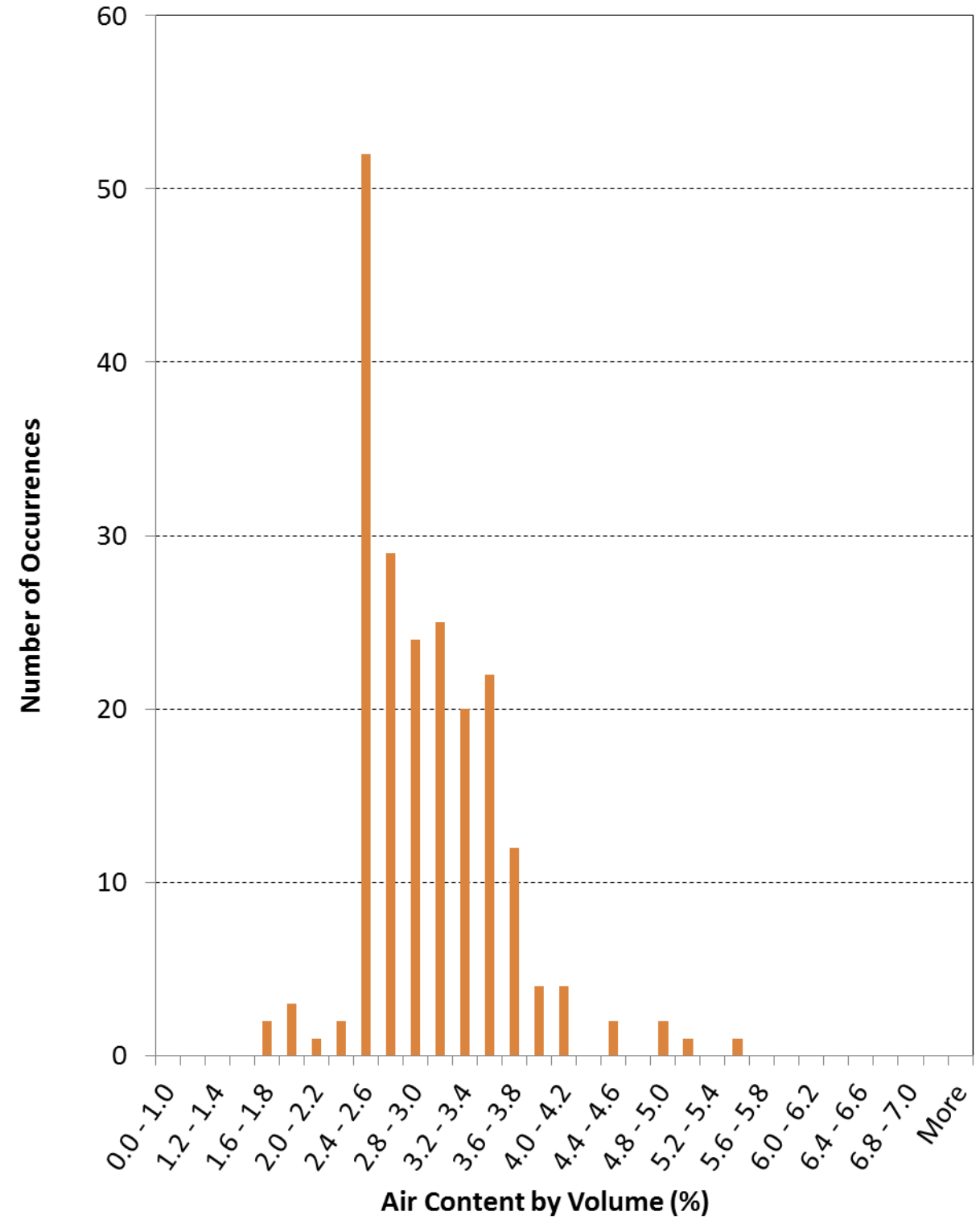

Figure C.4: Histogram of Air Contents for Plant D

Appendix D: Plant-Specific Slump Measurement Histograms

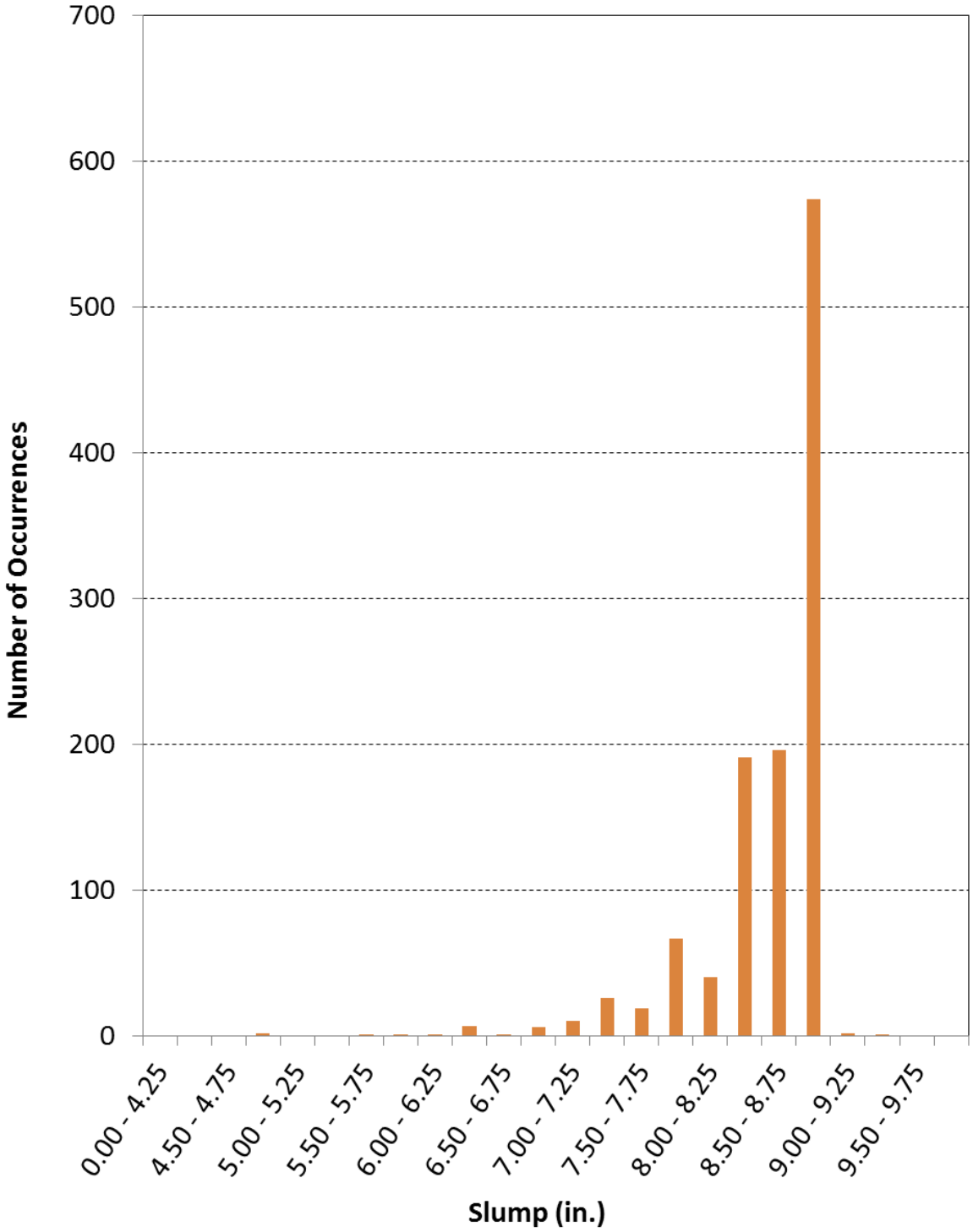

Figure D.1: Histogram of Slump Measurements for Plant A

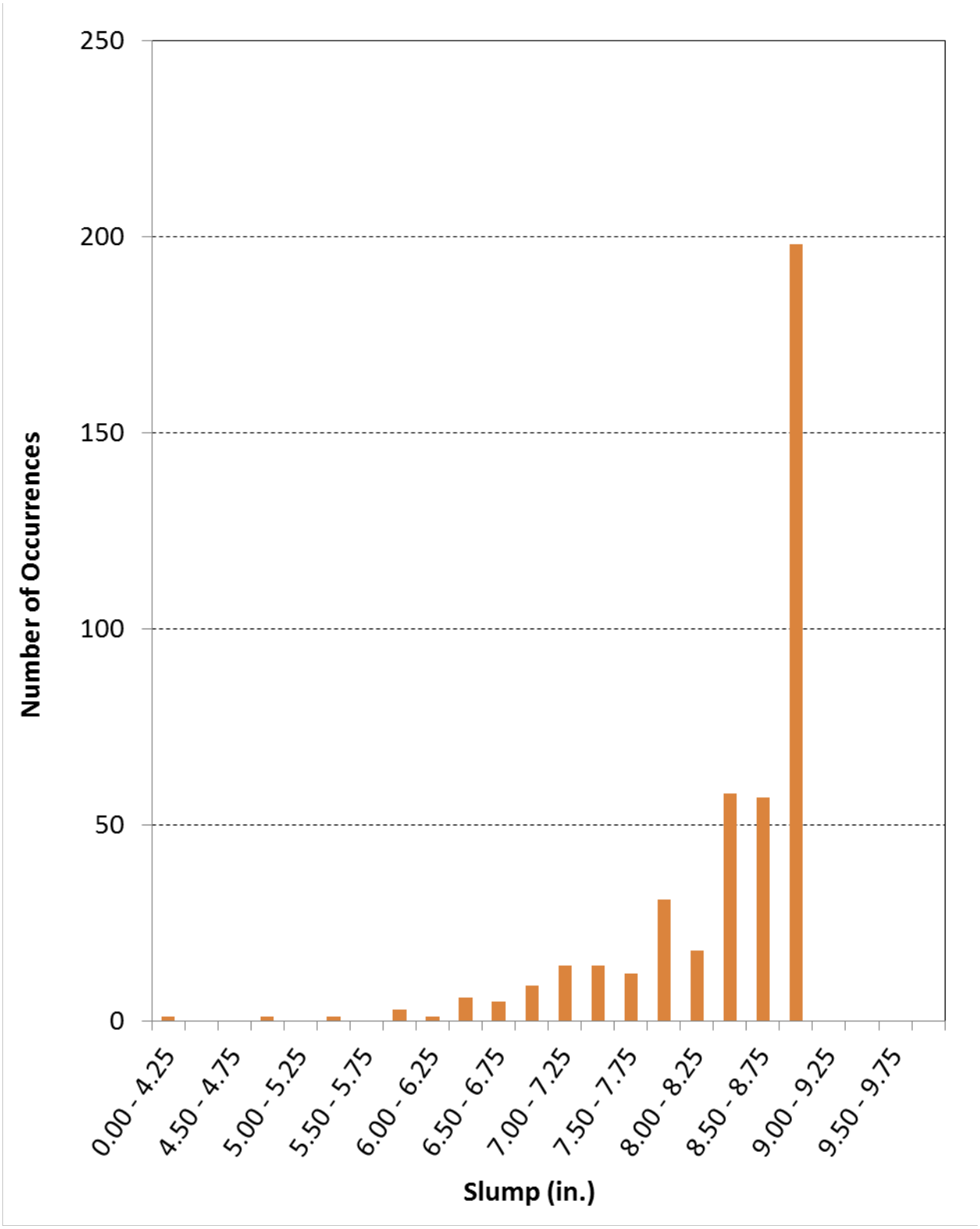

Figure D.2: Histogram of Slump Measurements for Plant B

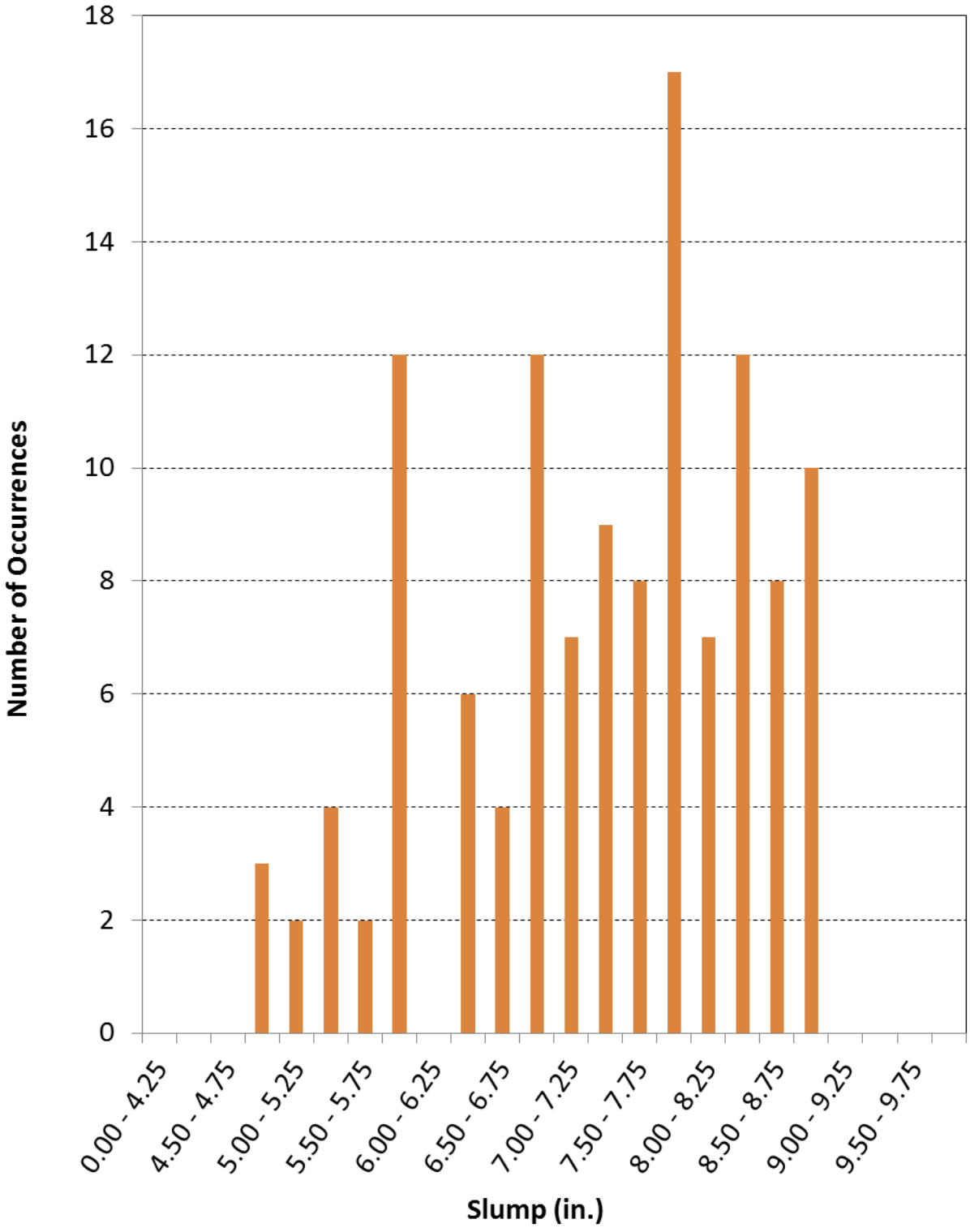

Figure D.3: Histogram of Slump Measurements for Plant C

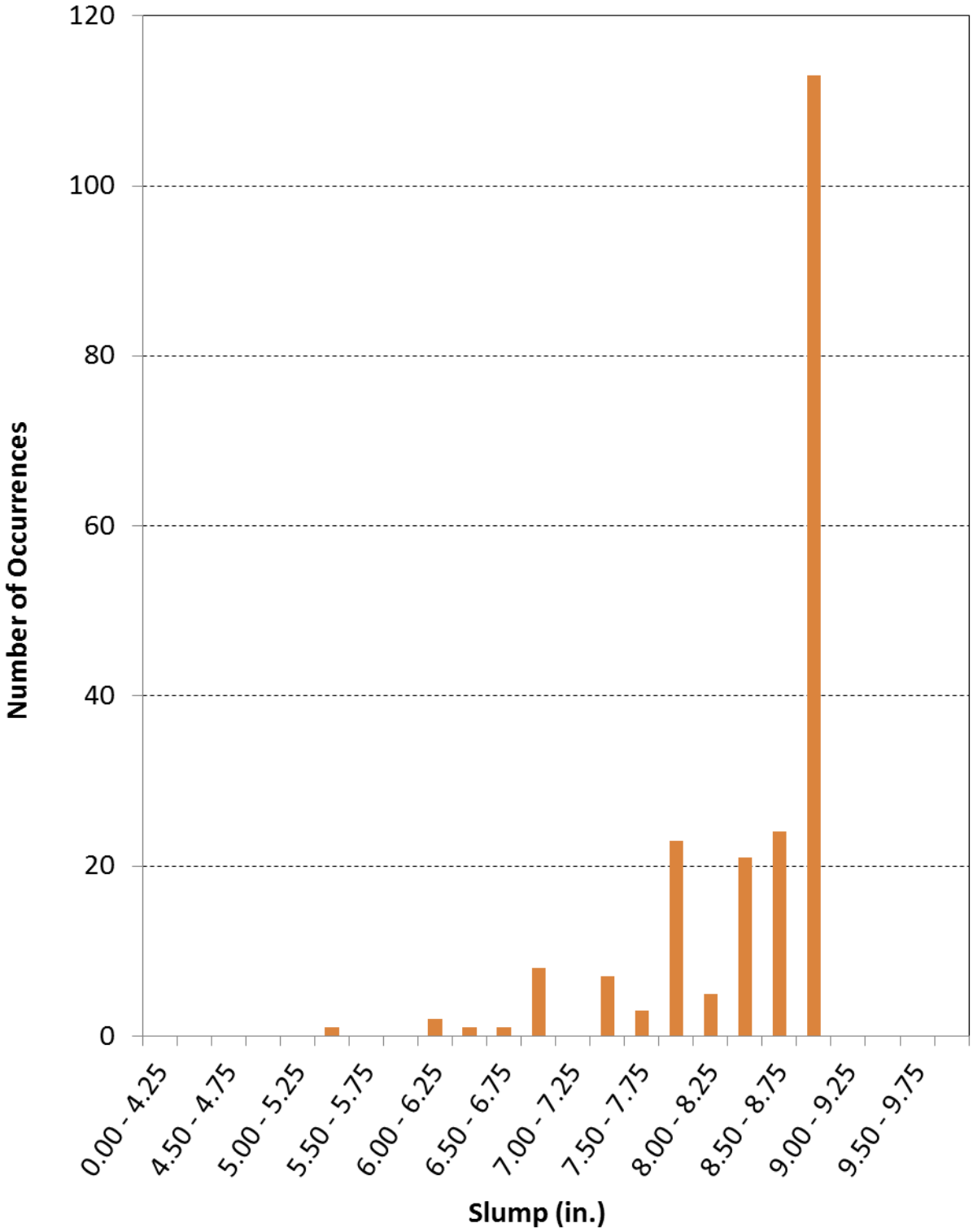

Figure D.4: Histogram of Slump Measurements for Plant D

Appendix E: Plant-Specific Release Strength Scatter Plots and Histograms

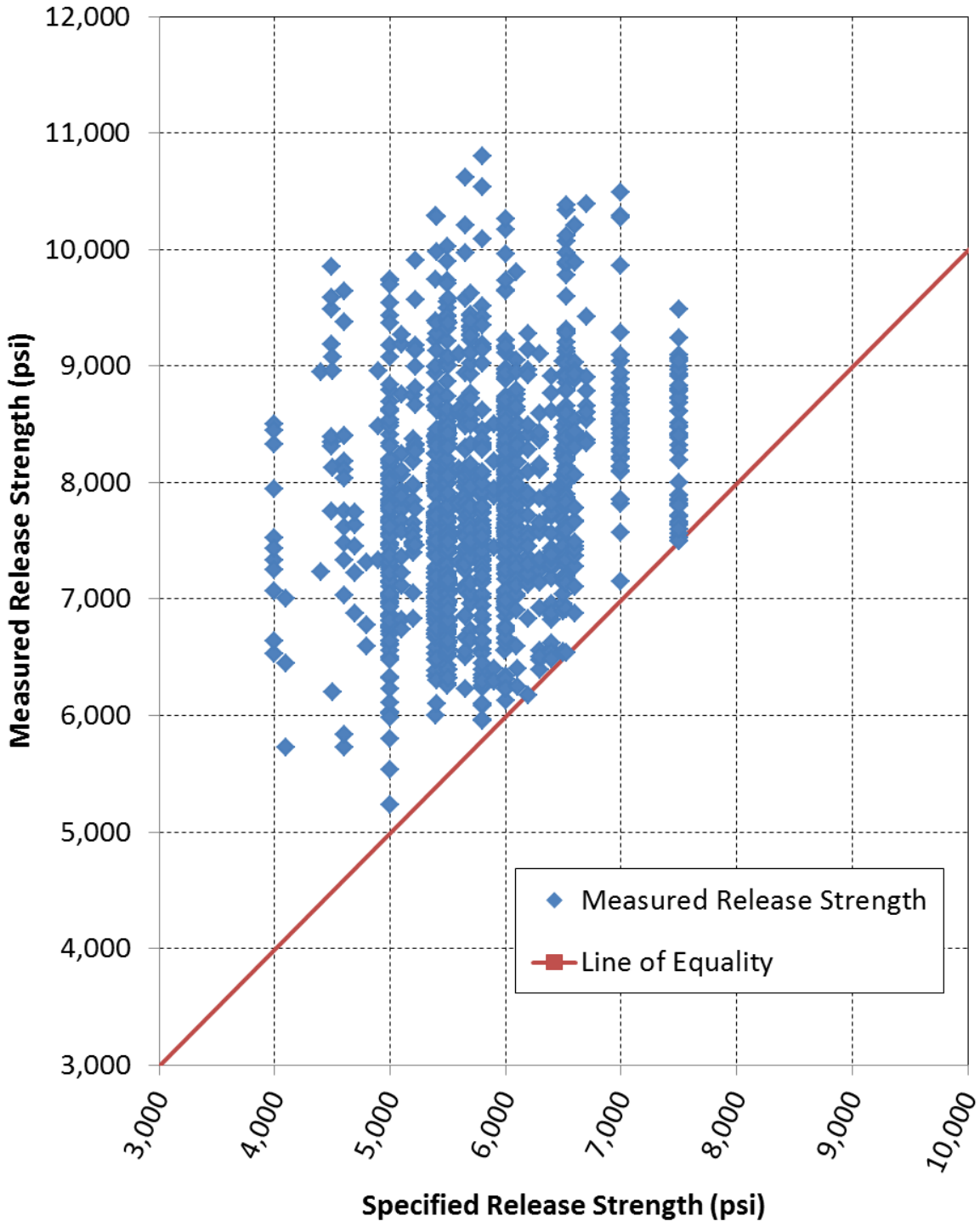

Figure E.1: Measured Release Strengths versus Specified Release Strengths for Plant A

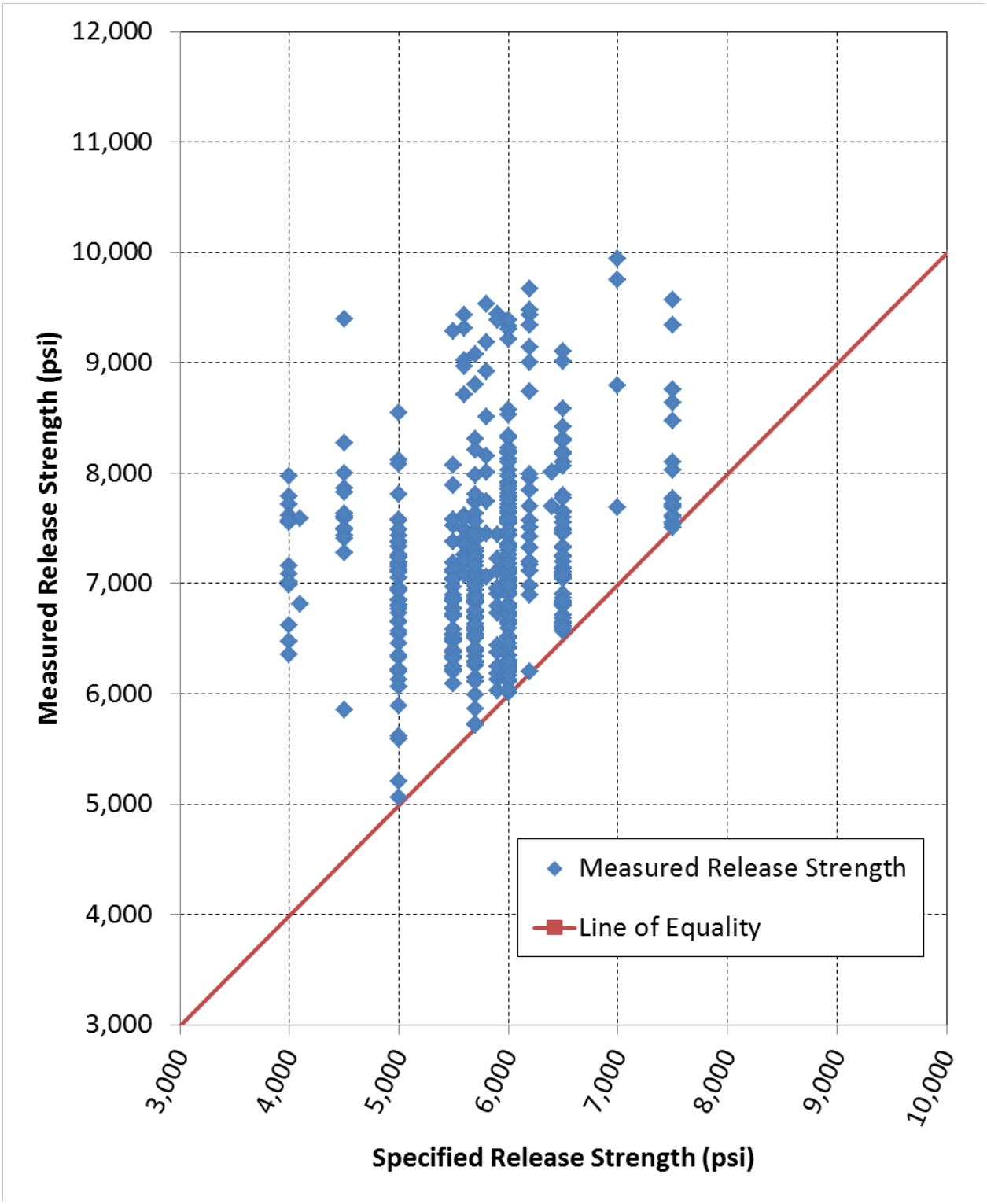

Figure E.2: Measured Release Strengths versus Specified Release Strengths for Plant B

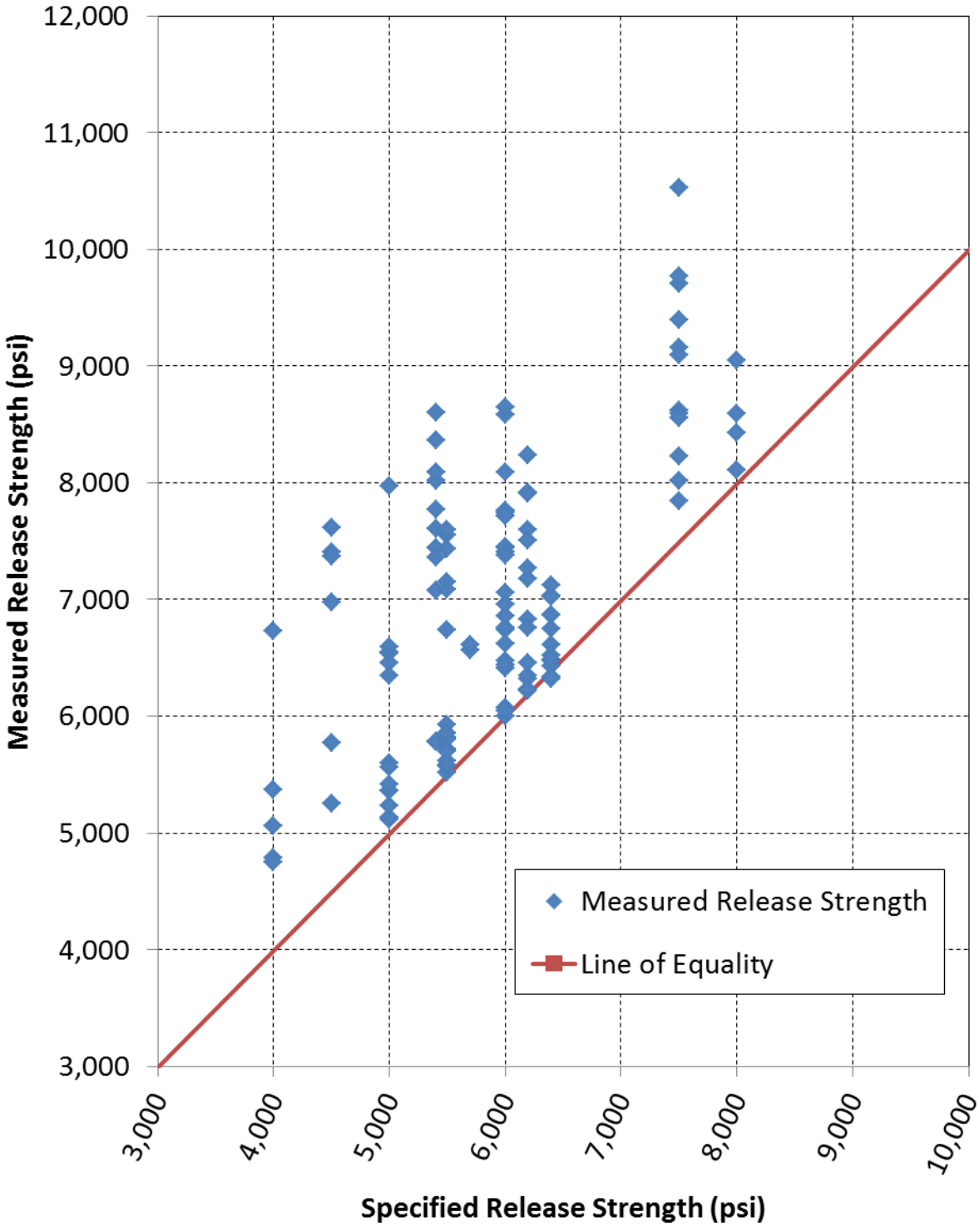

Figure E.3: Measured Release Strengths versus Specified Release Strengths for Plant C

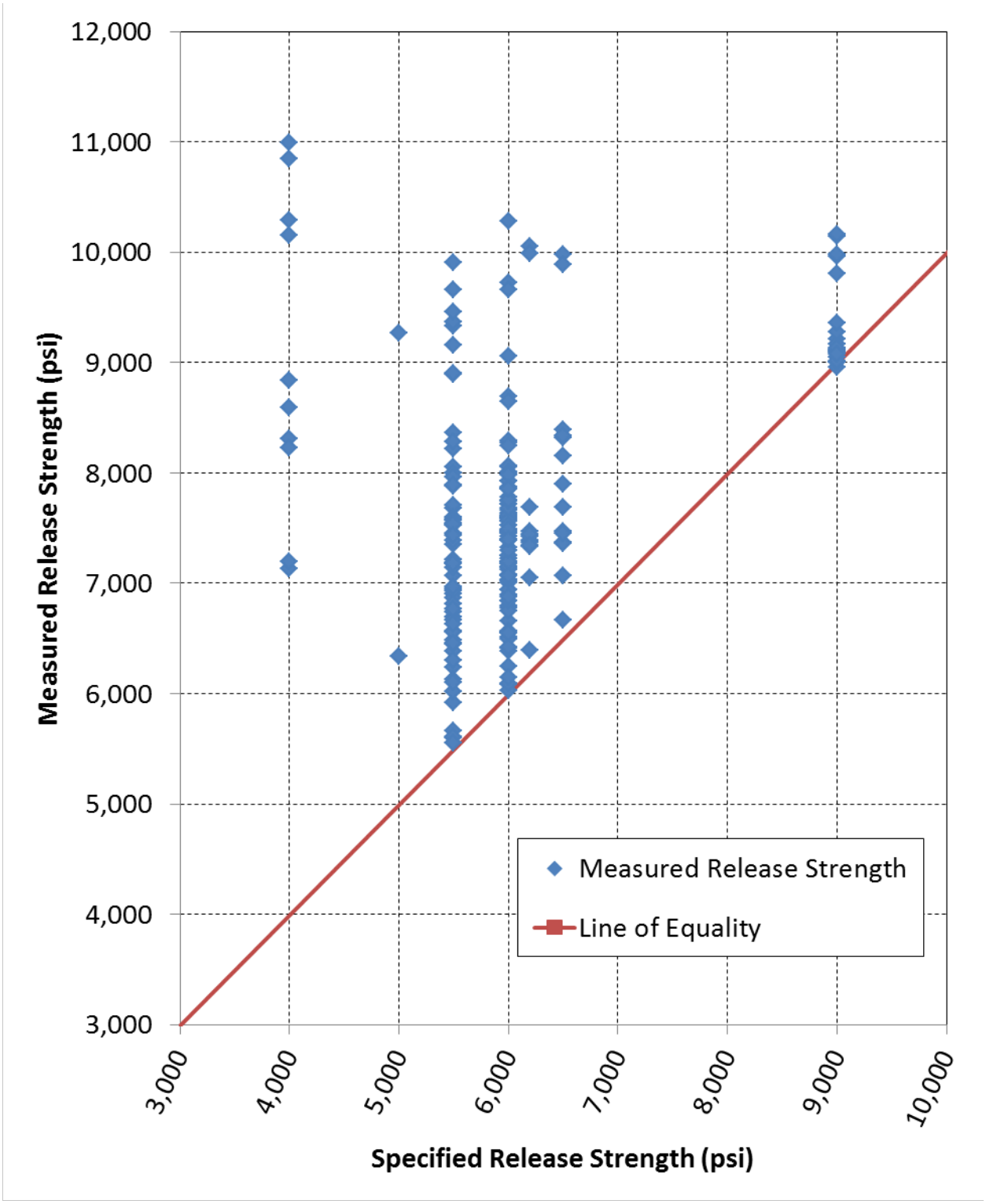

Figure E.4: Measured Release Strengths versus Specified Release Strengths for Plant D

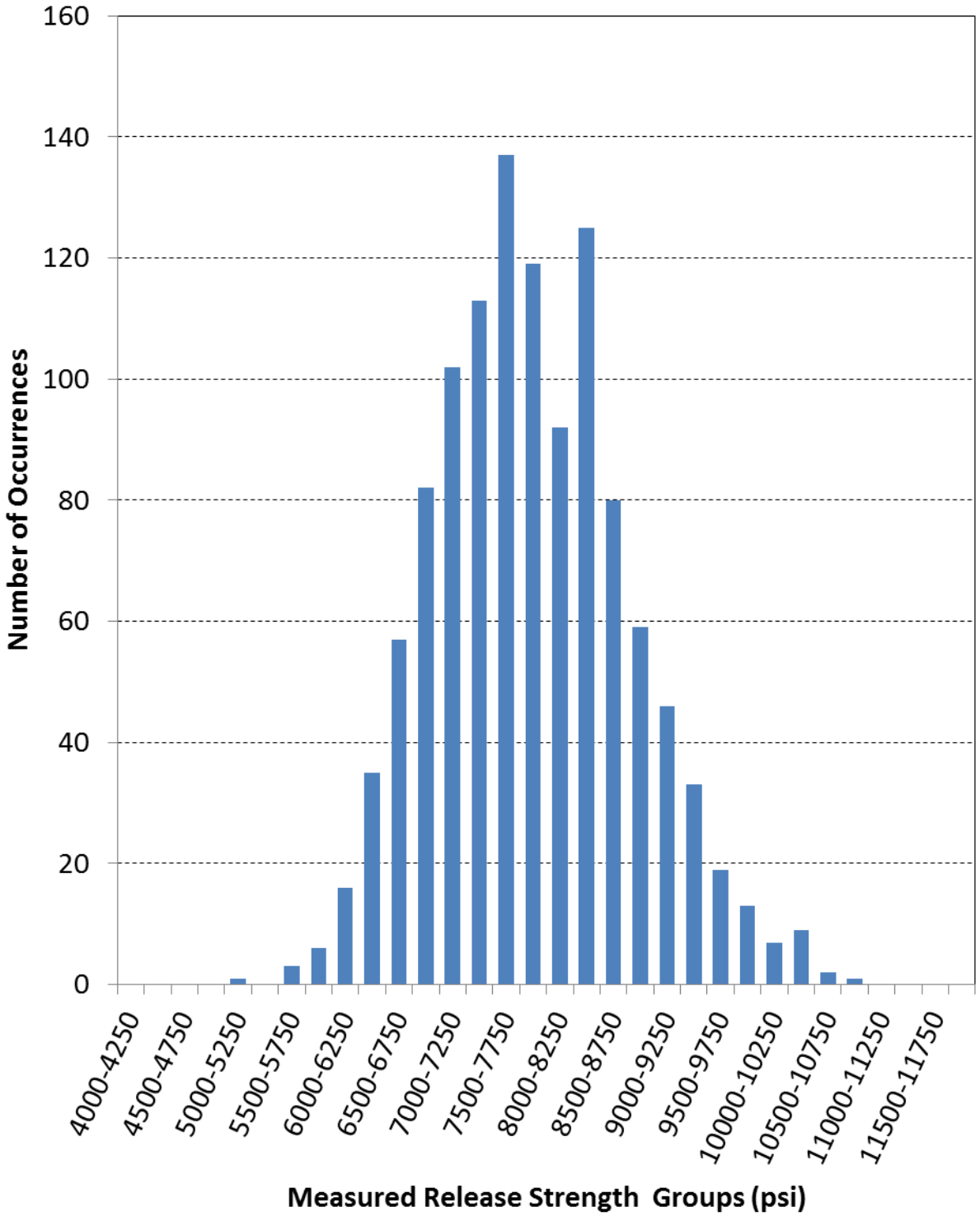

Figure E.5: Histogram of Measured Release Strengths from Plant A

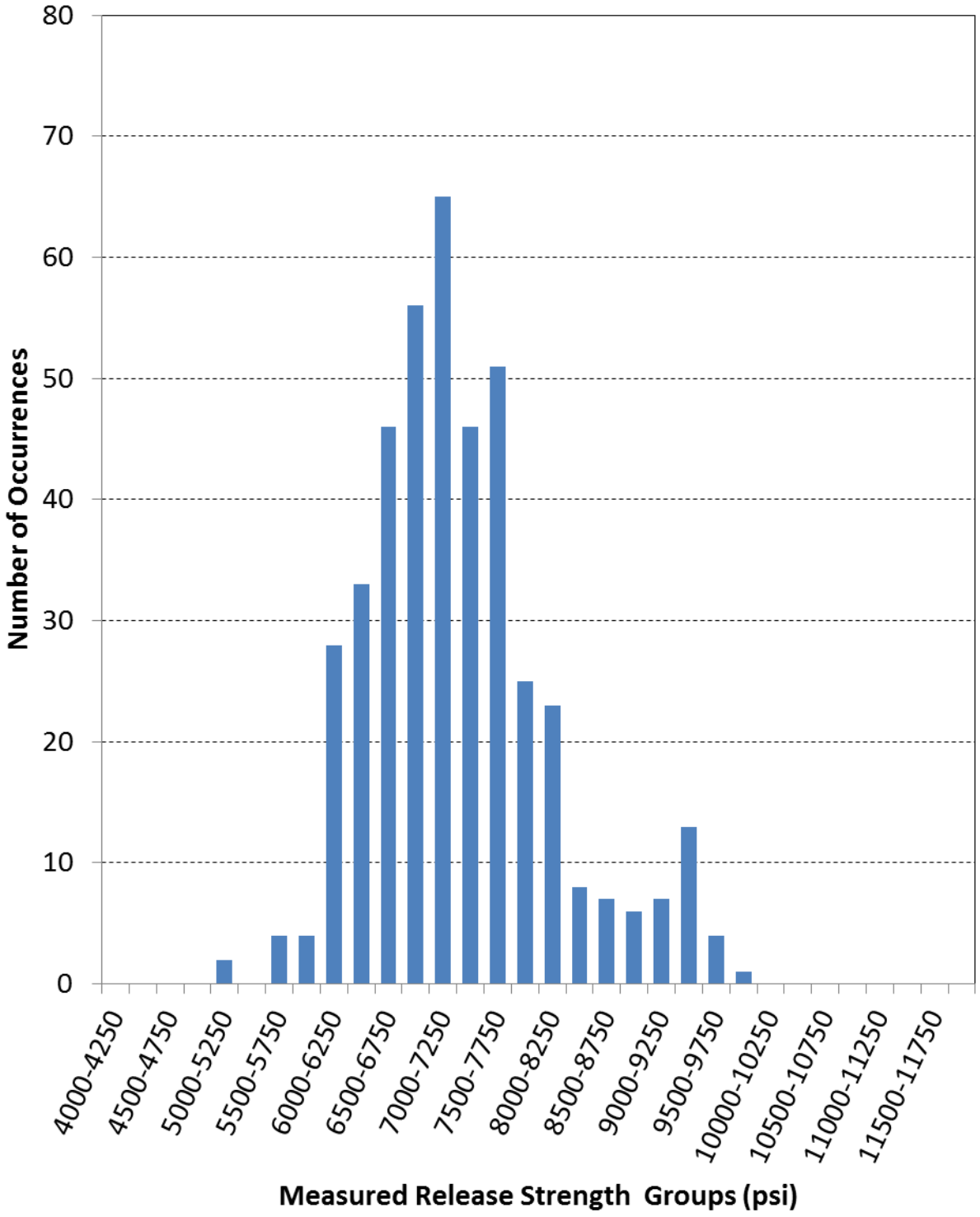

Figure E.6: Histogram of Measured Release Strengths from Plant B

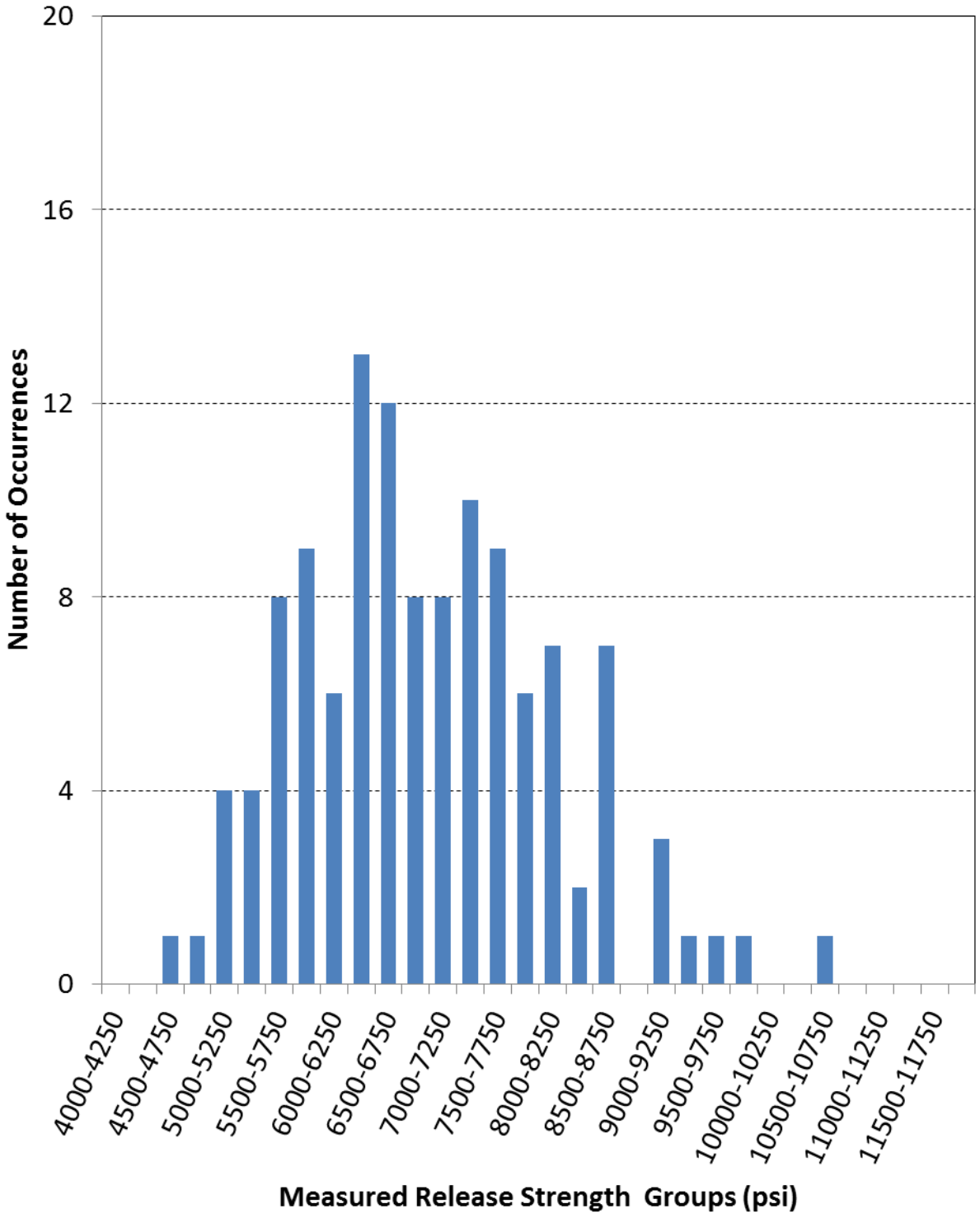

Figure E.7: Histogram of Measured Release Strengths from Plant C

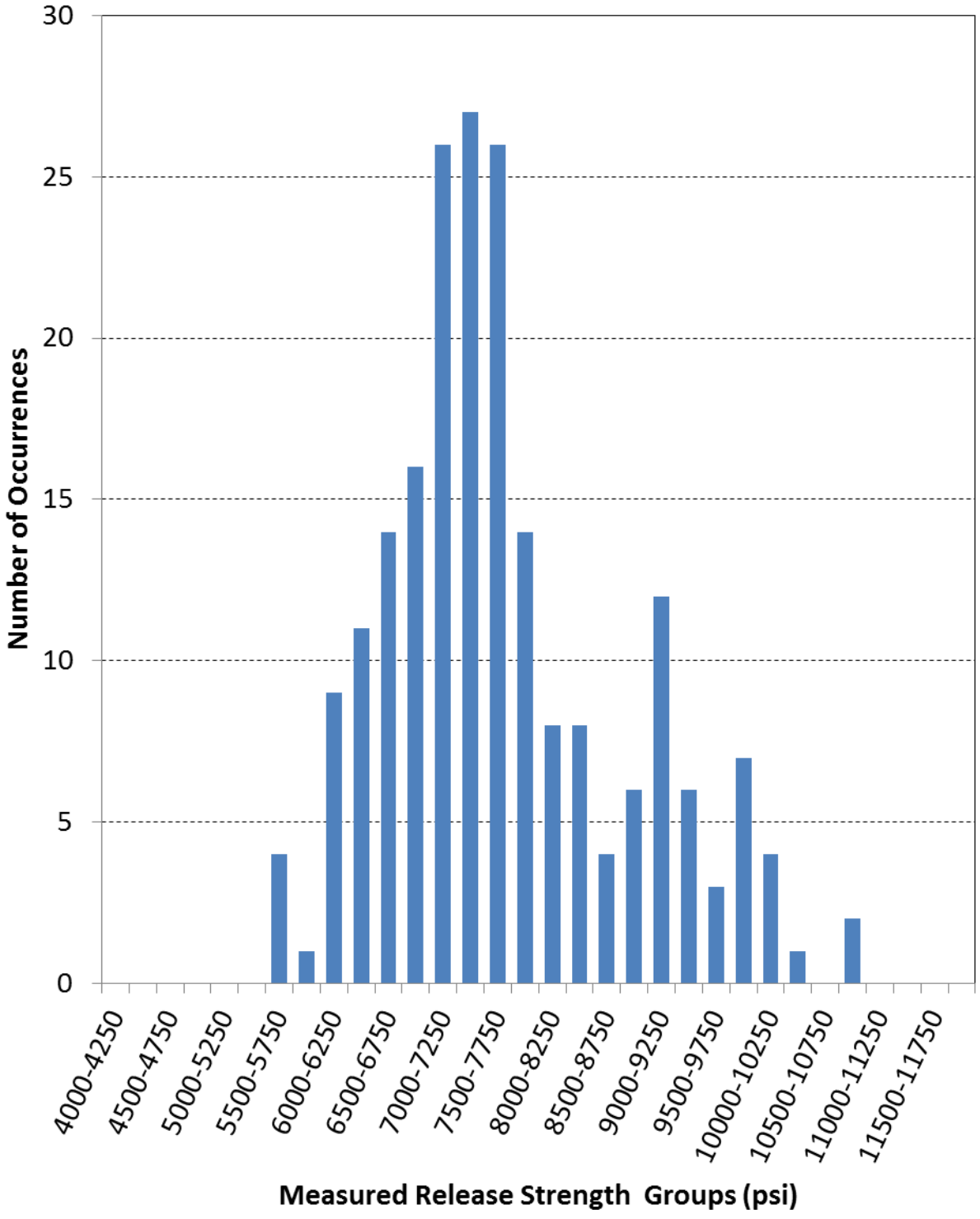

Figure E.8: Histogram of Measured Release Strengths from Plant D

Appendix F: Plant-Specific 28-Day Strength Scatter Plots and Histograms

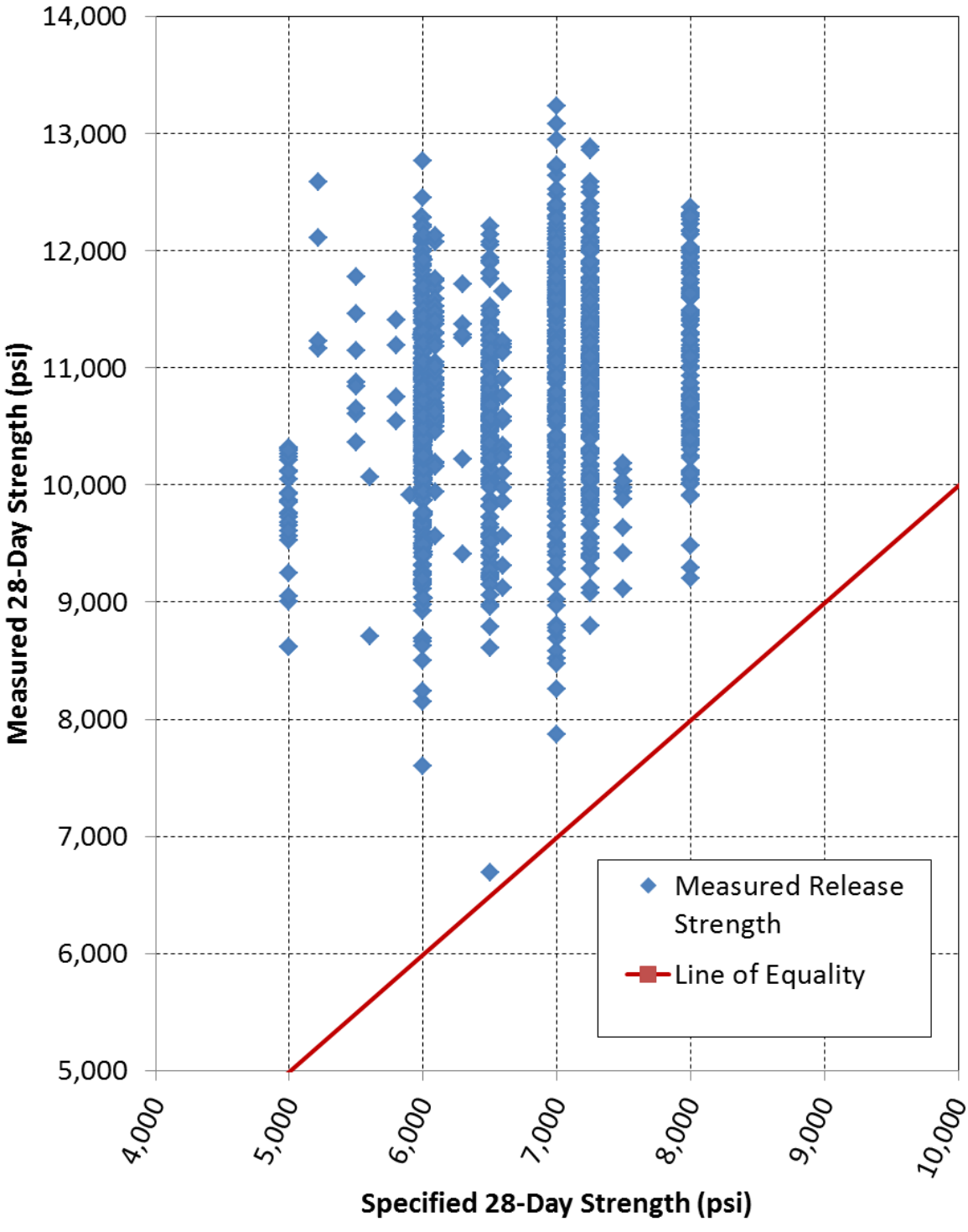

Figure F.1: Measured 28-Day Strengths versus Specified 28-Day Strengths for Plant A

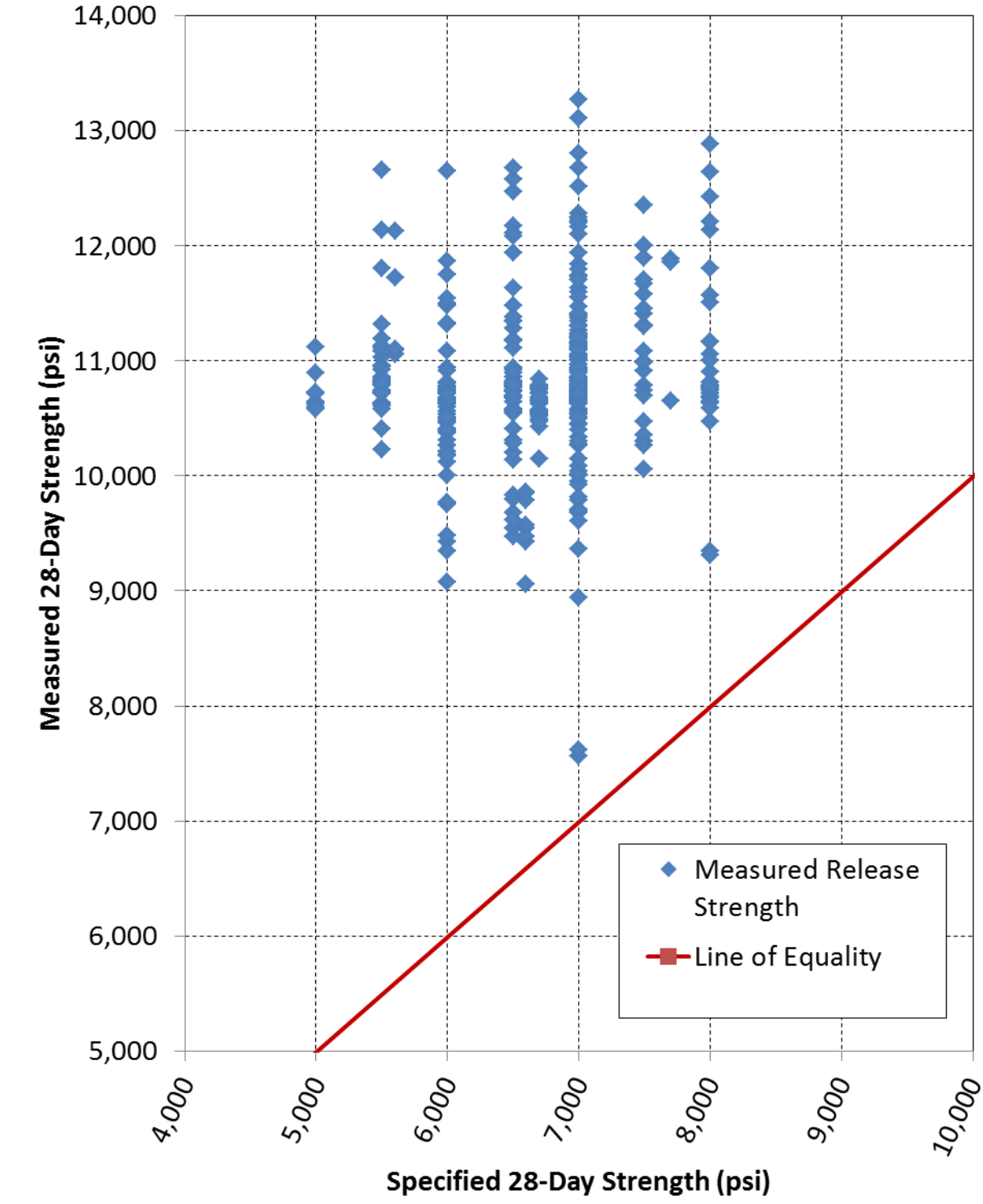

Figure F.2: Measured 28-Day Strengths versus Specified 28-Day Strengths for Plant B

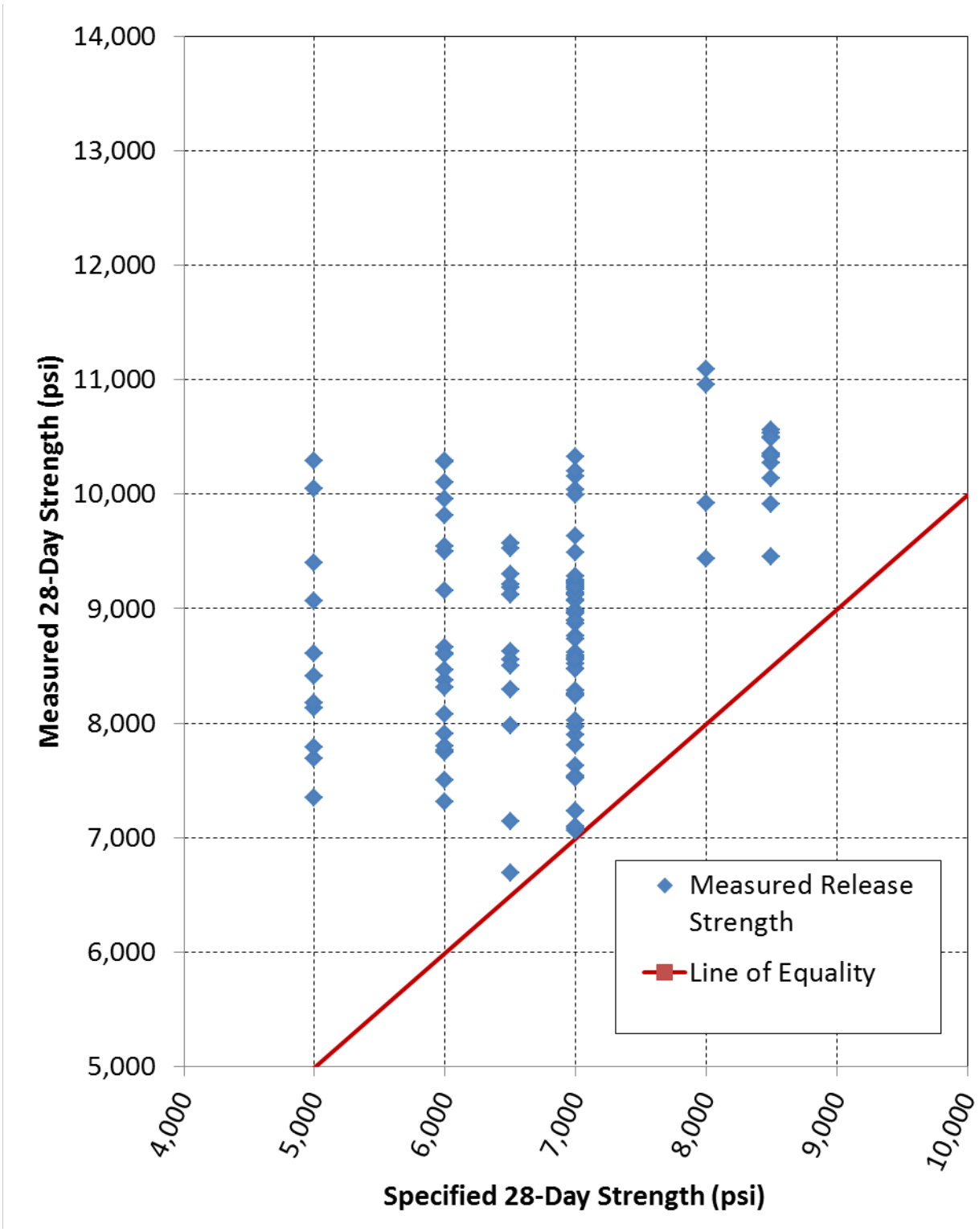

Figure F.3: Measured 28-Day Strengths versus Specified 28-Day Strengths for Plant C

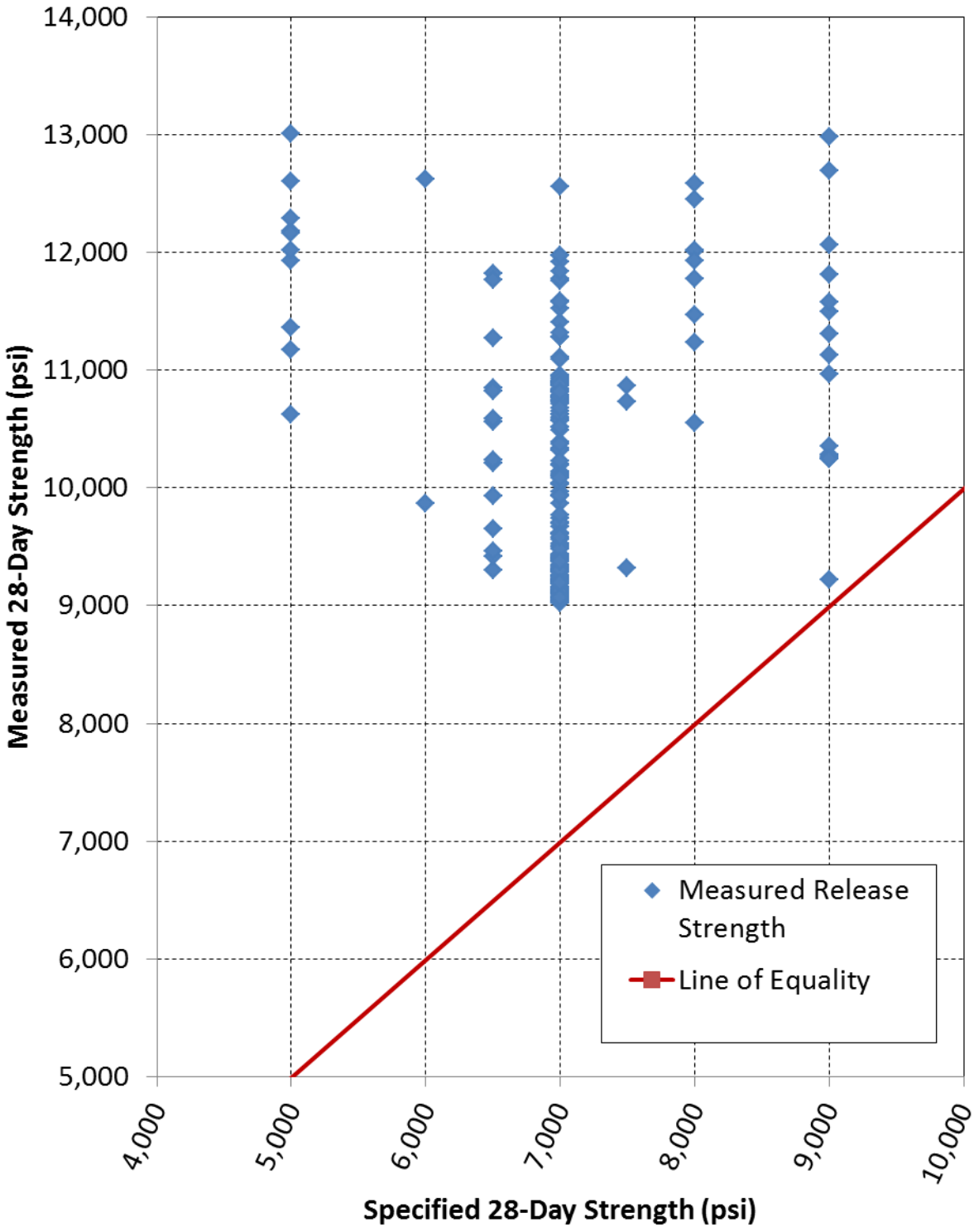

Figure F.4: Measured 28-Day Strengths versus Specified 28-Day Strengths for Plant D

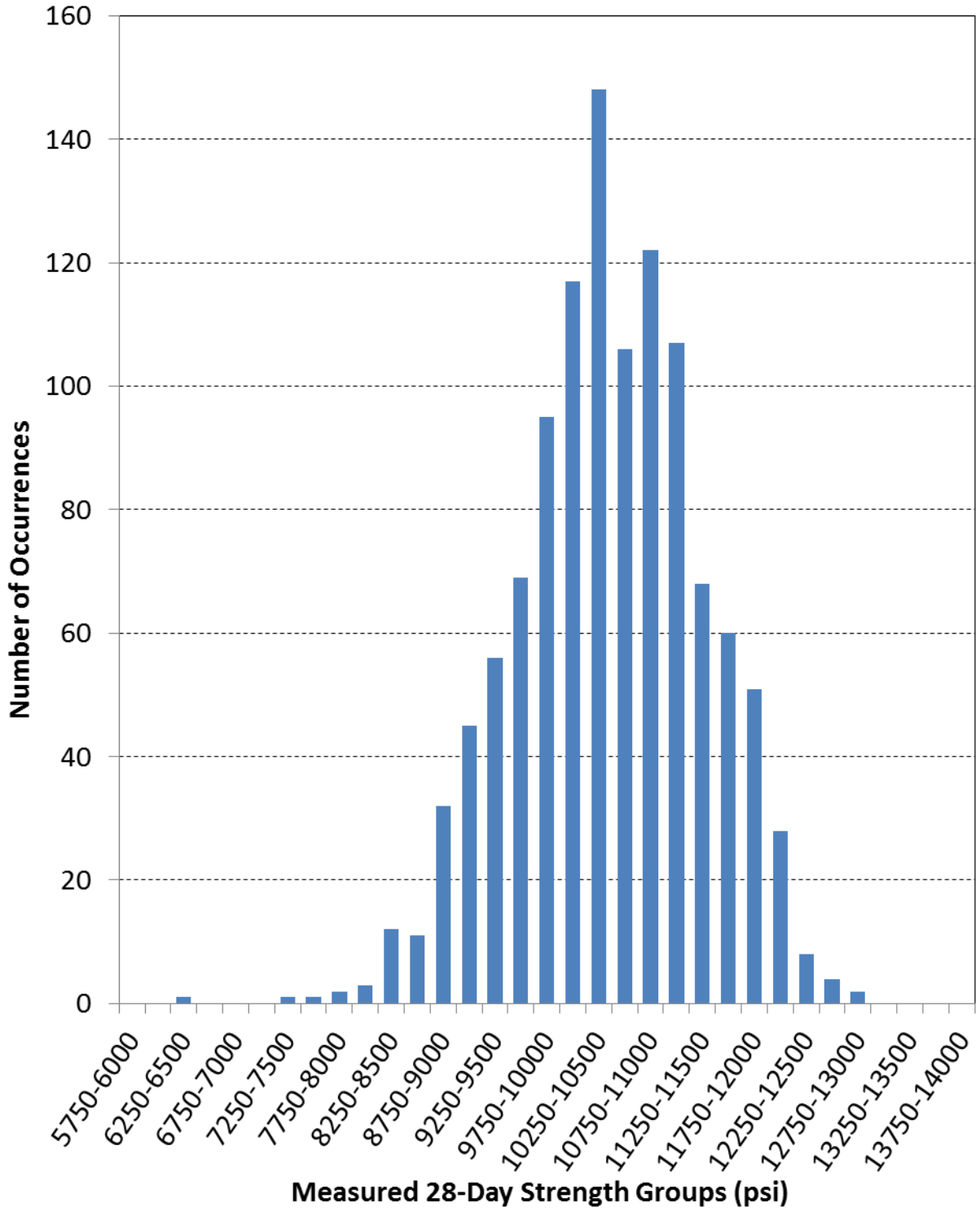

Figure F.5: Histogram of Measured 28-Day Strengths from Plant A

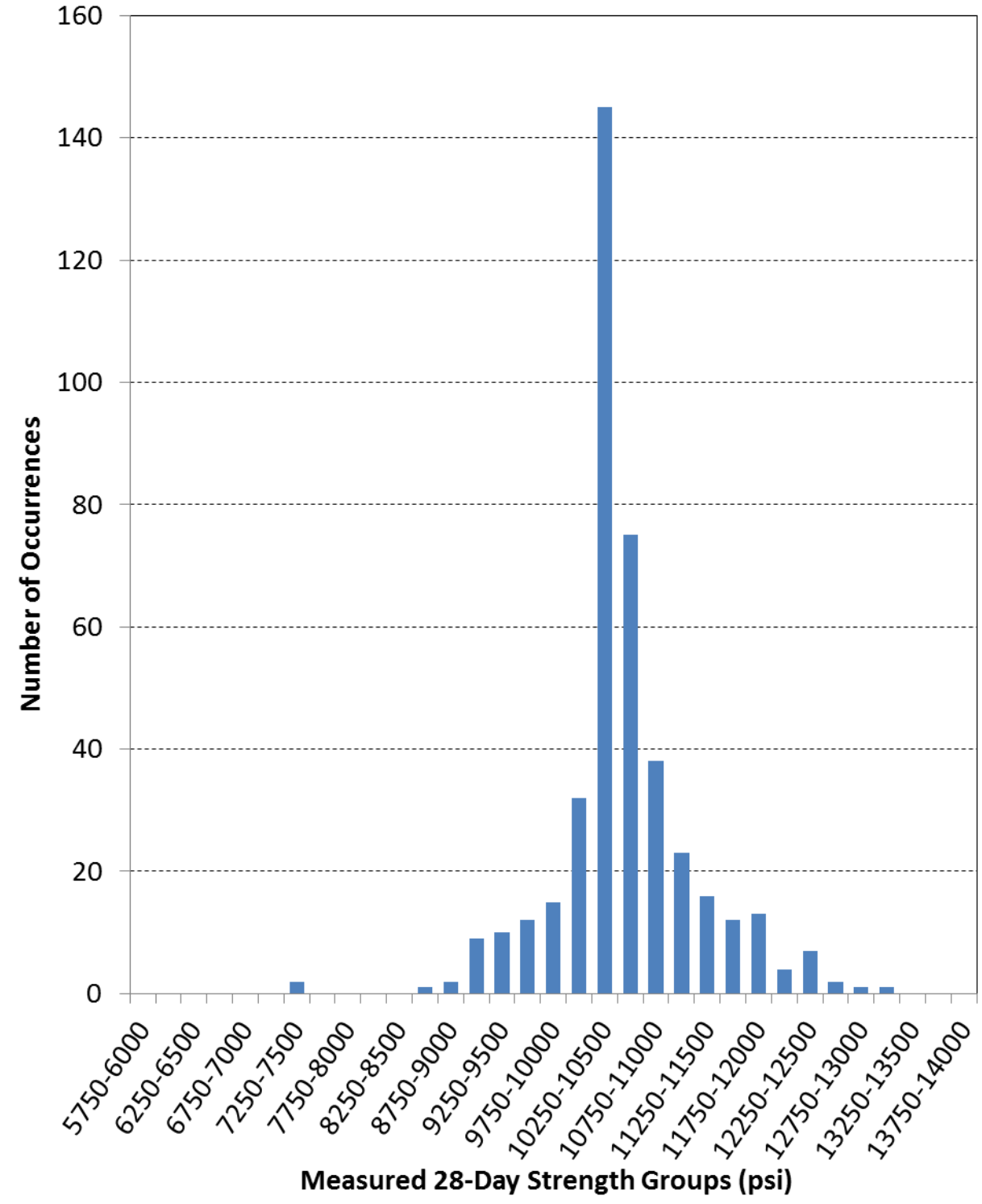

Figure F.6: Histogram of Measured 28-Day Strengths from Plant B

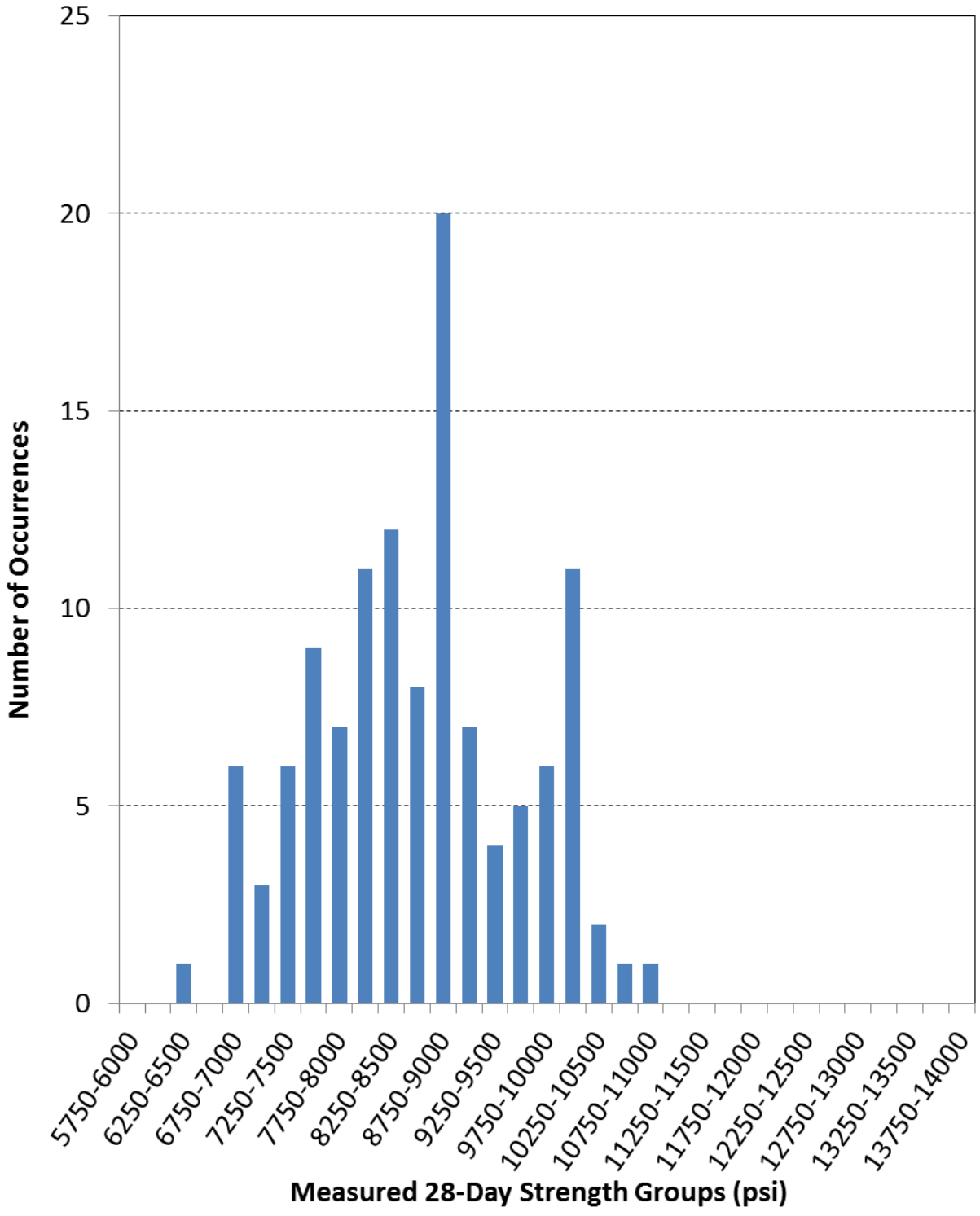

Figure F.7: Histogram of Measured 28-Day Strengths from Plant C

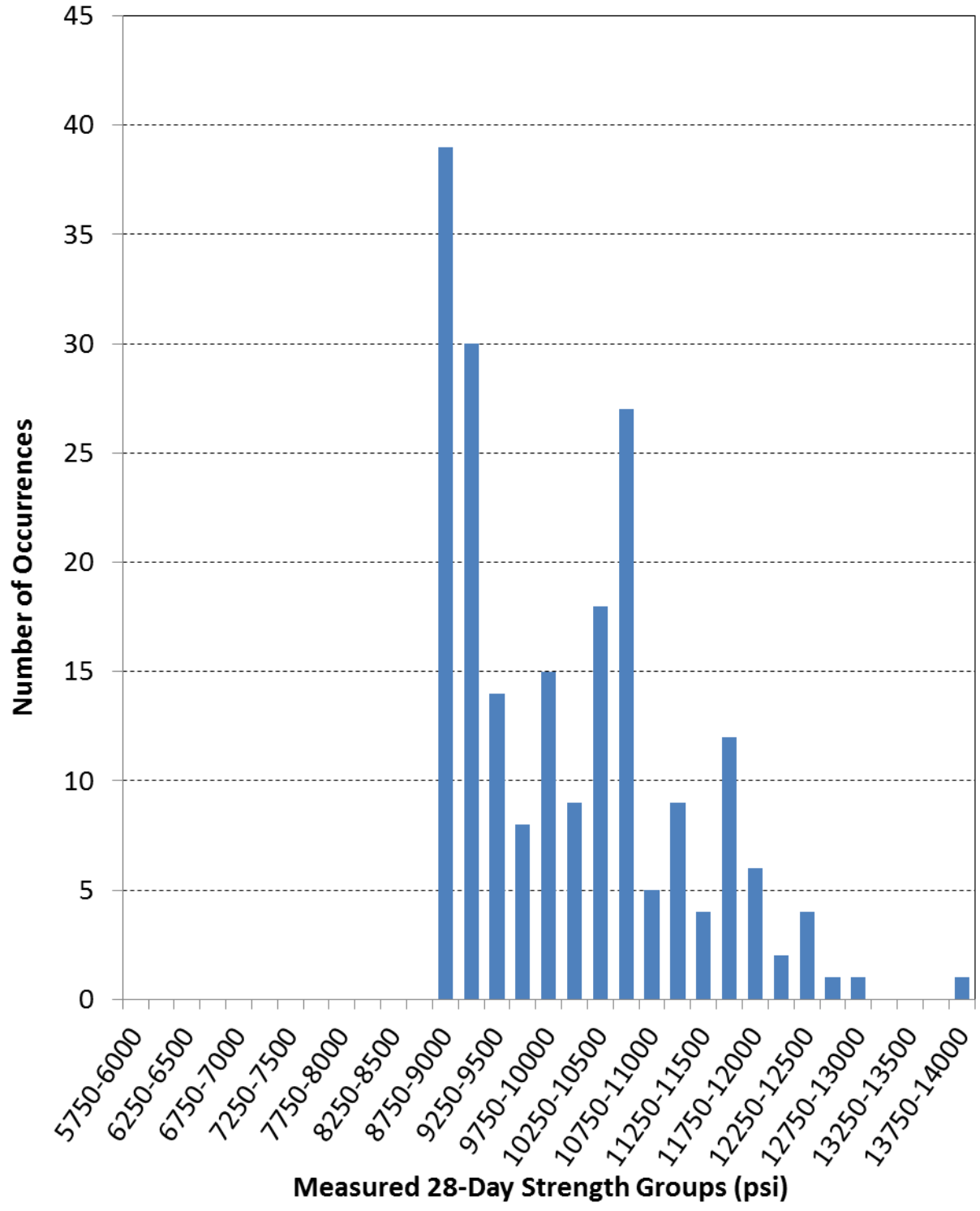

Figure F.8: Histogram of Measured 28-Day Strengths from Plant D

Appendix G: Plant-Specific Release Strength Distribution Tables

Table G.1: Plant A Release Strength Distributions – Bins Divided by f'_{ci}

Strength Bins	n	Sample Standard Deviation, s (psi)	Sample Mean, $\bar{x}$ (psi)	Sample Coefficient of Variance, COV (%)	Skewness Check, $\sqrt{\beta_1}$	Kurtosis Check, β_2
4000 psi $\leq f'_{ci} <$ 4500 psi	22	1120	7900	14.13	0.026	1.98
4500 psi $\leq f'_{ci} <$ 5000 psi	29	990	7710	12.85	-0.059	2.389
5000 psi $\leq f'_{ci} <$ 5500 psi	328	880	7660	11.49	0.423	3.097
5500 psi $\leq f'_{ci} <$ 6000 psi	302	950	7810	12.16	0.498	2.925
6000 psi $\leq f'_{ci} <$ 6500 psi	258	810	7830	10.35	0.209	2.794
6500 psi $\leq f'_{ci} <$ 7000 psi	127	880	8280	10.63	0.352	2.705
7000 psi $\leq f'_{ci} <$ 7500 psi	39	700	8600	8.13	0.945	4.101
7500 psi $\leq f'_{ci} <$ 8000 psi	50	570	8330	6.79	0.038	1.653
8000 psi $\leq f'_{ci} <$ 8500 psi	0	NA	NA	NA	NA	NA
8500 psi $\leq f'_{ci} <$ 9000 psi	0	NA	NA	NA	NA	NA
9000 psi $\leq f'_{ci} <$ 9500 psi	0	NA	NA	NA	NA	NA
Full f'_{ci} Range	1155	910	7870	11.52	0.3	2.913

Table G.2: Plant B Release Strength Distributions – Bins Divided by f'_{ci}

Strength Bins	n	Sample Standard Deviation, s (psi)	Sample Mean, $\bar{x}$ (psi)	Sample Coefficient of Variance, COV (%)	Skewness Check, $\sqrt{\beta_1}$	Kurtosis Check, β_2
4000 psi $\leq f'_{ci} <$ 4500 psi	16	500	7240	6.88	-0.33	1.669
4500 psi $\leq f'_{ci} <$ 5000 psi	14	740	7650	9.71	-0.058	4.697
5000 psi $\leq f'_{ci} <$ 5500 psi	47	720	6840	10.5	-0.279	3.156
5500 psi $\leq f'_{ci} <$ 6000 psi	136	860	7130	12.04	1.105	3.79
6000 psi $\leq f'_{ci} <$ 6500 psi	146	820	7340	11.15	0.737	3.35
6500 psi $\leq f'_{ci} <$ 7000 psi	50	660	7330	9	0.899	2.946
7000 psi $\leq f'_{ci} <$ 7500 psi	4	1030	9040	11.42	-0.321	0.934
7500 psi $\leq f'_{ci} <$ 8000 psi	17	650	8080	8.02	1.066	2.753
8000 psi $\leq f'_{ci} <$ 8500 psi	0	NA	NA	NA	NA	NA
8500 psi $\leq f'_{ci} <$ 9000 psi	0	NA	NA	NA	NA	NA
9000 psi $\leq f'_{ci} <$ 9500 psi	0	NA	NA	NA	NA	NA
Full f'_{ci} Range	430	840	7270	11.51	0.739	3.623

Table G.3: Plant C Release Strength Distributions – Bins Divided by f'_{ci}

Strength Bins	n	Sample Standard Deviation, s (psi)	Sample Mean, $\bar{x}$ (psi)	Sample Coefficient of Variance, COV (%)	Skewness Check, $\sqrt{\beta_1}$	Kurtosis Check, β_2
4000 psi $\leq f'_{ci} <$ 4500 psi	5	820	5340	15.28	0.844	1.785
4500 psi $\leq f'_{ci} <$ 5000 psi	6	980	6730	14.61	-0.504	1.192
5000 psi $\leq f'_{ci} <$ 5500 psi	25	1140	6600	17.31	0.208	1.515
5500 psi $\leq f'_{ci} <$ 6000 psi	19	750	6300	11.88	0.553	1.592
6000 psi $\leq f'_{ci} <$ 6500 psi	52	670	6970	9.66	0.651	2.527
6500 psi $\leq f'_{ci} <$ 7000 psi	0	NA	NA	NA	NA	NA
7000 psi $\leq f'_{ci} <$ 7500 psi	0	NA	NA	NA	NA	NA
7500 psi $\leq f'_{ci} <$ 8000 psi	12	800	8960	8.91	0.35	1.957
8000 psi $\leq f'_{ci} <$ 8500 psi	4	390	8550	4.58	0.188	1.077
8500 psi $\leq f'_{ci} <$ 9000 psi	0	NA	NA	NA	NA	NA
9000 psi $\leq f'_{ci} <$ 9500 psi	0	NA	NA	NA	NA	NA
Full f'_{ci} Range	123	1150	6960	16.58	0.442	2.884

Table G.4: Plant D Release Strength Distributions – Bins Divided by f'_{ci}

Strength Bins	n	Sample Standard Deviation, s (psi)	Sample Mean, $\bar{x}$ (psi)	Sample Coefficient of Variance, COV (%)	Skewness Check, $\sqrt{\beta_1}$	Kurtosis Check, β_2
4000 psi $\leq f'_{ci} <$ 4500 psi	10	1430	9060	15.76	0.05	1.314
4500 psi $\leq f'_{ci} <$ 5000 psi	0	NA	NA	NA	NA	NA
5000 psi $\leq f'_{ci} <$ 5500 psi	2	2070	7810	26.54	0	0.25
5500 psi $\leq f'_{ci} <$ 6000 psi	61	1050	7300	14.44	0.584	2.805
6000 psi $\leq f'_{ci} <$ 6500 psi	102	810	7440	10.92	1.253	5.535
6500 psi $\leq f'_{ci} <$ 7000 psi	14	960	8000	12.01	0.844	2.71
7000 psi $\leq f'_{ci} <$ 7500 psi	0	NA	NA	NA	NA	NA
7500 psi $\leq f'_{ci} <$ 8000 psi	0	NA	NA	NA	NA	NA
8000 psi $\leq f'_{ci} <$ 8500 psi	0	NA	NA	NA	NA	NA
8500 psi $\leq f'_{ci} <$ 9000 psi	0	NA	NA	NA	NA	NA
9000 psi $\leq f'_{ci} <$ 9500 psi	21	440	9300	4.72	0.795	2.395
Full f'_{ci} Range	210	1120	7700	14.53	0.42	1.685

Table G.5: Plant A Release Strength Distributions – Bins Divided by f_{ci}

Strength Bins	n	Sample Standard Deviation, s (psi)	Sample Mean, $\bar{x}$ (psi)	Sample Coefficient of Variance, COV (%)	Skewness Check, $\sqrt{\beta_1}$	Kurtosis Check, β_2
f_{ci} < 5500 psi	8	110	5270	2.17	-0.262	1.512
5500 psi ≤ f_{ci} < 6000 psi	29	140	5810	2.39	-0.698	2.461
6000 psi ≤ f_{ci} < 6500 psi	105	150	6270	2.37	-0.273	1.833
6500 psi ≤ f_{ci} < 7000 psi	230	140	6780	2.08	-0.308	2.016
7000 psi ≤ f_{ci} < 7500 psi	268	150	7250	2.05	-0.070	1.776
7500 psi ≤ f_{ci} < 8000 psi	261	140	7730	1.87	0.104	1.808
8000 psi ≤ f_{ci} < 8500 psi	143	140	8230	1.71	0.159	1.947
8500 psi ≤ f_{ci} < 9000 psi	70	150	8720	1.71	0.023	1.574
9000 psi ≤ f_{ci} < 9500 psi	27	130	9230	1.44	0.032	2.002
9500 psi ≤ f_{ci} < 10,000 psi	15	180	9700	1.82	0.551	1.634
10,000 psi ≤ f_{ci}	2	40	10,090	0.42	0.000	0.250
Full f_{ci} Range	1158	830	7420	11.17	0.298	3.195

Table G.6: Plant B Release Strength Distributions – Bins Divided by f_{ci}

Strength Bins	n	Sample Standard Deviation, s (psi)	Sample Mean, $\bar{x}$ (psi)	Sample Coefficient of Variance, COV (%)	Skewness Check, $\sqrt{\beta_1}$	Kurtosis Check, β_2
f_{ci} < 5500 psi	10	270	5240	5.24	-1.101	2.738
5500 psi ≤ f_{ci} < 6000 psi	56	130	5790	2.28	-0.315	1.893
6000 psi ≤ f_{ci} < 6500 psi	105	150	6300	2.37	-0.511	1.958
6500 psi ≤ f_{ci} < 7000 psi	105	140	6750	2.08	-0.152	1.860
7000 psi ≤ f_{ci} < 7500 psi	78	130	7180	1.85	0.497	2.271
7500 psi ≤ f_{ci} < 8000 psi	36	100	7660	1.30	0.393	1.981
8000 psi ≤ f_{ci} < 8500 psi	21	130	8250	1.54	-0.412	2.108
8500 psi ≤ f_{ci} < 9000 psi	14	150	8710	1.69	-0.049	1.161
9000 psi ≤ f_{ci} < 9500 psi	3	30	9230	0.35	-0.343	0.667
9500 psi ≤ f_{ci} < 10,000 psi	2	230	9680	2.41	0.000	0.250
10,000 psi ≤ f_{ci}	0	NA	NA	NA	NA	NA
Full f_{ci} Range	430	810	6800	11.96	0.717	3.735

Table G.7: Plant C Release Strength Distributions – Bins Divided by f_{ci}

Strength Bins	n	Sample Standard Deviation, s (psi)	Sample Mean, $\bar{x}$ (psi)	Sample Coefficient of Variance, COV (%)	Skewness Check, $\sqrt{\beta_1}$	Kurtosis Check, β_2
f_{ci} < 5500 psi	20	280	5120	5.44	-0.803	2.751
5500 psi ≤ f_{ci} < 6000 psi	16	120	5760	2.07	0.091	1.593
6000 psi ≤ f_{ci} < 6500 psi	22	140	6220	2.25	0.163	1.822
6500 psi ≤ f_{ci} < 7000 psi	19	120	6770	1.82	0.174	1.581
7000 psi ≤ f_{ci} < 7500 psi	22	140	7250	1.91	0.213	1.739
7500 psi ≤ f_{ci} < 8000 psi	13	120	7700	1.58	-0.300	1.428
8000 psi ≤ f_{ci} < 8500 psi	4	140	8190	1.76	0.168	1.001
8500 psi ≤ f_{ci} < 9000 psi	3	260	8800	3.00	-0.369	0.667
9000 psi ≤ f_{ci} < 9500 psi	3	90	9150	1.00	-0.208	0.667
9500 psi ≤ f_{ci} < 10,000 psi	0	NA	NA	NA	NA	NA
10,000 psi ≤ f_{ci}	1	NA	10,110	NA	NA	NA
Full f_{ci} Range	123	1080	6640	16.31	0.439	3.084

Table G.8: Plant D Release Strength Distributions – Bins Divided by f_{ci}

Strength Bins	n	Sample Standard Deviation, s (psi)	Sample Mean, $\bar{x}$ (psi)	Sample Coefficient of Variance, COV (%)	Skewness Check, $\sqrt{\beta_1}$	Kurtosis Check, β_2
f_{ci} < 5500 psi	2	180	5290	3.34	0.000	0.250
5500 psi ≤ f_{ci} < 6000 psi	24	150	5800	2.62	-0.456	1.890
6000 psi ≤ f_{ci} < 6500 psi	31	140	6260	2.31	-0.175	1.728
6500 psi ≤ f_{ci} < 7000 psi	55	150	6740	2.22	-0.001	1.680
7000 psi ≤ f_{ci} < 7500 psi	37	130	7200	1.80	0.540	2.167
7500 psi ≤ f_{ci} < 8000 psi	18	160	7690	2.03	0.319	1.425
8000 psi ≤ f_{ci} < 8500 psi	16	140	8250	1.75	-0.065	1.858
8500 psi ≤ f_{ci} < 9000 psi	12	140	8730	1.65	0.144	1.682
9000 psi ≤ f_{ci} < 9500 psi	12	130	9210	1.40	0.336	2.132
9500 psi ≤ f_{ci} < 10,000 psi	3	130	9650	1.35	-0.101	0.667
10,000 psi ≤ f_{ci}	0	NA	NA	NA	NA	NA
Full f_{ci} Range	210	1010	7120	14.16	0.659	2.739

Appendix H: Plant-Specific 28-Day Strength Distribution Tables

Table H.1: Plant A 28-Day Strength Distributions – Bins Divided by f'_c

Strength Bins	n	Sample Standard Deviation, s (psi)	Sample Mean, $\bar{x}$ (psi)	Sample Coefficient of Variance, COV (%)	Skewness Check, $\sqrt{\beta_1}$	Kurtosis Check, β_2
5000 psi $\leq f'_c <$ 5500 psi	31	850	10,010	8.52	1.139	4.741
5500 psi $\leq f'_c <$ 6000 psi	18	790	10,840	7.31	-0.732	3.837
6000 psi $\leq f'_c <$ 6500 psi	356	840	10,540	7.98	-0.221	2.989
6500 psi $\leq f'_c <$ 7000 psi	190	780	10,500	7.43	-0.712	5.111
7000 psi $\leq f'_c <$ 7500 psi	419	940	10,950	8.56	-0.324	2.813
7500 psi $\leq f'_c <$ 8000 psi	9	360	9810	3.63	-0.765	2.068
8000 psi $\leq f'_c <$ 8500 psi	127	740	11,090	6.64	-0.101	2.249
8500 psi $\leq f'_c <$ 9000 psi	0	NA	NA	NA	NA	NA
9000 psi $\leq f'_c$	0	NA	NA	NA	NA	NA
Full f'_c Range	1150	890	10,730	8.33	-0.212	3.07

Table H.2: Plant B 28-Day Strength Distributions – Bins Divided by f'_c

Strength Bins	n	Sample Standard Deviation, s (psi)	Sample Mean, $\bar{x}$ (psi)	Sample Coefficient of Variance, COV (%)	Skewness Check, $\sqrt{\beta_1}$	Kurtosis Check, β_2
5000 psi $\leq f'_c <$ 5500 psi	9	170	10,730	1.61	1.158	3.026
5500 psi $\leq f'_c <$ 6000 psi	38	500	11,000	4.5	1.572	5.321
6000 psi $\leq f'_c <$ 6500 psi	76	530	10,610	5.01	0.360	6.071
6500 psi $\leq f'_c <$ 7000 psi	90	680	10,680	6.37	0.514	4.183
7000 psi $\leq f'_c <$ 7500 psi	152	780	10,880	7.17	-0.398	6.925
7500 psi $\leq f'_c <$ 8000 psi	26	640	11,180	5.68	-0.024	1.767
8000 psi $\leq f'_c <$ 8500 psi	30	820	11,050	7.39	0.322	3.199
8500 psi $\leq f'_c <$ 9000 psi	0	NA	NA	NA	NA	NA
9000 psi $\leq f'_c$	0	NA	NA	NA	NA	NA
Full f'_cRange	421	700	10,830	6.45	0.095	5.893

Table H.3: Plant C 28-Day Strength Distributions – Bins Divided by f'_c

Strength Bins	n	Sample Standard Deviation, s (psi)	Sample Mean, $\bar{x}$ (psi)	Sample Coefficient of Variance, COV (%)	Skewness Check, $\sqrt{\beta_1}$	Kurtosis Check, β_2
5000 psi $\leq f'_c <$ 5500 psi	11	960	8630	11.16	0.420	1.692
5500 psi $\leq f'_c <$ 6000 psi	0	NA	NA	NA	NA	NA
6000 psi $\leq f'_c <$ 6500 psi	21	970	8750	11.03	0.253	1.583
6500 psi $\leq f'_c <$ 7000 psi	13	890	8590	10.38	-0.811	2.424
7000 psi $\leq f'_c <$ 7500 psi	60	800	8670	9.24	-0.194	2.543
7500 psi $\leq f'_c <$ 8000 psi	0	NA	NA	NA	NA	NA
8000 psi $\leq f'_c <$ 8500 psi	4	800	10,350	7.75	-0.104	0.699
8500 psi $\leq f'_c <$ 9000 psi	12	320	10,270	3.07	-1.409	4.074
9000 psi $\leq f'_c$	0	NA	NA	NA	NA	NA
Full f'_cRange	121	980	8890	11.01	0.028	2.286

Table H.4: Plant D 28-Day Strength Distributions – Bins Divided by f'_c

Strength Bins	n	Sample Standard Deviation, s (psi)	Sample Mean, $\bar{x}$ (psi)	Sample Coefficient of Variance, COV (%)	Skewness Check, $\sqrt{\beta_1}$	Kurtosis Check, β_2
5000 psi $\leq f'_c <$ 5500 psi	10	710	11,930	5.92	-0.367	2.008
5500 psi $\leq f'_c <$ 6000 psi	0	NA	NA	NA	NA	NA
6000 psi $\leq f'_c <$ 6500 psi	2	1940	11,250	17.29	0	0.25
6500 psi $\leq f'_c <$ 7000 psi	14	830	10,420	7.98	0.258	1.731
7000 psi $\leq f'_c <$ 7500 psi	151	850	10,020	8.50	0.640	2.369
7500 psi $\leq f'_c <$ 8000 psi	3	860	10,310	8.32	-0.373	0.667
8000 psi $\leq f'_c <$ 8500 psi	9	630	11,780	5.32	-0.546	2.189
8500 psi $\leq f'_c <$ 9000 psi	0	NA	NA	NA	NA	NA
9000 psi $\leq f'_c$	16	1250	11,300	11.07	0.531	2.591
Full f'_cRange	205	1060	10,330	10.28	0.684	2.826

Table H.5: Plant A 28-Day Strength Distributions – Bins Divided by f_c

Strength Bins	n	Sample Standard Deviation, s (psi)	Sample Mean, $\bar{x}$ (psi)	Sample Coefficient of Variance, COV (%)	Skewness Check, $\sqrt{\beta_1}$	Kurtosis Check, β_2
f_c < 8000 psi	3	620	7390	8.37	-0.304	0.667
8000 psi ≤ f_c < 8500 psi	4	140	8280	1.64	0.462	1.184
8500 psi ≤ f_c < 9000 psi	23	150	8750	1.76	0.232	1.733
9000 psi ≤ f_c < 9500 psi	73	140	9280	1.48	-0.150	1.842
9500 psi ≤ f_c < 10,000 psi	127	150	9760	1.55	-0.130	1.707
10,000 psi ≤ f_c < 10,500 psi	210	140	10,260	1.39	-0.132	1.809
10,500 psi ≤ f_c < 11,000 psi	255	140	10,720	1.28	0.221	1.835
11,000 psi ≤ f_c < 11,500 psi	229	150	11,240	1.33	0.069	1.732
11,500 psi ≤ f_c < 12,000 psi	131	140	11,740	1.21	0.063	1.856
12,000 psi ≤ f_c < 12,500 psi	80	120	12,190	1.00	0.315	2.092
12,500 psi ≤ f_c < 13,000 psi	13	140	12,690	1.14	0.277	1.658
13,000 psi ≤ f_c	2	110	13,160	0.81	0.000	0.250
Full f_c Range	1150	890	10,730	8.33	-0.212	3.070

Table H.6: Plant B 28-Day Strength Distributions – Bins Divided by f_c

Strength Bins	n	Sample Standard Deviation, s (psi)	Sample Mean, $\bar{x}$ (psi)	Sample Coefficient of Variance, COV (%)	Skewness Check, $\sqrt{\beta_1}$	Kurtosis Check, β_2
f_c < 8000 psi	2	40	7590	0.56	0.000	0.250
8000 psi ≤ f_c < 8500 psi	0	NA	NA	NA	NA	NA
8500 psi ≤ f_c < 9000 psi	1	NA	8940	NA	NA	NA
9000 psi ≤ f_c < 9500 psi	11	150	9340	1.58	-0.965	2.395
9500 psi ≤ f_c < 10,000 psi	20	120	9740	1.24	-0.115	1.888
10,000 psi ≤ f_c < 10,500 psi	46	150	10,280	1.46	-0.355	1.933
10,500 psi ≤ f_c < 11,000 psi	221	110	10,710	1.02	0.330	2.740
11,000 psi ≤ f_c < 11,500 psi	62	140	11,200	1.21	0.427	2.009
11,500 psi ≤ f_c < 12,000 psi	27	130	11,720	1.13	-0.001	1.772
12,000 psi ≤ f_c < 12,500 psi	20	120	12,200	1.00	0.507	2.759
12,500 psi ≤ f_c < 13,000 psi	9	110	12,680	0.86	0.422	2.178
13,000 psi ≤ f_c	2	110	13,190	0.86	0.000	0.250
Full f_c Range	421	700	10,830	6.45	0.095	5.893

Table H.7: Plant C 28-Day Strength Distributions – Bins Divided by f_c

Strength Bins	n	Sample Standard Deviation, s (psi)	Sample Mean, $\bar{x}$ (psi)	Sample Coefficient of Variance, COV (%)	Skewness Check, $\sqrt{\beta_1}$	Kurtosis Check, β_2
f_c < 8000 psi	25	350	7530	4.66	-0.498	2.223
8000 psi ≤ f_c < 8500 psi	17	130	8280	1.58	-0.160	2.141
8500 psi ≤ f_c < 9000 psi	22	170	8710	1.96	0.483	1.513
9000 psi ≤ f_c < 9500 psi	26	120	9220	1.26	0.907	2.876
9500 psi ≤ f_c < 10,000 psi	10	200	9740	2.05	0.054	1.004
10,000 psi ≤ f_c < 10,500 psi	16	130	10,250	1.22	-0.180	2.051
10,500 psi ≤ f_c < 11,000 psi	4	220	10,640	2.03	0.721	1.293
11,000 psi ≤ f_c < 11,500 psi	1	NA	11,090	NA	NA	NA
11,500 psi ≤ f_c < 12,000 psi	0	NA	NA	NA	NA	NA
12,000 psi ≤ f_c < 12,500 psi	0	NA	NA	NA	NA	NA
12,500 psi ≤ f_c < 13,000 psi	0	NA	NA	NA	NA	NA
13,000 psi ≤ f_c	0	NA	NA	NA	NA	NA
Full f_c Range	121	980	8890	11.01	0.028	2.286

Table H.8: Plant D 28-Day Strength Distributions – Bins Divided by f_c

Strength Bins	n	Sample Standard Deviation, s (psi)	Sample Mean, $\bar{x}$ (psi)	Sample Coefficient of Variance, COV (%)	Skewness Check, $\sqrt{\beta_1}$	Kurtosis Check, β_2
f_c < 8000 psi	0	NA	NA	NA	NA	NA
8000 psi ≤ f_c < 8500 psi	0	NA	NA	NA	NA	NA
8500 psi ≤ f_c < 9000 psi	0	NA	NA	NA	NA	NA
9000 psi ≤ f_c < 9500 psi	68	120	9230	1.34	0.127	1.948
9500 psi ≤ f_c < 10,000 psi	23	150	9720	1.58	0.284	1.601
10,000 psi ≤ f_c < 10,500 psi	24	120	10,220	1.21	0.115	2.076
10,500 psi ≤ f_c < 11,000 psi	45	130	10,770	1.21	-0.396	1.896
11,000 psi ≤ f_c < 11,500 psi	13	120	11,260	1.03	0.028	1.829
11,500 psi ≤ f_c < 12,000 psi	17	160	11,770	1.35	-0.352	1.641
12,000 psi ≤ f_c < 12,500 psi	8	160	12,150	1.29	0.731	1.989
12,500 psi ≤ f_c < 13,000 psi	6	160	12,670	1.23	1.144	2.532
13,000 psi ≤ f_c	2	800	13,580	5.89	0.000	0.250
Full f_c Range	206	1080	10,330	10.27	0.691	2.839

Appendix I: Plant-Specific Air-Adjusted Strength Distribution Tables

Table I.1: Plant A Release Strength Distributions – Air-Adjusted Data, Bins Divided by f'_{ci}

Strength Bins	n	Sample Standard Deviation, s (psi)	Sample Mean, $\bar{x}$ (psi)	Sample Coefficient of Variance, COV (%)	Skewness Check, $\sqrt{\beta_1}$	Kurtosis Check, β_2
4000 psi $\leq f'_{ci} <$ 4500 psi	22	1090	7510	14.49	0.058	1.716
4500 psi $\leq f'_{ci} <$ 5000 psi	29	840	7260	11.56	-0.223	2.5
5000 psi $\leq f'_{ci} <$ 5500 psi	328	790	7290	10.77	0.279	3.212
5500 psi $\leq f'_{ci} <$ 6000 psi	302	910	7330	12.46	0.47	3.16
6000 psi $\leq f'_{ci} <$ 6500 psi	258	740	7390	10.04	0.281	3.098
6500 psi $\leq f'_{ci} <$ 7000 psi	127	850	7780	10.94	0.296	2.865
7000 psi $\leq f'_{ci} <$ 7500 psi	39	640	7880	8.09	0.934	4.002
7500 psi $\leq f'_{ci} <$ 8000 psi	50	480	7690	6.25	0.209	1.969
8000 psi $\leq f'_{ci} <$ 8500 psi	0	NA	NA	NA	NA	NA
8500 psi $\leq f'_{ci} <$ 9000 psi	0	NA	NA	NA	NA	NA
9000 psi $\leq f'_{ci} <$ 9500 psi	0	NA	NA	NA	NA	NA
Full f'_{ci} Range	1155	830	7420	11.18	0.299	3.193

Table I.2: Plant B Release Strength Distributions – Air-Adjusted Data, Bins Divided by f'_{ci}

Strength Bins	*n*	Sample Standard Deviation, s (psi)	Sample Mean, $\bar{x}$ (psi)	Sample Coefficient of Variance, COV (%)	Skewness Check, $\sqrt{\beta_1}$	Kurtosis Check, β_2
4000 psi ≤ f'_{ci} < 4500 psi	16	560	6780	8.29	-0.209	1.627
4500 psi ≤ f'_{ci} < 5000 psi	14	750	7090	10.59	-0.044	3.469
5000 psi ≤ f'_{ci} < 5500 psi	47	740	6450	11.44	0.026	3.67
5500 psi ≤ f'_{ci} < 6000 psi	136	830	6660	12.44	0.983	3.63
6000 psi ≤ f'_{ci} < 6500 psi	146	800	6850	11.68	0.725	3.356
6500 psi ≤ f'_{ci} < 7000 psi	50	590	6900	8.55	0.732	2.678
7000 psi ≤ f'_{ci} < 7500 psi	4	1280	8650	14.82	-0.233	0.862
7500 psi ≤ f'_{ci} < 8000 psi	17	560	7550	7.45	0.801	2.418
8000 psi ≤ f'_{ci} < 8500 psi	0	NA	NA	NA	NA	NA
8500 psi ≤ f'_{ci} < 9000 psi	0	NA	NA	NA	NA	NA
9000 psi ≤ f'_{ci} < 9500 psi	0	NA	NA	NA	NA	NA
Full f'_{ci} Range	430	810	6800	11.96	0.717	3.735

Table I.3: Plant C Release Strength Distributions – Air-Adjusted Data, Bins Divided by f'_{ci}

Strength Bins	*n*	Sample Standard Deviation, s (psi)	Sample Mean, $\bar{x}$ (psi)	Sample Coefficient of Variance, COV (%)	Skewness Check, $\sqrt{\beta_1}$	Kurtosis Check, β_2
4000 psi ≤ f'_{ci} < 4500 psi	5	780	5100	15.2	0.737	1.645
4500 psi ≤ f'_{ci} < 5000 psi	6	1090	6820	16.04	-0.485	1.21
5000 psi ≤ f'_{ci} < 5500 psi	25	990	6390	15.44	-0.14	1.459
5500 psi ≤ f'_{ci} < 6000 psi	19	900	6120	14.65	0.29	1.44
6000 psi ≤ f'_{ci} < 6500 psi	52	600	6530	9.17	0.363	2.024
6500 psi ≤ f'_{ci} < 7000 psi	0	NA	NA	NA	NA	NA
7000 psi ≤ f'_{ci} < 7500 psi	0	NA	NA	NA	NA	NA
7500 psi ≤ f'_{ci} < 8000 psi	12	860	8530	10.13	0.068	1.749
8000 psi ≤ f'_{ci} < 8500 psi	4	380	8030	4.73	-0.469	1.125
8500 psi ≤ f'_{ci} < 9000 psi	0	NA	NA	NA	NA	NA
9000 psi ≤ f'_{ci} < 9500 psi	0	NA	NA	NA	NA	NA
Full f'_{ci} Range	123	1080	6640	16.31	0.439	3.084

Table I.4: Plant D Release Strength Distributions – Air-Adjusted Data, Bins Divided by f'_{ci}

Strength Bins	n	Sample Standard Deviation, s (psi)	Sample Mean, $\bar{x}$ (psi)	Sample Coefficient of Variance, COV (%)	Skewness Check, $\sqrt{\beta_1}$	Kurtosis Check, β_2
4000 psi ≤ f'_{ci} < 4500 psi	10	1220	8160	14.93	-0.072	1.364
4500 psi ≤ f'_{ci} < 5000 psi	0	NA	NA	NA	NA	NA
5000 psi ≤ f'_{ci} < 5500 psi	2	1620	7200	22.51	0	0.25
5500 psi ≤ f'_{ci} < 6000 psi	61	960	6760	14.25	0.743	2.875
6000 psi ≤ f'_{ci} < 6500 psi	102	760	6900	10.95	1.285	5.649
6500 psi ≤ f'_{ci} < 7000 psi	14	840	7380	11.4	0.678	2.328
7000 psi ≤ f'_{ci} < 7500 psi	0	NA	NA	NA	NA	NA
7500 psi ≤ f'_{ci} < 8000 psi	0	NA	NA	NA	NA	NA
8000 psi ≤ f'_{ci} < 8500 psi	0	NA	NA	NA	NA	NA
8500 psi ≤ f'_{ci} < 9000 psi	0	NA	NA	NA	NA	NA
9000 psi ≤ f'_{ci} < 9500 psi	21	420	8600	4.93	0.462	1.743
Full f'_{ci} Range	210	1010	7120	14.16	0.474	1.791

Table I.5: Plant A 28-Day Strength Distributions – Air-Adjusted Data, Bins Divided by f_c'

Strength Bins	n	Sample Standard Deviation, s (psi)	Sample Mean, $\bar{x}$ (psi)	Sample Coefficient of Variance, COV (%)	Skewness Check, $\sqrt{\beta_1}$	Kurtosis Check, β_2
5000 psi ≤ f_c' < 5500 psi	31	740	9560	7.74	0.970	3.998
5500 psi ≤ f_c'< 6000 psi	18	720	10,250	7.02	-1.151	4.130
6000 psi ≤ f_c' < 6500 psi	356	730	10,010	7.24	-0.477	3.717
6500 psi ≤ f_c' < 7000 psi	190	820	9900	8.31	-0.489	4.964
7000 psi ≤ f_c' < 7500 psi	419	880	10,300	8.51	-0.435	3.230
7500 psi ≤ f_c' < 8000 psi	9	330	9510	3.51	-0.244	1.350
8000 psi ≤ f_c' < 8500 psi	127	630	10,270	6.16	-0.296	2.662
8500 psi ≤ f_c' < 9000 psi	0	NA	NA	NA	NA	NA
9000 psi ≤ f_c'	0	NA	NA	NA	NA	NA
Full f_c'Range	1150	810	10,110	8.01	-0.350	3.664

Table I.6: Plant B 28-Day Strength Distributions – Air-Adjusted Data, Bins Divided by f'_c

Strength Bins	*n*	Sample Standard Deviation, s (psi)	Sample Mean, $\bar{x}$ (psi)	Sample Coefficient of Variance, COV (%)	Skewness Check, $\sqrt{\beta_1}$	Kurtosis Check, β_2
5000 psi ≤ f'_c < 5500 psi	9	280	9920	2.83	1.076	3.164
5500 psi ≤ f'_c< 6000 psi	38	490	10,260	4.77	0.810	3.344
6000 psi ≤ f'_c < 6500 psi	76	510	10,000	5.11	0.435	4.234
6500 psi ≤ f'_c < 7000 psi	90	640	9930	6.48	0.390	3.947
7000 psi ≤ f'_c < 7500 psi	152	770	10,150	7.56	-0.290	6.173
7500 psi ≤ f'_c < 8000 psi	26	480	10,430	4.60	0.179	1.853
8000 psi ≤ f'_c < 8500 psi	30	700	10,350	6.74	0.167	2.226
8500 psi ≤ f'_c < 9000 psi	0	NA	NA	NA	NA	NA
9000 psi ≤ f'_c	0	NA	NA	NA	NA	NA
Full f'_c Range	421	660	10,110	6.55	0.027	5.502

Table I.7: Plant C 28-Day Strength Distributions – Air-Adjusted Data, Bins Divided by f'_c

Strength Bins	n	Sample Standard Deviation, s (psi)	Sample Mean, $\bar{x}$ (psi)	Sample Coefficient of Variance, COV (%)	Skewness Check, $\sqrt{\beta_1}$	Kurtosis Check, β_2
5000 psi ≤ f'_c < 5500 psi	11	1210	8540	14.20	0.560	1.705
5500 psi ≤ f'_c < 6000 psi	0	NA	NA	NA	NA	NA
6000 psi ≤ f'_c < 6500 psi	21	900	8700	10.39	-0.262	1.864
6500 psi ≤ f'_c < 7000 psi	13	840	8080	10.43	-0.670	2.286
7000 psi ≤ f'_c < 7500 psi	60	880	8170	10.78	0.166	2.896
7500 psi ≤ f'_c < 8000 psi	0	NA	NA	NA	NA	NA
8000 psi ≤ f'_c < 8500 psi	4	720	9730	7.40	-0.468	1.066
8500 psi ≤ f'_c < 9000 psi	12	520	9770	5.29	0.138	3.113
9000 psi ≤ f'_c	0	NA	NA	NA	NA	NA
Full f'_c Range	121	1020	8490	12.02	0.086	2.388

Table I.8: Plant D 28-Day Strength Distributions – Air-Adjusted Data, Bins Divided by f_c'

Strength Bins	n	Sample Standard Deviation, s (psi)	Sample Mean, $\bar{x}$ (psi)	Sample Coefficient of Variance, COV (%)	Skewness Check, $\sqrt{\beta_1}$	Kurtosis Check, β_2
5000 psi ≤ f_c' < 5500 psi	10	500	10,750	4.62	-0.577	1.859
5500 psi ≤ f_c'< 6000 psi	0	NA	NA	NA	NA	NA
6000 psi ≤ f_c' < 6500 psi	2	1360	10,400	13.13	0	0.25
6500 psi ≤ f_c' < 7000 psi	14	710	9610	7.36	-0.290	1.861
7000 psi ≤ f_c' < 7500 psi	151	870	9310	9.30	0.402	2.500
7500 psi ≤ f_c' < 8000 psi	3	670	9290	7.16	-0.334	0.667
8000 psi ≤ f_c' < 8500 psi	9	550	10,580	5.17	-0.155	1.518
8500 psi ≤ f_c' < 9000 psi	0	NA	NA	NA	NA	NA
9000 psi ≤ f_c'	16	1090	10350	10.52	0.595	2.236
Full f_c'Range	205	960	9550	10.06	0.270	1.567

Appendix J: Additional In-Plant Strength-Growth Prediction Plots

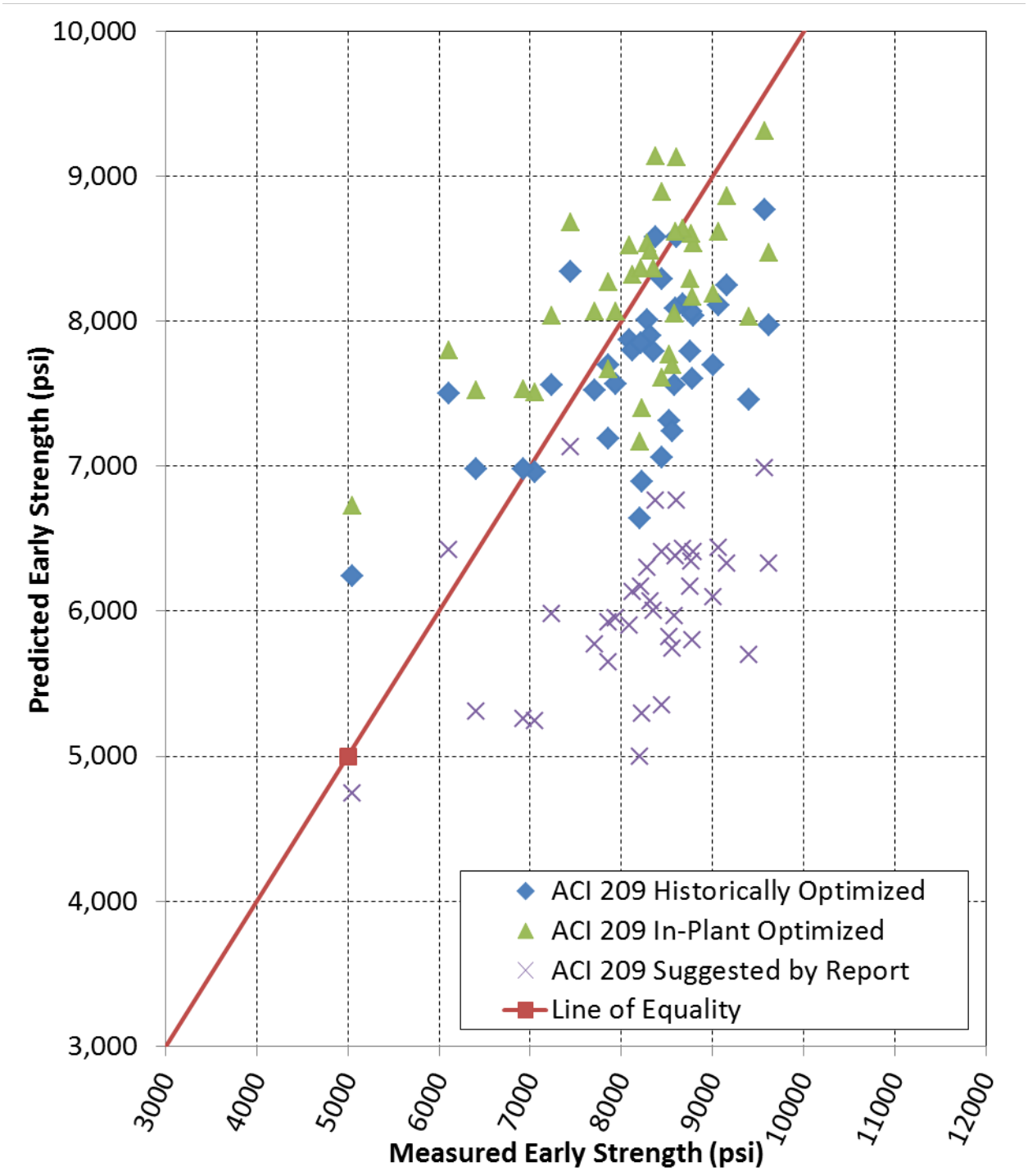

Figure J.1: ACI 209 Early Strength Predictions for In-Plant Data using Chronological Age

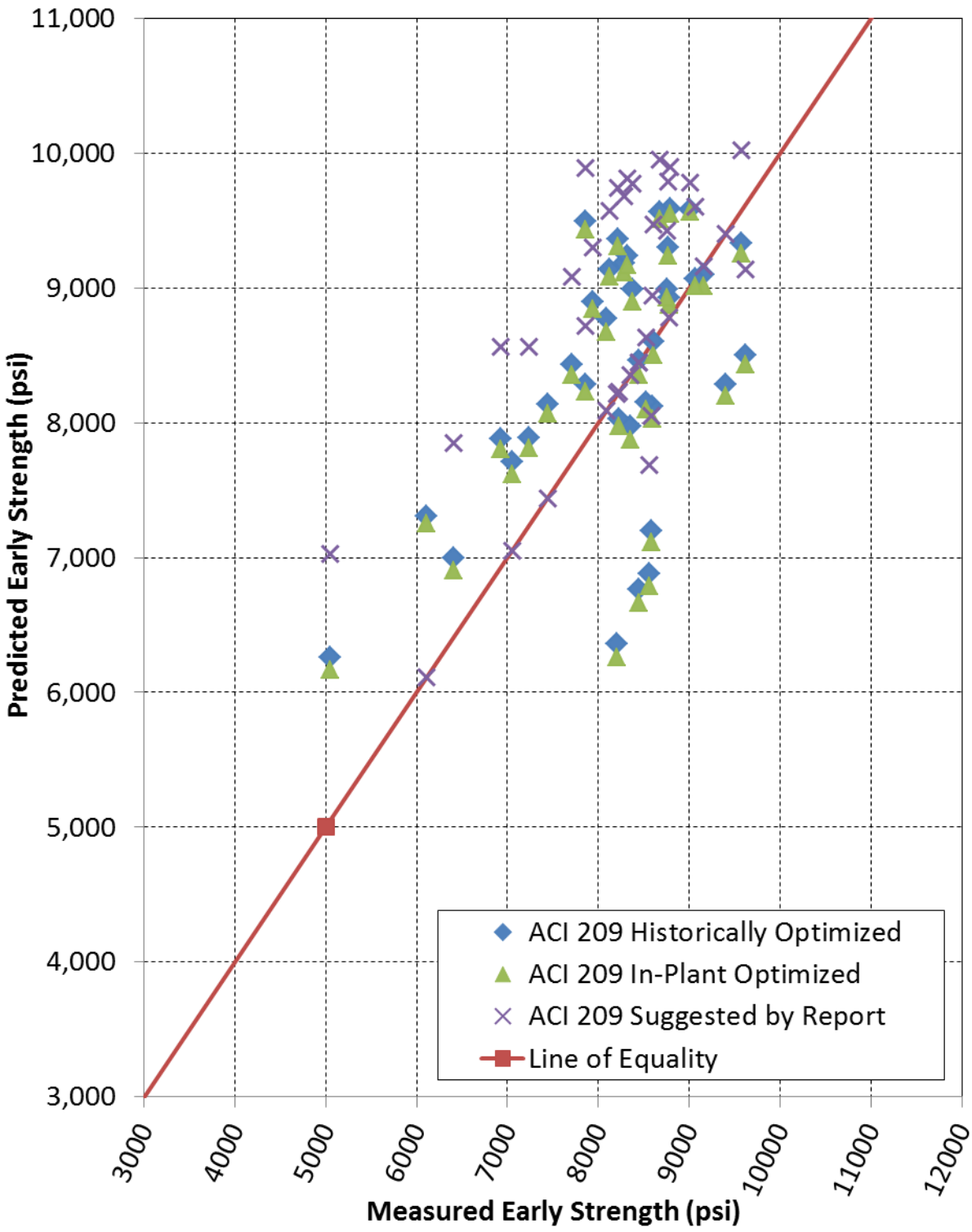

Figure J.2: ACI 209 Early Strength Predictions for In-Plant Data using Equivalent Age

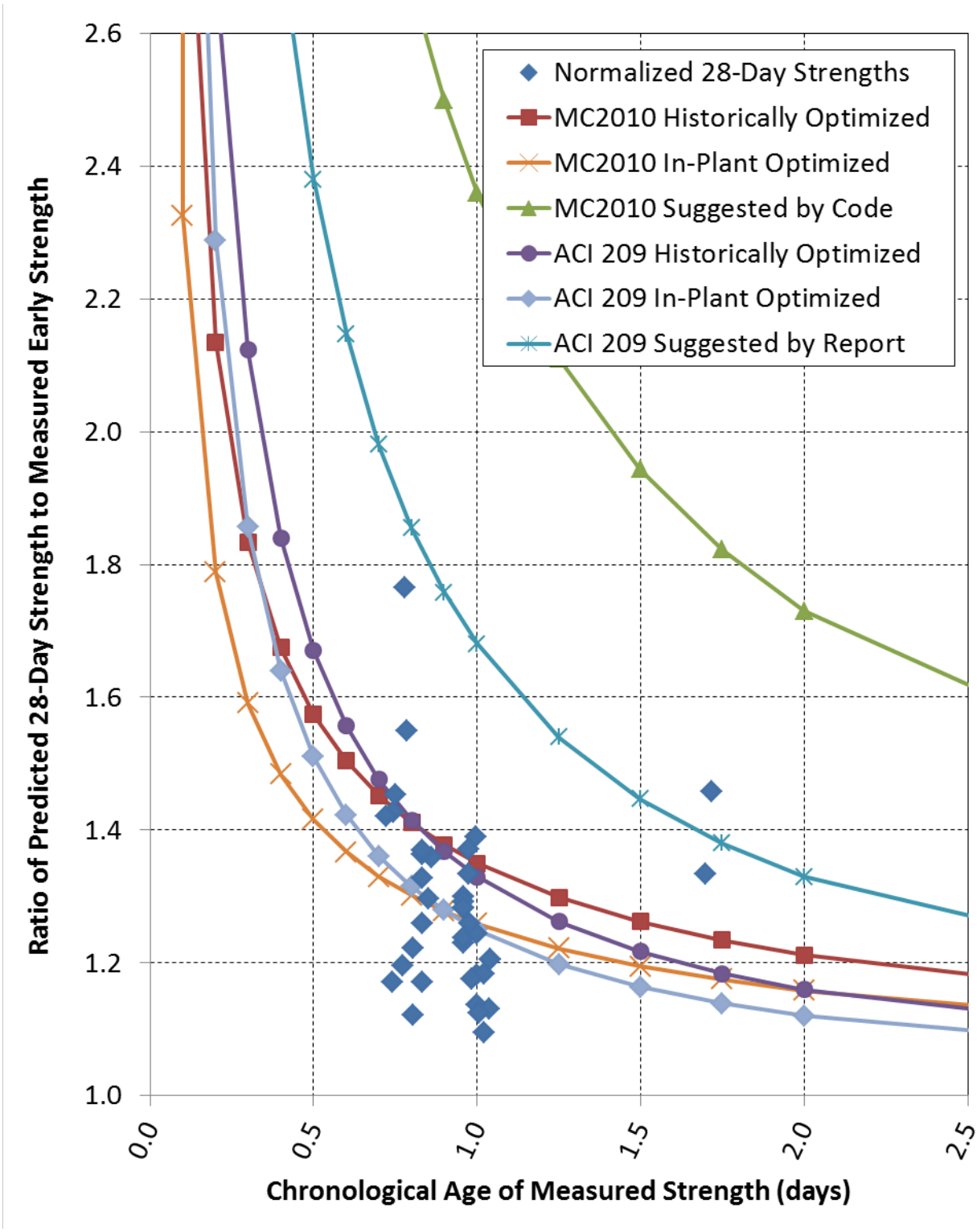

Figure J.3: Prediction Curves for In-Plant 28-Day Strengths with Chronological Age

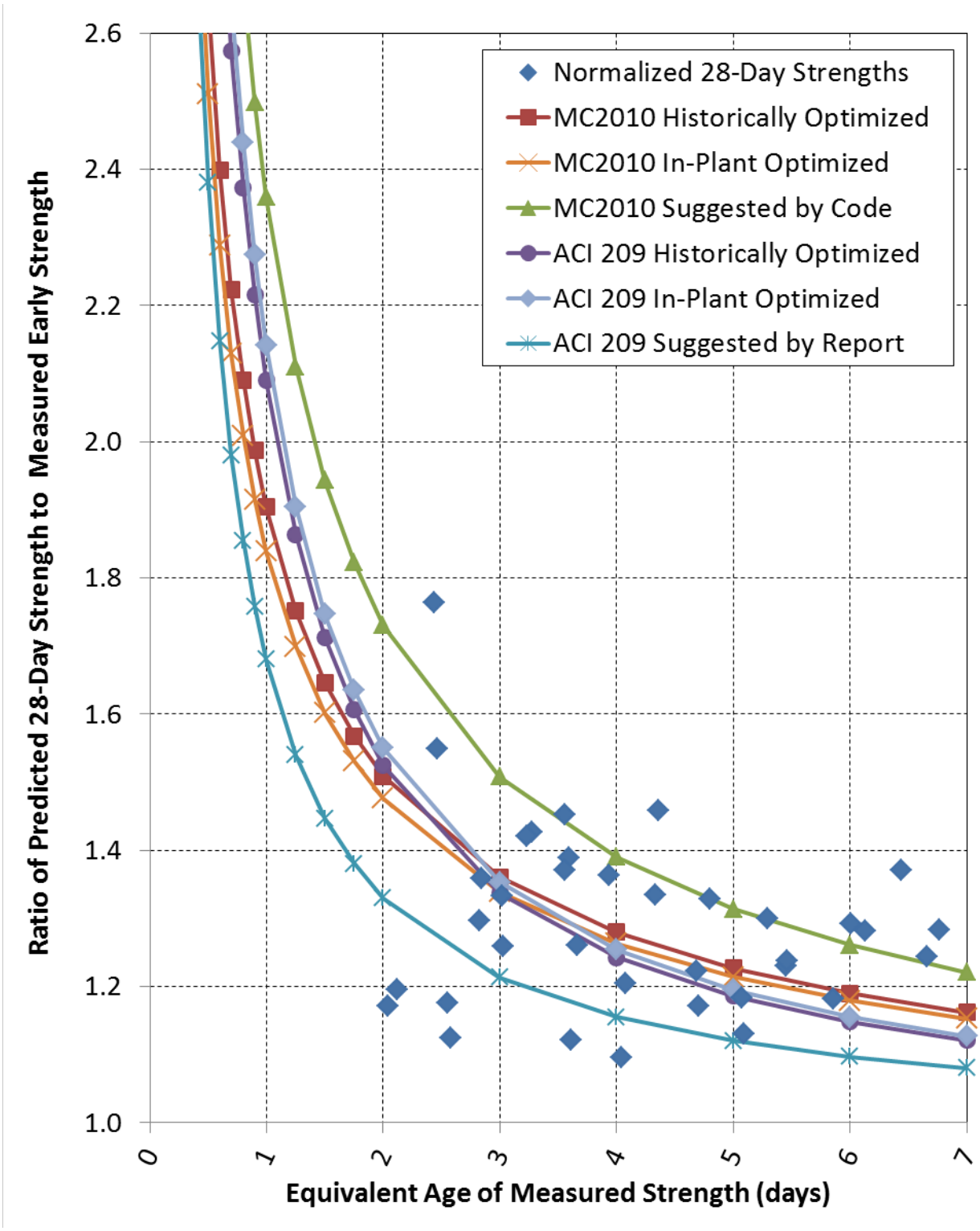

Figure J.4: Prediction Curves for In-Plant 28-Day Strengths with Equivalent Age

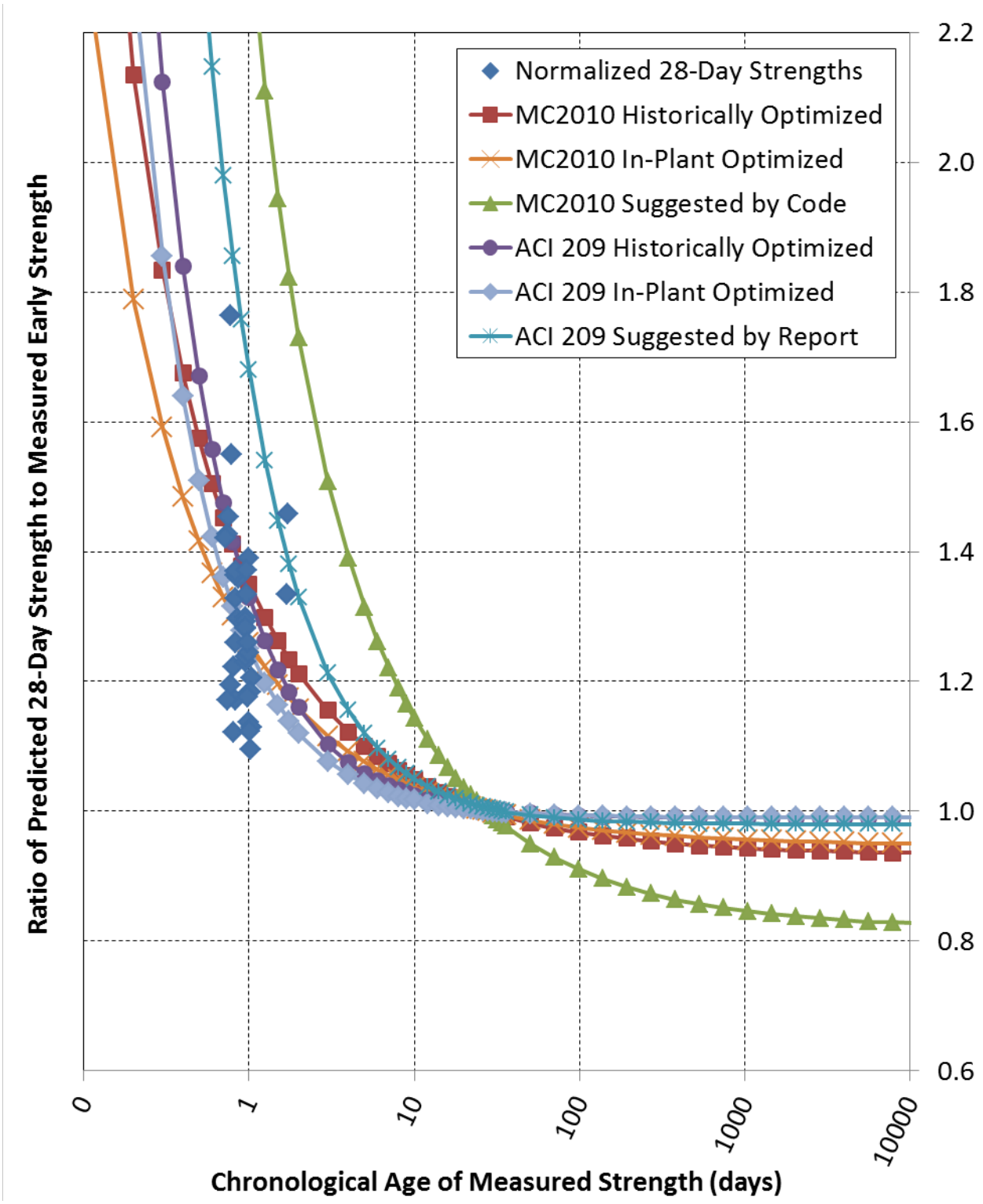

Figure J.5: Extended Prediction Curves for In-Plant 28-Day Strengths, Chronological Age

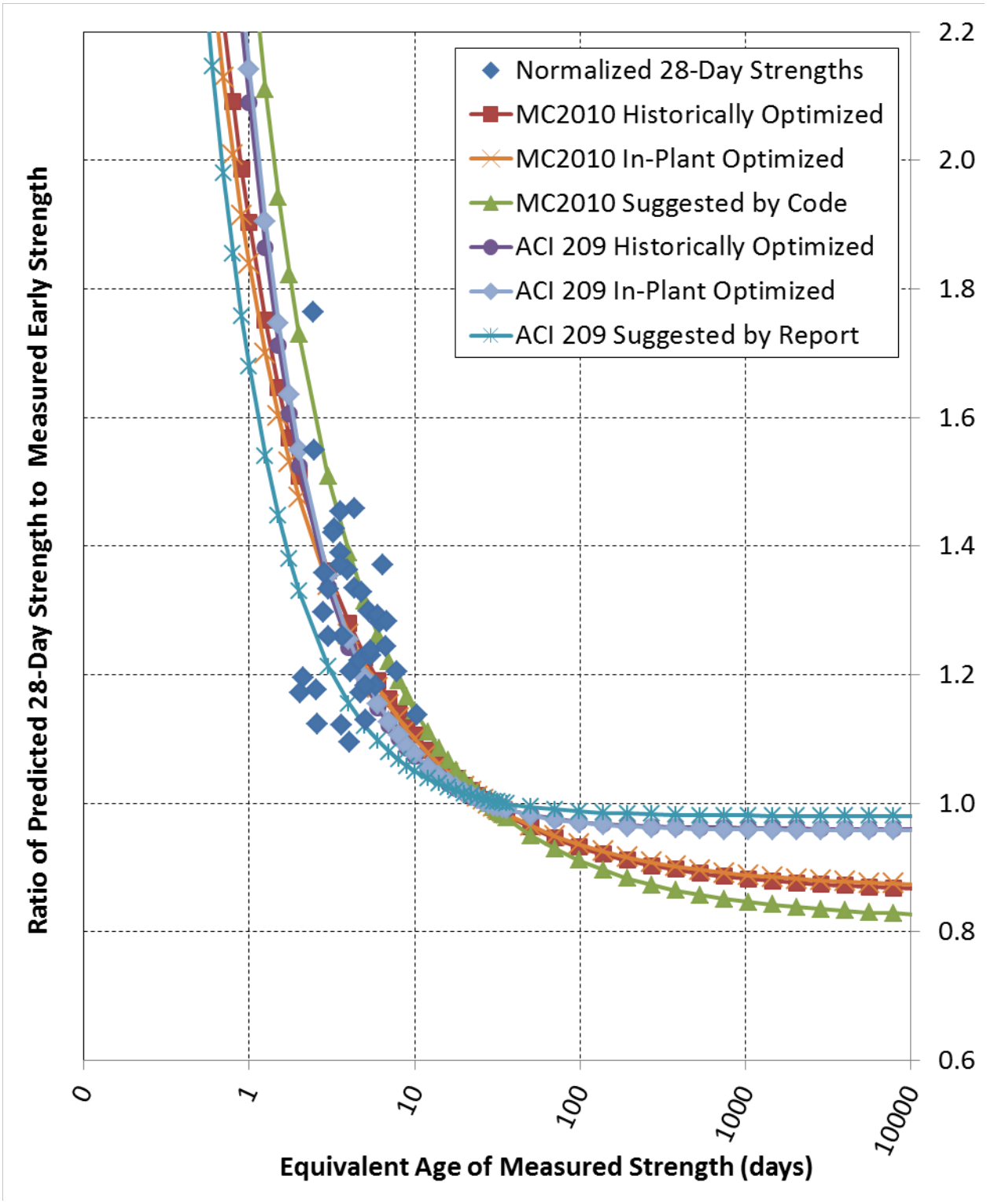

Figure J.6: Extended Prediction Curves for In-Plant 28-Day Strengths, Equivalent Age

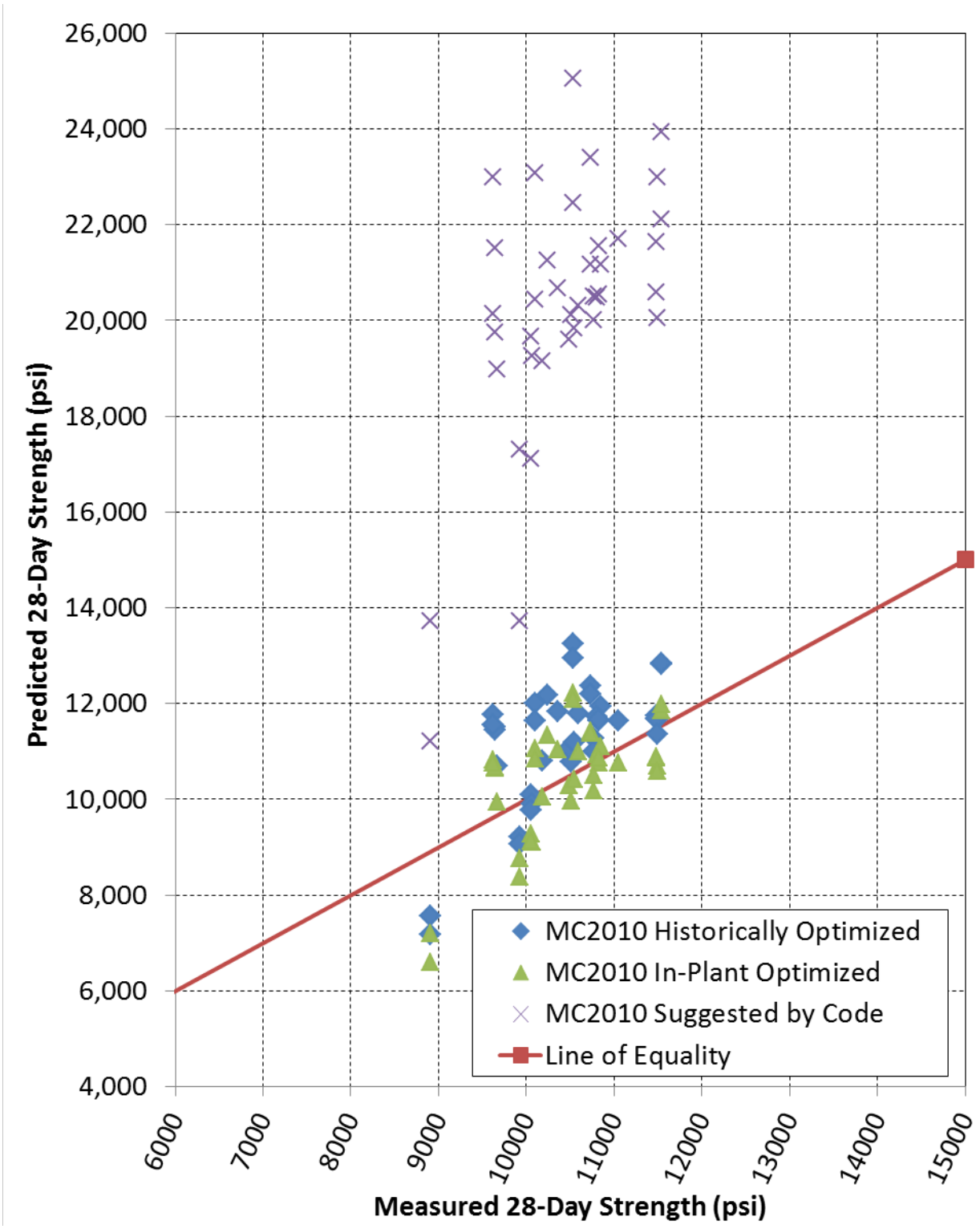

Figure J.7: MC2010 28-Day Strength Predictions for In-Plant Data using Chronological Age

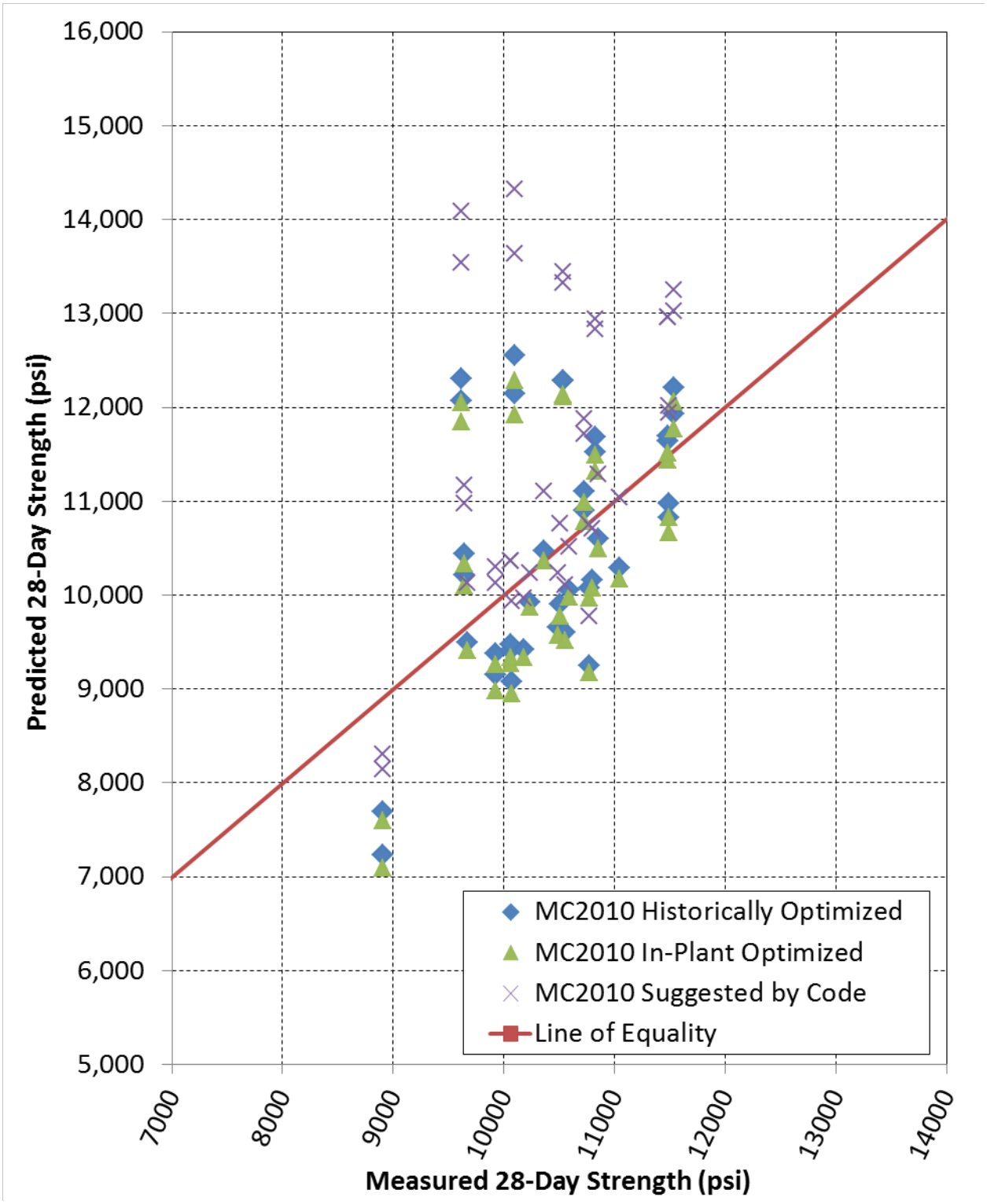

Figure J.8: MC2010 28-Day Strength Predictions for In-Plant Data using Equivalent Age

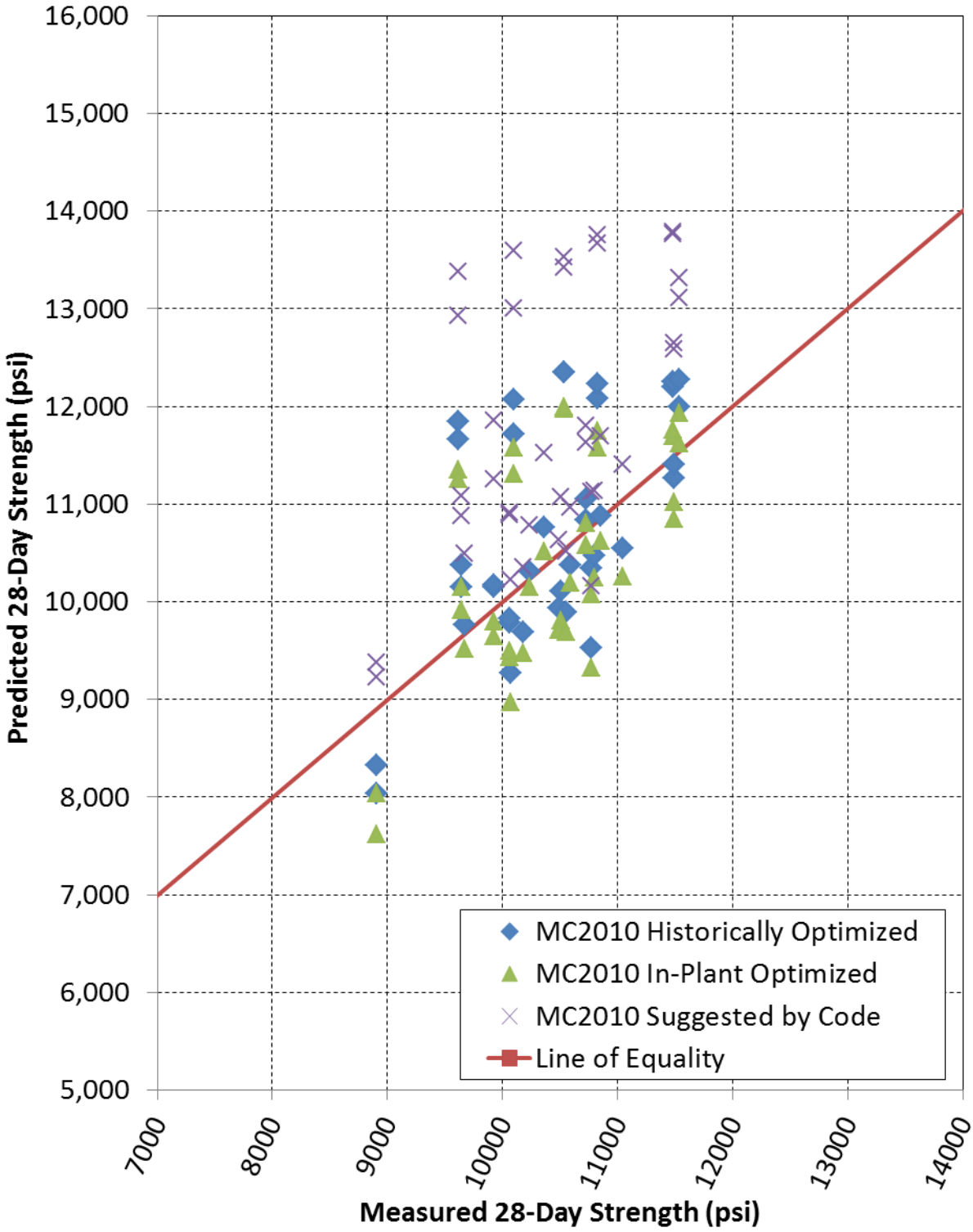

Figure J.9: MC2010 28-Day Strength Predictions for In-Plant Data using Adjusted EA

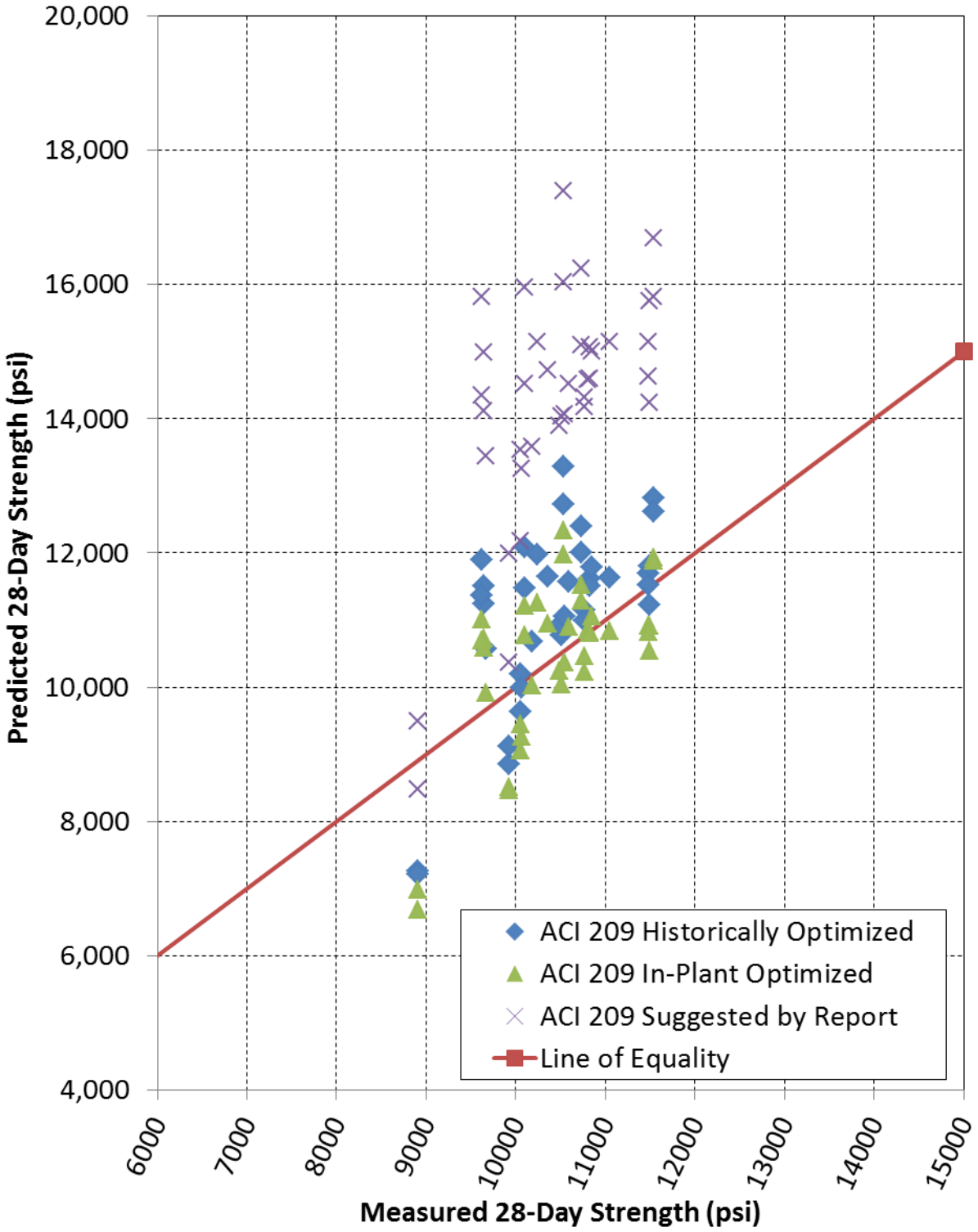

Figure J.10: ACI 209 28-Day Strength Predictions for In-Plant Data using Chronological Age

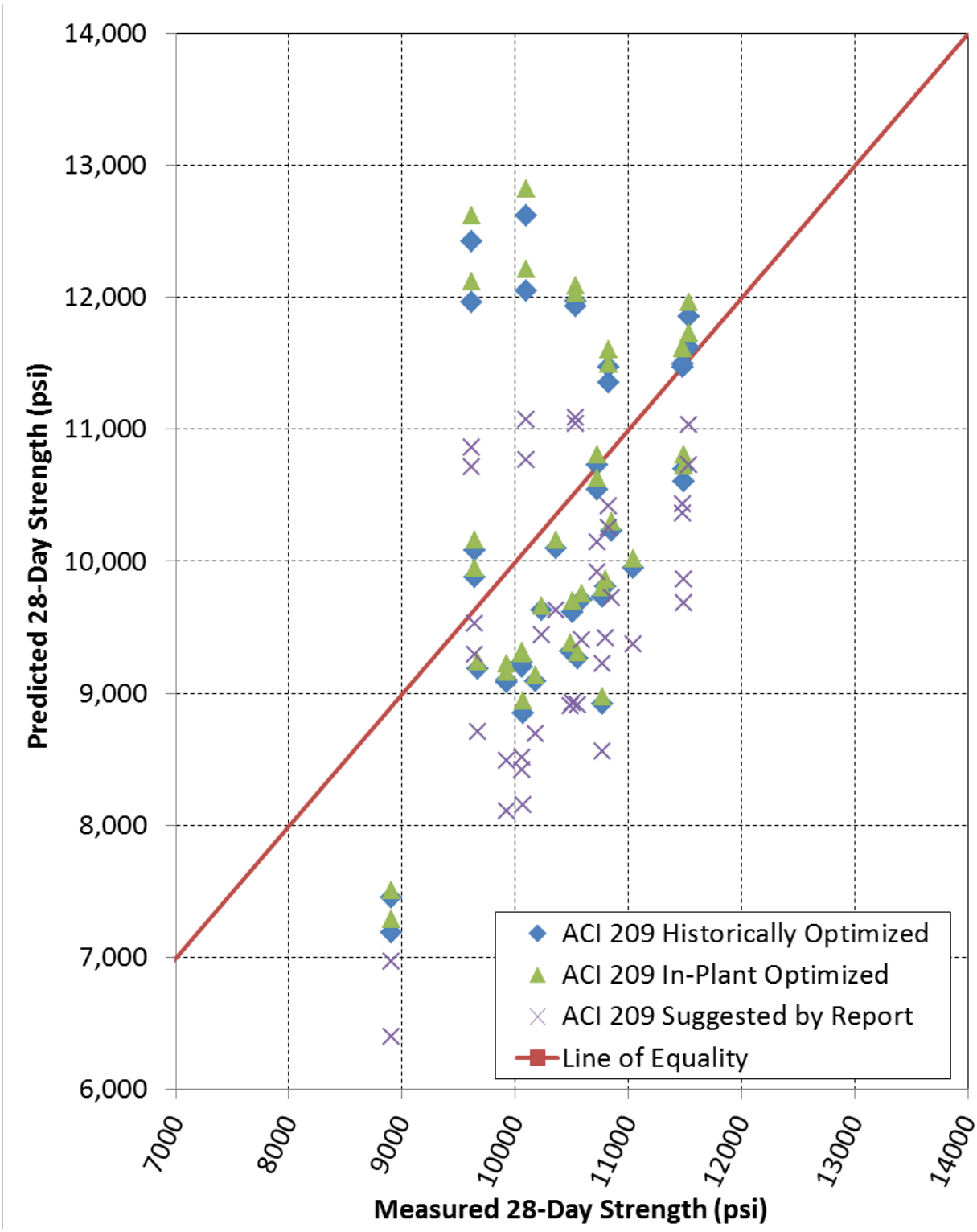

Figure J.11: ACI 209 28-Day Strength Predictions for In-Plant Data using Equivalent Age

Appendix K: Additional In-Plant Release Modulus Prediction Plots

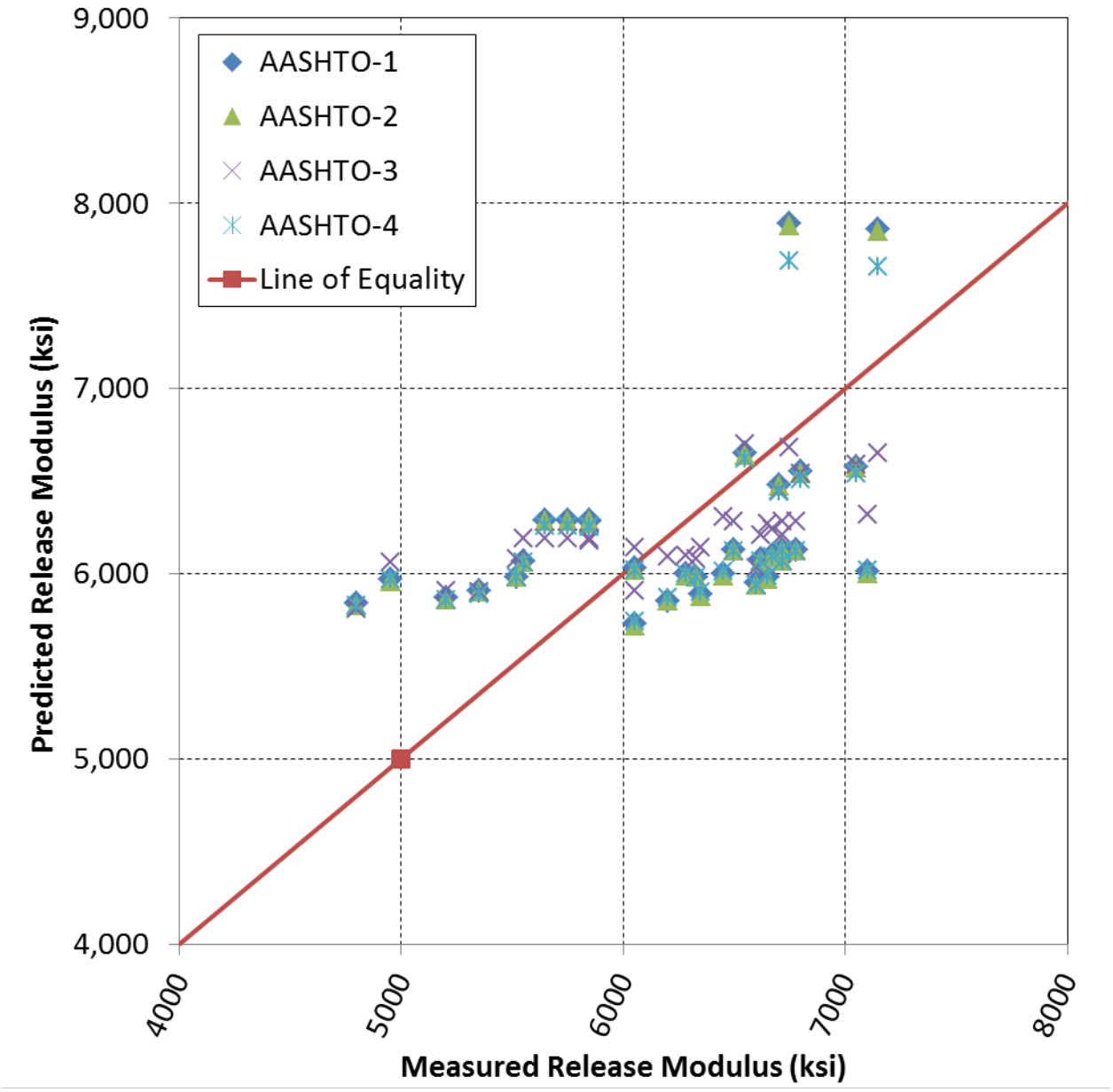

Figure K.1: Optimized AASHTO Release Modulus Predictions with Specified Strengths

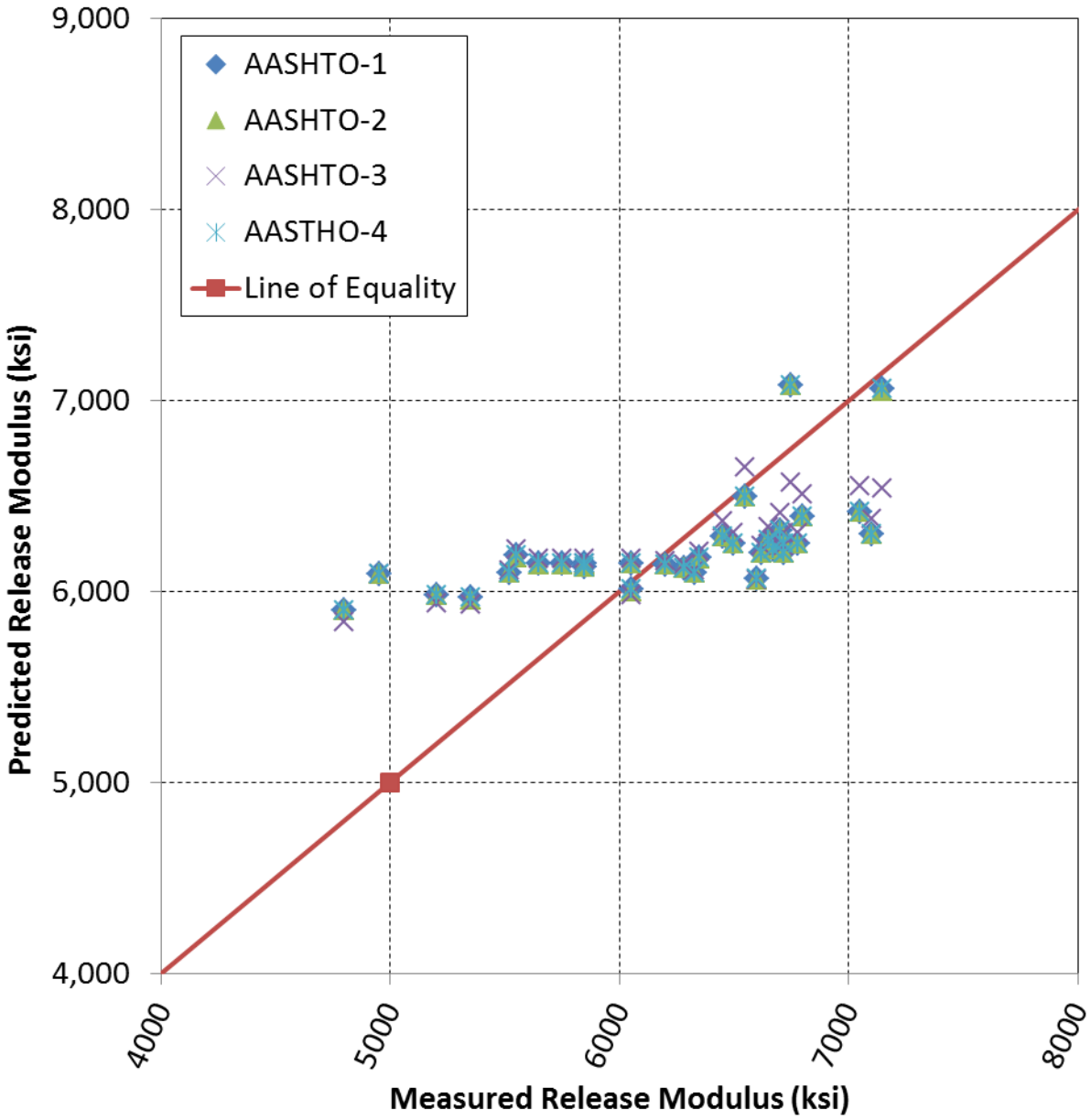

Figure K.2: Optimized AASHTO Release Modulus Predictions with Expected Strengths

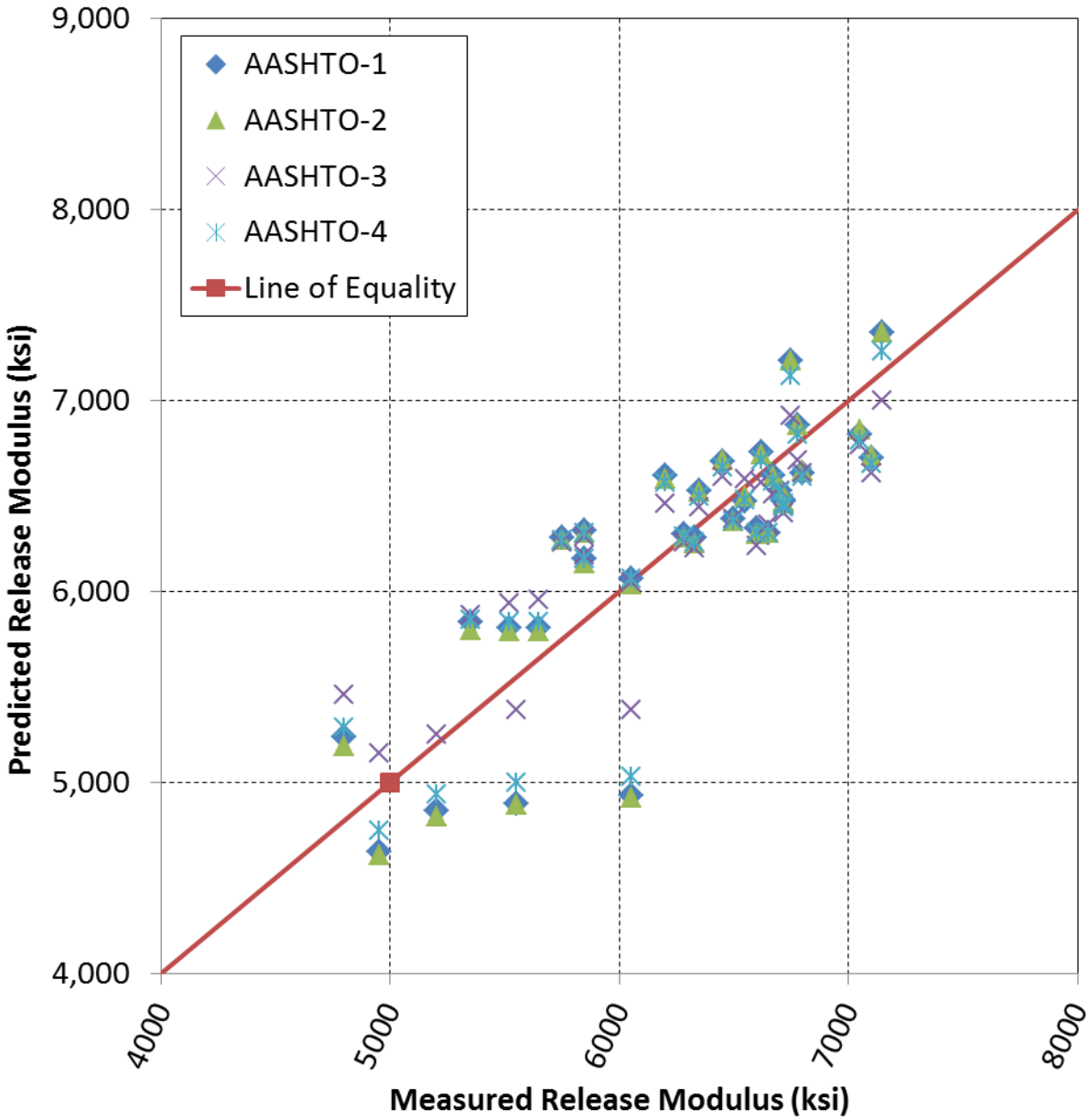

Figure K.3: Optimized AASHTO Release Modulus Predictions with Measured Strengths

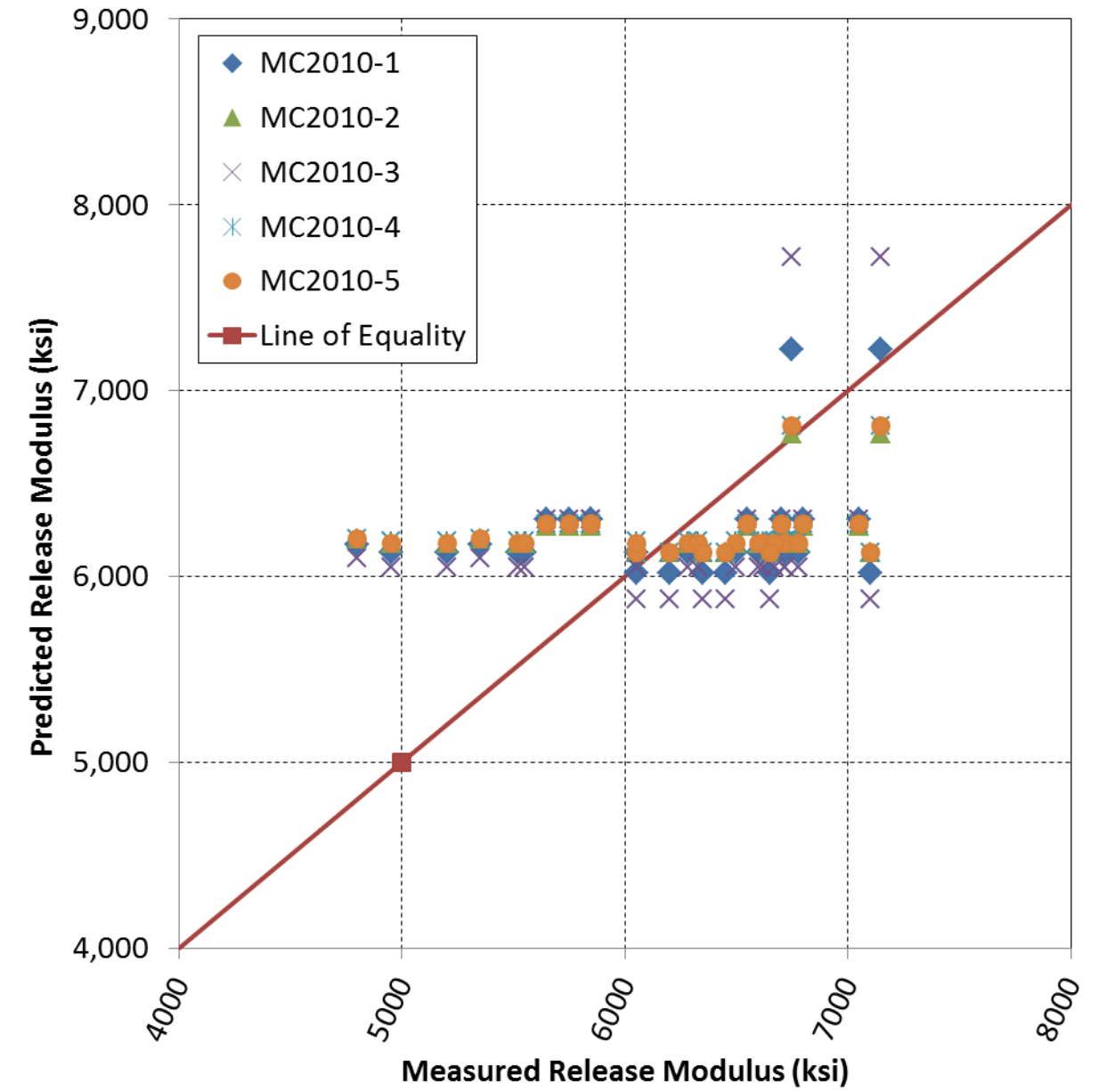

Figure K.4: Optimized MC2010 Release Modulus Predictions with Specified Strengths

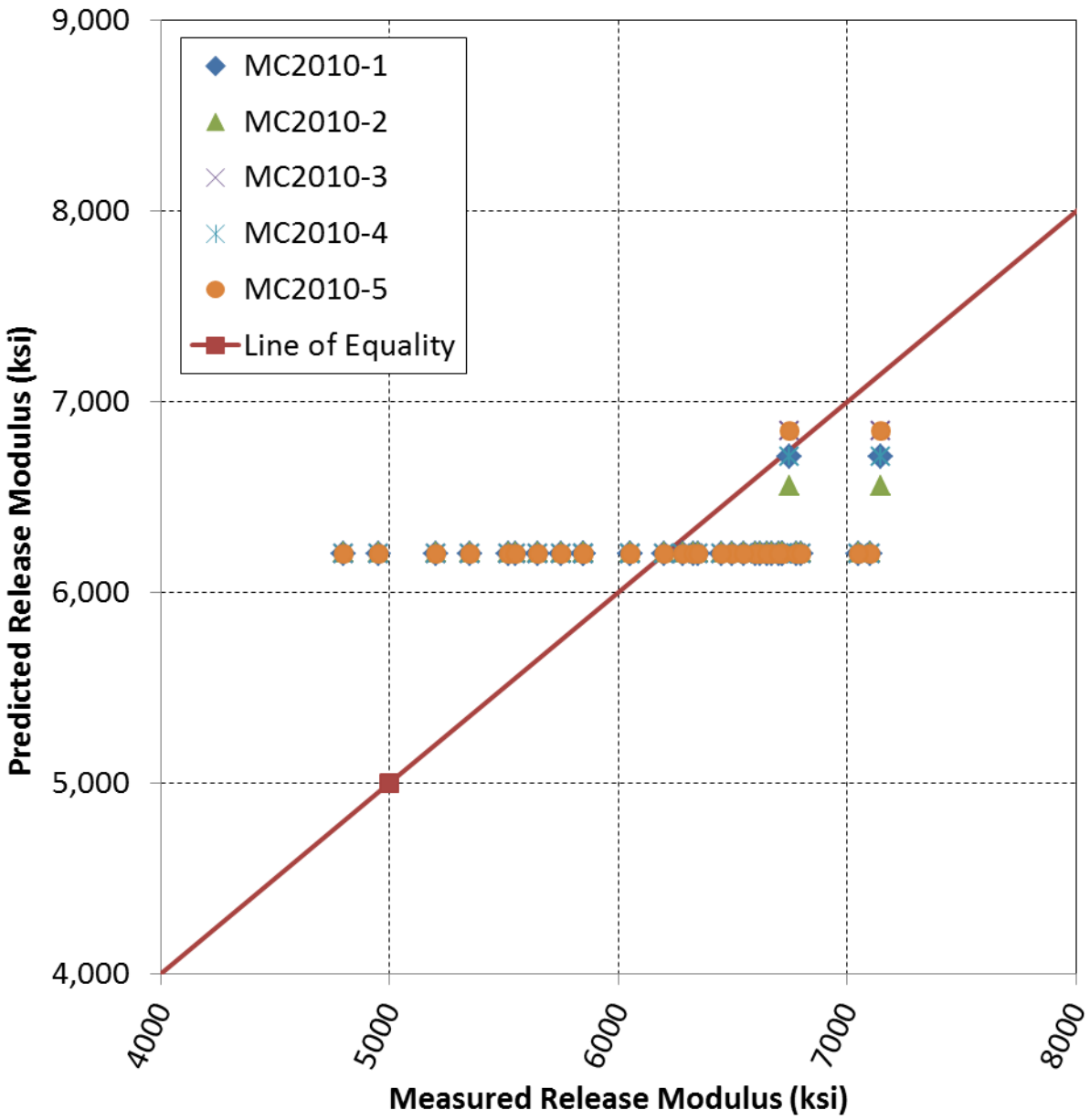

Figure K.5: Optimized MC2010 Release Modulus Predictions with Expected Strengths

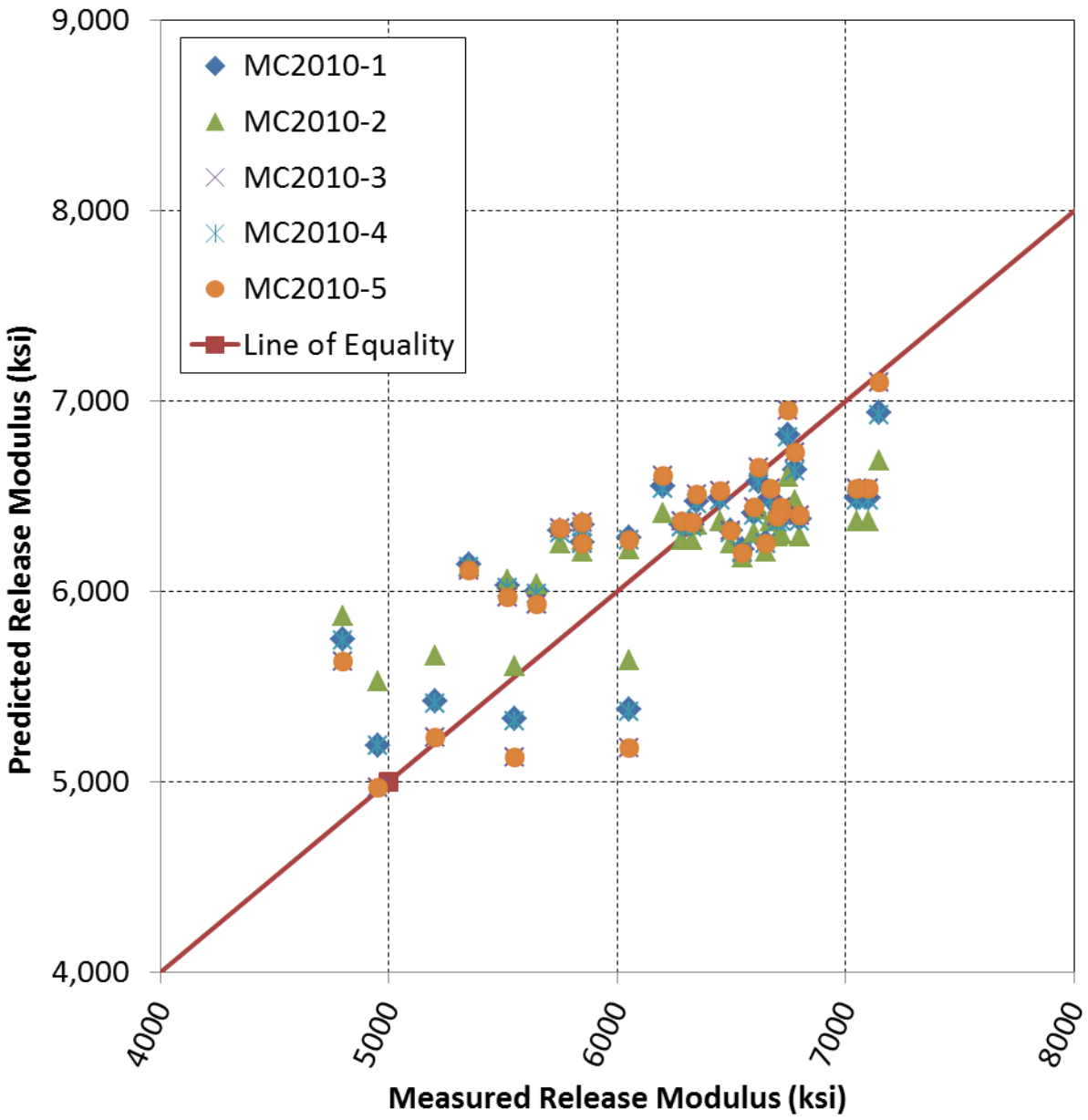

Figure K.6: Optimized MC2010 Release Modulus Predictions with Measured Strengths

Appendix L: In-Plant 28-Day Modulus Prediction Plots

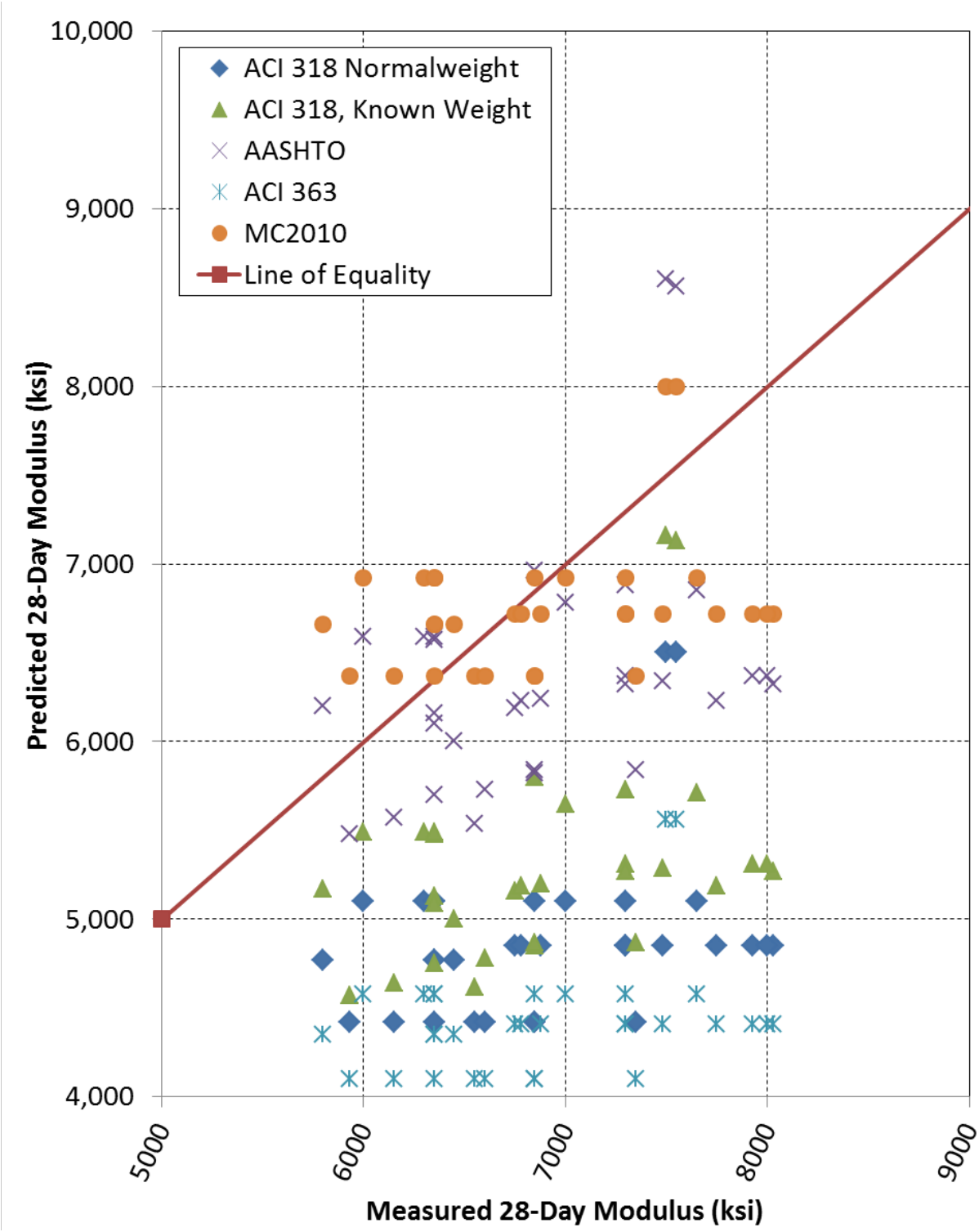

Figure L.1: 28-Day Modulus Predictions using Basic Equations, Specified Strength

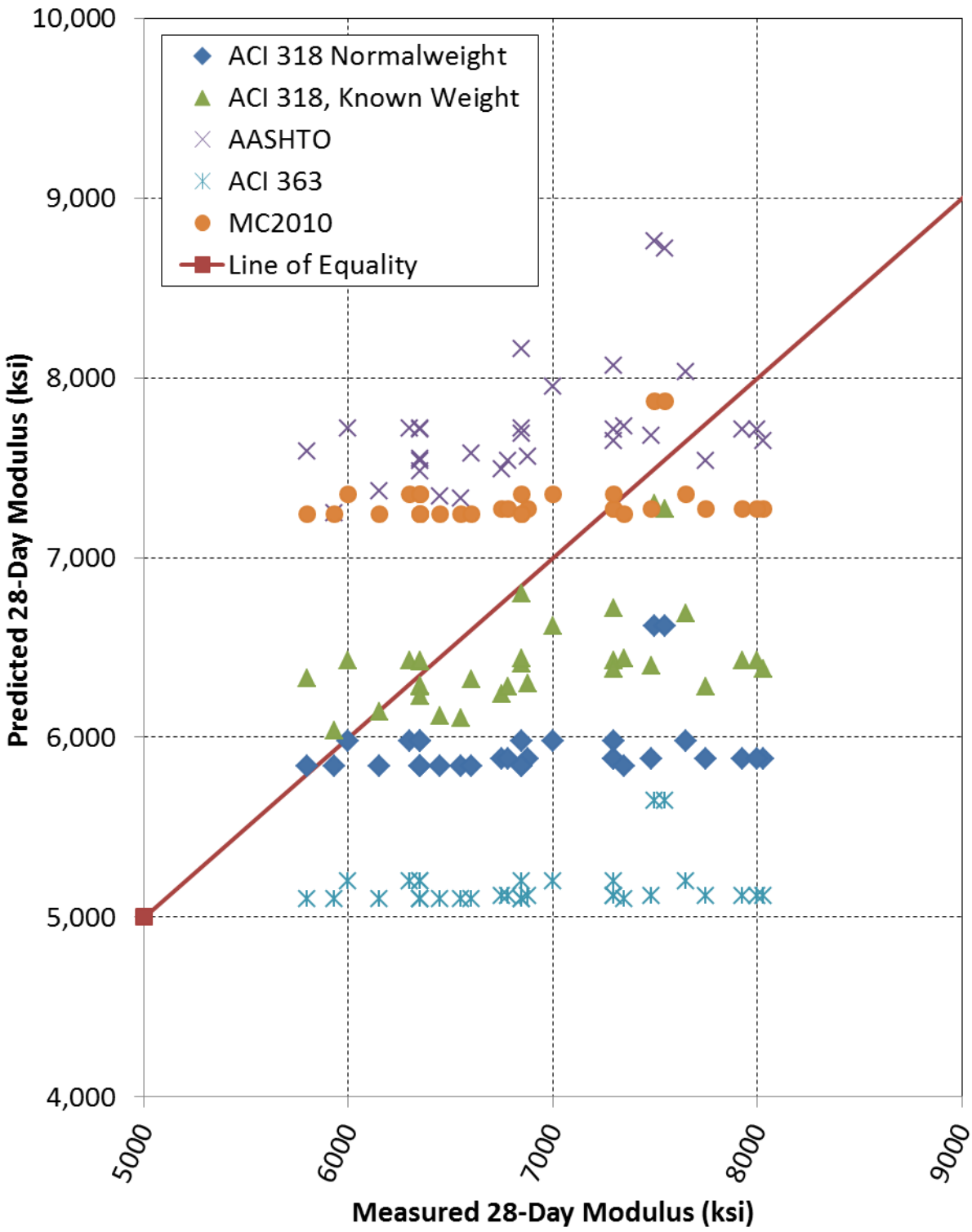

Figure L.2: 28-Day Modulus Predictions using Basic Equations, Expected Strength

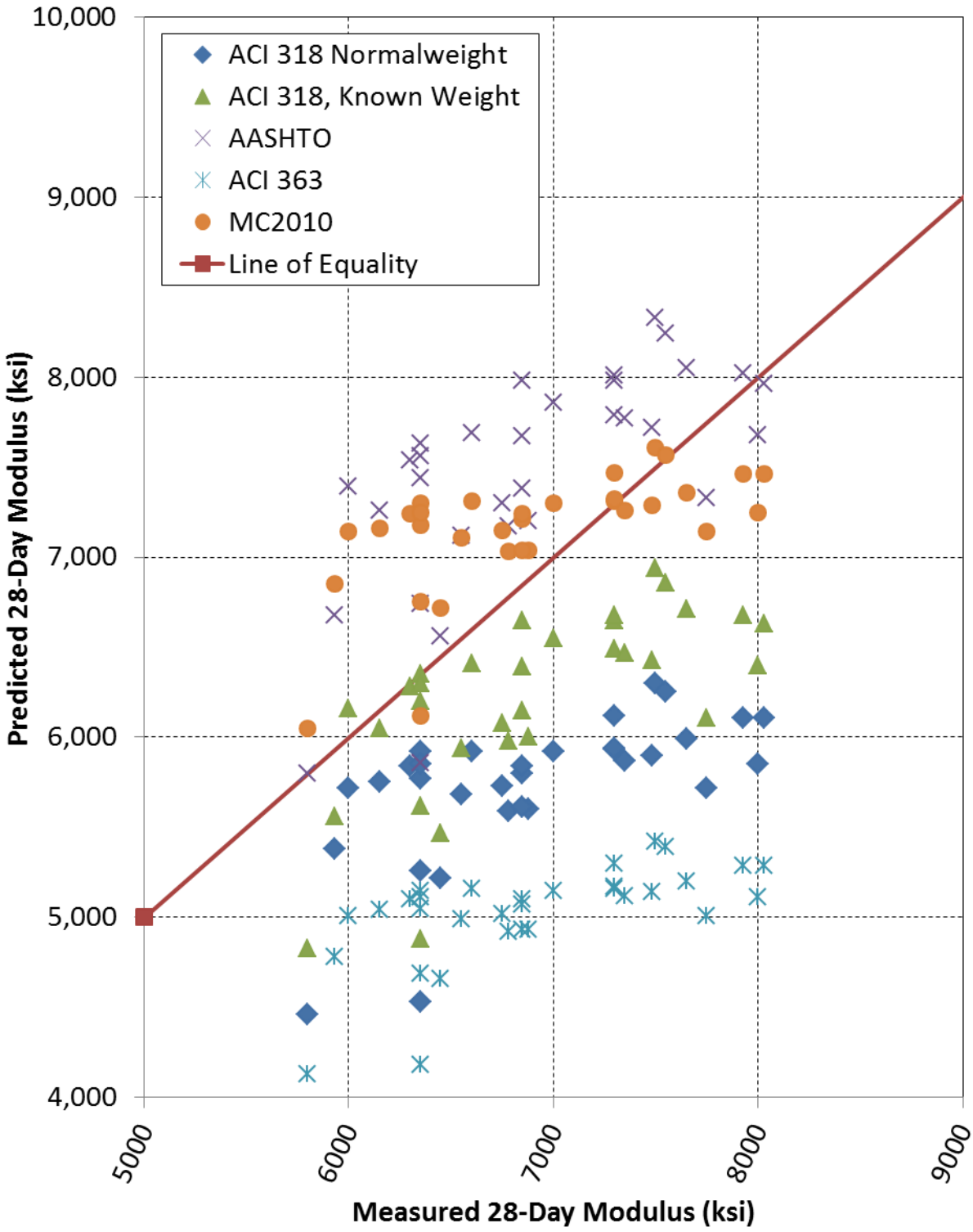

Figure L.3: 28-Day Modulus Predictions using Basic Equations, Measured Strength

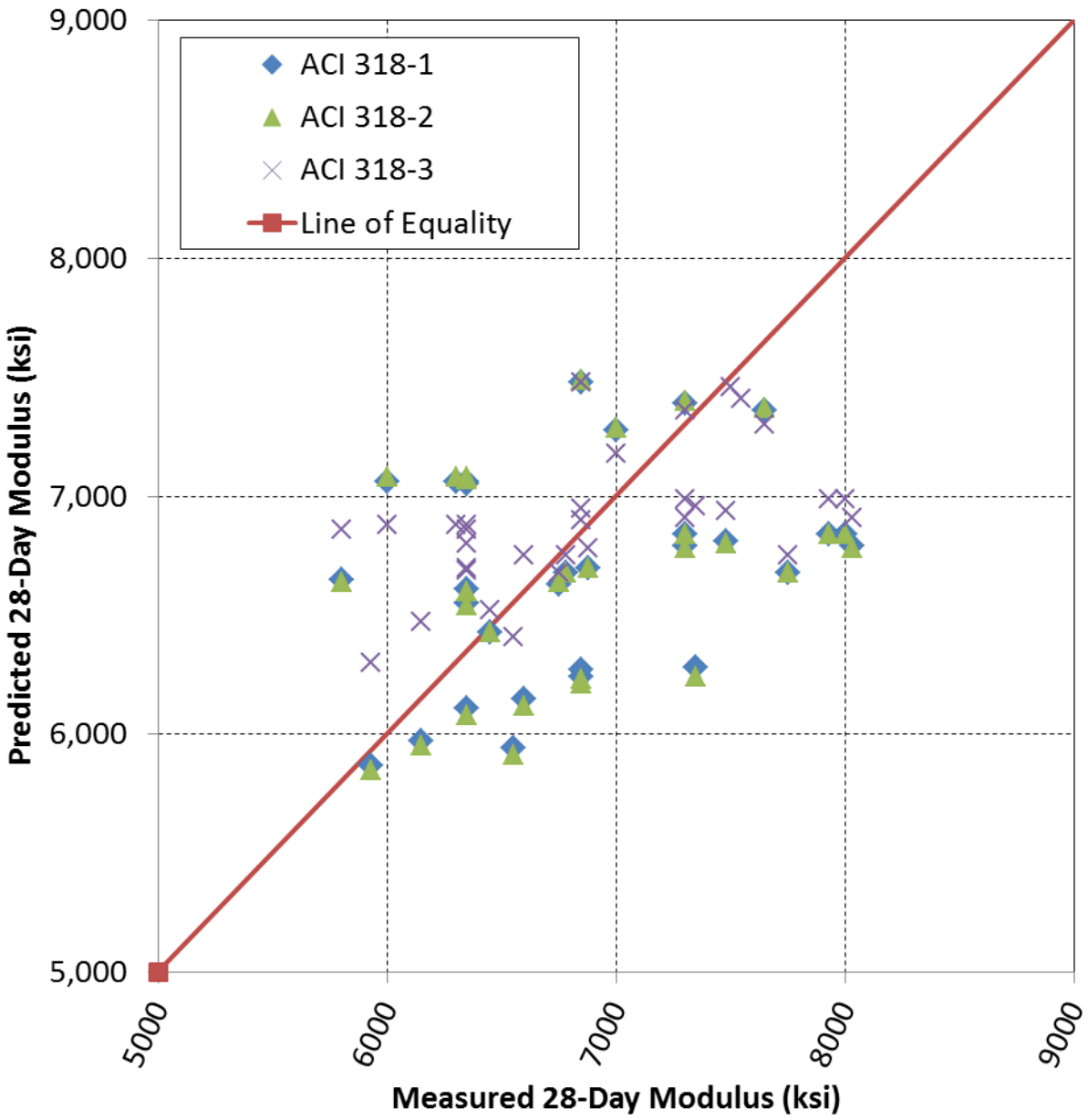

Figure L.4: Optimized ACI 318 28-Day Modulus Predictions with Specified Strengths

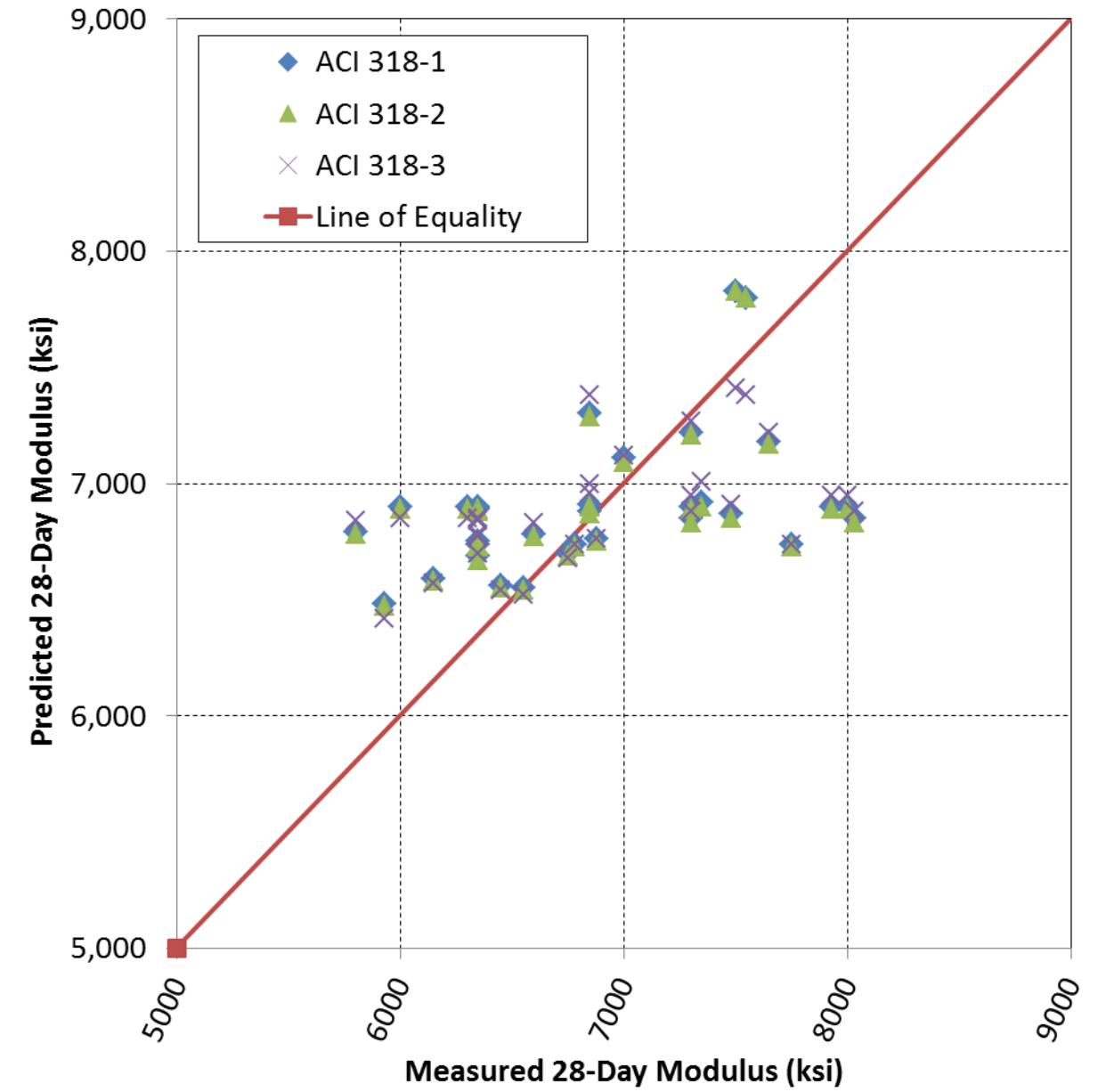

Figure L.5: Optimized ACI 318 28-Day Modulus Predictions with Expected Strengths

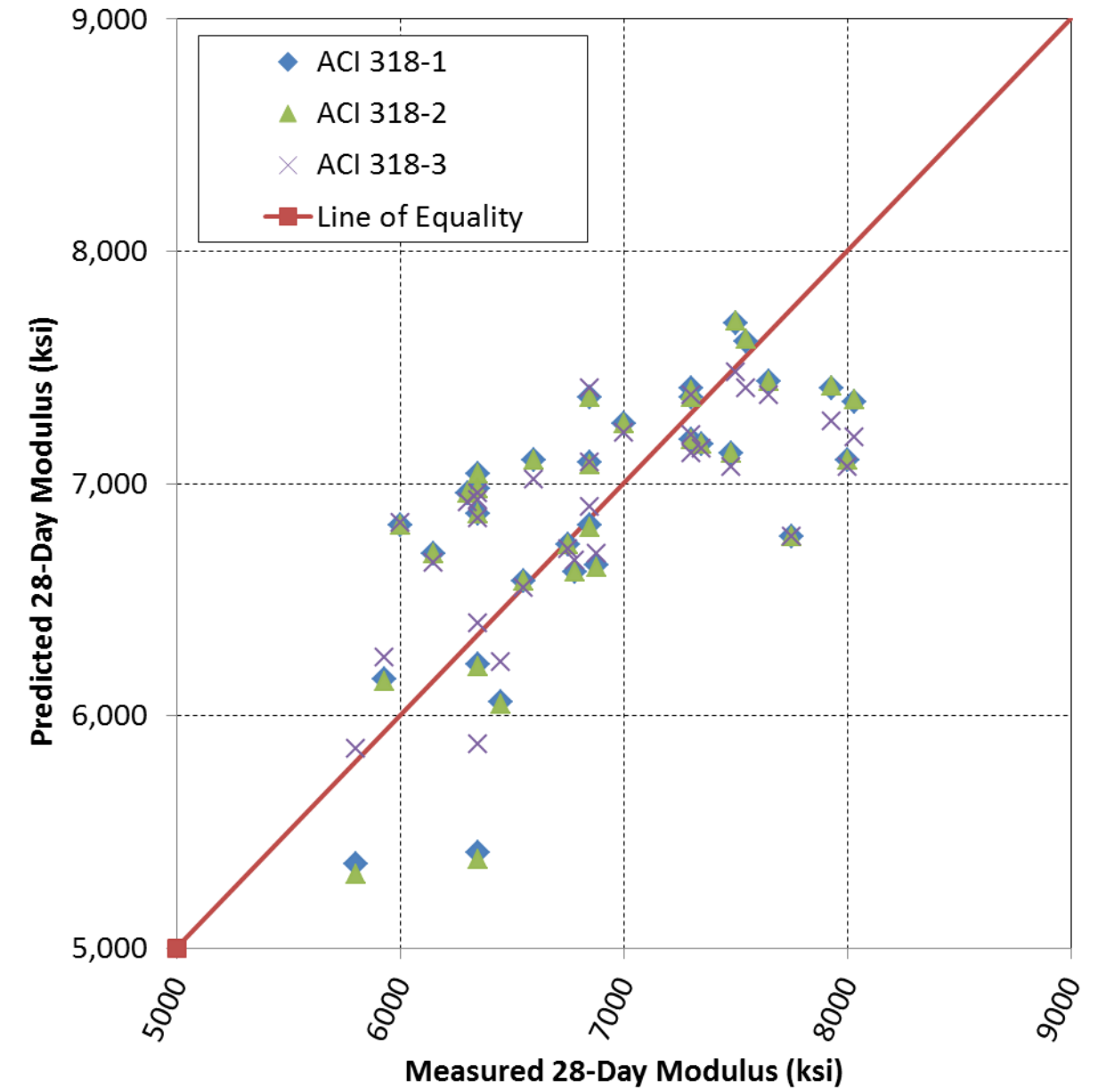

Figure L.6: Optimized ACI 318 28-Day Modulus Predictions with Measured Strengths

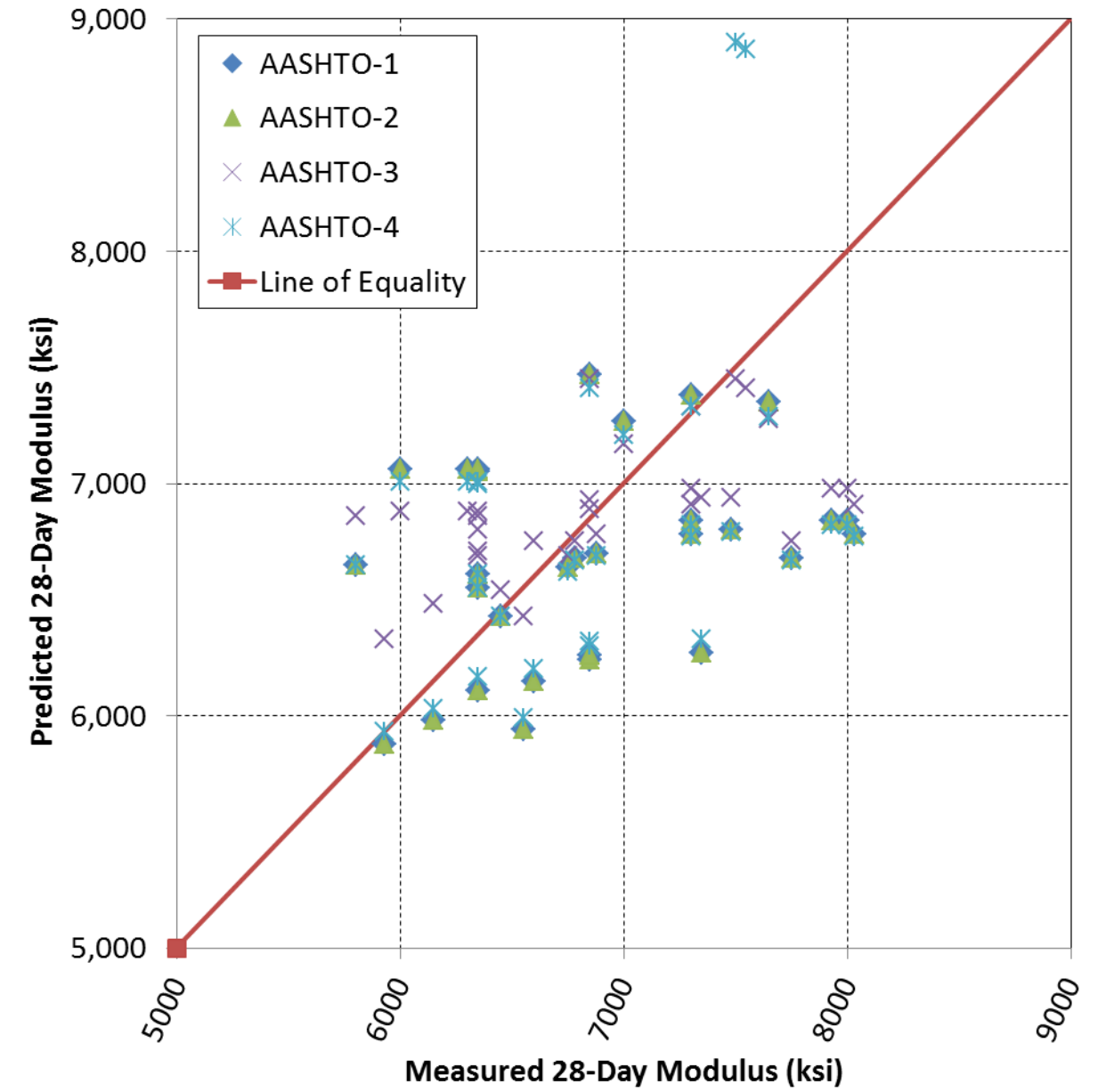

Figure L.7: Optimized AASHTO 28-Day Modulus Predictions with Specified Strengths

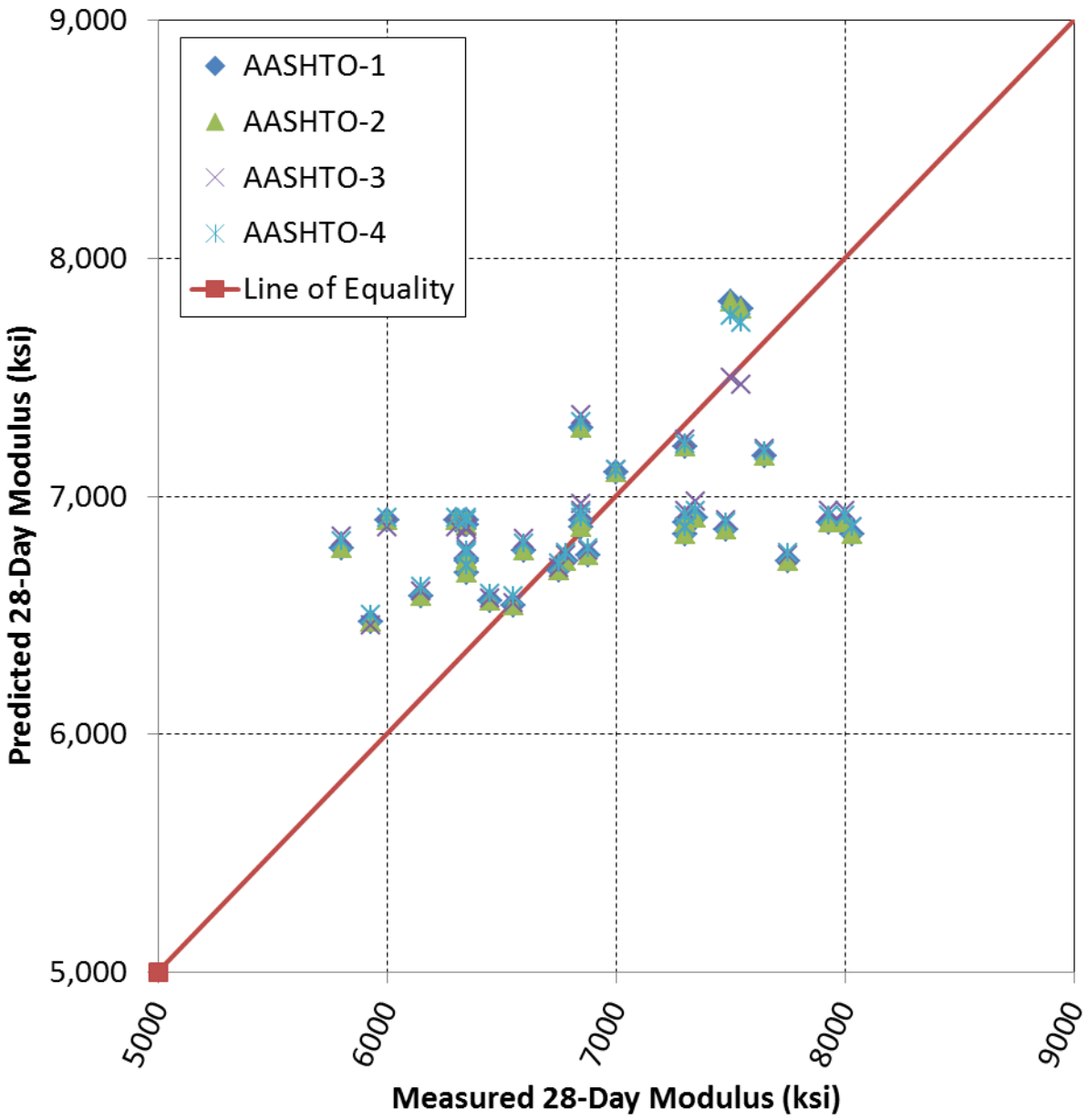

Figure L.8: Optimized AASHTO 28-Day Modulus Predictions with Expected Strengths

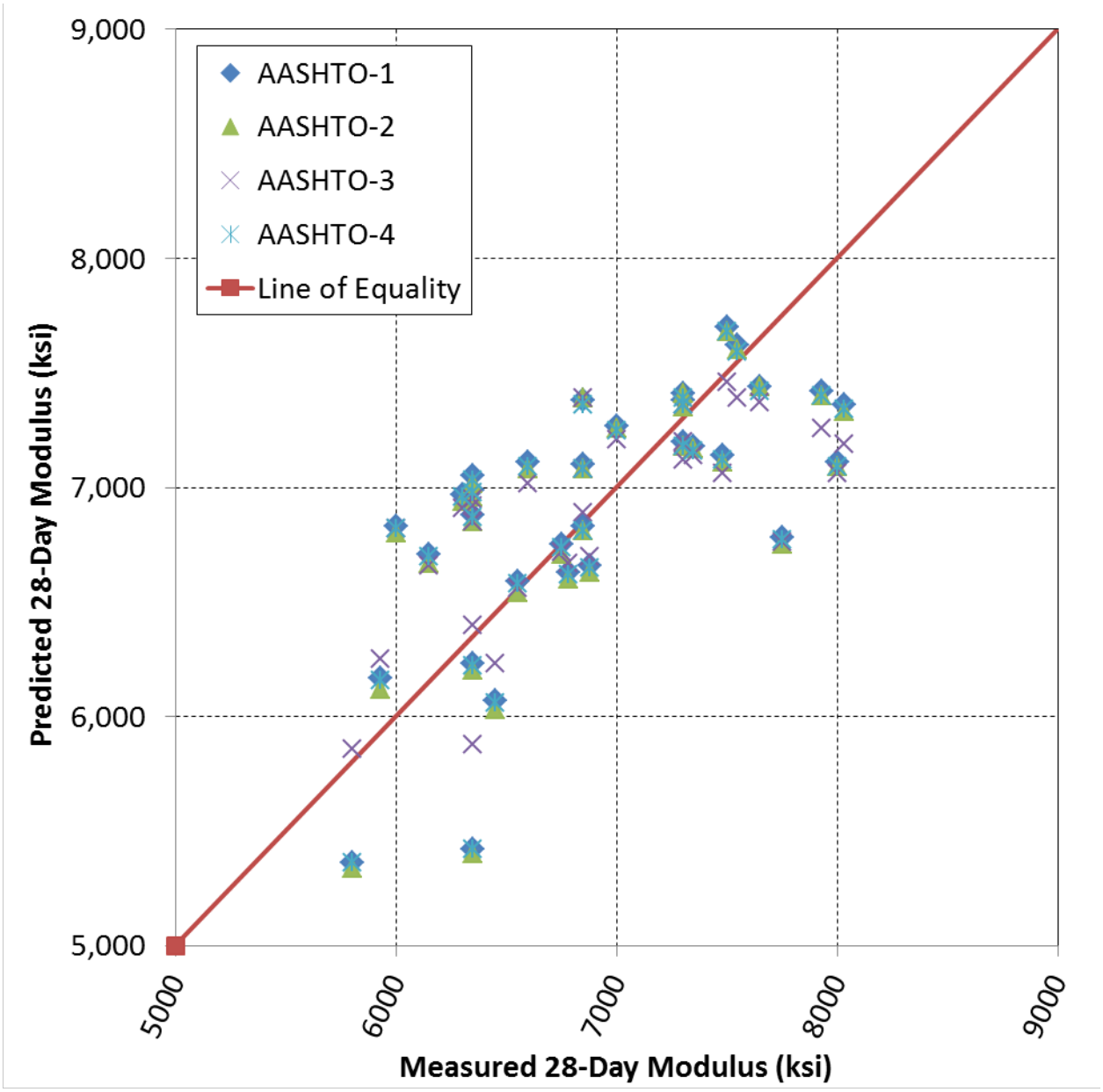

Figure L.9: Optimized AASHTO 28-Day Modulus Predictions with Measured Strengths

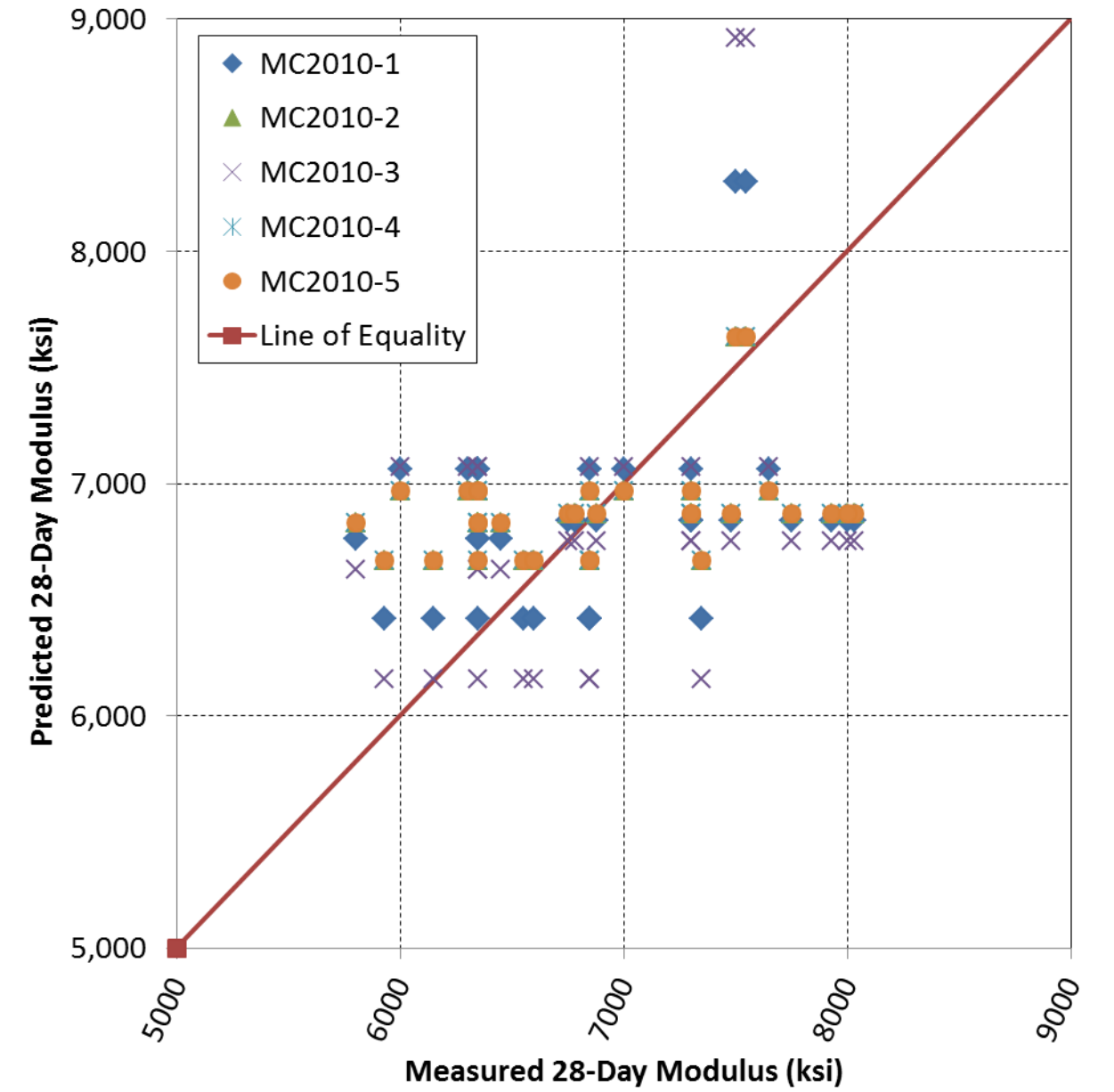

Figure L.10: Optimized MC2010 28-Day Modulus Predictions with Specified Strengths

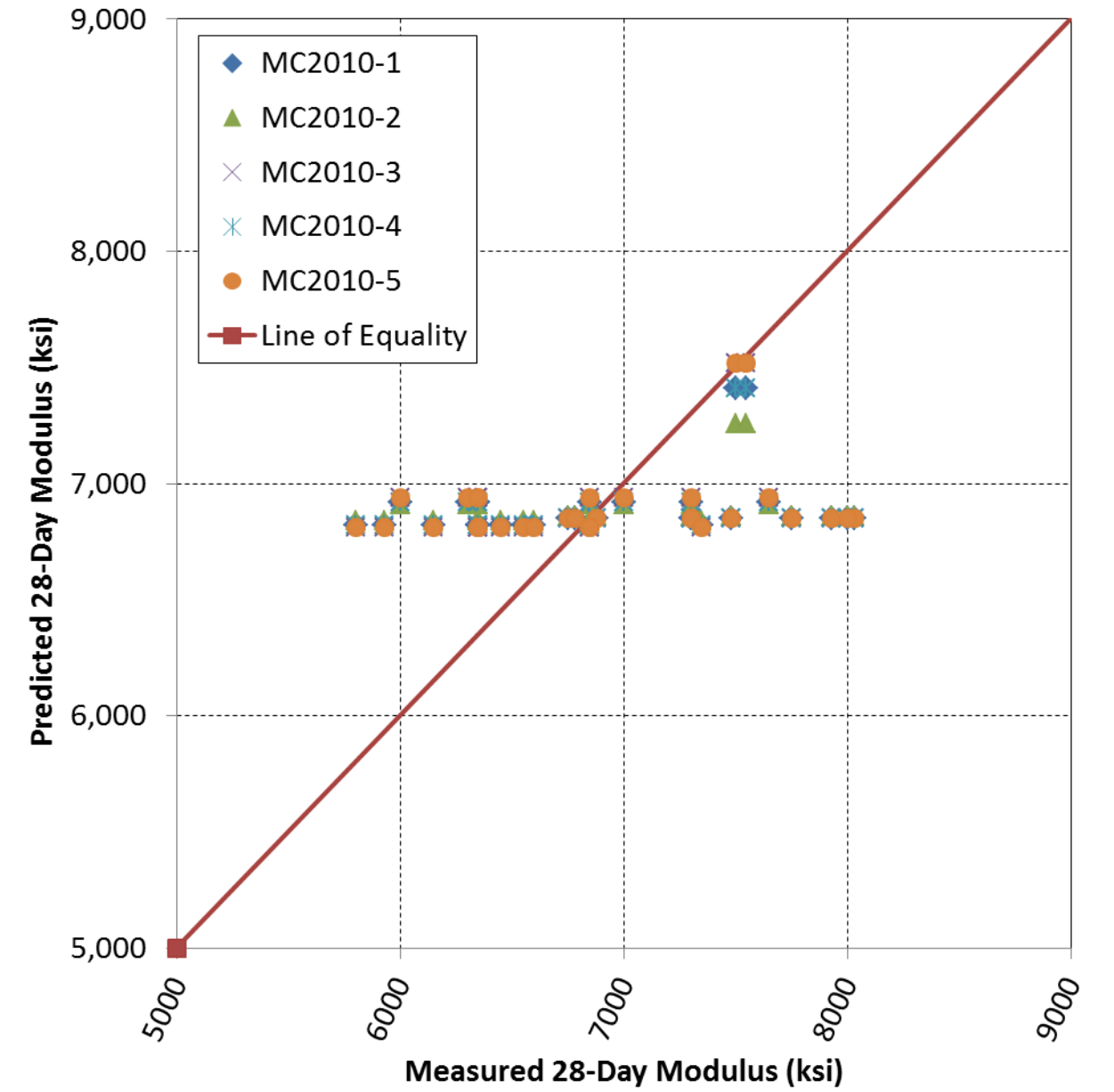

Figure L.11: Optimized MC2010 28-Day Modulus Predictions with Expected Strengths

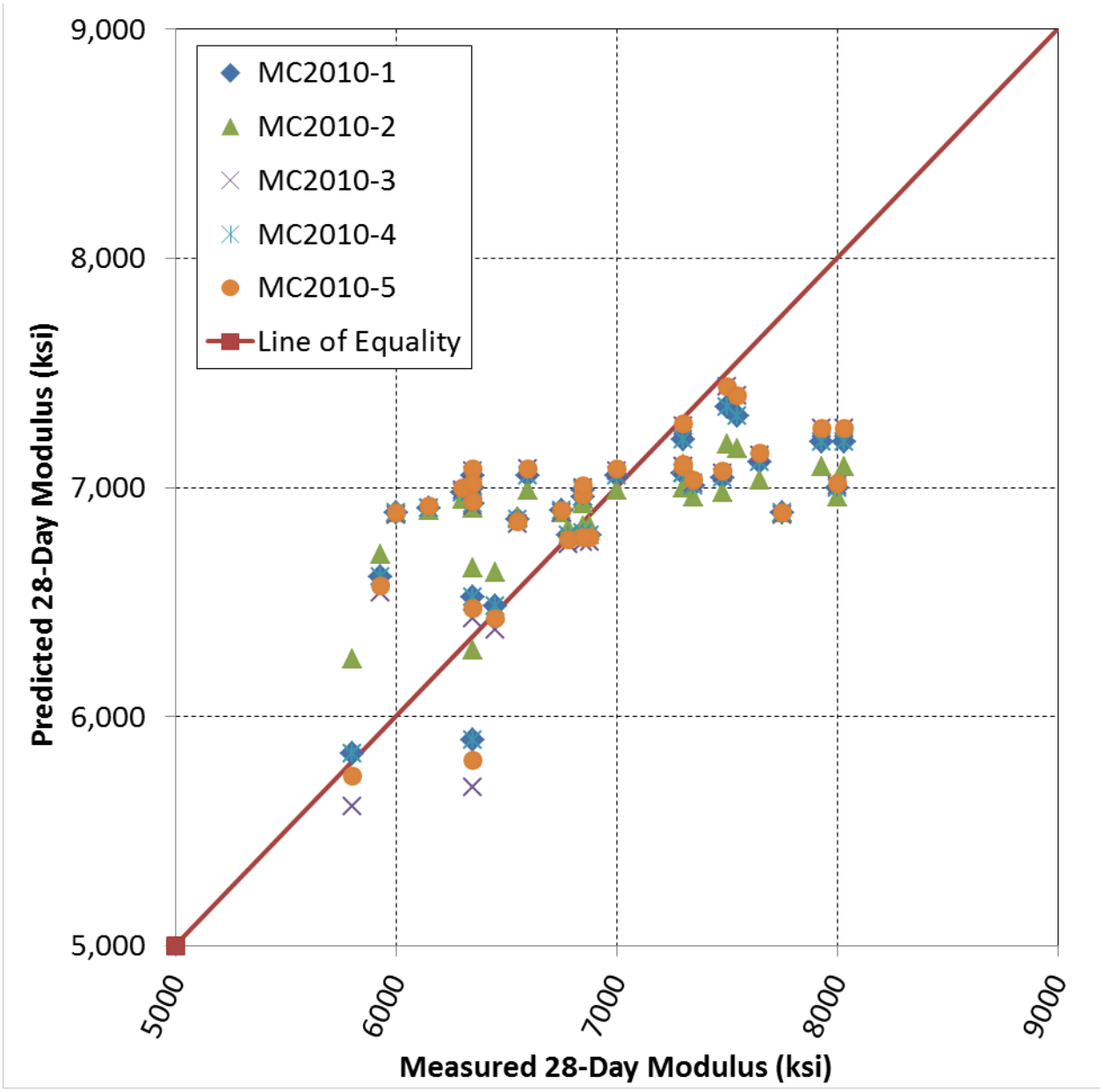

Figure L.12: Optimized MC2010 28-Day Modulus Predictions with Measured Strengths

Appendix M: In-Plant Data Summary

Table M.1: In-Plant Air Contents, Unit Weights, and Release Maturity Quantifications

Project Source	Concrete Type	Air Content (%)	Unit Weight (pcf)	Chronological Age at Release (hours)	Equivalent Age, at 73°F, at Release (hours)
Current-1	VC	3.6	147.2	41.3	104.7
Current-2	VC	2.9	148.3	40.8	104.1
Current-3	VC	3.0	152.1	20.7	68.3
Current-4	VC	2.5	152.8	20.4	67.9
Current-5	VC	4.0	150.5	17.9	78.5
Current-6	VC	2.5	152.8	17.4	77.5
Current-7	VC	3.0	152.1	20.0	88.0
Current-8	VC	2.5	152.8	19.3	86.6
Current-9	VC	3.8	150.8	20.0	112.9
Current-10	VC	2.8	152.4	19.3	112.5
Current-11	VC	4.4	149.9	18.5	50.8
Current-12	VC	4.0	150.5	17.8	49.0
Keske-1	VC	4.0	153.7	25.0	187.7
Keske-2	VC	4.4	153.2	23.0	130.8
Keske-3	VC	4.2	153.6	24.0	140.6
Keske-4	VC	3.9	154.1	23.0	127.0
Keske-5	VC	2.9	155.7	23.0	131.0
Keske-6	VC	3.4	155.2	20.0	115.2
Keske-7	VC	2.7	156.9	20.0	94.6
Keske-8	SCC	4.1	151.1	24.0	249.6
Keske-9	SCC	3.4	151.7	24.0	159.8
Keske-10	SCC	4.9	148.9	23.0	147.1
Keske-11	SCC	4.0	151.2	23.0	144.2
Keske-12	SCC	4.1	151.0	20.0	154.6
Keske 13	SCC	3.9	151.2	23.0	162.5
Keske-14	SCC	3.8	151.2	18.0	85.4
Boehm-1	VC	3.4	151.2	20.6	84.2
Boehm-2	VC	3.0	151.9	Unknown	Unknown
Boehm-3	SCC	3.8	148.5	22.8	67.4
Boehm-4	SCC	1.8	150.3	23.3	76.3
Boehm-5	SCC	1.5	153.6	23.3	90.2
Boehm-6	SCC	1.5	153.2	23.3	102.0

Table M.2: In-Plant Strengths and Measured Modulus of Elasticity Values

Project Source	Concrete Type	Specified Release Strength (psi)	Specified 28-Day Strength (psi)	Measured Release Strength (psi)	Measured Release Modulus (ksi)	Measured 28-Day Strength (psi)	Measured 28-Day Modulus (ksi)
Current-1	VC	5600	6000	6110	4800	8910	5950
Current-2	VC	5600	6000	7440	5350	9930	6550
Current-3	VC	5500	7250	8450	6700	11,480	8050
Current-4	VC	5500	7250	8350	6700	10,830	7300
Current-5	VC	5500	7250	7050	5500	10,060	7750
Current-6	VC	5500	7250	8090	6500	11,490	7950
Current-7	VC	5500	7250	9160	6600	11,540	7300
Current-8	VC	5500	7250	9400	6800	10,540	8000
Current-9	VC	5500	7250	8230	6800	9640	6900
Current-10	VC	5500	7250	8780	6650	10,730	7500
Current-11	VC	5500	7250	8450	6600	10,100	6750
Current-12	VC	5500	7250	8210	6350	9620	6800
Keske-1	VC	5200	6000	8790	7100	10,590	7350
Keske-2	VC	5200	6000	7860	6650	9670	6850
Keske-3	VC	5200	6000	8760	6450	10,360	6850
Keske-4	VC	6000	8000	8290	6700	10,770	7000
Keske-5	VC	6000	8000	8770	7050	10,850	7300
Keske-6	VC	6000	8000	8320	6800	11,050	7650
Keske-7	VC	6000	8000	7710	6550	10,510	6850
Keske-8	SCC	5200	6000	9010	6200	10,240	6350
Keske-9	SCC	5200	6000	8680	6350	10,800	6600
Keske-10	SCC	5200	6000	7940	6050	10,180	6150
Keske-11	SCC	6000	8000	8120	5750	10,490	6300
Keske-12	SCC	6000	8000	7860	5850	10,770	6350
Keske 13	SCC	6000	8000	8220	5850	10,550	6350
Keske-14	SCC	6000	8000	6930	5650	10,070	6000
Boehm-1	VC	5500	7000	4990	6050	6330	6350
Boehm-2	VC	5500	7000	4860	5550	6120	5800
Boehm-3	SCC	5500	7000	5110	5200	8390	6450
Boehm-4	SCC	5500	7000	4500	4950	8530	6350
Boehm-5	SCC	9000	13,000	10,190	6750	12,200	7500
Boehm-6	SCC	9000	13,000	10,720	7150	12,030	7550